

**CRANFIELD UNIVERSITY**

**SCHOOL OF ENGINEERING  
(COLLEGE OF AERONAUTICS)**

**Ph.D. Thesis**

**Academic years: 1998 - 2002**

**T. M. YOUNG**

**INVESTIGATIONS INTO THE OPERATIONAL  
EFFECTIVENESS OF HYBRID LAMINAR FLOW  
CONTROL AIRCRAFT**

**Supervisor: J.P. Fielding**

**October 2002**

© Cranfield University, 2002. All rights reserved. No part of this publication may be reproduced without the written permission of the copyright holder.

## ACKNOWLEDGEMENT

From 1996 to 2002, the author was responsible for the technical contribution of the University of Limerick, Ireland, to three collaborative Hybrid Laminar Flow Control (HLFC) research projects. These projects: HYLDA (Hybrid Laminar Flow Demonstration on Aircraft), HYLTEC (Hybrid Laminar Flow Technology) and ALTTA (Application of Hybrid Laminar Flow Technology on Transport Aircraft), provided the inspiration and background to the work presented in this thesis. The author acknowledges the financial support of the Commission of European Communities in funding these projects. The financial contribution of the University of Limerick towards the annual cost of Ph.D. registration and travel expenses is also gratefully acknowledged.

I wish to express my most sincere gratitude to everyone who helped and supported me in my research efforts over the past four years. In particular, I wish to thank Professor John Fielding, my supervisor, mentor and friend, for his encouragement and constructive suggestions. The enthusiasm of the HYLDA, HYLTEC and ALTTA research communities was truly infectious and I am grateful to this group of dedicated researchers for their inspiration and assistance. For their meticulous editing of the draft thesis, I wish to thank my wife, Fiona Young, my mother, Shirley Young and my good friend, Jim Borge. I will be forever indebted to my family, Fiona, Michael, Kieran and Christopher, for their love and support.

Trevor Young  
October 2002



Blank page

## ABSTRACT

Hybrid Laminar Flow Control (HLFC) is an active drag reduction technique that permits extended laminar flow on an aircraft surface at chord Reynolds numbers normally associated with turbulent flow. The operational effectiveness of HLFC aircraft relates to the probability of a partial or complete loss of laminar flow. Four factors were considered: (1) Ice particles in cirrus clouds; (2) Insect contamination; (3) Mechanical failure; and (4) Damage to the suction surfaces.

Two computer programs capable of determining the required fuel for a given mission profile have been developed for aircraft in the classes of the B757-200 and the A330-200. The programs were validated against published payload-range data, and modified to emulate the installation of a HLFC system, by incorporating changes to the drag polar, Specific Fuel Consumption (SFC) and Operating Empty Weight (OEW). Sensitivity studies were conducted. The results permit estimates to be determined of the trip fuel reduction of HLFC aircraft compared to equivalent turbulent aircraft.

A conceptual design of a HLFC system has been developed for the reference aircraft. A SFC penalty of 1.6% was determined for the B757-200 class aircraft (range: 3272nm, payload: 19147kg) and 2.1% for the A330-200 class aircraft (range: 5980nm, payload: 24035kg) for a system capable of reducing the drag by approximately 14%. The installed system weight represents 2.0% and 1.6% of the OEW for the B757-200 and A330-200 classes of aircraft respectively. The reduction in trip fuel, compared to the turbulent baseline vehicles, was estimated to be 7.4% for these conditions. To obtain the greatest benefit for a HLFC aircraft, the fuel planning must consider the probable time-in-cloud that will result in a loss of laminar flow. An optimised fuel planning approach, which requires a forecast of en route cirrus cloud, has been estimated to further reduce the trip fuel for long-range missions by 2.5 - 3.8%.

Blank page

## TABLE OF CONTENTS

<b>1</b>	<b>Introduction .....</b>	<b>1</b>
1.1	The Potential of Hybrid Laminar Flow Control .....	1
1.2	Financial Impact of Drag Reduction.....	2
1.3	Environmental Impact of Drag reduction .....	3
1.4	Technologies to Improve Efficiency and Reduce Emissions.....	5
1.5	Operational Effectiveness.....	10
1.6	Objectives and Analysis Model.....	10
1.7	Thesis.....	13
<b>2</b>	<b>Background: Hybrid Laminar Flow Control.....</b>	<b>15</b>
2.1	Introduction .....	15
2.2	Laminar Flow .....	15
2.3	LFC and HLFC Studies and Flight Test Campaigns .....	20
2.4	HLFC System .....	20
2.5	Contamination of the LFC Surface.....	23
<b>3</b>	<b>Computer Performance Model.....</b>	<b>26</b>
3.1	Introduction .....	26
3.2	Requirements for the “Baseline” Program.....	26
3.3	Performance theory.....	30
3.4	Computer Program .....	31
<b>4</b>	<b>Aircraft Performance Data .....</b>	<b>40</b>
4.1	Introduction .....	40
4.2	Boeing 757-200 Class Aircraft .....	40
4.3	Airbus 330-200 Class Aircraft.....	44
4.4	Model Validation.....	49
<b>5</b>	<b>Incorporation of HLFC System into Aircraft Models.....</b>	<b>56</b>
5.1	Introduction .....	56
5.2	Design Threshold Height in Climb.....	56
5.3	Correction Factors for HLFC.....	59
<b>6</b>	<b>Sensitivity Analysis .....</b>	<b>63</b>
6.1	Introduction .....	63
6.2	Methodology.....	63
6.3	Results of Sensitivity Studies on Trip Fuel .....	65
6.4	Theoretical Evaluation of Trip Fuel Sensitivity.....	68
<b>7</b>	<b>HLFC System Installation .....</b>	<b>74</b>
7.1	Introduction .....	74
7.2	HLFC System Design.....	74
7.3	Drag Reduction.....	75
7.4	SFC Increase Due to Suction System .....	81
7.5	Mass of HLFC System .....	92
<b>8</b>	<b>Ice Clouds .....</b>	<b>96</b>
8.1	Introduction .....	96
8.2	Transition due to Cirrus Clouds.....	96
8.3	Cloud Climatology .....	99
8.4	Fuel Planning and Weather forecasts.....	105
<b>9</b>	<b>Insect Contamination .....</b>	<b>109</b>
9.1	Introduction .....	109
9.2	Impact on Laminar Flow of Insect Contamination .....	109
9.3	Insect Environment and Distributions .....	112
9.4	Concepts for Contamination Mitigation .....	116
9.5	Krüger Flap / Shield .....	118
9.6	Liquid / Foam Systems .....	119
<b>10</b>	<b>Mechanical Failure, Damage and Durability .....</b>	<b>124</b>
10.1	Introduction .....	124
10.2	HLFC System (Mechanical) Failure.....	124
10.3	Damage to the Perforated Surface .....	128



10.4 Durability of the Perforated Surface .....	130
<b>11 Fuel Savings .....</b>	<b>136</b>
11.1 Introduction .....	136
11.2 Impact of Range on Potential Fuel Savings .....	136
11.3 Weather Forecasting and Optimised Fuel Planning .....	137
11.4 Contingency Fuel and Flight Planning .....	140
<b>12 Discussion .....</b>	<b>144</b>
12.1 State-of-the-art .....	144
12.2 HLFC Performance Models .....	145
12.3 Re-sizing Potential .....	145
12.4 Sensitivity Studies .....	146
12.5 HLFC System Installation .....	147
12.6 Cirrus Clouds and Fuel Savings .....	148
12.7 Insect Contamination .....	151
12.8 Mechanical Failure, Damage and Durability .....	151
<b>13 Conclusions .....</b>	<b>153</b>
<b>References .....</b>	<b>154</b>

## LIST OF APPENDICES

<b>A</b>	<b>Environmental Impact</b>
<b>B</b>	<b>HLFC Technology</b>
<b>C</b>	<b>Overview of Major LFC and HLFC Studies and Flight Test Campaigns</b>
<b>D</b>	<b>Fuel Planning and Payload-range</b>
<b>E</b>	<b>Aircraft Performance Theory</b>
<b>F</b>	<b>B757-200 class Aircraft Data</b>
<b>G</b>	<b>A330-200 class Aircraft Data</b>
<b>H</b>	<b>Performance Programs</b>
<b>I</b>	<b>HLFC Sensitivity Studies</b>
<b>J</b>	<b>HLFC System Installation</b>
<b>K</b>	<b>Cloud Encounters</b>
<b>L</b>	<b>Insect Contamination</b>
<b>M</b>	<b>Mechanical Failure, Damage and Durability Aspects of HLFC Systems and Suction Surfaces</b>
<b>N</b>	<b>Nomenclature, Definitions and Glossary</b>

## LIST OF FIGURES

	<b>Page</b>
Fig. 1-1 Aircraft fuel burn (redrawn after Birch, 2000)	6
Fig. 1-2 Aerodynamic efficiency improvement (redrawn after Schneider, 2000)	6
Fig. 1-3 Drag breakdown of typical transport aircraft (redrawn after Marec, 2000)	9
Fig. 1-4 Analysis model	12
Fig. 2-1 Pressure distribution on the upper surface of a NLF aerofoil, LFC aerofoil and HLFC aerofoil (redrawn after Joslin, 1998a)	16
Fig. 2-2 Boundaries of NLF and HLF (redrawn after Schrauf, 2001)	17
Fig. 2-3 Sketch illustrating HLFC system installation on wing, empennage and nacelle	19
Fig. 3-1 Flight profile for fuel planning of HLFC aircraft	29
Fig. 3-2 Flowchart of calculations for mode 1 "Weight"	34
Fig. 3-3 Flowchart of calculations for mode 2 "Range"	35
Fig. 3-4 Flowchart of calculations for mode 3 "Fuel"	36
Fig. 4-1 Drag polars used for B757-200 class aircraft	41
Fig. 4-2 SFC at 35000ft for B757-200 class aircraft	43
Fig. 4-3 Process adopted for establishing the database for the A330-200 class aircraft	44
Fig. 4-4 Estimated drag polars for A330-200 class aircraft	45
Fig. 4-5 Sketch illustrating actual and modelled Corrected fuel flow and SFC data	47
Fig. 4-6 Estimated corrected fuel flow at 35000ft for A330-200 class aircraft	48
Fig. 4-7 Estimated specific fuel consumption at 35000ft for A330-200 class aircraft	48
Fig. 4-8 Payload-range chart for B757-200 class aircraft MTOW 115670kg (255000lb)	53
Fig. 4-9 Payload-range chart for A330-200 class aircraft MTOW 233000kg (513650lb)	55
Fig. 5-1 Fuel consumed in climb to FL 350 for B757-200 class aircraft	57
Fig. 5-2 Relative pump power versus height for: (a) HYLDA nacelle (after Möller, 2001); (b) ALTTA A320 fin design (after Horstmann et al., 2002) and (c) Generic nacelle (analysed by the author)	58
Fig. 5-3 Influence of flight level on laminar flow extent for ALTTA fin	58
Fig. 5-4 HLFC corrections to basic performance program	60
Fig. 5-5 Drag and lift versus weight during cruise for B757-200 class aircraft	61
Fig. 6-1 Payload-range graph indicating points of interest	64
Fig. 6-2 Change in trip fuel due to changes in OEW, SFC & drag:- Case 1A	66
Fig. 6-3 Change in trip fuel due to changes in OEW, SFC & drag:- Case 1B	66
Fig. 6-4 Change in trip fuel due to changes in OEW, SFC & drag:- Case 2A	67
Fig. 6-5 Change in trip fuel due to changes in OEW, SFC & drag:- Case 2B	67
Fig. 7-1 HLFC system design process	75
Fig. 7-2 Drag approximation (based on ESDU 66031, 1995)	76
Fig. 7-3 $C_D$ versus $C_L^2$ for B7G7	78
Fig. 7-4 Estimated planform areas of suction panels for B757-200 class aircraft	84
Fig. 7-5 Estimated planform areas of suction panels for A330-200 class aircraft	85
Fig. 7-6 Schematic of proposed power generation for suction system	88
Fig. 7-7 SFC penalty per 100kW shaft power off-take for RB211-535E4 class engine (conditions: bleed air 0.25kg/s, datum power off-take 100kW)	90
Fig. 7-8 SFC penalty per 100kW shaft power off-take for Trent 772 class engine (conditions: bleed off-take 1.13 kg/s, datum power off-take 200kW)	90
Fig. 7-9 Principal dimensions and layout of HLFC system in right hand HTP of B757-200 class aircraft (established to estimate pump power and system mass)	95
Fig. 8-1 Hall criteria for X-21 at 40000ft, Mach 0.75 (redrawn after Davis et al., 1987)	98
Fig. 8-2 Correlation of cloud encounter with laminar flow for the Jetstar based on results from Davis et al. (1987). (Data reproduced as Table K-1, Appendix K.)	99
Fig. 8-3 Definitions for route data analysis of time in cloud	102
Fig. 8-4 Average time-in-cloud (based on data from Jasperson et al., 1984a)	103
Fig. 9-1 Loss of laminar flow resulting from insect impact on wing of B757-200 class aircraft	110
Fig. 9-2 Scanning Electron Microscope (SEM) images of insect impact tests on a perforated titanium plate - tested at the University of Limerick (after O'Donoghue, 2001)	111
Fig. 9-3 Insect vertical distribution data (redrawn after Croom and Holmes, 1985)	113



Fig. 9-4	<i>Number of insects on wing leading edges on eight aircraft, as observed at Schiphol Airport during 1988 (redrawn after Elsenaar and Haasnoot, 1992)</i>	115
Fig. 9-5	<i>HYLTEC SAAB 2000 flight aircraft, showing test specimens and their location</i>	116
Fig. 9-6	<i>Krüger shield on Jetstar Douglas test article (from Fischer et al., 1983)</i>	119
Fig. 10-1	<i>Schematic of HLFC control system architecture for HTP of B757-200 class aircraft (conceptual design devised to estimate system mass and reliability)</i>	126
Fig. 10-2	<i>Rain erosion rig, built by AS&amp;T (Young et al., 2001)</i>	131
Fig. 10-3	<i>SEM images showing rain erosion on Nd-YAG perforated carbon fibre epoxy specimens (Young et al., 2001)</i>	132
Fig. 10-4	<i>SEM images of laser drilled holes (diameter ~ 80µm) in aluminium alloy, following salt spray trials. Note cracking around hole edge (Young et al., 2001)</i>	132
Fig. 10-5	<i>(a) Test panels installed in holder (b) Detail showing normal and reverse taper</i>	134
Fig. 11-1	<i>Ratio of cruise fuel to block fuel and cruise plus climb fuel (above 20000 ft) for varying range</i>	137
Fig. 11-2	<i>Change in trip fuel compared to turbulent baseline aircraft for a given range</i>	139
Fig. 11-3	<i>B757-200 class aircraft: Fuel on landing at alternative airport versus loss of laminar flow, based on fuel planning that assumed 7% TIC</i>	142
Fig. 11-4	<i>B757-200 class aircraft: Fuel on landing at alternative airport versus loss of laminar flow, based on fuel planning that assumed 21% TIC</i>	142
Fig. 11-5	<i>A330-200 class aircraft: Fuel on landing at alternative airport versus loss of laminar flow, based on fuel planning that assumed 7% TIC</i>	143
Fig. 11-6	<i>A330-200 class aircraft: Fuel on landing at alternative airport versus loss of laminar flow, based on fuel planning that assumed 21% TIC</i>	143

## LIST OF TABLES

	<i>Page</i>
<i>Table 1-1 Estimated fuel efficiency improvements; baseline 1997 (IPCC, 1999)</i>	7
<i>Table 1-2 Reduction potential in aircraft fuel burn over a 20 year period</i>	8
<i>Table 1-3 Events that will impact fuel usage on HLFC aircraft</i>	11
<i>Table 3-1 Program modes of operation</i>	27
<i>Table 3-2 General program requirements</i>	27
<i>Table 3-3 Weight breakdown for program operation</i>	32
<i>Table 3-4 Functions of the individual sheets of the program</i>	37
<i>Table 3-5 Structure of master computing table</i>	38
<i>Table 4-1 Leading parameters for selected baseline (reference) aircraft</i>	40
<i>Table 4-2 Comparison of climb results from brake release to 35000ft</i>	42
<i>Table 4-3 B757-200 class aircraft mission results (program run in Range mode)</i>	52
<i>Table 4-4 MTOW and payload for the A330-200 (Airbus, 2000a)</i>	53
<i>Table 4-5 A330-200 class aircraft results (program run in Weight mode)</i>	54
<i>Table 5-1 Fuel flow correction factors</i>	62
<i>Table 6-1 Matrix of sensitivity studies undertaken</i>	64
<i>Table 6-2 Ground rules for sensitivity studies for B757-200 class aircraft</i>	65
<i>Table 6-3 Ground rules for sensitivity studies for A330-200 class aircraft</i>	65
<i>Table 6-4 Results of "spot check" to assess change in trip fuel</i>	68
<i>Table 6-5 Data for reference condition</i>	70
<i>Table 6-6 Summary of evaluations performed</i>	70
<i>Table 6-7 Impact of small change to end-of-cruise mass (<math>m_2</math>)</i>	72
<i>Table 6-8 Impact of small change to SFC</i>	72
<i>Table 6-9 Impact of small change to L/D</i>	73
<i>Table 7-1 Drag reduction for HLFC B757 (Boeing, 1982)</i>	79
<i>Table 7-2 Profile drag reduction for B757-200 class HLFC aircraft</i>	80
<i>Table 7-3 Profile drag reduction for A330-class project aircraft analysed by Wilson (1997)</i>	81
<i>Table 7-4 Suction system power requirement</i>	82
<i>Table 7-5 Estimated suction panel areas</i>	83
<i>Table 7-6 Suction system power requirement for design cruise height</i>	88
<i>Table 7-7 SFC change for shaft power off-take</i>	91
<i>Table 7-8 Estimate of SFC penalty for HLFC systems in B757-200 and A330-200 class aircraft</i>	91
<i>Table 7-9 Mass of HLFC system</i>	93
<i>Table 7-10 Mass of HLFC system (based on scaled values for HTP case study)</i>	94
<i>Table 8-1 Cloud definitions used for Jetstar flights (Davis et al., 1987)</i>	98
<i>Table 8-2 Summary of GASP cloud data (from Jaspersen et al., 1984a; 1984b)</i>	102
<i>Table 8-3 Influence of change in contingency fuel on trip fuel (Range: 2350nm)</i>	106
<i>Table 9-1 Literature review of major experiments evaluating liquid anti-contamination systems</i>	120
<i>Table 10-1 Estimate of the probability of failure of the HLFC system</i>	128
<i>Table 10-2 Rain erosion test results (Young et al., 2001)</i>	131
<i>Table 10-3 Materials evaluated</i>	134
<i>Table 10-4 Summary of important conclusions</i>	135
<i>Table 11-1 Matrix for studies - Optimised fuel planning</i>	138
<i>Table 11-2 Matrix for studies - Contingency fuel</i>	140



Blank page

# 1 INTRODUCTION

## 1.1 THE POTENTIAL OF HYBRID LAMINAR FLOW CONTROL

A completely laminar wing of a jet transport aircraft would have ~10% of the drag of a turbulent wing (Joslin, 1998a). This 90% reduction in the profile drag of the wing offers the potential for enormous economic and environmental benefit. The concept of Laminar Flow Control (LFC) relies on a relatively small amount of air being sucked through a perforated wing skin to suppress boundary layer instabilities. A Hybrid Laminar Flow Control (HLFC) wing has a forward section of LFC and an aft section that maintains the boundary layer in a laminar state by means of a favourable pressure gradient.

The successful development of a HLFC wing requires considerable research effort, covering many different engineering disciplines. The challenges faced by researchers include: the aerodynamic problem of modelling the behaviour of the boundary layer under various operating conditions and the design of the perforated wing structure, suction system, de-icing / anti-contamination systems and monitoring system. Although much of the early research effort focused on aerodynamic issues, in recent years a multi-disciplinary approach, covering the broad disciplines of aerodynamics, structures (and materials) and systems (including propulsion) has been needed to further develop the complete HLFC system.

Numerical techniques to predict laminar to turbulent transition have been progressively refined in recent years. Nevertheless, computational techniques still need to be bench-marked and this is normally achieved by wind tunnel testing. But in the particular case of HLFC, tunnel tests can produce overly pessimistic results due to higher turbulence levels. The extrapolation of tunnel results to flight conditions – to establish design parameters such as the laminar flow transition location, the optimum suction velocity and the critical sizes of roughness elements which will cause transition – has proven to be a very difficult task. As a consequence flight tests are unavoidable. The high costs associated with experimental flight testing are difficult to justify for any manufacturer; particularly when all elements of the problem are not well understood and the benefits are as yet not fully quantified. Technological progress hinges on a HLFC wing flight test campaign to validate the concepts and develop operational experience. However, such programmes are very expensive.

The potential rewards of laminar flow are considerable. Dziomba (1993) wrote, “any airframe manufacturer capable of putting this puzzle together and guaranteeing to the airlines reliable benefits through laminar flow under operational conditions will enjoy a significant competitive advantage within the future world aircraft market”. The laminar flow aircraft would have a greater range, lower direct operating cost, and lower atmospheric emissions than current turbulent designs. Schrauf (2001) of Airbus estimates that a 16% reduction in the total aircraft drag is possible, using HLFC on a long-range aircraft in the class of the A340. This would come from laminar flow on the



upper wing surface (~12%), empennage (~3%) and nacelles (~1%). These savings are significantly less than the theoretical drag reduction of 90% mentioned above, partly because the fuselage and lower wing surface are not included in the estimate, and partly because transport aircraft wings cannot be completely laminarised by this technique.

The successful implementation of HLFC is dependent on practical solutions being found for a number of technical and operational problems. The operational issues that have been explored by the author concern the consequences of potential failures of the HLFC system. Operational factors that may limit laminar flow, include: insect contamination on the leading edges, rain, ice particle impact during flight through cirrus clouds, dust storms and mechanical system failure. The problem is that the standard en route contingency fuel, generally taken to be 3 - 5% of the trip fuel as an operational reserve, is inadequate to cover the increase in fuel burn due to a total loss of laminar flow for the entire flight. The incidence rate of such events is thus of importance in establishing the benefits of HLFC technology. It will be demonstrated that the consequences of such failures depend significantly on the fuel planning approach adopted for HLFC aircraft operations. The requirements for current aircraft operations and the implications of such failures on the fuel savings potential of HLFC aircraft over comparable turbulent aircraft have been investigated.

## **1.2 FINANCIAL IMPACT OF DRAG REDUCTION**

### **1.2.1 Fuel saving**

Drag reduction due to HLFC lowers the aircraft's fuel consumption, which reduces the operating costs. The fuel saving (expressed as a percentage) can be expected to be lower than the percentage drag reduction; the actual amount depending on the mission range and operational conditions. Based on the 16% drag reduction mentioned above, it is estimated that the net fuel savings would be of the order of 10% for a long-range mission (see Chapter 11). The reasons why the block fuel<sup>1</sup> cannot be directly factored by the drag reduction percentage to give the fuel saving, are as follows:

- (1) The benefit of the drag reduction is eroded by an increase in aircraft system weight and the need to power the suction system, which will increase the power extracted from the engines.
- (2) The operation of the HLFC system cannot be guaranteed 100% of the time, due to the loss of laminar flow caused by flying through cirrus clouds and from insect impacts. Furthermore, its use is likely to be restricted to operations above ~20000ft. The block fuel elements of engine start, taxi, takeoff, initial climb and descent, will not be reduced.

---

<sup>1</sup> Block fuel: The total fuel used from engine start-up to shut-down.

- (3) The rate of fuel consumption at any point during the cruise is directly proportional to the weight of the aircraft at that time. (The rate of fuel burn is also proportional to the Specific Fuel Consumption (SFC) and inversely proportional to the aircraft's lift-to-drag ratio.) This means that for short cruise segments, the percentage fuel savings in the cruise would approach the percent drag reduction, but as the cruise range increases, so the percentage savings will drop.

### **1.2.2 Impact on Direct Operating Cost**

Fuel is a significant portion of an airline's Direct Operating Cost (DOC). For a long-range aeroplane this fraction is ~22%, according to Marec (2000). Using this factor of 22%, a 10% reduction in trip fuel would thus translate to a 2.2% reduction in DOC. Small changes in DOC however, can have a large impact on the net profit (the difference between net revenue and net costs) of an airline. It is obvious that when the parameter of interest is the difference between two large numbers, relatively small changes to these numbers will have a large influence on the result. To illustrate the gearing effect between fuel savings and net profit, it is assumed that: (1) A margin of 5% exists between net revenue and net costs for the airline (a value quoted by Schneider, 2000); (2) The Indirect Operating Cost (IOC) is approximately equal in magnitude to the DOC (Raymer, 1989). The 2.2% reduction in DOC would then imply a 21% increase in net profit.

Not included in the simple scenario outlined here, but relevant to this technology, is the potential increase in the aeroplane's price and the increased maintenance costs. These factors are of concern to potential clients of this technology, who will be required to weigh up the advantages of reduced fuel costs against the higher purchase price and maintenance costs. Taking a long-term view, it would be expected that as the Earth's fossil fuel stores become depleted, the price of fuel would increase, thus accounting for a larger portion of an airline's DOC. This would enhance the attractiveness of fuel reduction technologies.

## **1.3 ENVIRONMENTAL IMPACT OF DRAG REDUCTION**

### **1.3.1 Pollution**

Turbine-powered aircraft burn kerosene, and will continue doing so for the foreseeable future, because there are no alternative fuels that are as energy-intensive, easily stored and safe to house in a confined space (Moxon, 1999). From a global perspective, there are two environmental issues that require consideration as a consequence – fuel reserves and engine emissions. The reduction in the consumption of a limited natural resource – fossil fuel – is itself a laudable goal. Associated with the reduction in fuel burn is a reduction in the atmospheric pollution caused by aircraft operations.



The jet aircraft is a relative newcomer to the “club” responsible for producing gases hazardous to the environment, considering that there has been a steady build-up of CO<sub>2</sub> (carbon dioxide) since the start of the industrial age. By any measure, aviation is a small “player”, consuming only 2 - 3% of the total of fossil fuels consumed world-wide each year, according to the report *Aviation and the Global Atmosphere*<sup>2</sup> (IPCC, 1999). However, aircraft are unique in one respect. They operate in the upper troposphere and lower stratosphere, where important weather processes occur and where significant amounts of ozone (an important greenhouse gas) exist. For this reason their impact is particularly difficult to quantify. Aircraft affect the atmosphere by introducing gases and particles into it and by forming contrails. The emissions include greenhouse gases such as CO<sub>2</sub> and water, as well as chemically active gases, such as NO<sub>x</sub> (nitrogen oxides), which alter the naturally occurring greenhouse gases. The delicate balance between the amount of heat entering and leaving the atmosphere – a process that is critical to the earth’s climate – is affected by these pollutants, and researchers are just beginning to quantify their long-term effects. (Supplementary details on the dominant pollutants are given in Appendix A.)

### 1.3.2 Fuel burn

CO<sub>2</sub> and water are estimated to contribute about 35% of aviation’s impact on climate change (IPCC, 1999). A reduction in fuel burn will result in a proportional decrease in these elements, resulting in a direct reduction in environmental change. The remaining 65% is attributed mainly to the effects of NO<sub>x</sub> and contrails. For these factors, the causal relationship is more complex and the environmental impact significantly depends on other issues, like the prevailing climate, season, flight altitude and geographical location (IPCC, 1999). Fuel burn is thus not a precise measure of the potential for aircraft to affect climatic changes. Notwithstanding this limitation, fuel burn per passenger-km remains a good indicator of the relative environmental cost of alternative technologies.

According to the IPCC report (1999), global passenger air travel, as measured in terms of revenue passenger-km, has grown since 1960 at nearly 9% per annum. By 1997 it slowed to about 5% per year, a rate which was projected would continue until at least 2015. The total aviation fuel consumption was estimated to increase by ~3% per year over the same period; the difference, largely due to improved aircraft efficiencies. Air traffic growth in the immediate aftermath of the terrorist attack on the US in September 2001 – coupled with the general downturn in the world economy – has been negative. However, long term forecast growth rates are unlikely to be significantly changed due to these events.

---

<sup>2</sup> A study carried out at the request of the ICAO (International Civil Aviation Organisation) by the Intergovernmental Panel on Climate Change (IPCC) integrating much of the world-wide research that has been conducted to assess the effects of aircraft operations on climate and atmospheric ozone.



Hybrid Laminar Flow Control is one of a number of exciting techniques under study at present, which has the potential to produce a significant reduction in aircraft drag. The impact of this is illustrated by Schneider (2000), who concluded that a 1% reduction in aerodynamic drag for an A340 aircraft operating in the long-range mode will result in a saving of about 0.4 million litres of fuel per year, per aircraft, which would "save" the environment roughly 5000kg of noxious emissions.

### 1.3.3 Regulatory standards and measures

Existing aircraft pollution standards are mainly aimed at improving air quality around airports and there are no specific standards applying to emissions in the cruise. The production of CO (carbon monoxide), hydrocarbons, NO<sub>x</sub> and smoke in the landing / takeoff (LTO) cycle is restricted under existing engine regulations. The most recent agreement, the CAEP/4 standard, was ratified by ICAO (International Civil Aviation Organisation) members in 1998 (Duthie, 2001). The only international agreement that could potentially affect aviation emissions in cruise is the Kyoto Protocol<sup>3</sup>, which was aimed at stabilising greenhouse gas concentrations at a perceived level that would prevent dangerous long-term damage to the world's climatic system. However, the Protocol was not ratified by the US, and its use as a framework for world-wide aviation environmental policy is now considered unlikely.

## 1.4 TECHNOLOGIES TO IMPROVE EFFICIENCY AND REDUCE EMISSIONS

### 1.4.1 Aircraft fuel efficiency gains

Significant improvements in aircraft fuel efficiencies have been achieved since the start of the jet transport era, inaugurated by the de Havilland Comet in 1952. Condit (1996) of Boeing, observed that historically these improvements have averaged 1 - 2% per year for new production aircraft. Modern subsonic transonic aircraft are ~70% more fuel efficient per passenger-km than early jet aircraft (IPCC, 1999). The data in Fig. 1-1, reproduced from Birch (2000), supports this statement.

Szodruch (2001) reports that for Airbus Industrie's products, the ratio of trip fuel / distance has been reduced by ~37% over the preceding twenty years. These advances have been achieved through new engine, airframe and systems technologies. Over a 20 year period, the aerodynamic efficiency of new Airbus Industrie designs, as measured by the parameter  $(ML/D)_{max}$ , has increased by more than 30% compared to the A300, according to Schneider (2000). (See Fig. 1-2.)

---

<sup>3</sup> The Kyoto Protocol was adopted by the United Nations Framework Convention on Climate Change (UNFCCC) in December 1997 and requires Annex 1 (industrialised) countries to reduce their collective emissions of greenhouse gases by ~ 5% by the period 2008-2012, compared to 1990 levels (IPCC, 1999).



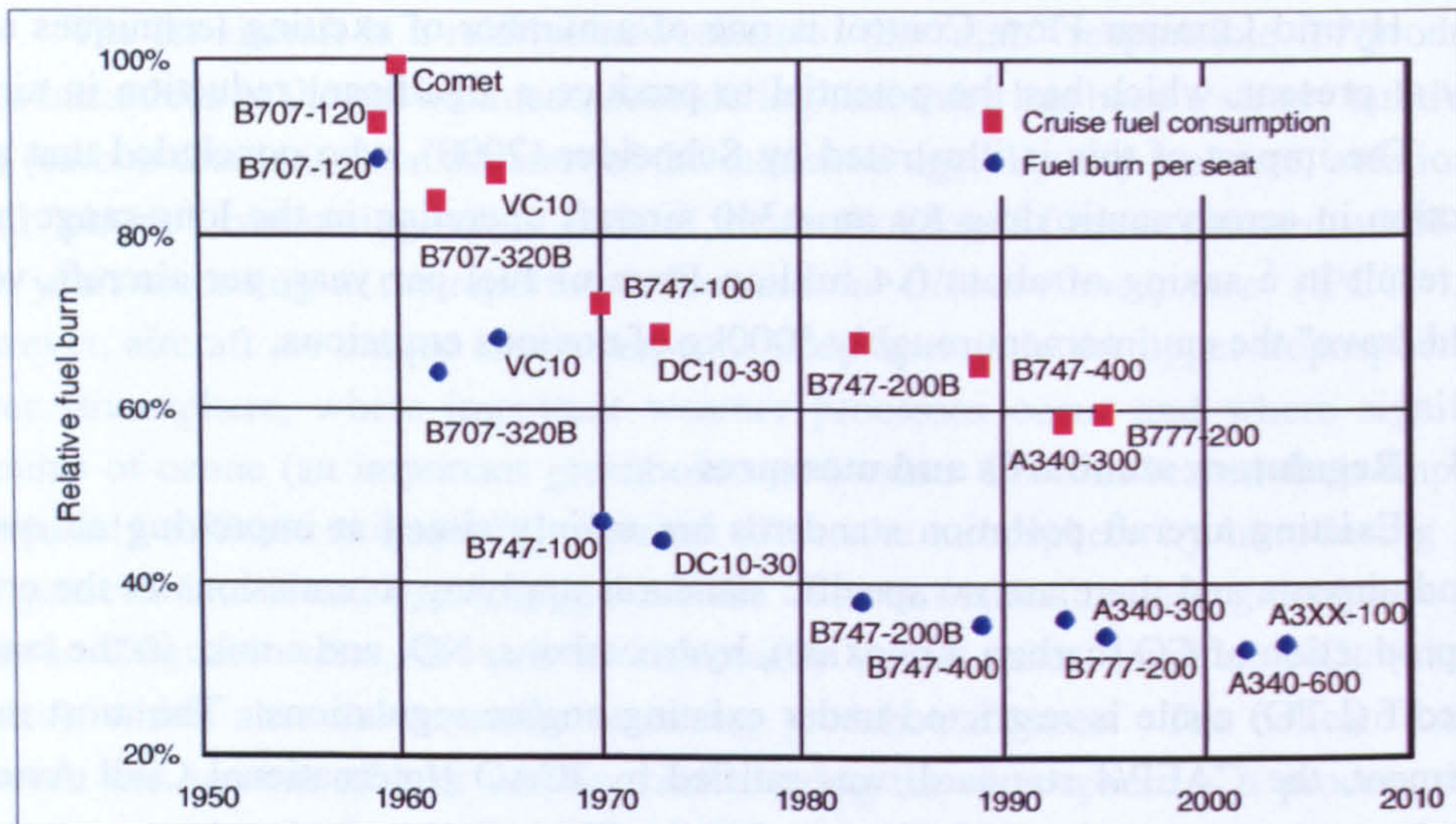


Fig. 1-1 Aircraft fuel burn (redrawn after Birch, 2000)

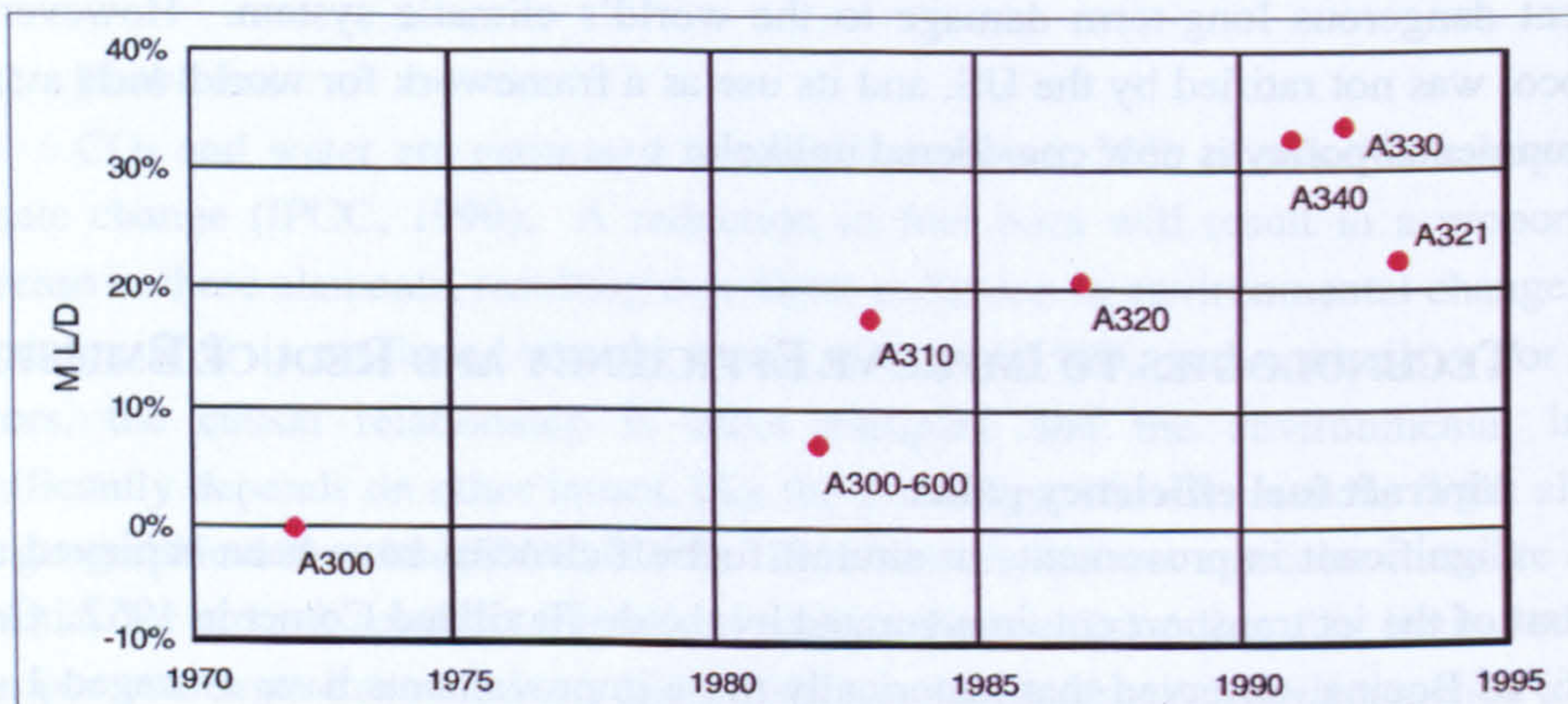


Fig. 1-2 Aerodynamic efficiency improvement (redrawn after Schneider, 2000)

Published in Jan. 2001, the report<sup>4</sup> *European Aeronautics: A vision for 2020*, which was prepared for the European Commission, sets as goals an ambitious 50% cut in fuel consumption and an 80% cut in NO<sub>x</sub> emissions for new aircraft. Set as an aspirational target, it was intended that this document would focus European research efforts and set a framework for the generation of strategic research agendas.

A number of researchers have made projections of future technological improvements. These vary from the pessimistic to the overly optimistic. One example is contained in the IPCC (1999) report. The estimated airframe, engine and total aircraft

<sup>4</sup> *European Aeronautics: A vision for 2020*:- a report prepared by a senior "group of personalities" for the European Commission, to establish a European aeronautics research agenda (CEC, 2001).



fuel efficiency improvements from the 1950s to 1997, as well as near term (to 2015) and longer term (to 2050) projections, are summarised in Table 1-1.

**Table 1-1** *Estimated fuel efficiency improvements; baseline 1997 (IPCC, 1999)*

Time period	Airframe	Propulsion	Total aircraft
1950 - 1997	30%	40%	70%
1997 - 2015	10%	10%	20%
2015 - 2050	25%	20%	40 - 50%

Gerhards and Szodrich (2000) of Airbus were more optimistic and stated that the potential exists for a greater than 50% net reduction in trip fuel / distance, over a 20 year time frame (see Table 1-2). This assertion was repeated by Schneider (2000) at the same forum in June 2000. Their forecast is roughly in line with the results of a study into the potential impact of changes in technology, on the development of air transport in the UK, conducted by Arthur D. Little Ltd in 2000. Forecasts contained in their confidential report (DETR/71861/01rep.doc, 2000) were reproduced by the *Greener by Design*<sup>5</sup> Technology Sub-Group (2001). Arthur D. Little Ltd. maintained that there could be a gain in fuel efficiency of 15 - 25% by 2005, of 25 - 40% by 2015, and of 50 - 70% by 2030. The *Greener by Design* Technology Sub-Group did not consider the aforementioned forecasts to be realistic. The Sub-Group "has come to a more conservative view than the IPCC of the reductions in fuel burn that are likely to be achievable in the long term if only economic factors shape the evolution of the dominant design". The report continues to explain that the dominant configuration (with conventional fuselage, low swept wings and engines podded under the wings) is a highly evolved design, which has limited scope for further improvement. It notes that of the 70% improvement in fuel efficiency over the 40 year interval, 53% came in the first 10 years.

The "law of diminishing returns" – in which further improvements become harder and harder to achieve with time – may well be validated in this situation, as new designs approach limits set by the laws of physics, or by practical constraints. An example of the latter is provided by Brown (1997) of Airbus, who indicated that the aspect ratio of the A380 (termed A3XX at the time of reporting) was restricted – impairing its potential aerodynamic efficiency – because of the need to comply with the ICAO Standard F for airport design (which effectively limits the wing span to 80m, to comply with existing gate sizes).

Birch (2000) reports that significant SFC improvements have been made over the past 40 years, through engine improvements in Thermal Efficiency (which depends significantly on the Turbine Inlet Temperature and Overall Pressure Ratio) and Propulsive Efficiency (which largely depends on the Bypass Ratio). The technological

<sup>5</sup> Greener by Design: Working Group established under the auspices of the UK Department of Trade and Industry in 2000, with participation by the Royal Aeronautical Society and the Society of British Aerospace Companies, to address environmental issues relating to the aviation industry.



progress is likely to slow as materials limitations and physical constraints in cooling technologies are approached. Birch (2000) predicts that for the conventional turbofan engine, the current improvement rate in efficiency of ~1% per year, is likely to reduce to ~0.5% per year by 2020.

**Table 1-2** *Reduction potential in aircraft fuel burn over a 20 year period (Gerhards and Szodruch, 2000)*

Contribution due to:	Notes	Reduction
<i>Lift dependent drag</i>	Multifunctional control surfaces, smart wing, higher aspect ratio, wingtip devices, vortex control.	~11%
<i>Friction drag</i>	Shock-boundary layer control, laminar flow, turbulence control.	~22%
<i>SFC improvements</i>	Improved engine technology.	~22%
<i>Weight reduction</i>	Materials and structures technologies applied to airframe and engine, and improved systems.	~8%
<i>Configuration</i>	Advanced or new configurations.	~4%
<b>Total</b>		<b>~67%</b>

#### 1.4.2 Airframe improvements

The airframe improvements are expected to come from many different areas. The relative weight of airframe structures will continue to reduce through the increased use of composite structures and low density materials, like aluminium-lithium and GLARE. Techniques in structural optimisation and enhanced manufacturing processes will allow further refinements in weight reduction.

Aircraft systems also offer the opportunity for weight reduction. In-flight entertainment system weight is likely to be reduced by new computer and communications technologies. Developments of electric systems replacing pneumatic systems, which rely on engine bleed air, have the potential to save fuel. Active pitch stability augmentation, wing load alleviation and variable camber devices (described by Mertens, 1999; 2000; for example) are some of the advanced airframe technologies which are likely to result in increased efficiency and lower fuel burn.

The reduction of drag through laminar flow is seen as one of the most promising of the technologies under investigation. This has enormous potential, as the friction drag can contribute almost 50% of the total drag on a modern transport aircraft, according to Thibert *et al.*, (1990) and Marec (2000), as shown in Fig. 1-3. Other drag reduction techniques such as riblets (Walsh, 1980; La Roche, 1998; for example), active shock control and adaptive wings (Stanewsky *et al.*, 1997; Stanewsky and Rosemann, 2000; for example) offer the potential for further fuel savings. Kumar and Hefner (2000) of NASA wrote "recent advances in materials, electronics, miniaturised sensors and actuators and increased understanding of three-dimensional unsteady flow physics have opened the door to new innovations in actively controlling macro- and micro-scale flow characteristics". They suggest that "this is truly a growth area in aerodynamics that



will allow for step increases in aerodynamic performance while, at the same time, dramatically reduce noise and emissions".

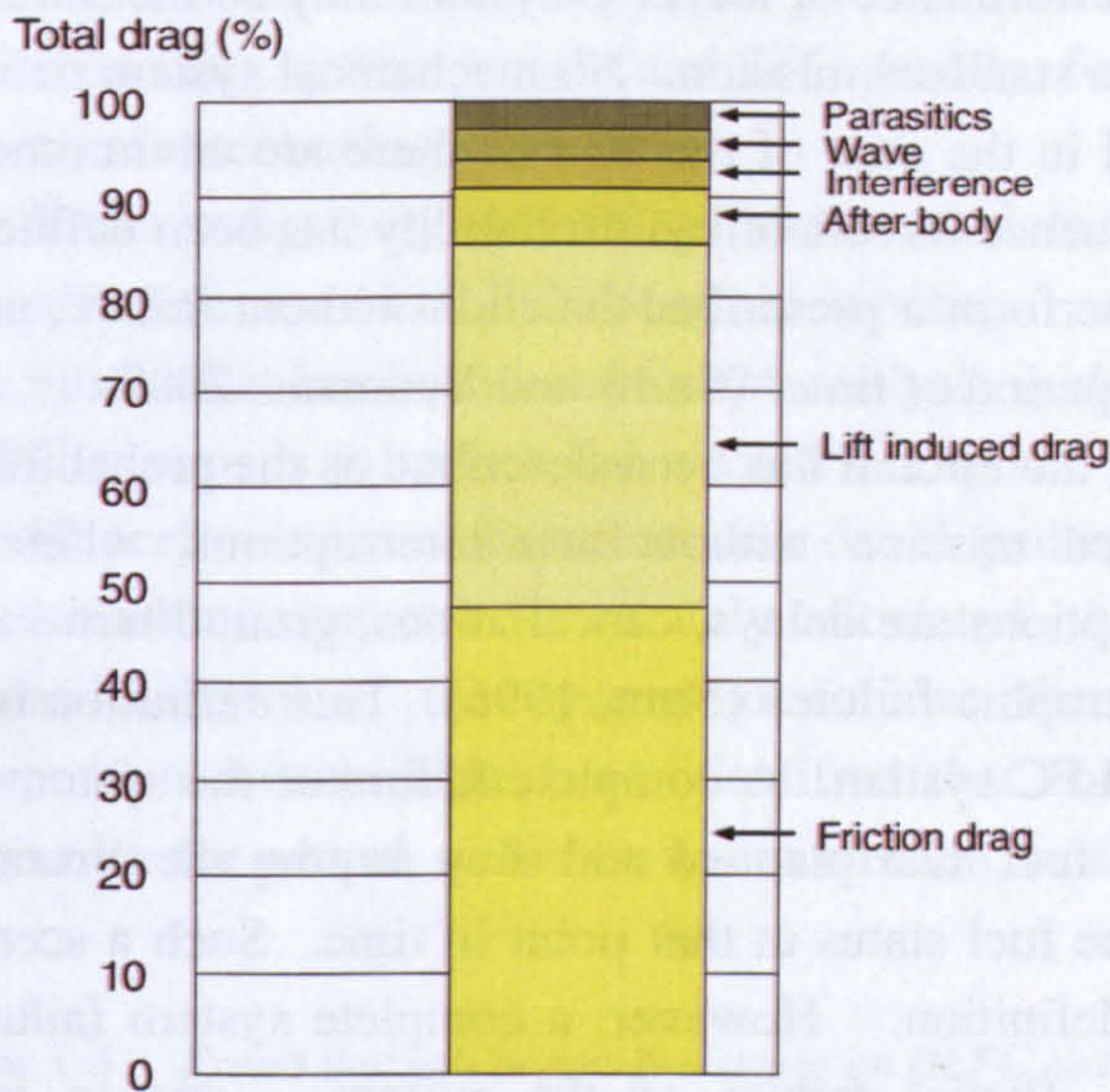


**Fig. 1-3** Drag breakdown of typical transport aircraft (redrawn after Marec, 2000)

### 1.4.3 Engine technologies

Significant efficiency gains have been achieved through jet engine improvements, which have seen SFC values cut nearly in half (Brasseur *et al.*, 1998). The high bypass ratio engines introduced into airline service in the 1970s and 1980s had much improved efficiencies and reduced CO<sub>2</sub> and HC emissions. Improved efficiencies achieved by increased engine Overall Pressure Ratio and higher combustor inlet temperatures however, result in higher NO<sub>x</sub> levels at high power settings (Birch, 2000). A delicate balance has to be met by the manufacturer to reduce both NO<sub>x</sub> emission (through improved combustor design) and to simultaneously reduce SFC. Research goals to achieve NO<sub>x</sub> emission levels 50% below current standards in 5 to 10 years, were mentioned in the IPCC report (1999).

### 1.4.4 Aircraft operations

Improvements in Air Traffic Management (ATM) and other operational procedures could reduce aviation fuel burn by between 8 and 18% (IPCC, 1999). A quarter of all flights in Europe in 1999 were delayed, according to Pusch (2001); improvements in ATC (Air Traffic Control) capabilities would lead to fewer delays and reduced holding times. Other operational measures to reduce fuel burn include: increased load factors, non-essential on-board weight reduction, reduction in auxiliary power usage and reduced taxi time.



## 1.5 OPERATIONAL EFFECTIVENESS

The effectiveness of an operational system is a function of the performance and the reliability of that system. The performance of a HLFC system may be measured by its ability to reduce the trip fuel for a standard mission. No mechanical system delivers 100% performance indefinitely, and in the case of the HLFC, there are environmental and mechanical factors that will influence its reliability. Reliability has been defined as "the probability that a system will perform a prescribed function without failure, under specified conditions, for a specified period of time" (Snow and Yeomans, 2000).

The operational reliability of the aircraft has been described as the probability of the aircraft completing its intended mission without any interruptions, where for transport aircraft operations, interruptions are delays, cancellations, ground turn-backs, air turn-backs, diversions and catastrophic failures (Nam, 1996). This definition is not particularly useful in assessing a HLFC system. A complete failure of the system will result in the aircraft burning more fuel than planned and may require the aircraft to divert or turn-back depending on the fuel status at that point in time. Such a scenario could be studied using the above definition. However, a complete system failure is only one possible failure mode. Partial failure of the system – due to insect contamination on one part of the wing, for example – will result in the system not delivering the target fuel burn reduction. This may not result in an operational interruption, but would nevertheless be construed as a partial failure. For a HLFC system, the failures may be defined as events that will result in a loss of laminar flow and increased fuel consumption. The factors that would cause this to happen are mechanical (i.e. systems failure or damage) and environmental (where the biggest concerns are insects, ice and rain).

For this study, the definition of Snow and Yeomans (2000) was found to be a convenient framework. The operational effectiveness of the HLFC system has been taken to mean the probability that the system will deliver a target fuel savings, under defined conditions, for a specified portion of the cruise, for a specified duration (i.e. number of flights). A critical element in the assessment of the HLFC system is the anticipated performance of the system. For example, if it is "only" expected that the system be fully functional for 90% of the cruise (and for the remaining 10% the wing will be turbulent) and the operational fuel planning is based on this assumption, then a failure will only be registered when the system is operational for less than 90% of the cruise.

## 1.6 OBJECTIVES AND ANALYSIS MODEL

Three sets of objectives were established for this work.

- (1) To develop computer performance models that are capable of accurately calculating the trip fuel for a given mission specification, and to use these models



to study the impact of HLFC on the trip fuel for user specified inputs, corresponding to alternative HLFC designs.

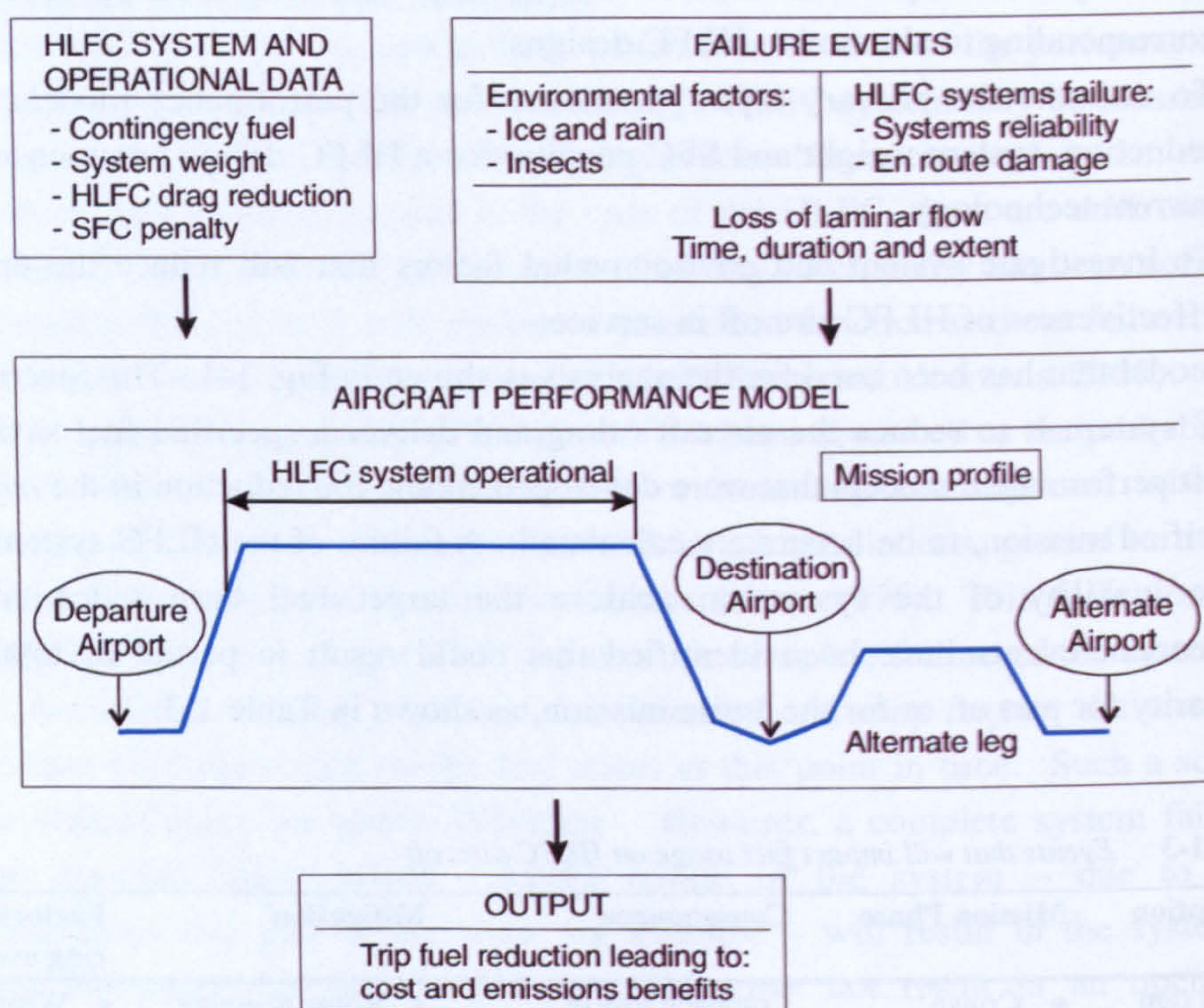
- (2) To estimate the primary input parameters for the performance models, i.e. drag reduction, system weight and SFC penalty, for a HLFC design commensurate with current technology.
- (3) To investigate system and environmental factors that will reduce the operational effectiveness of HLFC aircraft in service.

The model that has been used for the analysis is shown in Fig. 1-4. The function of the HLFC system is to reduce the aircraft's drag and deliver a specified fuel saving. The aircraft performance models that were developed enable the reduction in the *trip fuel* for a specified mission, to be accurately calculated. A failure of the HLFC system is taken as the inability of the system to achieve the target fuel burn reduction. Four independent events have been identified that could result in partial or total loss of laminarity for part of, or for the entire mission, as shown in Table 1-3.

**Table 1-3** *Events that will impact fuel usage on HLFC aircraft*

Description	Mission Phase	Consequence	Mitigation	Factors influencing event
Ice and rain	<ul style="list-style-type: none"> <li>• Cruise</li> <li>• Top of climb</li> </ul>	Complete loss of laminar flow for finite time.	<ul style="list-style-type: none"> <li>• Route planning</li> <li>• Pilot avoidance</li> </ul>	<ul style="list-style-type: none"> <li>• Weather</li> </ul>
Insect contamination	<ul style="list-style-type: none"> <li>• Takeoff</li> <li>• Initial climb</li> </ul>	Partial loss of laminar flow for entire mission.	<ul style="list-style-type: none"> <li>• On-board system</li> <li>• Cleaning by rain and ice</li> </ul>	<ul style="list-style-type: none"> <li>• Weather</li> <li>• Season</li> <li>• Location</li> </ul>
System failure	<ul style="list-style-type: none"> <li>• Takeoff</li> <li>• Climb</li> <li>• Cruise</li> </ul>	Partial or complete loss of laminar flow for remainder of mission.	<ul style="list-style-type: none"> <li>• System design</li> <li>• Maintenance</li> </ul>	<ul style="list-style-type: none"> <li>• System reliability</li> </ul>
Damage to perforated surface (e.g. bird strike)	<ul style="list-style-type: none"> <li>• Takeoff</li> <li>• Climb</li> <li>• Cruise</li> </ul>	Partial or complete loss of laminar flow for remainder of mission.	<ul style="list-style-type: none"> <li>• Route planning</li> <li>• Pilot action</li> <li>• Surface design</li> </ul>	<ul style="list-style-type: none"> <li>• Weather</li> <li>• Component design</li> </ul>





Element	Description	Comment
<b>Aircraft performance model</b>	This element is comprised of computer models that can accurately determine an aircraft trip fuel for user specified parameters of payload and range.	The fuel planning requirements and the performance model is described in Chapter 3. The aircraft data is described in Chapter 4.
<b>HLFC system and operational data</b>	This describes the performance benefits (in terms of drag reduction), the system weight and SFC penalty. The operational issues include the contingency fuel definition, aircraft speeds, etc.	This is presented in Chapters 5 and 7.
<b>Failure events</b>	This element serves to describe the failure events and is divided into two categories – environmental factors (insects, ice and rain) and systems failure / damage.	This is described in Chapters 8 to 10.
<b>Output</b>	The impact of HLFC on trip fuel for the envisaged scenarios is investigated.	Results of the sensitivity studies are presented in Chapters 6. Fuel savings under operational conditions are described in Chapter 11.

Fig. 1-4 Analysis model



## **1.7 THESIS**

### **1.7.1 Acknowledgement**

The research reported in this thesis took place from 1996 to 2002 at the University of Limerick (Limerick, Ireland) and at Cranfield University (Bedford, UK). During this time the author was responsible for the work contracted to the University of Limerick in three HLFC research projects, funded by the CEC (Commission of the European Communities) under the Fourth and Fifth Framework Programmes (see Appendix C). These projects were:

- Project HYLDA (Hybrid Laminar Flow Demonstration on Aircraft); 1996 – 1999.
- Project HYLTEC (Hybrid Laminar Flow Technology); 1998 – 2001.
- Project ALTTA (Application of Hybrid Laminar Flow Technology on Transport Aircraft); 2000 – 2002.

Although the substantive research reported herein took place outside of these programmes, the author derived considerable benefit from his involvement in these projects, as they provided a rich background to the work undertaken. The focus of the CEC research was the characterisation of HLFC suction panels and contamination alleviation / prevention of the laminar flow surfaces and there were certain common research elements. Where appropriate, relevant aspects of the CEC research have been reported herein and in all such cases, the contribution of collaborators has been noted.

### **1.7.2 Thesis structure**

Following the Introduction, an overview of the subject of HLFC is presented in Chapter 2. This is complemented by a more detailed description in Appendix B. Included is a review of boundary layer instabilities, Laminar Flow Control techniques, suction system design and a description of HLFC compatible anti-contamination and de-icing systems. In support of the technical description, a historical overview of the most significant projects undertaken in laminar flow control is presented in Appendix C. The progress made since the first LFC wind tunnel tests were conducted by NACA in 1939 is traced, with important research milestones mentioned. The landmark X-21A tests conducted in the mid-1960s, the Boeing 757 flight tests and the recent CEC sponsored research projects, are described.

Chapter 3 describes the development of a computer program for the evaluation of the trip fuel under standard operating conditions. The regulatory requirements for fuel planning are outlined. The generation of an aircraft performance database, representing aircraft in the class of the Boeing 757-200 and the Airbus 330-200, is described in Chapter 4. Supporting details are to be found in the appendices, i.e. fuel planning (Appendix D), performance theory (Appendix E), aircraft technical data (Appendices F and G) and the computer programs (Appendix H). The incorporation of the HLFC system into the computer program, for the purpose of assessing its impact on the trip fuel of the aircraft under standard conditions, is covered in Chapter 5. This is



followed by sensitivity analyses into the impact of SFC, aircraft mass and drag changes on the trip fuel, which are described in Chapter 6. The design of HLFC systems is a complex multi-disciplinary task. Estimates of the installation implications of this technology for the two aircraft models that were developed, are presented in Chapter 7.

Central to the issue of fuel savings is the laminar flow “failure modes” of cirrus cloud encounter and insect contamination of the leading edges. These two issues are described in Chapters 8 and 9 respectively. Supporting details are presented in Appendix K (cloud encounters) and Appendix L (insect contamination). Chapter 10 covers potential causes of mechanical failure and damage to the HLFC surfaces. Chapter 11 contains the results of the performance studies, in which fuel savings under model operating conditions were calculated.

A listing of nomenclature used and a glossary of technical jargon is included as Appendix N. A single CD containing two computer files: *B757class.123* and *A330class.123*, accompanies the thesis.

### 1.7.3 Units

The units that have been used for the aircraft *performance* calculations are “aviation” / British units. This resulted from the fact that the baseline aerodynamic and engine performance data (described in Appendix F) used to develop the computer models for calculating the mission fuel, were available in these units. The results reported in the main body of the thesis have been converted to SI units. As aircraft operations, by convention, express height in feet and speed in knots, these two measures have been used throughout the thesis. Conversion factors are provided in Table E-3 (Appendix E).

## **2 BACKGROUND: HYBRID LAMINAR FLOW CONTROL**

### **2.1 INTRODUCTION**

The transition from a laminar to turbulent boundary layer is marked by a sudden increase in the thickness of the boundary layer and a significant change in the local flow behaviour. The random variation of velocity and flow direction, within a turbulent boundary layer, is responsible for an order of magnitude increase in skin friction drag, compared to that of laminar flow. Efforts to delay this transition at the leading edge of the wing, empennage or nacelle to 50%, or even further back along the chord, have been the goal of many experiments, dating back to the late 1930s. Viewed by many as the ultimate challenge in aerodynamics, hundreds of theoretical and experimental research projects have been conducted world-wide. Whilst a complete understanding of the problem and the development of practical design solutions have been elusive, considerable technological progress has taken place, as the technology has matured in recent years.

In this chapter a brief overview of the principles of LFC and HLFC are presented. A more detailed review of the technology is included as Appendix B; the mechanisms for boundary layer transition are outlined, followed by a description of the aerodynamic principles, suction system architecture and anti-contamination systems, applicable to HLFC.

### **2.2 LAMINAR FLOW**

#### **2.2.1 Transition**

HLFC is being considered for the wing, horizontal tailplane, fin and engine nacelles of a jet transport aircraft. The flow over three of these surfaces – the wing, horizontal tailplane (HTP) and fin, is a complex 3D flow field, which is significantly influenced by leading edge sweep. The engine nacelle is different as there is essentially no sweep on the nose section. The laminar to turbulent flow transition mechanisms which exist due to sweep are thus not present on the nacelle. On the upper surface of a swept wing or on the empennage, there are three flow mechanisms or instabilities which need to be controlled to prevent transition: Tollmien-Schlichting (TS) instability, Cross-flow (CF) instability and Attachment Line Contamination (see section B.2, Appendix B).

#### **2.2.2 Natural Laminar Flow**

For smaller aircraft, laminar flow can be achieved by the aerofoil design alone. This so-called Natural Laminar Flow (NLF) is obtained by a wing profile that produces a progressive pressure drop (i.e. favourable gradient) resulting in flow acceleration and a delay in transition to approximately the point of minimum pressure. (See Fig. 2-1.)



NLF aerofoils are used extensively for gliders and for some GA (General Aviation) aircraft. They are also suitable for small aircraft with modest leading edge sweep, such as the Piaggio P180. Under the CEC sponsored ELFIN project (described in section C.8, Appendix C), NLF was successfully demonstrated at Mach 0.75 on a Fokker 100 aeroplane, using a wing glove. The boundaries of NLF are shown in Fig. 2-2.

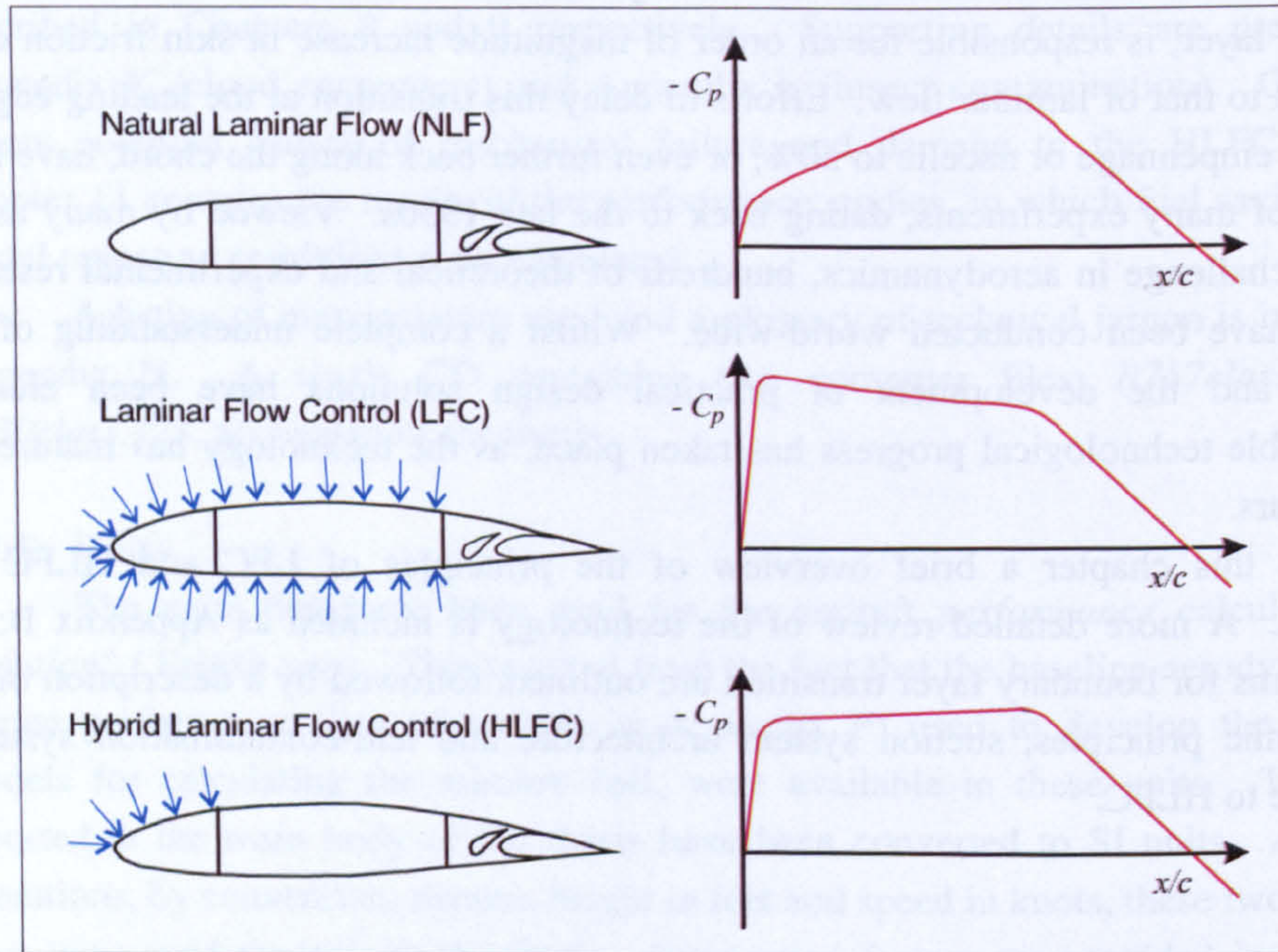


**Fig. 2-1** Pressure distribution on the upper surface of a NLF aerofoil, LFC aerofoil and HLFC aerofoil (redrawn after Joslin, 1998a)

### 2.2.3 Laminar Flow Control

Joslin (1998a) described Laminar Flow Control (LFC) as, “an active boundary layer control technique employed to maintain the laminar state at chord Reynolds numbers beyond that which is normally characterised as being transitional or turbulent in the absence of control”. Stabilisation of the boundary layer to delay transition can be achieved by a number of principles, including suction, blowing, thermal and the use of Micro-Electro-Mechanical Systems (MEMS) (Warsop, 1999; 2000; for example). Of these LFC systems, the one that has received greatest attention by researchers, is suction. The removal of a small amount of the air from within the boundary layer, through the skin via slots, or through a porous or perforated surface, can suppress all instabilities and maintain a laminar flow for extended distances over an aerodynamic surface. Significantly, this may be achieved on highly swept wings and also in the presence of an unfavourable pressure gradient.

The required flow rate through the porous or perforated surface is a function of the predominant instability at that point on the wing. Generally low suction rates are



required to suppress TS instabilities, while higher rates are required to suppress CF instabilities and Attachment Line Contamination. Details of the impact of suction on delaying transition are provided by, for example: Pfenninger and Reed (1966), Pfenninger (1977), Poll *et al.* (1992a), Arnal (1992), Hansen (1996) and Bokser *et al.* (1998). Suction has also been shown to relaminarise the flow following a disturbance (Henke *et al.*, 1993; Poll and Danks, 1994). The success of this depends on the state of the boundary layer at the point of transition and the nature of the disturbance.

The design implications of installing a suction system beneath the entire wing surface are considerable. It would result in a significant increase in structural complexity of the primary wing box, with a reduced space available for fuel and an increased overall wing weight. Techniques that rely on natural laminar flow over the wing box are thus preferential.

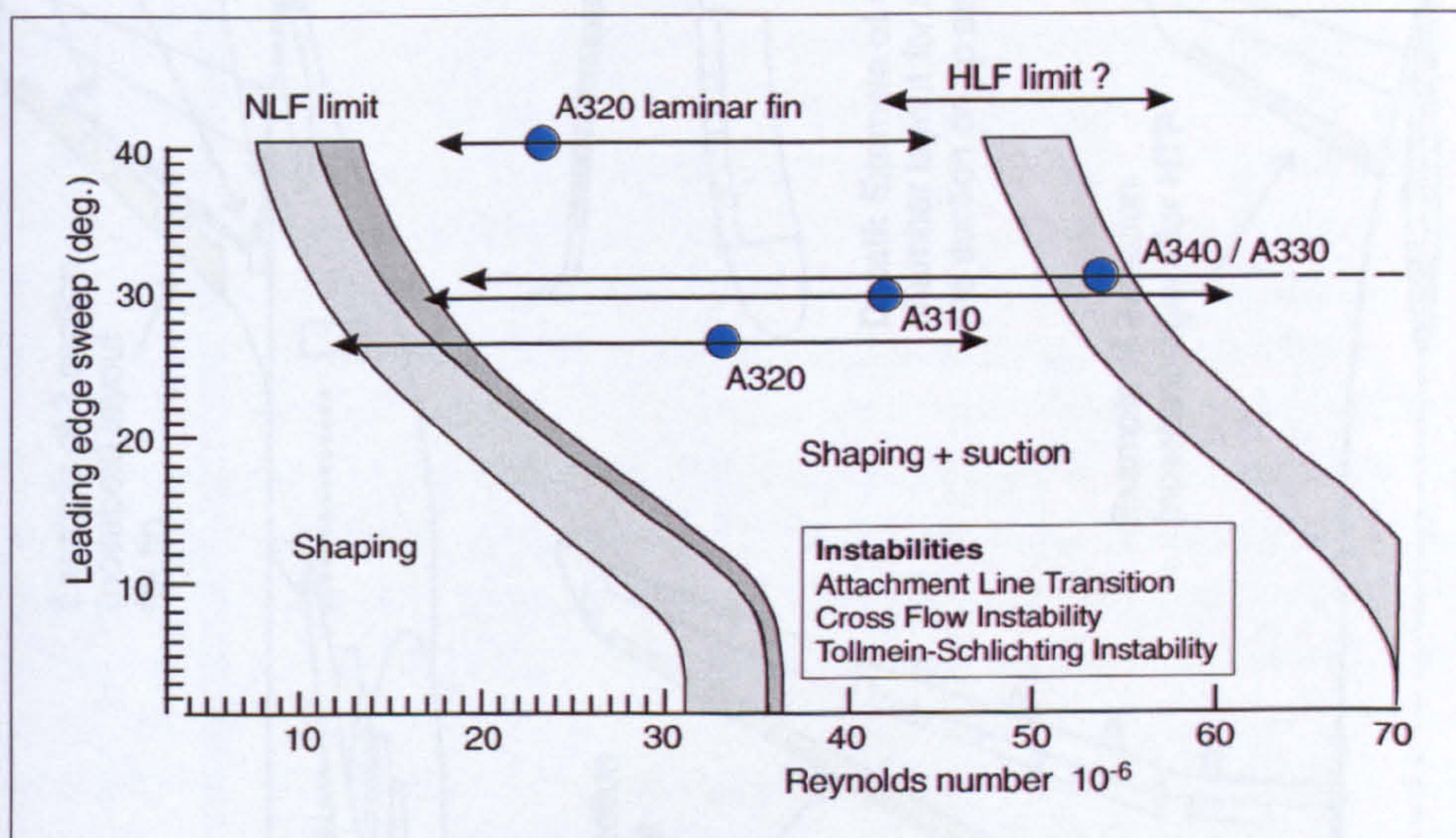


Fig. 2-2 Boundaries of NLF and HLF (redrawn after Schrauf, 2001)

### 2.2.4 Hybrid Laminar Flow Control

Hybrid Laminar Flow Control is a "hybrid" of full LFC and NLF. It relies on: (1) Suction being applied to the leading 10 - 20% of the chord (i.e. ahead of the front spar), to stabilise the flow; and (2) A correctly profiled contour, to generate a suitable pressure gradient, thus maintaining the laminar flow aft of the suction area. Transition is delayed by this technique, and may even occur aft of the 50% chord location, due to the combined effects of the local pressure gradient and Reynolds number.

The control of the boundary layer is achieved by bleeding air, at modest velocities of 0.1 to 0.3 m/s, through a perforated or porous skin surface by means of mechanical suction. The air is ducted beneath the skin through a network of chambers and pipes located in the leading edge section (D-box) of the wing, and finally exhausted.



As suction is limited to the forward part of the wing, HLFC avoids many of the structural problems associated with LFC; particularly as it does not interfere with the wing box section. It also requires a smaller and lighter suction system. These advantages make HLFC more suitable than full LFC for subsonic transport aircraft. The HLFC wing also has good aerodynamic performance in the fully turbulent mode, which is a significant advantage.

The principle of HLFC can be applied to the wing, empennage and engine nacelle, as shown in Fig. 2-3. The prevention of CF instability and Attachment Line Contamination requires that suction be applied to the leading edge of the wing or tailplane. However, the lip of an engine nacelle has no significant sweep and hence there is no need to apply suction at the nose of the nacelle. This makes for a simpler design solution. The flow is stabilised by applying suction aft of the lip section of the nacelle.







## **2.3 LFC AND HLFC STUDIES AND FLIGHT TEST CAMPAIGNS**

Braslow and Muraca (1978) and Braslow (1999), provide a historical review of early LFC experiments. The first LFC tests using suction are reported to have been conducted by NACA in 1939. The successful tests were followed in 1941 by the first LFC flight experiments, which were performed using a B-18 aircraft. An important milestone was reached with the USAF / Northrop X-21A flight programme, in the early-to mid-1960s. Valuable information regarding the practical problems of LFC accrued from these flight tests, which were supported by wind-tunnel tests and analytical study. Much of the current world-wide interest in laminar flow control stems from the test campaign conducted by NASA, Douglas Aircraft and Lockheed-Georgia, using a Jetstar (Lockheed C-140) aircraft from 1983 to 1986. In addition to demonstrating the viability of the LFC, the aircraft was flown in a Simulated Airline Service (SAS) study to evaluate LFC under operational conditions.

Since the mid-1980s, the research has largely focused on HLFC using suction. The first practical in-flight demonstration of HLFC on a transport aircraft took place using a modified Boeing 757 in 1990. Since then, HLFC has been demonstrated by two separate engine nacelle studies (on a GEAE nacelle installed on an A300 testbed and on a DLR/RR nacelle installed on a VFW 614 test aircraft), and most recently on the fin of an Airbus 320. Supersonic demonstration of HLFC was accomplished using a modified F-16XL aircraft, in 1996.

The American studies have primarily involved NASA, Lockheed, Douglas, Boeing, USAF and GEAE. As a result of the early US work, Boeing holds several patents in this area. In Europe the predominant research effort has been conducted by collaborative research teams, involving the former Airbus partners (Aerospatiale-Matra, BAE Systems, DASA and CASA), engine manufacturers (Snecma and Rolls-Royce), the European national research organisations (QinetiQ, DLR, FFA and ONERA) and supported by universities and smaller specialist aerospace companies. Most of these programmes were conducted with financial support of the Commission of European Communities (CEC). In addition, practical experience of HLFC has come from the work independently performed by Dassault Aviation and ONERA, using a Falcon 900 business jet. An overview of these tests and research programmes is presented in Appendix C.

## **2.4 HLFC SYSTEM**

### **2.4.1 System elements**

The complete HLFC system is comprised of four main elements:

- (1) The suction surface;
- (2) The suction system;
- (3) The monitoring system; and



(4) The anti-contamination system.

These elements will be considered briefly in this section.

### **2.4.2 Suction surface**

The suction surface and the plenum chambers underneath the skin represent the most significant engineering challenge in terms of the manufacture and maintenance of the HLFC system. A critical issue for the design of a complete HLFC wing is the structural joint that will be required between the suction surface and the laminar flow section aft of the suction surface. To prevent transition at this joint, manufacturing tolerances in terms of a step or gap at this, or at any other junction in the laminar flow region, will be substantially tighter than those used in the manufacturing process today.

Various means of producing a skin surface which will allow air to pass through it, have been studied as part of the laminar flow research that started in the late 1930s. These can be divided into three categories: (1) Porous materials, (2) Micro slotted surfaces, and (3) Discrete holes. The aerodynamic requirement is that air be sucked through the skin surface, with minimal pressure loss, and in a way that does not instigate transition of the boundary layer.

Slotted surfaces, which were used for many of the early LFC research projects (such as the Lockheed designed test article for the Jetstar, which featured a titanium skin with 27 rows of 0.1mm wide slots), cannot be considered for the more highly swept wings typical of a modern airliner (Joslin, 1998a). Perforated surfaces can be manufactured with holes of smaller dimensions than the aforementioned slots. Furthermore, hole orientation can be tailored to result in the least possible disruption of the flow. Electron beam drilling was used for the Douglas LFC Jetstar article. Drilling by Nd-Yag or Excimer laser has been the preferred technique for the more recent tests. The Boeing 757 tests and the recent European programmes (see Appendix C) have all used this method for the production of the suction surface. Ideally, the shape of the hole should be tapered with the larger diameter on the inside. The advantage of this is that should dust (or any other particulate matter) enter the hole, it will be sucked through and will not block the hole. This can be achieved by laser drilling, as the hole on the laser entry side is always bigger than on the exit side. Hole sizes and spacing vary from project to project. A typical hole exit diameter is  $\sim 60\mu\text{m}$  and the hole centre-to-centre distance is  $\sim 500\mu\text{m}$ .

Porous materials, like fabrics or sintered meshes, create even less disruption to the flow than slots or discrete holes. These materials tend however to have little structural integrity and stiffness. No successful design of such a surface with the necessary substructure has been developed.

Candidate materials for laser drilled surfaces have been evaluated as part of the experimental programmes described in Appendix C. (Details of the work conducted by the author in this regard are presented in Chapter 10). The materials include titanium, stainless steel, aluminium and carbon fibre composite. Titanium is regarded as the



prime candidate material, not only because it can be laser drilled with precision, but also because of the ability to form the material in the designed shape, its fatigue properties in the drilled condition, good impact resistance and durability.

### 2.4.3 Suction system

The function of the suction is to conduct the air bled from the external boundary layer to the pump and then finally to the exhaust. A series of narrow suction chambers (flutes or plenums, as they are also called) is required to run under the skin in a spanwise direction. The suction within the rows of chambers is tailored to suit the external flow conditions, characterised by pressure, pressure gradient and Reynolds number. This necessitates the installation of valves and /or calibrated orifices in the suction system, to provide the required pressure in each chamber. Tailoring of the suction flow may also be achieved by changing the hole size and / or spacing.

The suction chambers will convey the air to larger collection ducts or pipes, which will run to the pump. The material used for the suction chambers and the method of manufacture, have to be considered in an integrated manner with the selection of the skin material. Brazing, welding, adhesive bonding and superplastic forming, have all been considered for joining the suction chambers to the perforated skin. Providing a durable bond or junction between the skin and the chambers, without blocking too many holes, is the critical issue. The requirement for an almost airtight seal between the suction chamber and skin surface, further complicates the manufacturing process. A titanium substructure was used on the A320 fin test (section C.14, Appendix C) to eliminate problems with dissimilar materials.

The pump(s) which provide the necessary suction may theoretically be driven by bleed air or mechanical power off-take from the engine. Wilson (1997) compared the electrical and bleed air drive options, and concluded that an electrical drive was more efficient with approximately half of the SFC penalty of that of the bleed drive option. The author is of the opinion that Wilson had underestimated the SFC penalty for the electric system (see Chapter 7), implying that the difference would be less than the quoted value. Nevertheless, independent studies conducted during the HYLDA project (section C.16, Appendix C) came to the supporting conclusion that an electric induction motor driving an axial compressor, was the most efficient system. As the start-up power requirement for the system is high, consideration has been given to using bleed air to start the compressor.

An increase in fuel burn results from the increased power extraction from the engines, which in turn reduces the net performance benefit. The "exchange rate" of power off-take versus increase in SFC is assessed in Chapter 7.

### 2.4.4 Monitoring systems

The extent of the laminar flow on the skin can be measured in a number of ways. Hot film or hot wire sensors have been widely used in the wind tunnel and in-flight



experimental work described in Appendix C. Other techniques include infrared thermography, embedded microphones and liquid crystal transducers. The experimental determination of the extent of laminar flow can be measured using an array of evenly spaced small Pitot tubes (sometimes called a "rake"), mounted behind the laminar flow surface at a height of ~2mm off the surface. The total pressure, compared to the reading of a reference Pitot tube can be used to infer the chordwise extension of the laminar flow. In addition, static pressure ports have been used to measure the pressure on the external surface and in the suction chambers.

For a production aircraft the requirements are different. A robust monitoring system is required that will indicate to the pilot if the laminar flow design target is being achieved. The state of the HLFC system can be assessed by monitoring changes in pressure in the ducts. An alternative technique based on surface pressure fluctuations was explored by Wright and Nelson (2000). They were able to distinguish between laminar and turbulent flow on a LFC wind tunnel model, using miniature microphones. In principle, information on the static pressure in the ducts, the operating condition of the compressor, and the state of the boundary layer at selected locations, may be used in conjunction with the existing fuel monitoring system, to ensure that the pilot becomes aware of a HLFC system failure.

#### **2.4.5 Anti-contamination system**

Insect contamination and ice adherence are two crucial operational issues for HLFC aircraft. These are discussed in section 2.5. Considerable operational experience exists for de-icing and anti-icing systems on the leading edge of wings and on nacelles; however, very little experience is available on realistic insect contamination avoidance / cleaning systems. The prevention of insect and ice contamination may be achieved using a single system, or the functions may be separated, by having a barrier system for the insects and a hot air or liquid system for the ice. Various methods to prevent insects from disrupting the flow are reviewed in Chapter 9. These include "preventative" methods and "cleaning" methods. Although a wide range of concepts have been proposed and tested, most are impractical and only two are seriously considered as being operationally viable. These are:

- (1) A shield that either catches the insect or deflects its path away from the laminar flow surface; and
- (2) A continuous fluid discharge that prevents insects from adhering to the surface.

## **2.5 CONTAMINATION OF THE LFC SURFACE**

### **2.5.1 Contaminants**

Contamination of the leading edge and suction surface is a major operational concern for HLFC aircraft and leads to reduced system effectiveness. The problem is



not restricted to HLF systems, but impacts any laminar flow surface. Contamination can be caused by ice, rain, sand, insects and other airborne particles. The greatest concerns for HLFC operation are ice and insect contamination.

### 2.5.2 Ice formation

Roughness caused by ice has long been known to seriously degrade the aerodynamic characteristics of a wing surface. It encourages transition from laminar to turbulent flow upstream of where it would normally occur, increasing the drag. The problem of ice removal and ice prevention for a HLFC aircraft is a little different from that of a turbulent design. Firstly, ice on the aerofoil surface will have greater impact on the fuel consumption, due to the laminar flow transition and secondly, the de-icing / anti-icing system must be compatible with the design of the HLFC suction system.

There are essentially two de-icing / anti-icing systems used on jet aircraft – one is based on melting the ice by heating the surface, and the other is a liquid system that utilises a Freezing Point Depressant (FPD)<sup>6</sup>. The integration of the de-icing system and the anti-contamination system is discussed later in section 9.6.

### 2.5.3 Ice crystals

Ice crystals found in cirrus clouds pose a unique problem to HLFC aircraft. Transition may be induced by the wake of small particles moving through the boundary layer. This was widely documented following the X-21A LFC flight tests (described in section C.3, Appendix C). Davis *et al.* (1987; 1989) describe the impact of ice crystals on laminar flow, as encountered on the Jetstar flight test programme. It was reported that full laminar flow was regained almost immediately after the aircraft left the cloud. Further details on this effect are presented in Chapter 8.

### 2.5.4 Rain

Rain can result in a loss of lift and an increase in drag (Thompson, 1995). The rain's effect on aerodynamic performance is largely due to premature transition of the boundary layer, because of raindrops contacting the leading edge and forming craters (Luers, 1983). Water beads or rivulets may form, which contribute to surface roughness and increased skin friction. In the case of HLFC surfaces, rain blocks the holes and prevents the flow of air through the skin surface. The ducts have to be purged after the rain stops, before air may be sucked through the skin again. This has obvious flight implications and may limit HLFC operations to flight segments above ~20 000ft, on certain routes. This is discussed further in Chapter 5.

---

<sup>6</sup> Freezing Point Depressant (FPD) is a solution, usually glycol based, with the ability to prevent the formation of ice or to decompose pre-formed ice.



### **2.5.5 Airborne particles**

Dirt and dust can have two impacts, i.e. blocking of the holes and erosion of the aerodynamic surfaces. Humphreys (1992) assessed the potential impact of these elements. Using Sahara dust sizes as the particulate matter, he suggested that hole blockage would be unlikely, because the largest particles in Sahara dust represent only a fraction of the total size distribution and even these are less than the typical hole diameters of the suction surface. Potential difficulties could be encountered following severe dust storms or after volcanic activity. The HLFC system would have to be inactivated or the airflow reversed in such conditions. Flight trials conducted during the HYLTEC project concluded that HLFC perforated panels do not get blocked during flight to the extent that was previously feared and that flight through rain tends to clean the panels (see section M.4, Appendix M).

### **2.5.6 Insect contamination**

Insects striking the leading edge of laminar flow surfaces have long been recognised as one of the most significant problems associated with laminar flow. This threat is almost entirely confined to operations in close proximity to the ground and requires mitigation during the takeoff, initial climb, approach and landing. During these flight phases the aircraft speed is sufficient to cause the outer shell of the insect to rupture, releasing the body fluid onto the leading edge surface. This causes the insect, or parts of the insect body, to adhere to the aircraft skin. The residue can block the suction holes and can cause transition of the boundary layer, if its height exceeds the critical excrescence height for the laminar flow at the impact site. Details on insect contamination and proposed solutions for the mitigation of the problem are presented in Chapter 9.



### **3 COMPUTER PERFORMANCE MODEL**

#### **3.1 INTRODUCTION**

To study the impact of HLFC technology on the trip fuel, two computer performance models, capable of determining the fuel required for a specified mission, were developed. In this chapter a description of the computer program is presented. Two aircraft types were selected as baseline vehicles, representative of modern medium to long-range airliners (described in Chapter 4). The concept involved modelling the en route performance of these aircraft and then adapting these models to take into account the virtual installation of a HLFC system (Chapter 5). This modification involved a decrease in drag and a corresponding increase in SFC, during the part of the mission where the HLFC system would be operational, and an increase in the Operating Empty Weight (OEW), resulting from the installation of the system. All other design parameters were unchanged, including the wing planform and powerplant characteristics.

The HLFC aircraft models developed for this study did not take into account the potential that exists for re-sizing a new design to meet a given range and payload specification – which was the approach adopted in the studies reported by Lange (1987; 1988), Arcara *et al.* (1991) and Wilson (1997), for example. Instead, the HLFC models represent idealised "retrofit" aircraft with a longer range, rather than a new HLFC aircraft sized to meet the design range. In this respect, the study is similar to the approach adopted by Boeing (1982) or Atkin and Courtenay (2002). No account was taken of any physical space or structural limitations that may be imposed by the actual design. For example, the "installation" of the HLFC system did not reduce the space available in the wing for fuel, nor did any physical constraints in the wing D-box restrict the installation of the system; as Bieler and Swan (2000) stated would be the case for an A310 HLFC retrofit design.

#### **3.2 REQUIREMENTS FOR THE "BASELINE" PROGRAM**

##### **3.2.1 General requirements**

The main requirements of the turbulent baseline computer program were to determine the fuel consumed, distance covered and time elapsed for the baseline aircraft performing a standard mission according to a standard flight profile (described in section 3.2.2). The program was required to run in three modes, depending on the input data, as specified in Table 3-1. Furthermore, a set of general requirements pertaining to the operation of the program were set as targets for its development. These are itemized in Table 3-2.



**Table 3-1** *Program modes of operation*

Mode	Requirements
1 "Weight" mode	To compute the range for a user specific Brake Release Weight (BRW) and payload.
2 "Range" mode	To compute the BRW to satisfy a user specific range and payload.
3 "Fuel" mode	To compute the fuel required to fly a mission where the range, BRW and payload are specified, and to determine the tankered fuel <sup>7</sup> on landing at the alternate airport.

**Table 3-2** *General program requirements*

Parameter	Requirements
1 Accuracy	The predicted trip fuel values should match published data of the baseline aircraft to within 5%.
2 Repeatability	The variation in answers of the trip fuel calculation should not exceed 0.1% from different runs (with the same input data).
3 Robustness	With the input of valid data, the program should not crash under normal usage and if it does crash it should not damage the code in any way that prevents the program from running again.
4 Run time	The run time should be less than 3 minutes on a standard PC (500MHz processor or better).

### 3.2.2 Fuel planning requirements / regulations

Specific requirements exist in FAR 121 and JAR OPS 1 with regard to fuel planning, to ensure that all aircraft engaged in public transport flights meet a minimum standard of safety, deemed appropriate to the operation. The exact requirements depend on the operator (flag or domestic carrier), type of aircraft (turbine engine or turbo-prop), route planned (domestic or international), and the availability of alternate airports (if for any reason the aircraft is unable to land at the destination airport). As HLFC technology favours long-range missions where considerable time is spent in the cruise, the fuel planning requirements that have been used for the studies reported herein, conform to the requirements for international flights. Fuel planning policies for commercial transport aircraft are outlined in JAR OPS 1 Subpart D, section 1.255. The relevant sections of this document, including important definitions relating to the interpretations of the policy, have been reproduced in Appendix D.

For the purpose of flight planning, the flight profile can be divided into several legs as shown in Fig. 3-1. The ICAO provides recommendations for international flight operations. For aeroplanes equipped with turbo-jet engines, paragraph 4.3.6.3.2 (A) of ICAO Annex 6 applies, when an alternate airport is specified (Boeing, 1996). The requirements are: To fly to and execute an approach, and a missed approach, at the aerodrome to which the flight is planned, and thereafter:

- (1) To fly to the alternate aerodrome specified in the flight plan; and then

<sup>7</sup> The tankered fuel is defined here as the "extra" fuel on board the aircraft after landing at the alternate aerodrome (i.e. that which is over-and-above the contingency fuel) after completing a standard mission.



- (2) To fly for 30 minutes at holding speed at 1500 feet above the alternate aerodrome under standard temperature conditions, and approach and land; and
- (3) To have an additional amount of fuel sufficient to provide for the increased consumption, on the occurrence of any of the potential contingencies specified by the operator, to the satisfaction of the State of the operator. (Typically, a percentage of the trip fuel.)

The fuel, time and distance covered for each leg is determined. This may be based on historical data, as would be the case for the start-up and taxi fuel at a particular airport, or calculated for the specific route planned. For the purposes of the current study the segments of the mission during which the HLFC system would operate, are indicated in Fig. 3-1. The implementation of this is discussed in Chapter 5.

### 3.2.3 Contingency fuel (en route reserve)

At the planning stage, not all factors which could have an influence on the fuel consumption to the destination aerodrome can be foreseen. According to JAR OPS 1 Subpart D, section 1.255, contingency fuel is carried to compensate for items such as:

- (1) Deviations of an individual aeroplane from the expected fuel consumption data;
- (2) Deviations from forecast meteorological conditions; and
- (3) Deviations from planned routings and/or cruising levels/altitudes.

The contingency fuel may be either:

- (1) 5% of the planned trip fuel or,
- (2) 3% of the planned trip fuel, provided that an en route alternate aerodrome is available.

The 5% contingency is sometimes called *oceanic reserves*, whilst the 3% contingency is called *continental reserves*. For the studies conducted by the author and herein reported, a 5% contingency has been used. The one exception is recorded in Table 4-3 (Chapter 4), where a 3% contingency has been used in order to compare computed values against published results for the B757-200 aircraft.



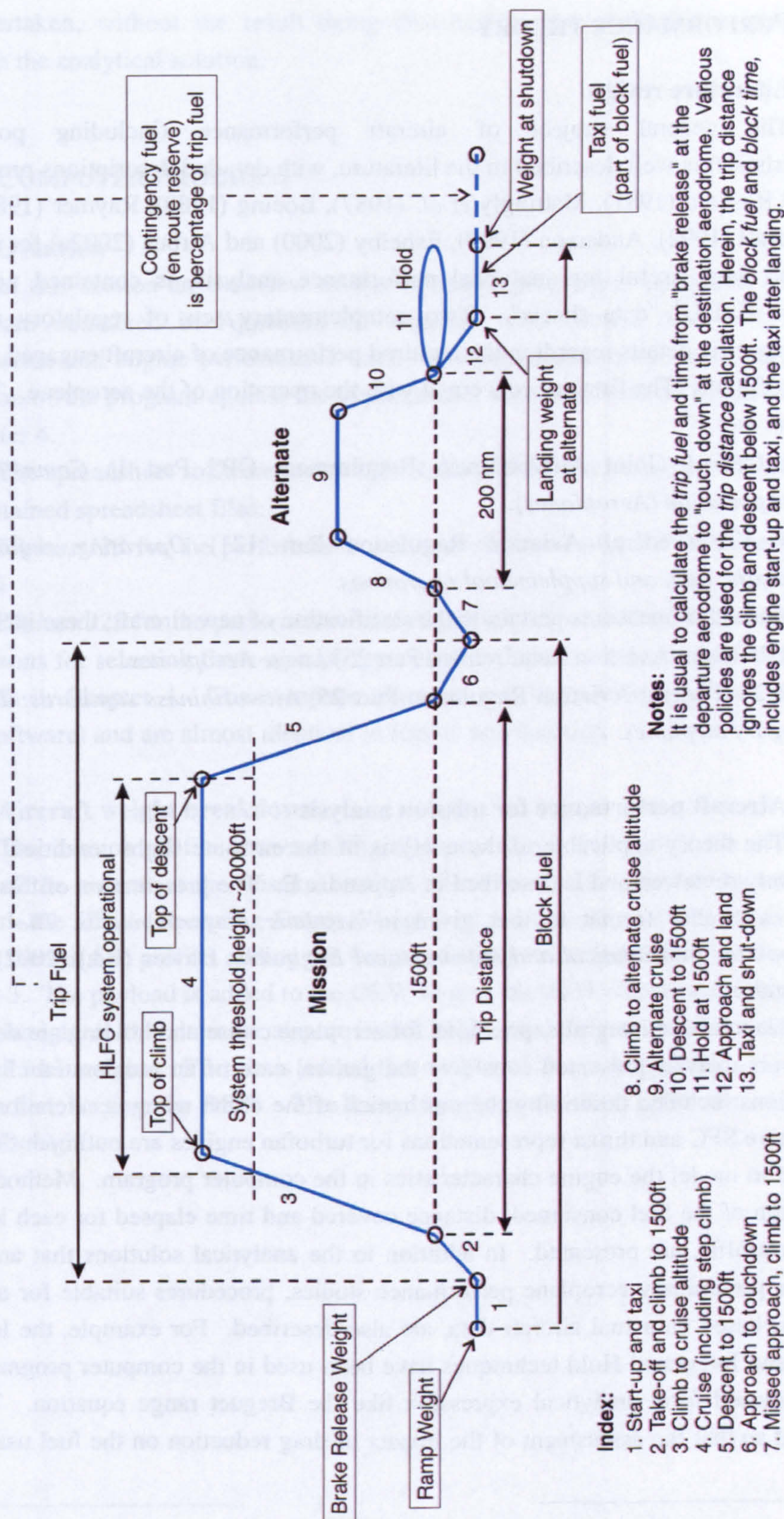


Fig. 3-1 Flight profile for fuel planning of HLC aircraft



### 3.3 PERFORMANCE THEORY

#### 3.3.1 Literature review

The general subject of aircraft performance (including powerplant characteristics) is well described in the literature, with detailed descriptions provided by Lan and Roskam (1981), Mattingly *et al.* (1987), Boeing (1989), Raymer (1989), Mair and Birdsall (1992), Anderson (1999), Eshelby (2000) and Airbus (2002a) for example. Validated data, useful for analytical performance analysis, is contained within the extensive ESDU<sup>8</sup> "data sheets". Two complementary sets of regulatory measures contain specific details regarding the required performance of aircraft engaged in public transport flights. The first are concerned with the operation of the aeroplane. The most important are:

- JAR OPS 1 (Joint Airworthiness Requirement OPS Part 1) *Commercial Air Transportation (Aeroplanes)*.
- FAR 121 (Federal Aviation Regulation Part 121) *Operating requirements: Domestic, flag, and supplemental operations*.

The second set of measures pertain to the certification of new aircraft; these include:

- JAR 25 (Joint Aviation Requirement Part 25) *Large Aeroplanes*.
- FAR 25 (Federal Aviation Regulation Part 25) *Airworthiness standards: Transport category airplanes*.

#### 3.3.2 Aircraft performance for mission analysis

The theory applicable to the analysis of the en route flight condition has been extensively reviewed and is described in Appendix E. The presentation of this material follows a similar format to that given in *Airplane Performance in The Standard Handbook for Aeronautical and Astronautical Engineers*, Davies (Ed.) (2002), written by the author.

Generalised integral expressions for aeroplane cruise and holding are developed. The climb analysis presented considers the general case of an accelerated climb, with expressions included describing the mechanics of the climb using acceleration factors. Alternative SFC and thrust representations for turbofan engines are outlined; these were required to model the engine characteristics in the computer program. Methods for the evaluation of the fuel consumed, distance covered and time elapsed for each leg of the mission profile, are presented. In addition to the analytical solutions that are usually used for preliminary aeroplane performance studies, procedures suitable for numerical analysis, based on actual aircraft data, are also described. For example, the Integrated Range and Integrated Hold techniques have been used in the computer program, rather than a closed form analytical expression like the Breguet range equation. This was required so that the assessment of the impact of drag reduction on the fuel usage could

---

<sup>8</sup> ESDU, 27 Corsham St., London. U.K.



be undertaken, without the result being distorted by the assumptions necessary to establish the analytical solution.

## 3.4 COMPUTER PROGRAM

### 3.4.1 Overview

In this section an overview of the computer program is presented. Complete details are contained in Appendix H, together with sample runs and tables of aerodynamic and engine performance data. The generation of the input data and the validation of the program against the requirements set out in section 3.2, are described in Chapter 4.

The spreadsheet software Lotus 123 (Release 9.6)<sup>9</sup> has been used to develop two self-contained spreadsheet files:

- (1) *B757class.123* for the performance analysis of the Boeing 757-200 class aircraft; and
- (2) *A330class.123* for the performance analysis of the Airbus 330-200 class aircraft.

The reasons for selecting these aircraft types and the baseline aircraft performance data are given in Chapter 4. The computer files are run independently (from within the Lotus software) and are almost identical in format and function.

### 3.4.2 Aircraft weight breakdown

The mission profile shown in Fig. 3-1 provides a framework for defining the weight of the aircraft at the mission stations of interest. The simplest approach is to start with the OEW (Operating Empty Weight) of the aircraft and to work backwards through the mission profile, adding the weight elements incrementally. This is shown in Table 3-3. The payload is added to the OEW to give the ZFW (Zero Fuel Weight). The landing weight at the alternate airport is the ZFW, plus the *contingency* fuel and the *tankered* fuel weights. To this is added the weight of the *holding* fuel, *alternate* fuel and *trip* fuel, to give the BRW. The Ramp weight is the BRW, plus the *start-up* and *taxi* fuel weight.

---

<sup>9</sup> Lotus 123, a product of the Lotus Development Corporation, Staines, Middlesex, UK.



Table 3-3 Weight breakdown for program operation

Weight breakdown	Comment
Operating Empty Weight (OEW)	The OEW is a fixed parameter for each aircraft type.
Payload	The <i>payload</i> is specified by the user.
Zero Fuel Weight (ZFW)	$ZFW = OEW + Payload$ .
Contingency fuel	The <i>contingency fuel</i> (en route reserve fuel) is a percentage of the trip fuel and is specified by the user.
Tankered fuel	The <i>tankered fuel</i> is zero for modes 1 and 2; however, for mode 3, the <i>tankered fuel</i> is the output of the calculation where both range and BRW are specified.
Land weight at alternate	$Land\ weight\ (alternate) = ZFW + Contingency\ fuel + Tankered\ fuel$ .
Holding (final reserve)	The <i>holding (final reserve) fuel</i> is calculated for the user specified conditions.
Alternate and land	The <i>alternate and land fuel</i> is calculated for the user specified conditions.
Trip fuel	The <i>trip fuel</i> is calculated for the user specified conditions.
Brake Release Weight (BRW)	$BRW = Land\ weight\ (alternate) + Final\ reserve\ fuel + Alternate\ and\ land\ fuel + Trip\ fuel$ .
Start-up and taxi	The <i>start-up and taxi fuel</i> is taken as a fixed quantity.
Ramp Weight	$Ramp\ weight = BRW + Start-up\ and\ taxi\ fuel$ .

### 3.4.3 Program logic

The program comprises a number of computational modules, which were written (and de-bugged) separately, to compute the *fuel*, *distance* and *time* for the climb, cruise, hold and descent legs of the mission. These were then integrated into a single program. Allowances were made for the remaining legs (i.e. start-up, taxi, takeoff, landing, etc.) so that fuel, distance and time could be determined from engine start, to touchdown at the alternate airport. The computation occurs sequentially, using the specified BRW (for program modes 1 and 3), or an assumed BRW (for mode 2) as the starting point. For each leg of the mission (defined in Fig. 3-1) the fuel is determined and the aircraft weight determined.

The climb was broken into intervals of 5000ft, or less. The essential problem with the climb calculation is that the weight at the end of the interval depends on the rate of climb in the interval (which is not constant) and this in turn depends on the weight. An iterative solution is thus required for each step of the climb. On inspection, it was found that two iterations permitted convergence within each interval. Following the climb calculation, the conditions at the TOC (top of climb) are established.

The next module considered the cruise. The determination of the cruise fuel and time can only be performed if the distance from the TOC to the TOD (top of descent) is known; however, at the start of the calculation this is not known, due to an uncertainty of the descent distance. An estimate of the TOC to TOD distance is used to compute a trial value for the cruise fuel and time, which is then used for the rest of the mission. The final result is compared to the specified mission, and an iteration follows which results in the correct TOC to TOD distance being determined. In the software a



“backsolve” feature<sup>10</sup> has been used to control the iteration for the cruise calculations, for both the main mission and for the alternate leg.

In mode 1, the payload is specified and the *range* is the unknown parameter. It is determined by iteration as shown in Fig. 3-2, where each iterative cycle determines the fuel required for a trial cruise distance. Convergence is attained when the available mission fuel is consumed. In the program this is achieved by subtracting the calculated total fuel (mission fuel plus reserves) and the payload from the BRW, to give a trial OEW value. The trial OEW is compared to the actual OEW for the aircraft and the difference used to adjust the cruise distance (TOC to TOD). The computation is repeated until convergence of within 0.01% of the weight is reached.

Where the range is specified (i.e. mode 2), a trial BRW is used as the starting point for the calculation. In this case the difference between the trial OEW and the actual OEW is used to adjust the trial BRW. As before, the computation is repeated until convergence of within 0.01% of the weight is reached. The process is reflected in the flowchart in Fig. 3-3.

When the aircraft lands at the alternate airport following a standard mission (including the hold) in the case of modes 1 or 2, the fuel on board the aircraft would exactly equal the en route contingency (reserve) fuel. In this analysis the mission fuel is calculated in such a way that this will be true. Obviously a departure during the “flight” from the planned mission would result in this not being the case.

For mode 3 (see Fig. 3-4) all three input parameters, i.e. BRW, range and payload are specified by the user. The parameter to be determined is the mission fuel. In this case the fuel on board at the time of landing at the alternate airport, will not in general be equal to the en route contingency fuel. The difference between the on-board fuel and the contingency fuel has been referred to herein, as the *tankered* fuel. This tankered fuel is in fact the unknown parameter that is determined for this program mode. The tankered fuel is the “extra” fuel on board after landing at the alternate aerodrome, following a standard mission. In modes 1 and 2 the tankered fuel is zero.

---

<sup>10</sup> Backsolve: Lotus 123 has a powerful built-in *backsolver* feature. This is an iterative solver function, that may be used when the numerical answer to a defined function is known, but the variable(s) needed to produce that answer, are not known.



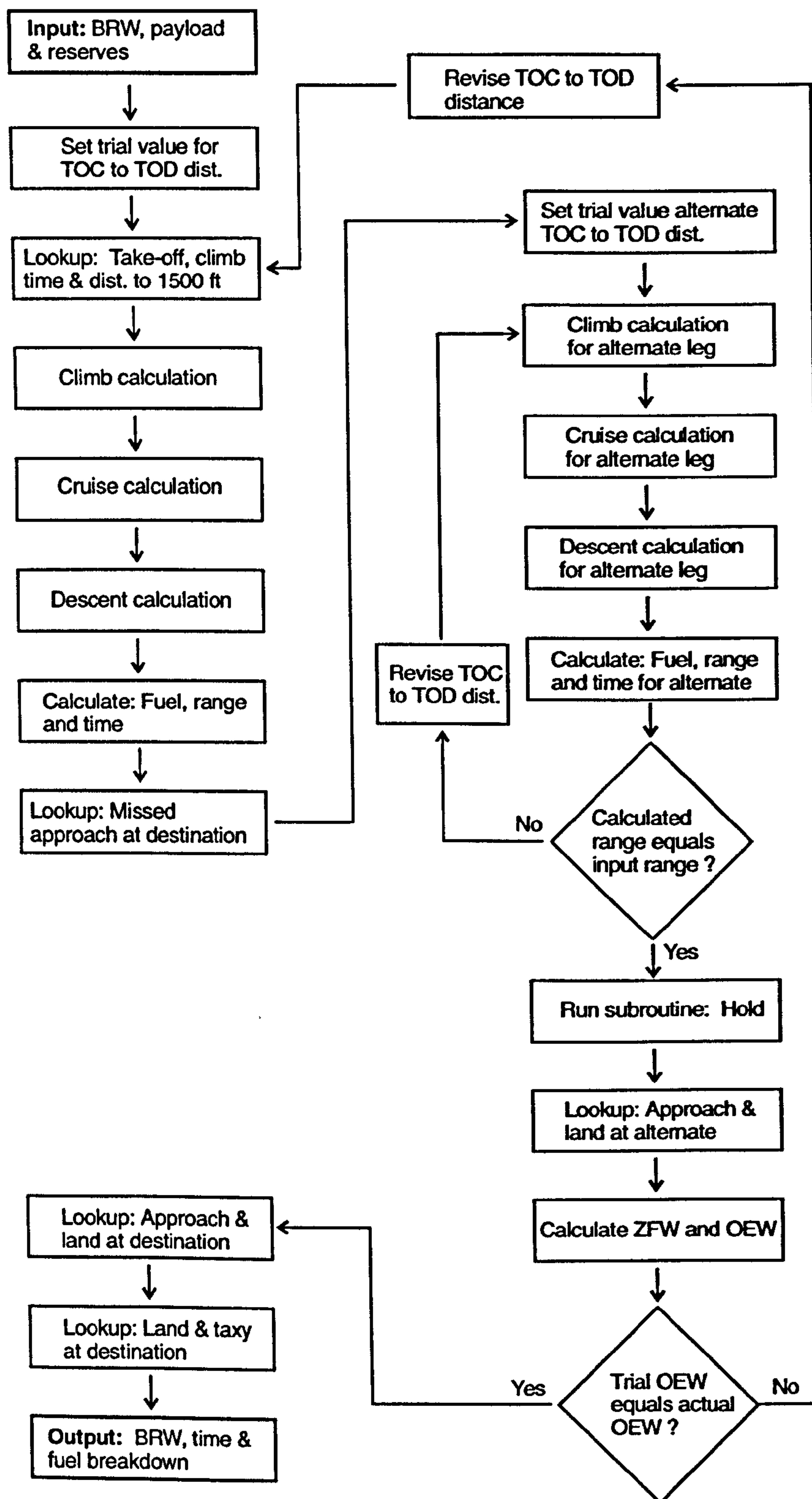


Fig. 3-2 Flowchart of calculations for mode 1 "Weight"



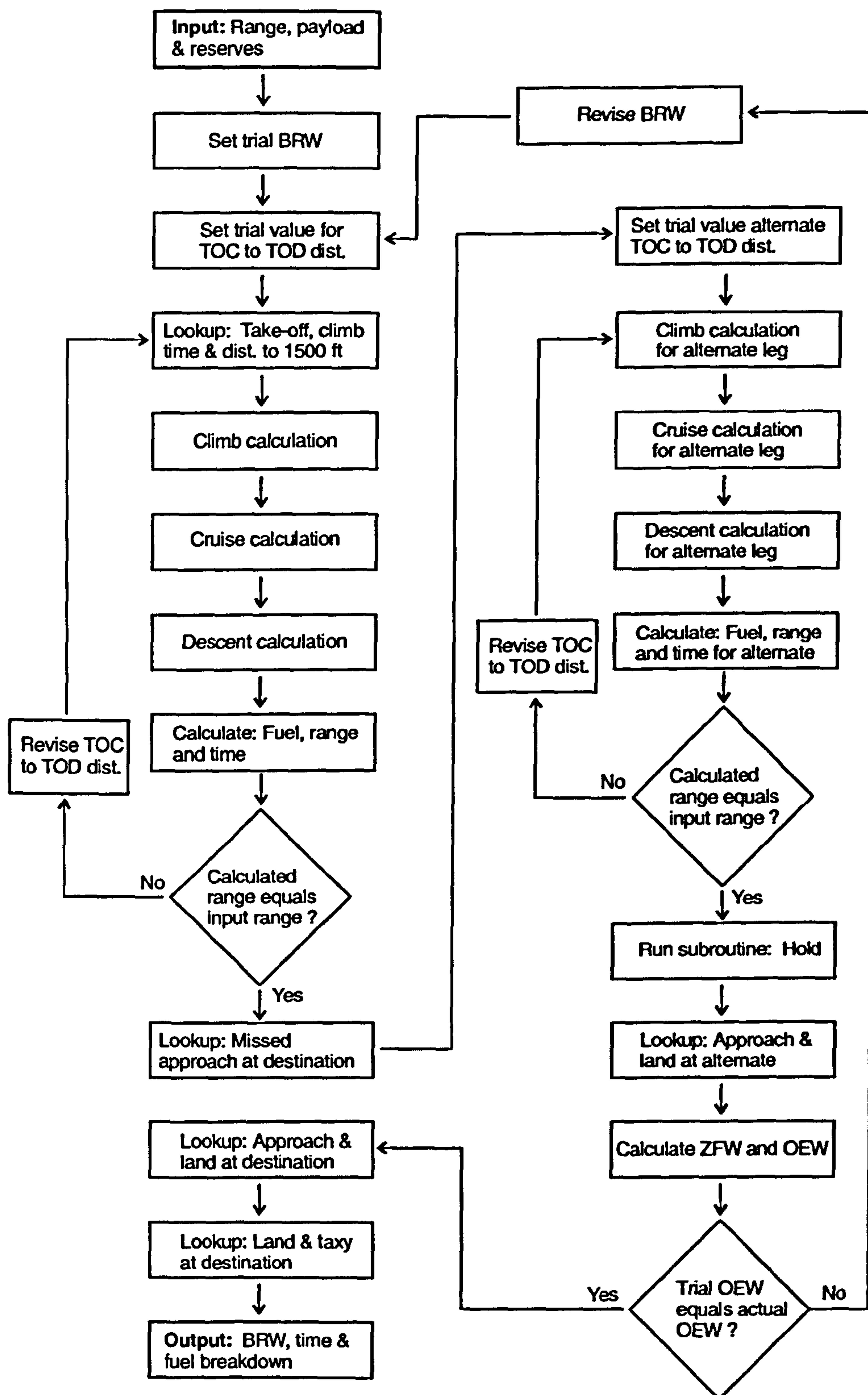


Fig. 3-3 Flowchart of calculations for mode 2 "Range"



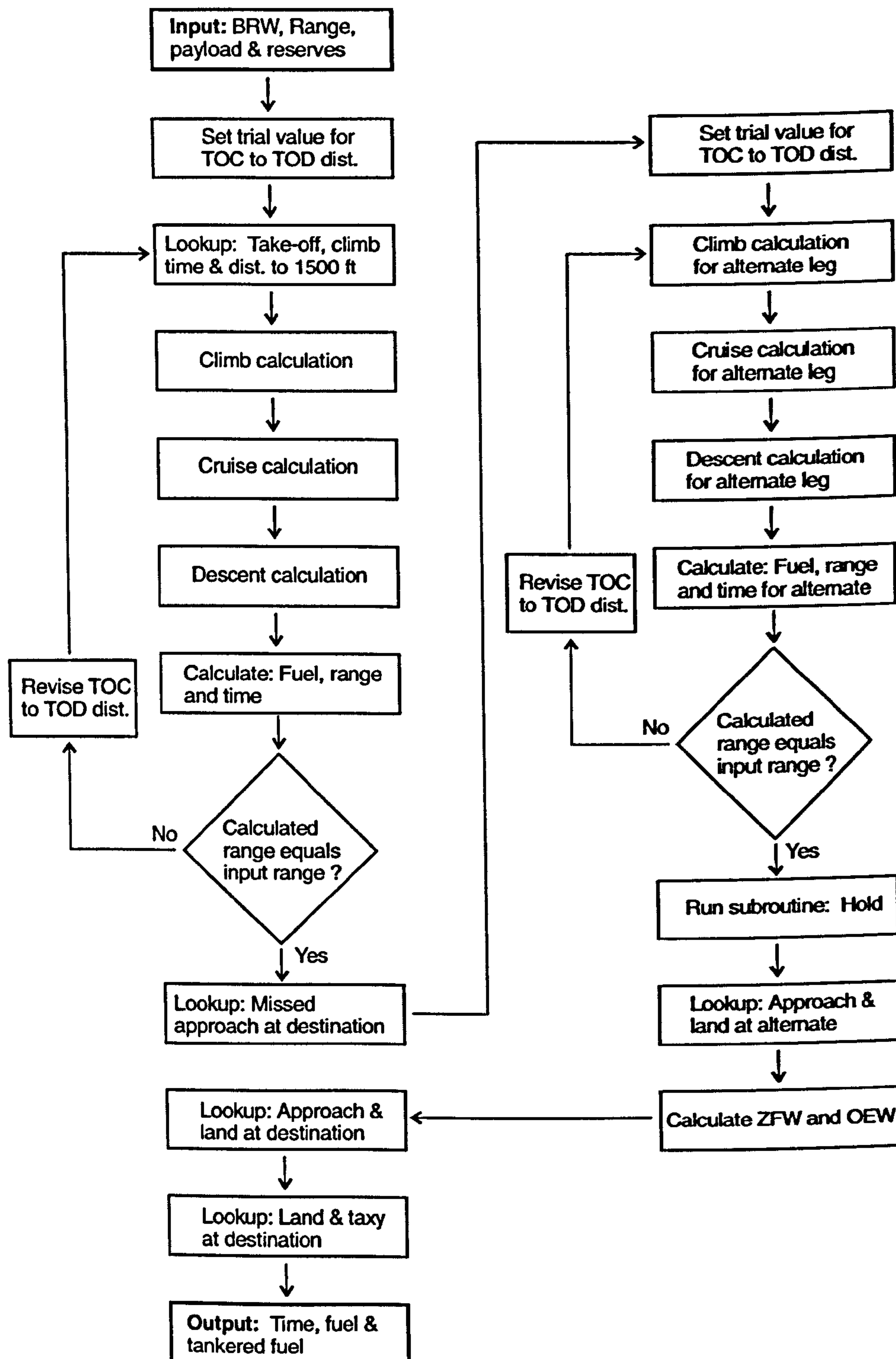


Fig. 3-4 Flowchart of calculations for mode 3 "Fuel"



### 3.4.4 Program structure

The two spreadsheet files *B757class.123* and *A330class.123* are almost identical. The few differences are described in Appendix H. Each file is comprised of 10 sheets (pages); the functions of which are outlined in Table 3-4. The user controls the program from sheet A, which has several elements including tables of aircraft and mission specific data, software buttons to run the different calculation modes, a master computing table, dialogue boxes and the macro (program) code. Sheets B, C and D contain the computational spreadsheets that evaluate the fuel, distance and time for the cruise, climb and hold legs, respectively. The aircraft specific data required for the calculations are located in *look-up* tables on sheets E, F, G and H. Sheet I contains International Standard Atmosphere (ISA) data, while sheet J has the program output.

**Table 3-4** *Functions of the individual sheets of the program*

Sheet	Function	Contents
A	Master sheet	Input tables, Master computing table, Macro code
B	Computational spreadsheets	Cruise calculations - mission and alternate
C	Computational spreadsheets	Climb and descent calculations - mission and alternate
D	Computational spreadsheets	Hold calculation
E	Look-up tables	Drag polar
F	Look-up tables	Corrected fuel flow
G	Look-up tables	Engine climb and idle data
H	Look-up tables	Hold Mach No., Initial climb data, Mission allowances
I	Look-up tables	ISA tables
J	Output	Results

### 3.4.5 Input tables

On sheet A, a table of aircraft specific data containing the wing reference area, OEW, maximum BRW and maximum fuel capacity, are specified. The aerodynamic and engine data for the aircraft are included in the look-up tables on sheets E, F, G and H. The establishment of the technical details of the two aircraft types required for the program, are summarized in section 4.4 (for the B757-200 class aircraft) and section 4.5 (A330-200 class aircraft).

If the program is to be run in either *Weight* or *Fuel* program modes, the BRW is specified. In all cases, the payload is required. Alternatively, if the range is specified, it may be run in either *Range* or *Fuel* program modes. The profile data of *climb speed schedule* and *cruise height*, alternate distance, hold time (final reserve) and the contingency (en route reserve) fuel percentage, must be entered.

For the evaluation of the impact of HLFC, a separate input table is available, which enables the user to specify the change to the aircraft's drag, fuel flow and weight, due to the installation of a virtual HLFC system. This is addressed in Chapter 5.

### 3.4.6 Master computing table

Central to the program operation is a Master computing table, illustrated in Table 3-5. For each leg of the mission, numbered 1 to 13 in Fig. 3-1, the calculated fuel



weight, time and distance (determined elsewhere in the program) are inserted. On alternative lines in the table, and indicated by the shaded cells, are "point" calculations corresponding to specific locations along the mission profile. These are summations of the values corresponding to the previous point and the values corresponding to the leg in question. In certain places in the table, the computation is not performed sequentially (e.g. the cruise fuel and time depends on the TOC to TOD distance, and a "backsolve" iterative routine is used).

**Table 3-5** Structure of master computing table

	Weight	Time	Distance
<b>MAIN MISSION:</b>			
<b>Ramp weight</b>			
1. Start-up and Taxi	<i>Fixed values for fuel &amp; time are used.</i>		<i>Distance is zero.</i>
<b>At brake release</b>			
2. Takeoff & Climb to 1500 ft	<i>Fuel and time determined from look-up table based on BRW.</i>		<i>Distance is zero.</i>
<b>At 1500ft</b>			
3. Climb to cruise altitude	<i>Fuel, time &amp; distance computed, based on instantaneous weight</i>		
<b>At TOC</b>			
4. Cruise	<i>Fuel, time &amp; distance computed, using "backsolve" routine, based on TOC to TOD distance.</i>		
<b>At TOD</b>			
5. Descent to 1500 ft	<i>Fuel, time &amp; distance computed, based on instantaneous weight.</i>		
<b>At 1500 ft</b>			
6. Approach	<i>Fixed values for fuel &amp; time are used.</i>		<i>Distance is zero.</i>
<b>Landed at Destination</b>			
13. Taxi & Shutdown	<i>Fixed values for fuel &amp; time are used.</i>		<i>Distance is zero.</i>
<b>Block weight/ time/ distance</b>			
<b>ALTERNATE:</b>			
<b>Depart for Alternate</b>			
7. Missed approach	<i>Fixed values for fuel &amp; time are used.</i>		<i>Distance is zero.</i>
<b>At 1500ft</b>			
8. Climb	<i>Fuel, time &amp; distance computed, based on instantaneous weight.</i>		
<b>At TOC for Alternate</b>			
9. Alternate cruise	<i>Fuel, time &amp; distance computed, using "backsolve" routine, based on TOC to TOD distance.</i>		
<b>At TOD for Alternate</b>			
10. Descent to 1500 ft	<i>Fuel, time &amp; distance computed, based on instantaneous weight.</i>		
<b>Overhead Alternate</b>			
11. Hold at 1500 ft	<i>Fuel, time &amp; distance computed, based on holding time.</i>		
<b>End Hold</b>			
12. Approach & Land	<i>Fixed values for fuel &amp; time are used.</i>		<i>Distance is zero.</i>
<b>Landed at Alternate</b>			

**Note:** The values in the shaded cells represent "point values" of the aircraft weight, cumulative time and distance, from the start. The values in the non-shaded cells represent the fuel consumed, time and distance for that leg (as identified in Fig. 3-1).



### 3.4.7 Program execution

To operate the program the selected file is opened from within the software package Lotus 123. It may be run in one of the three modes described in Table 3-1, depending on the nature of the problem and the input data. The user selects the required mode by clicking with the mouse on the appropriate software button, marked *Weight*, *Range* and *Fuel*, located on the master sheet (sheet A). A dialogue box displays a "busy" message during computation and a counter indicates the number of major iteration cycles performed. When the program terminates, the message indicates whether the convergence criterion was met.

The results, displayed on sheet A, are also appended to a template on sheet J, which is able to store up to 20 sets of results. This permits comparisons to be made between different runs, which are identified by a run number allocated sequentially and inserted at the top of each column in the table. A fourth software button on sheet A marked *Clear*, deletes all entries in the results table and prepares the table for a new study.



## 4 AIRCRAFT PERFORMANCE DATA

### 4.1 INTRODUCTION

The aircraft types used as turbulent baseline or reference models for the study were the Boeing 757-200 and Airbus 330-200. The B757 was selected as it had been the subject of a number of Boeing HLFC studies, and is the only aircraft of this class that has been flight tested with a HLF wing (see section C.6, Appendix C). The A330 aircraft type – which has about twice the Takeoff Weight (TOW) of the B757 and has a much longer range – is currently considered as a good candidate for a HLFC retrofit programme (along with its stablemate, the A340), should the technology continue developing and become financially viable during the life of the aircraft. Leading parameters for these two aircraft are indicated in Table 4-1 below.

As the performance characteristics of the aircraft models would not comply in all respects with those of the reference aircraft, a distinction is made herein, and the computer models are referred to as the *B757-200 class* aircraft and *A330-200 class* aircraft. An outline description of the aerodynamic and engine data for these models is presented in this chapter. Full details are given in Appendices F and G for the B757-200 and A330-200 classes of aircraft respectively.

**Table 4-1** *Leading parameters for selected baseline (reference) aircraft*

	<b>B757-200</b>	<b>A330-200</b>
Max. Takeoff Weight (MTOW)	115 660kg (255 000lb)	233 000kg (513 650lb)
Max. Zero Fuel Weight (MZFW)	85 280kg (188 000lb)	170 000kg (374 760lb)
Operating Empty Weight (OEW)	58 390kg (128 730lb)	120 500kg (265 640lb)
Max. structural payload*	26 890kg (59 270lb)	49 500kg (109 120lb)
Design (typical) mixed class seating	201	253
Range with design payload	3660nm (6782km)	6650nm (12322km)
Wing reference area	181.25m <sup>2</sup> (1951ft <sup>2</sup> )	361.58m <sup>2</sup> (3892ft <sup>2</sup> )
Max. fuel capacity	43630lt (11526USG)	139 090lt (36 750USG)

**Note:** See Tables F-1 and G-1 for referenced data on the B757-200 and A330-200 respectively.

\*Max. structural payload is MZFW minus OEW.

### 4.2 BOEING 757-200 CLASS AIRCRAFT

#### 4.2.1 Baseline aircraft database

Data from a Performance Engineer's Manual (PEM) (Boeing, undated) for a generic twin-engine jet, referred to as the B7G7 by Boeing, was used as the baseline database. The data is comparable to that of the first generation Boeing 757-200. The pertinent information included:

- (1) Drag polars;
- (2) Maximum climb thrust;
- (3) Corrected fuel flow;



- (4) Minimum idle in-flight thrust and fuel flow;
- (5) Fuel and the time from brake release to 1500ft;
- (6) Holding speeds at 1500ft.

The data was entered into a series of spreadsheet look-up tables. After validating the basic program (described in section 4.4), the data was modified to better represent the current generation B757-200 aircraft. An overview of the data and the methodology adopted to adjust / validate the data are presented in this section. Full details are contained in Appendix F.

#### 4.2.2 Aerodynamic data

The aerodynamic data was taken directly from the B7G7 PEM. The drag data was included in the database as a table of  $C_D$  values against  $C_L$  values (in steps of 0.05), for Mach numbers between 0.30 and 0.70 in steps of 0.05, and then from Mach 0.72 to 0.87 in steps of 0.1. The drag polars at selected Mach numbers are shown in Fig. 4-1.

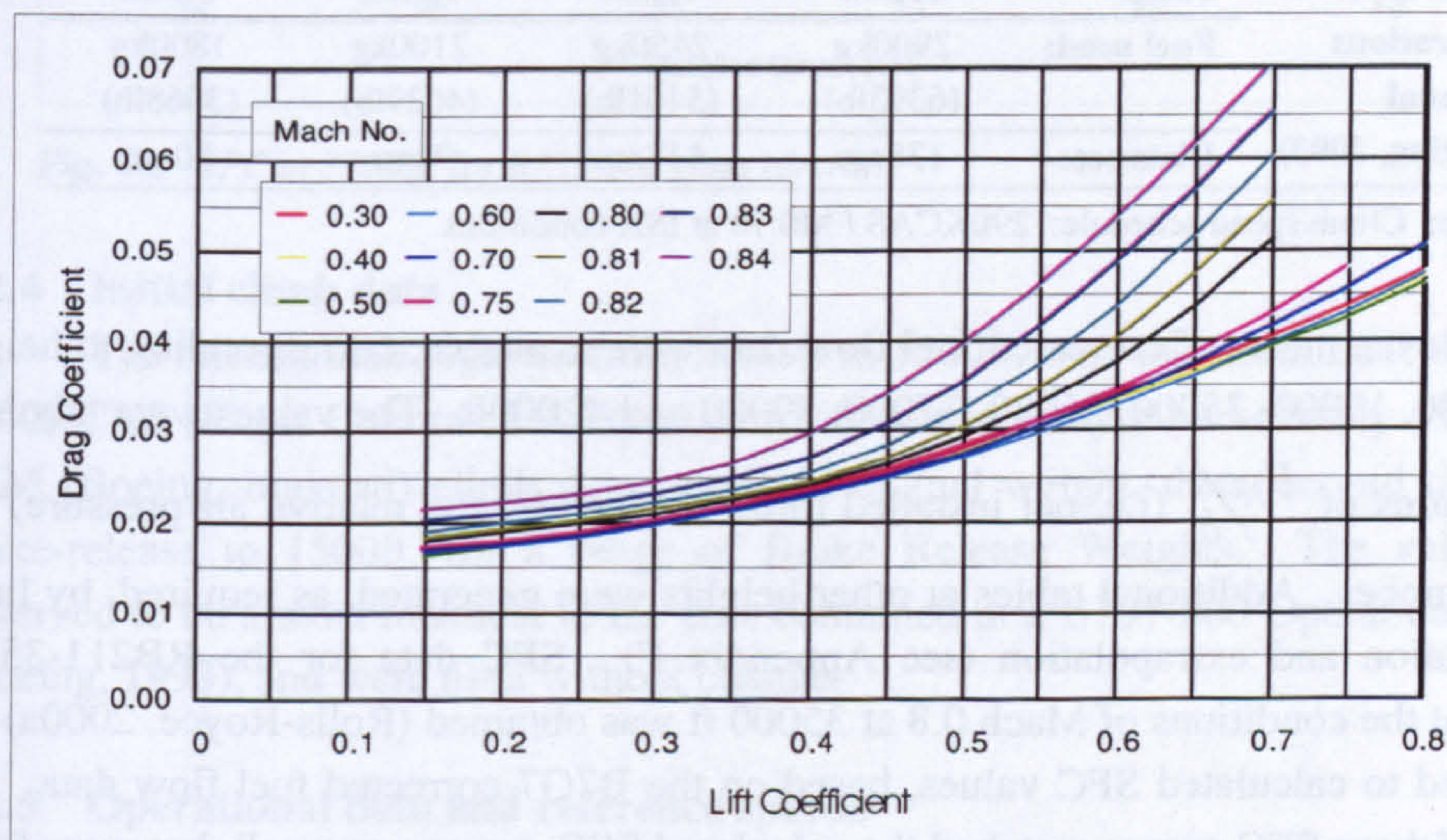


Fig. 4-1 Drag polars used for B757-200 class aircraft

#### 4.2.3 Engine data

The B757-200 has been fitted with three versions of the Rolls-Royce RB211-535 and two Pratt and Whitney 2000 series engines (see Table F-2, Appendix F). The engine data in the B7G7 PEM closely matched that of the RB211-535C engine in terms of SFC and thrust (Rolls-Royce, 1998). The approach adopted was to use this database as a reference, and to scale the data to get a database as close as possible to the more modern variant of this engine, the RB-211-535E4. This facilitated the en route performance of the computer model to be compared directly to that of the current generation B757-200.

The rate of climb (ROC) of an aircraft is dependent on the excess of thrust to drag, for a given weight and speed. (See equation [E-25], Appendix E.) Providing that



the drag data is correct, calculated time-to-climb values and distance to TOC values (for various weights) provide a mechanism to assess the climb thrust data. The computer program was used to calculate the time to climb to FL 350 (Flight Level 350), the fuel used and the distance covered for a range of Brake Release Weights. Following a number of trials, a scaling factor of 1.080 was selected, as this gave the best overall results (see Table 4-2). Also indicated in the table are the corresponding values taken from a B757-200 Operations Manual (Boeing, 1993), which was used as a reference.

**Table 4-2 Comparison of climb results from brake release to 35000ft**

Brake Release Weight ->		115000kg (253518lb)	105000kg (231473lb)	95000kg (209428lb)	85000kg (187383lb)
Calculated using performance model*	Time:	23.1min	19.0min	16.1min	13.7min
	Fuel used:	2875kg (6338lb)	2408kg (5309lb)	2054kg (4529lb)	1747kg (3852lb)
	Distance:	139.6nm	112.7nm	93.5nm	78.3nm
From B757 Operations Manual (Boeing, 1993)	Time:	23min	19min	16min	14min
	Fuel used:	2900kg (6393lb)	2450kg (5401lb)	2100kg (4629lb)	1800kg (3968lb)
	Distance:	138nm	113nm	94nm	80nm

\*Note: Climb speed schedule: 290KCAS / M0.78 at ISA conditions.

Seven tables of corrected fuel flow data were available, corresponding to heights of 0, 5000, 10000, 35000, 36089, 37000, 39000 and 42000ft. The values were tabulated as functions of  $F_N/\delta$  (i.e. net installed thrust divided by the relative air pressure) and Mach number. Additional tables at other heights were generated, as required, by linear interpolation and extrapolation (see Appendix F). SFC data for the RB211-353E4 engine at the conditions of Mach 0.8 at 35000 ft was obtained (Rolls-Royce, 2000a) and compared to calculated SFC values, based on the B7G7 corrected fuel flow data. The shape of these SFC curves matched the calculated SFC curves very well, but were found to be about 7% lower than the calculated values at the minimum point (i.e. the bottom of the "loop"). The ratio of the quoted SFC values of the RB211-535E4 and RB211-535C engines in cruise (see Table F-2, Appendix F) is 0.926. The B7G7 fuel flow data was scaled by this amount to bring it close to that of the baseline engine.

To validate the resulting trial database the trip fuel required for four fixed distances, at a given aircraft weight, was computed using the computer program. The results were compared to published values from a B757-200 Operations Manual (Boeing, 1993) for the identical mission conditions. The scaling factor was then revised in an iterative manner, until a good agreement between the trip time and trip fuel values was obtained. The selected scaling factor of 0.937 yielded the results presented later in Table 4-3. Although the computer program does not use SFC data implicitly (as it is based on the use of corrected fuel flow), it proved useful to establish these values at selected altitudes, for comparative purposes. An example is given in Fig. 4-2.



Small changes (of the order of 10%) to the engine idle thrust and fuel flow were observed to have a negligible impact on the computed trip fuel. The B7G7 data for idle thrust was thus used without change.

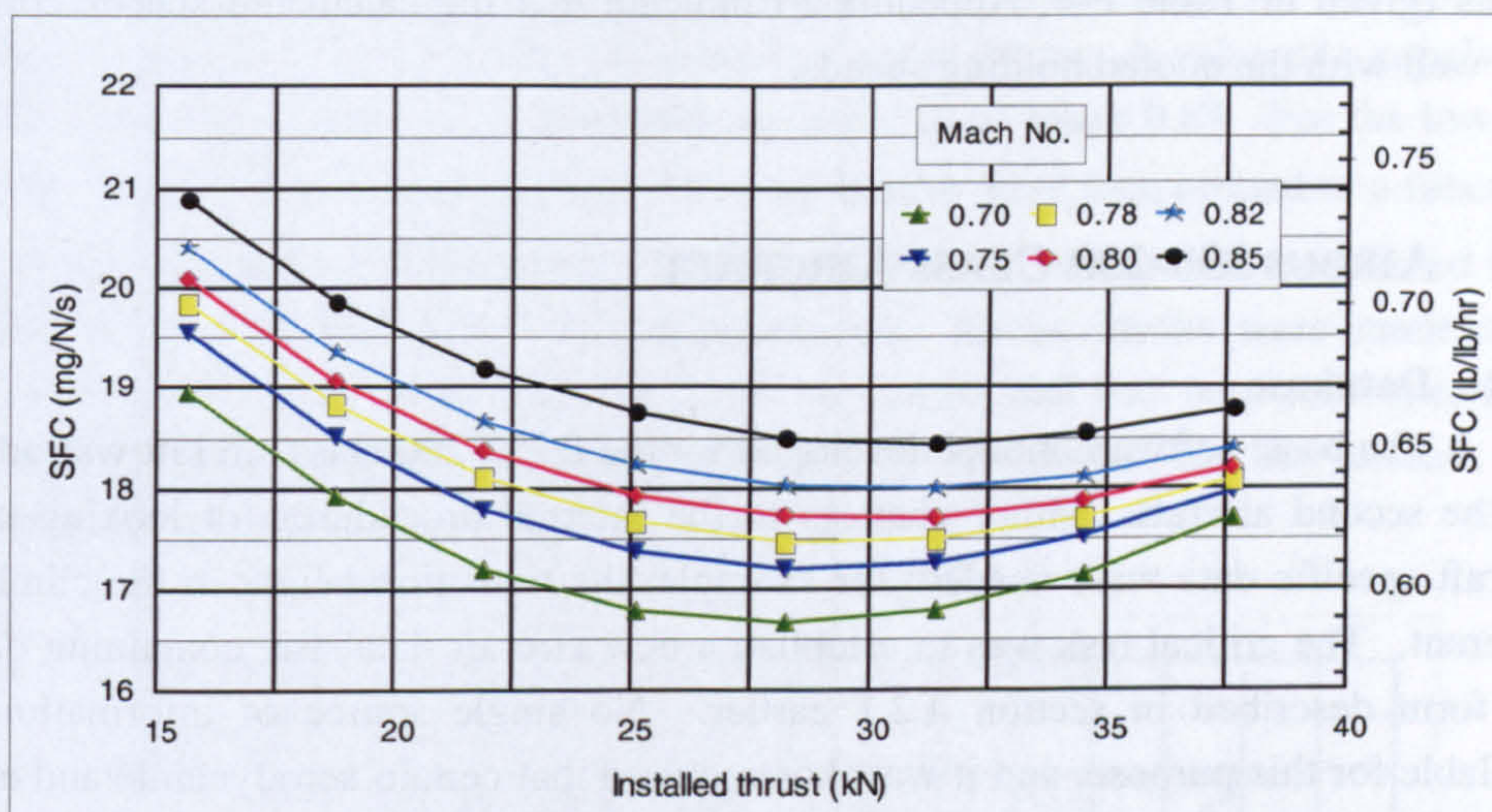


Fig. 4-2 SFC at 35000ft for B757-200 class aircraft

#### 4.2.4 Initial climb data

The initial climb segment from takeoff to 1500ft, with the aircraft accelerating to ~250KCAS (Knots Calibrated Airspeed), is difficult to analyse numerically. The B7G7 PEM (Boeing, undated) climb data consisted of fuel weight, distance and time, from brake-release to 1500ft, for a range of Brake Release Weights. The values were observed to be almost identical to the data contained in a B757-200 Operations Manual (Boeing, 1993), and were used without change.

#### 4.2.5 Operational data and reference speeds

The climb speed schedule<sup>11</sup> adopted for the B757-200 class aircraft was 250/290/M0.80. The FAA stipulates that a speed of 250KIAS (Knots Indicated Air speed) should not be exceeded below FL 100 (Boeing, 1993) and for this reason a 250KCAS speed limit was adhered to in the schedule. The height at which 290KCAS equalled Mach 0.80 was determined to be ~32100ft.

The speed for the alternate leg was set as the Maximum Range Speed (MRS). As this value was not indicated in the available documentation, the Specific Air Range (SAR) was calculated for FL 200 for different aircraft weights, typical of that which would be expected at the end of the cruise. From plots of these results (Fig. F-10, Appendix F), a speed of Mach 0.55 was deduced as the MRS.

<sup>11</sup> Climb speed schedule: The abbreviation 250/290/M0.80 implies that the aeroplane climbs at a CAS of 250kt until FL 100 is reached. Above this height the speed is held at 290kt CAS in the climb until Mach 0.80 is reached, and thereafter a constant Mach number is maintained. (See section E.3.3, Appendix E.)



The recommended holding Mach number at 1500ft for a range of aircraft weights was provided in the B7G7 PEM (Boeing, undated). As a cross-check with the aerodynamic data, the *green dot* speeds<sup>12</sup> were determined for these conditions. The results (given in Table F-4, Appendix F) indicate that the calculated speeds correlate very well with the quoted holding speeds.

### 4.3 AIRBUS 330-200 CLASS AIRCRAFT

#### 4.3.1 Database

The basic software model developed for the B757-200 class aircraft was adapted for the second aircraft. Minor changes to the internal procedures for looking up the aircraft specific data were needed; for example, the transition height in the climb was different. The critical task was to establish a new aircraft database, containing data of the form described in section 4.2.1 earlier. No single source of information was available for this purpose, and it was thus required that certain aerodynamic and engine data be "back-engineered" from published performance values.

The climb speed schedule, cruise speed and holding speeds were obtained from an A330 Operating Manual (Airbus, undated). The most important information for the purpose of calculating the trip fuel is the drag polar and the fuel flow data, and to a lesser extent, the climb thrust data. The database was established in an iterative manner, using scaled B7G7 values as input to the computer program, and then conducting checks of the results against available performance data. The process is illustrated in Fig. 4-3 and is explained in the sections that follow.

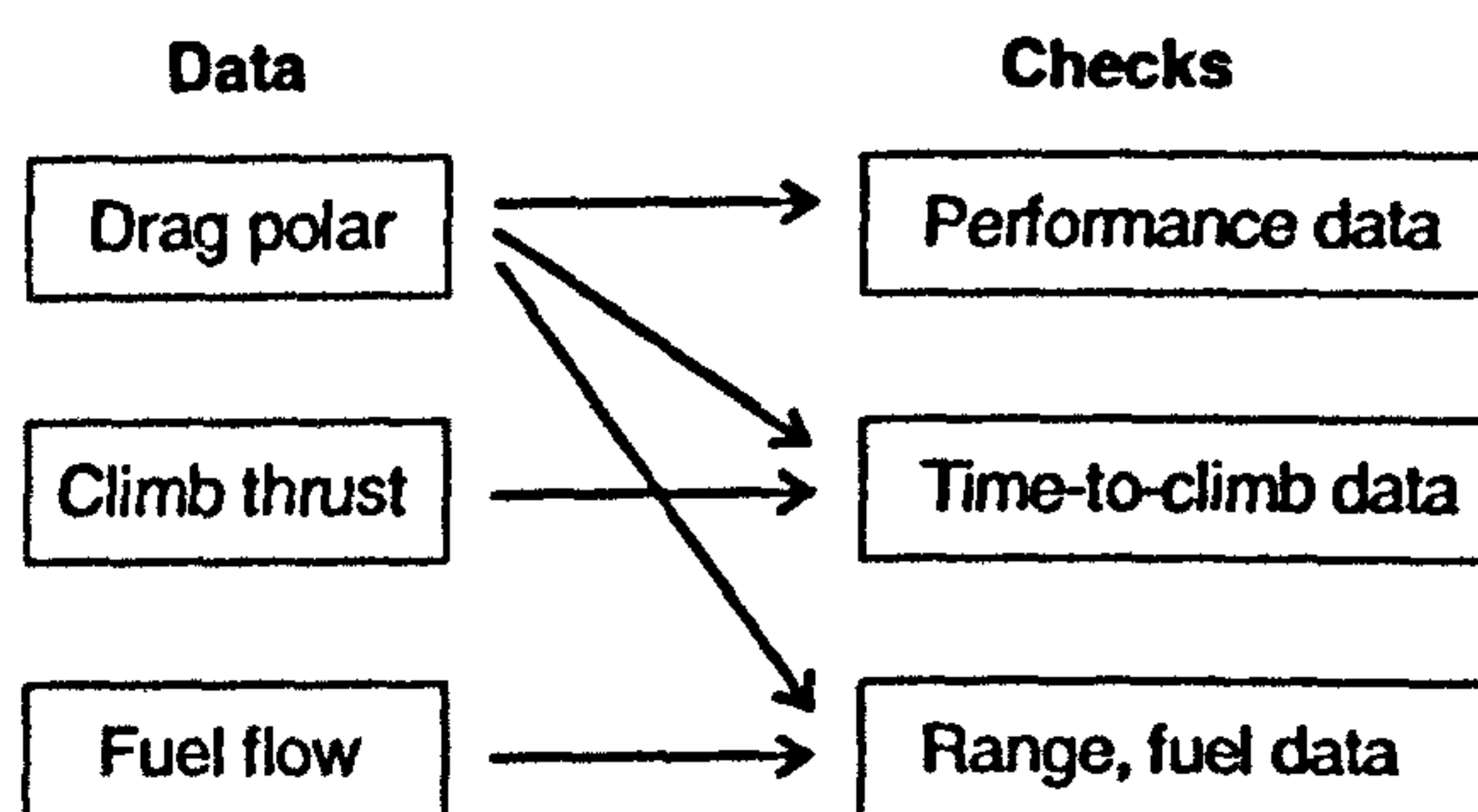


Fig. 4-3 Process adopted for establishing the database for the A330-200 class aircraft

#### 4.3.2 Drag polar

The approach adopted was to:

- (1) Develop a mathematical model of the B7G7 PEM drag data;
- (2) Adjust the calculated coefficients of this model to suit the A330-200 data.

A generic drag polar of the following form was used:

<sup>12</sup> Green dot speed: Operational reference speed that gives the best lift-to-drag ratio for the aeroplane at a particular mass.



$$C_D = K_1 + K_2 C_L^2 + K_3 C_L^n \quad \text{--- [4-1]}$$

Details of this drag representation are given in section 7.3. Coefficients  $K_1$ ,  $K_2$ ,  $K_3$  and  $n$  were determined for each Mach number ( $M$ ) where data for the B7G7 was available, using the "least squares" technique of curve fitting. A value of  $n$  equals 6 was found to give good correlation for Mach numbers up to Mach 0.84. For the low speed drag polar  $K_3$  was set equal to zero. The coefficients were then plotted as a function of Mach number, smoothed and scaled / adjusted to suit the data points established for the A330-200 class aircraft (Fig. G-2, Appendix G). Cross checks were made against available performance data, e.g. the best  $L/D$  ratio and the best  $L/D$  speed were determined and compared to the quoted holding conditions for the aircraft. The resulting drag polars are shown in Fig. 4-4 below.

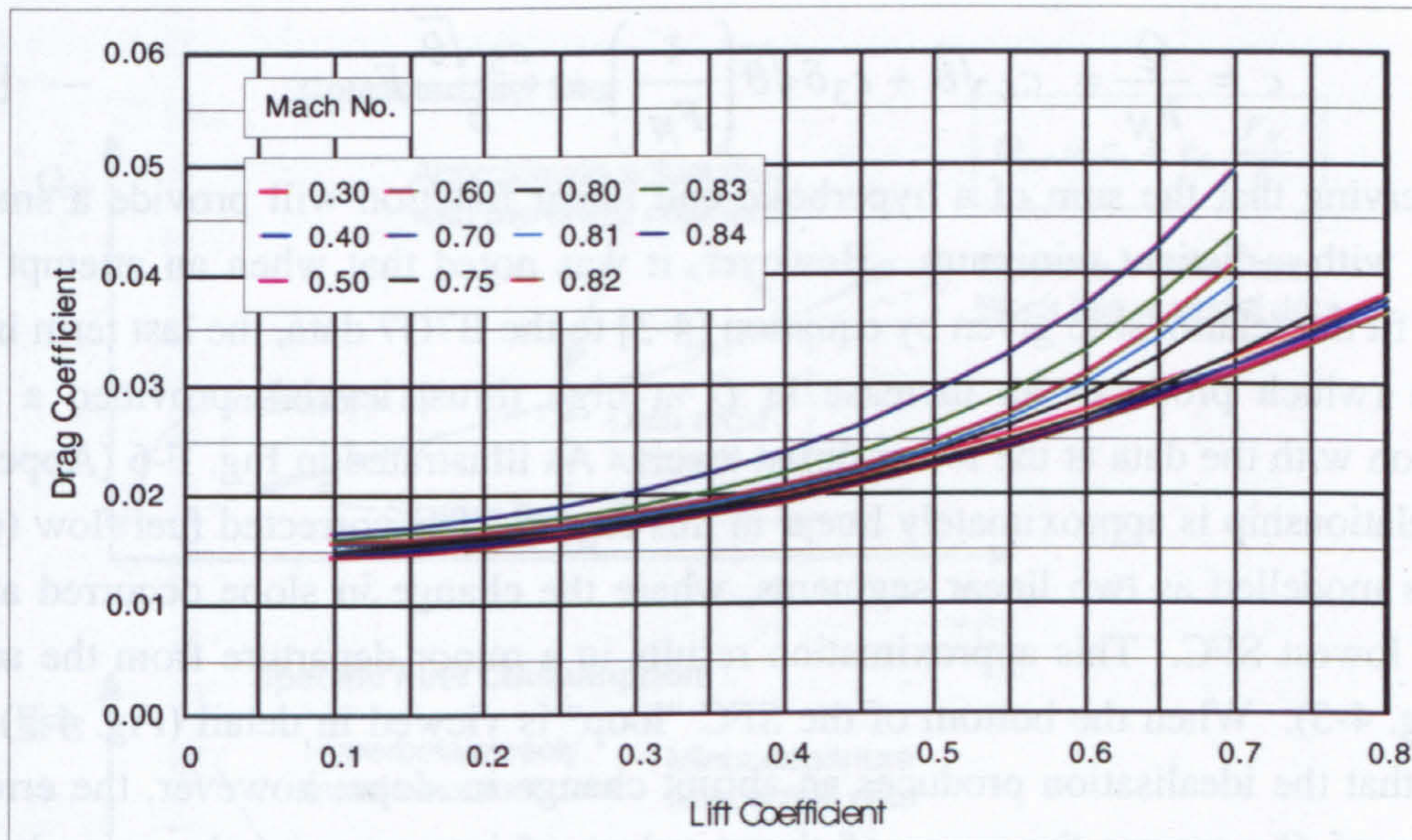


**Fig. 4-4** Estimated drag polars for A330-200 class aircraft

### 4.3.3 Engine data

The A330-200 can be fitted with three engines, which in terms of performance are very similar. Leading parameters of these engines are indicated in Table G-3 (Appendix G). The Rolls-Royce Trent 772 was selected as the baseline engine for the purposes of the performance model. The thrust of this engine is approximately 1.7 to 1.9 times greater than that of the RB211-535C, evaluated at the climb and takeoff conditions respectively. The B7G7 climb thrust data was scaled to produce a trial data table for the A330-200 class aircraft and installed in the software model. Following an identical approach to that described in section 4.2.3, the time and distance to reach a specified cruising altitude were calculated and compared to quoted A330-200 Operating Manual values (Airbus, undated). The scaling factor of 1.77 yielded the best results.



ESDU 73019 (1982) indicates that for a range of turbo-jet and turbo-fan engines, the manufacturers data for fuel flow at a given value of  $M$ , may be satisfactorily expressed by the relationship:

$$\frac{Q}{\delta\sqrt{\theta}} = c_3 + c_4\left(\frac{F_N}{\delta}\right) + c_5\left(\frac{F_N}{\delta}\right)^2 \quad \text{--- [4-2]}$$

where the fuel flow ( $Q$ ) and the net thrust ( $F_N$ ) are both corrected for atmospheric conditions ( $\delta$  and  $\theta$  represent the standard atmospheric pressure and temperature ratios respectively). The coefficients  $c_3$ ,  $c_4$  and  $c_5$  are constants for a specific engine and must be determined for each value of  $M$  of interest. It was noted that one advantage of this representation is that it provides the correct form of the SFC "loops", when plotted as a function of thrust. This is evident by re-writing equation [4-2] in terms of the Specific Fuel Consumption ( $c$ ):

$$c = \frac{Q}{F_N} = c_4\sqrt{\theta} + c_3\delta\sqrt{\theta}\left(\frac{1}{F_N}\right) + \frac{c_5\sqrt{\theta}}{\delta}F_N \quad \text{--- [4-3]}$$

and observing that the sum of a hyperbolic and linear function will provide a smooth function with a distinct minimum. However, it was noted that when an attempt was made to fit the relationship given by equation [4-3] to the B7G7 data, the last term in the equation (which produces an increase in  $Q$  at high thrust levels), provided a poor correlation with the data at the lower thrust levels. As illustrated in Fig. F-6 (Appendix F) the relationship is approximately linear in this region. The corrected fuel flow ( $Q_{cor}$ ) was thus modelled as two linear segments, where the change in slope occurred at the point of lowest SFC. This approximation results in a minor departure from the actual data (Fig. 4-5). When the bottom of the SFC "loop" is viewed in detail (Fig. 4-7) it is evident that the idealisation produces an abrupt change in slope; however, the error in the value of  $Q_{cor}$  across the range of thrust values of interest, was shown to have a negligible influence on the trip fuel. For the lower part of the line the equation:

$$Q_{cor} = \frac{Q}{\delta_t\sqrt{\theta_t}} = c_1 + c_2\left(\frac{F_N}{\delta}\right) \quad \text{--- [4-4]}$$

was used. This has a similar form to that recommended by Bert (1999). A "least squares" curve fit was used to determine  $c_1$  and  $c_2$  values for the range of Mach number and heights of interest for the B7G7 data, in order to establish the nature of the relationships. These coefficients were adjusted to suit available information for the baseline engine, thus establishing a trial database for the A330-200 class aircraft. It is evident from equation [4-4] that  $c_2$  has the same units as SFC and represents the slope of the line of fuel flow versus thrust. If  $c_1$  was equal to zero (or very small) then  $c_2$  relates directly to the SFC. Trial values of  $c_2$  were obtained by scaling the B7G7 data by a factor of 0.93, based on the fact that the more modern engine was about 7% more efficient than the older engine. (The details are given in section G.4, Appendix G.)



The cruise sub-routine of the computer performance model was then used with the trial fuel flow database to determine the fuel required for various cruise distances. These results were compared to the integrated range data, given in an A330 Flight Crew Operating Manual (Airbus, undated). Adjustments were made to the  $c_2$  fuel burn coefficients, until a correlation of within 1% was achieved. The resulting corrected fuel flow values for 35000ft are shown in Fig. 4-6. As a further check the SFC was determined for various speeds at a height of 35000ft (Fig. 4-7). The resulting plot of SFC versus thrust for Mach 0.82 showed a minimum at 50.3kN (11300lb), with a corresponding SFC value of 16.9mg/N/s (0.598lb/lb/hr). At a cruise thrust of 53.4kN (12000lb) the SFC was 17.1lb/lb/hr (0.602lb/lb/hr). These SFC values (representing the installed engine, with power and standard bleed air off-take) compared very well with the value of 16.5mg/N/s (0.584lb/lb/hr) given in Table G-3 (Table G) for the uninstalled engine, and the ~ 3% difference was deemed to be approximately correct.

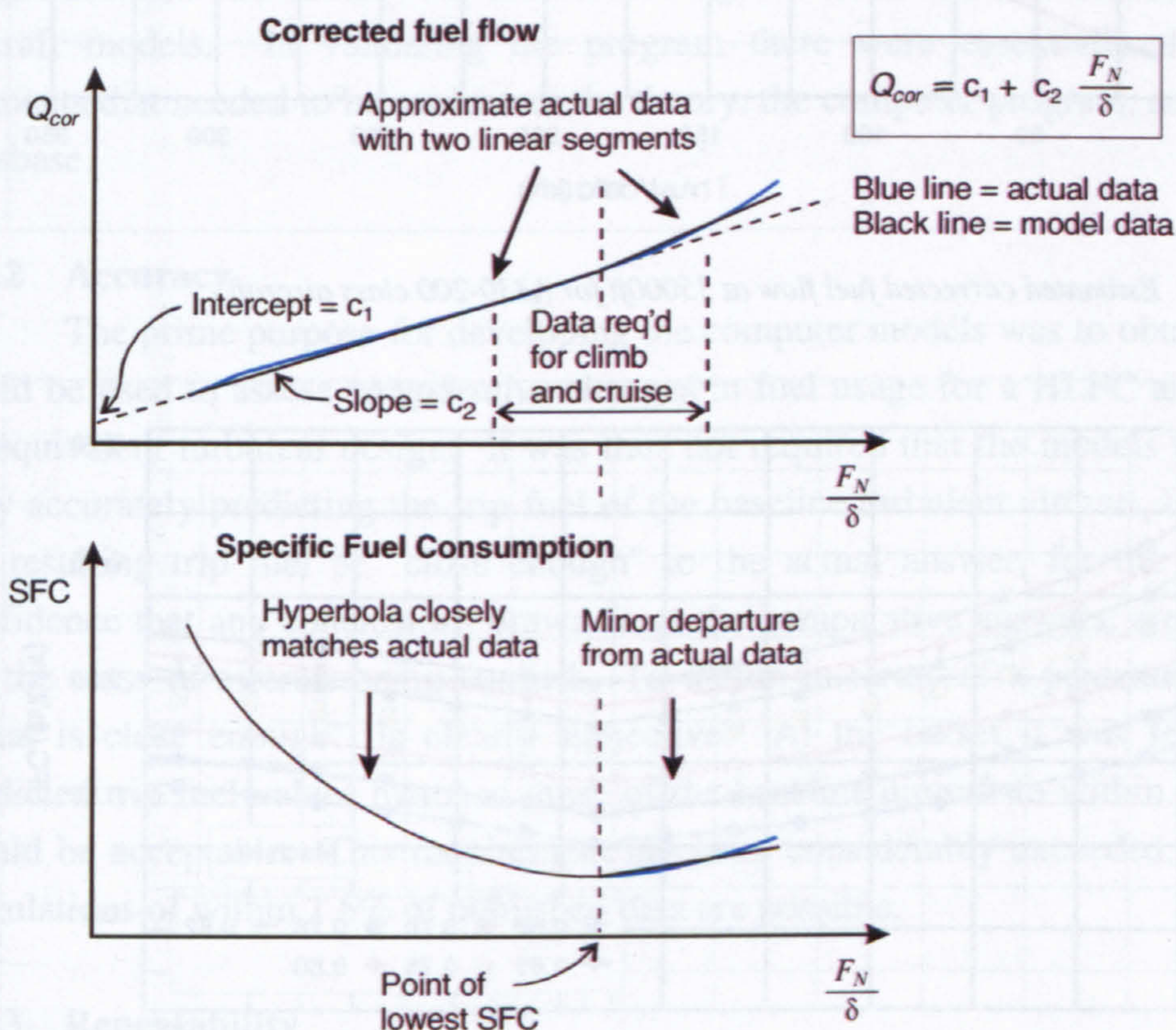


Fig. 4-5 Sketch illustrating actual and modelled Corrected fuel flow and SFC data

#### 4.3.4 Initial climb data

The initial climb data for the A330-200 class aircraft was based on the assumption that the time for the aircraft to accelerate from rest to 1500ft, would not vary significantly within this class of medium size twin-turbofan airliner. (Further details on the takeoff and climb-out are provided in section E.6, Appendix E and section G.5, Appendix G.) The fuel required for this portion of the mission was obtained by scaling the B757-200 class aircraft data by a factor of 1.77 (which was the value selected for the



climb thrust data). As the fuel consumed during this short segment of the mission is very small compared to the rest of the mission, this approximation was adequate. The resulting fuel and time data from brake-release to 1500ft are indicated in Fig. G-9 (Appendix G) for a range of Brake Release Weights.

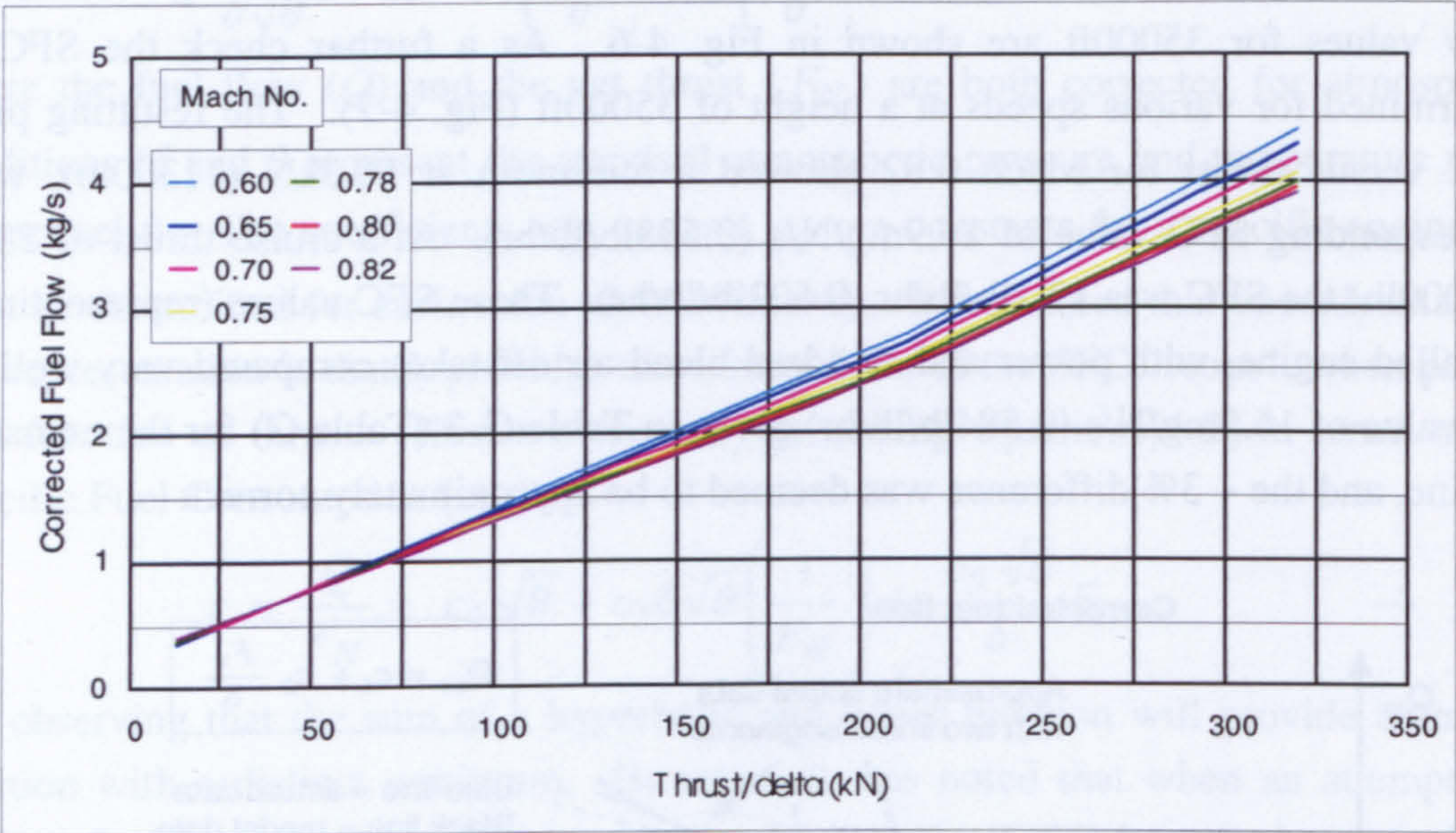


Fig. 4-6 Estimated corrected fuel flow at 35000ft for A330-200 class aircraft

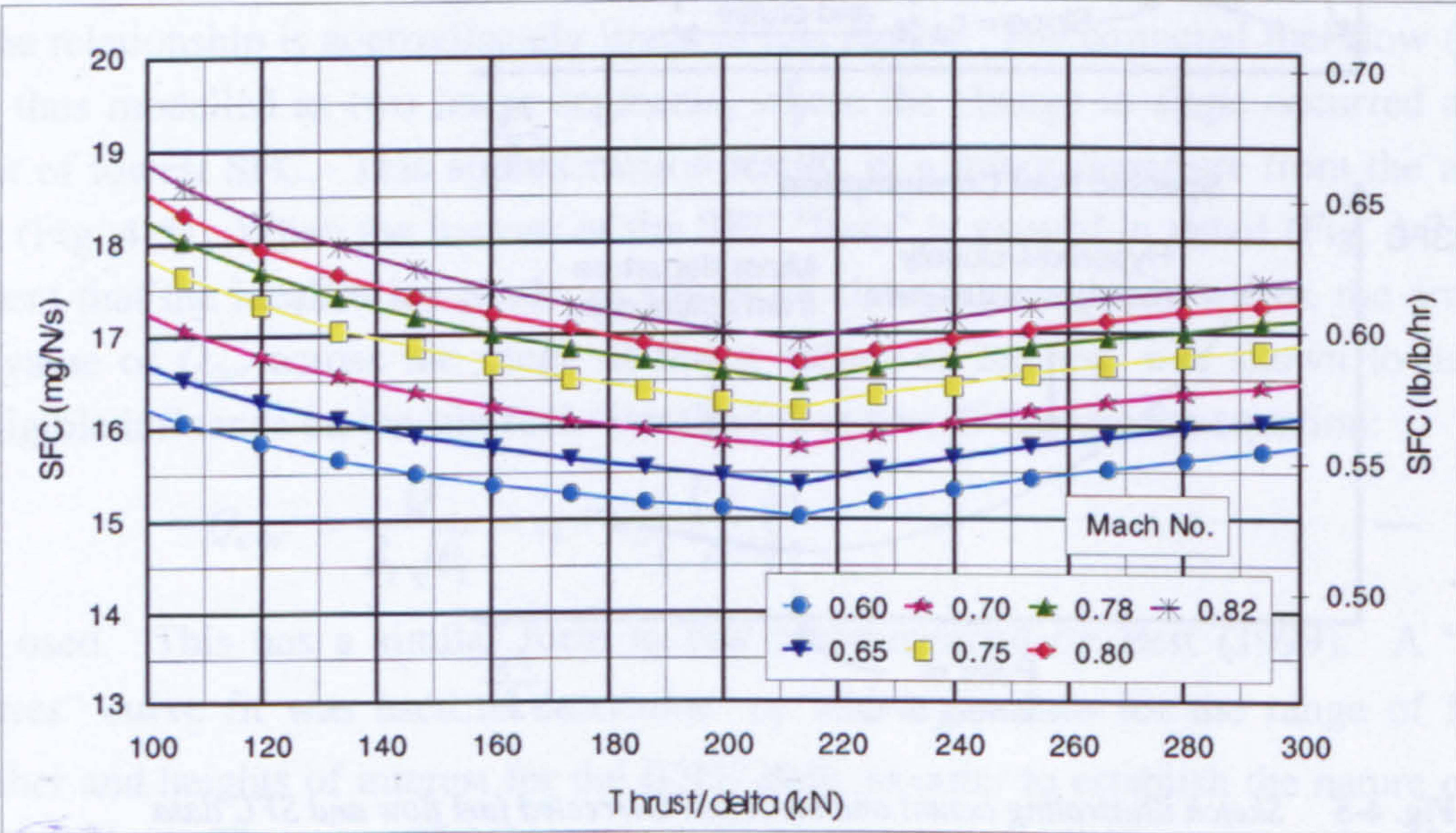


Fig. 4-7 Estimated specific fuel consumption at 35000ft for A330-200 class aircraft

4.3.5 Operational data and reference speeds

The climb speed schedule for the A330-200 class aircraft was 250/300/M0.80. The first transition height was 10000ft and the second transition was at ~31000ft (i.e. the height at which Mach 0.80 is reached for 300KCAS). In the identical manner to that described in section 4.2.5 for the B757-200 class aircraft, the SAR was calculated for



three aircraft weights, in order to establish the best cruise speed for the alternate leg. From these results (presented in Fig. G-10, Appendix G) it was evident that the MRS at 25000ft falls within the range Mach 0.58 to Mach 0.62. Mach 0.60 was selected for the alternate leg for the performance analysis.

The holding speeds were set as the green dot speeds, determined by plotting the  $L/D$  ratio against Mach number, for the range of weights of interest, at the holding height of 1500ft (Fig. G-11, Appendix G).

## 4.4 MODEL VALIDATION

### 4.4.1 Validation aspects

The general requirements, indicated in Table 3-2, i.e. accuracy, repeatability, robustness and run time, were assessed using the databases established for the two aircraft models. In validating the program there were essentially three separate elements that needed to be evaluated: the theory, the computer program, and the aircraft database.

### 4.4.2 Accuracy

The prime purpose for developing the computer models was to obtain a tool that could be used to assess *comparative* changes in fuel usage for a HLFC aircraft against an equivalent turbulent design. It was thus not required that the models be capable of very accurately predicting the trip fuel of the baseline turbulent aircraft, but rather that the resulting trip fuel be "close enough" to the actual answer, for the user to have confidence that any conclusions drawn from the comparative answers, are indeed valid for the class of aircraft being studied. To define in terms of a percentage deviation, "what is close enough", is clearly subjective. At the outset it was felt that if the predicted trip fuel values matched those of the baseline aircraft to within 5%, then this would be acceptable. This requirement has been considerably exceeded, and trip fuel calculations of within 1.5% of published data are possible.

### 4.4.3 Repeatability

Very small changes in the trip fuel can result from the failure of the HLFC system to operate for a small portion of the mission, and it is these small changes that are important in assessing the impact of the system failure. Hence, it was required of the program that it was capable of repeating the calculation with a high degree of accuracy. As the computer program functions by iterative solution, the result depends on the convergence criterion, set in the computer code. The general criterion used was that the calculated BRW should match the one used to predict the fuel usage to within 0.01%. Very small variations in the calculated trip fuel would thus result from different runs. It was useful to explore the magnitude of these variations, which were observed to



depend on the trip fuel. The ratio of the trip fuel weight to the BRW is a function of the trip distance. For a short trip distance of 1000nm (for the B757-200 class aircraft) the ratio is ~0.08. This ratio increases to ~0.34 for a 6600nm trip distance for the A330-200 class aircraft. The variation in answers of the trip fuel calculation would thus not exceed 0.1% for short distances and 0.03% for longer distances, based on the established convergence criterion (i.e. that the percentage variation in BRW would not exceed 0.01%). It was concluded that this criterion produced answers that were sufficiently similar for comparisons to be made between different runs.

#### **4.4.4 Robustness**

Robustness implies that the program is reliable, does not crash frequently and if it does crash, that it does not damage the source code in any way that prevents the program from running again. During program development, the main reason for the spreadsheet software to crash was due to a solver routine seeking a mathematical answer that was not possible. This tended to occur when the data being sought was outside of the range of values in the look-up tables. Within the bounds of reasonable input data, the program has been demonstrated to be extremely robust.

#### **4.4.5 Run time**

The run time depends on the convergence criterion (see discussion on repeatability above) and the proximity of the input TOC to TOD distance (entered by the user) relative to the final result. Run times are between 5 and 50 seconds (on a 500MHz PC). A cut-off at 50 outer loop iteration cycles was found to ensure that the program terminated if convergence was not achieved in less than about one minute.

#### **4.4.6 Theory**

The theory required for en route performance analysis was largely developed from the fundamental principles of mechanics of flight, as described in Appendix E. This was checked against reliable / validated sources. Use was made of Jet Transport Performance Methods (Boeing, 1989), Boeing Performance Course Notes (Boeing, 1996) and ESDU methods (ESDU 73018, 1980; ESDU 73019, 1982). Hand calculations for the climb, cruise, descent and hold segments of the mission, were first undertaken using Boeing PEM data and checked, where possible, against Boeing supplied solutions.

#### **4.4.7 Computer code**

The approach adopted was to develop a single spreadsheet table to analyse each leg of the mission separately (i.e. climb, cruise, descent and hold). Checks were made against the hand calculations (described earlier) for each leg of the mission. Many of the subroutine calculations could be checked directly against results presented in the Boeing Performance Course Notes (Boeing, 1996).



The individual spreadsheet tables were then integrated by means of the master computing table (see Table 3-5) and macro code written to enable the program to run in an iterative manner. To validate this element of the work, a second independently written software program was produced by another researcher (Straubinger, 2000). Although Straubinger worked under the direct supervision of the author, the actual software was independently written from the first model (which was not available to him). When the second model was evaluated using the B7G7 database, it yielded trip fuel results that differed by less than 0.1%, compared to the original model for the mission distances of interest (Schmidt, 2001).

#### **4.4.8 Data: B757-200 class aircraft**

The required trip fuel for various mission distances was initially calculated using the B7G7 database. These results were observed to be a few percent greater than comparative values for a current generation Boeing 757-200 as given in an Operations Manual (Boeing, 1993). A credible explanation for the differences between the results came from the observation that the Operations Manual was for an aeroplane fitted with modern RB211-353E4 engines, and the Boeing B7G7 engine data corresponded to an older engine (which, as mentioned earlier in section 4.2.3, would be comparable to the RB211-353C engine). By adjusting the fuel flow data (as described in section 4.2.3), the engine database was brought closer to that of the more modern engine.

Table 4-3 contains the results of five computer runs performed in the range mode (using the final revision of the database), for fixed trip distances of 1000, 1500, 2000, 2500 and 2900nm. Appended to the bottom of the table are the corresponding trip time and trip fuel values from the B757-200 Operations Manual (Boeing, 1993). In the Operations Manual, the trip fuel is based on the landing weight and does not consider the alternate leg and reserve fuel; however, the computer program requires these details in order to complete the computation. In assessing the trip fuel values, it should be noted that the Operations Manual contains procedures for rapidly obtaining approximate results. The "simplified flight planning" method is presented on a single chart and one graduation of the smallest scale on the fuel axis corresponds to 200kg. Assuming a one-graduation error margin, the trip fuel values from the Operations Manual should be considered as  $\pm 200\text{kg}$  (440lb). The trip time should similarly be indicated as  $\pm 6\text{min}$ . The calculated trip times are seen to be consistently less than the values from the Operations Manual and are within the 6 minute error band. This observed difference could possibly be due to different mission allowances (see Table H-12, Appendix H), which were not explicitly stipulated in the Operations Manual. The difference in the trip fuel values is shown to be no more 1.5%. These results provide reassurance that the model data is reasonably accurate.

Using the computer model the corners of the payload-range chart were calculated for the B757-200 class aircraft (see Fig. 4-8). This was necessary to establish the reference conditions for the sensitivity analysis presented in Chapter 6.



**Table 4-3**    *B757-200 class aircraft mission results (program run in Range mode)*

Run Number		1	2	3	4	5
Ramp Weight	kg	98404	102541	106877	111441	115314
Brake Release Weight	kg	98177	102314	106650	111215	115088
Payload	kg	26886	26886	26886	26886	26886
OEW	kg	58394	58394	58394	58394	58394
HLFC drag reduction		0.0000	0.0000	0.0000	0.0000	0.0000
HLFC fuel flow increase	%	0.00%	0.00%	0.00%	0.00%	0.00%
Contingency	%	3.0%	3.0%	3.0%	3.0%	3.0%
Range (Trip distance)	nm	1000	1500	2000	2500	2900
Trip fuel	kg	8538	12547	16753	21180	24932
Trip time	hr : min	02:22	03:28	04:33	05:38	06:31
Block fuel	kg	8946	12956	17161	21589	25340
Block time	hr : min	02:46	03:52	04:57	06:02	06:55
Alternate	nm	200	200	200	200	200
Hold time	hr : min	00:30	00:30	00:30	00:30	00:30

**Fuel Breakdown**

Start-up and taxi	kg	227	227	227	227	227
Trip fuel	kg	8538	12547	16753	21180	24932
Alternate and land	kg	2555	2557	2559	2561	2563
Final reserve (Holding)	kg	1548	1550	1551	1553	1561
Contingency fuel	kg	256	376	503	635	748
Tankered fuel	kg	0	0	0	0	0
Total fuel on board	kg	13124	17257	21593	26157	30030

**Trip Fuel Breakdown**

Takeoff, climb to 1500 ft	kg	374	393	412	432	451
Climb to cruise altitude	kg	1798	1932	2090	2280	2471
Cruise	kg	5897	9754	13783	18000	21541
Descent to 1500 ft	kg	287	287	287	287	288
Approach	kg	181	181	181	181	181
Total trip fuel	kg	8538	12547	16753	21180	24932

**Comparison to B757-200**

Trip time (Boeing, 1993)	hr : min	02:18	03:24	04:30	05:36	06:33
Difference		-2.90%	-1.96%	-1.11%	-0.60%	0.50%
Trip fuel (Boeing, 1993)	kg	8640	12740	16940	21340	25040
Difference		1.2%	1.5%	1.1%	0.7%	0.4%

**Notes:**

1. For the computer program, the OEW was taken as the "typical" OEW indicated by Boeing (1999b). Reserves were specified as International reserves with a 3% contingency (en route trip allowance), an overshoot, 200nm alternate diversion and a 30min hold at 1500ft.
2. Mission: Climb at 250/290/M0.8; Cruise at M0.80, FL 350; Alternate climb at 250/270; Alternate cruise at M0.55, FL 200; ISA + 0°C, zero wind; Mission allowances as per Table H-12 (Appendix H).
3. The payload was the maximum structural payload of 26890kg (59270lb).
4. The program was run in aviation / British units with weights in pounds; final results converted to kg.
5. The B757-200 quoted trip fuel and trip time values were taken from a "simplified flight planning" procedure in the B757 Operations Manual (Boeing, 1993) and should be considered as ±200kg and ±6min respectively. The trip fuel was based on the landing weight and therefore does not consider the reserve fuel.
6. The upper part of the climb speed schedule was indicted as M0.78 in the B757-200 Operations Manual (Boeing, 1993), whilst the computer model used M0.80.



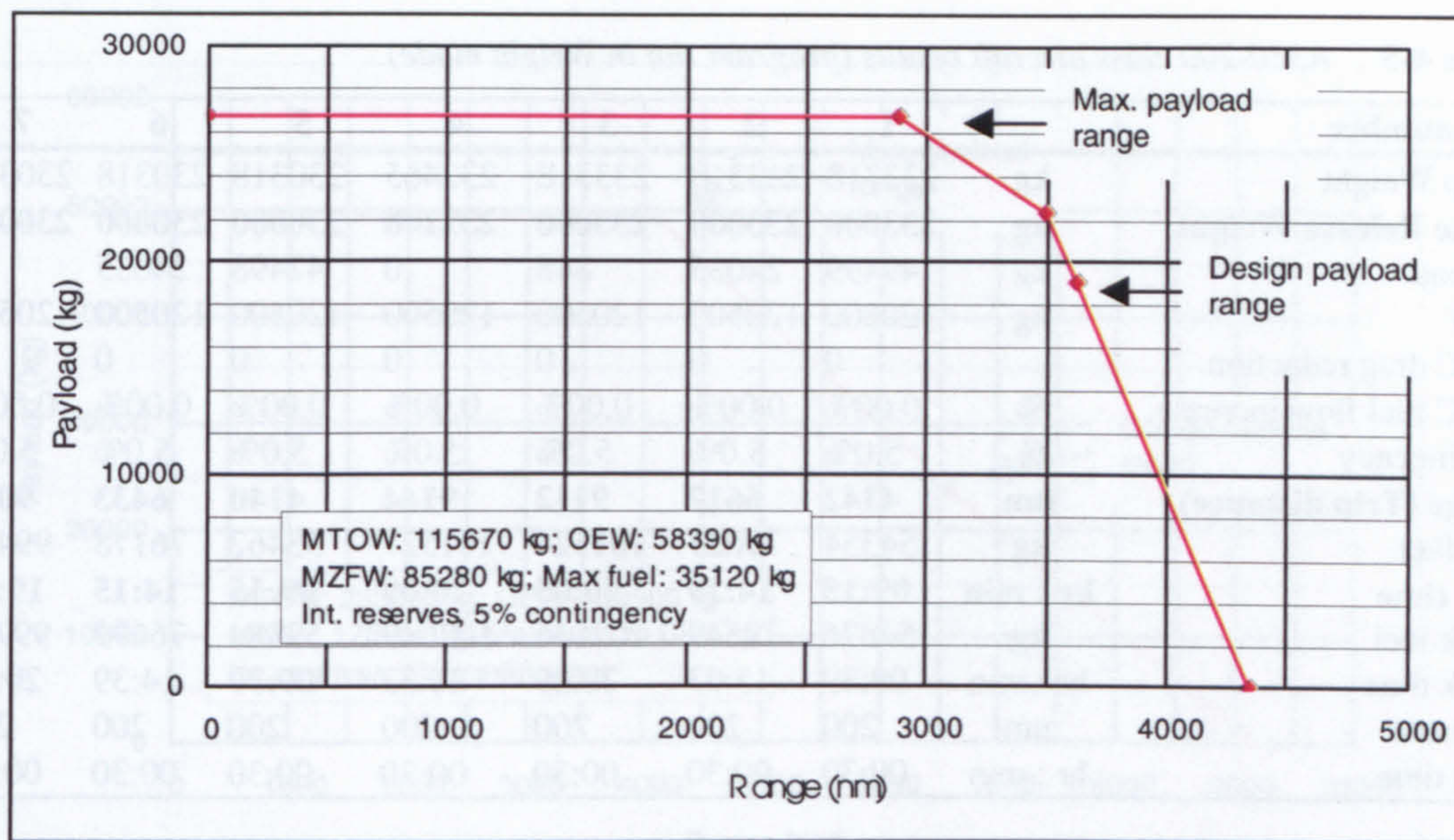


**Fig. 4-8** Payload-range chart for B757-200 class aircraft MTOW 115670kg (255000lb)

#### 4.4.9 Data: A330-200 class aircraft

A check of the accuracy of the model was undertaken, by comparing the results to those presented in the "Airbus 330 Briefings" (Airbus, 2000a). The corners of payload-range envelope were determined using the computer model for two aircraft variants, designated herein as variant A and B (see Table 4-4). In this case the BRW was known and trip distance had to be determined. The results table from the performance analysis has been reproduced in Table 4-5. Appended to the bottom of the table are values from the A330-200 payload-range diagram (Airbus, 2000a). The range values of 6650nm and 6450nm (for variants A and B respectively) were indicated explicitly on the graph for the baseline passenger configuration (given as 253 passengers plus baggage), but the other four values had to be scaled off the graph, and as such could not be considered more accurate than about  $\pm 100$ nm. Nevertheless, it is seen that the calculated range values fall within 1.5% of the values given for the baseline aircraft.

Fig. 4-9 is a payload-range chart for the A330-200 class aircraft, based on the calculated values corresponding to a MTOW of 233000kg.

**Table 4-4** MTOW and payload for the A330-200 (Airbus, 2000a)

	MTOW	Max. structural payload
<b>Variant A</b>	233000kg (513650lb)	49500kg (109120lb)
<b>Variant B</b>	230000kg (507040lb)	47500kg (104710lb)



Table 4-5 A330-200 class aircraft results (program run in Weight mode)

Run number		1	2	3	4	5	6	7
Ramp Weight	kg	233318	233318	233318	232465	230318	230318	230318
Brake Release Weight	kg	233000	233000	233000	232148	230000	230000	230000
Payload	kg	49499	24035	848	0	47498	24035	0
OEW	kg	120500	120500	120500	120500	120500	120500	120500
HLFC drag reduction		0	0	0	0	0	0	0
HLFC fuel flow increase	%	0.00%	0.00%	0.00%	0.00%	0.00%	0.00%	0.00%
Contingency	%	5.0%	5.0%	5.0%	5.0%	5.0%	5.0%	5.0%
Range (Trip distance)	nm	4142	6617	9112	9144	4140	6433	9006
Trip fuel	kg	54354	79027	101524	101527	53462	76178	99475
Trip time	hr : min	09:15	14:39	20:05	20:09	09:15	14:15	19:51
Block fuel	kg	54876	79549	102046	102049	53984	76699	99996
Block time	hr : min	09:39	15:03	20:29	20:33	09:39	14:39	20:15
Alternate	nm	200	200	200	200	200	200	200
Hold time	hr : min	00:30	00:30	00:30	00:30	00:30	00:30	00:30

Fuel Breakdown

Start-up and taxi	kg	318	318	318	318	318	318	318
Trip fuel	kg	54354	79027	101524	101527	53462	76178	99475
Alternate and land	kg	3834	3592	3307	3301	3795	3591	3300
Final reserve (Holding)	kg	2098	1895	1749	1744	2077	1894	1743
Contingency fuel	kg	2718	3951	5076	5076	2673	3809	4974
Tankered fuel	kg	0	0	0	0	0	0	0
Total fuel	kg	63321	88783	111973	111966	62325	85790	109809

Trip Fuel Breakdown

Takeoff, climb to 1500 ft	kg	798	798	798	798	798	798	798
Climb to cruise altitude	kg	5478	5478	5478	5422	5285	5285	5285
Cruise	kg	47321	72026	94565	94627	46624	69371	92711
Descent to 1500 ft	kg	553	521	479	477	551	520	477
Approach	kg	204	204	204	204	204	204	204
Total trip fuel	kg	54354	79027	101524	101527	53462	76178	99475

Comparison to A330-200

Range (Airbus, 2000a)	nm	4200	6650	9100	9100	4200	6450	9000
Difference		-1.38%	-0.50%	0.13%	0.48%	-1.43%	-0.26%	0.07%

Notes:

1. The OEW was taken as the "typical airline" OEW as indicated by Airbus (2001a). Reserves were specified as International reserves with a 5% contingency (en route trip allowance), an overshoot, 200nm alternate diversion and a 30min hold at 1500ft.
2. Mission: Climb at 250/300/M0.80; Cruise at M0.8, FL 370/410; Alternate climb at 250/270; Alternate cruise at M0.60, FL 250; ISA + 0°C; Mission allowances as per Table H-12 (Appendix H).
3. Run numbers 1, 2, 3 and 4 correspond to variant A, and runs 5, 6 and 7 are for variant B.
4. Runs 3 and 4 were at maximum fuel capacity of 111970kg (246830lb). (Variant B did not reach the fuel limit.)
5. The design or "baseline" payload was given as 253 passengers plus baggage with a passenger "allowance" weight of 95kg (209.4lb) as indicated by Airbus (2000a); which gave a payload of 24035kg (52985lb). This was used for runs 2 and 6.
6. The program was run in aviation / British units with weights in pounds; final results converted to kg.
7. The A330-200 range values were taken from a payload-range chart contained in the "Airbus 330 Briefings" (Airbus, 2000a). The range values of 6650nm and 6450nm (for the two variants) were indicated on the graph for the "baseline" payload but the other range values were scaled off the graph (and as such are not more accurate than  $\pm 100$ nm).



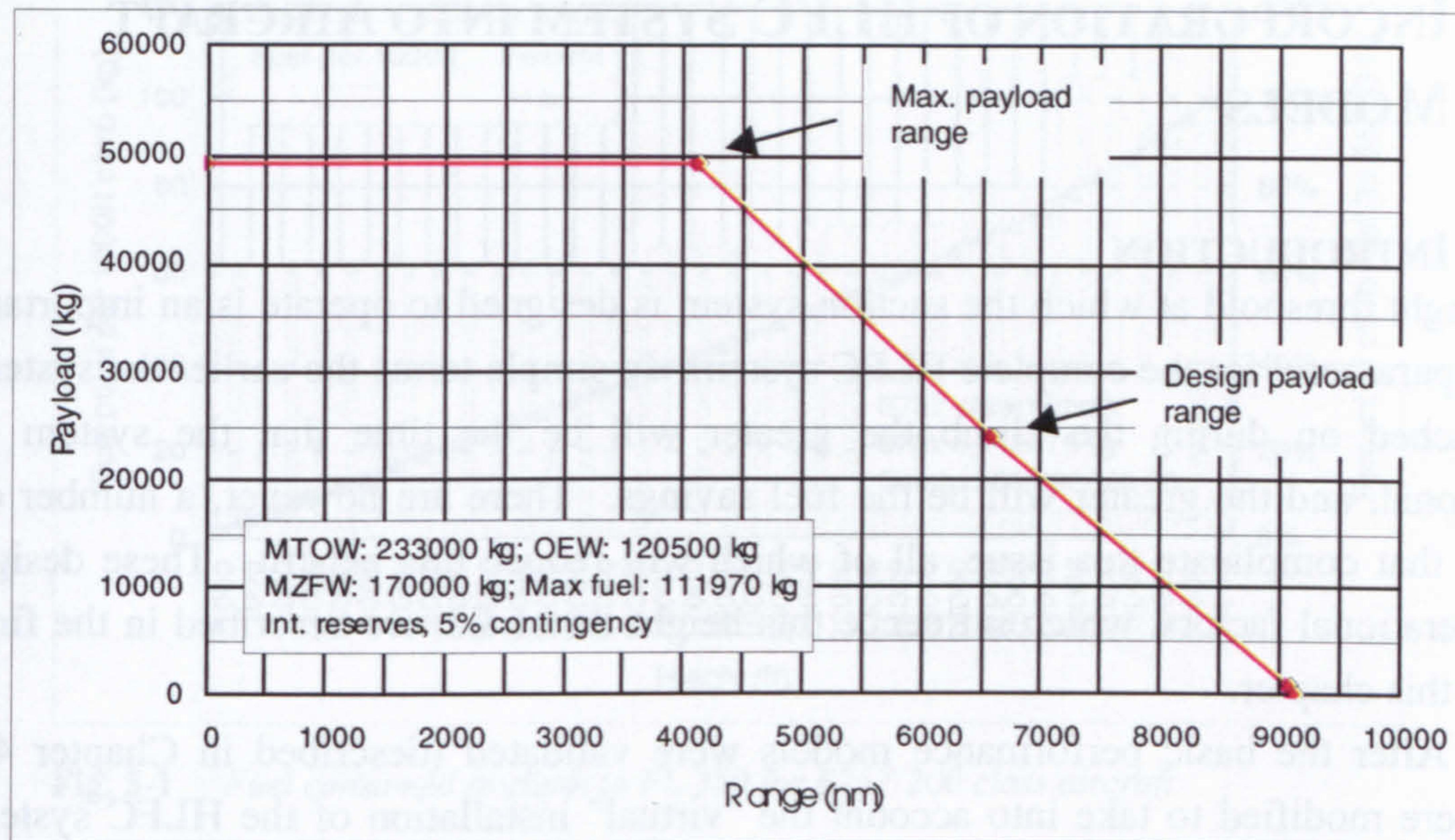


**Fig. 4-9** Payload-range chart for A330-200 class aircraft MTOW 233000kg (513650lb)

#### 4.4.10 Conclusion - Validation of the models

As the purpose of the computer models was to obtain comparative, rather than absolute reductions in fuel, it was felt that these checks were sufficient to conclude that the models were performing in a robust and consistent manner and could be used to study the relative impact of HLFC on fuel burn.



## **5 INCORPORATION OF HLFC SYSTEM INTO AIRCRAFT MODELS**

### **5.1 INTRODUCTION**

The height threshold at which the suction system is designed to operate is an important design parameter for the complete HLFC system. In simple terms the earlier the system is switched on during the climb the greater will be the time that the system is operational, and the greater will be the fuel savings. There are however, a number of factors that complicate this issue, all of which will reduce this benefit. These design and operational factors, which influence this height threshold, are described in the first part of this chapter.

After the basic performance models were validated (described in Chapter 4), they were modified to take into account the "virtual" installation of the HLFC system and its operation above the threshold height. A description of the approach adopted for incorporating these changes in the program is presented in section 5.3 of this chapter. The methods used for estimating the magnitude of these changes are described in Chapter 7.

### **5.2 DESIGN THRESHOLD HEIGHT IN CLIMB**

#### **5.2.1 Potential for fuel savings**

The advantage of applying HLFC to the upper part of the climb is illustrated in Fig. 11-1 (Chapter 11), where it is seen to be particularly important to medium range missions. To explore the impact of switching the system on at various heights, the B757-200 class aircraft performance model was used to assess the rate at which fuel is burnt, following a takeoff at maximum BRW and a climb speed schedule of 250/290/M0.8. The fuel consumed per 1000ft in a climb is not exactly constant, as indicated in Fig. 5-1. The climb speed schedule, which changes from a constant CAS (calibrated airspeed) to a constant Mach number at ~29000ft, is responsible for the observed change at this height. The fuel consumed from 20000ft to an initial cruise altitude of 35000ft, is ~51% of the total climb fuel; this reduces to ~37% for a threshold of 25000ft and to ~21% for 30000ft.

#### **5.2.2 Cloud occurrence during climb**

High level clouds have a base above 20000ft and are composed largely of ice crystals, rather than water particles (Thom, 1997). These are limited to cumulonimbus and cirrus cloud types. By designing the HLFC system to operate above this height threshold, a significant operational advantage will be gained, as the system will not have to be purged of water which could get sucked in during the climb.



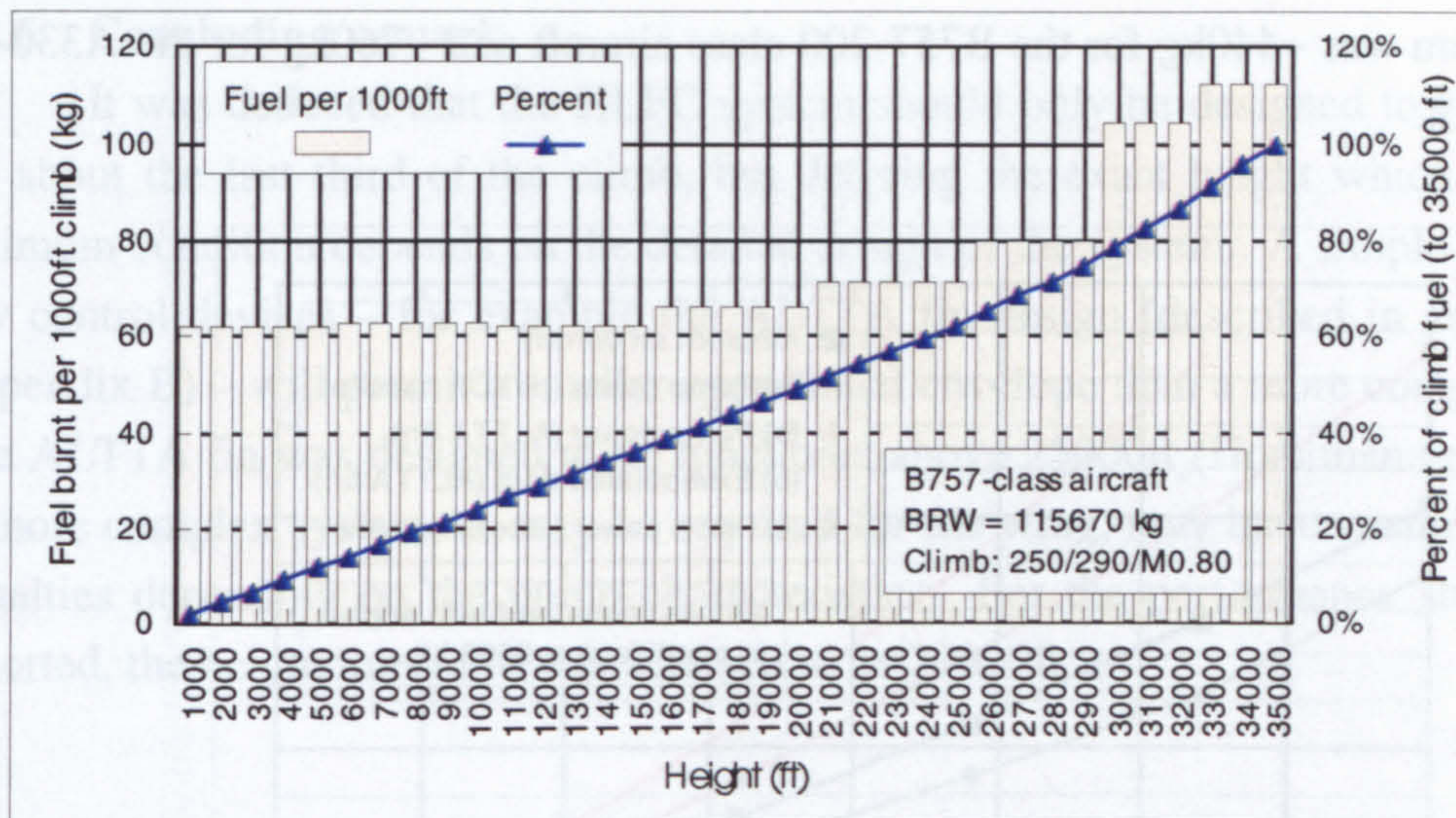


**Fig. 5-1** Fuel consumed in climb to FL 350 for B757-200 class aircraft

### 5.2.3 Power requirement

The power required for the suction system depends significantly on the air density and will thus reduce with increasing altitude. The results of three separate studies are given in Fig. 5-2. In each case the estimated pump power for the HLFC suction system was normalised with respect to the power required at a height of 35000ft.

- (a) The required pump power was estimated by Möller (2001) for the HLFC system designed for the HYLDA nacelle (see section C.16). These values were recalculated by the author using the design parameters and methodology established by Möller.
- (b) Horstmann *et al.* (2002) report on the design of a simplified HLFC fin for the A320 aeroplane – a study conducted as part of project ALTTA. The results given in Fig. 5-2 were taken from Horstmann *et al.* (2002) and normalised.
- (c) Using the methods outlined in Appendix J, the author determined the power requirement for a generic HLFC engine nacelle.

The results of (a), (b) and (c) are shown in Fig. 5-2. It is seen that the power required reduces approximately in line with air density. At 20000ft, the HLFC system will consume ~1.6 to 2.2 times the power required for the cruise condition, whereas at 25000ft, it will consume ~1.3 to 1.7 times that required for cruise.

### 5.2.4 System mass influence

The mass of the pump system (and associated power generation) will depend on the maximum power required; a lighter and smaller system will be required if the threshold height is close to the cruise height. The actual difference in mass will depend on the off-design performance characteristics of the selected pump. The order of magnitude of this influence can be established by considering the results of the HLFC mass estimation exercise described in Chapter 7. It was estimated that the mass of the



pump system was ~440kg for the B757-200 class aircraft and ~760kg for the A330-200 class aircraft.

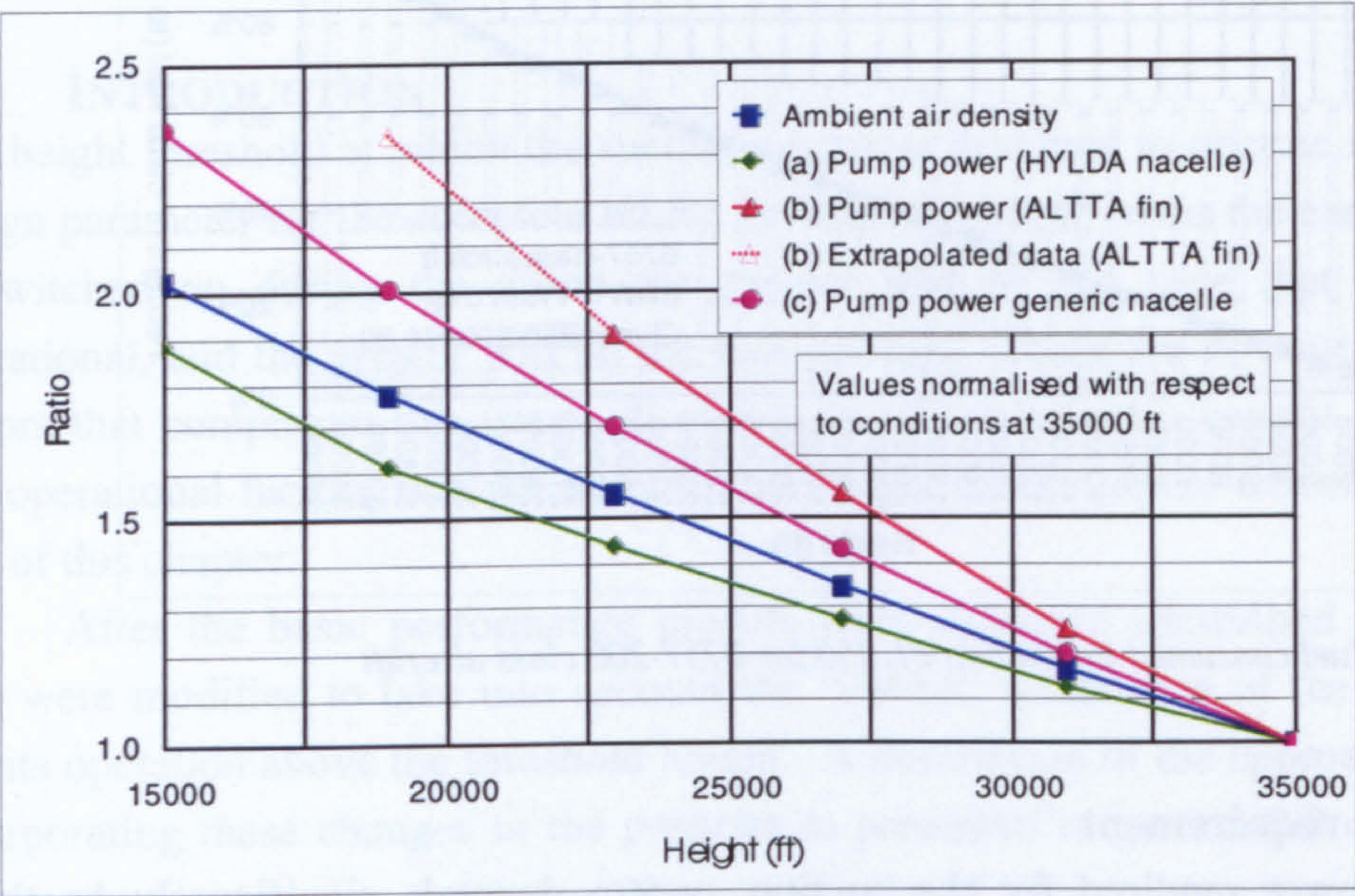


**Fig. 5-2** Relative pump power versus height for: (a) HYLDA nacelle (after Möller, 2001); (b) ALTTA A320 fin design (after Horstmann *et al.*, 2002) and (c) Generic nacelle (analysed by the author)

### 5.2.5 Laminar flow extent

With all other factors constant (e.g. Mach number, suction system design, etc.), the lower chord Reynolds number associated with higher flight levels results in a significantly greater extent of laminar flow on the chord ( $x/c$ ). Design data for the ALTTA A320 fin concept, reported by Horstmann *et al.* (2002), are reproduced in Fig. 5-3. It is evident that at 25000ft, the laminar flow extends to ~83% of that which would be achieved by the same system, under the same conditions, but at the cruise height of 35000ft.

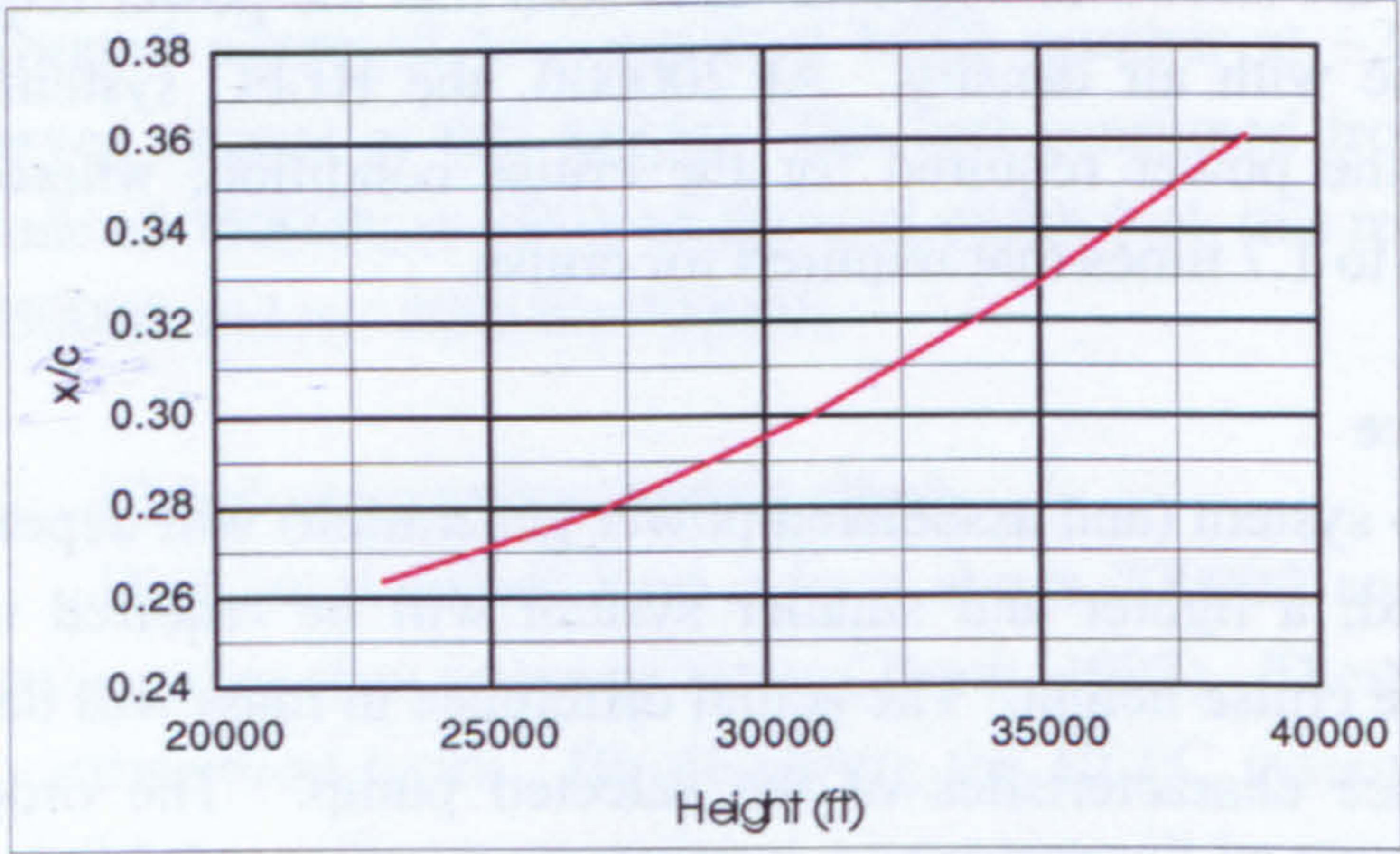


**Fig. 5-3** Influence of flight level on laminar flow extent for ALTTA fin (redrawn after Horstmann *et al.*, 2002)



### 5.2.6 Concluding remark

It was deduced that the HLFC system should only be designed to be functional for about the last third of the climb, but defining the exact height which reflects the optimum condition depends on the detailed design of the system. A simple system with few control devices – for example the ALTTA fin design (described in section B.5.3, Appendix B) – will permit a smaller operational envelope than a more complex system. The ALTTA fin was designed to be functional above 25000ft (Horstmann *et al.*, 2002). A more complex system, as may be required for the wing, may have smaller off-design penalties depending on the pump characteristics. For the performance studies herein reported, the height threshold was selected to be 20000ft.

## 5.3 CORRECTION FACTORS FOR HLFC

### 5.3.1 Computer program changes

Before the two computer models (described in Chapter 4) could be used to assess the impact of HLFC on the trip fuel, it was necessary to modify the programs. Three sets of input fields were created to allow the user to account for:

- (1) The mass of the HLFC system;
- (2) The drag reduction; and
- (3) The SFC increase.

The mechanisms by which these changes were incorporated into the programs are discussed in this section. Estimates of the magnitude of these changes are described in Chapter 7 and Appendix J.

### 5.3.2 System mass penalty

The mass penalty due to the HLFC system must be entered into the computer program on the master sheet (i.e. sheet A) by the user. This is the total system mass and includes all HLFC system components, installation allowances for brackets, looms, etc. and all fluids (as may be required for the anti-contamination system). Estimates for the mass penalty are presented in section 7.5. In the program the installed system mass is added to the OEW for the basic aircraft. If the payload is constant, then the increase will imply a greater TOW, and hence an increased fuel burn.

Certain missions are MTOW limited. Combinations of payload and range, where this is the case, can be seen on the upper right hand boundary of the payload-range diagram, depicted in Fig. D-2 (Appendix D). The MTOW values used in the computer models were identical to the values given in Table 4-1 for the two baseline aircraft. In the program, these values were not permitted to increase when the OEW increased. The consequence is that the difference between the MTOW and the OEW – which is the amount available for the payload and the fuel – is reduced. This imposes a restriction on the available fuel that can be taken on board, if the payload does not



change. The range calculated for a fixed payload in this situation will thus be affected by: (1) The increase in OEW, which will increase the TOW and hence the fuel burn; and (2) The reduced fuel limit, resulting from the increased OEW and fixed MTOW. This issue is discussed further in Chapter 6, where the influence of OEW changes on the resulting trip fuel is investigated.

### 5.3.3 Mission stations for HLFC system corrections

The computer programs were adapted to introduce the effects of HLFC on the upper part of the climb above 20000ft, as shown in Fig. 5-4. This part of the mission was divided into four segments and correction factors may be individually allocated to each station. During the cruise, the performance of the aircraft is evaluated at 21 stations. The factors can be individually applied at these stations or they may be applied uniformly to the entire cruise. In this way, the impact of a loss of laminar flow for a portion of the mission may be assessed.

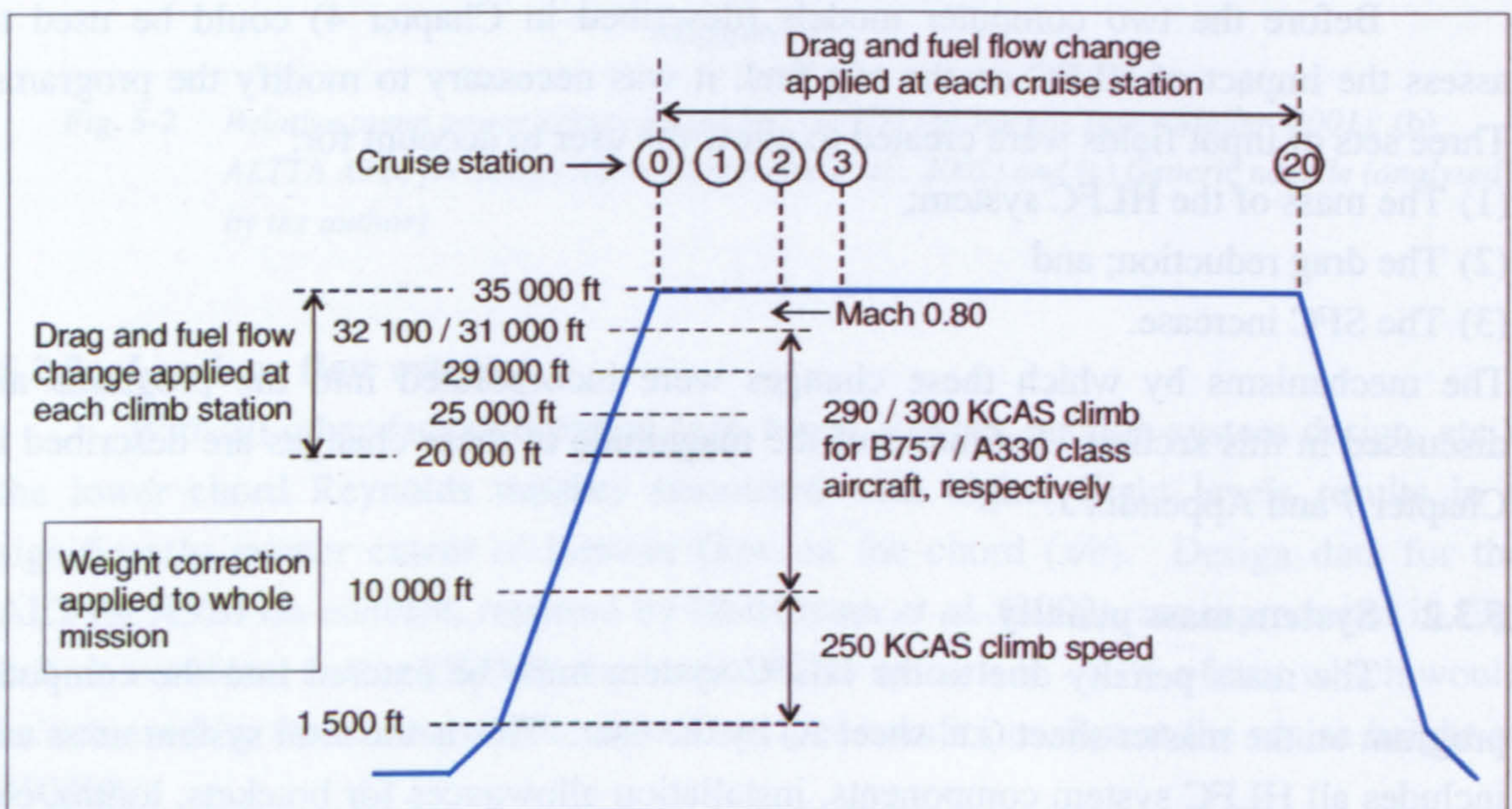


Fig. 5-4 HLFC corrections to basic performance program

### 5.3.4 Drag reduction

The user enters the drag reduction due to the HLFC system as a change in drag coefficient ( $\Delta C_{D_{HLFC}}$ ), rather than as a percentage reduction in drag. Estimates of the drag reduction for the two classes of aircraft considered are given in section 7.3. In the program the total aircraft drag coefficient is determined at each station and the drag amount  $\Delta C_{D_{HLFC}}$  is subtracted. This approach was adopted because the profile drag ( $C_{D_p}$ ) is reduced by the delay in the laminar to turbulent flow transition, but the lift-dependent drag component is essentially unchanged in the presence of the LFC system (Sawyers and Wilson, 1996).



During the cruise the aircraft's weight decreases which, at constant speed and height, results in a steady decrease in the lift coefficient and a corresponding reduction in the lift-dependent drag. These relationships are illustrated in Fig. 5-5, obtained using the B757-200 class aircraft program. By maintaining a constant profile drag reduction, the percentage reduction in drag increases with time during the cruise, as the profile drag becomes a larger portion of the total drag.

The mean drag coefficient during the cruise (determined at the 21 cruise stations) for the turbulent baseline aircraft, has been used as a reference parameter. It has been useful in some cases to express the drag reduction ( $\Delta C_{D_{HLFC}}$ ) as a fraction of this mean value. This approach has been used in the sensitivity studies described in Chapter 6.

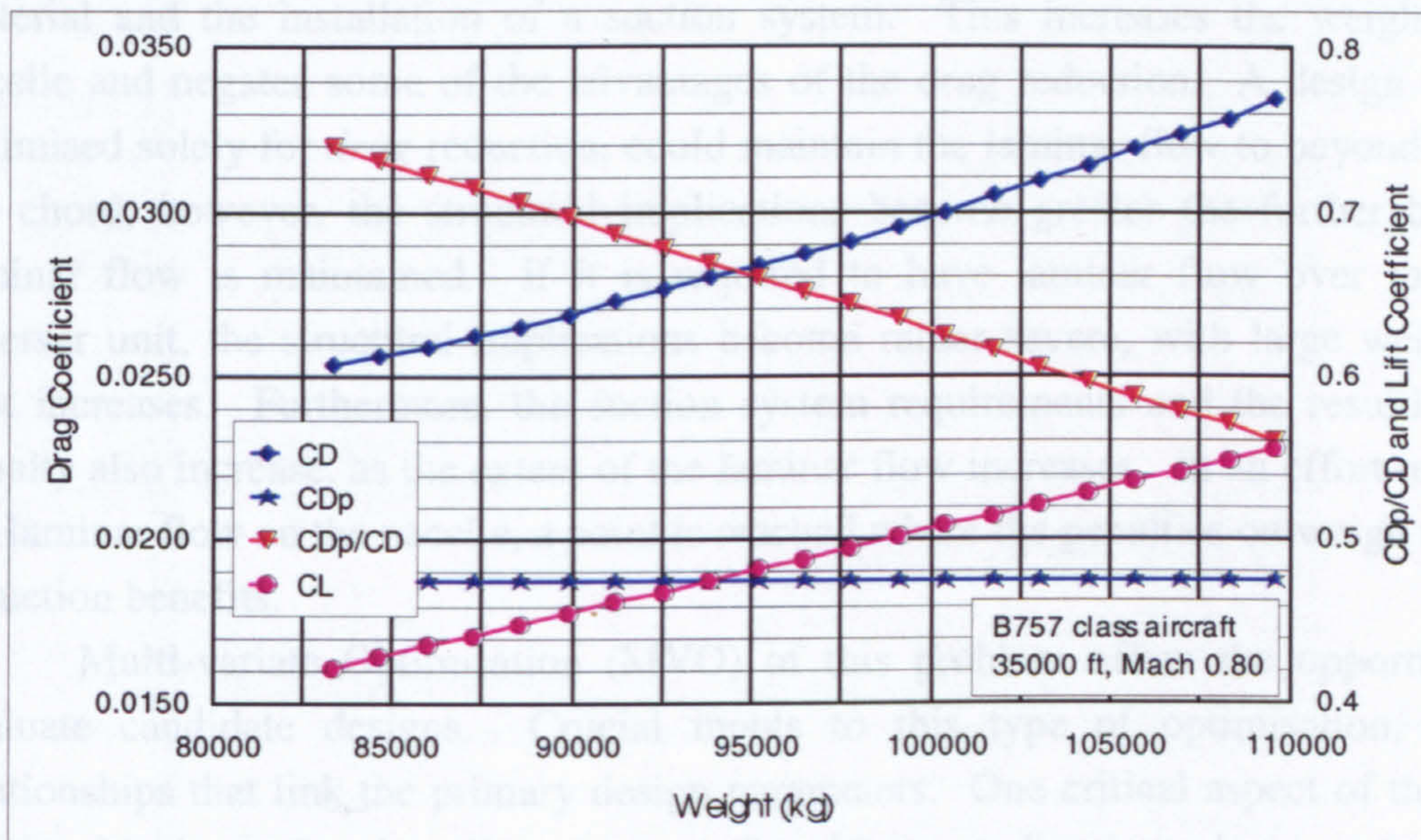


Fig. 5-5 Drag and lift versus weight during cruise for B757-200 class aircraft

### 5.3.5 Specific fuel consumption

In the program the fuel flow at each station is determined from look-up tables based on the aircraft's thrust. The HLFC system fuel penalty is incorporated as a percentage increase in the fuel flow, at the user selected stations. On the master sheet, an input table is provided that enables the user to specify the percentage increase at each station. The estimation of the SFC penalty is described in section 7.4.

The required pump power necessary to produce the desired panel flow velocity and hence drag reduction, reduces with height. This was taken into account in the program by multiplying the cruise fuel flow penalty by a scaling factor, which reduced with increasing height. The values given in Table 5.1 are based on the analysis presented in Appendix J.



**Table 5-1    *Fuel flow correction factors***

B757-200 class A/C		A330-200 class A/C	
Flight segment	Fuel flow scale factor	Flight segment	Fuel flow scale factor
Cruise	1.0	Cruise	1.0
32100 to 35000 ft	1.1	31000 to 37000 ft	1.1
29000 to 32100 ft	1.2	29000 to 31000 ft	1.2
25000 to 29000 ft	1.4	25000 to 29000 ft	1.4
20000 to 25000 ft	1.7	20000 to 25000 ft	1.7



## 6 SENSITIVITY ANALYSIS

### 6.1 INTRODUCTION

The design of a HLFC system for the wing, empennage or nacelle of an airliner, is a multi-disciplinary task, for which a range of design solutions are possible. The development of an "optimum" design is a non-trivial task, due to the high degree of inter-dependence that exists between the structural, aerodynamic and systems design parameters. Consider, for example, candidate design solutions for a HLFC engine nacelle. For most modern high by-pass ratio engines, the nacelle incorporates a large amount of carbon fibre epoxy composite material in its manufacture. The air-loads on the nacelle are comparatively low and the structure represents a highly optimised light-weight design. The incorporation of a HLFC system requires a more robust skin material and the installation of a suction system. This increases the weight of the nacelle and negates some of the advantages of the drag reduction. A design solution optimised solely for *drag* reduction, could maintain the laminar flow to beyond 50% of the chord; however, the structural implications become greater the further back the laminar flow is maintained. If it is required to have laminar flow over the thrust reverser unit, the structural implications become rather severe, with large weight and cost increases. Furthermore, the suction system requirements and the resulting SFC penalty also increase, as the extent of the laminar flow increases. In an effort to extend the laminar flow on the nacelle, a point is reached where the penalties outweigh the drag reduction benefits.

Multi-variate Optimisation (MVO) of this problem offers the opportunity to evaluate candidate designs. Crucial inputs to this type of optimisation, are the relationships that link the primary design parameters. One critical aspect of this inter-relationship is explored in this chapter. Sensitivity studies have been performed to evaluate the impact on *trip fuel*, due to changes to the OEW, SFC and  $C_D$ .

### 6.2 METHODOLOGY

Three sets of calculations to determine the trip fuel were performed for selected combinations of payload and range, using the computer models described in Chapter 4 and modified as described in Chapter 5.

- (1) The OEW was increased in small steps, whilst the SFC and  $C_D$  were unchanged.
- (2) The SFC was incrementally increased, whilst the OEW and  $C_D$  were unchanged.
- (3) The  $C_D$  was reduced, whilst the SFC and OEW were unchanged.

The SFC and drag changes were implemented above 20000ft for the main mission (not the alternate leg), but the mass change affected the OEW of the aircraft. For each "flight", the lowest BRW was determined for the specified range (using the *Range* program mode), which ensured that the smallest fuel quantity was calculated each time.



The resulting change in *trip fuel* was determined as a percentage of the fuel required for the baseline turbulent model and plotted against the variable parameter.

Two points on the payload-range graph were selected for analysis for each aircraft type. The first corresponded to the maximum structural payload (point A) and the second was at a typical design payload (point B), as shown in Fig. 6-1. Both points were taken close to the maximum range, at about 90% of the permissible range at that payload. The points were not selected on the boundaries of the payload-range graph, to avoid encountering a weight or fuel capacity limitation when considering either increased SFC or OEW.

In the case of the A330-200 class aircraft, the maximum range at the design payload (point C) was on the boundary where the range was restricted by maximum structural weight; whereas for the B757-200 class aircraft, it was restricted by fuel tank capacity. This combination of variables meant that 12 studies were undertaken, as illustrated in Table 6-1.

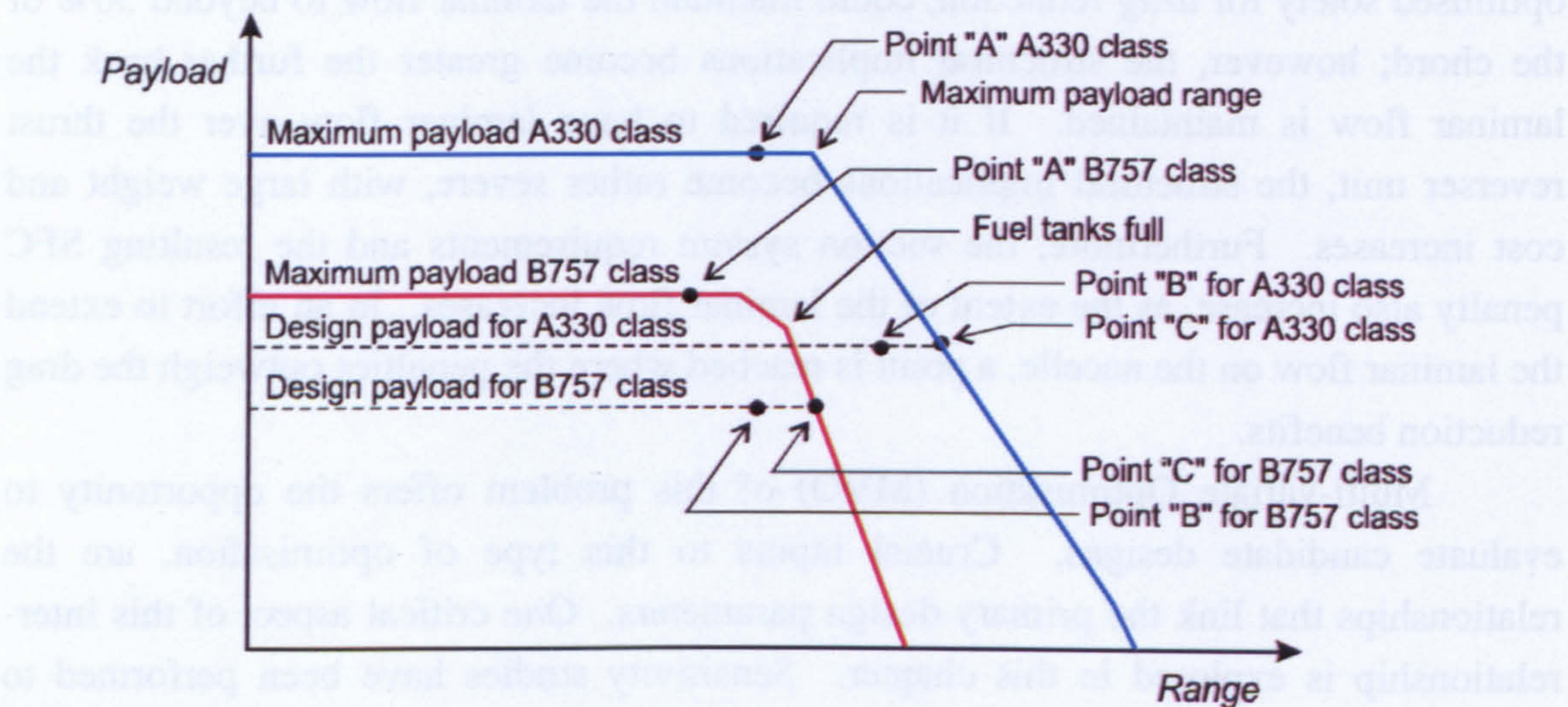


Fig. 6-1 Payload-range graph indicating points of interest

Table 6-1 Matrix of sensitivity studies undertaken

Case	Aircraft type	Range (nm)	Payload (kg)	OEW changed SFC & $C_D$ unchanged	SFC changed OEW & $C_D$ unchanged	$C_D$ changed OEW & SFC unchanged	Results given in figure:
1A	B757-200	2603	26886	√	√	√	Fig. 6-2
1B	class A/C	3272	19147	√	√	√	Fig. 6-3
2A	A330-200	3745	49500	√	√	√	Fig. 6-4
2B	class A/C	5980	24035	√	√	√	Fig. 6-5



## 6.3 RESULTS OF SENSITIVITY STUDIES ON TRIP FUEL

### 6.3.1 B757-200 class aircraft

The constraints and input variables for the studies are given in Table 6-2. Results for cases 1A and 1B are shown in Figures 6-2 and 6-3 respectively. The illustrative result in the nomogram corresponds to a 2% increase in OEW, a 2% SFC penalty and a 14% reduction in total drag (based on the mean drag in cruise for the turbulent baseline aircraft, for the distance and aircraft weight of interest).

**Table 6-2** *Ground rules for sensitivity studies for B757-200 class aircraft*

<b>Weights:</b>	The basic OEW is 58394kg (128730lb). Point A (Fig. 6-1) represents the maximum structural payload of 26886kg (59270lb) and ~90% of the max. range at the MTOW. Point B represents the "baseline" payload of 19147kg (42210lb), based on 201 passengers plus baggage at a passenger "allowance weight" of 95.3kg (210lb) and ~90% of the max. range at the max. fuel limit.
<b>Mission:</b>	Climb / descent at 250/290/M0.8; Cruise at Mach 0.8 at FL 350; Alternate climb / descent at 250/270; Alternate cruise at Mach 0.55 at FL 200; ISA + 0°C, zero wind; Mission allowances as per Table H-12 (Appendix H).
<b>Reserves:</b>	International reserves with 5% contingency (en route trip allowance), an overshoot, 200nm alternate diversion and 30min hold at 1500ft.
<b>Drag reduction:</b>	The drag reduction was based on a percentage of the mean drag determined for the cruise for the turbulent baseline aircraft for the distance and weight of interest, i.e. as a percent of $C_D = 0.03015$ for case 1A and $C_D = 0.02841$ for case 1B.

### 6.3.2 A330-200 class aircraft

The constraints and input variables for the studies are given in Table 6-3. Results for case 2A and case 2B are shown in Figures 6-4 and 6-5 respectively.

**Table 6-3** *Ground rules for sensitivity studies for A330-200 class aircraft*

<b>Weights:</b>	The basic OEW was 120500kg (265640lb). Point A (Fig. 6-1) corresponds to the maximum structural payload of 49500kg (109120lb) and ~90% of the max. range at the MTOW. Point B represents the "baseline" payload of 24035kg (52985lb) i.e. 253 passengers plus baggage, at a passenger "allowance" weight of 95kg (209.4lb) and ~90% of the max. range at the MTOW.
<b>Mission:</b>	Climb / descent at 250/300/M0.8; Cruise at Mach 0.8 at FL 370 / 410; Alternate climb / descent at 250/270; Alternate cruise at Mach 0.60; ISA + 0°C; Mission allowances as per Table H-12 (Appendix H).
<b>Reserves:</b>	International reserves with 5% contingency (en route trip allowance), an overshoot, 200nm alternate diversion and 30min hold at 1500ft.
<b>Drag reduction:</b>	The drag reduction was based on a percentage of the mean drag determined for the cruise for the turbulent baseline aircraft for the distance and weight of interest, i.e. as a percent of $C_D = 0.02821$ for case 2A and $C_D = 0.02588$ for case 2B.



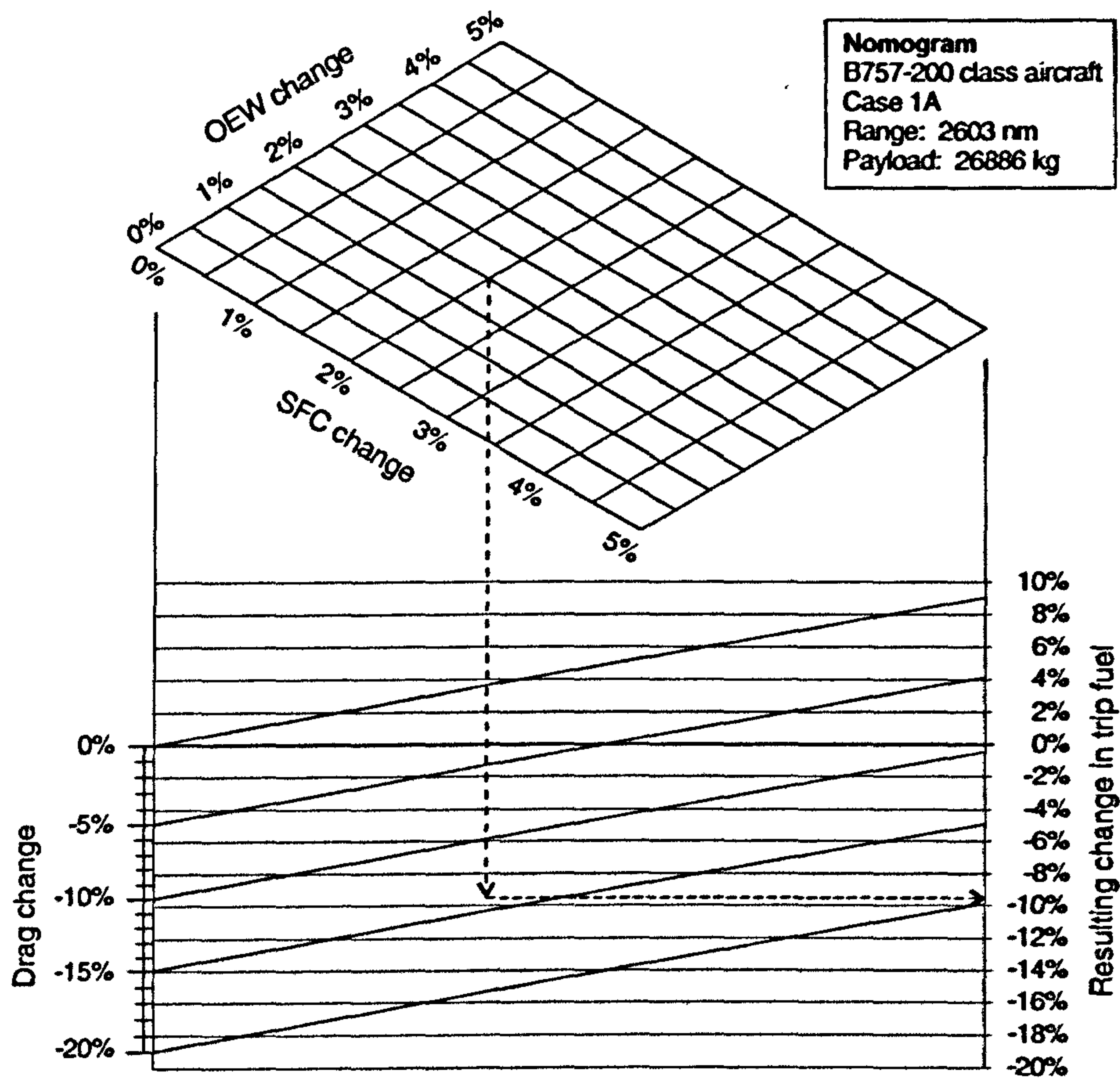


Fig. 6-2 Change in trip fuel due to changes in OEW, SFC & drag:- Case 1A

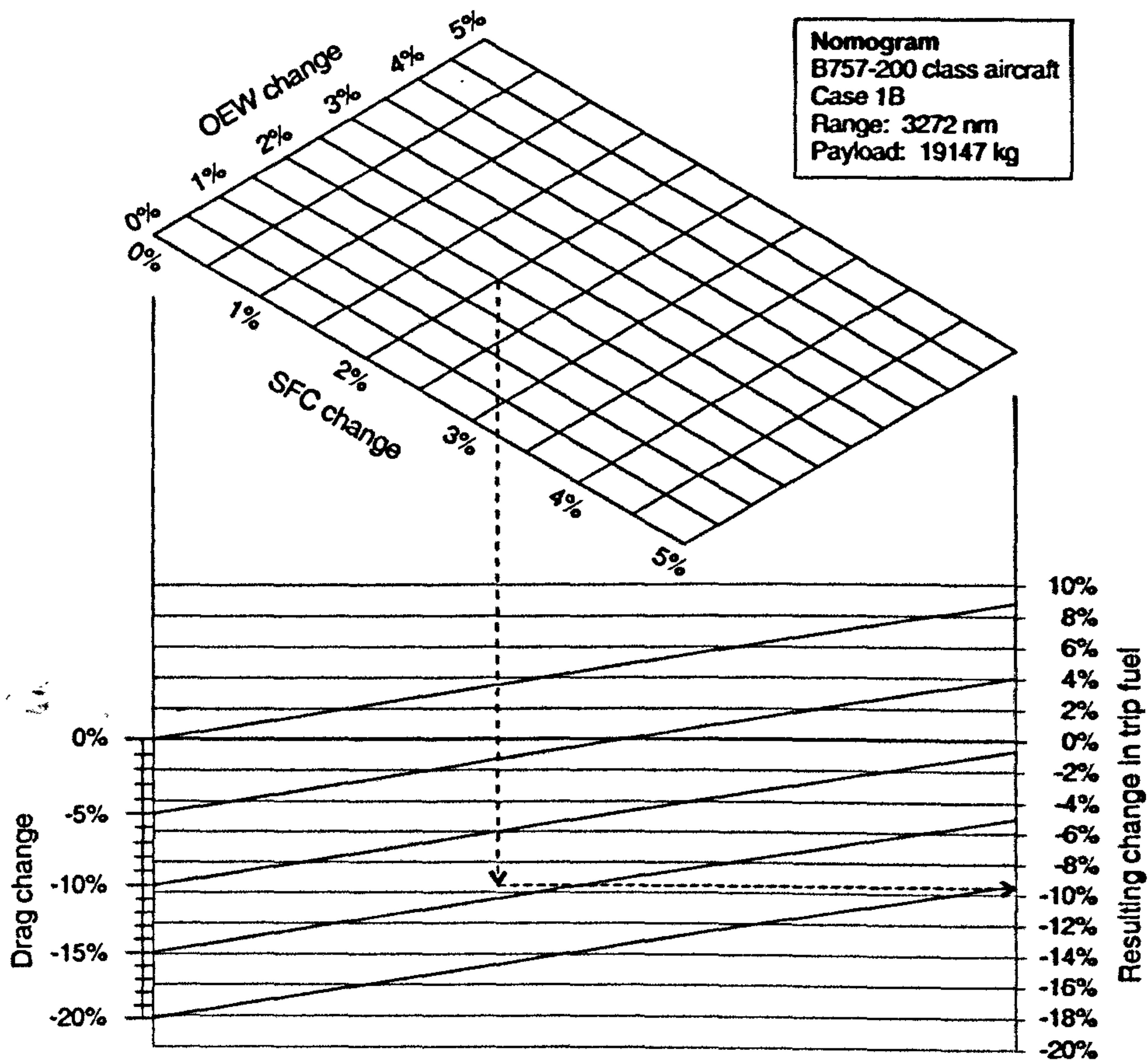


Fig. 6-3 Change in trip fuel due to changes in OEW, SFC & drag:- Case 1B



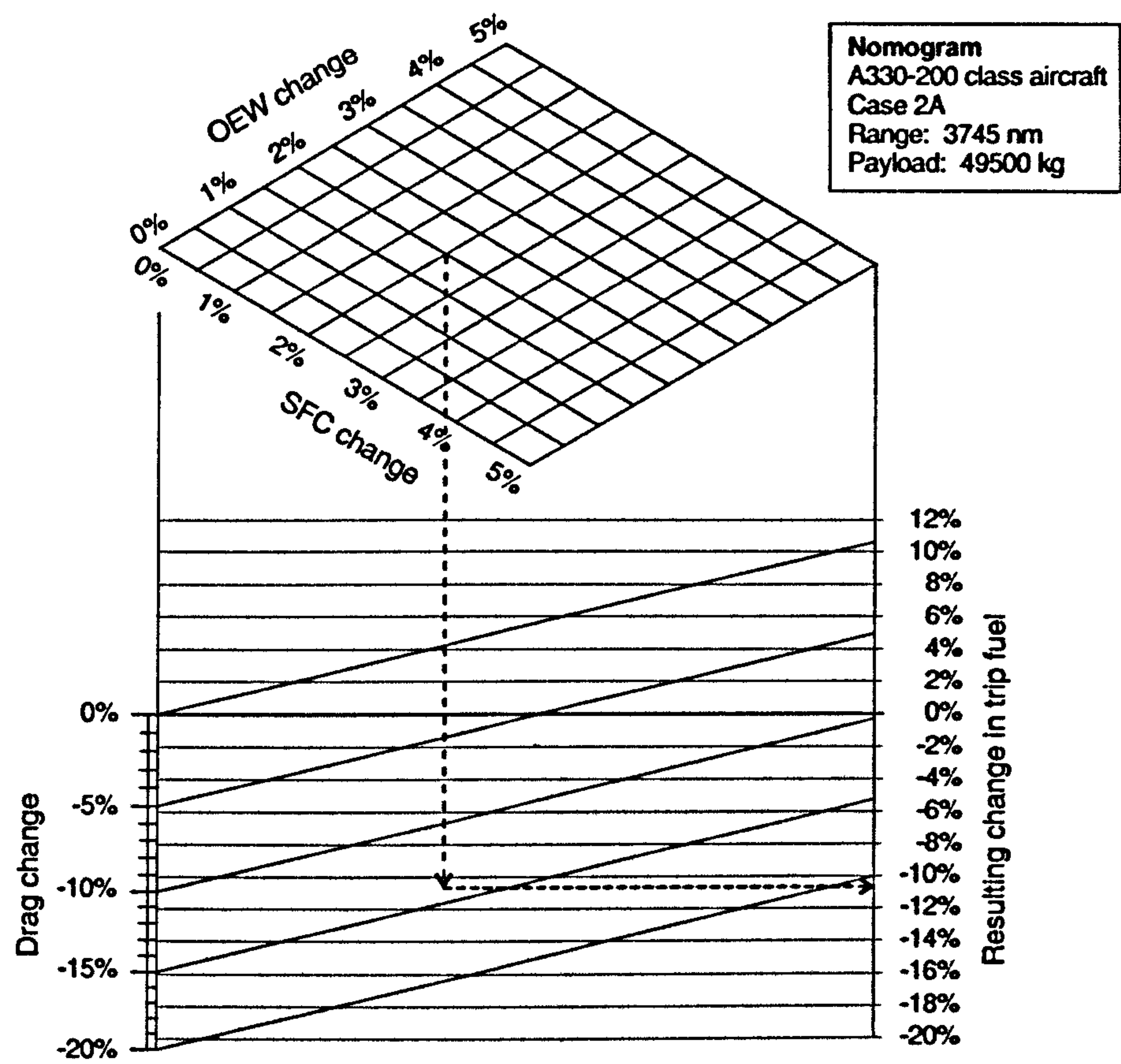


Fig. 6-4 Change in trip fuel due to changes in OEW, SFC & drag:- Case 2A

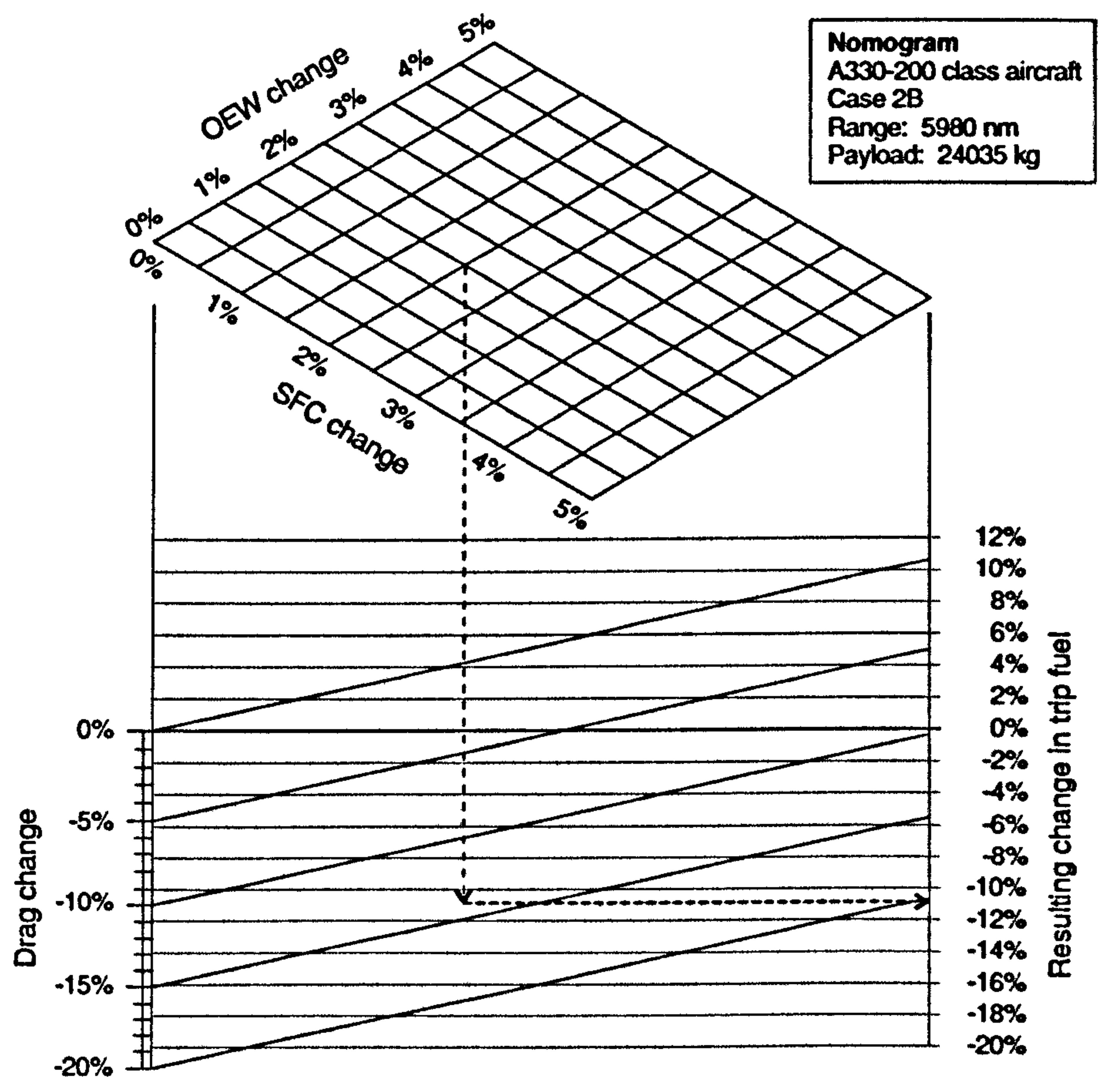


Fig. 6-5 Change in trip fuel due to changes in OEW, SFC & drag:- Case 2B



6.3.3 Assessment of linear independence

The approach adopted above was to separate the effects of the three input parameters and to treat them as linear independent variables. An estimate of the trip fuel saving due to the combined effect of all three parameters can be obtained by adding the results of the three parameters, as presented in Figures 6-2 to 6-5 for the two cases considered. To explore the accuracy of this method for the range and payload conditions selected, the computer models were run with a simultaneous input of a 2% increase in OEW, a 2% increase in SFC and a 14% decrease in drag. The results from these "combined" analyses are shown in Table 6-4, together the results from the approximate method. It is seen that the answers differ by less than 1%, indicating that reasonable answers can be obtained from the approximate method. This inter-relationship is further explored in section 6.4.

Table 6-4 Results of "spot check" to assess change in trip fuel

	B757-200 class A/C		A330-200 class A/C	
	Case 1A	Case 1B	Case 2A	Case 2B
Change in trip fuel due to:				
2% increase in OEW	1.42%	1.32%	1.83%	1.74%
2% increase in SFC	2.09%	2.16%	2.11%	2.46%
14% change in drag	-13.08%	-12.98%	-14.84%	-15.04%
Total	-9.56%	-9.51%	-10.90%	-10.85%
"Combined" computer run:	-10.05%	-9.98%	-11.49%	-11.53%

6.4 THEORETICAL EVALUATION OF TRIP FUEL SENSITIVITY

6.4.1 Objective

The objective of this evaluation was to investigate mathematically the impact on fuel burn during cruise, due to an active drag reduction technology that will simultaneously increase the SFC and  $L/D$  ratio, whilst adding weight to the aircraft. Whereas the approach in section 6.3 was to use the computer model to evaluate the sensitivity of *trip fuel* due to individual and combined changes to the input parameters, the approach taken in this section was to explore this relationship *mathematically* for the *cruise* only. The idea was to establish expressions that could be used to generalise the results obtained earlier for the two selected aircraft. Further details and the derivation of all equations are presented in Appendix I. The critical results are given here in section 6.4.

6.4.2 Numerical expression for small changes

If it is assumed that  $m_2$  (end-of-cruise mass),  $\bar{E}$  (mean lift-to-drag ratio) and  $\bar{c}$  (mean SFC) are independent during cruise, then a linear expression for small change may be written as follows:



$$\frac{\delta m_f}{m_2} = \left( \frac{\partial m_f}{\partial m_2} \right) \frac{\delta m_2}{m_2} + \left( \frac{\partial m_f}{\partial \bar{c}} \right) \frac{\delta \bar{c}}{m_2} + \left( \frac{\partial m_f}{\partial \bar{E}} \right) \frac{\delta \bar{E}}{m_2} \quad \text{--- [6-1]}$$

where  $m_f$  is the fuel used in cruise and  $\frac{\delta m_f}{m_2}$  represents a relative change in the fuel burn due to small changes in the variables  $m_2$ , SFC and  $L/D$ . To determine mathematical expressions for the partial derivatives  $\left( \frac{\partial m_f}{\partial m_2} \right)$ ,  $\left( \frac{\partial m_f}{\partial \bar{c}} \right)$  and  $\left( \frac{\partial m_f}{\partial \bar{E}} \right)$  the Breguet range equation was used. This equation permits the range ( $R$ ) to be calculated for a specified fuel mass ( $m_f$ ). One form of this equation (as derived in section E.4, Appendix E) is:

$$R = \frac{V\bar{E}}{\bar{c}g} \log_e \left( \frac{m_1}{m_2} \right) \quad \text{--- [6-2]}$$

For the analysis of the impact of a HLFC system, it is required that the expression be written the other way around, with the fuel mass expressed in terms of the cruise range. It is possible to derive this in terms of either the start-of-cruise mass ( $m_1$ ) or the end-of-cruise mass ( $m_2$ ), as shown in Appendix I. Expressing the fuel required in terms of the end-of-cruise mass yields the following expression:

$$m_f = \left( e^{\frac{R\bar{c}g}{V\bar{E}}} - 1 \right) m_2 \quad \text{--- [6-3]}$$

Partial derivatives with respect to:  $m_2$ ,  $\bar{E}$  and  $\bar{c}$  were determined from this equation (details in Appendix I) and substituted into equation [6-1], to yield the following expression:

$$\frac{\delta m_f}{m_2} = \left( e^{\frac{R\bar{c}g}{V\bar{E}}} - 1 \right) \frac{\delta m_2}{m_2} + \left( e^{\frac{R\bar{c}g}{V\bar{E}}} \frac{R\bar{c}g}{V\bar{E}} \right) \frac{\delta \bar{c}}{\bar{c}} - \left( e^{\frac{R\bar{c}g}{V\bar{E}}} \frac{R\bar{c}g}{V\bar{E}} \right) \frac{\delta \bar{E}}{\bar{E}} \quad \text{--- [6-4]}$$

The change in fuel burn due to a fixed change in aircraft mass (i.e. the first partial derivative in equation [6-4]) is the same as that presented by Shustrov (1998). Similar sensitivity relationships are given in the Cranfield University lecture note DAeT95122 (Cranfield University, undated), attributed to Le Claire (1986); however, they are not in the same form, nor derived in the same manner as that given in Appendix I. Equation [6-4] is very convenient as the changes to  $m_2$ ,  $\bar{E}$  and  $\bar{c}$  are expressed in non-dimensional terms. The impact on fuel burn can thus be determined from relative (or percentage changes) to  $m_2$ ,  $\bar{E}$  and  $\bar{c}$ .

### 6.4.3 Results from small change equation

Equation [6-4] was evaluated against results obtained from the computer program with the B757-200 class aircraft data. The cruise segment was considered in



isolation (see section H.4, Appendix H) and used to evaluate the fuel required to cover the distance of 2350nm at Mach 0.80 at 35000ft (ISA conditions). The end-of-cruise mass ( $m_2$ ) was used as the control parameter and was set equal to 90996kg (200600lb). This cruise condition is very close to that of Point “A” on the payload-range graph, given in Fig. 6-1. The end-of cruise mass would be a typical end of cruise weight for the B757-200 class aircraft, irrespective of the cruise distance. The start-of-cruise mass ( $m_1$ ) was sought using the "backsolve" software feature for the specified cruise distance. The output from the program included mean values of  $\bar{c}$  and  $\bar{E}$  calculated as the average of 21 data points established during the cruise (as illustrated in Table E-2 in Appendix E). Critical results are given in Table 6-5.

Table 6-5 Data for reference condition

Range	TAS	Mean SFC	$\bar{E}$	$m_1$	$m_2$	$m_f$
4355km (2350nm)	237.4m/s (461.1kt)	17.74mg/N/s (0.6264lb/lb/hr)	16.89	109914kg (242306lb)	90996kg (200600lb)	18919kg (41706lb)

Using the mean values given in Table 6-5 above, it follows from equation [6-4] that:

$$\frac{\delta m_f}{m_2} = 0.20807 \frac{\delta m_2}{m_2} + 0.22836 \frac{\delta \bar{c}}{\bar{c}} - 0.22836 \frac{\delta \bar{E}}{\bar{E}}$$

The relative change in fuel mass  $\frac{\delta m_f}{m_2}$  was assessed using this equation for small

changes to  $m_2$ ,  $\bar{c}$  and  $\bar{E}$  as indicated below in Table 6-6. The results are given in Tables 6-7 to 6-9, where they can be compared to the results obtained from the computer model.

Table 6-6 Summary of evaluations performed

Parameter	Reported at the bottom of:
$m_2$ varied from 0 to 5%	Table 6-7
$\bar{c}$ varied from 0 to 5%	Table 6-8
$\bar{E}$ varied from 0 to ~22%	Table 6-9

6.4.4 Results from computer model

The relative change in fuel mass  $\frac{\delta m_f}{m_2}$  was determined directly using the computer program for small changes to the governing parameters. The results are given in Tables 6-7, 6-8 and 6-9. In each case only one governing parameter was changed, while the others were kept constant. The end-of-cruise weight ( $m_2$ ) could be changed directly in the computer program and the impact assessed (see Table 6-7).



For the SFC sensitivity study the *fuel flow* was factored within the database as the SFC could not be directly controlled. This was increased in steps of 1%, from 0 to 5%. As the range did not change, the start-of-cruise mass ( $m_1$ ) increased by a small amount representing the increased on-board fuel. This meant that the thrust also increased a little in the cruise to compensate for the increased drag. The mean SFC for each computer run was calculated and compared to the baseline condition (i.e. run number 1 in Tables 6-7 to 6-9). The percentage increases in  $\bar{c}$ , as expected, closely follow the percentage increases in fuel flow; but, as shown in Table 6.8, there is a minor difference in the third significant figure (e.g. a 5.00% increase in fuel flow resulted in a 5.01% increase in  $\bar{c}$ ).

For the last set of calculations (Table 6-9) the *drag coefficient* was reduced within the database in equal steps. The mean lift-to-drag ratio during cruise was calculated, and the percentage increase determined with respect to the baseline condition. These percentage changes in  $\bar{E}$  could then be compared to the resulting change in fuel.

#### 6.4.5 Discussion of results

The results of the formulation given by equation [6-4], were compared to results obtained from the computer model, which took into account the coupling between the input parameters. The following was noted:

- (1) For a 5% increase in  $m_2$  equation [6-4] yielded a 1.04% increase in the ratio  $\frac{m_f}{m_2}$ ;

this compared fairly well to the 1.27% change obtained using the computer model. It is evident that as the weight increases both  $C_L$  and  $C_D$  would increase and at the higher  $C_L$  values the  $L/D$  ratio would be lower. The impact is small, but is evident in the table. The higher drag would require a proportionally greater thrust and this would change the SFC. The mean SFC is shown to vary by a very small amount.

- (2) For a 5% increase in SFC equation [6-4] gave a 1.15% increase in the ratio  $\frac{m_f}{m_2}$ ;

this compared very well to the 1.17% change from the computer model. As the weight increase (due to the increased fuel requirement) is small, the mean  $L/D$  ratio does not change much.

- (3) The impact of a change in  $L/D$  ratio was similarly investigated using equation [6-4]; however, the correlation with the computer model was not as good as that observed for the SFC change. For a 10.2% increase in  $L/D$ , equation [6-4] yielded a -2.33% change in fuel mass, versus a -1.94% change obtained using the computer program. With reduced fuel load due to the lower drag, the aircraft is lighter at all



times during the cruise. This will change the SFC at each point during the cruise, as is evident from Fig. E-5 (Appendix E). The mean SFC increases in this particular situation; however, due to the non-linearity of SFC changes in cruise, this result cannot be regarded as a general observation.

Table 6-7    *Impact of small change to end-of-cruise mass ( $m_2$ )*

Computer run:	1	2	3	4	5	6
Range (nm)	2350.0	2350.0	2350.0	2350.0	2350.0	2350.0
$\bar{C}$ (mg/N/s)	17.74	17.74	17.74	17.74	17.75	17.76
$\bar{C}$ change	0.00%	-0.01%	-0.01%	0.00%	0.03%	0.08%
$\bar{E}$	16.886	16.863	16.834	16.801	16.764	16.722
$\bar{E}$ change		-0.14%	-0.31%	-0.50%	-0.72%	-0.97%
$m_1$ (kg)	109914	111036	112168	113309	114460	115621
$m_2$ (kg)	90996	91906	92816	93726	94636	95545
$m_2$ change	0.00%	1.00%	2.00%	3.00%	4.00%	5.00%
$m_f$ (kg)	18919	19131	19352	19583	19824	20076
$\frac{\Delta m_f}{m_2}$	0.00%	0.233%	0.477%	0.731%	0.995%	1.27%
Results from equation [6-4]:						
$\frac{\Delta m_f}{m_2}$	0.00%	0.208%	0.416%	0.624%	0.832%	1.04%

Table 6-8    *Impact of small change to SFC*

Computer run:	1	2	3	4	5	6
Range (nm)	2350.0	2350.0	2350.0	2350.0	2350.0	2350.0
$\bar{C}$ (mg/N/s)	17.74	17.92	18.10	18.28	18.45	18.63
$\bar{C}$ change	0.00%	1.00%	2.00%	3.01%	4.01%	5.01%
$\bar{E}$	16.886	16.883	16.879	16.875	16.871	16.867
$\bar{E}$ change		-0.02%	-0.04%	-0.06%	-0.09%	-0.11%
$m_1$ (kg)	109914	110126	110339	110552	110766	110981
$m_2$ (kg)	90996	90996	90996	90996	90996	90996
$m_2$ change	0.00%	0.00%	0.00%	0.00%	0.00%	0.00%
$m_f$ (kg)	18919	19130	19343	19556	19771	19986
$\frac{\Delta m_f}{m_2}$	0.00%	0.233%	0.466%	0.701%	0.936%	1.17%
Results from equation [6-4]:						
$\frac{\Delta m_f}{m_2}$	0.00%	0.229%	0.458%	0.687%	0.916%	1.15%



Table 6-9    *Impact of small change to L/D*

Computer run:	1	2	3	4	5	6	7
Range (nm)	2350.0	2350.0	2350.0	2350.0	2350.0	2350.0	2350.0
$\bar{c}$ (mg/N/s)	17.74	17.77	17.81	17.87	17.96	18.06	18.18
$\bar{c}$ change	0.00%	0.14%	0.38%	0.73%	1.21%	1.79%	2.48%
$\bar{E}$	16.886	17.420	17.997	18.609	19.273	19.984	20.754
$\bar{E}$ change	0.00%	3.16%	6.58%	10.20%	14.14%	18.34%	22.91%
$m_1$ (kg)	109914	109311	108717	108149	107593	107054	106524
$m_2$ (kg)	90996	90996	90996	90996	90996	90996	90996
$m_2$ change	0.00%	0.00%	0.00%	0.00%	0.00%	0.00%	0.00%
$m_f$ (kg)	18919	18315	17722	17153	16597	16058	15528
$\frac{\Delta m_f}{m_2}$	0.00%	-0.663%	-1.32%	-1.94%	-2.55%	-3.14%	-3.73%
Results from equation [6-4]:							
$\frac{\Delta m_f}{m_2}$	0.00%	-0.722%	-1.50%	-2.33%	-3.23%	-4.19%	-5.23%

6.4.6    Concluding remark

One objective of the study was to explore the use of a simple mathematical relationship that could be used to generalise the results established in the thesis for the two selected aircraft types, to other aircraft. It was concluded that the change in the fuel consumed during the cruise, due to small changes in: (1) aircraft mass, (2) SFC, and (3) lift-to-drag ratio, may be satisfactorily approximated by equation [6-4].



## 7 HLFC SYSTEM INSTALLATION

### 7.1 INTRODUCTION

To accurately predict the performance benefits of a HLFC aircraft requires comprehensive design details of the installed system, which were not available for the study herein reported. In this chapter a simplified analysis process is described. By virtue of the methods used – which would be consistent with a *conceptual* design study – the accuracy of the results given in this chapter are not at the same level as those presented in the previous three chapters, where very detailed analyses were undertaken. The drag reduction, SFC penalty and system weight values, described here for the B757-200 class and A330-200 class HLFC aircraft models, should thus be seen as illustrative estimates, determined as input data for the performance programs.

### 7.2 HLFC SYSTEM DESIGN

#### 7.2.1 Design process

The design of a HLFC system is a large, complex, multi-disciplinary undertaking, which is characterised by a high degree of interdependence between the various system components. Various elements of the process have been described by: Lachmann (1961), Boeing (1982), McDonnell Douglas (1983), Jones (1985), Wilson (1997), Joslin (1998a), Boeing (1999a), Schrauf and Horstmann (2000), and Atkin and Courtenay (2002), for example. The primary elements of the design process are illustrated in Fig. 7-1.

#### 7.2.2 Existing designs

Although HLFC systems have been designed and installed in a limited number of transport aircraft (e.g. in a Boeing 757 wing, a GEAE / Rohr Industries nacelle and in an Airbus 320 fin), no complete system covering the wing, empennage and nacelle has been produced for a single aircraft. More importantly, these systems were experimental, developed with a clear goal to demonstrate the viability of the concept and to take measurements that would facilitate the development of better design tools. Furthermore, the designs incorporated "off-the-shelf" aircraft components (e.g. pumps, valves; etc.) and whereas this approach led to reduced project costs, it did not represent the lightest or simplest solution. These test articles do not represent a production standard design. The impact of this is that: (1) There is a very small database of tested hardware upon which design studies can be based; and (2) The database cannot be used verbatim, because it does not represent a production solution.

The "paper" design which best represents a production solution is the one currently being developed for the A320 fin as part of project ALTTA (see sections B.5.5, Appendix B and C.18, Appendix C). Described by Schrauf and Kühn (2001) and



by Horstmann *et al.* (2002), this design incorporates a much simpler suction system. By comparison, the first A320 HLFC fin (see section C.14, Appendix C) had nine suction chambers ahead of the front spar; each chamber was connected by a duct to the "collector" duct for the suction pump, which was located in the passenger cabin. Control valves and flow meters in the ducts permitted the pressure in individual chambers to be actively controlled by a central computer. In the ALTTA fin concept, there is only one suction chamber, which is the leading edge D-box. The mass flow controlling elements are the perforated outer skin and a series of calibrated orifices in an inner sheet (Fig. B-19, Appendix B). The suction pump is placed in the nose box. According to Horstmann *et al.* (2002), the system is "designed to be fully self-adapting for a certain range of Mach numbers, flight levels and yaw angles".

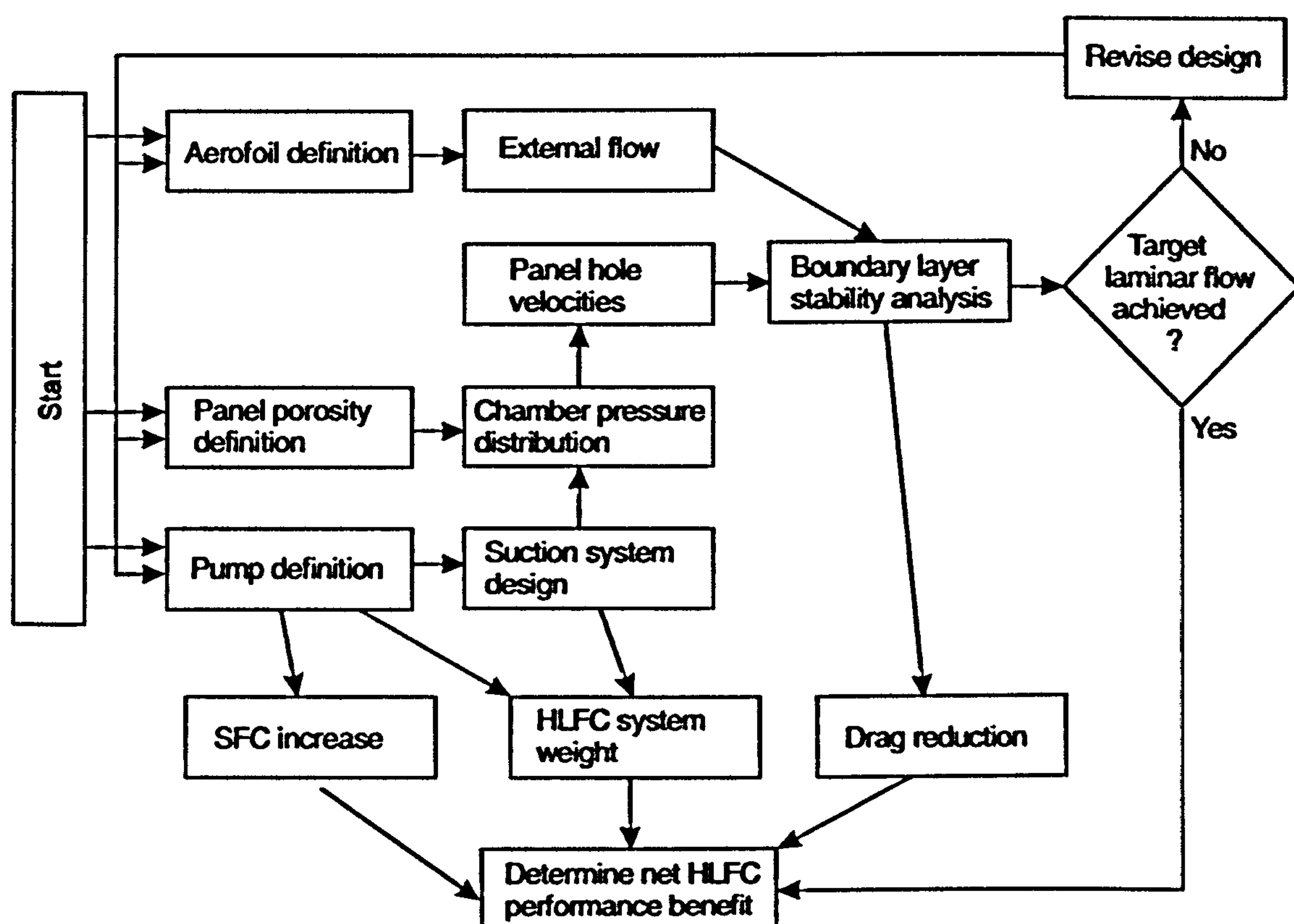


Fig. 7-1 HLFC system design process

## 7.3 DRAG REDUCTION

### 7.3.1 Drag breakdown

The purpose of the HLFC system is to delay the laminar to turbulent transition of the boundary layer, resulting in a reduction in the skin friction drag (which is a major component of the profile drag). It was necessary to model the aircraft's drag mathematically before the influence of the profile drag reduction could be incorporated. The subdivision of an aircraft's drag may be represented in a number of ways, as



outlined in section E.9 (Appendix E). As a matter of convenience the drag coefficient of the complete aircraft is frequently approximated by the expression:

$$C_D = C_{D_0} + K C_L^2 \quad \text{--- [7-1]}$$

where  $C_{D_0}$  is the *lift-independent* drag coefficient and  $K$  is the *lift-dependent* drag factor. Actual drag polars will usually differ from this idealised parabolic form, particularly at high or low angles of attack (AOA) and at high Mach numbers. ESDU 66031 (1995) describes the drag relationship for a plane symmetrical-section wing in terms of two parabolic segments. This is illustrated on a plot of  $C_D$  versus  $C_L^2$  in Fig. 7-2. Up to a certain value of the lift coefficient ( $C_{L_K}$ ) the variation of  $C_D$  with  $C_L^2$  is linear and can be represented by the slope  $k_1$ . Above  $C_{L_K}$  the slope is given by  $k_2$ , where  $k_2 > k_1$ .

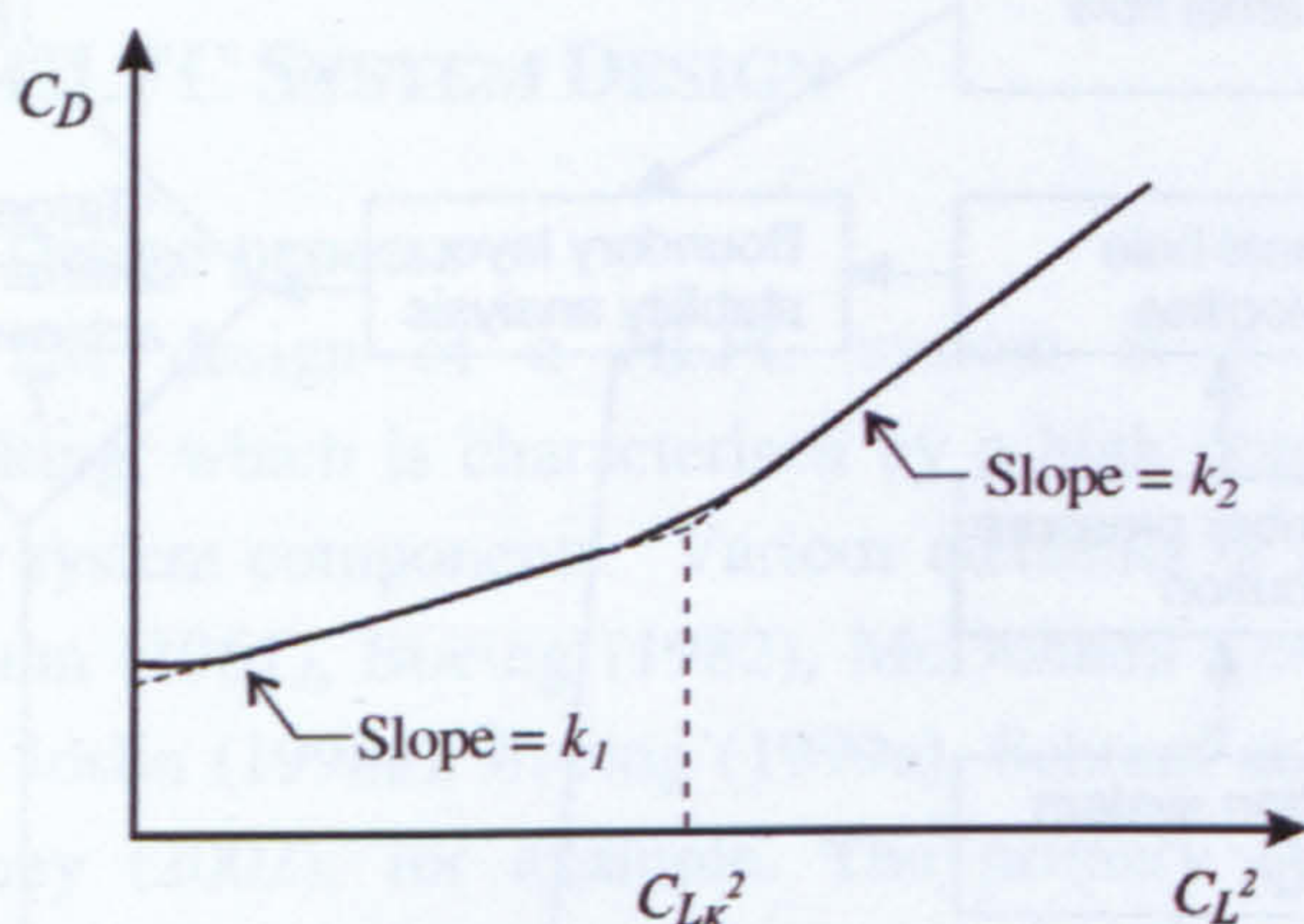


Fig. 7-2 Drag approximation (based on ESDU 66031, 1995)

### 7.3.2 Model drag polars

The  $C_D$  versus  $C_L$  relationship shown in Fig. 7-2 requires five unknown quantities to be determined in order to represent experimental data. Plots of  $C_D$  against  $C_L^2$  were prepared using the B7G7 PEM data for each Mach number so that slope and intercepts on the axis of the two segments could be ascertained. It soon became clear that the point where the slope changed (i.e.  $C_{L_K}$ ) was not easily discernible on the graphs. Instead the slopes increased gradually above a certain  $C_L$  value – which was itself a function of Mach number. It was also apparent that to achieve a smooth curve, the two segments needed to be “blended”, rather than to be allowed to meet at a sharp corner. This complicated the mathematical model without offering any advantage. The approach was abandoned in favour of the one described below.

ESDU 66031 (1995) describes unpublished Hawker Siddeley Aviation work, which indicated that “in some cases a term in  $C_L^4$  is not negligible” in drag



representation. The results of Ardonceau (1994) indicated that a good fit with the experimental data of elliptic and crescent wing planforms was obtained by including polynomial terms to the power of 3 and 4. Yajnik and Subbaiah (1976) showed that the drag polar of the YF-16 fighter aircraft with manoeuvre flaps extended (i.e. with a cambered section), is well represented by the following equation:

$$C_D = K_1 + K_2 C_L^2 + K_3 C_L^n \quad \text{--- [7-2]}$$

with the exponent  $n$  evaluated numerically to be in the range 3.4 to 4.2. This is simpler than the approach described earlier, as there are only four values to be determined for each drag polar. The approach was explored to model the B7G7 PEM drag data. The values of  $K_1$ ,  $K_2$ ,  $K_3$  were considered to be only functions of Mach number, and a single value of  $n$  was sought that would provide the best overall fit to the data for all Mach numbers. In this representation  $K_1$  is not exactly the same as  $C_{D_0}$  (the true zero lift drag coefficient). Wing sections with substantial camber result in the minimum drag point occurring at a small positive value of  $C_L$ , rather than at  $C_L = 0$  (see section E-9, Appendix E). No data was available to model the drag around the  $C_L = 0$  region, and the value of  $K_1$  was taken as a "best fit" extrapolation of the data to the  $C_L$  axis.

The coefficients  $K_1$ ,  $K_2$ ,  $K_3$  and  $n$  were determined for each Mach number, where B7G7 data was available. Initially, the "least squares" technique of curve fitting was used to establish the coefficients. The value of  $n$  was observed to be mostly in the region of 4 to 7, for the Mach number range considered. Trial values of  $n = 4$  (as selected by Yajnik and Subbaiah, 1976) and  $n = 6$  were then used to model the drag data. For the low speed drag polars,  $K_3$  was set equal to zero. A value of  $n = 6$  was selected, as it was found to provide the best overall representation of the data; it resulted in a surprisingly good correlation for speeds up to Mach 0.84, when appropriate values of  $K_3$  were selected.

Using a plot of  $C_D$  versus  $C_L^2$  for Mach 0.30, the low speed value of  $K_1$  was ascertained by extrapolating the line to  $C_L = 0$  and the value of  $K_2$  was determined from the slope of the line. At this Mach number  $K_3 = 0$  and the drag polar is well represented by a parabola. The same approach was adopted for the higher Mach numbers to obtain trial values for  $K_1$  and  $K_2$  by only considering low  $C_L$  data points. At the higher  $C_L$  values, the actual data departed from the straight line which would represent the parabolic drag polar. The lift coefficient at which the data departed from the parabolic drag polar was noted to progressively reduce as the Mach number increased (Fig. 7-3). It was found that this could be modelled by progressively increasing the value of  $K_3$  with Mach number. This was done by graphical inspection of superimposed plots of the modelled and actual data. Small adjustments were made to



the coefficients to ensure that the model accurately represented the data in the region of greatest interest (i.e. around  $C_L = 0.5$ ).

From about Mach 0.60 onwards, a very small increase in  $K_1$  was needed to represent the data and at about Mach 0.79, a rapid increase in  $K_1$  was required to model the compressibility drag rise. Increases in  $K_2$  and  $K_3$  were also required (representing the lift dependent wave drag contribution). After determining the "best fit" values for  $K_1$ ,  $K_2$  and  $K_3$  for each Mach number, the coefficients were plotted as functions of Mach number and then smoothed "by hand". This was intended to prevent spurious data points from distorting the model.

The final step was to use the revised coefficients to generate drag polars, which were compared to the original data by calculating the percentage deviation at each data point. The accuracy of the model could be judged by the following statistics: For the 329 data points on the  $C_D$  versus  $C_L$  table, more than 60% of the modelled  $C_D$  values fell within 0.5% of the original data and for nearly 90% of the data points, the modelled values were within 2%.

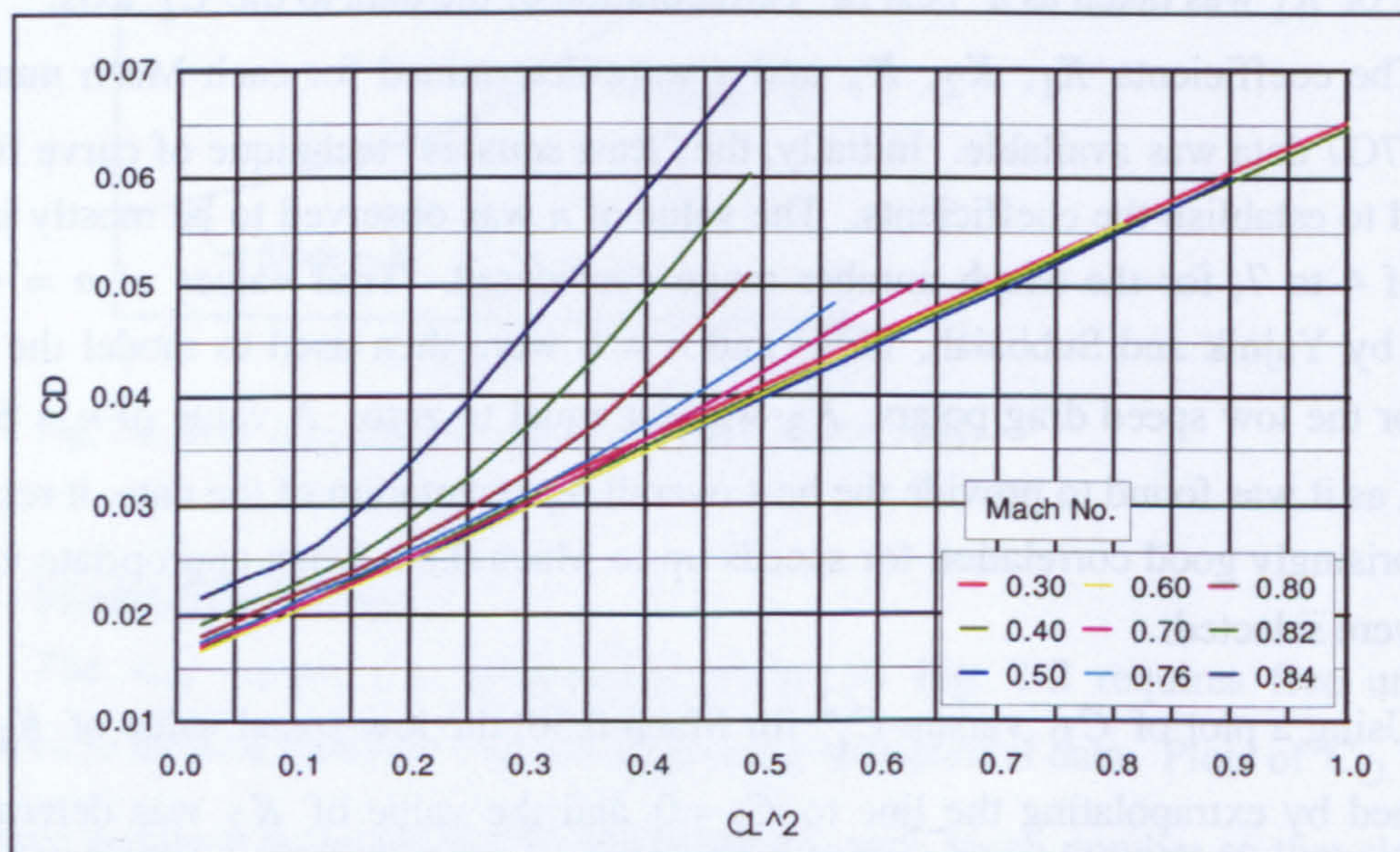


Fig. 7-3  $C_D$  versus  $C_L^2$  for B7G7

### 7.3.3 B757-200 class aircraft HLFC drag reduction

Under contract to NASA, the Boeing Preliminary Design Department in 1981 - 1982 undertook a HLFC study using the Boeing 757-200 aircraft as the baseline vehicle. Conceptual design modifications involving system and structural changes were developed. Estimates of the weight increase, suction power and drag reduction were determined. The ground rules for the study required that the wing planform, thickness and spanwise lift distribution of the B757-200 baseline aircraft be matched by the wing of the HLFC aircraft. These restrictions meant that the resulting concept did not reflect



a fully optimised HLFC aircraft. It was stated that, "the present baseline aircraft has a relatively small wing (optimised for turbulent flow) and that a HLFC airplane designed for the same mission probably would have a larger wing; hence, the impact of the laminarization could be larger" (Boeing, 1982). A laminar flow wing was developed by Boeing to provide the target pressure distribution. "The drag reduction due to HLFC was estimated on the basis of boundary layer calculations performed at three spanwise locations on the wing. These gave the local section profile drag coefficients for fully turbulent flow and for partly laminar flow. Interpolation of the three local sections profile drag coefficients gave the spanwise drag distributions from which the total wing profile drag was obtained by integration." (Boeing, 1982) At the cruise altitude of 37000ft, the laminar flow on the upper surface near to the fuselage side extended from the leading edge to ~55% of the chord, and the extent of laminar flow increased linearly with span station to reach a maximum of 60% chord at the ~65% semi-span position; outboard of this point it was maintained at 60% of the chord. For the lower surface, the flow extended to 38% chord at the fuselage side, increasing to 60% chord at the 70% semi-span station. Allowances were made for a loss of laminar flow due to turbulent contamination from the body, wingtips, engine pylons and the flap track fairings. The local section profile drag coefficients were evaluated for the design case of Mach 0.80 at 37000ft, for a gross aircraft lift coefficient of 0.50. The values were integrated to yield the overall wing profile drag, which was used to determine the reduction in drag due to the HLFC system (Table 7-1). Also shown in the table is the drag reduction with HLFC applied to the empennage. This assumed 50% chord laminarization.

**Table 7-1** Drag reduction for HLFC B757 (Boeing, 1982)

HLFC applied to:	$\Delta C_D$
<b>Wing:</b>	
Upper wing surface only	0.00225
Lower wing surface only	0.00110
<b>Upper &amp; lower wing surface</b>	<b>0.00335</b>
<b>Empennage:</b>	
Vertical tail	0.00050
Horizontal tail	0.00080
<b>Complete empennage</b>	<b>0.00130</b>

Note: For M0.80, 37000ft,  $C_L = 0.50$ .

More recent studies conducted by Airbus indicated that achieving laminar flow on the lower wing surface is improbable (for example Robert, 1992; Sawyers and Wilson, 1996); however, it has been demonstrated that it is possible on an engine nacelle. Tegarden (1996) reported on the GE / Rohr HLFC nacelle study (Appendix C.10) and indicated that a 40% drag reduction on the nacelle was deemed to be achievable, provided that the manufacturing problems associated with gaps, steps and manufacturing tolerances could be overcome. Meyer (2000) of Rolls-Royce stated that for the HYLDA nacelle (see Appendix C.16) it was predicted that laminar flow would



extend to "almost" 50% of the nacelle chord, resulting in a 35% reduction in nacelle friction drag. The nacelle profile drag coefficient for the B757 was given as 0.00164 (Boeing, 1982). Based on this data, a value of 37% drag reduction was used for the current study, which implied a drag saving of 6 drag counts for the aircraft.

The drag reduction for the desired configuration, i.e. HLFC on the upper wing, empennage and nacelles, was obtained by removing the contribution of the lower wing surface from the Boeing study (1982) and adding the contribution of the nacelles (Table 7-2). This gave a profile drag reduction of 0.00415 or 22.1%.

The profile drag coefficient for the turbulent baseline aircraft is given as 0.01875. This is a little greater than the value of  $K_1$  used to model the drag at Mach 0.80, as described earlier in section 7.3.2. The total drag coefficient for the baseline B757-200 at Mach 0.80 was given as 0.0308 for a lift coefficient of 0.50 (Boeing, 1982). This compared very well to the drag model described in section 7.3.2, where the drag is 0.0295 under the same conditions.

The mean drag coefficient during cruise, for a trip distance of 3636nm at the design payload (i.e. point "C" on the payload-range diagram given in Fig. 6-1) and at Mach 0.80, was evaluated to be 0.0290 using the computer model. Using this as a reference condition, the HLFC drag reduction of 41.5 counts represents 14.3% of the total drag.

**Table 7-2** *Profile drag reduction for B757-200 class HLFC aircraft*

	<b>Turbulent Baseline</b>	<b>Percent of total</b>	<b><math>\Delta C_{Dp}</math></b>	<b>Percent reduction</b>	<b>New <math>C_{Dp}</math></b>
Upper wing	0.00453	24.2%	0.00225	49.7%	0.00228
Lower wing	0.00241	12.9%	0.00000	0.0%	0.00241
<b>Total wing</b>	<b>0.00694</b>	<b>37.0%</b>	<b>0.00225</b>	<b>32.4%</b>	<b>0.00469</b>
Vertical tail	0.00128	6.8%	0.00050	39.1%	0.00078
Horizontal tail	0.00181	9.7%	0.00080	44.2%	0.00101
<b>Total empennage</b>	<b>0.00309</b>	<b>16.5%</b>	<b>0.00130</b>	<b>42.1%</b>	<b>0.00179</b>
Nacelles	0.00164	8.7%	0.00060	36.6%	0.00104
Fuselage	0.00653	34.8%	0.00000	0.0%	0.00653
Struts & flap tracks	0.00055	2.9%	0.00000	0.0%	0.00055
<b>Totals</b>	<b>0.01875</b>	<b>100%</b>	<b>0.00415</b>	<b>22.1%</b>	<b>0.01460</b>

### 7.3.4 A330-200 class aircraft drag reduction

Wilson (1997) modified a MVO computer program to study the application of HLFC to jet transport aircraft (see section B.7.9, Appendix B). A number of conventional aircraft types were selected to provide a baseline from which the benefits of HLFC could be assessed. One of these project aircraft was based on the A330. The results of the profile drag calculation for five separate studies conducted using the MVO code with this baseline aircraft are reproduced in Table 7-3. Number 1 is the turbulent baseline model, whilst numbers 2 to 6 represent HLFC aircraft models. The parts of the aircraft that were laminarised in each study are indicated in the table, along with the



corresponding reduction in aircraft profile drag. In the analysis performed by Wilson (1997) the aircraft was re-sized for each study to meet a given mission specification. The implication of this is that the profile drag reduction was influenced by the change in aircraft size. However, the change was small, as indicated by the wing reference areas in Table 7-3. The reduction in profile drag is ~25%, corresponding to a configuration with HLFC applied to the upper wing surface, fin, HTP (horizontal tailplane) and nacelles. This is seen to be very similar to the corresponding value of 22.1% given in Table 7-2 for the B757-200 class aircraft.

The value of  $K_1$  used to model the drag polar at Mach 0.80 for the A330-200 class aircraft, as described in section G.3 (Appendix G) was 0.01509. Based on a 25% reduction in profile drag, it was estimated that the HLFC system would reduce the aircraft's drag by 37.7 drag counts. At the reference condition used before (i.e. point "C" on Fig. 6-1), the mean drag at Mach 0.8 was evaluated to equal 0.02666, using the computer model. This reduction represents ~ 14.1% of the aircraft's total drag.

The drag reduction estimates given in this section may be compared to the results of other studies and tests. A review of such work is presented in section B.7 of Appendix B. Supporting data to the estimate of Wilson (1997) comes from Schrauf (2001) and Schrauf and Kuhn (2001), who recently indicated that a reduction of 16% is possible for a long-range aircraft in the class of the A340.

**Table 7-3** *Profile drag reduction for A330-class project aircraft analysed by Wilson (1997)*

No.	Description	$S \text{ (m}^2\text{)}$	$C_{D_p}$	$\Delta C_{D_p}$	(%)
1	Turbulent baseline A/C	373	0.01451		
2	HLFC on: Wing (upper surface)	366	0.01223	0.00228	15.7%
3	HLFC on: Fin	372	0.01415	0.00036	2.5%
4	HLFC on: HTP	372	0.01388	0.00063	4.3%
5	HLFC on: Nacelle	370	0.01412	0.00039	2.7%
Sum of items 2 - 5				0.00366	25.2%
6	HLFC on: Wing (upper surface), fin, HTP, nacelle	363	0.01087	0.00364	25.1%

## 7.4 SFC INCREASE DUE TO SUCTION SYSTEM

### 7.4.1 Equivalent drag approach

The impact of the power required to drive the suction system on the overall performance of the aircraft can be considered in two ways. Firstly, the power can be described as an equivalent drag term. The use of a "common currency" (i.e. drag) enables the net performance benefit to be established at a selected *design point*, taking into account the power of the HLFC system. This approach was adopted by Atkin and Courtenay (2002), for example, who explored the net benefits for an A310 HLFC retrofit design. For the B757 study (Boeing, 1982) with HLFC on the upper and lower wing surfaces, the suction drag was estimated to be  $C_{D_s} = 0.00027$ . This equivalent



drag represents 8% of the estimated 0.00335 reduction in profile drag due to the HLFC system on the wings.

The alternative approach, which is more difficult to implement, involves: (1) Determining the estimated power required to drive the pumps; (2) Estimating the increase in fuel flow as a result of this power takeoff; (3) Determining the reduction in trip fuel for the mission distance. Whereas the first approach is very useful for comparing alternative HLFC design options, the latter results in a more accurate calculation of the trip fuel saving for a particular design option.

7.4.2 Previous studies

A summary of quoted suction power requirements for previous studies is given in Table 7-4. Although the table provides a general order of magnitude for the suction power, the data is of little real value in establishing the power requirement for a new study. There are two reasons for this. Firstly, old estimates of the flow rate required to stabilise the flow (e.g. the B757 HLFC study, as described by Boeing, 1982) were later shown to be too high and lower flow rates have been demonstrated to be satisfactory in flight tests. Secondly, the suction power depends significantly on the detailed design of the suction system and this information is not always explicitly stated in the literature.

Table 7-4     *Suction system power requirement*

	MTOW (kg)	Suction power (kW)	HLFC configuration	Reference
B757 HLFC	99800	126	Wing upper surface	Boeing (1982)
B757 HLFC	99800	206	Wing upper & lower surface	Boeing (1982)
Large twin (HLFC-2)	23950 - 271720	224	Wing, HTP, fin, nacelle	Arcara <i>et al.</i> (1991)
Long-range Quad	206900	297	Wing (upper), HTP, fin, nacelle	Wilson (1997)
A310 HLFC retrofit	150000	190	Wing (partial upper), HTP, fin	HYLTEC (2000)

7.4.3 Estimate of suction panel areas

The first step in establishing the suction power was to estimate the planform areas of the suction surfaces. The extent of laminar flow on the wing, fin, HTP and nacelle was based on previous studies (as described in Appendix C). The results are shown in Fig. 7-4 and Fig. 7-5, for the B757-200 and A330-200 classes of aircraft respectively. The principal dimensions indicated in these figures (e.g. the wing and tailplane span) correspond to published details of the Boeing 757-200 and Airbus 330-200 (see Fig. F-1, Appendix F and Fig. G-1, Appendix G). However, certain secondary dimensions (e.g. the nacelle diameter and the aerofoil leading edge radius), had to be estimated from scaled drawings, or inferred from other data.

The chordwise extent of the suction panels is restricted by structural considerations, particularly the location of the forward spar, which is typically located at ~20% of the chord. Table 7-5 contains a summary of the calculated areas. Also



indicated in the table are the suction panel *wetted* areas. The empennage wetted areas were 2.11 times those of the corresponding planform areas; the scaling factor was evaluated so as to account for the aerofoil profile and for the lower / opposite surface. The suction panel on the wing starts just below the leading edge (to ensure a laminar stagnation line) and extends to ~17.5% of the chord along the upper surface, as illustrated in the wing detail given in Fig. 7-4. A factor of 1.15 was established to account for this. There is no requirement for suction on the nacelle lip, due to the absence of sweep. The suction area was based on the product of the suction panel length (estimated to be 18% of the nacelle length) and a mean circumference.

**Table 7-5**    *Estimated suction panel areas*

	Scaling factor	B757-200 class A/C		A330-200 class A/C	
		Planform suction area (m <sup>2</sup> )	Wetted suction area (m <sup>2</sup> )	Planform suction area (m <sup>2</sup> )	Wetted suction area (m <sup>2</sup> )
Wing (port)	1.15	11.39	13.10	24.47	28.14
Wing (starboard)	1.15	11.39	13.10	24.47	28.14
HTP (port)	2.11	3.11	6.56	4.65	9.81
HTP (starboard)	2.11	3.11	6.56	4.65	9.81
Fin	2.11	5.04	10.63	5.74	12.11
Nacelle (port)			4.42		7.09
Nacelle (starboard)			4.42		7.09
Total			58.8		102.2



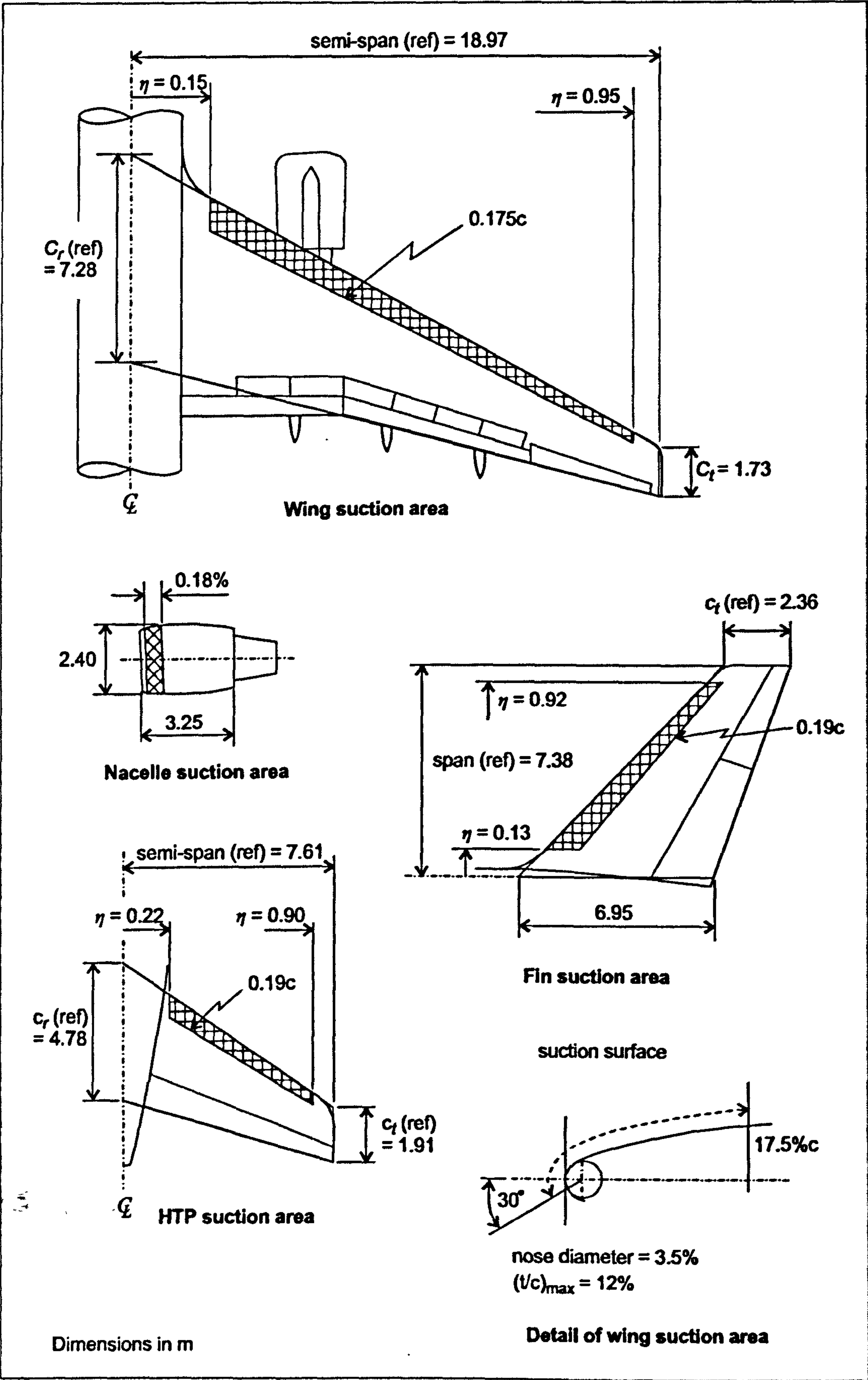


Fig. 7-4 Estimated planform areas of suction panels for B757-200 class aircraft



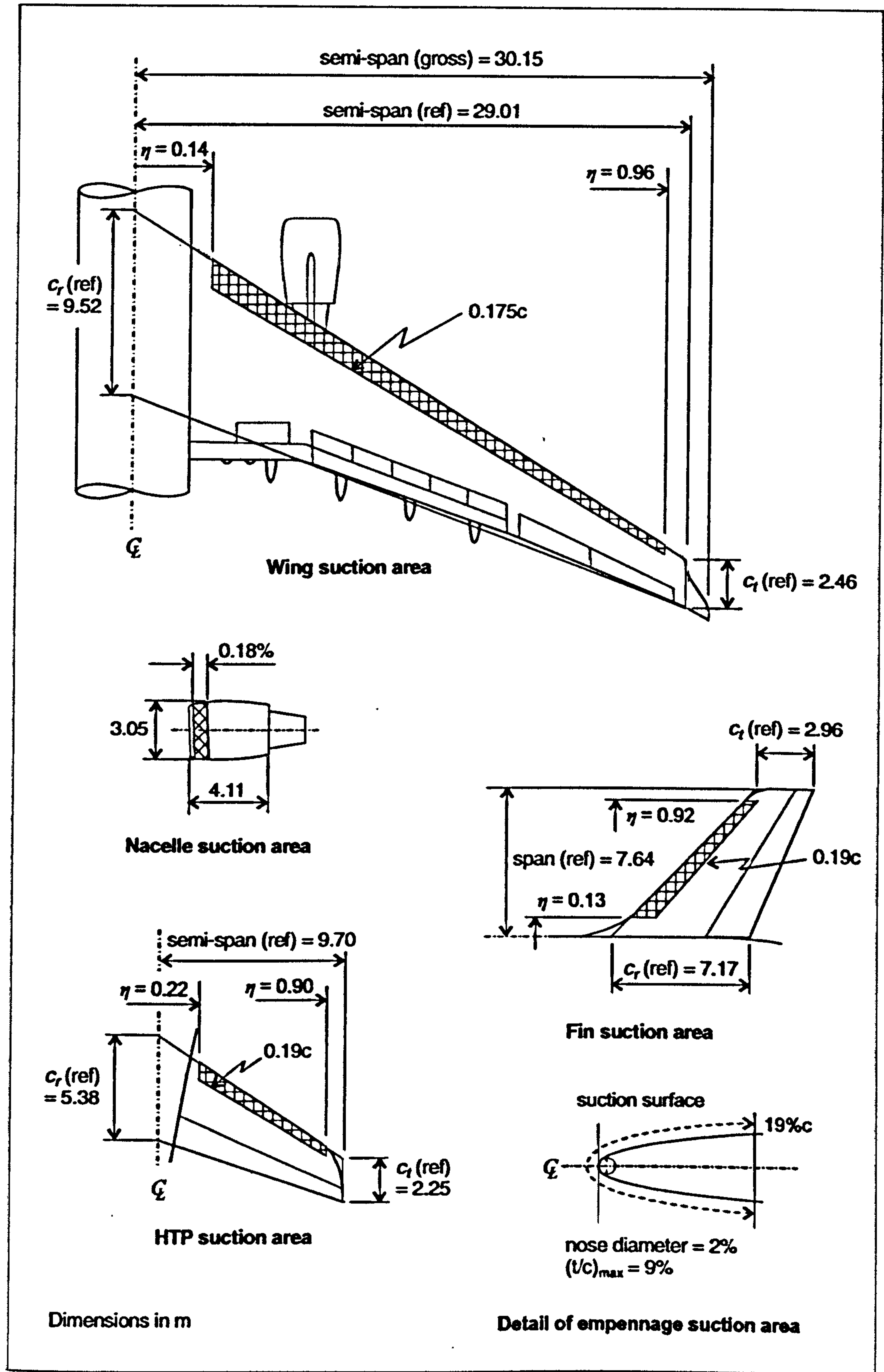


Fig. 7-5 Estimated planform areas of suction panels for A330-200 class aircraft



#### 7.4.4 Pump power

From an overall system perspective, the pressure loss through the suction system is a fundamental design issue, as it has a large bearing on the net performance benefit of the HLFC system. An approach that may be used to analyse a defined suction system is outlined in section J.2 (Appendix J). It is not possible to implement this approach fully for a conceptual design study, as detailed knowledge of the installed suction system is required. A simplified analysis has been undertaken for the B757-200 and A330-200 classes of aircraft. This is described in this section.

According to Atkin and Courtenay (2002), the required pump power can be determined using the following expression:

$$P_{pump} = \frac{\dot{m} c_p T_{in}}{\eta_{pump}} \left\{ \left( \frac{P_{in}}{P_{out}} \right)^{\frac{\gamma-1}{\gamma}} \left( 1 + \frac{\gamma-1}{2} M^2 \right) - 1 \right\} \quad \text{--- [7-2]}$$

where:  $P_{pump}$  is the pump power,  $\dot{m}$  is the mass flow rate,  $c_p$  is the specific heat capacity at constant pressure,  $T_{in}$  is the stagnation temperature at the design altitude conditions,  $\eta_{pump}$  is the overall pump efficiency (representing both mechanical and isentropic efficiencies),  $\gamma$  is the ratio of specific heats and  $M$  is the exit flow Mach number. The ratio  $\left( \frac{P_{in}}{P_{out}} \right)$  is the total pressure ratio across the pump. (This equation is repeated as [J-11] in Appendix J, where further details are given.)

An estimate of the pump power may be obtained using equation [7-2] if two critical parameters can be established for the particular design, viz. the total mass flow through the suction system and the pump pressure ratio. The mass flow rate ( $\dot{m}$ ) is given by the equation:

$$\dot{m} = \rho V_w S_{panel} \quad \text{--- [7-3]}$$

where:  $\rho$  is the air density,  $V_w$  is the panel velocity (or the mean velocity of air through the suction surface) and  $S_{panel}$  is the panel area.

The panel velocity is the critical output parameter resulting from the boundary layer stability analysis (see section B.3.5, Appendix B). This is dependent on the suction chamber layout, chamber pressure distribution and the external flow characteristics (which depend on the aerofoil profile). The chordwise extent of the laminar flow – which dictates the drag reduction – is thus dependent on all of these factors. The use of a mean panel velocity to estimate the pump power for a project design study, without undertaking this non-trivial investigation, is thus a rough approximation. The accuracy of the result will depend on the database used for estimating  $V_w$ . The velocities that have resulted from studies conducted in the HYLDA, HYLTEC and ALTTA projects (described in Appendix C) are of the order of 0.1 to 0.3 m/s.



The design pressure ratio across the pump depends on the suction panel porosity (see section B.4.5, Appendix B) and the detailed design of the suction system. For example, a simplified system, such as the ALTTA fin concept (see section 7.2.2 and B.5.3, Appendix B), will have a lower pressure loss than the more complex system installed in the B757 wing (Boeing, 1999a). System components, such as flow monitoring instrumentation and control valves, have been seen to substantially influence the pressure losses in the system.

The HTP of the B757-200 class aircraft was selected as a reference design for the assessment of the suction system installation. Using the dimensions of the suction surfaces defined in Fig. 7-4, a conceptual layout of a suction system was developed, enabling the principal dimensions of the ducts to be determined. A detailed flow analysis was performed on the system for a cruise altitude of 35000ft, as described in section J.2 (Appendix J). The results, given in the order of the sequential analysis undertaken, are recorded in Table J-2 (Appendix J). The estimated pump power for the HTP (one side) was 16.9kW for a panel velocity of 0.13m/s and the pump pressure ratio was evaluated to be 1.60. The pressure ratio was observed to be a little higher than the results calculated for a HLFC nacelle, based on HYLDA nacelle design parameters provided by Möller (2001). Conversely, greater pressure ratios would be expected for a HLFC wing design, where greater upstream losses would result from the more complex ducting system.

It was assumed that the calculated pressure ratio of 1.60 for the HTP would represent an average value for all components (i.e. wing, empennage and nacelle), for both classes of aircraft. The summary of results presented in Table 7-6 was obtained using equation [7-2] (details given in section J.2.6, Appendix J), and is based on a panel flow velocity ( $V_w$ ) of 0.13 m/s, a pump pressure ratio of 1.60, an exhaust Mach number of 0.20 and a compressor efficiency ( $\eta_{compressor}$ ) of 0.80.

Studies conducted during the HYLDA project (Appendix C.16) came to the conclusion that an electric induction motor driving a turbo compressor was the most efficient suction device for this application. This was also the solution adopted for the B757 study (Boeing, 1982). Based on a motor efficiency ( $\eta_{motor}$ ) of 0.80, the power required for the electric motors was determined. The results are given in Table 7-6.



**Table 7-6** Suction system power requirement for design cruise height

	Suction panel area (m <sup>2</sup> )	Mass flow (kg/s)	Suction power (kW)	Compressor efficiency	Motor efficiency	Pump power (kW)
<b>B757-200 class A/C</b>						
Wing (both sides)	26.20	1.293	43.8	0.8	0.8	68.4
HTP (both sides)	13.12	0.648	21.9	0.8	0.8	34.3
Fin	10.63	0.525	17.8	0.8	0.8	27.8
Nacelle (both)	8.84	0.436	14.8	0.8	0.8	23.1
Sum ->	58.8					153.6
<b>A330-200 class A/C</b>						
Wing (both sides)	56.28	2.777	94.1	0.8	0.8	147.0
HTP (both sides)	19.62	0.968	32.8	0.8	0.8	51.3
Fin	12.11	0.598	20.2	0.8	0.8	31.6
Nacelle (both)	14.18	0.700	23.7	0.8	0.8	37.0
Sum ->	102.2					266.9

#### 7.4.5 Engine power off-take

The power for the electric motors would come from a re-sized Integrated Drive Generator (IDG). As the start-up power requirement for the compressor is high, consideration has been given to using bleed air to drive an air turbine, which will start the compressor. Thereafter, the air turbine will be disconnected. A schematic of this hybrid system is shown in Fig. 7-6.

The steady state power off-take from the gearbox is given by:

$$P_{shaft\ gearbox} = \frac{P_{pump}}{\eta_{gen}} = \frac{P_{shaft\ compressor}}{\eta_{gen} \eta_{motor}} = \frac{P_{suction}}{\eta_{gen} \eta_{motor} \eta_{compressor}} \quad \text{--- [7-4]}$$

According to Rolls Royce (2000b), the efficiency of a modern Integrated Drive Generator ( $\eta_{gen}$ ) is of the order of 0.65 to 0.75. A mean value of 0.70 has been used later in section 7.4.6.

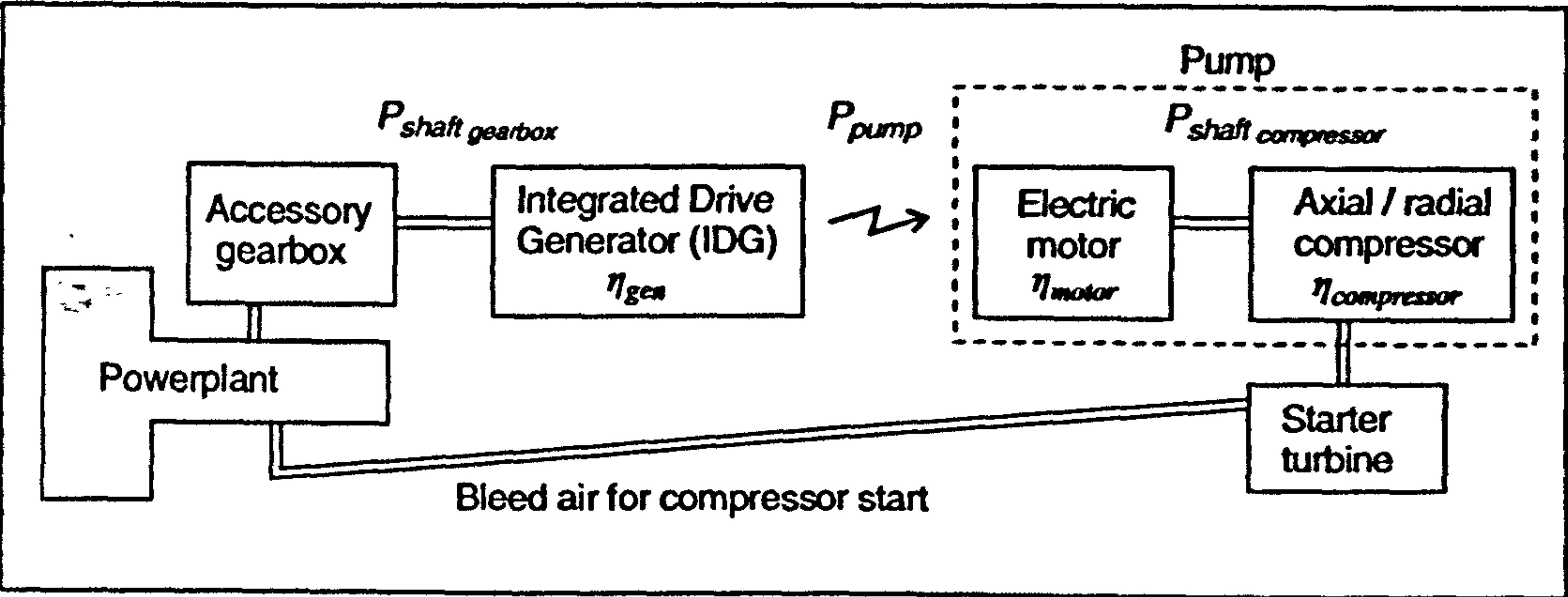


**Fig. 7-6** Schematic of proposed power generation for suction system



#### 7.4.6 SFC penalty for suction power

The approach adopted to establish the "exchange rate" between power off-take and SFC increase comprised a review of available data and the use of the Cranfield University Turbomatch engine modelling computer program. For the two reference engines, the Rolls-Royce RB211-535E4 and the Trent 772, the Turbomatch software was used to assess this relationship<sup>13</sup>. Available data, including takeoff SLS thrust and SFC, bypass ratio, pressure ratio and mass flow, were used to establish generic engine models. The model input parameters were then revised to get the SFC in cruise to within ~2% of the values established in Appendices F and G, for the two engines. The control (design point) data and full details of the study are described in section J.5 (Appendix J). As the engine models do not comply in all respects with the reference engines, a distinction is made herein and the model engines are referred to as the *Trent 772 class* engine and *RB211-535E4 class* engine. The final results are given in Figures 7-7 and 7-8.

It is observed that the SFC penalty decreases monotonically with increasing engine thrust and that the altitude variation (37000 to 41000ft for the Trent 772 model) had only a minor influence on the SFC penalty. For the B757-200 class aircraft, the cruise would typically commence with a thrust of ~32.5kN, reducing to ~24.5kN by the end of a medium range cruise (Fig. 7-7). The mid-cruise point would correspond to a SFC penalty of ~0.74% per 100kW power off-take. For the A330-200 class aircraft the cruise would typically commence at 37000ft, with a thrust requirement of ~55kN, reducing for a long-range cruise to ~36kN at 41000ft (Fig. 7-8). A mean SFC penalty of 0.54% per 100kW shaft power off-take was estimated for the A330-200 class aircraft.

By comparison, Boeing used a conservative value of 1% SFC increase for the 103kW power extraction (required from each engine for the pumps) for the HLFC study, based on the B757 (Boeing, 1982). Wilson (1997) also investigated the percentage reduction in the SFC due to shaft power off-take using the Turbomatch program. He explored the SFC penalty by modelling the Trent 775, CF6-80C2-A2 and CFM-56-5C-2 engines (Table 7-7). By comparison, his results are consistently lower than those given above. This can be explained by noting that his analysis was based on the maximum rated engine thrust. Using the trend established in Fig. 7-7, it would be expected that the SFC penalty at a typical mid-cruise thrust would be ~30% higher than that at the maximum rated cruise thrust. Taking this correction into account would bring the results of Wilson roughly into line with those given above.

---

<sup>13</sup> It is acknowledged that P. Laskaridis, School of Engineering, Cranfield University, provided assistance in modelling the engines using the Turbomatch program (Jan. 2002).



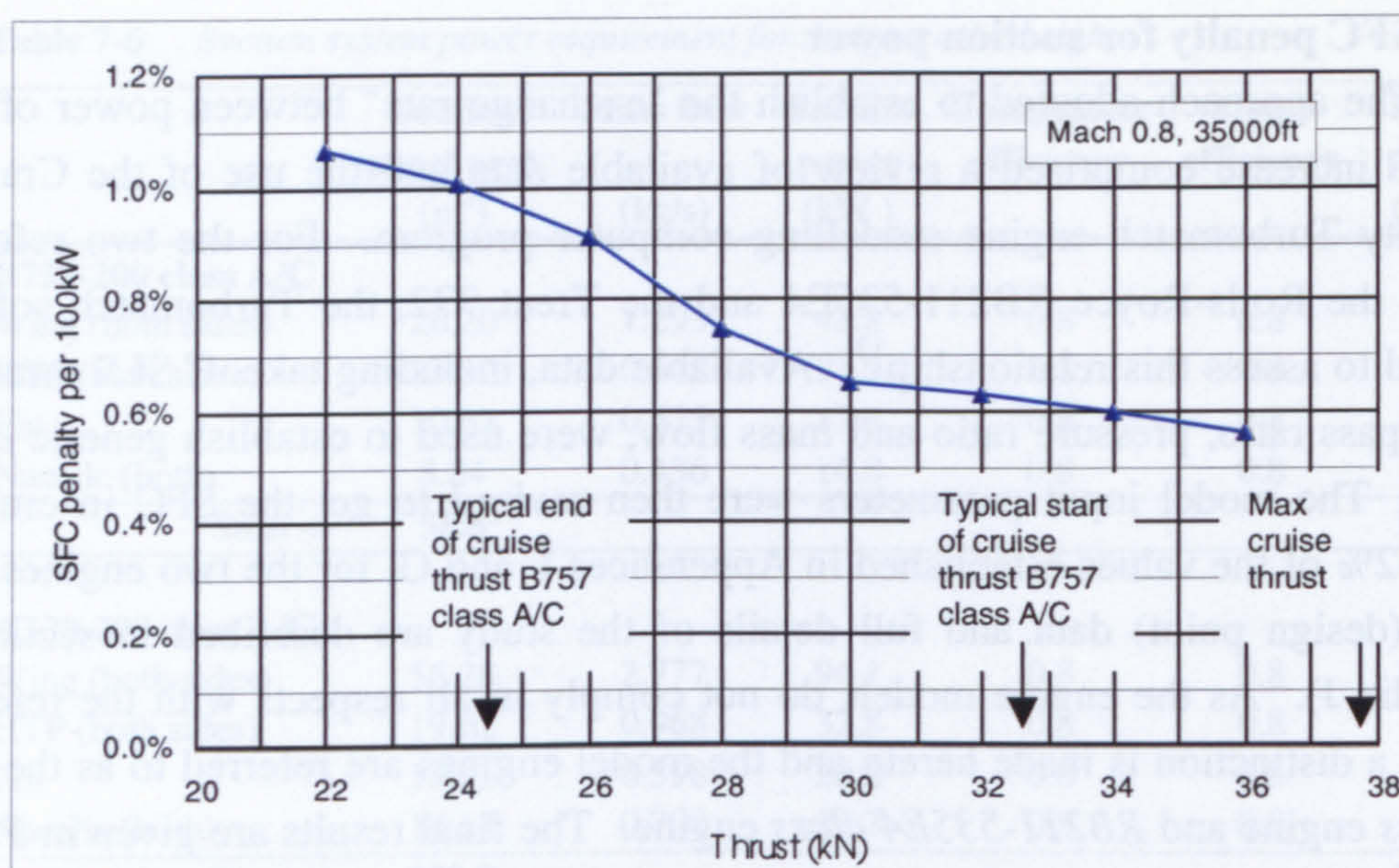


**Fig. 7-7** SFC penalty per 100kW shaft power off-take for RB211-535E4 class engine (conditions: bleed air 0.25kg/s, datum power off-take 100kW)

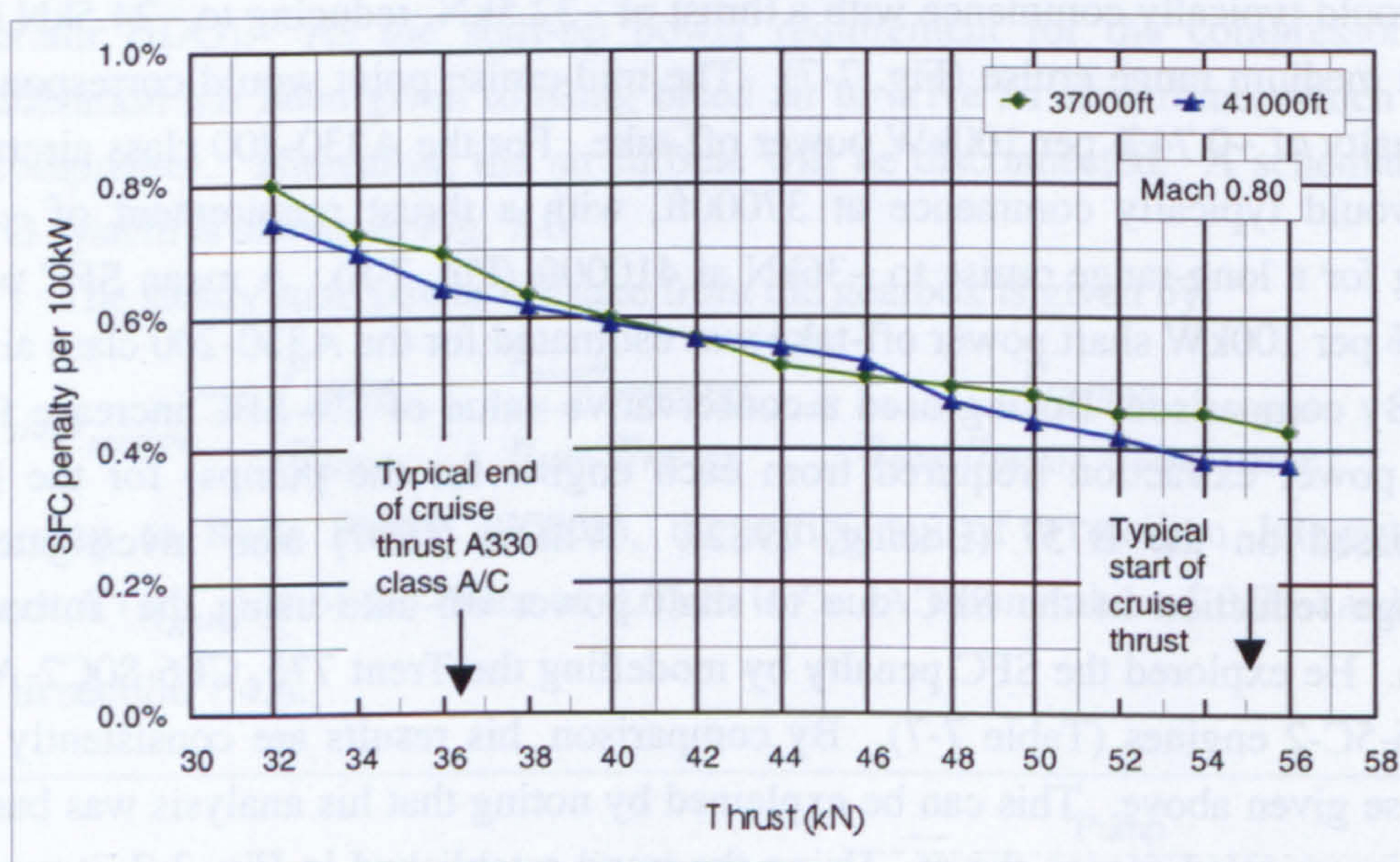


**Fig. 7-8** SFC penalty per 100kW shaft power off-take for Trent 772 class engine (conditions: bleed off-take 1.13 kg/s, datum power off-take 200kW)

Also shown in Table 7-7 is the data for the RB211-22. This was the first generation RB211 engine and had slightly different design parameters to the newer -535E4 engine (Rolls-Royce, 1998). Nevertheless, it was expected that the SFC penalty would be reasonably close to the results given in Fig. 7-7, and this was confirmed. Furthermore, the author was informed that the SFC penalty would be in the region of ~0.7% per 100kW for an engine in the class of the RB211 at typical cruise thrust (Rolls-Royce, 2000a). This is consistent with the results shown in Fig. 7-7. The Trent 500



(installed on the A340) is an engine of lower thrust but higher bypass ratio than the Trent 772. The SFC penalty given in Table 7-7 is seen to be consistent with that determined using the Turbomatch software.

Based on the established "exchange rates" of power off-take to SFC penalty, the increases in SFC for the B757-200 and A330-200 classes of aircraft have been calculated for the estimated suction pump power requirements (Table 7-8).

**Table 7-7** *SFC change for shaft power off-take*

Engine	SFC change per 100kW off-take	Thrust	Source
Trent 775 model*	0.40%	51.1kN (max. cruise thrust)	Wilson (1997)
CF6-80C2-A2 model*	0.35%	50.5kN (max. cruise thrust)	Wilson (1997)
CFM-56-5C-2 model*	0.59%	30.9kN (max. cruise thrust)	Wilson (1997)
RB211-22	0.46%	39.5kN (max. cruise thrust)	Rolls-Royce (1968)
Trent 500	0.49%	Cruise thrust at Mach 0.82	Rolls-Royce (2000b)

\* Modelled by Wilson (1997) using Turbomatch program

**Table 7-8** *Estimate of SFC penalty for HLFC systems in B757-200 and A330-200 class aircraft*

Engine	Pump power required for HLFC (kW)	$\eta_{gen}$	Engine shaft power off-take for HLFC (kW)	SFC change per 100kW shaft power off-take at mid-cruise thrust	SFC increase at mid-cruise thrust
RB211-535E4 class	153.6	0.70	219.4	0.74%	1.62%
Trent 772 class	266.9	0.70	381.3	0.54%	2.06%
Note ->	1	2	3	4	

Notes:

1. Results from Table 7-6.
2. Efficiency taken as mid-range value for IDG efficiencies (Rolls-Royce, 2002b).
3. Evaluated using equation [7-4].
4. Taken as mid-cruise SFC penalty from Fig. 7-7 and Fig. 7-8.

#### 7.4.7 SFC penalty versus equivalent drag

To complete the investigation into the pump power required for the HLFC system, the result for the B757-200 class aircraft was cross-checked against the result reported by Atkin and Courtenay (2002), using the equivalent drag approach mentioned in section 7.4.1. The results of the sensitivity study for case 1B (described in Chapter 6) were used. For a 1.62% SFC change (reported in Table 7-8 above) the increase in trip fuel for these conditions (i.e. 3272nm and 19147kg payload) is ~1.74%, which is equivalent to a 1.81% increase in drag. These values can be estimated from the nomogram in Fig. 6-3. If the net drag reduction at the mid-cruise point for this aircraft is taken as 14.3% (section 7.3.3), then the pump power penalty will reduce the drag benefit by ~12.7%. Atkin and Courtenay (2002) reported that for their study (which



was based on the laminarisation of part of the A310 aircraft wing), the pump "drag" reduced the laminar flow drag benefit by ~15%.

## 7.5 MASS OF HLFC SYSTEM

### 7.5.1 Mass estimation approaches

The mass of a HLFC system can be estimated in two ways for a conceptual design study:

- (1) Using a reference parameter such as the MTOW, the system mass can be estimated by scaling results derived from previous studies / projects (i.e. a top-down approach);
- (2) The system architecture can be defined, and a system mass determined by summing the estimated component mass values and adding an allowance for the installation of the components (i.e. a bottom-up approach).

The difficulty with the first approach is that there is very little data available about HLFC systems in the required configuration; and the problem with the second approach is that it is dependent on a detailed definition of the complete system being available.

### 7.5.2 Mass estimate based on parametric data

Arcara *et al.* (1991) report on a NASA study conducted to evaluate the application of HLFC to a 300 passenger long-range twin-engine conceptual design (see section B.7.7, Appendix B). The estimated system weight was 0.51% of the MTOW. Similar studies were conducted by Wilson (1997), who investigated the impact of HLFC on five different classes of aircraft. The results are given in Table 7-9 as items 2 to 6. The system weight values were observed to fall within a narrow range from 0.77 to 1.02% of the MTOW, with a mean of 0.89%. As the OEW had been used as the reference parameter in Chapter 6, it was convenient to "translate" the ratios in Table 7-9 to equivalent values in terms of OEW. The ratio of OEW to MTOW is ~0.51, based on quoted values for the B757-200 and A330-100 aircraft (see Tables F-1 and G-1, in Appendices F and G respectively). This ratio is consistent with the data compiled by Roskam (1985) for this class of aircraft. The estimated mean system weight is therefore 1.74% of OEW.

For all of these studies HLFC was considered on the wing, empennage, and nacelles. Using the mean value of the results of Wilson, the HLFC system mass was estimated for the B757-200 and A330-200 classes of aircraft. These results are given as items 7 and 8 in Table 7-9.



**Table 7-9** *Mass of HLFC system*

No.	Aircraft type	$W_{TO}$ (kg)	$\Delta W_{HLFC}$ (kg)	$\frac{\Delta W_{HLFC}}{W_{TO}}$	$\frac{\Delta W_{HLFC}}{W_{OEW}} *$	Reference / Note
1	Long-range twin	1289946	6600	0.51%	1.00%	Arcara <i>et al.</i> (1991)
2	Regional jet	44661	375	0.84%	1.65%	Wilson (1997)
3	Short-range twin	71943	552	0.77%	1.50%	Wilson (1997)
4	Medium range twin	198710	2022	1.02%	2.00%	Wilson (1997)
5	Long-range quad	206839	1776	0.86%	1.68%	Wilson (1997)
6	Super jumbo	489612	4657	0.95%	1.87%	Wilson (1997)
<b>The mean value for items 2 - 6 is:</b>				<b>0.89%</b>	<b>1.74%</b>	
7	B757-200 class A/C	115660	1029	0.89%	1.74%	Estimate based on mean
8	A330-200 class A/C	233000	2074	0.89%	1.74%	Estimate based on mean

Notes:

\* Based on fixed ratio of OEW to MTOW of 0.51

 $\Delta W_{HLFC}$  is the increase in A/C weight due to the HLFC system for: wing, empennage and nacelles.

### 7.5.3 Mass estimate based on system components

The alternative "bottom-up" approach requires a complete definition of the HLFC system. Again, the HTP for the B757-200 class aircraft was used as a reference case. The system layout is shown in Fig. 7-9. Mass estimates for the individual components were established under four headings or mass groups, i.e. (1) Suction surface, ducts and valves; (2) Control and monitoring system; (3) Pump system and power generation; and (4) Anti-contamination system.

The wetted surface area (given in Table 7.5) and diameter and length of the suction system ducts (given in Table J-2, Appendix J) had been estimated as part of pump power calculation. This enabled the mass of the perforated skin and the ducting to be determined. It was assumed that the skin would be made from titanium, which would replace the existing aluminium skin. It was also assumed that a liquid / foam anti-contamination system would be used. Estimates were made for the mass of the system components and an installation factor of 10 - 15% was included as a provision for brackets, fasteners, additional access panels, etc. The complete mass breakdown is given in section J-6 (Appendix J). The installed system mass for the HTP (one side) was estimated to be 148kg.

For each of the four mass groups a scale factor was determined by dividing the mass of the group by the estimated pump power for the HTP. These scale factors were then used to estimate the mass of HLFC system installations in the wing, empennage and nacelle, for both classes of aircraft. The results are given in Table 7-10. The one departure from this process concerned the anti-contamination system of the wing. It was assumed for the purpose of the mass estimate that a Krüger flap would be used. Boeing (1982) determined that this change of the leading edge device for the B757-200 would result in a mass reduction of ~150kg. However, the report also indicated that changes to the trailing edge devices may be required, which would reduce the mass saving. It was assumed for the current study that there would be no overall mass change



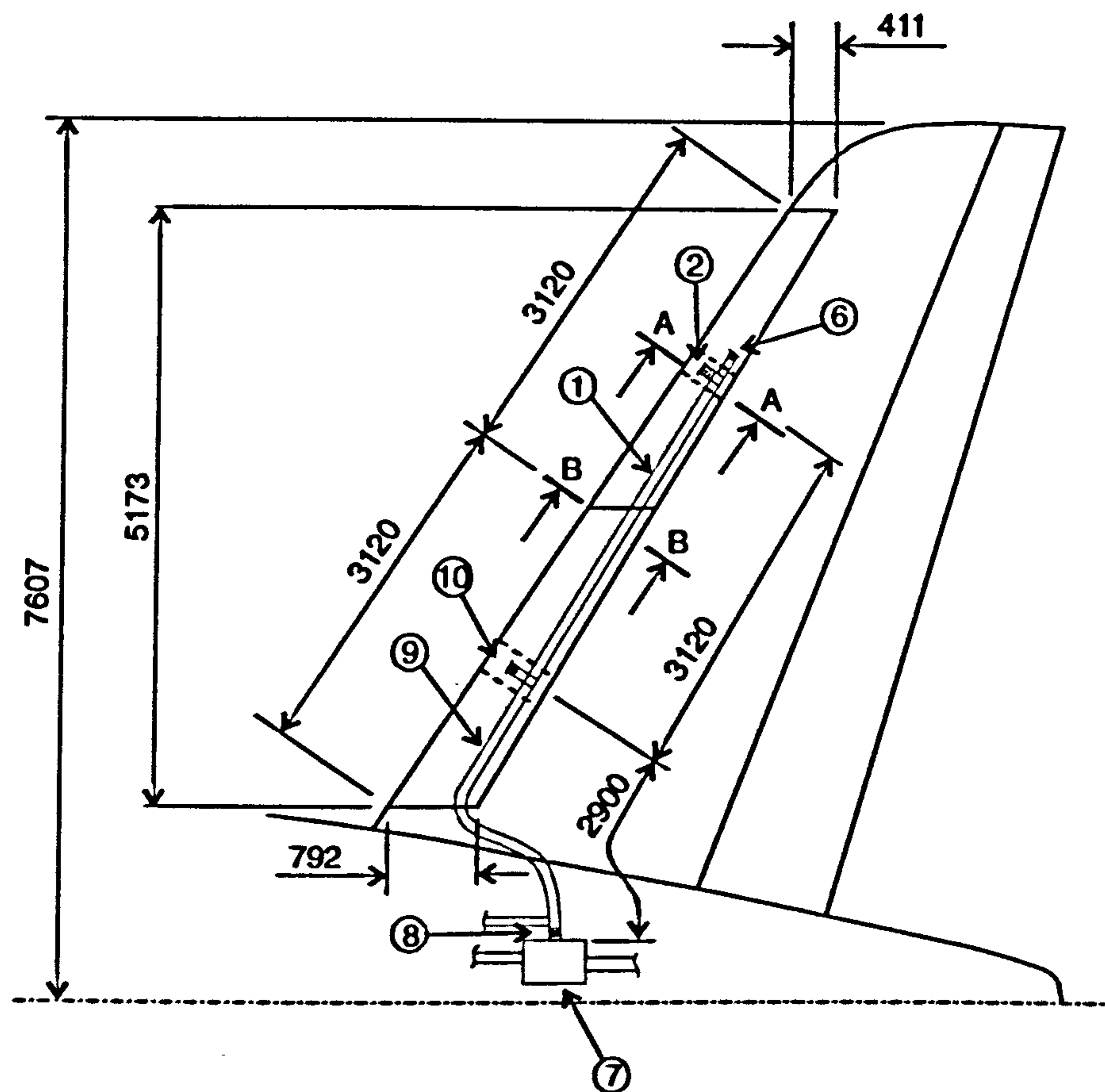
for the wing leading and trailing edge devices. There is a further requirement for anti- / de-icing on the wing surface. This was based on a hot air transpiration technique (described by Boeing, 1999; and Humphreys and Horstmann, 2000; for example), whereby a reverse flow of hot air is blown through the suction system. (The same system would be used to purge the ducts of water.) A provision for additional valves and ducting has been made.

The installed system weight represents 2.00% and 1.62% of the OEW, for the B757-200 and A330-200 classes of aircraft respectively. These values are seen to be similar to the estimates of Wilson (1997). Due to the nature of the estimation techniques adopted it would be expected that these results would be accurate to  $\pm 15\%$ .

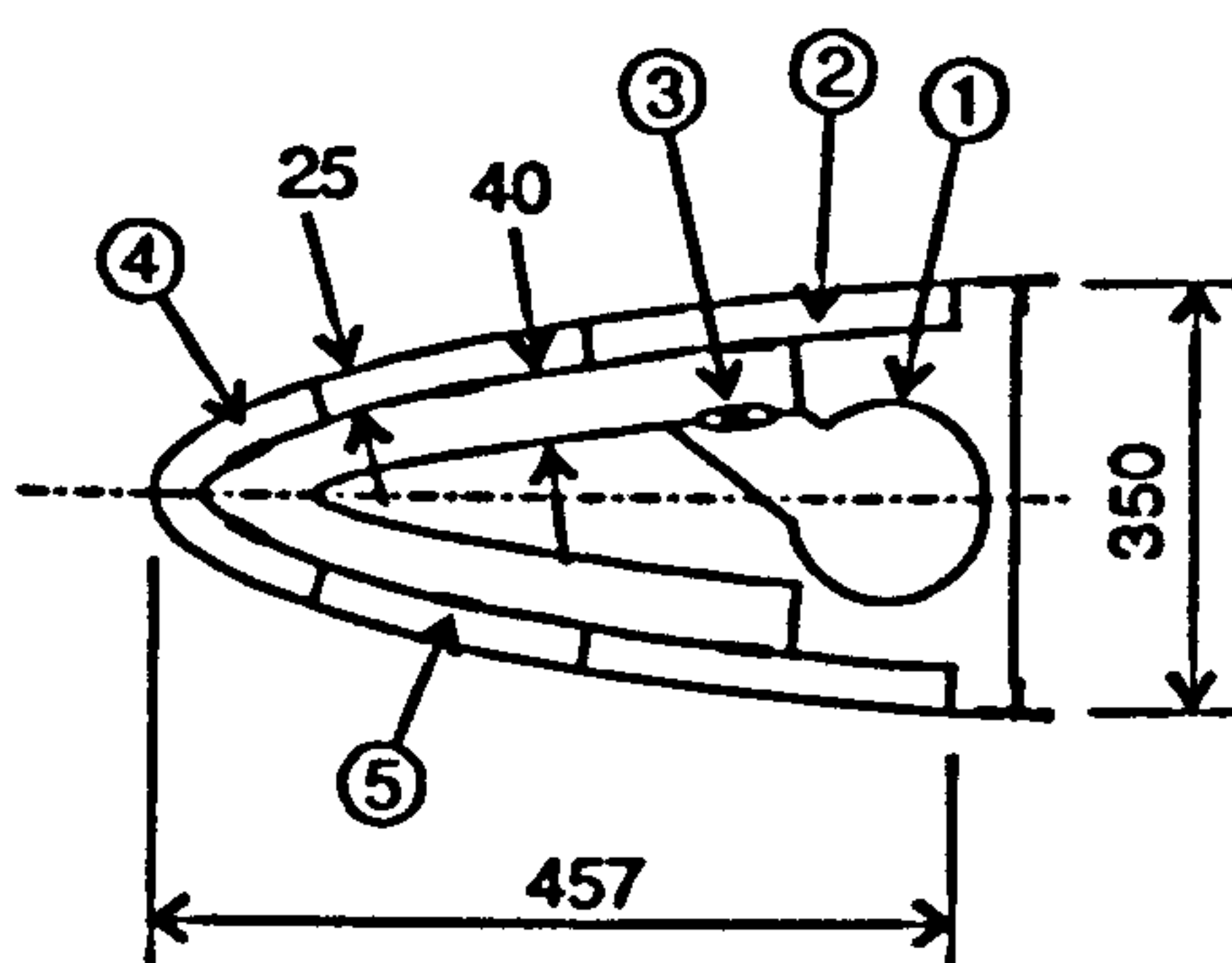
**Table 7-10** *Mass of HLFC system (based on scaled values for HTP case study)*

	Pump power (kW)	Surfaces ducts & valves (kg)	Control system (kg)	Pump system & Power (kg)	Decontamination system (kg)	Anti- / de-icing system (kg)	Totals (kg)
<b>B757-200 class A/C</b>							
Wing (both sides)	68.4	152.3	73.5	195.4		11.0	432
HTP (both sides)	34.3	76.3	36.8	97.9	84.1		295
Fin	27.8	61.8	29.8	79.3	68.1		239
Nacelle (both)	23.1	51.4	24.8	65.9	56.6		199
sum ->	153.6						1165
<b>A330-200 class A/C</b>							
Wing (both sides)	147.0	327.2	157.8	419.8		15.0	920
HTP (both sides)	51.3	114.1	55.0	146.4	125.7		441
Fin	31.6	70.4	34.0	90.3	77.6		272
Nacelle (both)	37.0	82.4	39.8	105.8	90.8		319
sum ->	266.9						1952
Scale factor ->		2.23 (kg/kW)	1.07 (kg/kW)	2.86 (kg/kW)	2.45 (kg/kW)		

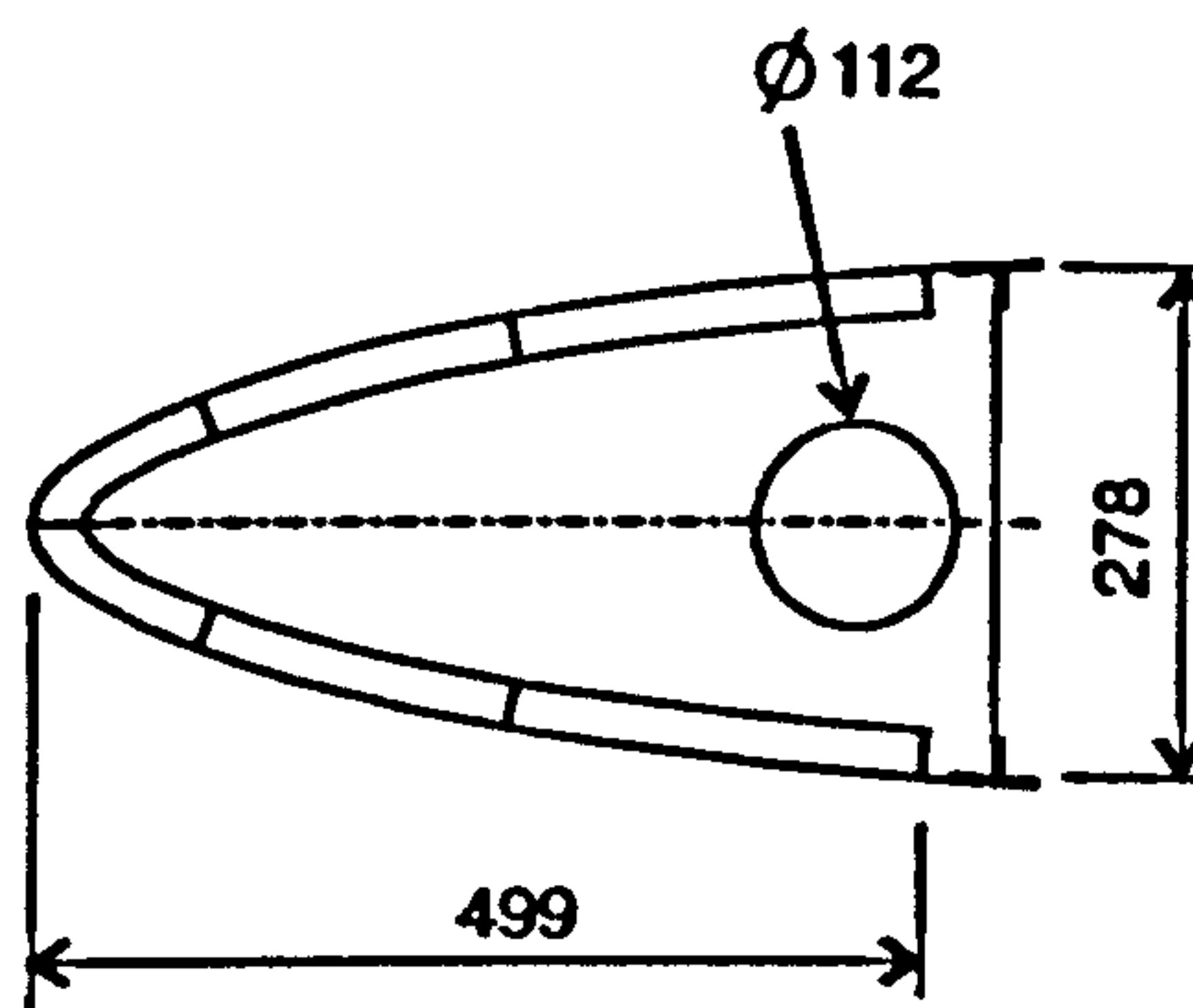




**HLFC system installation in right hand HTP**



**Section AA: Detail of nosebox at connector duct**



**Section BB: Detail of nosebox**

- |                        |                        |
|------------------------|------------------------|
| ① Transfer duct no. 1  | ⑥ Over pressure valve  |
| ② Connector duct no. 1 | ⑦ Suction device       |
| ③ Control valve        | ⑧ Shut-off valve       |
| ④ Suction chamber      | ⑨ Transfer duct no. 2  |
| ⑤ Orifice              | ⑩ Connector duct no. 2 |

Not to scale

Dimensions in mm

**Fig. 7-9** Principal dimensions and layout of HLFC system in right hand HTP of B757-200 class aircraft (established to estimate pump power and system mass)



## 8 ICE CLOUDS

### 8.1 INTRODUCTION

Having explored the potential that exists for fuel reduction using HLFC technology, the focus of the study shifted to the investigation of environmental and mechanical factors that could impact the operational effectiveness of HLFC aircraft, by reducing the *ideal* fuel savings (described in Chapter 6). The first issue studied was the phenomenon whereby flight through cirrus clouds has been known to temporarily disrupt laminar flow. There are three aspects of this issue that are explored in this chapter. The first deals with the effect of cloud particles on LFC, the particle size and the particle concentrations that are needed to produce a transition of the boundary layer (section 8.2). The second part concerns the cloud climatology on typical airline routes (section 8.3). In this regard, it is necessary to address the fundamental questions: what is the probability of cloud encounter on airline routes, and what is its variability with altitude, season, and location? As part of this study, a model – in terms of cloud frequency – is established which may be used to assess the probable loss of laminar flow on typical airline routes. Lastly, the ability of Meteorological Services to forecast cirrus at these altitudes to the desired resolution is investigated (section 8.4). Supporting details regarding the data capture and the analysis of clouds are included in Appendix K.

### 8.2 TRANSITION DUE TO CIRRUS CLOUDS

#### 8.2.1 Flight test data

The loss of laminar flow due to cirrus clouds was extensively reported following the X-21A and the Jetstar flight tests (see sections C.3 and C.4 of Appendix C). In later flight tests, flights were specifically conducted away from clouds because of the instrumentation used to detect the laminar flow, and little or no substantive data was recorded.

#### 8.2.2 X-21A flight experience

The USAF sponsored Northrop X-21A flight test programme (described in section C.3, Appendix C) evaluated laminar flow using two experimental aircraft (Fig. C-1). At a cruise condition of Mach 0.75 and 40 000ft it was observed that laminar flow was lost whenever the aircraft penetrated cirrus clouds, with horizontal visibilities estimated to be about 1.5 - 3 km (Davis and Fischer, 1983). It was noted that this was a reversible phenomenon and laminar flow was restored almost immediately after the aircraft left the cloud. Furthermore, laminar flow was observed to be partially degraded or erratic when the aircraft flew through light cirrus haze, even where the horizontal visibility was as great as 80km.



The X-21A observations were investigated by Hall (1964), who suggested that ice crystals (which make up the cirrus clouds) entering a laminar boundary layer shed turbulent vortices, which caused the transition. He analysed the path of columnar ice crystals<sup>14</sup> of length-to-diameter ratio of 2.5, impinging on an elliptical approximation of the leading edge of the X-21A wing. The results indicated that for the flight condition of Mach 0.75 at 40000ft, particles shorter than 4 $\mu$ m follow the streamlines. With increasing size, the inertia forces prevail over the aerodynamic forces and the particles penetrate the boundary layer; however, breakdown of the laminar flow does not result until the particles reach a critical size. Significantly, particles of this critical size must be present in sufficiently large numbers to cause boundary layer transition.

The key factors which would determine whether any given cloud encounter would cause total or partial loss of laminar flow are: (1) The particle size; (2) The concentration of particles in the air; and (3) The time it would take the particles to travel through the boundary layer. It is convenient to describe the latter two parameters as the particle flux. Fig. 8-1 (attributed to Hall, 1964; but redrawn using data from Davis *et al.*, 1987) is one result for the flight condition of Mach 0.75 at 40000ft. The abscissa variable is the equivalent melted diameter (EMD) and the ordinate is the particle concentration. It is seen that particles smaller than 33 $\mu$ m EMD or a concentration of less than  $\sim 500\text{m}^{-3}$ , produce no effect (regions 1 and 2), and with increasing size and concentration there is an increasingly detrimental effect on laminar flow. Partial loss would occur if the concentration of particles greater than 33 $\mu$ m EMD exceeded  $\sim 500\text{m}^{-3}$  (region 3). The lower threshold between partial loss and no loss was based on a 10% laminar flow loss. Ice crystals greater than 33 $\mu$ m EMD with concentrations greater than  $\sim 10^5\text{m}^{-3}$  resulted in a total loss of laminar flow (region 4). The critical particle size, it was noted, was smaller at lower altitudes.

For the X-21A flight tests, it was demonstrated that the ice crystals were generally larger than the critical size. The duration of a particle passing through the boundary layer was shown to be sufficient to initiate turbulence, and the predicted flux of ice particles in cirrus clouds with a visibility of 5 000 to 10 000ft, was high enough to cause the observed loss of laminar flow (Hall, 1964; Davis *et al.*, 1987). Davis *et al.* (1987) caution against the generalisation of these results to other aircraft, and note that the regions on the plot are "functions of airfoil leading edge shape and sweep, and of aircraft speed and altitude". Joslin (1998a) in reviewing this issue, indicated that transition induced by the wake of a particle was a local effect, independent of the usual parameters (e.g. pressure gradient) influencing boundary layer transition.

---

<sup>14</sup> Ice crystals in cirrus clouds occur in several crystalline forms (habits). The columnar variety is only one such form, as described in Appendix K.



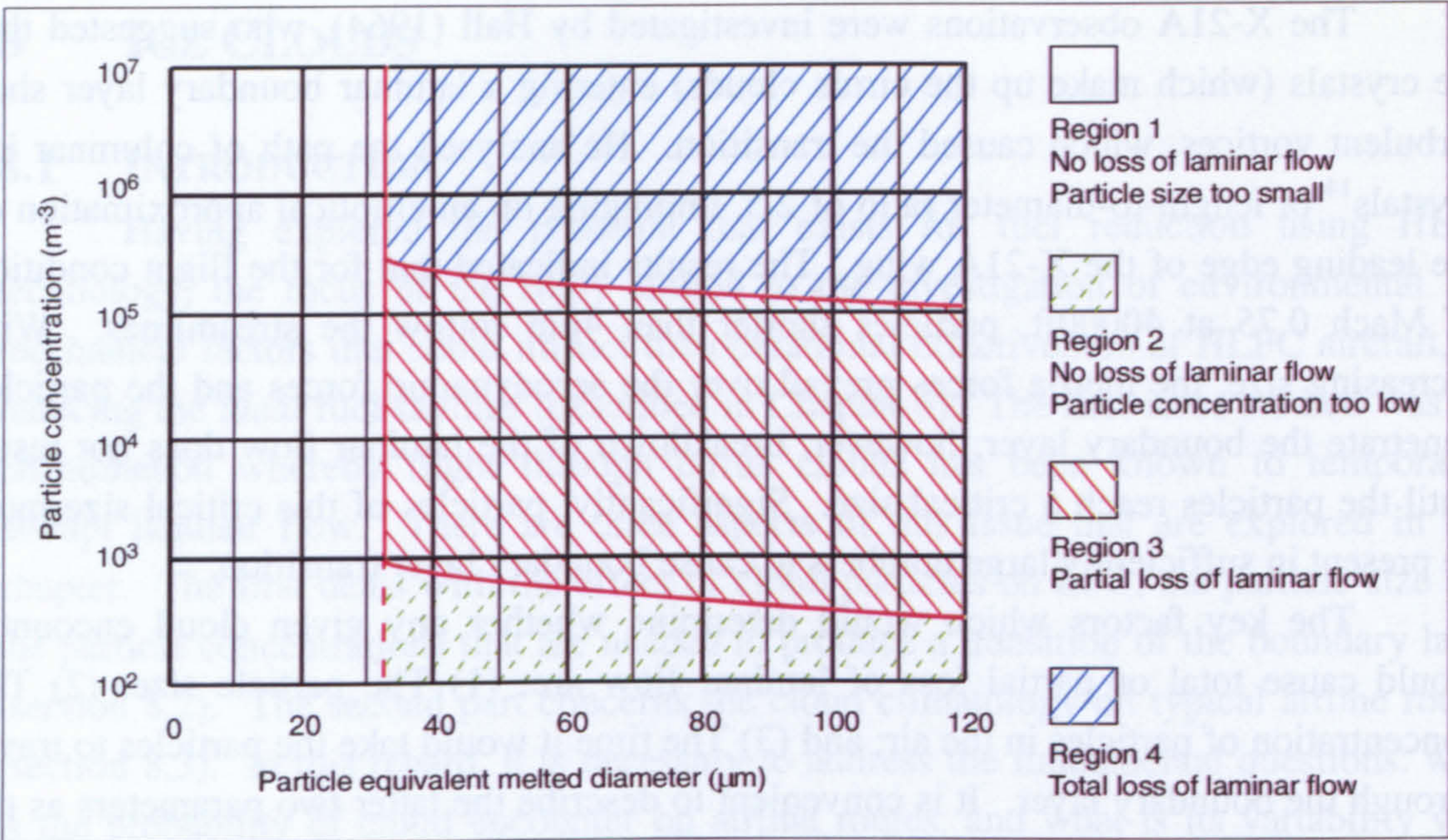


Fig. 8-1 Hall criteria for X-21 at 40000ft, Mach 0.75 (redrawn after Davis et al., 1987)

8.2.3 Jetstar flight testing

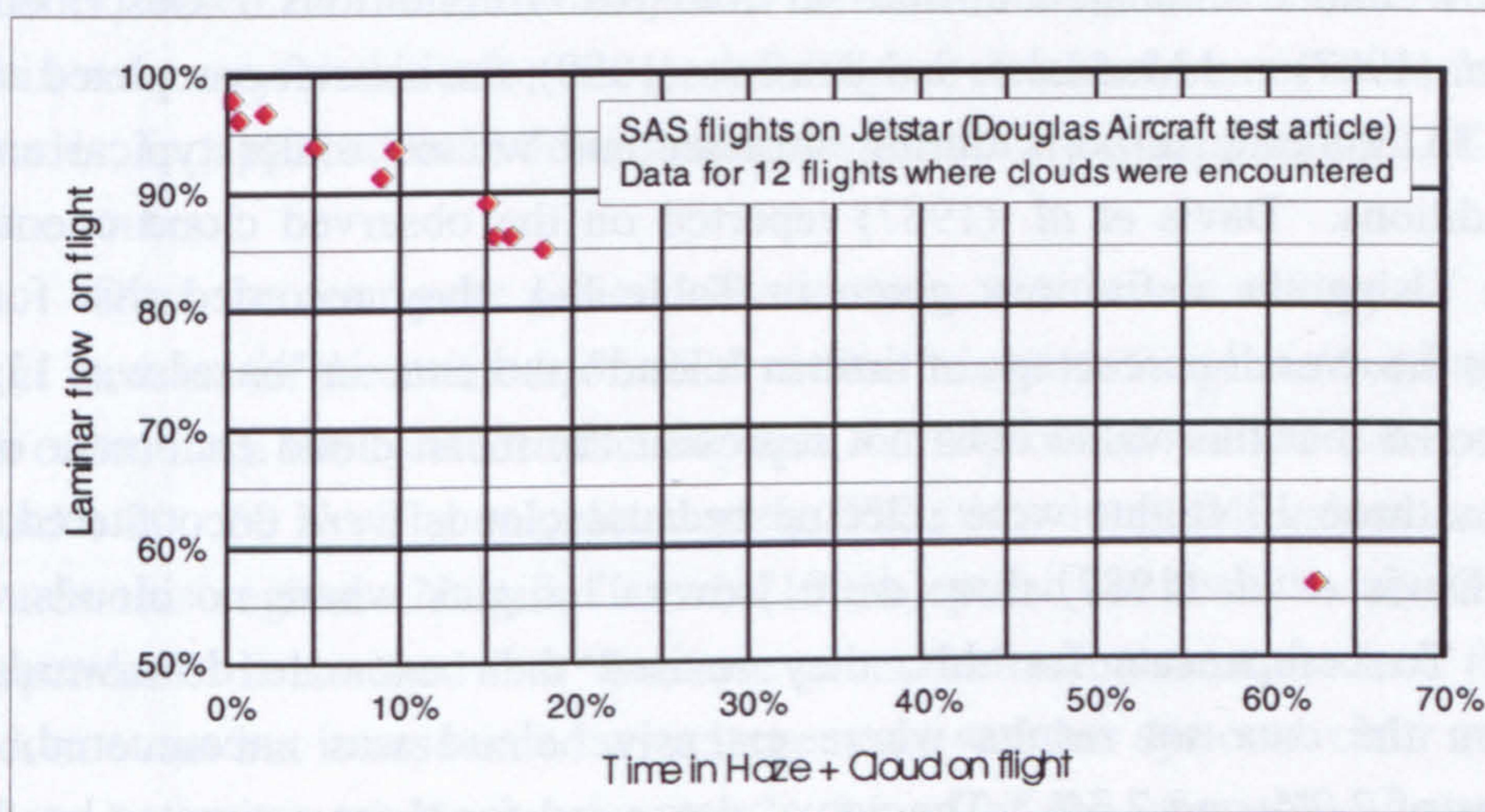
Davis and Fischer (1983) indicate that one of the goals of the LEFT (Leading-Edge Flight Test) experiment was to develop, through operational experience, plots such as those shown in Fig. 8-1 for the Jetstar aircraft. This, it was intended, would allow a limited validation of the Hall criteria (developed for the X-21A) and would explore its extension to other aircraft. Concurrent measurements of laminar flow and ice particle concentrations were made (Davis et al., 1987). The extent of laminar flow on the wing surface was measured using an array of evenly spaced small Pitot tubes (commonly referred to as a "rake"), mounted behind the LFC test article, at a distance of ~1.8mm off the surface. Ice particles were identified using a spectrometer and charging patch. Davis et al. (1987) report that the degree of laminar flow on the test articles changed simultaneously as the aircraft entered visible cloud. As indicated in Table 8-1 a concentration of particles of more than 1000m<sup>-3</sup>, with a size larger than 60μm, was taken as "in-cloud", whilst a concentration of between 0 - 1000m<sup>-3</sup> was taken as "in haze". Fig. 8-2, generated by the author using the results of Davis et al. (1987), shows the correlation of cloud encounter with measured laminar flow (on the Douglas Aircraft test article) for 12 flights, where significant cloud amounts were encountered.

Table 8-1 Cloud definitions used for Jetstar flights (Davis et al., 1987)

Definition	Particle size	Concentration
Cloud	> 60μm	> 1000 m <sup>-3</sup>
Haze	> 60μm	0 to 1000 m <sup>-3</sup>
Clear	> 60μm	0 m <sup>-3</sup>



Davis *et al.* (1987) concluded that the data showed "Hall criteria-like" behaviour in that increasing particle concentrations led to progressively smaller degrees of laminar flow. They stated that the Jetstar observations validated qualitatively the Hall criteria, but cautioned that this was only a limited validation because the aerofoil shape, altitude and Mach number conditions were different to those for which the original Hall figure was derived.



**Fig. 8-2** Correlation of cloud encounter with laminar flow for the Jetstar based on results from Davis *et al.* (1987). (Data reproduced as Table K-1, Appendix K.)

#### 8.2.4 Falcon HLF flights

In some recent laminar flow tests, flights were specifically conducted away from clouds because of the instrumentation used to detect the laminar flow. Tribot (2001) of Dassault, when questioned by the author on this issue, stated that there were no observations of a loss of laminar flow during the Falcon 50 and Falcon 900 NLF and HLF flight tests (see section C.5 and C.9 Appendix C), as "no flights were done in such conditions because of the measurement techniques used on each glove (i.e. hot film technique, which is very sensitive to humidity)".

### 8.3 CLOUD CLIMATOLOGY

#### 8.3.1 Cloud encounter probability

The *average* time that an aircraft will spend in cloud is an important parameter in establishing the net benefit of HLFC technology. The earliest estimate of the time that a LFC aircraft would spend in cirrus clouds, resulting in a loss of laminar flow, was established by Snyder (1964) of the USAF, following the X-21A observations. Fowell and Antonatos (1965), reporting on the work of Snyder, state that "for a number of specific routes of practical interest for aircraft operations, an aircraft might be expected to be in cloud only about 3% to 6% of the time". More detailed information comes



from the Jetstar experiments and from measurements taken on board commercial aircraft during routine service (for reasons other than for the study of laminar flow). These studies are reviewed in this chapter.

### 8.3.2 Jetstar Simulated Airline Service (SAS) data analysis

The NASA Jetstar LEFT programme evaluated the effectiveness and practicality of laminar flow under simulated airline service (SAS) conditions. Described by Maddalon *et al.* (1987) and Maddalon and Braslow (1990), the aircraft completed about 62 flights to 33 domestic airports during summer and winter, under typical airline operating conditions. Davis *et al.* (1987) reported on the observed cloud encounter environment. Using the definitions given in Table 8-1, they recorded that for 13 selected flights the overall percentage of time in "cloud" plus time in "haze" was 11.4%. It should be noted that this value does not represent the mean cloud encounter of all SAS flights, as those 13 flights were selected because clouds *were* encountered, and according to Davis *et al.* (1987) there were "several" flights where no clouds were encountered. To compensate for this, they revised their estimate downwards by removing from the data set results where extensive cloud was encountered, thus yielding values of 7.2% and 7.3%. The actual data used for these estimates has been reproduced in Table K-1 (Appendix K). It was concluded by Davis *et al.* (1987), that the figure of 7.2% is "probably an upper bound on the likelihood of cloud encounter on an overall basis".

### 8.3.3 Global Atmospheric Sampling Program (GASP) data acquisition

The most complete set of measured cloud encounter and particle concentration data available to date on airline routes was obtained during the NASA Global Atmospheric Sampling Program (GASP) from March 1975 to June 1979. Conducted by the NASA Lewis Research Center for the US Department of Transportation, meteorological and trace-constituent measurements of ambient atmospheric conditions were taken aboard four Boeing 747 airliners in routine commercial service world-wide (Perkins and Gustafsson, 1975; Gustafsson *et al.*, 1979).

The cloud particle measurements were taken by light-scattering particle counters installed on the aircraft. Some 88000 cloud encounter measurements were made on more than 3000 flights (Davis and Fischer, 1983). Observations of 256 seconds were recorded at nominal 5 or 10 minute intervals, at altitudes above 20000ft. For each observation, the number of seconds that the aircraft was "in-cloud" was determined. The cloud detection threshold was established on the basis of visual observation of light haze. This resulted in an "in-cloud" registration whenever the local aggregate particle concentration, for all particles with diameters greater than  $3\mu\text{m}$ , was greater than  $66\,000\text{ m}^{-3}$  (Jasperson *et al.*, 1984a; 1984b).



### 8.3.4 Application of GASP data to LFC aircraft

A statistical analysis to predict the probability of cloud encounter on airline routes and its variation with altitude, season and location, was subsequently undertaken by NASA. Results based on a subset of the data were reported by Nastrom *et al.* (1981a; 1981b). Davis and Fischer (1983) and later Jasperson *et al.* (1984a; 1984b; 1985), presented more detailed and updated analyses of the GASP cloud encounter statistics, based on the entire database of 88000 samples. The data were analysed to obtain summary statistics on the probability of cloud encounter at commercial airliner altitudes, for application in determining the feasibility of employing LFC on long-range airline routes.

Over the four-year period observations were made during all seasons with a slight increase in the number of observations made in winter and spring. Most of the data came from the Northern Hemisphere, with about 3/4 of the data coming from the latitudes 20 - 60 N. The calculated mean TIC (time-in-cloud) values are thus weighted towards this region. Nastrom *et al.* (1981b) point out that the observations are not independent. It is stated that "because general cloudiness or the lack thereof, is not a random event but is associated with large scale weather systems, clear and cloudy areas tend to have appreciable areal extent". Many of the climatology observations were consistent with expectation and could be related to global-scale meteorological circulations.

The working assumption that NASA researchers had made for the purpose of assessing the viability of LFC, was that no laminar flow would be lost in clear air and that 100% loss would occur whenever the aircraft flew through visible cloud. What constituted a "cloud" in the GASP data did not exactly match the Hall limits. By considering particle size distribution data, Jasperson *et al.* (1984a; 1984b) concluded that the estimated concentrations of particles greater than the Hall limit of 33 $\mu$ m EMD in the GASP "in-cloud" data, were sufficiently high to cause a loss of laminar flow.

The definitions used in the route analysis of the cloud data are defined in Fig. 8-3. The data analysis indicated that the average fraction of time in cloud on a single flight ( $TIC_f$ ) varied depending on the route, altitude and season. Jasperson *et al.* (1984a; 1984b; 1985) observed that flight in clear air (i.e.  $TIC_f = 0\%$ ) was the most frequent occurrence, that a  $TIC_f$  value of 100% was never measured, and that the frequency of  $TIC_f$  values usually decreased monotonically as the  $TIC_f$  increased. It was reported that the observed behaviour could be modelled using a gamma probability density distribution (details given in section K.4, Appendix K). Table 8-2 reproduced from Jasperson *et al.* (1984a; 1984b), is a summary of the probability of cloud encounter on seven routes, at various altitude bands, established using this model. It is seen in this table that the probability of the aircraft encountering clouds for any route / altitude, for more than 10% of a flight, was less than 34%. This is shown by the value of 66% for the US West Coast / NW Europe route at the 28500 - 33500ft altitude band. For the extreme condition, corresponding to a cloud encounter of more than 50% of a flight, the



probability was estimated to be 1.4% for the worst case (again at the West Coast / NW Europe route).

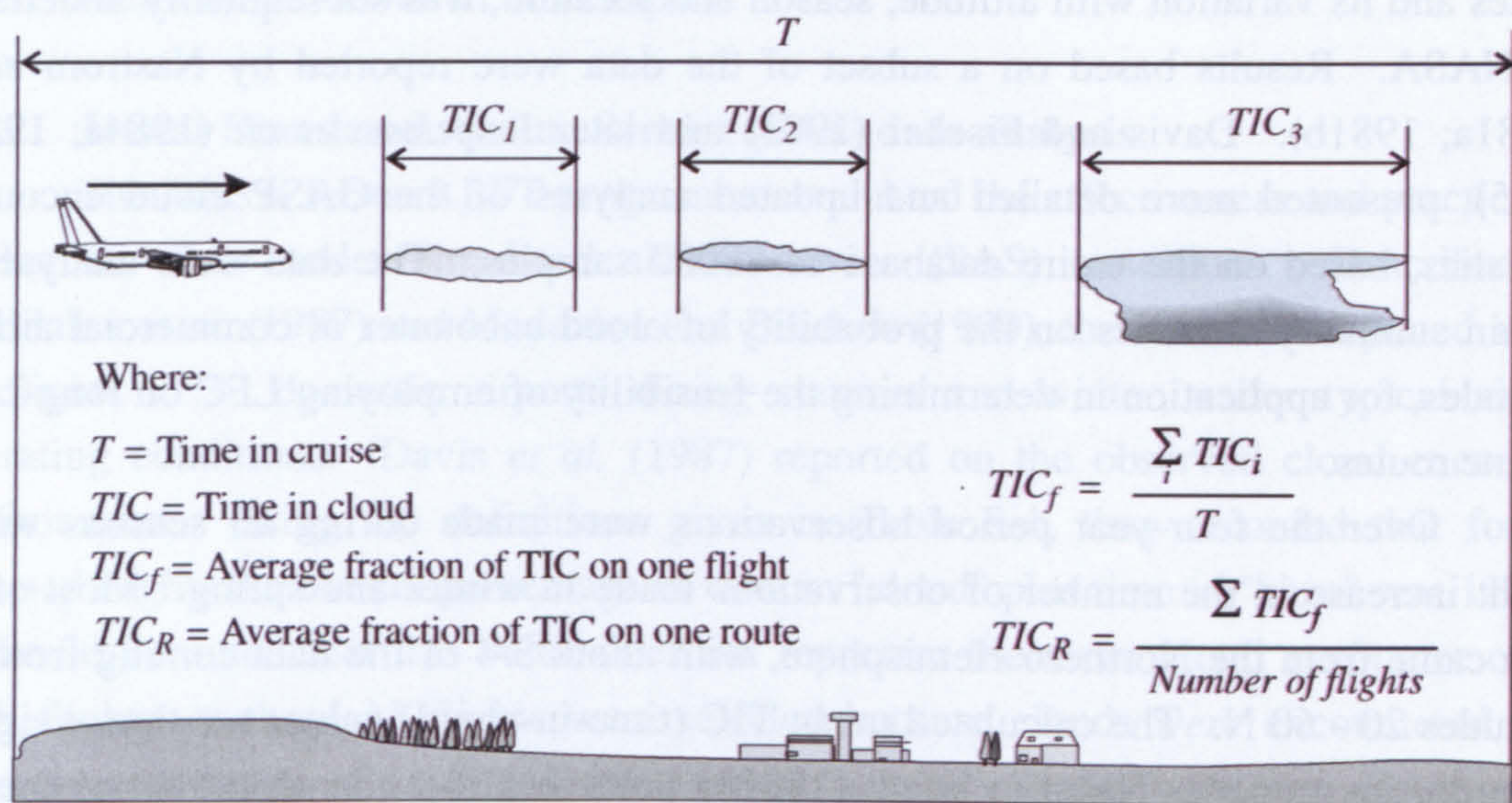


Fig. 8-3 Definitions for route data analysis of time in cloud

Table 8-2 Summary of GASP cloud data (from Jaspersen et al., 1984a; 1984b)

Route	Altitude band (1000ft)	No. of flights	Probability (%) of $TIC_f$					$TIC_R\%$
			<1%	<5%	<10%	<25%	<50%	
California - Hawaii	28.5-33.5	22	17.3	47.6	67.8	91.1	98.8	9.4
	33.0-38.5	177	24.7	62.8	82.6	97.9	100.0	5.5
	38.5-43.5	2	-	-	-	-	-	-
E Coast (USA)	28.5-33.5	3	-	-	-	-	-	-
W Coast (USA)	33.0-38.5	58	20.1	53.8	74.1	94.7	99.6	7.5
	38.5-43.5	13	41.3	86.0	97.2	100.0	100.0	2.4
W Coast (USA) - NW Europe	28.5-33.5	6	16.7	46.2	66.0	90.1	98.6	9.9
	33.0-38.5	26	38.6	83.1	96.0	99.9	100.0	2.7
	38.5-43.5	26	37.7	82.2	95.6	99.9	100.0	2.8
E Coast (USA) - NW Europe	28.5-33.5	38	17.5	47.8	67.8	91.3	98.9	9.3
	33.0-38.5	99	19.5	52.3	72.6	94.0	99.4	7.9
	38.5-43.5	24	33.5	76.9	92.9	99.7	100.0	3.4
Australia - SE Asia	28.5-33.5	16	18.7	50.6	70.8	93.0	99.3	8.4
	33.0-38.5	20	18.0	49.0	69.1	92.1	99.1	8.9
	38.5-43.5	-	-	-	-	-	-	-
W Coast (USA) - Japan	28.5-33.5	4	-	-	-	-	-	-
	33.5-38.5	30	31.3	73.8	90.9	99.5	100	3.8
	38.5-43.5	14	43.5	87.9	97.9	100.0	100.0	2.2
Japan - W Coast (USA)	28.5-33.5	-	-	-	-	-	-	-
	33.0-38.5	12	18.0	49.0	69.1	92.1	99.1	8.9
	38.5-43.5	29	32.2	75.3	91.9	99.7	100.0	3.6

8.3.5 Route average cloud encounter data

The route average time-in-cloud ( $TIC_R$ ) values are also indicated in Table 8-2. The values varied from 2.2% (US W Coast / Japan route, at 38500 - 43000ft) to 9.9%



(US W Coast / NE Europe, at 28500 - 33500ft). For most routes the lower altitude bands experienced greater cloud incidence than the higher altitude bands. The exception was the Australia to SE Asia route, where, like other subtropical routes, the tropopause would lie well above the cruise altitudes, resulting in the higher altitude bands encountering more cirrus cloud than the lower altitude bands. The low value of 2.8%  $TIC_R$  corresponding to the upper flight level band, for the US W Coast to NW Europe route, is attributed to the low tropopause at the northern latitudes traversed on this route.

The probability distribution of cloud on a particular route is illustrated for the US E Coast / NW Europe route by Jasperson *et al.* (1984a). Fig. 8-4 represents the modelled values (using the gamma probability density distribution) for the two flight level bands. (There were 99 flights in the sample for the upper flight level and 38 flights in the lower flight level bands.) For approximately 50% of the flights, the average TIC was between 0 and 5% for the two flight level bands. The percentage falls off rapidly for increasing average TIC. Averages of the two modelled values were calculated by the author and are recorded in Table K-2 (Appendix K). These values were used as the idealised model of probable cloud encounter reported herein.

A conservative assumption (error allowance) has been made regarding the cloud encounter model that was used for these studies. The upper value of the TIC band (Fig. 8-4) was used for each case, e.g. 5% TIC was taken to correspond to 50.3% of the cases, rather than a value within the 0 - 5% band. This implies that the model represents a level of cloudiness greater than that actually measured for that particular route.

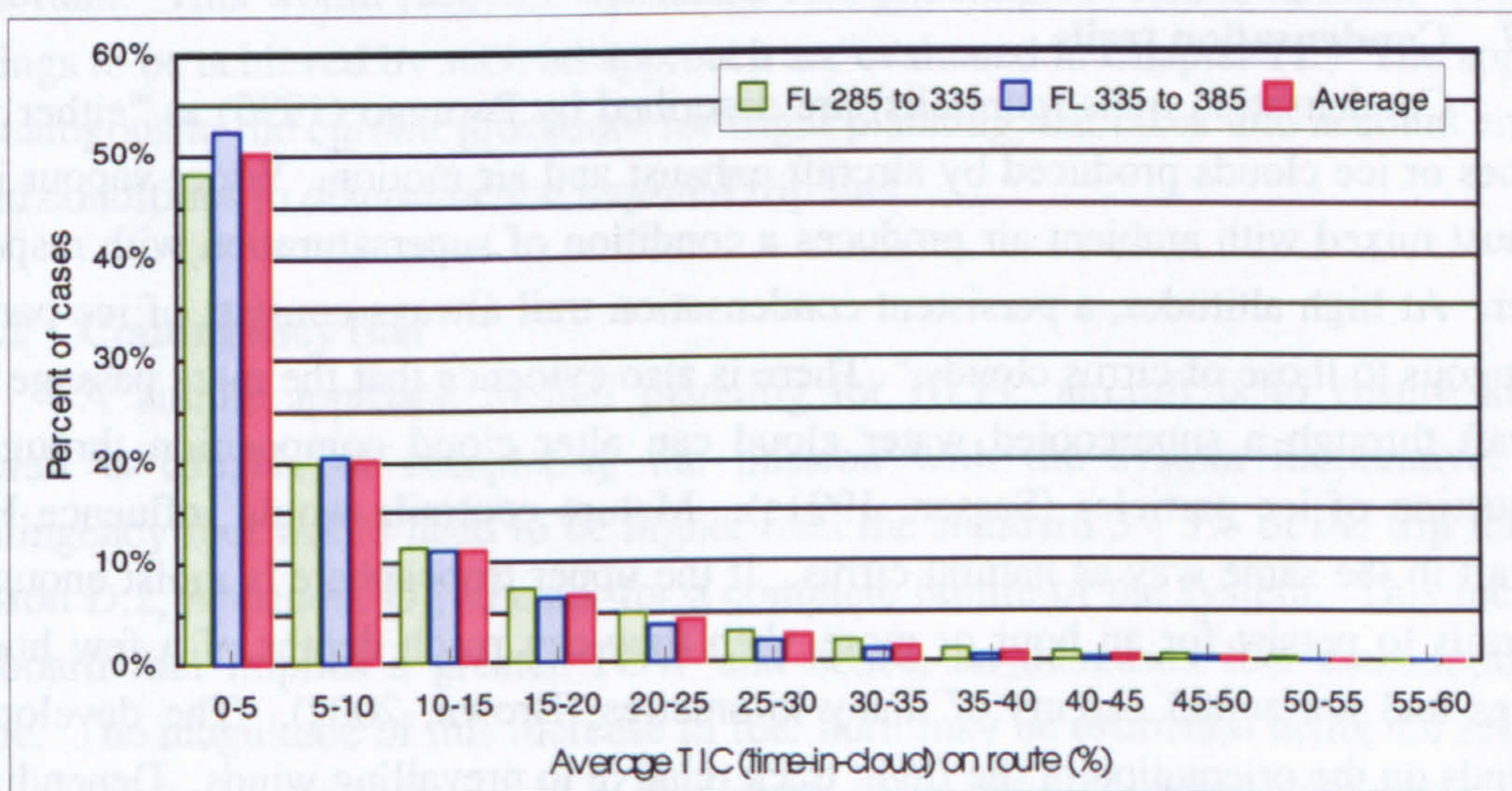


Fig. 8-4 Average time-in-cloud (based on data from Jasperson *et al.*, 1984a)

### 8.3.6 Change in cirrus with time

Although the GASP research provides extensive data on cirrus cloud on aircraft flight routes, the database represents atmospheric conditions in the late 1970s and this



changes with time. There is strong scientific opinion that global cloud amount, and in particular cirrus cloud, is increasing (Angell *et al.*, 1984; London, 1991; Parungo *et al.*, 1993; Parungo, 1995). Parungo (1995) claims that “with increasing aircraft traffic, plus anthropogenic pollution over the past half century, a positive trend for total cloud amount in general, and cirrus amounts in particular, should be expected”. A study by Angell *et al.* (1984) concluded that there was a 3.7% increase in cloudiness over the contiguous United States during the 33-year interval 1950 – 1982. Parungo (1995) determined annual mean oceanic cirrus cloud amounts for the period 1950 to 1981. Three general patterns were identified: (a) from 1951 - 1962, no discernible changes; (b) from 1962 - 1967, a negative trend; and (c) from 1967 - 1981, a positive trend. It is indicated that these changes “may be natural variations, or anthropogenic effects or combinations of both”. Parungo (1995) calculated the change to be 2.0% for the Northern Hemisphere and 0.8% for the Southern Hemisphere, over the 14-year interval from 1967 - 1981. Further details are given in section K.2 of Appendix K.

To forecast a change in global cirrus cloud amounts, so as to assess its impact on future HLFC aircraft operations based on the data reviewed, is speculative. The data does however, indicate the order of magnitude of possible change, which, based on a simple average of the later results of Parungo (1995), indicates a rate of increase of cirrus for the globe of about 1% per decade. If the rate of increase remained the same, an increase of ~3.3% would be expected from 1979 (when the GASP data was recorded) to the present time. It was concluded that the order of magnitude of this change is within the error allowance made above in establishing the cloud encounter model.

### 8.3.7 Condensation trails

Condensation trails (contrails) are described by Parungo (1995) as “either water plumes or ice clouds produced by aircraft exhaust and air motion. Water vapour in the exhaust mixed with ambient air produces a condition of supersaturation with respect to water. At high altitudes, a persistent condensation trail always consists of ice particles analogous to those of cirrus clouds.” There is also evidence that the mere passage of an aircraft through a supercooled water cloud can alter cloud composition through the production of ice particles (Sassen, 1991a). Mature contrails would influence HLFC aircraft in the same way as natural cirrus. If the upper troposphere is moist enough for contrails to persist for an hour or more, then they can reach depths of a few hundred metres and horizontal extents of many kilometres (Brown, 2002). The development depends on the orientation of the flight track relative to prevailing winds. Depending on the temperature and humidity conditions, contrails may coalesce, becoming indistinguishable from cirrus clouds and covering thousands of square kilometers.

In 1992 contrails were estimated to cover ~0.1% of the Earth’s surface on an averaged basis, with larger regional values associated with the popular air routes (IPPC, 1999). Although contrail formation is extremely small compared to natural cloud



formation, contrails often occur in clusters in geographical regions that are cold and humid and have a substantial amount of air traffic, such as central Europe.

It is speculated that because of the limited vertical extent of the contrail, it may be a viable option for a HLFC aircraft to climb / descend a few thousand feet, to get out of the influence of another aircraft flying ahead of it at the same flight level.

## 8.4 FUEL PLANNING AND WEATHER FORECASTS

### 8.4.1 Fuel planning

Routine fuel planning requirements for airline operations must take into account *expected* meteorological conditions and furthermore, the contingency fuel must be sufficient for deviations from the forecast conditions. These requirements, as stipulated in JAR OPS 1 and FAR 121 (details given in Appendix D) pertain to current generation turbulent aircraft engaged in public transport operations. Whereas the principle of drag reduction technologies being incorporated in newer generation aircraft is commonplace, HLFC technology is somewhat different as the en route drag reduction depends on an environmental condition, i.e. the time spent in cloud.

To obtain the greatest benefit for a HLFC aircraft, the fuel planning must consider the *probable* TIC that will result in a loss of laminar flow for that particular mission. The presence of cirrus cloud on airline routes is of little interest for current aircraft operations; however, for HLFC aircraft the ability to forecast cirrus cloud is important. This would facilitate optimised fuel planning for HLFC aircraft. (The fuel savings to be achieved by such an approach are evaluated in Chapter 11.) The approach is analogous to the current procedure for flight planning that takes into account en route wind conditions to determine the required trip fuel.

### 8.4.2 Contingency fuel

A simple approach to fuel planning for HLFC aircraft is to ensure that the aircraft is capable of completing the mission with the system inoperative. The contingency fuel would need to be higher than the standard 3 - 5% of the trip fuel (see section D.2, Appendix D), to cater for a complete failure of the system. This increased on-board fuel implies a greater TOW and hence, an increased fuel consumption en route. The magnitude of this increase in fuel burn may be estimated using the results of the sensitivity analysis presented in Chapter 6. Two simplifications are made: (1) The Breguet range equation is used; (2) The trip fuel is based on a cruise segment equal to the trip distance (i.e. no climb or descent). The validity of these simplifications is explored in section E.4 (Appendix E).

In section I.2 (Appendix I) the partial derivative representing the change in cruise fuel with respect to a change in the mass of aircraft was determined. Using this relationship, it was possible to derive an expression for the change in trip fuel ( $m_f$ ),



resulting from a change in the contingency fuel (which is expressed as a percentage of the trip fuel). The variable  $x$  is introduced to define the contingency fuel, viz.

Contingency fuel =  $x m_f$

Equation [I-13] derived in section I.3 (Appendix I) is repeated:

$$\frac{\delta m_f}{m_f} = \frac{(e^\beta - 1) \delta x}{1 - (e^\beta - 1) \delta x} \quad \text{where } \beta = \frac{R \bar{c} g}{V E} \quad \text{--- [8-1]}$$

where  $m_f$  in this equation is the initial trip fuel and  $\delta x$  is the relative change in contingency fuel. Using the data for the B757-200 class aircraft given in Table 6-5 for a range of 2350nm, equation [8-1] was evaluated for incremental changes in the contingency fuel. The results are recorded in Table 8-3 below. They indicate that if the contingency fuel increases from 5 to 10% of the trip fuel, then an additional ~1% of the previous trip fuel will be consumed in transporting that contingency fuel over the distance of 2350nm. This penalty will increase with increased trip distances. Fuel planning procedures for HLFC aircraft that will ensure safe operation, without the penalty of a substantial increase in contingency fuel will maximise the benefits of this technology.

Table 8-3 Influence of change in contingency fuel on trip fuel (Range: 2350nm)

Change in contingency fuel ( $\delta x$ )	1.0%	2.0%	3.0%	4.0%	5.0%
Relative change in fuel burn $\left(\frac{\delta m_f}{m_f}\right)$	0.21%	0.42%	0.63%	0.84%	1.05%

8.4.3 Operational Numerical Weather Prediction (NWP)

It is evident that the ability of Numerical Weather Prediction (NWP) models to forecast the presence of ice clouds – with microphysical properties that would degrade laminar flow – is an important operational concern for HLFC aircraft. This issue was explored by the author in conjunction with Brown<sup>15</sup> (Young *et al.*, 2002).

Current *operational* NWP models are unable to directly provide information on ice particle size or concentration. As such, these models are not able to provide a forecast of en route geographical regions where the particle size and concentration would exceed a particular size and concentration criterion (e.g. corresponding to the limits proposed by Hall). The required data that would be needed by HLFC aircraft to plan a mission would thus not be routinely available.

Current models describe ice clouds using only a single model variable, the ice water content (IWC). However, more advanced models are being developed, which include some form of prognostic representation of ice cloud (i.e. one in which the ice cloud properties are described by one or more variables of the numerical model). The

<sup>15</sup> P. Brown, Cloud Physics Research, Met Office, Cody Technology Park, Farnborough, Hampshire, UK.



benefit of this approach is improved simulation capability, particularly with regard to the representation of supercooled stratocumulus cloud and freezing rain, and increased high-altitude ice cloud amounts (Wilson and Ballard, 1999).

Another limitation of current operational models when being considered for use in flight planning for HLFC aircraft, is the vertical grid resolution of 1km used for modelling the incidence of cirrus. This is a problem with regard to predicting cloud incidence at particular flight levels. A finer vertical grid resolution would be a significant advantage, if for example it were possible to distinguish cloudy from cloud-free flight levels. However, this is not possible at present. Improvements in this regard are likely as "increased computer power is likely to be directed at this issue in the near to medium future" (Brown, 2002). Observations of the size distribution of ice crystals as a function of altitude in a cloud system typically show an increasing concentration of larger particles at lower altitudes (Field, 1999; 2000). This corresponds to the growth of ice particles by aggregation as they fall from the levels near cloud tops at which they are nucleated, and can be represented by an exponential size distribution (Field, 1999; 2000). Brown (2002) contends that such particle size distributions would allow a "relatively crude estimate" to be made of the number concentration of ice particles exceeding a critical size threshold, for a given value of the IWC at any grid-point at which ice cloud was forecast to occur.

#### 8.4.4 Research models

There are a number of numerical cloud models used for research purposes, in which more complex representations of cloud ice are employed. Brown (as reported in Young *et al.*, 2002) describes some of these models:

"One such approach is the representation of each of a number of different classes of ice particle (for example, pristine crystals, aggregates and rimed particles) with a separate prognostic variable for each (Caniaux *et al.* 1994). A further step is the use of so-called "dual-moment" schemes, which have separate prognostic variables for each of two moments of the particle size spectrum, typically particle number concentration and IWC. The scheme described by Swann (1998) uses dual-moment representation for three separate ice classes. Finally comes the representation of a large number of discrete size classes for ice particles (Chen and Lamb, 1994). Each of these has some ability to provide more detailed quantitative information on the occurrence of larger ice particles. The latter is computationally the most complex and will remain beyond the capabilities of operational NWP models for the foreseeable future. However, operational developments based on the other two approaches are being investigated for their potential value in providing improved descriptions of ice cloud as the horizontal grid resolution decreases from a typical value of around 60km used in current global models towards the value of around 15km in current typical regional forecasting models. Hogan *et al.* (2001) and Mace *et al.* (1998) have examined the ability of the global NWP model of the European



Centre for Medium Range Weather Forecasting (ECMWF) to predict the occurrence of cloud above a fixed geographical location, as a function of altitude and time. Cloud occurrence was determined using a vertically-pointing millimetre-wave radar, operated at sites in central southern England and north central Oklahoma respectively. These studies show that the model already has a large degree of skill in predicting cloud occurrence at both locations, although with some systematic biases in the timing of certain cloud types at the latter site." (Young *et al.*, 2002.)



## **9 INSECT CONTAMINATION**

### **9.1 INTRODUCTION**

Following early flight testing of LFC aircraft (see Appendix C) it was concluded that the leading edge of the wing must be protected from contamination during takeoff and landing, for the initial part of the climb and for the last part of the descent. Mechanical protection, in the form of a shield or cover was thought to be necessary. Recent flight tests, however, have indicated that the perforated surfaces do not get blocked by insects to the extent previously thought. Flight through rain and ice, it would appear, cleans the laminar flow surfaces to some extent. The use of fluids and coatings have also proven to be very effective in terms of the preventing insect contamination on the leading edges of HLFC surfaces.

This chapter reviews the issue of insect contamination and mitigation methods, and reports on environmental factors known to influence insect distributions.

### **9.2 IMPACT ON LAMINAR FLOW OF INSECT CONTAMINATION**

#### **9.2.1 Impact on HLFC surfaces**

Insect residue can impact the flow on HLFC suction surfaces in three ways:

- (1) The residue of a single insect impact on the surface will cause transition, if its height exceeds the critical height (determined for an excrescence on the surface, at that particular point on the laminar flow surface).
- (2) The residue blocks the suction holes, and if the area of contamination is sufficiently large, the lack of suction over that area will cause transition. Non-uniform suction caused by partial blockage of the holes, particularly that in a spanwise direction, is of concern, as it can result in longitudinal instabilities.
- (3) A cluster of insect debris – as may occur over an extended period of operation, or by flying through an insect swarm – could create sufficient surface roughness to cause transition.

The consequence of insect contamination on a HLFC surface depends on the location of the impact. If an insect impacts on the attachment line of a swept wing or empennage, then laminar flow over the entire outboard section of the surface may be lost. Suction, in some cases, may be successful in relaminarising the flow. If the impact is not on the attachment line, but is on the suction panel or laminar flow surface, then a wedge-shaped area of turbulent flow, aft of the impact site, will result. This will have an included angle of 14 - 16 degrees (as shown in Fig. B-20, Appendix B).

Using the wing of the B757-200 class aircraft as an example, the size of the turbulent zone aft of the insect debris was estimated. The chordwise extent of the laminar flow that is shown in Fig. 9-1 was based on Boeing's B757 study (Boeing, 1982). The largest possible turbulent area would correspond to an impact near to the



wing root, as shown in Fig. 9-1. This would reduce the laminar flow planform area in this example, from  $38.18\text{m}^2$  to  $36.33\text{m}^2$ , a reduction of  $\sim 4.8\%$ . By assuming that the laminar flow drag is 10% of the turbulent flow drag, it was estimated that this change would result in a 5.4% increase in the profile drag of the upper wing surface. Based on the details presented in Table 7-2, the upper surface profile drag is  $\sim 8.6\%$  of the total drag of the HLFC aircraft at a typical cruise weight. Hence, the total drag would increase by approximately 0.5%.

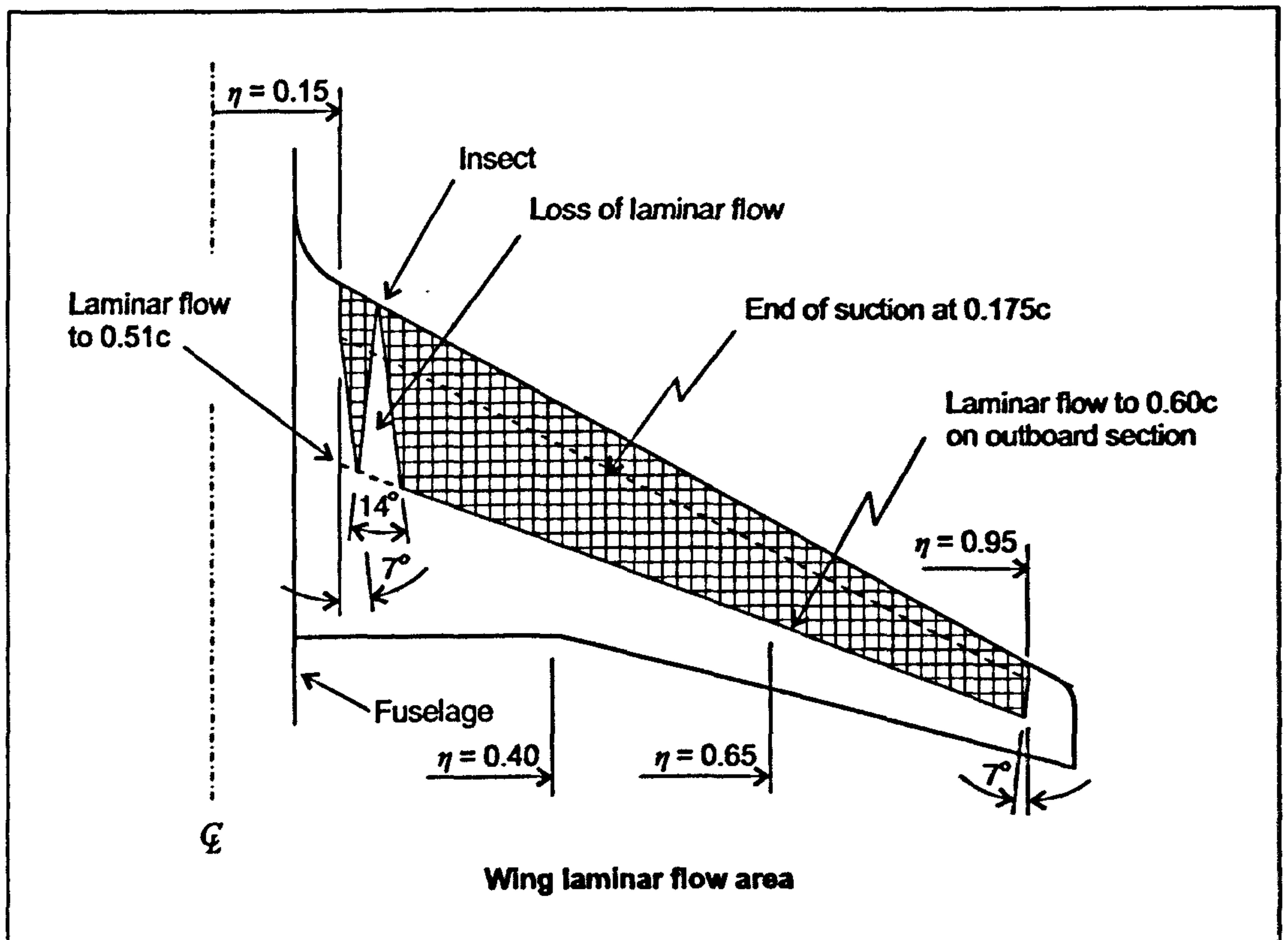
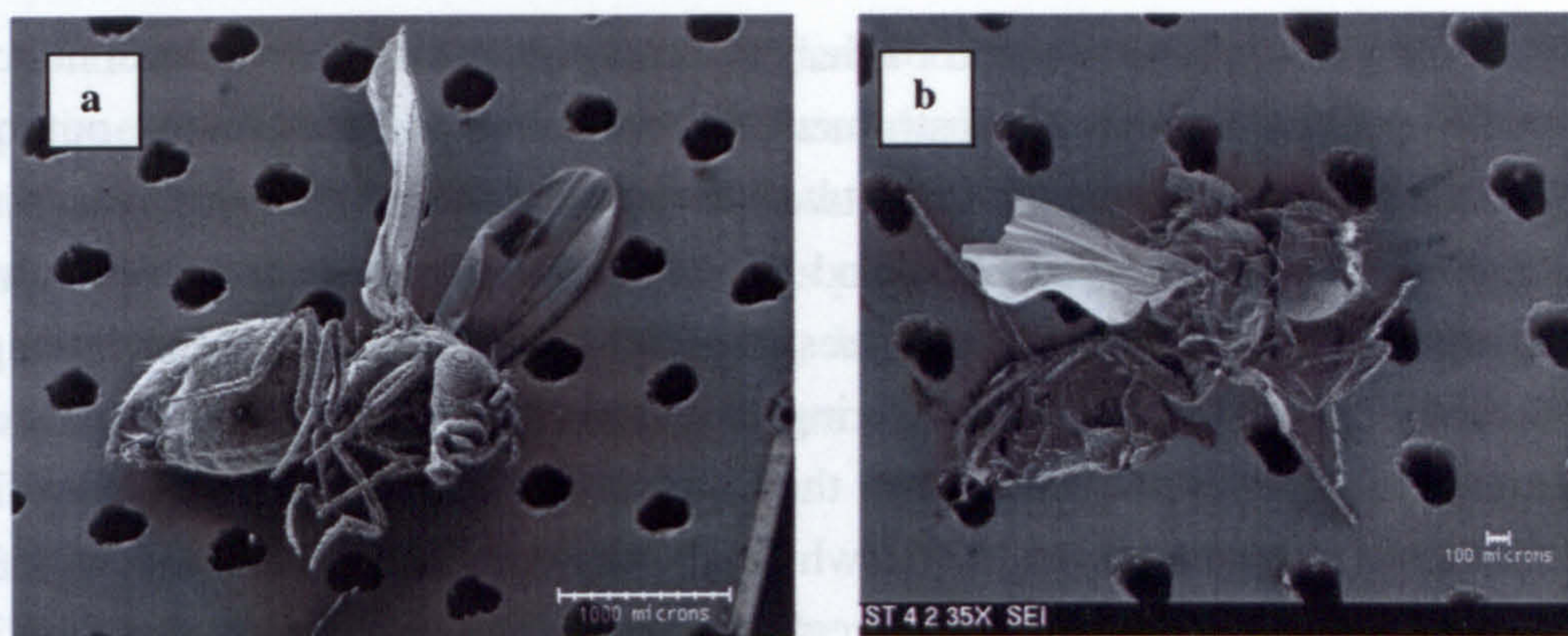


Fig. 9-1 Loss of laminar flow resulting from insect impact on wing of B757-200 class aircraft

### 9.2.2 Insect physiology

An insect's body is composed of two major parts: the exoskeletal cuticle and the blood (haemolymph). The haemolymph is not bound in vessels, but circulates freely through the insect's body. Physically, the haemolymph is a clear liquid with a high content of amino acids and proteins. If the speed of impact on the leading edge is sufficiently high, the exoskeletal cuticle will be ruptured. The haemolymph, which is then released onto the suction surface, acts as glue, binding parts of the insect's body to aircraft skin. This may cause hole blockage and a build-up of residue due to aggregation of insect biochemicals. Fig. 9-2 contains Scanning Electron Microscope (SEM) images of insect impact tests conducted at the University of Limerick (details given in Appendix L) using a custom designed airgun.





**Fig. 9-2** Scanning Electron Microscope (SEM) images of insect impact tests on a perforated titanium plate - tested at the University of Limerick (after O'Donoghue, 2001)

### 9.2.3 Insect impact distribution

*Roughness Due to Insects* by Coleman (1961) is a comprehensive study of the issue of insect contamination. One element of Coleman's investigation, which was studied by conducting wind tunnel tests, concerned the nature of insect debris build-up on the leading edge of wings. The highest excrescence on the wing occurred near the stagnation point, as might be expected. Coleman (1961) reported that the streamwise distribution of insect matter followed a distinct pattern, with "a narrow region at the front of the wing where the insects adhere more or less intact, followed by an expansive region where the insects are ruptured more or less, and the residue is predominantly fluid deposits (haemolymph)". Maresh and Bragg (1984) studied the trajectories of insects, as they would impact the leading edge, by modelling the insect characteristics and the airflow over the aerofoil. They noted that lighter insects were more influenced by the flowfield around the aerofoil and strike further back along the chord.

### 9.2.4 Critical height to cause transition

The height of the insect residue that remains on the surface is a function of the insect size, impact angle and speed of impact. If this exceeds a critical value, transition occurs. The critical roughness height, which is a characteristic of the flowfield, is described as the "height that an isolated 3D element must protrude into the laminar boundary layer to cause transition to turbulent flow" (Maresh and Bragg, 1984). The critical height is reported to be variable, depending on the Reynolds number, the stability status of the boundary layer (and hence, the relative position of the three-dimensional element on the wing) and even on outer flow disturbances (Kühn, 1998).

Data on the critical height of a roughness element that will trigger transition on NLF aerofoils comes from wind tunnel and flight tests. Marsden (1978) simulated insect excrescence on an aerofoil, by using artificial "bugs" made from adhesive tape of height 0.38mm and diameter 4.8mm. He reported a significant increase in drag for a contamination pattern of "bugs" placed on the leading edge and at 12mm and 152mm



behind the leading edge. Peterson and Fisher (1978) describe tests that were conducted by NASA using a Jetstar aircraft, instrumented to detect transition on the outboard leading-edge flap. A direct correlation between insect debris on the leading edge and loss of laminar flow was observed. Eiss and Wightman (1983) of NASA, in reviewing these test results, reported that insect residues ranging from 0.1mm to 0.4mm in height, were "collected" on the leading edges during low flights over agricultural fields, and that transition resulted due to residues "at the bottom of the height range". The field study of Elsenaar and Haasnoot (1992), which involved visual inspections of insect contamination on the leading-edges of aircraft at Schiphol airport (see section 9.3.3) used a critical height of 0.3mm as the criterion for the assessment of boundary layer transition.

For HLFC surfaces, there exists very little reliable data on critical excrescence heights. This is due in part to the difficulty in extrapolating measured wind tunnel test results to free stream conditions. It is recognised that the leading edge region from the stagnation line to about 15% chord location, is the most vulnerable region. As the flow extends further back, the critical height is reported to approximately double at 50% chord (Kühn, 1998). Tests conducted during the A320 HLFC flight trials (see section C.14, Appendix C) assessed the impact of excrescence on laminar flow, by sticking small circular "patches" to the fin surface. However, little has been published regarding these results.

### 9.2.5 Self-cleaning

Anecdotal evidence from airlines indicate that flight through rain and ice tends to clean the wing surface to some extent, removing insect debris and leaving residues of a reduced thickness on the wing leading edge. Maddalon *et al.* (1987), describing the Jetstar SAS flight tests, confirm this to be true, and report that "insect debris tended to erode with time, and that passing through cloud cover allowed a natural washing of the surface". Henke (2000) reported that this was also observed with the A320 fin tests.

## 9.3 INSECT ENVIRONMENT AND DISTRIBUTIONS

### 9.3.1 Impact speeds

The speed at which insects will rupture on impact is related to the anatomy and mass of the insect. For example, the fruit fly, *Drosophila*, used by Coleman (1959) in a series of laboratory tests, was reported to rupture on impact, at a speed of ~27kt. Lower speeds of 21 - 23kt were measured for other types of insects. The fruit fly shown in Fig. 9-2a was fired at 90° to the test plate at a speed of 20kt (O'Donoghue, 2001). The insect was observed to be only lightly attached to the plate, and it was evident from the SEM image that the exoskeletal cuticle was intact. Humphreys (1992) suggests that the threshold speed for contamination on an actual wing is considerably higher and should



be based on the impact trajectory. He deduced a threshold speed of ~40kt, using the experimental results of Croom and Holmes. Airline operational policy places an upper limit on the taxi speed. It is understood that a maximum speed of 20kt is typical, thus protection will not be required during this phase. The protection system must therefore be extended / switched on during taxi, before the takeoff has commenced and be retracted / switched off after the aircraft has climbed out of the region of threat.

### 9.3.2 Insect height distributions

The distribution of insects in the atmosphere has been of keen interest to researchers for many years. Hardy and Milne (1938) reported on the vertical distribution of insects, which were caught in nets, although this work was conducted for the purpose of studying insect behaviour and not for assessing their potential threat to novel drag reduction techniques that were emerging at that time. After reviewing the data of Coleman (1961), Humphreys (1992) concluded that for a LFC aircraft, "50 - 60% of the insects would be collected during the ground run and the balance at low altitude during climb and descent. Under normal conditions, the number collected above 1000ft feet [would be] negligible".

Croom and Holmes (1985; 1986) of NASA, conducted a study of insect distributions and the atmospheric conditions that affect these distributions, by flying a modified Cessna 206 aircraft over a marshy area. The population density of insects was determined at five heights, with each data point representing an average of the data at that height. Croom and Holmes (1985) correlated their results against a "curve fitting" of Coleman's data and demonstrated a good agreement between the results (Fig. 9-3). Croom and Holmes (1985) concluded that "insect contamination protection for laminar flow airplanes is probably not necessary above about 500ft".

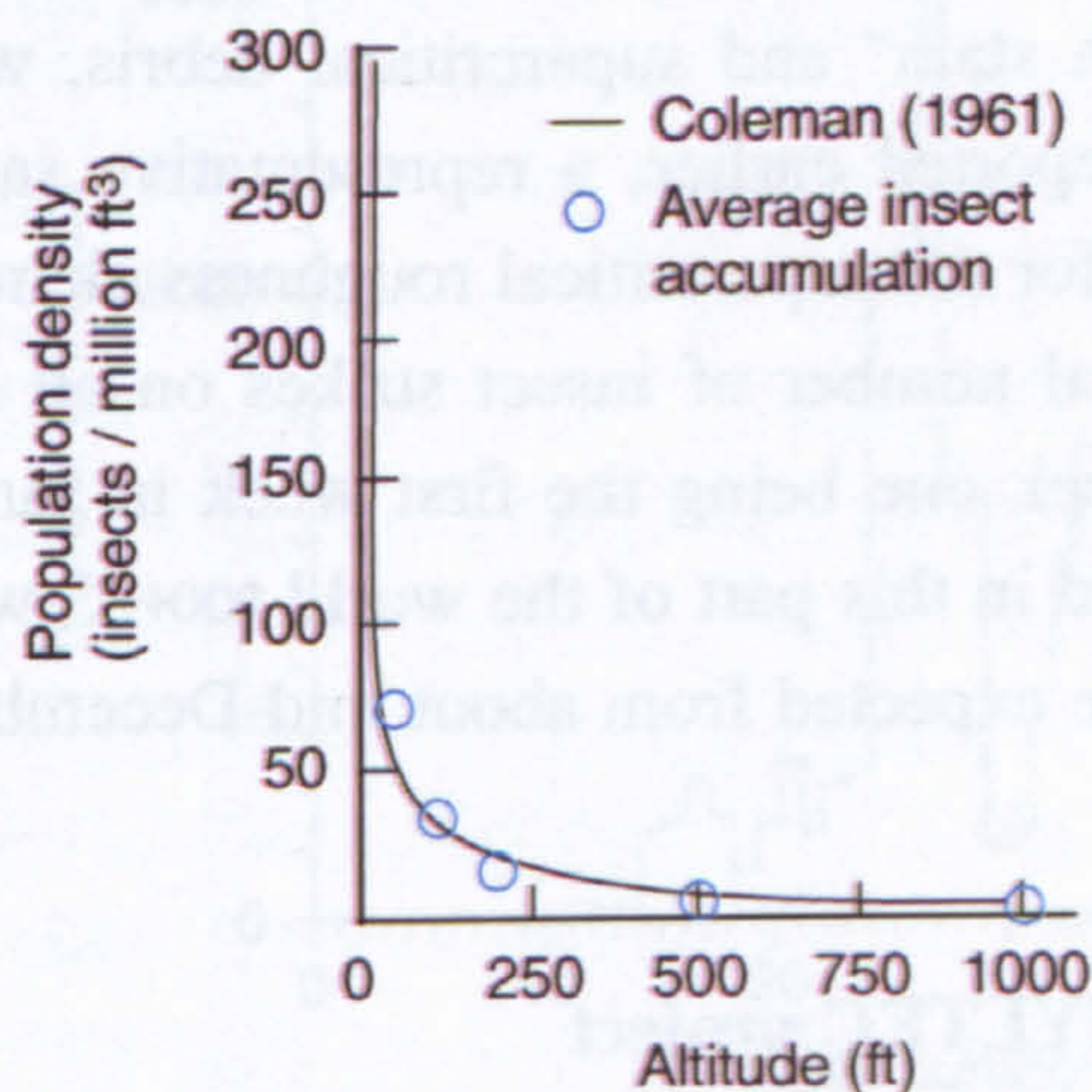


Fig. 9-3 Insect vertical distribution data (redrawn after Croom and Holmes, 1985)



### 9.3.3 Environmental and seasonal factors

In general, the airborne population density of insects will be affected by local terrain, temperature, humidity, wind and season. Under certain atmospheric conditions, increased rates of insect accumulation may be expected. Coleman (1961) indicated that favourable conditions for airborne insect activity were light wind (5 - 10kt) and high humidity, and that a peak in population density could be expected at a temperature of ~25°C. The strong dependence on atmospheric temperature is borne out by the results of Croom and Holmes (1985), which indicate that outside of the temperature band of 21 - 29°C, very little insect activity was evident.

The simple distribution shown in Fig. 9-3 of insect population density dropping off with increasing height, would be expected to have regional anomalies. During the daytime, airborne insects can be carried to altitudes of hundreds of metres by convection motion of the atmosphere (Johnson, 1969). At night, there is an absence of convection and insects must maintain height by active flight. Drake and Farrow (1988) describe the influence of a nocturnal temperature inversion – which may have a height of several hundred metres – on insect migration. At the top of the temperature inversion, a local maximum in wind speed often occurs, and insect concentrations were reported to sometimes occur at this height. Riley *et al.* (1995), report on the aerial densities of migrating insect species, and report that windborne migrations of hundreds of kilometres are possible.

The problem of insect contamination on HLFC aircraft is thus expected to have distinct regional and seasonal patterns. A field study conducted by Elsenaar and Haasnoot (1992) at Schiphol airport involved weekly inspections – for a one year period – of the leading edges of eight aircraft, to count the number of insect strikes. These aircraft, consisting of three types (i.e. DC-9, B737 and F-28) were engaged in routine short and medium range operations in Europe. A distinction was made between subcritical strikes, described as a "thin protein stain" and supercritical debris, where "some of the insect body was visible". As reported earlier, a representative sample established a height of 0.3mm as the threshold for the supercritical roughness elements. The results, given in Fig. 9-4, indicate the total number of insect strikes on all eight aircraft, plotted as a function of time, with week one being the first week in January 1988. It is evident that the problem is restricted in this part of the world to ~35 weeks of the year, and almost no contamination can be expected from about mid-December to about mid-April.

### 9.3.4 Insect contamination investigation - HYLTEC project

As part of the HYLTEC project (see section C.17, Appendix C), a SAAB 2000 aircraft (Fig. 9-5) was fitted with two test panels on the outer wing leading edges, and a Liquid Contamination Control System (LCCS) was installed. The tests commenced in August 1999, with the aircraft flying standard passenger service routes in Northern Europe, for a period of 20 months; the objective being to investigate contamination and



durability aspects of HLFC. The test vehicle, methodology and preliminary results, were described by Humphreys and Totland (2000), and by Humphreys (2001).

Four organisations were involved: AS&T<sup>16</sup> was responsible for the design and manufacture of the LCCS, the test panels and holders; SAAB Aerospace (Linköping, Sweden) jointly with AS&T, for certification and system installation; SAAB Aerospace for the management of the flight tests, inspections and data acquisition; SAS for aircraft operation; and the University of Limerick for the analysis of the insect contamination data and for the post flight-test inspection of the perforated panels. The work performed at the University of Limerick was conducted under the direction of the author, and is described herein, in two parts. The insect contamination work is described in this chapter (with supporting details given in Appendix L) and the durability of the perforated test panels is described in Chapter 10 (with details in Appendix M).

A weekly inspection of the panels for insect contamination was performed using a rating scale to categorise the extent of the contamination. Weekly averages of temperature, dew point and barometric pressure were calculated based on daily weather reports obtained from the Swedish meteorological office for the majority of the flight destinations. During the warmer months (i.e. April to September), when average temperatures ranged from approximately 10 to 20°C, relatively high levels of contamination were evident. Conversely, there was no contamination during the cold months, when the average temperatures fell below freezing (i.e. November to February). For the temperate period of March / April, and October, some insect activity was evident (see Fig. L-6, Appendix L). These results were observed to be broadly in line with those of Elsenaar and Haasnoot (1992). Further details on this work are given in Appendix L.

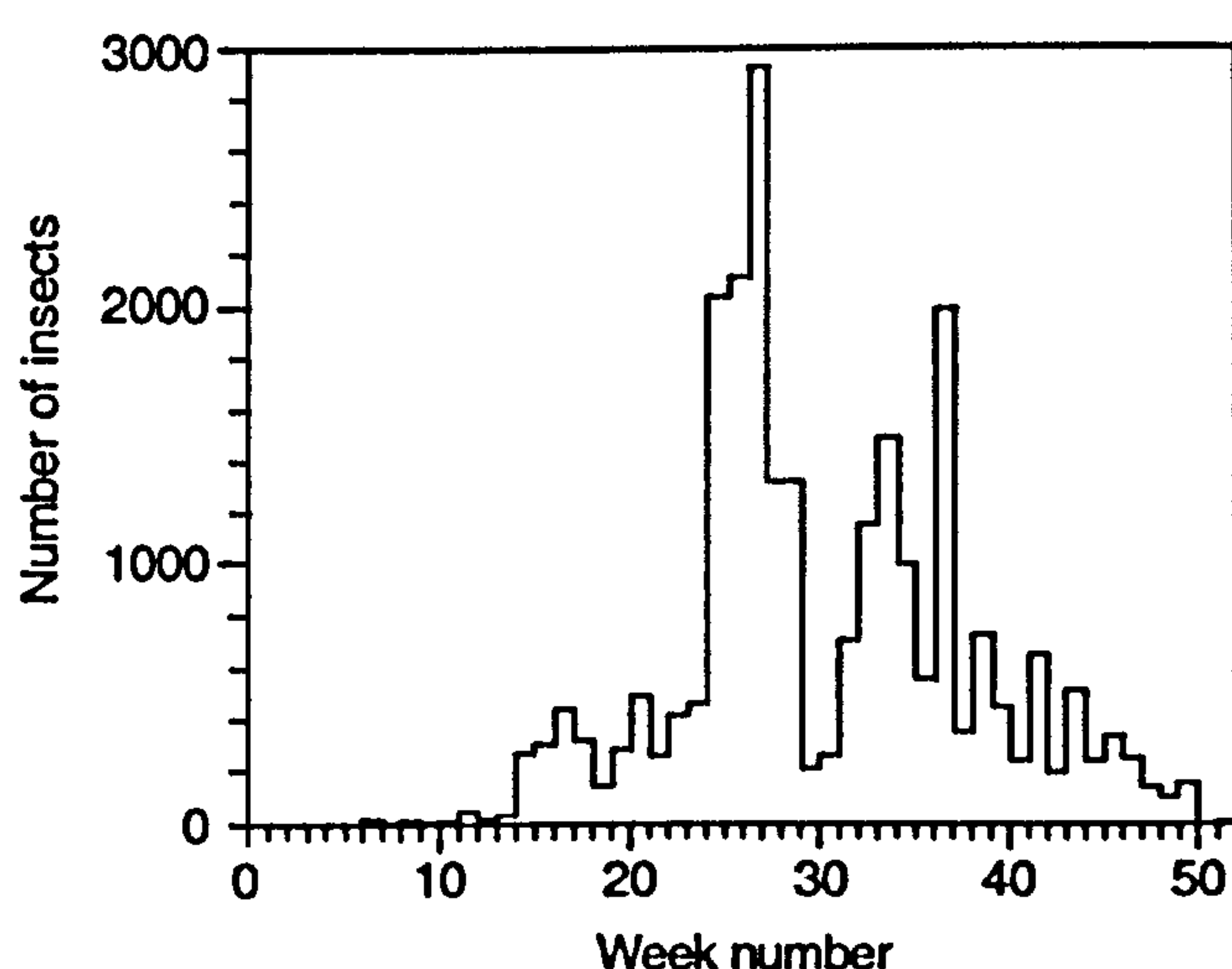


**Fig. 9-4** *Number of insects on wing leading edges on eight aircraft, as observed at Schiphol Airport during 1988 (redrawn after Elsenaar and Haasnoot, 1992)*

<sup>16</sup> AS&T: Aerospace Systems and Technology, Consett, Co. Durham, UK.





**Fig. 9-5** *HYLTEC SAAB 2000 flight aircraft, showing test specimens and their location (from Humphreys and Totland, 2000)*

## 9.4 CONCEPTS FOR CONTAMINATION MITIGATION

### 9.4.1 Background

There have been many attempts at solving the problem of insect contamination disrupting laminar flow. Coleman (1961) discusses a number of alternative techniques, including “preventative” and “cleaning” methods. A NASA sponsored study of LFC concepts conducted by McDonnell Douglas (1983) evaluated the practicality of alternative methods. Joslin (1998a) provides a current overview of the subject. In spite of the broad range of techniques investigated, the fact remains that the majority of these ideas are impractical for operational aircraft. A number of methods are briefly reviewed in this section.

### 9.4.2 Cover

The light-weight cover made from paper or mylar, for example, could be removed from the leading edge after takeoff, leaving a clean surface. An early report on the use of this method was by Gray and Davies (1952), who indicated that it was used to protect the leading edge on a King Cobra aircraft during laminar flow tests conducted by the RAE (Royal Aircraft Establishment). Runyan *et al.* (1987) describe how a paper covering was pulled into the cabin of a Boeing 757 when it reached ~5000ft during NLF flight tests. The concept is simple and is suitable for experimental flight tests, but is not an operational solution.

### 9.4.3 Scrapers and wipers

Coleman (1961) reported on the work of Beech and Nicholas (1953), describing the use of scrapers / wipers. Practical design problems exist with this concept, as the



device must be either jettisoned or retracted into the wing structure for high-speed flight.

#### 9.4.4 Fluid layer

The surface is protected by a fluid layer, which is removed by shear stress at high wind speeds. A related technique also explored by Coleman (1961), is based on the principle of a soluble film, which could be removed by heating, or by flushing the surface with water. Solutions of glycerine, glycerine and gelatine, and soap and methanol, were evaluated.

#### 9.4.5 Flexible surface

Wortmann (1974) demonstrated that a flexible surface, made of an elastic material, would deform under impact by the insect, thus absorbing some of the kinetic energy and reducing the risk of a rupture of the insect shell. Damage of the flexible surface by rain and hail was indicated as a major concern.

#### 9.4.6 Coatings

Peterson and Fisher (1978) reported on the flight experimentation of "superslick" coatings on a Jetstar aircraft. Segments of the leading edge flap were covered with Teflon and hydrophobic coatings. The results indicated that none of the coatings showed a significant reduction in insects adhering to the test surfaces. Eiss *et al.* (1985) demonstrated that the issue of insect contamination is fundamentally a problem of adhesion prevention. This was supported by tests on aluminium plates, coated with polymers of various surface energies, which were mounted in a jig on top of an automobile. Siochi *et al.* (1987) investigated the use of hydrophobic surfaces. The research was directed at the use of non-stick polymers and elastomers. Tegarden (1996) reported on the testing of a GE (General Electric) proprietary silicone coating (originally developed for the US Navy to prevent the fouling of underwater vessels). The post impact insect debris height was measured to be less than 0.05mm (i.e. below the critical height); however, concern regarding the durability of the coating due to hail impact was highlighted.

#### 9.4.7 Shield

A shield that extends forward in front of the leading edge, to either deflect or block insects from striking the laminar flow surface, is a good solution; provided that it can also be designed to double as a Krüger flap, in the classical role as a high lift device. The shield would then be retracted after the aircraft climbs out of the insect threat region. One drawback is that it becomes virtually impossible to maintain laminar flow on the lower surface. This concept is described in more detail in section 9.5.



#### 9.4.8 Continuous liquid discharge

Coleman (1961) and later Peterson and Fisher (1978) reported that a continuous liquid spray was effective in preventing insect contamination. This has been substantiated by a number of subsequent experiments, where the continuous discharge of fluids through a porous leading edge has been employed (see section 9.6).

#### 9.4.9 Concluding remark

The Jetstar LFC trials (see section C.4, Appendix C) evaluated two systems, which at that time were regarded as being the most promising, viz. a Krüger flap / shield and a liquid discharge system. These two options are still regarded as being the most practical of the alternatives for addressing this problem. It is interesting to note that both systems were selected for further evaluation more than 15 years later at part of the HYLTEC Do228 test campaign (see section C.17, Appendix C).

### 9.5 KRÜGER FLAP / SHIELD

The Krüger flap solution has been the subject of much theoretical and experimental work. Significant investigations are mentioned in the brief review of the topic provided in this section. The most complete evaluation of the concept was undertaken by NASA and Douglas Aircraft. A Krüger flap was installed on the right wing of the LFC Jetstar (shown in Fig. 9-6). This was reported to be very successful in keeping the leading edge of the wing free of contamination (Fischer *et al.*, 1983; Maddalon and Braslow, 1990).

Tamigniaux *et al.* (1987) tested the effectiveness of a Krüger flap as an insect shield in a wind tunnel. Insects were injected into the tunnel upstream of the model. The results showed that the lighter insects impacted further aft of the stagnation line than heavier insects, indicating that, as expected, heavier insects have straighter trajectories. Impacts at angles of less than 7° were reported to have left negligible insect debris on the surface to disrupt the boundary layer.

The leading edge of the B757 HLFC demonstrator was modified to include a Krüger flap, for high lift and insect protection (Collier, 1993). De-icing was facilitated by a hot air system. The flap was reported to have successfully protected the upper wing surface. In Europe, a Krüger flap was designed and tested in a wind tunnel as part of the LARA project (Dziomba, 1993). The effectiveness of the concept was later evaluated on a Do228 aircraft as part of the HYLTEC project (see Fig. C-14, Appendix C). In this case, the flap was fastened to the wing structure and could not be retracted during the test flights.

The Krüger flap solution is, however, not without its problems. It is mechanically more complex than a slat, particularly if comparable maximum lift performance is required. Lynch and Klinge (1991) of Douglas Aircraft Company



identified a number of concerns regarding the use of a Krüger flap instead of a slat in this role.

- (1) It is stated that the folding "bull-nose" of the Krüger flap is not as desirable a shape as that which can be achieved with a variable camber Krüger or slat, and hence greater deflections will be required (with ensuing reductions in maximum lift capability and increased drag).
- (2) Ice protection system requirements are effectively doubled, as the Krüger flap is unable to protect the wing in all flight conditions, but the slat can perform this function.
- (3) The Krüger flap cannot be used in the same way as a slat, to tailor the stall characteristics if they are found to be unacceptable during flight tests. In addition, the traditional "fixes" of vortex generators and fences will not be available. It was however noted that fly-by-wire controls offer the opportunity to get around some of these problems, but not without some performance penalty (Lynch and Klinge, 1991).

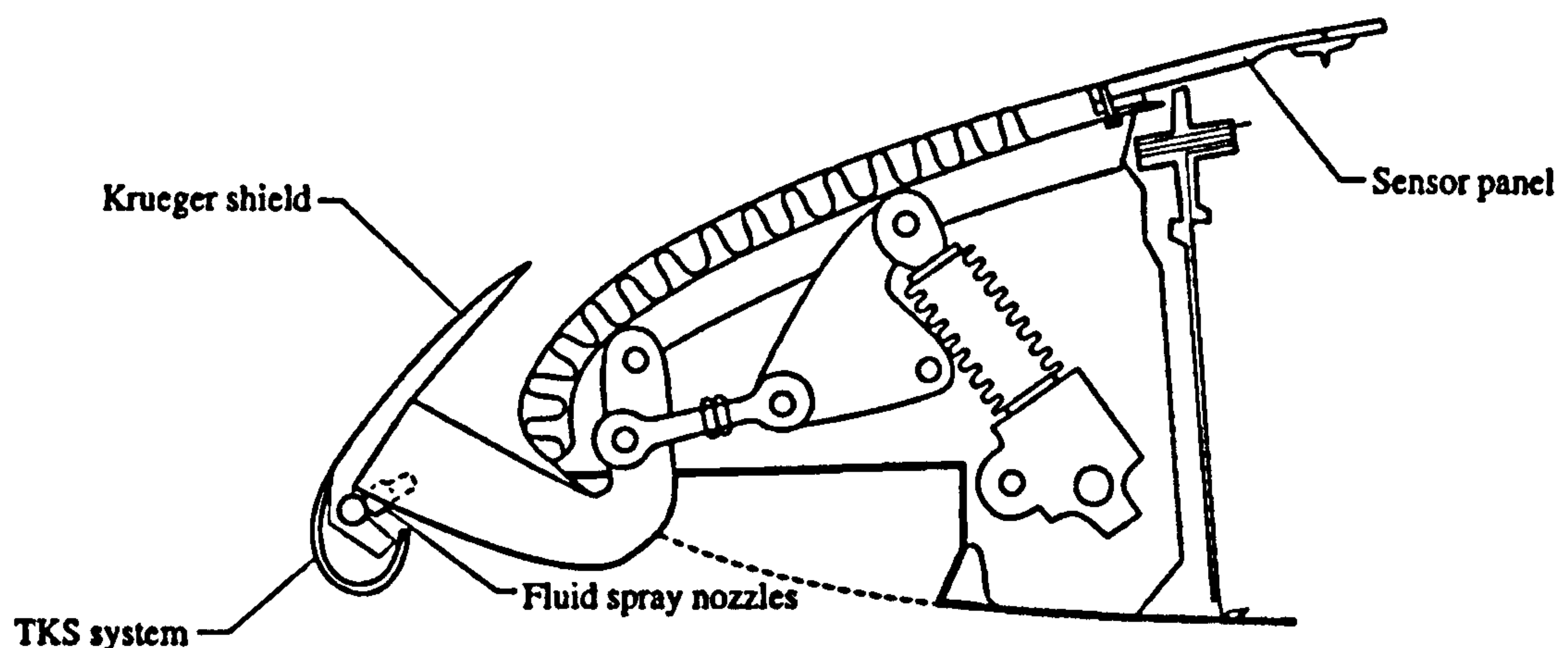


Fig. 9-6 Krüger shield on Jetstar Douglas test article (from Fischer et al., 1983)

## 9.6 LIQUID / FOAM SYSTEMS

### 9.6.1 Review of experimental research

The effectiveness of a continuous liquid spray in preventing insect contamination has been successfully demonstrated during a number of experimental test campaigns, as indicated in the review summary (Table 9-1).

### 9.6.2 Fluids for anti-contamination

The use of a Freezing Point Depressant (FPD) such as the glycol based fluids mentioned in Table 9-1, enables a single system to provide both icing protection and insect contamination control. A further advantage of these fluids comes from the fact that glycol systems are reported to be solvents for insect proteins (Croom and Holmes,



1985; Wagner *et al.*, 1988). A feature that has been previously reported (and independently confirmed at the University of Limerick) is that for effective protection, the surface must be wet before the insect impact occurs. This is enhanced by adding a surfactant to the solution, which aids in the spreading of the liquid over the surface, preventing dry patches on the surface. It also implies that the system must be switched on during taxiing, to allow time for the surface to be coated before the takeoff is commenced.

**Table 9-1** *Literature review of major experiments evaluating liquid anti-contamination systems*

Test vehicle	Comment	Reference
Wind tunnel	Water and 10% "teepol" surfactant supplied to test surface via small tubes.	Coleman (1961)
Jetstar	Continuous flow of water delivered by forward facing spray nozzles. Large volumes of water required for successful protection.	Peterson and Fisher (1978)
Wind tunnel	Ethylene glycol and ethylene glycol / water solutions applied through porous and perforated surfaces to evaluate anti-contamination and fluid system design.	McDonnell Douglas (1983)
Jetstar	(1) Starboard wing: Anti-icing fluid sprayed on upper wing surface from nozzles mounted on Krüger shield. (2) Port wing: Fluid pumped out of suction slots. 60 / 40 percent mixture of propylene glycol methyl ether / water used.	Maddalon <i>et al.</i> (1987), Lange (1987), Maddalon and Braslow (1990)
Cessna 206	TKS ice protection system adapted for tests. 80 / 20 percent solution of monoethylene glycol / water reported to be very effective during flight trials.	Croom and Holmes (1985, 1986)
Falcon 50	TKS de-icing system used to apply monopropylene glycol liquid to wing leading edge. System reported to be very effective, reducing "pollution" to zero.	Bulgubure and Arnal (1992)
LFU 205	Liquid anti-contamination evaluated as part of LARA project.	Dziomba (1993)
ATTAS HLF nacelle	Anti-contamination system, based on TKS anti-icing system, incorporated into leading edge of HLF panel.	Barry (1995), Mullender and Reidel (1996)
Do228	Mixture of glycol alcohol and water pumped through laser perforated leading edge skin on NLF glove.	Horstmann <i>et al.</i> (1996)
Falcon 900	Anti-icing and anti-contamination system installed in wing leading edge.	Fiton (2000)
SAAB 2000	Anti-icing fluid pumped through perforated titanium test panel on wing leading edge. Contamination reduced to "almost zero" during flight tests.	Humphreys and Totland (2000), Humphreys (2001)
Do228	No results published.	Test article described by Humphreys and Horstmann (2000)

### 9.6.3 Additives to anti-contamination fluids

It was reported (in the experiments mentioned in Table 9-1) that the removal of pre-impacted insect residue from the surface by the application of these fluids, had not



been successful. The development of a system capable of both protecting and cleaning the laminar flow surface was the objective of a study conducted at the University of Limerick. The research, which took place from 1998 - 2000, by O'Donoghue<sup>17</sup>, Pembroke<sup>18</sup>, O'Dwyer<sup>19</sup> and the author, was part of the HYLTEC project. Further details of this work are given in Appendix L. The objectives of the study were:

- (1) To investigate the effect of surfactants on the physical properties of anti- /de-icing fluids and to screen commercially available products for optimum performance;
- (2) To investigate the use of enzymes as additives in fluid compositions, by comparative screening of enzyme activity in FPD / water mixtures; and
- (3) To investigate the effectiveness of these fluids for insect adhesion mitigation, using a custom-built airgun, designed to fire insects onto stationary test plates.

### *Objective 1*

Surfactants had been used in a number of previous contamination experiments, including the early work of Coleman (1961); however, a comprehensive study of their use for this particular application had not been reported in the literature. A series of surfactants were examined by assessing their ability to reduce the surface tension of solutions of the Type I de-icing agent TKS-80 and the Type II anti-icing agent Kilfrost ABC-3. The results indicated that the fluorinated products outperform the non-fluorinated products, and that a number of Zonal fluorosurfactants were found to be particularly effective.

### *Objective 2*

The idea of adding enzymes – to break up the insect debris and aid in their removal – to anti-contamination fluids, had been suggested by Humphreys (1996); however, no laboratory study regarding the viability of the concept had previously been conducted.

Protein degrading enzymes (proteases) require water to catalyse the degradation of their substrate, which in this case is the insect debris. It was postulated that certain proteases added to FPD / water solutions, would be able to degrade insect proteins, thus encouraging the removal of debris from the wing. The screening experiments of candidate products indicated that the most resilient enzyme was Subtilisin Carlsberg, or commercial preparations of it. It was observed that the optimum temperatures for activity of this enzyme, were in the region of 40 - 50°C in ethylene glycol / water solutions (results recorded in Fig. L-1, Appendix L). Regarding the operational implementation of this concept, this is a serious concern as the controlling of the fluid temperature on the wing would be a non-trivial design problem.

---

<sup>17</sup> D. O'Donoghue (principal researcher), postgraduate student, CES Department, University of Limerick.

<sup>18</sup> T. Pembroke, CES Department, University of Limerick, Ireland.

<sup>19</sup> T. O'Dwyer, CES Department, University of Limerick, Ireland.



### *Objective 3*

An airgun was designed and constructed to test the best performing surfactant and enzyme solutions, by firing insects (at speeds of up to 150km/hr) onto laser perforated titanium test plates. (The insects were caught in the field or bred in the laboratory.) In all cases it was found that the emission of fluids onto already contaminated plates failed to remove insect residues, whilst pre-wetting the plates prevented the adhesion and debris build-up. (Photographic images recording one set of trials are given in Fig. L-4, Appendix L). Results from UV-visible spectroscopic measurement of solutions used in dissolution test fluids, showed that, irrespective of the duration of exposure of contaminated surfaces to test fluids protein dissolution and the cleaning effect of wind was improved by the presence of enzymes. However, when compared to the dramatic difference which pre-wetting makes to adhesion, the impact of this mechanism was small. It was concluded that there would be no additional benefit to be achieved by the addition of enzymes to insect contamination preparations, particularly when the requirement for temperature control was taken into account.

#### **9.6.4 Foam system**

Humphreys and Horstmann (2000) explain why it is necessary to use foam, rather than a liquid, where suction on the attachment line is required.

“Liquid transpiration through a porous zone within the leading edge is commonly used for ice protection on smaller aircraft and has been used experimentally for insect contamination avoidance, on laminar flow aerofoils, with good results. However, for applications where attachment line suction is required, it is not practical to exude liquid directly through the plenum chamber skin. There are two reasons for this: Firstly, the skin porosity required for boundary layer suction is incompatible with that required to control the dispersal of the relatively low flow rate of liquid that is required for ice and insect protection. Secondly, the volume of the plenum chamber is unnecessarily large for liquid dispersal, this implies a large mass of liquid to fill the plenum at start-up and the need to remove this liquid before suction can be established. Apart from the obvious weight and liquid usage disadvantages, undesirable time delays would also result at start-up and shut down. These incompatibilities and disadvantages can be overcome if the liquid can be transported through plenum chamber and skin in a foamed state.”

For the Do228 trials the foam was generated using a porous hard foam separator. High-pressure air was expanded through the hard foam tube into liquid covering the downstream surface.

#### **9.6.5 Fluid consumption**

The factors that need to be taken into consideration in estimating the required on-board quantity of insect anti-contamination fluid, are:



- (1) The flow rate, which depends on the design of the dispensing system, the fluid type, and whether or not a surfactant has been added;
- (2) The time duration that the system will be functioning during the takeoff and landing phases; and
- (3) The number of LTO cycles that must be catered for by a single filling of the fluid reservoir.

Estimates of the fluid flow rates necessary to protect a wing leading edge from insect contamination vary considerably. Tests conducted by Peterson and Fisher (1978) using a pure water system indicated that prohibitively large volumes were needed. The use of FPDs – aided in some cases by the addition of a surfactant – considerably reduced the amount of fluid needed. Laboratory tests conducted by McDonnell Douglas (1983), indicated that  $\sim 9$  lt/min per  $\text{m}^2$  of perforated area was required to "maintain surface wetness". This flow rate (which has later been demonstrated to be excessive) would impose a significant weight penalty on a HLFC aircraft. Croom and Holmes (1985) demonstrated during the Cessna 206 flight trials that substantially lower fluid quantities were adequate. They reported that flow rates of 0.55 - 1.1 lt/min per  $\text{m}^2$  of wing frontal area, of mono-ethylene glycol / water solution, were required for a 68 - 82% reduction in insect accumulation.

Humphreys (1992) estimated the fluid usage for a B747 size aircraft using the data from Croom and Holmes (1985). He concluded that a total of 76 lt/min (49 lt/min on the wings, 21 lt/min on the empennage and 6 lt/min on the engine nacelles) would be required for each flight. Humphreys estimated the time required for protection to be 11.6 min per flight (9.6 min for taxi; 1.0 for takeoff and climb; 1.5 for landing). The weight of the fluid equates to  $\sim 0.4\%$  of the OEW of the aircraft. This estimate has also erred on the side of caution, as it is most unlikely that insect protection will be required for the indicated taxi time.

The results of the fluid usage of the LCCS on the HYLTEC SAAB 2000 test aircraft (Fig. 9-5) are presented in section L.3.6 (Appendix L). The average fluid consumption, measured during the trials, was equivalent to 0.11 lt/min per metre of span. Based on an estimated frontal area of the test section, this translates to  $\sim 0.4$  lt/min per  $\text{m}^2$  of wing frontal area; a figure which is seen to be a little less than the lower value quoted by Croom and Holmes (1985).

Regarding the time required for system operation, Humphreys' estimate of  $\sim 12$  min per operation (for a B747 size aircraft) is roughly double the average time used for the SAAB 2000. As the rate of climb of the SAAB 2000 would not be dissimilar to an airliner, the difference is attributed to the longer taxi times, associated with the aircraft type operating from a major airport.



## 10 MECHANICAL FAILURE, DAMAGE AND DURABILITY

### 10.1 INTRODUCTION

In this chapter consideration is given to what may go wrong during a flight, resulting in partial or complete failure of the HLFC system. The first two issues – mechanical failure and damage – could be assessed by considering historical data and by looking at the probability of such occurrences. The durability of HLFC suction surfaces has been considered in an entirely different manner. In this regard, experimental results of work conducted during the HYLDA and HYLTEC projects (see sections C.16 and C.17, Appendix C) are presented.

As no production standard HLFC system has been designed, it has been necessary to postulate a representative design in order to assess the consequences of system failure. The actual components that would be used would be similar to components currently used for other aircraft systems (e.g. the Environmental Control System). Component failure rates could thus be estimated from maintenance data taken from existing systems.

### 10.2 HLFC SYSTEM (MECHANICAL) FAILURE

#### 10.2.1 Introduction

Developing a representative and credible system architecture of the HLFC system, for the purpose of conducting a reliability analysis, is a difficult task for three reasons:

- (1) No *production* standard HLFC system has been designed and all available information available relates to *experimental* installations. For these experiments the designers were not particularly concerned about the system's complexity or weight. Furthermore, the systems incorporated some means of measuring and adjusting the flow rates within individual chambers. This will not be required for a production system. The hardware (e.g. valves and pumps) were mostly off-the-shelf equipment, selected on the basis of availability and cost, and would not necessarily be representative of a production system.
- (2) In spite of the considerable research effort that has taken place over the past 20 years, in the USA and in Europe, there is still no clear-cut direction as to what will be the optimum design solution. There are a few multi-disciplinary design problems (e.g. the anti-contamination / de-icing system) that require further study before a synthesised production standard design can be produced.
- (3) Much of the research work conducted in the USA by Boeing (and other partners) and in Europe by Airbus (and partners) is confidential, and as a result, there is limited information in the public domain.



Notwithstanding these limitations, a representative system design – developed in concept only – was produced in order to explore the consequences of component failures. The design is not intended to represent an optimum solution, but rather a typical solution containing the major system components, developed for the purpose of undertaking this analysis.

### 10.2.2 HLFC system description

The conceptual layout for the HTP of the 757-200 class aircraft, developed for the purposes of estimating the suction power and system mass (described in Chapter 7), was extended by considering the control and monitoring system functions. The system block diagram, shown in Fig. 10-1, reflects the architecture of the design. The HLFC system has the following features:

- (1) The laser perforated titanium outer skin covers two nosebox sections. Each nosebox has six suction chambers as shown in Fig. 7-9 (Chapter 7). The two suction chambers at the leading edge (numbers 3 and 4) are used to convey the anti-contamination foam to the external surface. A shut-off valve (SOV) is required for each of these chambers.
- (2) There is one collector duct per nosebox. The air is conveyed from each suction chamber, through a calibrated orifice, to one of the collector ducts. These ducts – running in the chordwise direction – carry the air to a transfer duct, which is installed approximately parallel to the front spar in the HTP leading edge. At the junctions of the collector ducts and the transfer duct, a control valve is installed to regulate and balance the flow in the system. The transfer duct has an over-pressure valve (OPV) and a SOV installed.
- (3) The pump system consists of starter air turbine, an electric motor and an axial compressor. The starter turbine is driven by bleed air and has an in-line pressure regulating and shut-off valve (PRSOV).
- (4) The system has a purge capability. Bleed air enters the "suction" system at a junction on the main transfer duct, after passing through a filter and a PRSOV.
- (5) The control and monitoring system has a HLFC computer (electronic controller), which receives and sends information to the flight management computer. It receives data from the flow sensors (i.e. temperature, pressure, flow rate) and manages the control and shut-off valves.
- (6) The anti-contamination system consists of a pump, motor, reservoir, foam generators (which mix the liquid with bleed air) and a SOV.



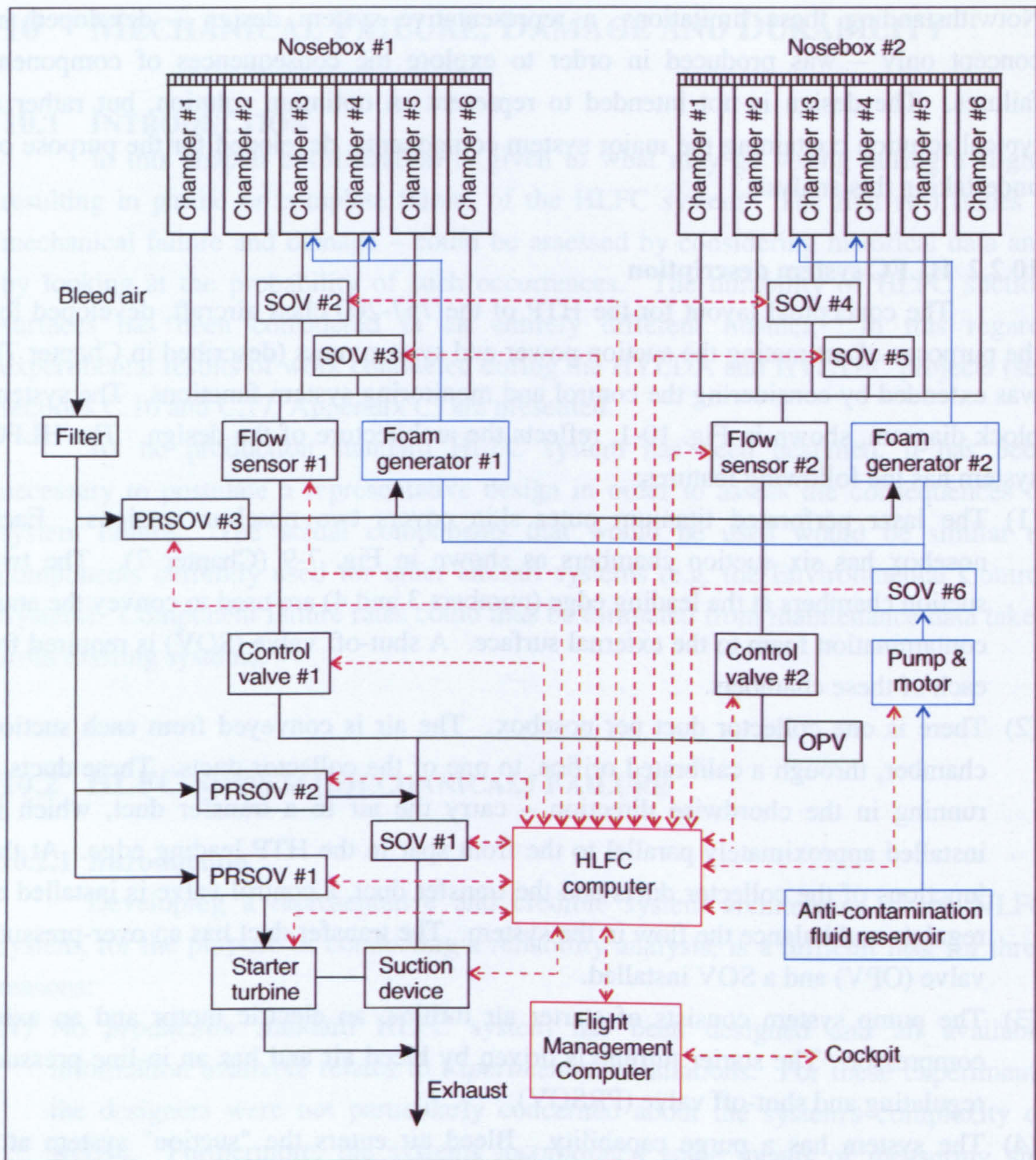


**Fig. 10-1** Schematic of HLFC control system architecture for HTP of B757-200 class aircraft (conceptual design devised to estimate system mass and reliability)

### 10.2.3 Component failure rate data

There were a number of factors that limited the accuracy of the system reliability calculation. The process adopted in establishing component failure rate data and the inherent limitations of the process are discussed below.

- (1) No production HLFC system has been built. Indicative reliability data for the HLFC components was obtained by considering similar components installed in in-service airliners, in the ECS (Environmental Control System), fuel system or de-icing system, for example.



- (2) The use of MTBUR (Mean Time Between Unscheduled Removal) data for the purpose of estimating the failure rate of a new system can produce a pessimistic result. Some of the reports consulted (e.g. British Airways, 1991; British Aerospace, 1979) only included components that were suspected of having failed. No data was recorded on similar, but not identical, components that were not removed.
- (3) Not all components that get removed would have actually failed. Data from a Boeing (1976) report for the B747 indicated that the "percentage justification" of component removal was of the order of 65 - 85%. A mean value of 75% was used to estimate the failure rates from the quoted removal rates (i.e. assuming a "no fault found" rate of 25%).
- (4) Newer components to be installed in future generations of aircraft are likely to be more reliable, due to ongoing technical improvements. A factor of 5% per decade was assumed.

Data on the selected reference components is given in Table M-1 (Appendix M). The removal rates were obtained from the MTBUR values and then divided by the two factors described in (3) and (4) above. The resulting failure rates were taken as indicative values for new components.

#### 10.2.4 System reliability analysis

Practical use of the data (Table M-1, Appendix M) was made by assuming a constant life-time failure rate. The component reliability could thus be represented by the Negative Exponential distribution. The reliability of the component, which may be taken as being the same as the Survivor Function  $S(t_1)$  for the time interval  $t_1$ , is thus given by:

$$\text{Component reliability} = S(t_1) = \int_{t_1}^{\infty} \lambda e^{-\lambda t} dt = e^{-\lambda t_1} \quad \text{--- [10-1]}$$

where  $t$  is the time variable and  $\lambda$  is the failure rate (Snow and Yeomans, 2000). In terms of system reliability, there are four modes of operation that need to be addressed:

- (1) The start-up mode;
- (2) The normal suction mode;
- (3) The purging operation; and
- (4) The anti-contamination mode.

An estimate of the system reliability may be obtained by assuming that all components function in series. The probability of system failure per flight hour, for a system that has series dependence, can be estimated by summing the component unreliability values for the time interval  $t_1 = 1 \text{ hr}$ , i.e.

$$\text{Probability of system failure} = \sum_{\text{components}} (1 - e^{-\lambda}) \quad \text{--- [10-2]}$$



The results are given in Table 10-1. It is seen that in the normal suction mode, the probability of failure is of the order of  $3.7 \times 10^{-4}$  per flight hour (i.e. one failure per 2700 flight hours). For the other modes, the analysis indicates that one failure would occur for every 3600hrs (start-up), 4700hrs (purge) and 3200hrs (anti-contamination). However, these modes would have a relatively short time of operation, occurring once or twice per LTO cycle. The failure rates should be modified by a duty cycle factor, based on the ratio of operating time to cycle mission time (MIL-STD-756B, 1981). This implies that the failure rates per flight hour would be lower than those indicated in Table 10-1 for these modes.

**Table 10-1** *Estimate of the probability of failure of the HLFC system*

	Rate per 1000hr	Probability of failure for:				Based on ref. component number*
		Start-up mode	Suction mode	Purge mode	De- Contamination	
Flow sensor #1	0.029		2.85E-05			1
Flow sensor #2	0.029		2.85E-05			1
Control valve #1	0.023		2.34E-05	2.34E-05		3
Control valve #2	0.023		2.34E-05	2.34E-05		3
SOV #1	0.014		1.43E-05	1.43E-05		6
SOV #2	0.014		1.43E-05	1.43E-05	1.43E-05	6
SOV #3	0.014		1.43E-05	1.43E-05	1.43E-05	6
SOV #4	0.014		1.43E-05	1.43E-05	1.43E-05	6
SOV #5	0.014		1.43E-05	1.43E-05	1.43E-05	6
OPV	0.014		1.42E-05	1.42E-05		7
Motor (suction pump)	0.050	5.00E-05	5.00E-05			8
Compressor (pump)	0.038	3.75E-05	3.75E-05			9
Starter turbine	0.028	2.78E-05				11
PRSOV #1	0.042	4.17E-05				13
PRSOV #2	0.042	4.17E-05	4.17E-05	4.17E-05	4.17E-05	13
Filter	0.000	0.00E+00		0.00E+00	0.00E+00	-
HLFC computer	0.038	3.75E-05	3.75E-05	3.75E-05	3.75E-05	16
Foam generator	0.000				0.00E+00	-
Motor (de-cont.)	0.050				5.00E-05	8
Pump (de-cont.)	0.067				6.67E-05	18
SOV #6	0.014		1.43E-05		1.43E-05	6
PRSOV #3	0.042	4.17E-05			4.17E-05	13
Sum ->		2.78E-04	3.70E-04	2.12E-04	3.09E-04	
One system failure per :		3600 hrs	2700 hrs	4725 hrs	3237 hrs	

\* Note: Reference component data is given in Table M-1 (Appendix M)

## 10.3 DAMAGE TO THE PERFORATED SURFACE

### 10.3.1 Introduction

The most likely cause of in-flight damage to the suction surface is bird impact. Current certification requirements in terms of impact damage are based on retaining structural integrity following an impact. In addition to this requirement a surface dent would also be of concern, as it could cause transition of the boundary layer. A single



impact may result in a wedge-shaped area of turbulent flow, aft of the impact site (similar to that shown in Fig. 9-1). A severe impact that caused a rupture in the skin would likely cause a complete failure of the laminar flow control for that surface. The consequence of damage on the leading edge is difficult to assess in general terms. It may result in a turbulent boundary layer developing on the attachment line and hence a total loss of laminar flow on the affected outboard wing panel. On the other hand, notches and bumps on the leading edge have been shown to prevent attachment line contamination (Reneaux *et al.*, 1996). It is therefore possible that certain dent shapes on the leading edge will have little influence on the laminar flow.

To assess the probability of a bird strike on the laminar flow surfaces, statistical data of impacts on commercial aircraft wings, nacelles and empennages, were sought. This enabled a preliminary evaluation of the probability of damage to the laminar flow surfaces to be established.

### 10.3.2 Probability of damage

*Wildlife Strikes to Civil Aircraft in the United States, 1990 - 1999* (Cleary *et al.*, 2000) is a summary report from the FAA National Wildlife Strike Database (FAA, 2001). Wildlife strikes are divided into bird strikes (~ 97.6%) and mammals (~2.4%). The aircraft operator could be identified for nearly 90% of the reported cases, providing the following breakdown by operator type: commercial operators (82%), business (13%), private (4%) and government/police (<1%). Of the 27 433 incidences attributed to birds (over the ten-year period), ~33% struck either the wing, engine or tail (data reproduced in Table M-2, Appendix M). The engine was seen to have a significant portion of the total, which is understandable, as birds get sucked into the engines. The engine nacelle is much less likely to be struck than the engine itself; however, it was not possible to separate the occurrences where the impact was on the nacelle from the data. The 33% value is thus an upper limit of the percentage of cases where the surfaces of interest (i.e. wing, empennage and nacelle) were struck.

An estimate of the number of bird strikes on the wing, engine or tail on commercial aircraft was obtained by multiplying 0.82 by 0.33 by 27 433, to give a total of 7423. Only ~17% of the bird impacts in the data resulted in damage to the aircraft structure (data reproduced as Table M-3, Appendix M). Using this factor, it is estimated that no more than 1262 commercial aircraft were damaged on the surfaces of interest during the ten-year period.

The number of USA commercial operations<sup>20</sup> over this time-frame was approximately 129 million (Cleary *et al.*, 2000). This enabled an estimate of the incident rate to be established. It was determined that the incident rate, where damage to the wing, engine or tail occurred, was approximately 10 strikes per million

---

<sup>20</sup> Operation: Either a takeoff or a landing.



operations. This estimate is likely to be an upper limit, as strikes to the engine itself were included in the data.

## 10.4 DURABILITY OF THE PERFORATED SURFACE

### 10.4.1 Introduction

The design and manufacture of the suction surface and its supporting substructure are critical elements in the development of HLFC technology. A review of the subject, by the author with Humphreys<sup>21</sup> and Fielding<sup>22</sup>, titled *Investigation of Hybrid Laminar Flow Control (HLFC) Surfaces* (Young *et al.*, 2001), outlines the design requirements, candidate materials and manufacturing considerations for suction panels. Selected parts of this manuscript are reproduced in section B.4 of Appendix B.

There has been a major concern that the porosity of the panels will change with time once the aircraft enters service. The issue of blockage of the holes by airborne particles and insects has been raised by many researchers. In the context of aircraft operations, the problem has been described by, for example: Maddalon and Wagner (1985), Meifarth and Heinrich (1992), Humphreys (1992; 1996; 1999) and Wilson and Jones (1996). An aspect which is equally worrying, but less well documented, concerns the opening up of the holes under the combined influence of corrosion and rain-/ ice-induced erosion. The increased porosity will alter the pressure distributions within the suction chambers, and could, if the holes get large enough, result in premature transition of the boundary layer.

### 10.4.2 HYLDA erosion and corrosion tests<sup>23</sup>

#### 10.4.2.1 Rain erosion tests

To evaluate the rain impact resistance of laser drilled materials during the HYLDA project (see section C.16 of Appendix C), a series of erosion tests were carried out. Humphreys designed and manufactured a rain erosion rig (Fig. 10-2) and the author was responsible for specimen preparation and the post-test inspection of the specimens. These specimens, of diameter 25mm, were clamped in a holder, at the end of a rotating arm. A rain-fall rate of 25mm per hour was used, with an average droplet size of ~1mm.

Four materials were tested (Table 10-2). The thermoset composite specimens were fabricated from seven layers of Fiberite 914C carbon fibre unidirectional material, and were tested in a perforated and non-perforated condition. The thermoplastic

<sup>21</sup> B. Humphreys, Aerospace Systems and Technology, Consett, Durham, UK.

<sup>22</sup> J. Fielding, School of Engineering, Cranfield University, Cranfield, Bedfordshire, UK.

<sup>23</sup> Previously reported by Young *et al.* (2001). Selected parts have been reproduced in this section.



composite specimens were perforated APC-2, a carbon fibre composite of PEEK (poly-etheretherketone). The aluminium specimens were anodised aircraft-grade clad aluminium alloy (L166). The titanium specimen was CP. Specimens were drilled with a Nd-Yag laser, using the single pulse method and Argon was used as the shielding gas.

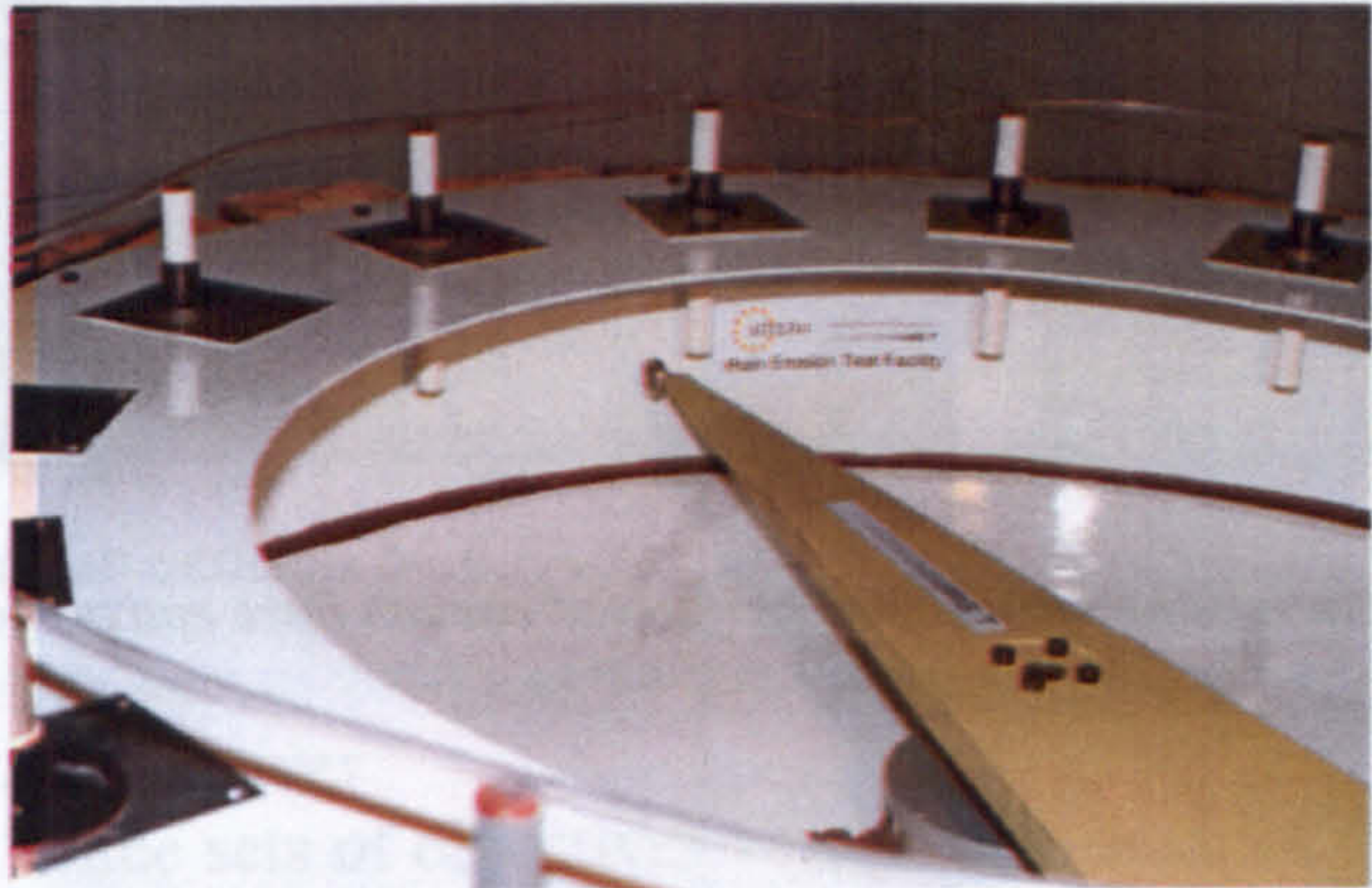


**Fig. 10-2** Rain erosion rig, built by AS&T (Young et al., 2001)

10.4.2.2 Rain erosion test results

A qualitative assessment of the life of the specimens was possible by using the aluminium specimen – which was similar to what is used on leading edges of current wings and nacelles – as a benchmark. Defining the limit of the “useful life” in the test was subjective. Humphreys decided to stop the test when fibre bundles were being removed from the composite specimens or when pitting – visible to the naked eye – started to occur on the metal specimens. The relative performance of the different materials is presented in Table 10-2.

Titanium was largely unaffected by the erosion impacts and displayed essentially no damage after 36 hours of continuous testing. The carbon fibre thermoset composite material, however, displayed very poor erosion resistance. Fig. 10-3a shows the commencement of damage, from after just a few minutes. Loose fibres on the surface are seen to have broken off at the hole edges, initiated by the heat damage to the resin in this region. After approximately 30 minutes, fibres were removed between adjacent holes (Fig. 10-3b). The laser drilled thermoplastic material also suffered some fibre removal, but this was considerably less than that of the carbon fibre epoxy specimens. After 11 hours, the perforated thermoplastic material was similar in damage to the carbon fibre epoxy specimens after 30 seconds, under the same conditions.

**Table 10-2** Rain erosion test results (Young et al., 2001)

Materials	Rain erosion resistance
Perforated carbon fibre epoxy composite	Very poor
Non-perforated carbon fibre epoxy composite (unpainted)	Poor
Perforated PEEK thermoplastic composite	Fair
Anodised L166 Alclad aluminium (non-perforated)	Good
Perforated titanium	Excellent



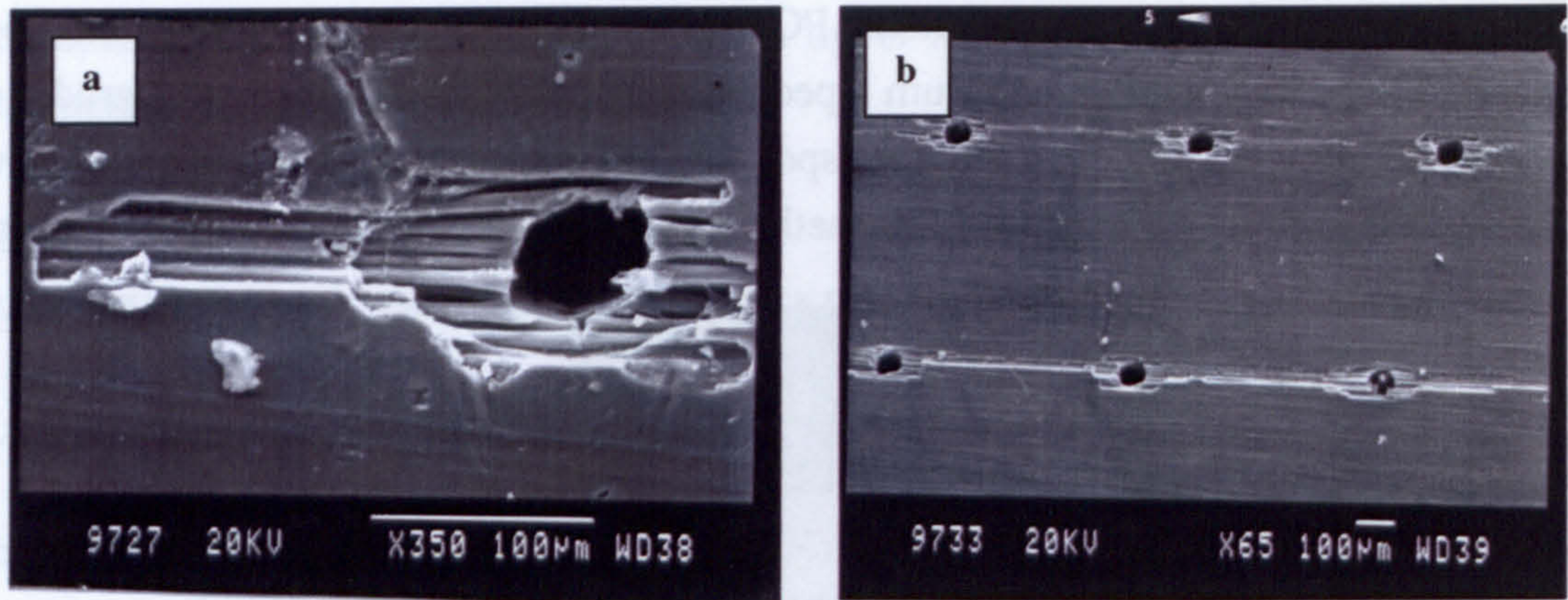


**Fig. 10-3** SEM images showing rain erosion on Nd-YAG perforated carbon fibre epoxy specimens (Young et al., 2001)

#### 10.4.2.3 Salt spray corrosion tests

To investigate the nature of corrosion of perforated aluminium, a 1mm thick panel of anodised non-clad L166 aluminium was drilled by Nd-YAG laser, and subjected to a salt spray test in accordance with ASTM B117 standard, by HAL Consultants<sup>24</sup> (1998), under contract to the author. The salt solution, of 5% NaCl in de-ionised water, was used on a “once-through” basis, with an average run-off rate of 2.6ml per day. The cycling was continuous over five days, thereafter the sample was removed. The panels, inspected at the University of Limerick, indicated signs of corrosion and damage at the edges of the holes (Fig. 10-4). The results supported the concern that unprotected perforated aluminium would have poor long-term corrosion resistance. However, it was not possible to correlate the exposure time in the salt spray cabinet, to an equivalent flight time. This issue was further explored in the HYLTEC project (see section 10.4.3).

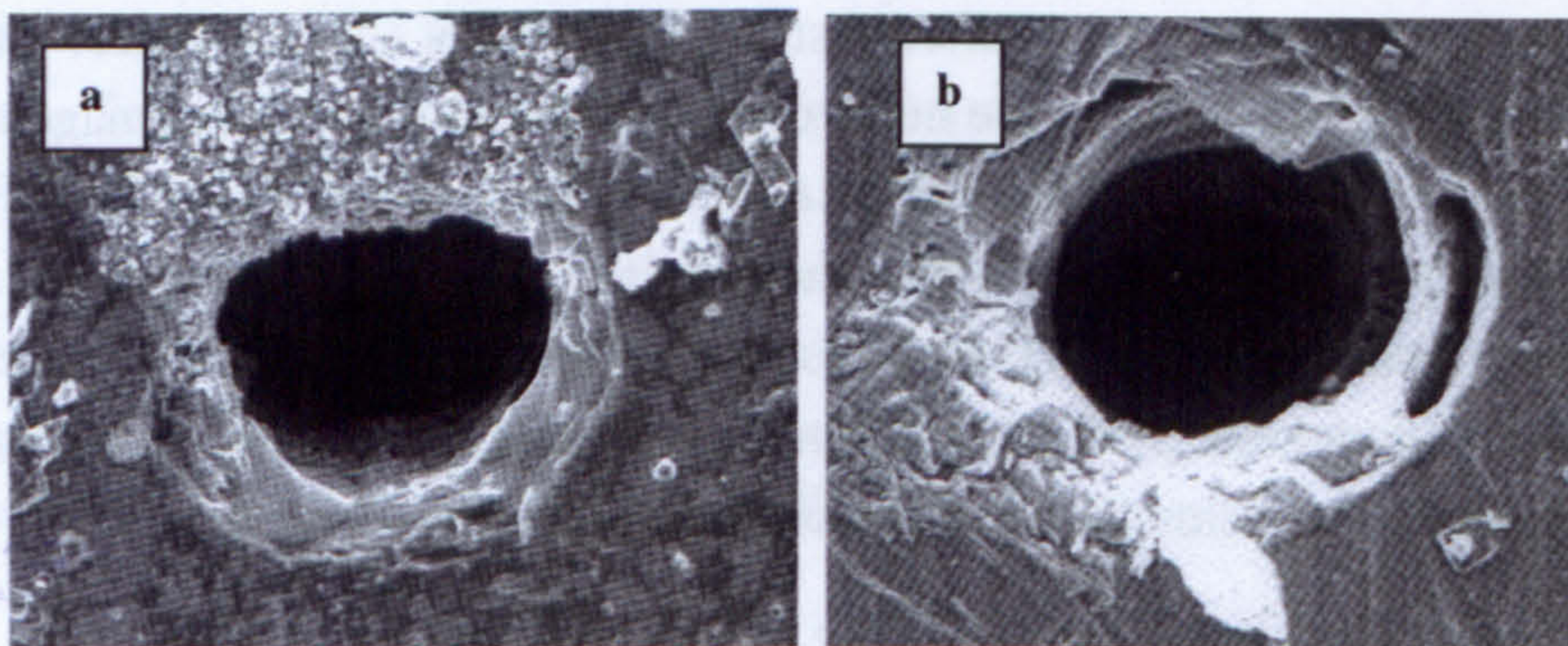


**Fig. 10-4** SEM images of laser drilled holes (diameter ~ 80µm) in aluminium alloy, following salt spray trials. Note cracking around hole edge (Young et al., 2001)

<sup>24</sup> Manchester, UK



### 10.4.3 HYLTEC durability tests<sup>25</sup>

#### 10.4.3.1 Introduction

As a part of the HYLTEC project a SAAB 2000 aircraft (Fig. 9-5, Chapter 9) was fitted with a number of small laser drilled test panels on the wing leading edge. The objective was to investigate contamination and durability aspects of candidate HLFC suction surfaces. The contamination aspects are described in Chapter 9. The University of Limerick was responsible for the post flight-test inspection and analysis of the panels, which was conducted under the direction of the author. An overview of the research and conclusions reached are described in this section, with further details provided in section M.4 (Appendix M).

#### 10.4.3.2 Objectives

Three sets of objectives were established for the post flight-test inspection of the panels. These were:

1. To examine the panels for cracking and corrosion using optical and scanning electron microscopy;
2. To measure the hole sizes using an optical technique and to statistically analyse the data to ascertain if the hole sizes changed due to exposure on the aircraft;
3. To determine the pressure loss versus flow rate characteristics of the different panels and to relate, if possible, the results to the measured hole sizes.

#### 10.4.3.3 Description of materials

The materials that were evaluated were: hard anodised non-clad aluminium, chromic acid anodised non-clad aluminium, titanium and APC-2 (Table 10-3). An aluminium panel – which was not installed on the aircraft – was used as a reference. The titanium panel was in two sections – one section had the laser exit (i.e. the small holes) on the outside (i.e. normal taper) and the other section was reversed. This enabled a comparative assessment of the hole sizes to be made. All panels were drilled with a Nd-YAG laser using the single pulse method and Argon as the shielding gas. The panels were pressed, rolled to shape and installed in the holder (Fig. 10-5), which was then attached to the leading edge of the port wing.

---

<sup>25</sup> *Durability of Hybrid Laminar Flow Control (HLFC) Surfaces*, by Young, Mahony, McClafferty, Corish, Humphreys and Totland (in press) describes this investigation, and summarises the major results.



Table 10-3 Materials evaluated

No.	Description	Material	Notes	Exposure on aircraft
1	Hard anodised aluminium	Non-clad L166, ~0.9mm thick	Sulphuric acid anodised	18 months*
2	Anodised aluminium	Non-clad L166, ~0.9mm thick	Chromic acid anodised	20 months
3	Titanium - normal taper	Commercially pure, ~0.9mm thick	Laser exit (small hole) on the outer face	20 months
4	Titanium - reverse taper	Commercially pure, ~0.9mm thick	Laser entry (large hole) on the outer face	20 months
5	APC-2	Carbon fibre PEEK, ~ 0.9mm thick		2 months
6	Reference panel	Non-clad L166, ~0.9mm thick	Drilled at the same time as panel 2.	nil

\* Panel removed after 18 months and replaced by APC-2 panel.

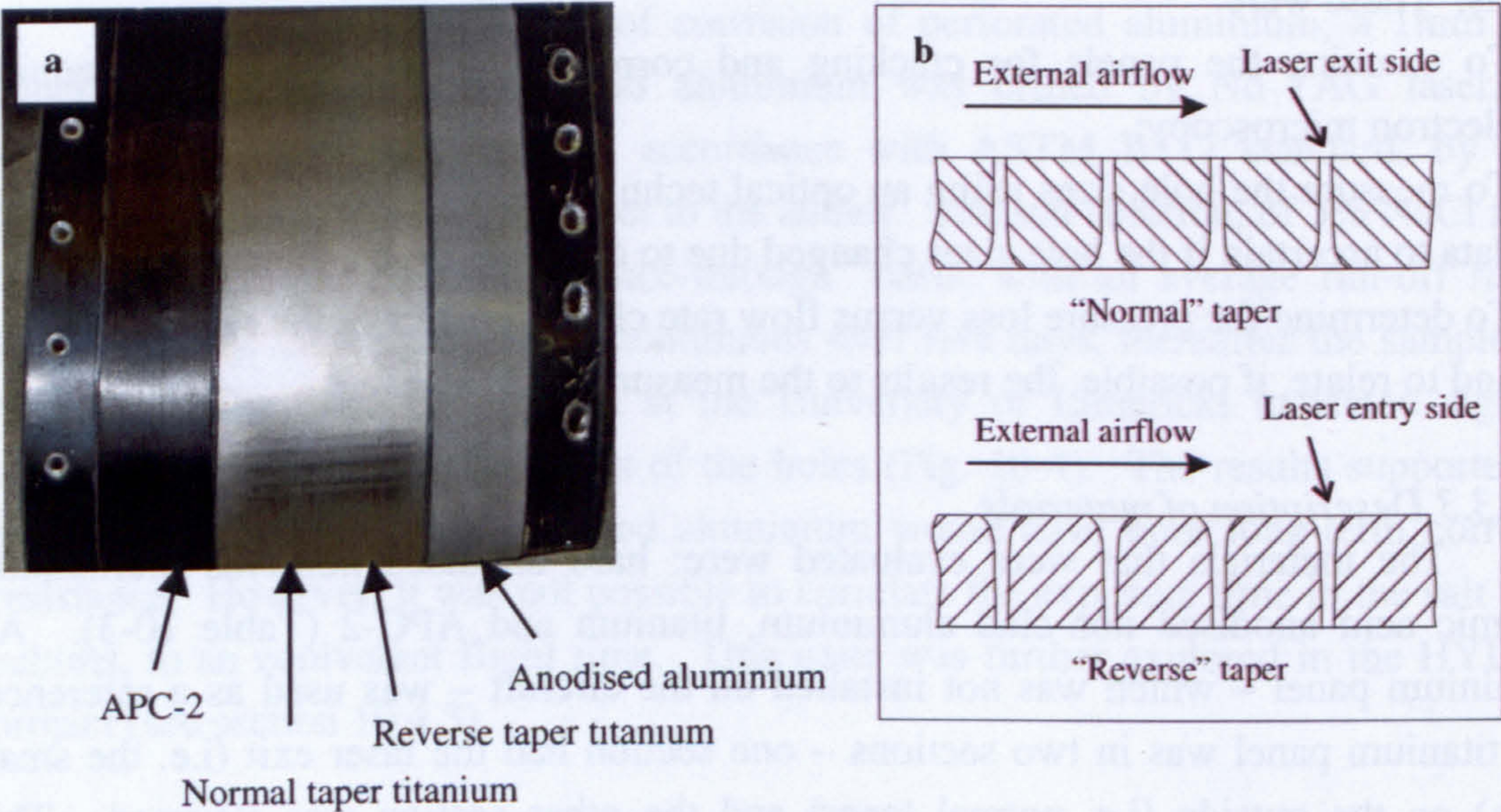


Fig. 10-5 (a) Test panels installed in holder (b) Detail showing normal and reverse taper

10.4.3.4 Results

1. Titanium was the most durable material tested. The panel surface showed no evidence of degradation after the flight trials. No cracking was observed during extensive microscopy of sectioned specimens. The hole sizes, measured on a titanium surface that was exposed on the leading edge, were statistically similar to the holes on the inside of the panels (which were not exposed to the rain / ice impacts).
2. Both the anodised (chromic acid) and hard anodised (sulphuric acid) aluminium panels displayed evidence of corrosion and micro-cracking. The reference panel was observed to be free of cracks, implying that any residual cracks in the recast laser around the hole were too small to be identified. It was thought that the cracks



- may have been initiated by the drilling and forming process, and that a significant "opening up" of the cracks occurred whilst exposed on the leading edge.
3. On the basis of the ANOVA<sup>26</sup> analysis performed, it was concluded that the holes on the exterior of the aluminium panel (laser exit side) were significantly larger on the test panel than on the reference panel. Although the holes on the laser entry side were also larger on the test panel, the relative amount was less, and the mean hole sizes could be considered as not being significantly different. It was concluded that the in-flight exposure was responsible for this increase in hole size on the external surface.
  4. After just two months exposure to operational conditions, the laser drilled APC-2 composite material demonstrated relatively poor durability, with noticeable amounts of fibre being removed between holes on the surface.

10.4.3.5 Conclusions

A summary of important conclusions regarding the three material types is given below in Table 10-4.

Table 10-4 *Summary of important conclusions*

Material	Conclusion
Titanium	The panel showed no evidence of degradation. Titanium remains the only viable choice for HLFC suction surfaces, where the attachment line is perforated.
Aluminium	The results effectively eliminate aluminium as a candidate material for this application.
APC-2 (carbon fibre PEEK)	Further trials will be required, to get a definitive answer as to the viability of using APC-2, or a similar thermoplastic material, for an engine nacelle - where oblique rain / ice impacts occur.

<sup>26</sup> ANOVA (analysis of variance): Statistical analysis technique.



## **11 FUEL SAVINGS**

### **11.1 INTRODUCTION**

It has been argued by the author (for example, Young and Fielding, 2000; 2001) that the calculation of the required trip fuel for HLFC aircraft and the prediction of fuel savings to be achieved by this technology, should be based on the probable loss of laminar flow during the flight and not on the requirement that an HLFC aircraft be capable of completing the mission in the “turbulent mode”. This approach requires knowledge of the system reliability and a forecast of the en route cirrus cloud at the planned cruise altitudes. The impact on the potential fuel savings of HLFC compared to a turbulent baseline aircraft, if such information were available, is assessed in this chapter.

### **11.2 IMPACT OF RANGE ON POTENTIAL FUEL SAVINGS**

HLFC is essentially a technology that will save fuel during the cruise; obviously this will favour long-range missions over short-range operations. The impact of range on the fuel-saving potential of HLFC may be assessed by considering the ratio of cruise fuel to block fuel. The results for the B757-200 and A330-200 classes of aircraft illustrated in Fig. 11-1, were obtained using the performance models described in Chapter 4 (based on the design payloads, International reserves and a 5% contingency fuel). Data for the A340 aircraft, as reported by Robert (1992) of Airbus, is also shown on the figure as a comparison. These values were read off a graph and would thus only be accurate to  $\pm 2\%$ . Furthermore, details on the payload and reserves were not provided by Robert; nevertheless, the percentages are seen to be very similar to those calculated for the A330-200 class aircraft.

It is evident that for a range of less than 500nm, the cruise fuel represents less than ~45% of the total fuel burn. At these shorter distances, the taxi, climb and descent fuel elements constitute a significant portion of the total block fuel. As the range increases, the cruise fuel / block fuel ratio increases. For 3000nm, which represents an average long-range mission for the A340 according to Robert (1992), it is seen that the ratio is ~ 85%. A more accurate picture of the fuel saving potential of HLFC is obtained by including the fuel burned during the upper part of the climb (herein selected to be above 20000ft) with the cruise fuel. This increases the ratio to ~59% at 500nm (for the B757-200 class aircraft) and to ~ 90% for a range of 3000nm.

In conclusion, it is seen that the opportunity to save fuel with this technology is extremely limited for flights of less than ~1000nm, where these relatively small theoretical fuel savings are further reduced by practical considerations of increased SFC and aircraft weight.



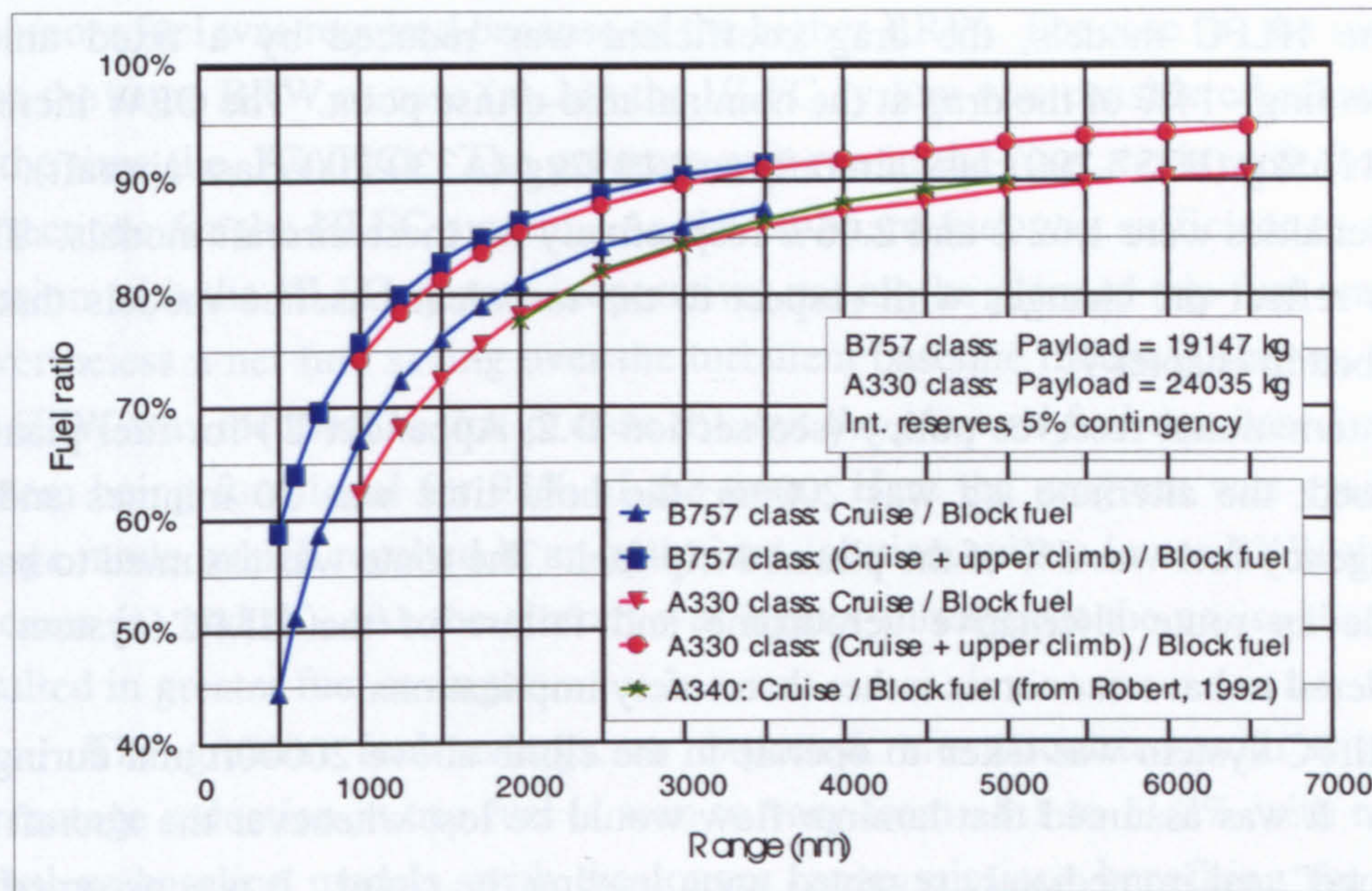


**Fig. 11-1** Ratio of cruise fuel to block fuel and cruise plus climb fuel (above 20000 ft) for varying range

## 11.3 WEATHER FORECASTING AND OPTIMISED FUEL PLANNING<sup>27</sup>

### 11.3.1 Rationale

The route average time-in-cloud (TIC) during cruise, as reported by Jaspersen *et al.* (1984a), varied from a low of 2.2 to 9.9% based on GASP data. These route average TIC values and the widely quoted estimate of 7% TIC of Davis *et al.* (1987) have previously been used in support of the economic viability of HLFC, by assuming that laminar flow will, on average, occur during most of the flight (say about 93%). There is, however, an important secondary influence that should also be taken into account in determining the net fuel savings achievable with HLFC technology. It concerns the optimisation of the fuel planning. During flight the rate of fuel consumption depends directly on the weight of the aeroplane. If credit is taken for the drag reduction due to the HLFC system during the *fuel planning* for a mission, then the aircraft will have a lower takeoff weight and it will be lighter throughout the cruise, significantly reducing the trip fuel. It is this reduction in trip fuel due to the lighter takeoff weight that is quantified in this section.

### 11.3.2 Ground rules

- (1) A fixed payload of 19147kg (B757-200 class aircraft) and 24035kg (A330-200 class aircraft) was used, corresponding to the design payload weights specified for cases 1B and 2B in Table 6-1.

<sup>27</sup> A very similar study using slightly different input data, was reported by the author in *The Impact of Cloud Encounter on Hybrid Laminar Flow Control Aircraft Operations* (Young *et al.*, 2002).



- (2) For the HLFC models, the drag coefficient was reduced by a fixed amount representing ~14% of the drag at the nominal mid-cruise point. The OEW increases were 1165kg (B757-200 class aircraft) and 1952kg (A330-200 class aircraft). The SFC penalties were 1.62% and 2.06% respectively for these aircraft models. These values reflect the changes with respect to the turbulent baseline models that are described in chapter 7.
- (3) The International reserves policy (see section D.2, Appendix D) for fuel planning was used; the alternate leg was 200nm; the hold time was 30 minutes and the contingency fuel was 5% of the planned trip fuel. The route was assumed to have a suitable en route alternative aerodrome and failure of the HLFC system was considered to have economic rather than safety implications.
- (4) The HLFC system was taken to operate in the climb above 20000ft and during the cruise. It was assumed that laminar flow would be lost whenever the aircraft was "in cloud" and immediately regained upon leaving the cloud. It was assumed that the pumps would be running during this time and hence the SFC penalty was imposed from the 20000ft point in the climb, until the TOD (top of descent).
- (5) Three range values were considered for each aircraft type (Table 11-1), corresponding to: (1) The distances of 3272nm and 5980nm, for the B757-200 and the A330-200 classes of aircraft respectively (i.e. point "B" in Fig. 6-1); (2) Two-thirds of these distances; and (3) One-third of these distances. The TIC was 7% of the time that the HLFC system was operational.

**Table 11-1** *Matrix for studies - Optimised fuel planning*

	B757-200 class aircraft			A330-200 class aircraft		
	(1)	(2)	(3)	(1)	(2)	(3)
Range (nm)	3272	2181	1091	5980	3987	1993
Payload (kg)	19147	19147	19147	24035	24035	24035
Increase in OEW (kg)	1165	1165	1165	1952	1952	1952
Increase in SFC	1.62%	1.62%	1.62%	2.06%	2.06%	2.06%
Change in drag	0.00415	0.00415	0.00415	0.00377	0.00377	0.00377

### 11.3.3 Results of trip fuel calculations

The output of the trip fuel calculations is summarized in Fig. 11.2. For each aircraft type three trip distances were evaluated, yielding six sets of results. Initially the program was run in the *Range* mode (for each aircraft and distance combination) to establish the fuel required for the turbulent baseline model. Three approaches were then followed to calculate the difference in trip fuel between the HLFC aircraft and the corresponding turbulent baseline model. For case (a) the HLFC system was considered inoperative for the whole flight. The program was run in the *Range* mode and it iterated to find the lowest fuel quantity (and hence lowest BRW) that would satisfy the mission. The negative change in fuel (Fig. 11.2) reflects the impact of the installation of the HLFC system, which would increase the aircraft's Zero Fuel Weight (ZFW) and the fact



that more fuel was required because of the higher BRW. For case (b) the model was run with the same BRW as case (a), but the HLFC system was considered effective for 93% of the time (i.e. 7% TIC). The program was run in the *Fuel* mode with the appropriate corrections for the HLFC system. As the on-board fuel was sufficient to complete the mission with the HLFC system inoperative, not all the planned trip fuel was consumed; nevertheless a net fuel saving over the turbulent baseline model is shown. For case (c) the ZFW was identical to that of case (b), but the *planned fuel* was based on the HLFC system being functional for 93% of the time. Here the program was again run in the *Range* mode, which resulted in an optimised solution, with a lower BRW than that used in cases (a) and (b). As the aircraft was lighter throughout the cruise than case (b), it resulted in greater fuel savings.

The greatest fuel savings, as expected, are associated with case (c). The percentage reduction in trip fuel is seen to vary from ~8.1 to 11.2% with respect to the turbulent baseline models, with the longer range missions benefiting the greatest. It should be noted that these predicted fuel savings depend significantly on the assumptions made regarding the drag reduction, OEW increase and SFC penalty, as discussed in Chapter 7.

An objective of this particular study was to explore the impact of carrying fuel that does not get used. This is seen as the difference between the results of case (c) and (b). It is evident that as the trip distance increases, the difference between (c) and (b) gets greater. For the shortest mission the difference between the fuel savings determined for case (c) and those for case (b), is 0.6% and 0.5% (for the B757-200 and A330-200 classes of aircraft respectively). This rises to 2.5% and 3.8% respectively for the longest mission considered for each aircraft type.

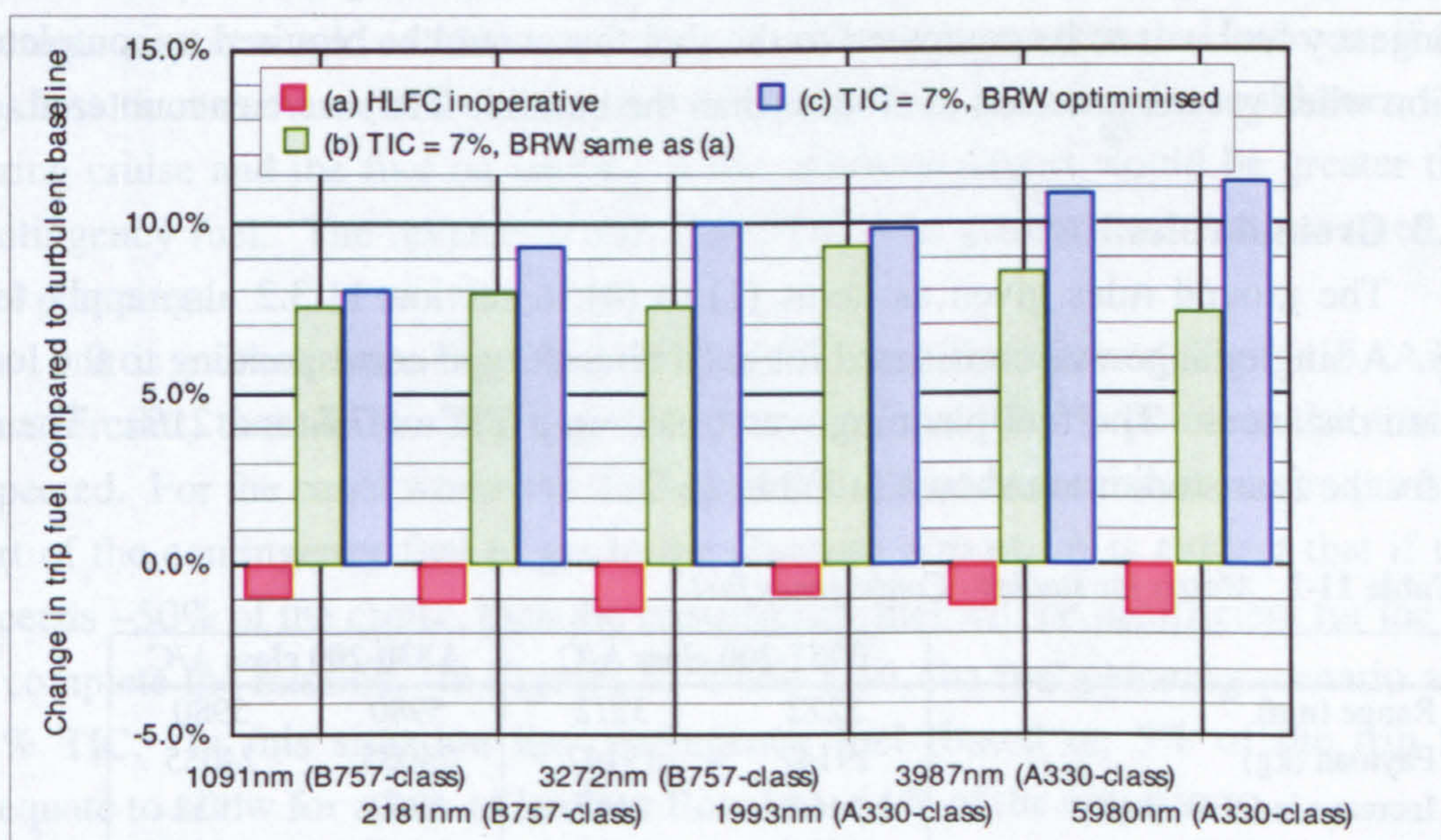


Fig. 11-2 Change in trip fuel compared to turbulent baseline aircraft for a given range



## 11.4 CONTINGENCY FUEL AND FLIGHT PLANNING

### 11.4.1 Introduction

Establishing the precise fuel quantity required for a HLFC aircraft requires knowledge of the fraction of the cruise that the system will not be operating due to the incidence of cloud. In an ideal situation, it would be possible to forecast the cloud patterns for flight planning in a way that is routinely done for winds. There are however a number of reasons why this is presently a much more difficult task. Spang *et al.* (2001) state that “around the tropopause cirrus clouds are optically thin and not detectable in the visible or reported by ground based weather observers. These clouds are also very difficult to observe for nadir-looking instruments and are often described as subvisual cirrus clouds.” Furthermore, these cloud layers can be very thin and to forecast the cloud at the planned flight level will require a high degree of accuracy.

A precise forecast of clouds may not be possible; however, in terms of the objectives of planning safe and efficient flight, it may also not be necessary. Nastrom *et al.* (1981b) remark that “because general cloudiness or the lack thereof, is not a random event but is associated with large scale weather systems, clear and cloudy areas tend to have appreciable areal extent”. Cirrus climatology has strong seasonal and geographical variations which are well understood (see section K.4, Appendix K). These observations allude to the suggestion that a conservative TIC estimate could be used for planning the fuel requirement of HLFC aircraft.

### 11.4.2 Objective

The objective was to explore the use of a baseline TIC value that could be used for flight planning for the two classes of aircraft. The magnitude of the standard contingency fuel was to be compared to the fuel that would be required to complete the mission when greater amounts of clouds (than the baseline TIC) were encountered.

### 11.4.3 Ground rules

The ground rules given as items (1) to (4) in section 11.3.2 also apply to this study. A single range was considered for each aircraft type corresponding to the longest mission distances. The fuel planning was based on a TIC of 7% and 21%. The input data for the four studies are shown in Table 11-2.

**Table 11-2** Matrix for studies - Contingency fuel

	B757-200 class A/C		A330-200 class A/C	
Range (nm)	3272	3272	5980	5980
Payload (kg)	19147	19147	24035	24035
Increase in OEW (kg)	1165	1165	1952	1952
Increase in SFC	1.62%	1.62%	2.06%	2.06%
Change in drag	0.00415	0.00415	0.00377	0.00377
Assumed TIC for fuel planning	7%	21%	7%	21%
Results given in:	Fig. 11-3	Fig. 11-4	Fig. 11-5	Fig. 11-6



Trip fuel calculations were performed allowing for a loss of laminar flow ranging from 0% to ~50% of the time that the HLFC system was operational.

#### 11.4.4 Method

Two fuel planning scenarios were explored, corresponding to an anticipated TIC of 7% and 21%. Based on the assumption that there would be a loss of laminar flow for this fixed percentage of the time, the required trip fuel and the aircraft's BRW were determined for the specified mission range and payload. The program was then re-run several times with the BRW (and total fuel) determined from the first computer run, but each time the program was set so that the model would encounter different "actual" TIC during the cruise. This varied from 0 to 50%. As expected, the "actual" fuel burn in the general case did not exactly match the planned fuel. The results that were of interest, included: (1) The fuel that would be on-board the aircraft, if it continued flying and landed at the alternate aerodrome, after the alternate leg and the hold; (2) The planned contingency fuel.

#### 11.4.5 Results

Figures 11-3 to 11-6 contain plots of the calculated fuel on landing at the alternate airport, versus the loss of laminar flow. The ordinate variable is the "actual" TIC expressed as a percentage of the HLFC operational time (i.e. the time from the 20000ft point in the climb to the TOD). For each of the four studies, the planned contingency fuel is shown.

If the en route conditions (in terms of TIC) were exactly the same as those assumed for the planning of the flight, and the aircraft was forced to divert to an alternate airport (again as per the planned mission), then the fuel on landing at the alternate airport would exactly equal the planned contingency fuel. However, if the TIC was less than that assumed for the fuel planning, then the aircraft would burn less fuel during cruise and the fuel on landing at the alternate airport would be greater than the contingency fuel. The reverse is true if the TIC was greater than that assumed for the fuel planning.

It is evident from Fig. 11-3 (B757-200 class aircraft) and Fig. 11-5 (A330-200 class aircraft) that the two fuel quantities are equal for the 7% point on the abscissa, as expected. For the cases where the TIC exceeded 7% of the cruise, it was required to use part of the contingency fuel to get to the alternate airport. It is evident that if the TIC exceeds ~50% of the cruise, then the contingency fuel will be insufficient for the aircraft to complete the mission. In Figures 11-4 and 11-6, the fuel planning scenario assumed 21% TIC. In this situation the contingency fuel (based on 5% of the trip fuel) is adequate to allow for a loss of laminar flow for ~64% of the cruise.



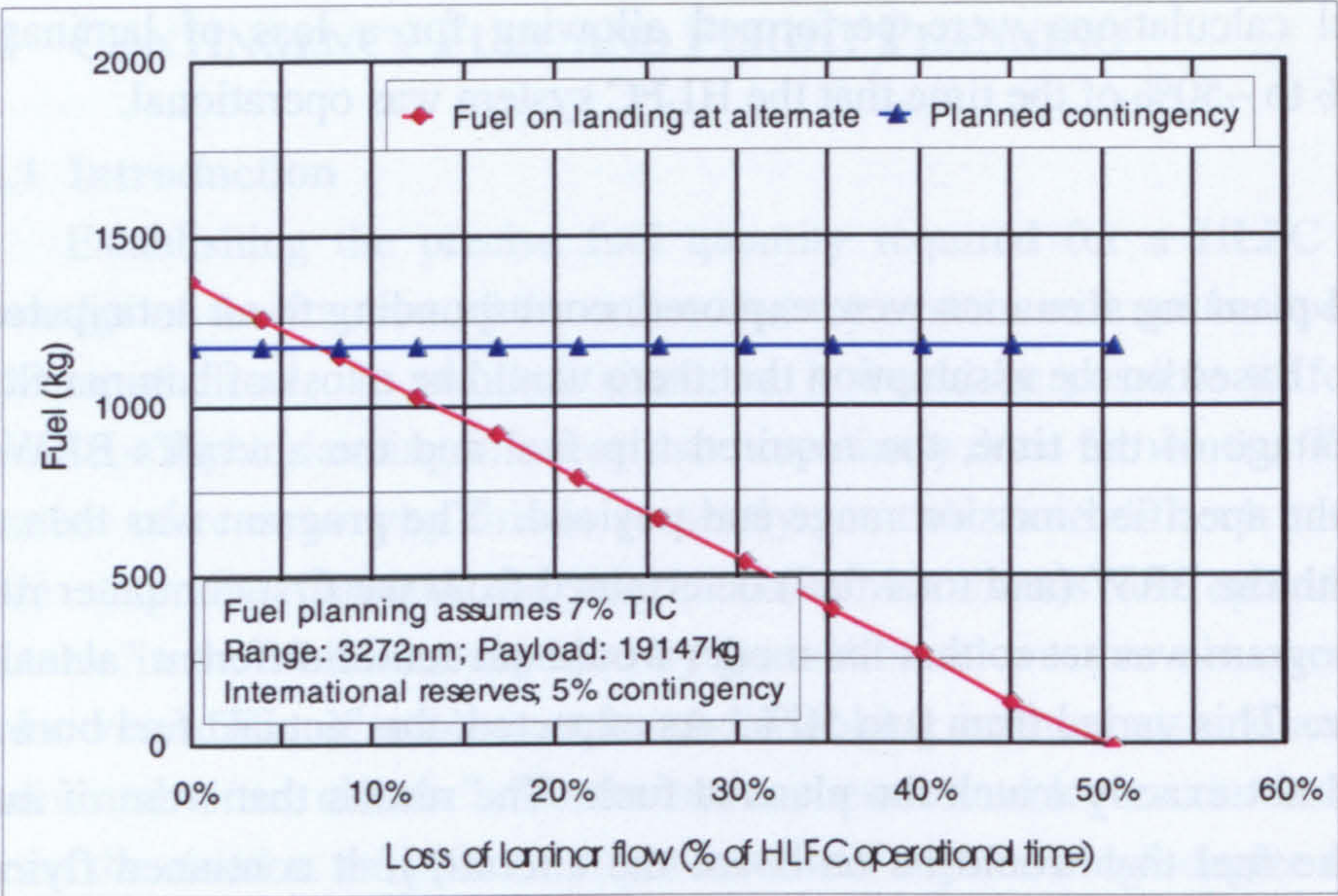


**Fig. 11-3** B757-200 class aircraft: Fuel on landing at alternative airport versus loss of laminar flow, based on fuel planning that assumed 7% TIC

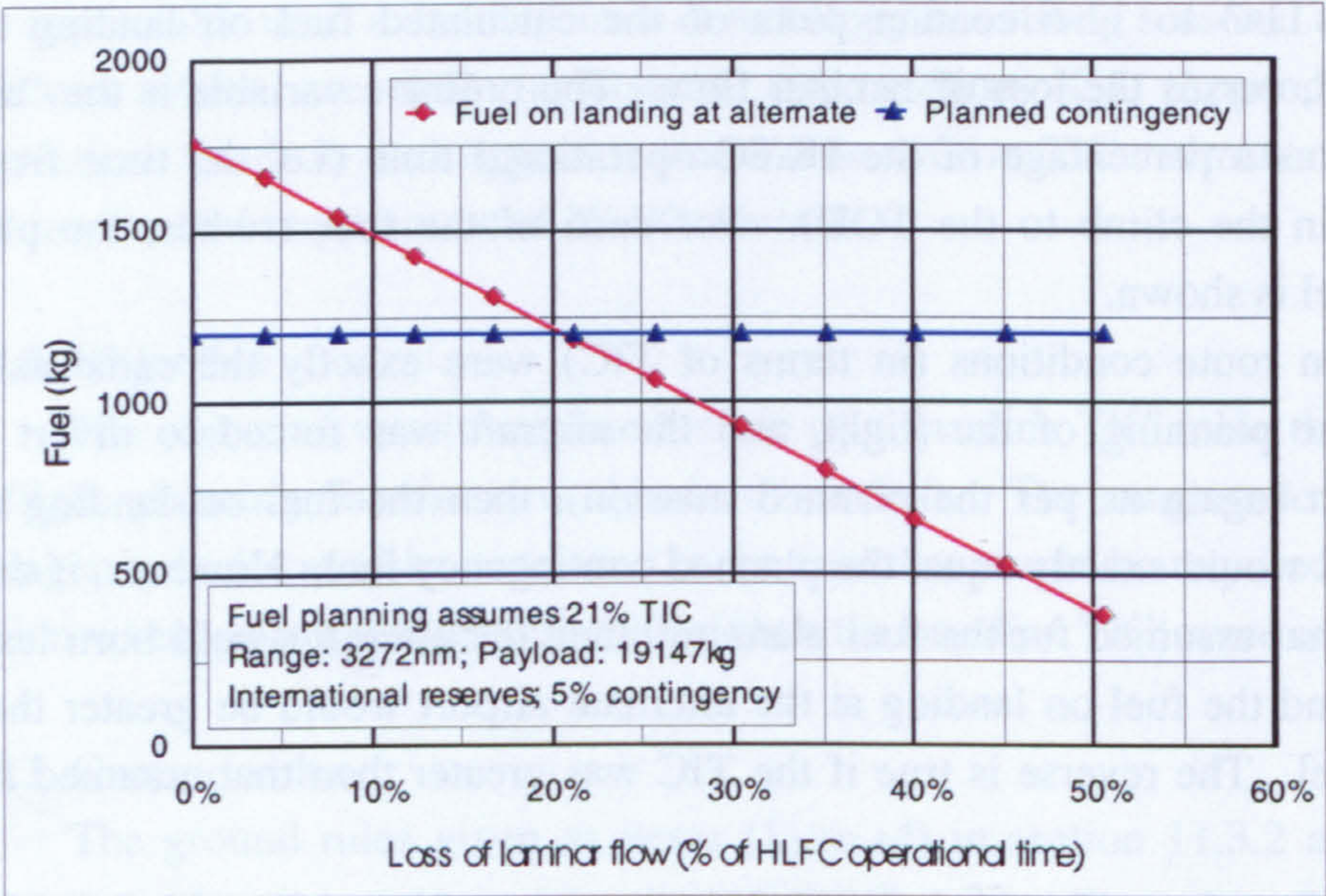


**Fig. 11-4** B757-200 class aircraft: Fuel on landing at alternative airport versus loss of laminar flow, based on fuel planning that assumed 21% TIC



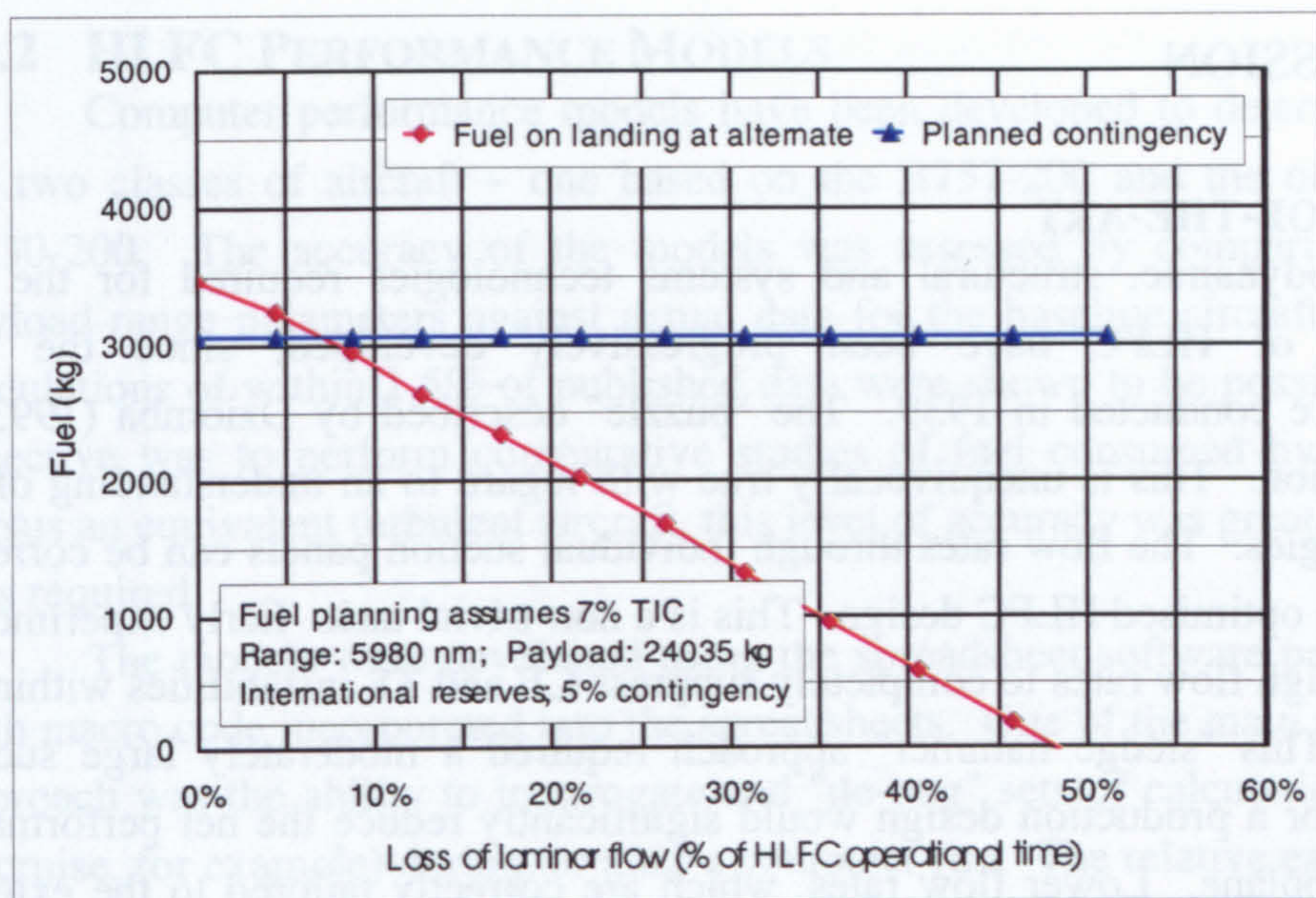


**Fig. 11-5** A330-200 class aircraft: Fuel on landing at alternative airport versus loss of laminar flow, based on fuel planning that assumed 7% TIC

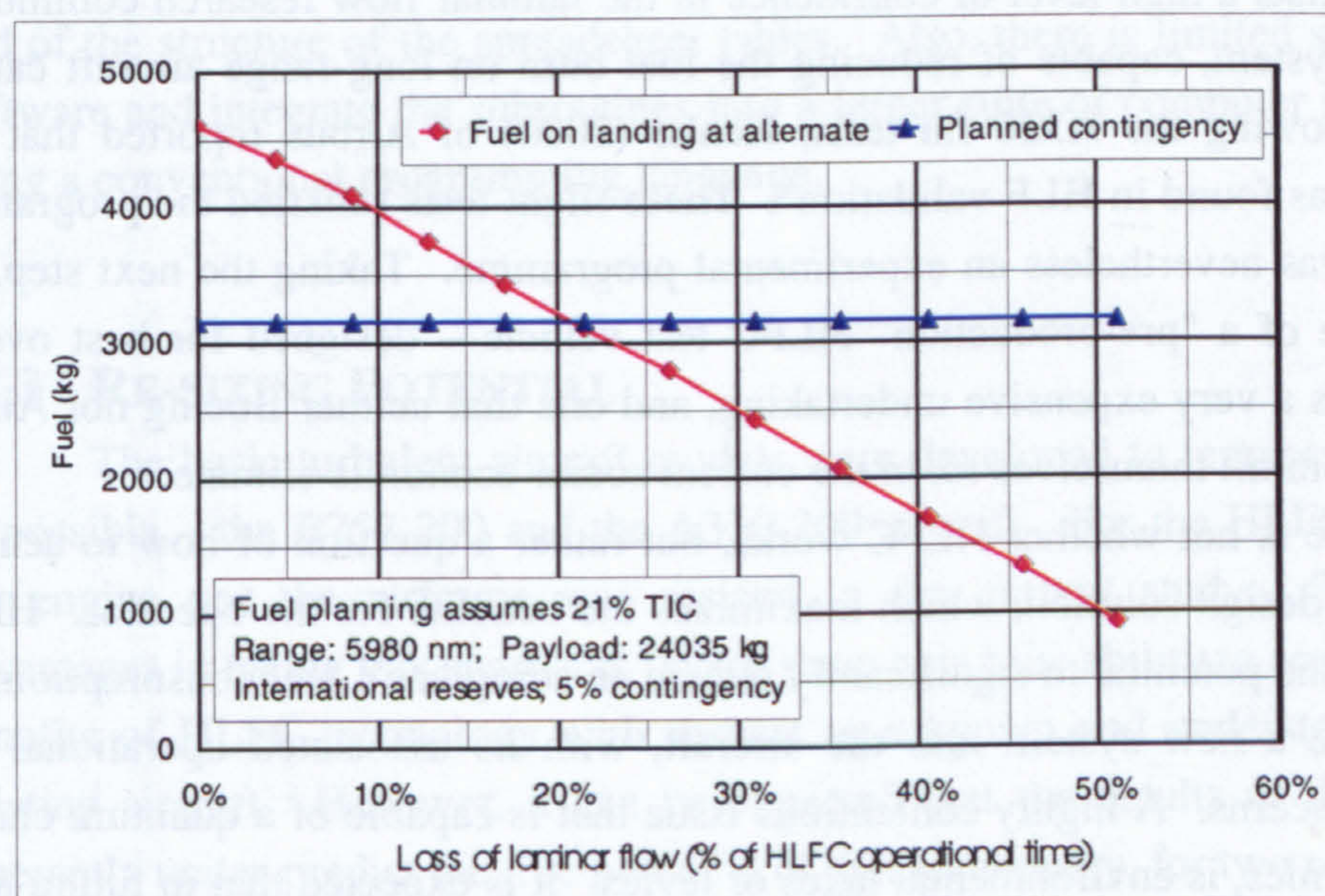


**Fig. 11-6** A330-200 class aircraft: Fuel on landing at alternative airport versus loss of laminar flow, based on fuel planning that assumed 21% TIC



## 12 DISCUSSION

### 12.1 STATE-OF-THE-ART

The aerodynamic, structural and systems technologies required for the full implementation of HLFC have been progressively developed, since the first experiments were conducted in 1939. The "puzzle" described by Dziomba (1993) is nearing completion. This is unequivocally true with regard to an understanding of the critical technologies. The flow rates through individual suction panels can be correctly calculated for an optimised HLFC design. This is a non-trivial task. Early experimental work relied on high flow rates to completely suppress CF and TS instabilities within the suction zone. This "sledge hammer" approach required a moderately large suction system, which for a production design would significantly reduce the net performance gain for the aeroplane. Lower flow rates, which are correctly tailored to the external flow condition, would permit instabilities to grow within the suction region, but without reducing the extent of laminar flow. The reduced mass flow implies a smaller suction system of lower weight and reduced SFC penalty.

There exists a high level of confidence in the laminar flow research community that a reliable system, capable of reducing the fuel burn on long-range aircraft can be produced. Following the A320 fin tests, Henke (2000) of Airbus reported that "no show-stopper was found in HLF validation". These flight tests satisfied the programme objectives. It was nevertheless an experimental programme. Taking the next step, i.e. the manufacture of a "pre-production" HLFC test vehicle – designed for best overall performance – is a very expensive undertaking, and one that neither Boeing nor Airbus are willing to commit themselves to, in the current social-economic climate.

The issue is not whether HLFC works, but rather a question of how to achieve the best overall design solution, which maximizes the benefits for the operator. HLFC technology has the potential to significantly reduce an aeroplane's fuel consumption, but it will introduce a new system into the aircraft, with its associated operational and maintenance concerns. A highly contentious issue that is capable of a quantum change in airline economics, is environmental taxes or levies. It is expected that in future more environmentally conscious governments will have the polluters pay for the environmental damage they cause, and in this way, aviation will become responsible for its share of greenhouse gases. No government has yet introduced such an emission levy (or carbon-fuel tax); however, the concept has received considerable attention. There has been "exhaustive consideration, which is still continuing", by the ICAO Committee on Aviation Environmental Protection (CAEP) of the "possibilities for using economic measures – fuel tax, levies, or trading, for instance – to reduce CO<sub>2</sub> emissions" according to Duthie (2001) of CAEP. The imposition of such levies will serve to stimulate the development of more efficient aircraft, and could swing the balance in favour of active drag reduction technologies, such as HLFC.



## 12.2 HLFC PERFORMANCE MODELS

Computer performance models have been developed to determine the trip fuel for two classes of aircraft – one based on the B757-200 and the other based on the A330-200. The accuracy of the models was assessed by comparing the calculated payload-range parameters against actual data for the baseline aircraft types. Trip fuel calculations of within 1.5% of published data were shown to be possible. As the main objective was to perform comparative studies of fuel consumed by a HLFC aircraft versus an equivalent turbulent aircraft, this level of accuracy was greater than that which was required.

The models were developed using the spreadsheet software package Lotus 123, with macro code incorporated into the spreadsheets. One of the main advantages of this approach was the ability to interrogate and "de-bug" sets of calculations (for the climb or cruise, for example) during, or after a computer run. The relative ease with which the input data, computational cells and results can be manipulated, makes this software package a very effective tool for this type of modelling. However, the open nature of the software can also be a limitation. For example, it cannot be treated as a "black box" routine. It is necessary that the user has an understanding of the computational process and of the structure of the spreadsheet tables. Also, there is limited scope to adapt the software and integrate the subroutines into a larger suite of computer programs, written using a conventional programming language.

## 12.3 RE-SIZING POTENTIAL

The basic turbulent aircraft models were developed to represent – as accurately as possible – the B757-200 and the A330-200 aircraft. For the HLFC models, neither the engine nor the airframe was resized in the current study. There are certain advantages in taking this approach; one of them being the ability to accurately assess the benefits of HLFC technology with respect to a known and understood baseline – an existing aircraft. However, it can be expected that the results of this approach will inherently under-predict the true potential of this technology, for two reasons.

- (1) The correct matching of an engine to an airframe should see the engine / airframe combination being most efficient at the design cruise condition. This was seen to be true for the B7G7 database, which was used as the baseline for the B757-200 class aircraft model. The bottom of the SFC "loop" corresponded approximately to the required cruise thrust at Mach 0.80 at an altitude of 35000ft. Herein lies the anomaly. If the thrust was reduced (due to the HLFC drag reduction), then the SFC would increase as the engine would no longer be operating at the optimum thrust level, even though the fuel flow to the engine would be reduced. If an alternative engine was selected – one that was matched to be most efficient at the reduced thrust level – then it would have a comparatively lower fuel burn when the HLFC system was operating. However, the full potential of this factor may not be



achievable because of other requirements for the engine of a HLFC aircraft. For example, the takeoff thrust would be essentially unchanged; however, the power off-take would be substantially increased. Furthermore, the off-design condition associated with an inoperative HLFC system needs to be considered. These factors could be taken into account as an extension of the work herein described, and the magnitude of this effect on the fuel consumption could thus be quantified.

- (2) Aircraft are fundamentally characterised by their payload-range capability. A HLFC aircraft, correctly sized to meet a given payload-range target, would be slightly lighter than a comparable turbulent design. The so-called "snowball" effect<sup>28</sup> has not been considered. In other words, the HLFC technology has been evaluated in terms of its idealised retrofit potential in the current study. New HLFC aircraft, designed to meet a given payload-range specification, would show a greater fuel saving compared to an equivalent turbulent model than that determined herein, for comparable HLFC system parameters.

## 12.4 SENSITIVITY STUDIES

### 12.4.1 Analysis conducted using computer model

In the current study the objective function has been the trip fuel consumed for a given range. Factors related to HLFC that could influence this parameter for medium- to long-range sectors have been investigated. Three sets of calculations were undertaken to determine the trip fuel for selected combinations of payload and range values.

- (1) The OEW was progressively increased, whilst the SFC and  $C_D$  were unchanged.
- (2) The SFC was increased, whilst the OEW and  $C_D$  were unchanged.
- (3) The  $C_D$  was reduced, whilst the SFC and OEW were unchanged.

For each mission calculation, the lowest BRW was determined for the specified range, which ensured that the smallest fuel quantity was calculated. The resulting change in trip fuel was determined as a percentage of the fuel required for the baseline turbulent model. For example, it was shown that a 2% increase in OEW, 2% increase in SFC and a 14% decrease in drag, would reduce the trip fuel by 9.5 - 10.9%, depending on the range and aircraft type.

Two points on the payload-range graph were selected for analysis for each aircraft type. The first corresponded to the maximum structural payload and the second was at a typical design payload (see Fig. 6-1, Chapter 6). Both points were at ~90% of the maximum range (for the turbulent baseline aircraft) at that payload. The points were not selected on the boundaries of the payload-range graph, to avoid encountering an

---

<sup>28</sup> Snowball effect: This describes the cycle of weight increases that occur in the design of a new aircraft, for a given range specification. It implies that a less efficient aircraft will burn more fuel, which will result in more fuel being carried, which will imply a heavier aircraft, and yet more fuel being consumed.



aircraft weight or fuel capacity limitation, when considering either increased SFC or OEW. In a comparable study undertaken by BAE Systems for the A310 aircraft (BAE Systems, 2000), they did not take this into account, and it is the conclusion of the author that the performance benefits of HLFC are underestimated in their study as a direct consequence.

The sensitivity studies that have been performed are seen as an important set of results emanating from the current study. The results – which are presented as nomograms – will facilitate a rapid determination of the trip fuel saving to be established for changes to the OEW, SFC and  $C_D$ . This application of these results is not restricted to laminar flow control, but is valid for any active drag reduction technique. The results will enable more accurate MVO studies of HLFC aircraft to be conducted.

The underlying assumption of linear independence of the three parameters (i.e. SFC, OEW and  $C_D$ ) was explored by comparing the results obtained by adding the individual contributions from the sensitivity studies, against those obtained by running the computer model with a simultaneous input of the parameters. The approximate, linearised method was observed to underestimate the fuel savings (of the HLFC aircraft compared to the turbulent baseline aircraft) by approximately 0.6% compared to the more accurate "combined" analysis, for the four cases considered.

#### 12.4.2 Mathematical model

To extend the results of the sensitivity analyses performed using the computer models to other aircraft types, a mathematical relationship was derived. It was shown that the impact on cruise fuel burn can be satisfactorily estimated from relative (or percentage changes) to  $m_2$  (end of cruise mass),  $\bar{E}$  (mean lift to drag ratio) and  $\bar{c}$  (mean SFC), using equation [6-4]. This is a convenient formulation as the changes to  $m_2$ ,  $\bar{E}$  and  $\bar{c}$  are expressed as non-dimensional terms, i.e.

$$\frac{\delta m_f}{m_2} = \left( e^{\frac{R\bar{c}g}{V\bar{E}}} - 1 \right) \frac{\delta m_2}{m_2} + \left( e^{\frac{R\bar{c}g}{V\bar{E}}} \frac{R\bar{c}g}{V\bar{E}} \right) \frac{\delta \bar{c}}{\bar{c}} - \left( e^{\frac{R\bar{c}g}{V\bar{E}}} \frac{R\bar{c}g}{V\bar{E}} \right) \frac{\delta \bar{E}}{\bar{E}}$$

### 12.5 HLFC SYSTEM INSTALLATION

The estimation of the drag reduction, SFC penalty and system weight, associated with the installation of the HLFC system (Chapter 7) was undertaken in order to establish representative input data for the performance programs. For the B757-200 and A330-200 classes of aircraft, reasonably accurate information was available for the drag and weight changes associated with HLFC. However, the SFC penalty arising from the need to drive the suction pumps required further investigation for two reasons: (1) It was poorly described in the literature; (2) Previous work, such as the Boeing 757 studies



(Boeing, 1982; Collier, 1993; Boeing 1999a) utilised higher suction rates than those which are now known to be necessary.

The approach adopted was to consider one part of the aircraft, the HTP of the B757-200 class aircraft, and to develop a conceptual HLFC design. The internal flow analysis which was conducted (Appendix J) enabled the pump pressure ratio to be estimated. It was then assumed that this pressure ratio would be the same for the other parts of the aircraft. Using the estimated mass flow, which was based on the suction surface area and a mean panel velocity, the suction pump power could be estimated for each part of the aircraft. This approach would be expected to yield an accurate estimate for the entire empennage, but a less accurate estimate for a wing or nacelle, because of detail design differences between the various system installations. For example, the mean panel flow velocity for the engine nacelle would be expected to be lower than that required for the empennage, as there is no need to suck at the leading edge (due to the absence of sweep).

The results of the suction pump analysis conducted for the HTP were observed to depend significantly on the pressure losses in the ducts, valves, meters, etc. Detail design changes to the system would have a large influence on the calculated pump pressure ratio, which in turn would have an effect on the pump power requirement. Only by precisely specifying the installed system components can this uncertainty be eliminated. The SFC penalty resulting from the power off-take associated with the requirement to drive the pump could be established with much greater confidence. The results obtained for the two reference engines, the RB211-535E4 and Trent 772, using the Cranfield University Turbomatch software could be correlated to other information available to the author. An approximately linear increase in SFC change per 100kW power off-take was evident during the cruise (associated with a progressive reduction in thrust). This fact has not always been taken into account by other researchers – if the maximum engine thrust is used, rather than a mean cruise thrust, the consequence is an underestimate of the SFC penalty.

## 12.6 CIRRUS CLOUDS AND FUEL SAVINGS

### 12.6.1 Cloud climatology

The operational effectiveness of HLFC aircraft is reduced by the presence of cirrus clouds, which are known to temporarily destroy the laminar flow. Based on measurements taken during the GASP, the route average TIC was seen to vary from ~2.2 to ~9.9% for the routes flown. Davis *et al.* (1987) concluded from the Jetstar test data, that a figure of 7.2% is "probably an upper bound on the likelihood of cloud encounter on an overall basis". These values are the best available information regarding the *average* time that a HLFC aircraft is likely to spend in cloud over an extended period of operation. However, it is possible to encounter substantially greater



cloud amounts, albeit not very often. The probability distribution of cloud on a particular route was assessed by Jaspersen *et al.* (1984a), based on the GASP data. For approximately 50% of the flights, the flight average TIC was between 0 and 5%. The percentage falls off rapidly for increasing flight average TIC. If there is uncertainty regarding the expected TIC on a particular flight, then sufficient fuel must be provisioned during the flight planning for the worst possible case. This additional fuel increases the takeoff weight and results in a greater trip fuel. This is particularly significant for long-range missions.

### 12.6.2 Optimised fuel planning and cloud forecast

Based on the estimated HLFC system design parameters (Chapter 7), it was calculated that there would be a ~7.4% reduction in trip fuel, compared to the turbulent baseline vehicles (at the design payload and 90% of the maximum range). The fuel planning for this scenario was based on the conservative requirement that the aircraft be capable of completing the mission with the HLFC system inoperative and without using the contingency fuel. However, a forecast of en route cirrus cloud would permit a reduced fuel load, by eliminating the requirement to take on board fuel that would not be required. A further decrease in trip fuel of ~2.5% for the B757-200 class aircraft (range: 3272nm; payload: 19147kg) and ~3.8% for the A330-200 class aircraft (range: 5980nm, payload: 24035kg) would then be possible.

This optimised fuel planning approach requires an accurate forecast of en route cirrus cloud, a capability that does not exist in current operational NWP models. Brown<sup>29</sup> was of the opinion "that IWC data from the global model, combined with climatological information on particle concentrations obtained from both observations and high-resolution models, would give adequate information to assess whether or not cloud forecast at a particular level would be of sufficient density to degrade the HLFC performance". More extensive studies of the kind described in section 8.4.4 (Chapter 8), would however be required in order to fully understand the potential of: (1) Improvements in the representation of ice cloud microphysics, (2) Reduced horizontal and vertical grid spacing, on the accuracy of cloud forecasts. The development of reliable meteorological models to forecast cirrus clouds for operational fuel planning is required to ensure optimum fuel provisioning for HLFC aircraft. It was noted that the planned development path for such models would provide an improved capability to meet this need, when it arises (Young *et al.*, 2002).

### 12.6.3 Contingency fuel and cloud incidence

The purpose of the study described in section 11.4 (Chapter 11) was to compare the amount of contingency fuel to the fuel that would be required to accommodate a complete failure of the HLFC system for a portion of the cruise. For a fixed range and

---

<sup>29</sup> P. Brown, Cloud Physics Research, Met Office, Cody Technology Park, Farnborough, Hampshire, UK.



payload, two scenarios were considered in the planning of the fuel requirement, which would determine the BRW. It was assumed that the HLFC system would be 100% effective for: (1) 93% of the HFLC operational time (i.e. from 20000ft in the climb to the Top of Descent), (2) 79% of the HFLC operational time. The first scenario corresponded to the widely quoted “upper limit” estimate of 7% TIC and the second corresponded to a three-fold increase in this amount. The fuel planning was based on standard International fuel reserves (Fig. 3-1). A contingency fuel of 5% of the trip fuel was calculated (which in turn was based on the HLFC system being functional for the prescribed portion of the flight).

For different “actual” amounts of cloud encountered in the cruise, the on board fuel was determined when the aircraft landed at the alternate airport, following a standard mission. The results are given in Figures 11-3 and 11-4 (B757-200 class aircraft) and Figures 11-5 and 11-6 (A330-200 class aircraft). For the situation where the TIC exceeded the anticipated amount, it was required to use part of the contingency fuel to get to the alternate airport. In the case of a 7% anticipated TIC, it was seen that if the actual TIC did not exceed ~50%, then the contingency fuel would be inadequate. The probability of this cloud amount being encountered on a particular flight is ~0.5%, based on the cloud model described in Chapter 8. For the second scenario, the contingency fuel is adequate to allow for a loss of laminar flow for ~64% of the HLFC operational time. The second scenario is more conservative than the first and has a slightly greater trip fuel. It is evident that the fuel savings potential of this technology can only be accurately calculated by considering, in detail, the operational fuel planning. This is particularly true for long-range missions, where the penalty of carrying fuel that does not get used is significant.

A baseline assumption made for the study herein described is that failure of the HLFC system would have economic and not safety implications. This is a valid assumption, which has precedence within the existing fuel planning requirements (Appendix D). According to JAR OPS 1, an aeroplane may not be released for takeoff if, following a failure of a power unit or loss of pressurisation at the most critical point along the route, the aeroplane is unable to: (1) Descend as necessary and proceed to an adequate aerodrome; and (2) Hold there for 15 minutes at 1500ft (450m) above aerodrome elevation; and (3) Make an approach and landing. In the event that the planned fuel load, including reserves (i.e. contingency, alternate and final holding fuel) are inadequate to accommodate this requirement for the planned route, then *additional* fuel must be taken onboard. An identical approach should apply to HLFC aircraft, in that a total system failure at the most critical point should not prevent the aircraft from safely reaching either the destination or a suitable alternate airport. The analysis presented in section 11.4 may be used to assess this requirement. For a fuel planning approach based on: (1) The HLFC system being operational for 93% of the time; (2) A 5% contingency fuel; it was shown that the aircraft would be able to land at the alternate



airport (after routing via the destination airport and holding for 30min) following HLFC system failure at the cruise mid-point.

## 12.7 INSECT CONTAMINATION

The gap that exists between the slat and the mainplane when it is closed is a problem for HLFC, as it will be very difficult to maintain laminar flow over the junction. Even if it were possible to produce a slat design that keeps this gap within the required tolerances, it is doubtful that this could be maintained over the life of the aircraft. The consequence is that a Krüger flap – which will not affect the upper surface airflow in the retracted position – will probably be required. This change will have a knock-on effect on the design of the other high lift devices on the wing and may penalise the high  $C_L$  performance of the aircraft. In the extended position a Krüger flap has been demonstrated – in the wind tunnel (Tamigniaux *et al.* 1987; Dziomba, 1993; for example) and in flight (Fischer *et al.*, 1983; Collier, 1993) – to be a very effective shield in preventing insects from spoiling the laminar flow surface. For the empennage and nacelle, a liquid / foam system may be used. Recent laboratory and flight tests conducted as part of the HYLTEC and ALTTA projects have re-affirmed the belief that these systems can be very effective.

Whilst the threat of insects causing a transition of the boundary layer is substantially reduced with these systems, it is not entirely eliminated for three reasons:

- (1) The liquid / foam system does not prevent insect debris from sticking to the surface 100% of the time.
- (2) The system will be designed to provide protection when the aircraft is near to the ground, but insects will occasionally be encountered at higher altitudes.
- (3) Due to the seasonal nature of insect activity, there is a very low probability of insect contamination during winter and hence the system may not be operated during these times.

It should thus be expected that a small amount of contamination would infrequently occur.

## 12.8 MECHANICAL FAILURE, DAMAGE AND DURABILITY

### 12.8.1 System architecture

The HLFC system for the aircraft is likely to be comprised of a number of independent sub-systems, one for each major surface (i.e. starboard wing, port wing, starboard nacelle, etc.). This layout is driven by weight considerations; however, it also leads to a redundant system architecture, where a loss of laminar flow on one part of the aircraft will not affect the other parts. In the case of the HTP and fin, this may not be



entirely true, as detail design considerations could eliminate some component duplication (for example in the anti-contamination system).

### **12.8.2 Mechanical failure and system reliability**

To establish the order of magnitude of the potential reliability of a HLFC system, it was necessary to develop a conceptual design of a representative system. The reference design was the HTP of the B757-200 class aircraft. As no production HLFC system has been built, component failure rates were estimated based on MTBUR (Mean Time Between Unscheduled Removal) data for similar components, used for other aircraft systems. Two further idealisations / assumptions were made: (1) That the component reliability could be represented by a Negative Exponential distribution; and (2) That all components required for a particular mode of operation could be represented by a series function. It was estimated (see Table 10-2) that in the normal suction mode, the probability of failure is of the order of  $3.7 \times 10^{-4}$  per flight hour (i.e. one failure per 2700 flight hours).

### **12.8.3 Damage due to bird impact**

Depending on the location of the impact and the severity of the damage, the consequences of a bird strike on the leading edge of a laminar flow surface could vary from negligible to a complete loss of laminar flow on the affected surface. Structural damage to the wing leading edge would likely cause a loss of laminar flow from the impact site, outboard along the wing surface. Damage that results in a rupture of the suction surface would disrupt the suction air flow for that part of the aircraft and cause a total loss of laminar flow on the affected part.

Using data from the FAA National Wildlife Strike Database (FAA, 2001), it was estimated that the incident rate where damage to the laminar flow regions on the aircraft might occur, would be no more than 10 strikes per million operations. This should be regarded as an upper limit as the data also included strikes to the engine itself.

### **12.8.4 Durability of suction surfaces**

The critical issue regarding the durability of the suction surface is whether the holes will change in size over a prolonged period of exposure. Tests conducted during the HYLDA and HYLTEC projects indicated that titanium is the only viable choice of material for HLFC suction surfaces, where the leading edge is perforated. A laser perforated titanium panel showed no evidence of degradation after 18 months of exposure on the leading edge of the SAAB 2000 test aircraft. The same test programme effectively eliminated aluminium as a candidate material due to extensive surface erosion / corrosion and internal cracking. For a nacelle application, it would be desirable to use a composite material to reduce the weight penalty associated with the use of titanium. However, further trials are required to get a definitive answer as to the viability of using APC-2, or a similar thermoplastic material, for this application.



## 13 CONCLUSIONS

1. Trip fuel calculations of within 1.5% of published data are possible, using the computer performance models that were developed, based on the B757-200 and A330-200 aeroplane types. The results of sensitivity studies – conducted using these models to quantify the influence on trip fuel, of changes to the aircraft's OEW (Operating Empty Weight), SFC (Specific Fuel Consumption) and drag – provide a rapid means of determining the fuel saving potential of HLFC technology.
2. An installed HLFC system, capable of reducing the total aeroplane drag by ~14%, was estimated to increase the OEW by ~2.0% and the mean SFC by ~1.6%, for an aeroplane in the class of the B757-200. For an A330-200 class aeroplane, the OEW increase was 1.6% and the mean SFC increase was 2.1%. Based on these results, the trip fuel reduction was 10.0% for the B757-200 class aircraft (range: 3272nm; payload: 19147kg) and ~11.2% for the A330-200 class aircraft (range: 5980nm, payload: 24035kg). The system weight estimation assumed that an active flow control system would be required. Should the simplified suction system concept currently being evaluated as part of the ALTTA project prove to be viable, then the system weight would be reduced.
3. The probability of mechanical failure of the suction system (for one part of the aircraft) was determined to be of the order of  $3.7 \times 10^{-4}$  per flight hour. The incident rate where bird strike damage to the laminar flow regions might occur, was estimated to be no more than 10 strikes per million operations.
4. Titanium has been confirmed as the only viable choice of material for the suction surfaces where the leading edge is perforated. No degradation of the material was observed following 18 months of flight tests, whereas aluminium test panels were observed to have extensive erosion / corrosion and internal cracking.
5. Considering the relative probabilities of failure of the HLFC system and the consequence of these failures, it was concluded that flight through cirrus cloud would be the dominant operational concern and would over-ride the other issues considered (viz. insect contamination, mechanical system failure and in-flight damage arising from bird strikes).
6. A fuel planning policy that makes provision for the system to be inoperative for 7% of the HLFC operational time (i.e. from 20000ft to the Top of Descent) would enable the aircraft to complete long-range missions using the en route contingency fuel (set as 5% of trip fuel), when the TIC (time-in-cloud) was 50%. The probability of encountering this cloud amount on a particular flight is ~0.5%.
7. To obtain the greatest benefit for a HLFC aircraft, the fuel planning must consider the probable TIC that will result in a loss of laminar flow for that particular mission. This requires a forecast of cirrus cloud for the route. This is not possible with current operational Numerical Weather Prediction models; however, this capability could be developed from current state-of-the-art research models, if the need arose.



## REFERENCES

- Abbott, I.H. and von Doenhoff, A.E. (1959). *Theory of Wing Sections*, Dover, New York.
- Airbus (2000a). A330 Briefing, Document No. AI/CM 310.0015/98, Marketing Division, Airbus Industrie, Blagnac, France, June 2000.
- Airbus (2000b). A310 Briefing, Document No. AI/CM 310.0096/98 issue 3, Marketing Division, Airbus Industrie, Blagnac, France, June 2000.
- Airbus (2001a). A330-200 Specifications, Airbus Industrie,  
URL: <http://www2.airbus.com/products/>, web-site accessed 26<sup>th</sup> Aug 2001.
- Airbus (2001b). Aircraft Maintenance Manual, Aircraft Type: A330, Airbus Industrie, July 2001.
- Airbus (2002a). Getting to Grips with Aircraft Performance, Flight Operations Support and Line Assistance, Airbus Industrie, Jan. 2002.
- Airbus (2002b). Multimedia Gallery: A330 General arrangements, Airbus Industrie,  
URL: <http://www.airbus.com/media/> web-site accessed 23<sup>rd</sup> July 2002.
- Airbus (2002c). Personal correspondence with Aircraft Systems engineer, Airbus Industrie, Oct. 2002.
- Airbus (undated). Flight Crew Operating Manual A330-200, SEQ. 147, Airbus Industrie.
- Anderson, J.D., Jr. (1999). *Aircraft Performance and Design*, McGraw-Hill.
- Anderson, B.T. and Bohn-Meyer, M. (1992). Overview of Supersonic Laminar Flow Research on F-16XL Ships 1 and 2, SAE Paper 921994.
- Angell, J.K., Korshover, J. and Cotton, G.F. (1984). Variation in United States Cloudiness and Sunshine, *Journal of Climate and Applied Meteorology*, Vol. 23 (1984), pp. 752 -761.
- Anon (1992). First Laminar Flow Flight Tests Prove Drag Reduction Potential: ELFIN Project Leads the Way for European Laminar Aircraft, *Aircraft Engineering*, Jan. 1992, pp. 5 - 7.
- Arcara, P.C., Jr., Bartlett, D.W. and McCullers, L.A. (1991). Analysis for the Application of Hybrid laminar Flow Control to a Long-Range Subsonic Transport Aircraft, SAE Paper 912113, pp. 1 - 15.
- Ardonceau, P.L. (1994). Aerodynamic Properties of Crescent Wing Planforms, *Journal of Aircraft*, Vol. 31, No. 2, pp. 462 - 465.
- Arnal, D. (1992). Boundary Layer Transition: Prediction, Application to Drag Reduction, AGARD Report 786, Special course on Skin Friction Drag Reduction, pp. 5.1 - 5.59.
- Arnal, D. (1994). Boundary Layer Transition: Predictions Based on Linear Theory, AGARD Report 793, Special course on Progress in Transition Modeling, pp. 2.1 - 2.63.
- Arthur D. Little Ltd. (2000). Study into the Potential Impact of Changes in Technology on the Development of Air Transport in the UK, DETR/71861/01rep.doc. (Cited in: *Greener by Design*, 2001).
- ASM (1980). *Metals Handbook*, Eighth Edition Vol. 2 - Heat Treating, Cleaning and Finishing, American Society for Metals (ASM), Metals Park, Ohio.
- ASTM B117. Standard Practice for Operating Salt Spray (Fog) Apparatus, ASTM International, 100 Barr Harbour St., West Conshohocken, Pennsylvania, USA.
- Atkin, C. (2000). New Aerodynamic Approach to Suction System Design, CEAS / DragNet European Drag Reduction Conference, Potsdam, 19-21 June 2000, Notes on Numerical Fluid Mechanics, Springer, Vol. 76, pp. 55 - 63.
- Atkin, C. (2001). Personal correspondence with Dr. Chris Atkins, QinetiQ, Farnborough, UK, 25<sup>th</sup> July 2001.
- Atkin, C.J. and Courtenay, W.J.A. (2002). Predicting the Cruise Performance of a Retrofit Hybrid Laminar Flow Control System, CEAS Aerospace Aerodynamics Research Conference, Paper 90, Cambridge, 10 - 12 June 2002.
- BAE Systems (2000). HYLTEC Document to Support Technical Report 33, Confidential report for HYLTEC partners, TR-35, Aug. 2000. (Unpublished)



- Barrett, R.V., Richards, J. and Eustace, R. (1996). Alleviation of the Drag Penalty incurred by Insect Contamination using the Existing Suction System of a Hybrid Laminar Flow Nacelle, Second European Forum on Laminar Flow Technology, Bordeaux, June 1996, pp. 8.28 - 8.40.
- Barry, B. (1995). Application of Laminar-flow Technology Could Improve Fuel Economy at High Speeds, *ICAO Journal - Aerodynamics*, March 1995, pp. 15 - 17.
- Beech, G. and Nicholas, W.M. (1953). A Mechanical Type of Scraper For Dealing With Insect Contamination of Aircraft Wings, Unpublished Armstrong Whitworth Report No. W.T. 53/18. (Cited in Coleman, 1961).
- Bert, C.W. (1999). Range and Endurance of turboprop, turbofan, or piston-propeller aircraft having wings with or without camber, *Journal of Aircraft Design*, 2(1999), pp. 183 - 190.
- Bewick, C. (2001). Personal correspondence with Ms. Clare Bewick, Engineer, Rolls-Royce plc., Derby, UK, 3<sup>rd</sup> June 2001.
- Bhutiani, P.K., Keck, D.F., Lahti, D.H. and Stringas, M.J. (1993). Investigating the Merits of a Hybrid Laminar Flow Nacelle, The Leading Edge, General Electric Company, Spring 1993, pp. 32 - 35. (Cited in Joslin, 1998a).
- Bieler, H. (1999a). HYLTEC Hybrid Laminar Flow Technology, brochure prepared for Paris Airshow, June 1999, Department Aerodynamic Design Methods, DaimlerChrysler Aerospace Airbus, D-28183 Bremen, Germany. (Unpublished)
- Bieler, H. (1999b). Drag Reduction Workshop - Technology Status and Market Review, DragNet European Drag Reduction Workshop, Toulouse, June 1999. (Unpublished)
- Bieler, H. and Swan, P. (2000). Retrofit studies based on the Airbus A310 for HLFC Application on Aircraft, CEAS / DragNet European Drag Reduction Conference, Potsdam, 19 - 21 June 2000, Notes on Numerical Fluid Mechanics, Springer Vol. 76, pp. 64 - 70.
- Bieler, H., Swan, P. and Humphreys, B. (2002). The HYLTEC Project - A Hybrid Laminar Flow Technology Investigation, CEAS Aerospace Aerodynamics Research Conference, Cambridge, 10 - 12 June 2002.
- Birch, N.T. (2000). 2020 vision: The prospects for large civil aircraft propulsion, *Aeronautical Journal*, Aug. 2000, pp. 347 - 352.
- Boeing (1976). B747 Airline Service Experience, Report No. D6-13050-862R8, Boeing Commercial Airplane Company.
- Boeing (1982). Hybrid Laminar Flow Control Study: Final Technical Report, NASA CR-165930, Boeing Commercial Airplane Company, Oct. 1982.
- Boeing (1989). Jet Transport Performance Methods Reference D6-1420, The Boeing Company, May 1989.
- Boeing (1993). Operations Manual – Boeing 757-200 Volume III, The Boeing Company, May 1993.
- Boeing (1996). Performance Engineer General Course Notes - Volumes No. 1 and 2, The Boeing Company, Mar. 1996.
- Boeing (1999a). High Reynolds Number Hybrid Laminar Flow Control (HLFC) Flight Experiment, NASA CR-1999-209325 / CR-1999-209326, Boeing Commercial Airplane Group, April 1999.
- Boeing (1999b). Boeing 757-200 Background Information, Boeing Commercial Airplane Group, URL: <http://www.boeing.com/commercial/757-200>, accessed on 13<sup>th</sup> Aug. 1999.
- Boeing (2001). Boeing 757-200, EPD V3.06a, Boeing Commercial Airplane Group.
- Boeing (undated). Performance Engineers Manual 7G7, Boeing Commercial Airplane Group.
- Bokser, V.D., Babuev, V. Ph., Kiselev, A., Ph., Mikeladze, V.G. and Shapovalov, G.K. (1998). Experimental Investigation of the Application of Hybrid Laminar Flow Control to Large Scale Swept Wing Models at Subsonic Speeds, 21<sup>st</sup> Congress of the International Council of Aeronautical Sciences (ICAS), Melbourne, ICAS-A98-31544, 13 - 18 Sep. 1998.
- Bowes, G.M. (1974). Aircraft Lift and Drag Prediction and Measurement, in AGARD Lecture Series 67, *Prediction Methods for Aircraft Aerodynamic Characteristics*, Report AD-780-608, May 1974.



- Braslow, A.L.** (1999). A History of Suction-Type Laminar Flow Control with Emphasis on Flight Research, NASA Monograph in Aerospace History No. 13.
- Braslow, A.L.** and **Muraca, R.J.** (1978). A perspective on Laminar-Flow Control, Air Transportation: Technical Perspectives and Forecasts Conference, AIAA, Los Angeles, CA, 21 - 24 Aug. 1978.
- Brasseur, G., Amanatidis, G.T.** and **Angeletti, G.** (Editors) (1998). European Scientific Assessment of the Atmospheric Effects of Aircraft Emissions, European Commission DG XII, Science, Research, Development Environment and Climate Programme, *Atmospheric Environment*, Vol. 32, No. 13, July 1998, pp. 2327 - 2422.
- British Aerospace** (1979). HS. 125 Component Performance and Reliability, British Aerospace, Aircraft Group, Hatfield, Hertfordshire, UK, 12<sup>th</sup> June 1979.
- British Airways** (1991). B767 Component Performance Report, British Airways, Quality Control Group, London Heathrow Airport, UK.
- Brown, A.** (1997). Large Subsonic Transports and Military Aircraft, VI - Very Large Civil Transport, in Progress in Astronautics and Aeronautics A97-26201, Vol. 172, AIAA, pp. 144 - 156.
- Brown, P.R.A.** (2002). Personal correspondence with Mr. Philip Brown, Manager Cloud Physics Research Group, The Met Office, Cody Technology Park, Farnborough, UK, Jan 2002.
- Bulgubure, Ch.** (1999). Laminar Flow Wing Design Applied to Business Jets, DragNet European Drag Reduction Workshop, Toulouse, June 1999. (Unpublished)
- Bulgubure, Ch.** and **Arnal, D.** (1992). Dassault Falcon 50 Laminar Flow Flight Demonstrator, First European Forum on Laminar Flow Technology, Hamburg, 16 - 18 Mar. 1992, DGLR-Bericht 92-06, pp. 11 - 18.
- Caniaux G., Redelsperger, J-L.** and **Lafore, J-P.** (1994). A numerical study of the stratiform region of a fast-moving squall line: 1. General description and water and heat budgets, *Journal of Atmospheric Sciences*, Vol. 51, No. 14, pp. 2046 - 2074.
- CEC** (1998). Climate Change – Towards an EU Post-Kyoto Strategy, Communication COM (1998) 353, Commission of the European Communities (CEC), June 1998.
- CEC** (2001). European Aeronautics: A vision for 2020, "Report of the Group of Personalities", Commission of the European Communities (CEC), ISBN 92-894-0559-7, Jan. 2001.
- Chen J.P.** and **Lamb, D.** (1994). Simulation of cloud microphysical and chemical processes using a multicomponent framework: I Description of the microphysical model. *Journal of the Atmospheric Sciences*, 51 (1994), pp. 2613-2630.
- Cleary, E.C., Wright, S.E.** and **Dolbeer, R.A.** (2000). Wildlife Strikes to Civil Aircraft in the United States 1990 - 1999, FAA National Wildlife Strike Database Serial Report No. 6, Sep. 2000.
- Coleman, W.S.** (1959). The Characteristics of Roughness from Insects as Observed for Two - Dimensional Incompressible Flow Past Aerofoils, *Journal of AeroSpace Science*, May 1959. (Cited in Humphreys, 1992).
- Coleman, W.S.** (1961). Roughness due to Insects, *Boundary Layer and Flow Control*, Vol. II, Lachmann, G.V. (Ed.), Pergamon Press.
- Collier, F.S., Jr.** (1993). An Overview of Recent Subsonic Laminar Flow Control Flight Experiments, AIAA-93-2987, in conference proceedings: Fluid Dynamics Conference, Orlando, July 1993.
- Condit, P.** (1996). Performance, Process and Value: Commercial Aircraft design in the 21<sup>st</sup> Century, The Boeing Company, World Aviation Congress and Exposition, Los Angeles.
- CORDIS** (2001). Data base, Community Research & Development Information Service (CORDIS) of the Commission European Community, URL: <http://www.cordis.lu/en/home.html>, web-site accessed 16<sup>th</sup> Dec. 2001.
- Cranfield University** (undated). Analysis of the Fuel Penalties of Airframe Systems, Lecture note DAeT 95122, College of Aeronautics, Cranfield University. (Unpublished)



- Croom, C.C. and Holmes, B.J. (1985). Flight Evaluation of an Insect Contamination Protection System for Laminar Flow Wings, SAE 850860, General Aviation Aircraft Meeting and Exposition, Wichita, April 1985, pp. 4.486 - 4.494.
- Croom, C.C. and Holmes, B.J. (1986). Insect Contamination Protection For Laminar Flow Surfaces, Langley Symposium on Aerodynamics, Vol. 1, Dec. 1986, pp. 539 - 555.
- Daimler-Benz Aerospace (1995). HYLDA (Hybrid Laminar Flow Demonstration on Aircraft) Part B RTD Proposal Description, Proposal to the European Commission under the Industrial and Materials Technologies Framework, Daimler-Benz Aerospace Airbus, March 1995. (Unpublished)
- Davies, M. (Ed.) (2002). *The Standard Handbook for Aeronautical and Astronautical Engineers*, McGraw-Hill, New York.
- Davis, R.E. (1982). Probability of Laminar Flow Loss because of Ice Crystal Encounters, in conference proceedings: Laminar Flow Control: 1981 Research and Technologies Studies, NASA CP 2218, pp. 75 - 93.
- Davis, R.E. and Fischer, M.C. (1983). Cloud Particle Effects on Laminar Flow and Instruction for their Measurement Aboard a NASA LFC Aircraft, AIAA 83-2734, in conference proceedings: AIAA 2nd Flight Testing Conference, Las Vegas, 16 - 18 Nov. 1983, pp. 1 - 10.
- Davis, R.E. and Fischer, M.C. (1986). Cloud Particle Effects on Laminar Flow in the NASA LEFT Program: Preliminary Results, AIAA 86-9811.
- Davis, R.E., Maddalon, D.V. and Wagner, R.D. (1987). Performance of Laminar Flow Leading Edge Test Articles in Cloud Encounters, *Research in Natural Laminar Flow and Laminar-Flow Control*, Editors Hefner, J.N. and Sabo, F.E., NASA CP-2487, Part 1.
- Davis, R.E., Maddalon, D.V., Wagner, R.D., Fisher, D.F. and Young, R. (1989). Evaluation of Cloud Detection Instruments and Performance of Laminar-Flow Leading-Edge Test Articles during NASA Leading-Edge Flight Test Program, NASA TP-2888.
- Drake, V.A. and Farrow, R.A. (1988). The Influence of Atmospheric Structure and Motions on Insect Migration, *Annual Review Entomology* 33 (1988), pp. 183 - 210.
- Duthie, E. (2001). ICAO Regulation: Meeting Environmental Need? Fourth Community Aeronautical Days Conference, Hamburg, Germany, 29 - 31 Jan. 2001; Proceedings in Air & Space Europe, No. 3/4, Vol. 3, pp. 27 - 28.
- Dziomba, B. (1993). European Laminar Flow Projects, in conference proceedings: Aeroday 93: Second Community Aeronautics R&D Conference, Naples, Oct. 1993, pp. 3 - 16.
- Eiss, N.S., Jr. and Wightman, J.P. (1983). A Fundamental Approach to the Sticking of Insect Residues to Aircraft Wings:- Semi-annual technical report, NASA-CR-173063, July 1983.
- Eiss, N.S., Jr., Wightman, J.P., Gilliam, D.R. and Siochi, E.J. (1984). A Fundamental Approach to the Sticking of Insect Residues to Aircraft Wings- Annual Technical Report NASA-CR-173721, April 1984.
- Ellis, J.E. and Poll, D.I.A. (1996). Laminar and Laminarizing Boundary Layers by Suction Through Perforated Plates, 2<sup>nd</sup> European Forum on Laminar Flow Technology, Bordeaux, June 1996, pp. 8.17 - 8.27.
- Elsenaar, A. and Haasnoot, H.N. (1992). Survey on Schiphol Airport of the Contamination of Wing Leading Edges of Three Different Aircraft Types under Operating Conditions, First European Forum on Laminar Flow Technology, Hamburg, 16 - 18 March 1992, DGLR-Bericht 92-06, pp. 256 - 261.
- ESDU 66031 (1995). Introductory sheet on subcritical lift-dependent drag of wings, amendment (C), 27 Corsham St., London, Nov. 1995.
- ESDU 70020 (1970). Non-dimensional Approach to Engine Thrust and Airframe Drag for the Analysis of Measured Performance Data: Aircraft with Turbo-jet and Turbo-fan Engines, ESDU, 27 Corsham St., London, Sep. 1970.
- ESDU 72018 (1972). International Standard Atmosphere (-2000 to 105 000ft, Data in SI Units, ESDU, 27 Corsham St., London, May 1972.



- ESDU 73018 (1980). Introduction to estimation of range and endurance, amendment (a), ESDU, 27 Corsham St., London, Oct. 1980.
- ESDU 73019 (1982). Approximate methods for estimating cruise range and endurance: aeroplanes with turbo-jet and turbo-fan engines, amendment (c), ESDU, 27 Corsham St., London, May 1982.
- ESDU 77022 (1986). Equations for Calculation of International Standard Atmosphere and Associated Off-Standard Atmospheres, ESDU, 27 Corsham St., London, amendment (B) Feb. 1986.
- ESDU 85029 (1985). Calculation of Ground Performance in Take-off and Landing, ESDU, 27 Corsham St., London.
- ESDU 97016 (1997). Estimation of Airframe Drag by summation of Components: Principles and Examples, ESDU, 27 Corsham St., London, Sep. 1997.
- Eshelby, M.E. (2000). *Aircraft Performance - Theory and Practice*, Arnold.
- Etchberger, F.R. (1983). LFC Leading Edge Glove Flight - Aircraft Modification Design, Test Article Development and Systems Integration, NASA CR 172136, Lockheed-Georgia Company, Nov. 1983.
- FAA (2001). Wildlife Strike Database, William J. Hughes Technical Center, Federal Aviation Administration (FAA),  
URL: [http://wildlife-mitigation.tc.faa.gov/public\\_html/index.html](http://wildlife-mitigation.tc.faa.gov/public_html/index.html), web-site accessed 10 Dec. 2001.
- Fabian, P. and Pruchniewicz, P.G. (1977). Meridional Distribution of Ozone in the Troposphere at Northern Midlatitudes, *Journal of Geophysical Research*, Vol. 82, pp. 2063 - 2073.
- FAR 25 (Federal Aviation Regulation Part 25), Airworthiness standards: Transport category airplanes, Federal Aviation Administration (FAA), Washington, DC.
- FAR 121 (Federal Aviation Regulation Part 121) *Operating requirements: Domestic, flag, and supplemental operations*, Federal Aviation Administration (FAA), Washington, DC.
- Field, P.R. (1999). Aircraft Observations of Ice Crystal Evolution in Altostratus Cloud, *Journal of Atmospheric Sciences*, Vol. 56, June 1999, pp. 1925 - 1941.
- Field, P.R. (2000). Bimodal Ice Spectra in Frontal Clouds. *Quarterly Journal of the Royal Meteorological Society*, 126 (2000), pp. 379 - 392.
- Fischer, M.C., Wright A.S. and Wagner R.D. (1983). A Flight Test of Laminar Flow Control Leading Edge Systems, NASA TM-85712.
- Fischler, J.E., *et al.* (1986). Laminar Flow Control Perforated Wing Panel Development, NASA CP 178166, Douglas Aircraft Company, CA., Oct. 1986.
- Fiton, J. (2000). Lessons Learnt from Dassault's Falcon 900 HLF Demonstrator, CEAS / DragNet European Drag Reduction Conference, Potsdam, 19 - 21 June 2000, Notes on Numerical Fluid Mechanics, Springer, Vol. 76, pp. 37 - 38.
- Fowell, L.R. and Antonatos, P.P. (1965). Some results from the X-21A Program Part 2, Laminar Flow Control Flight Test Results, *Recent Developments in Boundary Layer Research*, AGARDograph 97.
- Gerhards, R. and Szodruch, J. (2000). Industrial Perspectives of Drag Reduction Technologies, CEAS / DragNet European Drag Reduction Conference, Potsdam, 19 - 21 June 2000, Notes on Numerical Fluid Mechanics, Springer, Vol. 76, pp. 259 - 266.
- Gaster, M. (1965). A simple Device for Preventing Contamination on Swept Leading Edges, *Journal of the Royal Aeronautical Society*, Vol. 69, Nov. 1965, pp. 788 - 789.
- Gray, W.E. and Davies, H. (1952). Note on the Maintenance of Laminar Flow Wings, R. & M. No. 2485, British A.R.C. (Cited in Joslin, 1998a.)
- Gray, W.E. (1952). The Effect of Wing Sweep on Laminar Flow, Tech. memo. Aero 255, RAE. (Cited in Braslow, 1999.)
- Greener by Design (2001). Air Travel - Greener by Design: The Technology Challenge, Report of the Technology Sub-Group (Green J.E., Chairman), Conducted under the aegis of the UK Department of Trade and Industry Foresight Programme; available from Society of British Aerospace Companies Ltd., London.



- Gregory, N. (1961). Research on Suction Surfaces for Laminar Flow, *Boundary Layer and Flow Control*, Vol. 2, Lachmann G.V. (Ed.), Pergamon Press, pp. 924 - 960.
- Gustafsson, U.R.C., Perkins, P.J., Nyland, T.W., Tiefermann, M.W. and Dudzinski, T.J. (1979). Airborne Atmospheric Sampling System, Learning to use our environment: 25<sup>th</sup> Annual technical meeting, Seattle, 30 April - 2 May 1979, Institute of Environmental Sciences, pp. 48 - 57.
- HAL Consultants (1998). Effects of Salts on Aluminium – Results of Preliminary Study Carried out for University of Limerick, by HAL Consultants, Manchester, UK, 25<sup>th</sup> July 1998. (Unpublished)
- Hall, G.R. (1964). On the Mechanics of Transition Produced by Particles Passing Through an Initially Laminar Boundary Layer and Estimated Effect on the LFC Performance of the X-21 Aircraft, Northrop Corp. (Cited in: Davis, 1982; Davis *et al.*, 1983; 1986; 1987; Joslin, 1998a).
- Hansen, H. (1996). The effect of Suction on Transition – Lessons learned from the ELFIN I S1 Wind Tunnel Test, 2<sup>nd</sup> European Forum on Laminar Flow Technology, Bordeaux, June 1996, pp. 8.41 - 8.57.
- Hardy, A.C. and Milne, P.S. (1938). Studies in the Distribution of Insects by Aerial Currents - Experiments in Aerial Tow-netting from Kites, *J. Anim. Ecol.* Vol. 7, No. 2, pp. 199 - 229. (Cited in Joslin, 1998a)
- Henke, R. (1999). A320 HLF Fin Flight Tests Completed, *Air & Space Europe*, Vol. 1, No. 2, pp. 76 - 79.
- Henke, R. (2000). Airbus A320 HLF Fin Flight Tests, CEAS / DragNet European Drag Reduction Conference, Potsdam, 19 - 21 June 2000, Notes on Numerical Fluid Mechanics, Springer, Vol. 76, pp. 31 - 36.
- Henke, R., Bieler, H., Garcon, F. and Priest, J. (1993). Hybrid Laminar Flow Control: The ELFIN Wind tunnel Test Campaign, in conference proceedings: Aeroday 93 Second Community Aeronautics R&D Conference, Naples, Oct. 1993, pp. 17 - 24.
- Henke, R., Capbern, P., Davies, A., Hinslinger, R. and Santana, J. (1996). The A320 HLF Fin Programme: Objectives and Challenges, Second European Forum on Laminar Flow Technology, Bordeaux, June 1996, pp. 12.1 - 12.11.
- Heymsfield, A.J. (1986). Ice Particles Observed in a Cirriform Cloud at -83°C and Implications for Polar Stratospheric Clouds, *Journal of the Atmospheric Sciences*, Vol. 43, pp. 851 - 855.
- Heymsfield, A.J. and Platt (1984). A Parameterization of the Particle Size Spectrum of Ice Clouds in Terms of the Ambient Temperature and Ice Water Content, *Journal of the Atmospheric Sciences*, Vol. 41, No. 5, pp. 846 - 855.
- Heymsfield, A.J. and McFarquhar, G.M (1996). High Albedos of the Cirrus in the Tropical Pacific Warm Pool: Microphysical Interpretations from CEPEX and from the Kwajalein, Marshall Islands, *Journal of the Atmospheric Sciences*, Vol. 53, No. 17, pp. 2424 - 2451.
- Heymsfield, A.J., McFarquhar, G.M., Collins, W.D., Goldstein, J.A., Valero, F.P.J., Spinhirne, J., Hart, W. and Pilewskie (1998). Cloud Properties leading to Highly reflective tropical cirrus: Interpretations from CEPEX, TOGA, COARE and Kwajalein, Marshall Islands, *Journal of Geophysical Research*, Vol. 103, No. D8, pp. 8805 - 8812, April 1998.
- Hickey, D. (2001). Simulation of Safety and Reliability of a HLFC System on Aircraft, Final year project report (Supervisor Young, T.), University of Limerick, Ireland, April 2001.
- Hobbs, P.V. (1974). *Ice Physics*, Oxford University Press, Oxford.
- Hobbs, P.V. and Rango, A.L. (1985). Ice Particle Concentrations in Clouds, *Journal of Atmospheric Science*, Vol. 42, No. 23 (1985), pp. 2523 - 2549.
- Hogan, R.J., Jakob, C. and Illingworth, A.J. (2001). Comparison of ECMWF winter-season cloud fraction with radar-derived values. *Journal of Applied Meteorology*, 40 (2001), pp. 513 - 525.
- Holmes, B.J., Obara, C.J., Martin, G.L., Domack, C.S. (1985). Manufacturing Tolerances for Natural Laminar Flow Airframe Surfaces, SAE Paper 850863



- Holmes, B.J. and Obara, C.J. (1992). Flight Research on Natural Laminar Flow Applications, in *Natural Laminar Flow and Laminar Flow Control*, Ed. Barnwell, R.W. and Hussaini, M.Y., Springer-Verlag, pp. 73 - 142.
- Horstmann, K-H., Körner, H., Wagner, B. and Welte, D. (1996). Natural laminar Flow Flight Test Investigation for Commuter Aircraft Application, Second European Forum on Laminar Flow Technology, Bordeaux, June 1996, pp. 2.19 - 2.30.
- Horstmann, K-H., Schrauf, G., Sawyers, D., Sturm, H. (2002). A simplified Suction System for a HLFC Leading Edge Box of an A320 Fin, CEAS Aerospace Aerodynamics Research Conference, Paper 91, Cambridge, 10 - 12 June 2002.
- Humphreys, B. (1992). Contamination Avoidance For Laminar Flow Surfaces, First European Forum on Laminar Flow Technology, Hamburg, 16 -18 Mar. 1992, DGLR-Bericht 92-06, pp. 262 - 269.
- Humphreys, B. (1996). Development of Decontamination Systems for Hybrid Laminar Flow Applications, Second European Forum on Laminar Flow Technology, Bordeaux, June 1996, pp. 9.3 - 9.12.
- Humphreys, B. (1999). Operational Aspects for HLF Technology, DragNet European Drag Reduction Workshop, Toulouse, June 1999. (Unpublished)
- Humphreys, B. (2001a). Working towards the Ideal Laminar Flow Structure, Fourth Community Aeronautical Days Conference, Hamburg, Germany, 29 - 31 Jan. 2001; Proceedings in Air & Space Europe, No. 3/4, Vol. 3, pp. 101 - 104.
- Humphreys, B. (2001b). HYLTEC Laminar Flow Flight Tests - Extending Operational Experience, DragNet European Drag Reduction Workshop, Cranfield University, U.K., 25 - 26 June 2001. (Unpublished)
- Humphreys, B. (2002). Personal correspondence with Mr. Bryan Humphreys, Aerospace Systems and Technology, Consett, Co. Durham, UK, Aug - Sep 2002.
- Humphreys, B.E. and Horstmann, K-H. (2000). Flight Testing of a HLF Wing with Suction, Ice-Protection and Anti-contamination Systems, CEAS / DragNet European Drag Reduction Conference, Potsdam, 19 - 21 June 2000, Notes on Numerical Fluid Mechanics, Springer, Vol. 76, pp. 39 - 51.
- Humphreys, B.E. and Totland, E.J. (2000). SAAB 2000 In-service Test of Porous Surfaces for HLFC, CEAS / DragNet European Drag Reduction Conference, Potsdam, 19 - 21 June 2000, Notes on Numerical Fluid Mechanics, Springer, Vol. 76, pp. 89 - 98.
- Humphreys, B.E, Totland, E.J, Young, T.M., Corish, J. and Whooley, A. (2002). In-service Test of Laminar Flow Materials and De-Contamination System for Hybrid Laminar Flow Control, HYLTEC TR-64. (Confidential report prepared for HYLTEC partners.)
- HYLTEC (2000). HYLTEC (Hybrid Laminar Flow Technology) Workshop on Laminar Flow Control - Operational Aspects, Co-ordinators: Bieler, H., Cliffe, B., Young, T. and Horstmann, K-H., Proceedings distributed to HYLTEC partners, Braunschweig, Sep. 2000. (Unpublished)
- IPCC (1999). Aviation and the Global Atmosphere, A Special Report of the Intergovernmental Panel On Climate Change (IPCC), Penner J. *et al.* (Ed.) Cambridge University Press, 1999.
- ISO 2533 (1975). *Standard Atmosphere*, International Organization for Standardization.
- Jackson, P. (1997). *Jane's All the World's Aircraft 1997-98*, Jackson, P. (Ed.), Jane's Information Group, Butler and Tanner, London.
- Jagger, D.H. and Davies A.J. (1996). Design and Engineering Issues of a Hybrid Laminar Flow Wing, Second European Forum on Laminar Flow Technology, Bordeaux, June 1996, pp. 12.17 - 12.32.
- JAR 25, *Joint Airworthiness Requirements Part 25*, European Joint Aviation Authorities (JAA), Hoofdorp, The Netherlands.
- JAR OPS 1, *Joint Airworthiness Requirements OPS 1*, European Joint Aviation Authorities (JAA), Hoofdorp, The Netherlands.



- Jasperson, W.H., Nastrom, G.D., Davis, R.E. and Holderman, J.D. (1984a). GASP Cloud Encounter Statistics: Implications for Laminar Flow Control Flight, *Journal of Aircraft*, Nov. 1984, pp. 851 - 857.
- Jasperson, W.H., Nastrom, G.D., Davis, R.E. and Holderman, J.D. (1984b). GASP Cloud and Particle Encounter Statistics and their application to LFC Aircraft Studies, NASA TM 85835.
- Jasperson, W.H., Nastrom, G.D., Davis, R.E. and Holderman, J.D. (1985). Variability of Cloudiness at Airline Cruise Altitudes from GASP Measurements, *Journal of Climate and Applied Meteorology*, Vol. 42, Jan 1985, pp. 74 - 82.
- Jenkinson, L.R., Simpkin, P. and Rhodes, D. (1999). *Civil Aircraft Design*, Arnold Publishers.
- Johnson, C.G. (1969). *Migration and Dispersal of Insects by Flight*, Methuen, London. (Cited by Riley, *et al.* 1995.)
- Jones, R.I. (1985). The Implications of Laminar Flow Control for Long Range Transport Aircraft, PhD. Thesis, College of Aeronautics, Cranfield Institute of Technology, UK.
- Joslin, R.D. (1998a). Overview of Laminar Flow Control, NASA TP-1998-208705, Langley Research Centre, Oct. 1998.
- Joslin, R.D. (1998b). Aircraft Laminar Flow Control, *Annual Review of Fluid Mechanics*, Vol. 30, pp. 1 - 29.
- Juillen, J.C. and Arnal, D. (1994). Experimental Study of Boundary Layer Suction Effects on Leading Edge Contamination along the Attachment Line of a Swept Wing, IUTAM Symposium on Laminar-Turbulent Transition, Sendai, Sep. 1994, pp. 173 - 180.
- Khain, A., Ovtchinnikov, M., Pinsky, M., Pokrovsky, A. and Krugliak, H. (2000). Notes on the State-of-the-art Numerical modeling of Cloud Microphysics: A review, *Journal of Atmospheric Research*, 55(2000), pp. 159 - 224.
- Kühn, W. (1998). Surface and Cleanliness Requirements, Co-ordination Memorandum : HYLDA-025, Daimler Benz Aerospace Airbus, Bremen. (Unpublished)
- Kumar, A. and Hefner, J.N. (2000). Future challenges and opportunities in aerodynamics, *Aeronautical Journal*, Aug. 2000, pp. 365 - 373.
- Lachmann, G.V. (1961). *Boundary Layer and Flow Control, Its principles and Application*, Vol. 2, Pergamon Press, 1961.
- Lambert, M. (1992). *Jane's All the World's Aircraft 1992-93*, Lambert, M. (Ed.), Jane's Information Group, Butler and Tanner, London.
- Lan, C-T.E. and Roskam, J. (1981). *Airplane Aerodynamics and Performance*, Roskam Aviation and Engineering Corp.
- Lange, R.H. (1984). Design Integration for Laminar Flow Control for Transport Aircraft, *Journal of Aircraft*, Vol. 21 No. 8, pp. 612 - 617.
- Lange, R.H. (1987). Lockheed laminar Flow Control Systems Development and Applications, in symposium proceedings: Research in Natural Laminar Flow and Laminar-Flow Control Symposium, Virginia, March 1987, Proceedings Ed. Hefner, J.N. and Sabo, F.E., NASA CP-2487, pp. 53 - 77.
- Lange, R.H. (1988). Application of Hybrid Laminar Flow Control to Global Range Military Transport Aircraft, Lockheed report LG87ER0145, NASA-CR-181638.
- La Roche, U. and Palffy (1998). Oblique Grooves Avoiding Laminar Flow Separation on Bodies in Positive Pressure Gradients, 21<sup>st</sup> Congress of the International Council of Aeronautical Sciences (ICAS), Melbourne, 13 - 18 Sep. 1988, ICAS-A98-31546.
- Laskaridis, P. (2002). Personal correspondence with Mr. Panagiotis Laskaridis, PhD Student, School of Engineering, Cranfield University, UK, Feb. 2002.
- Le Claire, R. (1986). Energy Management Fuel Weight Penalty of Aircraft Systems, BAe-KSE-R-GEN-1334, BAe Kingston-Upon-Thames, June 1986. (Cited in Cranfield University, Lecture note DAeT 95122, undated).



- London, J., Warren, S. and Hahn, C.J. (1991). Thirty Year Trend of Observed Greenhouse Clouds over the Tropical Oceans, *Journal: Advances in Space Research*, Vol. 11 No. 3, pp. 45 - 49.
- Luers, J.K. (1983). Wing Contamination: Threat to safe Flight, *Astronautics and Aeronautics*, Vol. 21, Nov. 1983.
- Lynch, F.T. and Klinge, M.D. (1991). Some Practical Aspects of Viscous Drag Reduction Concepts, in conference proceedings: Aerospace Technology, SAE, Long Beach, CA, 23 - 26 Sep 1991.
- Lynch, K.D., Sasson, K., Starr, D. Stephens, G. (2002). *Cirrus*, Oxford University Press, New York.
- Mace, G.M., Jakob, C. and Moran, K.P. (1998). Validation of hydrometeor occurrence predicted by the ECMWF model using millimeter wave radar data. *Geophysical Research Letters*, 25 (1998), pp. 1645 - 1648.
- Maddalon, D.V. (1991). Hybrid Laminar-Flow Control Flight Tests, NASA TM-4331.
- Maddalon, D.V. and Braslow, A.L. (1990). Simulated Airline Service Flight Tests of Laminar Flow Control with Perforated Surface Suction System, NASA TP-2966, Mar. 1990.
- Maddalon, D.V., Fisher, D.F., Jennett, L. and Fischer, M.C. (1987). Simulated Airline Service Experience with Laminar-Flow Control Leading-Edge Systems, Research in Natural Laminar Flow and Laminar-Flow Control Symposium, Virginia, Mar. 1987, Proceedings Ed. Hefner, J.N. and Sabo, F.E., NASA CP-2487, pp. 195 - 218.
- Maddalon, D.V. and Poppen, W.A., Jr. (1986). Design and Fabrication of Large Suction Panels with Perforated Surfaces for Laminar Flow Control testing in a Transonic Wind Tunnel, NASA TM-89011, Aug. 1986.
- Maddalon, D.V. and Wagner, R.D. (1985). Operational Considerations for Laminar Flow Aircraft, Laminar Flow Aircraft Certification Workshop, Wichita 15 - 16 April, Proceedings published as NASA CP-2413, Williams, L.J. (Ed.). pp. 247 - 268.
- Maestrati, J. and Bulgubure, Ch. (1996). Laminar Flow for business Jets: Falcon 900 HLFC Demonstrator, Second European Forum on Laminar Flow Technology, Bordeaux, June 1996, p. 11.3.
- Mahony, B. (2002). Characteristics of Hybrid Laminar Flow Control Suction Surfaces, B.Eng. Final Year Project Report (Supervisor: Young, T.), Department of Mechanical and Aeronautical Engineering, University of Limerick, Ireland, May 2002.
- Mair, W.A. and Birdsall, D.L. (1992). *Aircraft Performance*, Cambridge University Press, Cambridge.
- Marec, J-P. (2000). Drag Reduction: A Major Task for Research, CEAS / DragNet European Drag Reduction Conference, Potsdam, 19 - 21 June 2000, Notes on Numerical Fluid Mechanics, Springer, Vol. 76, pp. 17 - 28.
- Marengo, A., Thouret, V., Nédélec, P., Smit, H., Helten, M., Kley, D., Karcher, F., Simon, P., Law, K., Pyle, J., Poschmann, G., Von Wrede, R., Hume, C and Cook, T. (1998). Measurement of Ozone and Water Vapor by Airbus in-service Aircraft: The MOZAIC airborne program, An Overview, *Journal of Geophysical Research*, Vol. 103 (1998), Oct. 1998, pp. 25631 - 25642.
- Maresh, J.L. and Bragg, M.B. (1984). The Role of Aerofoil Geometry in Minimizing the Effect of Insect Contamination of Laminar Flow Sections, in conference proceedings: AIAA Second Applied Aerodynamics Conference, Seattle, Aug. 1984, AIAA 84-2170.
- Marsden D.J. (1978). Wind Tunnel Tests of a Slotted Flapped Wing Section, *Canadian Aeronautics and Space Journal*, Vol. 24, Mar. - Apr. 1978, pp. 83 - 91.
- Massey, B.S. (1983). *Mechanics of Fluids*, 5<sup>th</sup> edition, Van Nostrand Reinhold, Berkshire, UK.
- Mattingly, J.D., Heiser, W. and Daley, D.H. (1987). *Aircraft Engine Design*, American Institute of Aeronautics and Astronautics (AIAA), Washington DC.
- MatWeb (2002). Material Property Data, URL: <http://www.matweb.com>, accessed 23<sup>rd</sup> Aug. 2002.
- McClafferty, A. (2002). Characterisation of Flow Through Hybrid Laminar Flow Control Suction Surfaces, B.Eng. Final Year Project Report (Supervisor: Young, T.), Department of Mechanical and Aeronautical Engineering, University of Limerick, Ireland, May 2002.



- McDonnell Douglas (1983). Evaluation of Laminar Flow Control Systems Concepts for Subsonic Commercial Transport Aircraft, NASA CR 159251, McDonnell Douglas Corp., Douglas Aircraft Company, CA, June 1983.
- Meade, L.E., Kays, A.O., Ferrill, R.S., Young, H.R. (1977). Development of the Technology for the Fabrication of Reliable Laminar Flow Control Panels, Prepared for NASA by Lockheed-Georgia Company, Georgia, NASA CR-145168, Feb. 1977.
- Meifarh, K.U. and Heinrich, S. The Environment for Aircraft with Laminar Flow Technology within Airline Service, First European Forum on Laminar Flow Technology, Hamburg, 16 -18 Mar. 1992, DGLR-Bericht 92-06, pp. 251 - 255.
- Mertens, J. (1999). Adaptive Wing Project ADIF and Related Activities, DragNet European Drag Reduction Workshop, Toulouse, June 1999. (Unpublished)
- Mertens, J. (2000). Next Steps Envisaged to Improve Wing Performance of Commercial Aircraft, CEAS / DragNet European Drag Reduction Conference, Potsdam, 19 - 21 June 2000, Notes on Numerical Fluid Mechanics, Springer, Vol. 76, pp. 246 - 255.
- Meyer, P. (2000). Application of HLF Technology to Civil Nacelle, CEAS / DragNet European Drag Reduction Conference, Potsdam, 19 - 21 June 2000, Notes on Numerical Fluid Mechanics, Springer, Vol. 76, pp. 107 - 114.
- Miller, D.S. (1990). *Internal Flow Systems*, 2<sup>nd</sup> Edition, BHRA, The Flow Engineering Centre, Cranfield, Bedford, UK.
- MIL-STD-756B (1981). Reliability Modelling and Prediction, Military Standard, Department of Defense of the USA, Nov. 1981.
- Mitchell, D. (1994). A Model Predicting the Evolution of Ice Particle Size Spectra and Radiative Properties of Cirrus Clouds. Part 1: Microphysics, *Journal of the Atmospheric Sciences*, March 1994, Vol. 51, No. 6, pp. 797 - 816.
- Molitor, P. and Young, T. (2002). Adhesives Bonding of Glass Fibre Reinforced Composite Material to Titanium Alloy, *International Journal of Adhesion and Adhesives*, 22 (2002) pp. 101 – 107.
- Möller, W. (2001). Personal correspondence with Dr. Werner Möller, Nord-Micro, Frankfurt, July 2001.
- Moxon, J. (1999). Aircraft and the Environment: Burning Issues, *Flight International*, 20 - 26 Oct. 1999.
- Mullender, A.J., Lecordix, A.J., Lecossais, E., Godard, J.L. and Hepperle, M. (1996). The ELFIN II and LARA HLF Nacelles: Design Manufacture and Test, Second European Forum on Laminar Flow Technology, Bordeaux, June 1996, Proceedings pp. 5.31 - 5.48.
- Mullender, A.J. and Reidel, H. (1996). A Laminar Flow Nacelle Flight Test Programme, Second European Forum on Laminar Flow Technology, Bordeaux, June 1996, Proceedings pp. 2.31 - 2.49.
- Nam, G.W. (1996). Development of Safety and Reliability Prediction Methodology for Aircraft Systems and Common Cause Failures, Ph.D. Thesis, Cranfield University, U.K., 1996.
- Nastrom, G.D., Holderman, J.D., Davis, R.F. (1981a). Cloud Encounter and Particle-Concentration Variabilities from GASP Data, NASA TP-1886.
- Nastrom, G.D., Holderman, J.D. and Davis, R.E. (1981b). Cloud Encounter and Particle Density Variabilities from GASP Data, AIAA-81-0308, AIAA 19<sup>th</sup> Aerospace Sciences Meeting, St. Louis, 12 - 15 Jan. 1981.
- Nord-Micro (2002). Personal correspondence with engineering staff, Nord-Micro, Frankfurt/Main, Germany, Oct.2002.
- NWRC (2001). FAA Wildlife Strikes to Civil Aircraft in the United States, National Wildlife Research Center (NWRC) Ohio Field Station, USA,  
URL: <http://www.lrbcg.com/nwrscandusky/Strike.html>, web-site accessed 10 Dec. 2001.
- O'Donoghue, D. (2001). The Investigation of the Potential of Fluorosurfactants and Proteolytic Enzymes in Water Organic C-solvent Systems for Aircraft Wing Contamination Alleviation, M.Sc. thesis, University of Limerick, March 2001.



- O'Donoghue, D., Pembroke, T. O'Dwyer, T. and Young, T. (2001). The Investigation of Surfactant and Enzyme Formulations for Alleviation of Leading Edge Contamination on Hybrid Laminar Flow Surfaces, HYLTEC Technical Report 43, University of Limerick, Feb. 2001. (Confidential report.)
- O'Donoghue, D., Pembroke, T., Young, T. and O'Dwyer, T. (2000). Novel Environmentally Friendly Formulations for Alleviation of Leading Edge Contamination on Hybrid Laminar Surfaces, CEAS / DragNet European Drag Reduction Conference, Potsdam, 19 - 21 June 2000, Notes on Numerical Fluid Mechanics, Springer, Vol. 76, pp. 351 - 358.
- O'Donoghue, D., Young, T., Pembroke, T. and O'Dwyer, T. (2002). An Investigation of Surfactant and Enzyme Formulations for the Alleviation of Insect Contamination on Hybrid Laminar Flow Control (HLFC) Surfaces, *Journal of Aerospace Science and Technology*, 6 (2002) pp. 19 - 29.
- O'Driscoll, D., Hardwick, J., Young, T. and Ryan, J. (2000). Lightning Strike of Perforated Carbon Fibre Epoxy Laminar Flow Panels, *Journal of Composites Technology and Research*, 22(2) (2000) pp.71 - 75.
- Parungo, F. (1995). Ice Crystals in High Clouds and Contrails, *Journal of Atmospheric Research*, 38(1995), pp. 249 - 262.
- Parungo, F., Boatman, J., Sievering, H., Wilkison, S and Bruce, B., 1993, Trend in Global Marine Cloudiness and Anthropogenic Sulphur, *Journal of Climate*, 1(1993), pp. 434 - 440.
- Perkins, P. and Gustafsson, U.R.C. (1975). An Automated Atmospheric Sampling System Operating on 747 Airliners, NASA TM X-71790.
- Peterson, J.B. and Fisher D.F. (1978). Flight Investigation of Insect Contamination and its Alleviation, CTOL Transport Technology Conference, Langley Research Centre, Virginia, NASA CP 2036, Feb. - Mar. 1978, pp. 357 - 363.
- Pfenninger, W. (1977). Laminar Flow Control - Laminarization, in *Special Course on Concepts for Drag Reduction*, von Karman Institute, Belgium, 28 Mar. - 1 Apr. 1977, AGARD Report No. 654.
- Pfenninger, W. (1982). Design Considerations of Long-Range and Endurance LFC Airplanes with Practically all Laminar Flow, NASA CR-173234.
- Pfenninger, W. and Reed, V.D. (1966). Laminar Flow Research and Experiments, *Astronautics and Aeronautics*, AIAA, Vol. 4, No. 7, July 1966, pp. 44 - 50.
- Poll, D.I.A. and Danks, M. (1994). Relaminarisation of the Swept Wing Attachment Line by Surface Suction, IUTAM Symposium on Laminar-Turbulent Transition, Sendai, Sep. 1994, pp. 137 - 144.
- Poll, D.I.A., Danks, M. and Davies, A.J. (1992a). The effect of Surface Suction near the Leading Edge of a Swept-back wing, Paper 92-01-029, First European Forum on Laminar Flow Technology, 16 - 18 March 1992.
- Poll, D.I.A., Danks, M. and Humphreys, B.E. (1992b). The Aerodynamic Performance of Laser Drilled Sheets, First European Forum on Laminar Flow Technology, Hamburg, 16 - 18 Mar. 1992. DGLR-Bericht, 92-06, pp. 274 - 277.
- Povinelli, F.P., Klineberg, J.M. and Kramer, J.J. (1976). Improving Aircraft Energy Efficiency, *Astronautics and Aeronautics* (AIAA), Feb. 1976, pp. 19 - 31.
- Price, S. (1998). Information (Relevant to HLFC) on Insect Populations in the Atmosphere, Project Report, British Aerospace Airbus, July 1998. (Unpublished)
- Priest, J. and Paluch, B. (1996). Design Specification and Inspection of Perforated Panels for HLF Suction Systems, Second European Forum on Laminar Flow Technology, Bordeaux, June 1996, pp. 6.20 - 6.46.
- Pusch, C. (2001). Air Traffic Management, Fourth Community Aeronautical Days Conference, Hamburg, 29 - 31 Jan. 2001; Proceedings in Air & Space Europe, No. 3/4, Vol. 3, pp. 255 - 257.
- Raymer, D. (1989). *Aircraft Design: A conceptual approach*, American Institute of Aeronautics and Astronautics (AIAA), Washington DC.



- Reneaux, J. and Blanchard, A. (1992). The Design and Testing of an Airfoil with Hybrid Laminar Flow Control, First European Forum on Laminar Flow Technology, Hamburg, 16 -18 Mar. 1992, DGLR-Bericht 92-06, pp. 164 - 174.
- Reneaux, J., Preist, J., Juillen J.C. and Arnal, D. (1996). Control of Attachment Line Contamination, Second European Forum on Laminar Flow Technology, Bordeaux, June 1996, pp. 8.3 - 8.16.
- Riley, J.R., Reynolds, D.R., Mukhopadhyay, S., Ghosh, M.R. and Sarkar, T.K. (1995). Long-distance Migration of Aphids and other Small Insects in Northeast India, *European Journal of Entomology*, 92(1995), pp. 639 - 653.
- Robert, J-P. (1992). Hybrid Laminar Flow Control – A Challenge for a Manufacturer, First European Forum on Laminar Flow Technology, 16 -18 Mar. 1992, pp. 294 - 308.
- Rolls-Royce (1968). *Performance Specification and Installation Notes RB.211-22*, Rolls-Royce, Derby, UK, July 1968.
- Rolls-Royce (1998). *Aero data*, Publication No. TS1491, Rolls-Royce, Derby, UK, Feb. 1998.
- Rolls-Royce (2000a). Personal correspondence with Rolls-Royce engineers, May, 2000.
- Rolls-Royce (2000b). ALTTA Task 2.1: Power Source Options for HLC System Installation on a Trent 500, Report No. IAR01031, 20 Oct. 2000. (Unpublished)
- Roskam, J. (1985). *Airplane Design Part I*, Roskam Aviation and Engineering Corp., Ottawa, KA.
- Runyan, L.J., Bielak, G.W., Behbehani, R., Chen, A.W. and Rozendaal, R.A. (1987). NLF Glove Flight Test Results, *Research in Natural Laminar Flow and Laminar-Flow Control*, Ed. Hefner, J.N. and Sabo, F.E., NASA CP-2487, part 3, pp. 795 - 818.
- Sassen, K. (1991a). Aircraft-produced Ice Particles in Highly Supercooled Altocumulus Cloud, *Journal of Applied Meteorology*, Vol. 30, June 1991, pp. 765 - 775.
- Sassen, K. (1991b). Corona Producing Cirrus Cloud Properties Derived from Polarization Lidar and Photographic Analyses, *J. of Appl. Opt.*, Vol. 30 (1991), pp. 3421 - 3428. (Cited in Lynch *et al.*, 2002).
- Sawyers, D.M. and Wilson, R.A.L. (1996) Assessment of the Impact of Hybrid Laminar Flow on Large Subsonic Aircraft, Second European Forum on Laminar Flow Technology, Bordeaux, June 1996, pp. 3.3 - 3.17.
- Schmidt, C. (2001). Performance Assessment of Hybrid Laminar Flow Control (HLFC) Aircraft, *Diplomthesis* (Supervisor: Young, T.), University of Applied Sciences in Hamburg / University of Limerick, Ireland.
- Schneider, W. (2000). The importance of Aerodynamics in the Development of Commercially Successful Transport Aircraft, CEAS / DragNet European Drag Reduction Conference, Potsdam, 19 - 21 June 2000, Notes on Numerical Fluid Mechanics, Springer, Vol. 76, pp. 9 - 16.
- Schrauf, G. (2001). Towards Operational HLFC Flight Tests - Status of Laminar Flow Technology, DragNet European Drag Reduction Workshop, Cranfield University, U.K., 25 - 26 June 2001.
- Schrauf, G., Bieler, H., and Thiede, P. (1992). Transition Prediction - The Deutsche Airbus View, First European Forum on Laminar Flow Technology, Hamburg, 16 - 18 Mar. 1992, DGLR-Bericht, 92-06, pp. 73 - 81.
- Schrauf, G. and Horstmann, K-H. (2000). Linear Stability Theory Applied to Natural and Hybrid Laminar Flow Experiments, CEAS / DragNet European Drag Reduction Conference, Potsdam, 19 - 21 June 2000, Notes on Numerical Fluid Mechanics, Springer, Vol. 76, pp. 157 - 162.
- Schrauf, G. and Kühn, W. (2001). Future Needs and Laminar Flow Technology, Fourth Community Aeronautical Days Conference, Hamburg, 29 - 31 Jan. 2001; Proceedings in Air & Space Europe, No. 3/4, Vol. 3, pp. 98 - 100.
- Schrauf, G., Perraud, J., Lam, F., Stock, H.W., Vitiello, D. and Abbas, A. (1996). Transition Prediction with Linear Stability Theory – Lessons Learned from the ELFIN F100 Flight Demonstrator, Second European Forum on Laminar Flow Technology, Bordeaux, June 1996, pp. 8.58 - 8.71.



- Schwab, U. (1992). Electron Beam Drilled Holes for Laminar Flow Control, First European Forum on Laminar Flow Technology, Hamburg, 16 - 18 Mar. 1992, DGLR-Bericht 92-06, pp. 270 - 273.
- Shipley, P.P., Lecordix, J-L., Godard, J-L. and Rossow, C-C. (1993). The Design Optimisation of a Hybrid Laminar Flow Nacelle, Aerodays 93: Second Community Aeronautics R&D Conference, Naples, Oct. 1993.
- Shustrov, Y.M. (1998). "Starting mass" - a complex criterion of quality for aircraft on-board systems, *Journal of Aircraft Design*, 1(1998), pp. 193 - 203.
- Siochi E.J., Eiss, N.S., Gilliam, D.R., Wightman, J.P. (1987). A Fundamental Study of the Sticking of Insect Residues to Aircraft Wings, *Journal of Colloid & Interface Science*, Vol. 115, No. 2, pp. 346 - 356.
- Smith, B.A. (1995). F-16XL Flights Could Aid in HSCT Design, *Aviation Week and Space Technology*, 23 Oct. 1995.
- Snow, J.E. and Yeomans, D.G. (2000). Reliability Analysis Short Course, College of Aeronautics, Cranfield University, U.K., 20 - 24 Nov. 2000. (Unpublished).
- Snyder, J.L. (1964). Effect of Clouds on LFC Operations, Ops/Analysis, Directorate of Operations Research report, Deputy for Studies and Analysis, Systems Engineering Group, Research and Technology Division, Wright Patterson Air Force Base, Ohio, Dec. 1964. (Cited in Fowell and Antonatos, 1964).
- Sprang, R., Reise, M., Eidmann, G., Offermann, D. and Wang, P.H. (2001). A Detection Method for Cirrus Clouds using Crista 1 and 2 Measurements, *Journal Adv. Space Research*, Vol. 27, No. 10, pp. 1629 - 1634.
- Stanewsky, E., Délery, J., Fulker, J., Geissler, W. (Ed.) (1997). EUROSHOCK – Drag Reduction by Passive Shock Control, Notes on Numerical Fluid Mechanics, Vol. 56, Vieweg & Sohn, Braunschweig.
- Stanewsky, E. and Rosemann, H. (2000). Aspects of Shock Control and Adaptive Wing Technology, CEAS / DragNet European Drag Reduction Conference, Potsdam, 19 - 21 June 2000, Notes on Numerical Fluid Mechanics, Springer, Vol. 76, pp. 221 - 228.
- Straubinger, G. (2000). Development of an Aircraft Performance Model for the Prediction of Trip fuel and Trip time for a Generic Twin Engine Jet Transport Aircraft, *Diplom thesis*, (Supervisor: Young, T.), University of Applied Sciences in Hamburg / University of Limerick, Ireland.
- Swann, H. (1998). Sensitivity to the representation of precipitating ice in CRM simulations of deep convection. *Atmospheric Research*, 48 (1998), pp. 415 - 435.
- Szodruch, J. (2001). Aircraft Drag Reduction as an Answer to the Global Challenges, Fourth Community Aeronautical Days Conference, Hamburg, 29 - 31 Jan. 2001; Proceedings in Air & Space Europe, No. 3/4, Vol. 3, pp. 93 - 97.
- Tamigniaux, T.L.B., Stark, S.E., Brune, G. W. (1987). An Experimental Investigation of the Insect Shielding Effectiveness of a Krueger Flap/Wing Airfoil Configuration, 5th AIAA, Applied Aerodynamics Conference, Monterey, CA, 17 - 19 Aug. 1987, pp. 601 - 606.
- Tegarden, F.W. (1996). Hybrid Laminar Flow Nacelles - A Test for the Future, Engine-Airframe Integration Conference, Royal Aeronautical Society, Bristol, 10 - 11 Oct. 1996, pp. 11.1 - 11.11.
- Thibert, J.J., Reneaux, J. and Schmitt, V. (1990). Onera activities on Drag Reduction, 17<sup>th</sup> Congress of the International Council of Aeronautical Sciences, Stockholm, ICAS 90-3.6.1, pp. 1053 - 1064.
- Thibert, J.J., Quast, A. and Robert, J.P. (1992). The A320 Laminar Flow Fin Program, First European Forum on Laminar Flow Technology, Hamburg, 16 - 18 Mar. 1992, DGLR-Bericht 92-06, pp. 19 - 25.
- Thom, T. (1997). *The Air Pilot's Manual. Vol. 2, Aviation Law and Meteorology*, Airline, UK.
- Thompson, B.E., Jang, J. and Dion, J.L. (1995). Wing performance in Moderate Rain, *Journal of Aircraft*, Vol. 32, No. 5, Sep. - Oct. 1995.
- Timetal (1997). Specification sheet for Timetal 15-3 Titanium Alloy, Broadway, Denver, Colorado.



- Tribot, J-P. (2001). Personal correspondence with Mr. Jean-Pierre Tribot, Engineer, Dassault Aviation, Mérignac, France, 23 Oct. 2001.
- Wagner, R.D. and Fischer, M.C. (1983). Developments in the NASA Transport Aircraft Laminar Flow Program, AIAA-83-0090, AIAA 21<sup>st</sup> Aerospace Sciences Meeting, Reno, 10 - 13 Jan. 1983.
- Wagner, R.D., Maddalon, D.V., Bartlett, D., Collier, F.S., Jr. and Braslow A.L. (1992). Laminar Flow Flight Experiments - A Review, Barnwell, R.W. and Hussaini, M.Y. (Ed.), Springer-Verlag, pp. 23 - 72.
- Wagner, R.D., Maddalon, D.V., Fisher, D.F. (1988). Laminar Flow Control Leading Edge Systems in Simulated Airline Service, 16<sup>th</sup> Congress of the International Council of Aeronautical Sciences (ICAS), Jerusalem, 28 Aug. - 2 Sep. 1988, pp.1-11.
- Walsh, M.J. (1980) Drag Characteristics of V-groove and Transverse Curvature Riblets, in Viscous Drag Reduction, AIAA 168 - 184, Washington, DC.
- Wang, P-H., Minnis, P., McCormick, P., Kent, G.S. and Skeens, K.M (1996). A 6-Year Climatology of Cloud Occurrence Frequency from Stratospheric Aerosol and Gas Experiment II Observations (1985 - 1990), *Journal of Geophysical Research* Vol. 101, Dec. 1996, pp. 29407 - 29429.
- Wang, P-H., Minnis, P., McCormick, P., Kent, G.S., Yue, G.K., Young, D.F., Skeens, K.M (1998). A Study of the Vertical Structure of Tropical Optically Thin Clouds from SAGE II Observations, *Journal of Atmospheric Research* 47-48 (1998) pp. 599 - 614.
- Warsop, C. (1999). An investigation into the Viability of MEMS on Aircraft (AEROMEMS), DragNet European Drag Reduction Workshop, Toulouse, June 1999. (Unpublished).
- Warsop, C. (2000). Current Status and Prospects for Turbulent Flow Control, CEAS / DragNet European Drag Reduction Conference, Potsdam, 19 - 21 June 2000, Notes on Numerical Fluid Mechanics, Springer Vol. 76, pp. 269 - 277.
- Wentz, W.H., Jr., Ahmed, A. and Nyenhuis, R. (1985). Further Results of Natural Laminar Flow Flight Test Experiments, SAE Paper 850862, SAE SP-621, pp. 37 - 50.
- Whites, R.C., Sudderth, R.C. and Wheldon, W.G. (1966). Laminar Flow Control on the X-21, *Astronautics and Aeronautics*, AIAA, Vol. 4, No. 7, July 1966. pp. 38 - 43.
- Williams, N.R. (1982). SPF/DB Titanium LFC Porous Panel Concepts, in Laminar Flow Control: 1981 Research and Technologies Studies, Maddalon, D.V. (Ed.), NASA CP 2218, pp. 111 - 117.
- Williams, S.W. and Marsden P.J. (1996). New Laser Drilling Techniques for Porous Surfaces, Second European Forum on Laminar Flow Technology, Bordeaux, June 1996, pp. 9.13 - 9.22.
- Wilson, D.R. and Ballard, S.P. (1999). A microphysically based precipitation scheme for the UK Meteorological Office Unified Model. *Quarterly Journal of the Royal Meteorological Society*, 125 (1999), pp. 1607 - 1636.
- Wilson, R.A.L. and Jones, R.I. (1995). Project Design Studies on Aircraft Employing Natural and Assisted Laminar Flow Technologies, SAE 952038, Aerotech 95, Los Angeles, Sep. 1995.
- Wilson, R.A.L. and Jones, R. (1996). Operational and Certification Considerations for Subsonic Transport Aircraft with Hybrid Laminar Flow Control, in Second European Forum on Laminar Flow Technology, Bordeaux, June 1996, pp. 11.27 - 11.39.
- Wilson, R.A.L. (1997). The Introduction of Laminar Flow to the Design and Optimisation of Transport Aircraft, PhD thesis, Cranfield University, U.K.
- Wilson, V.E. (1982). SPF/DB Titanium Concepts for Structural Efficiency, in Laminar Flow Control: 1981 Research and Technologies Studies, Maddalon, D.V. (Ed.), NASA CP 2218, pp. 95 - 110.
- Wortmann F.X. (1974). A Method for Avoiding Insect Roughness on Aircraft (Installation of Highly Elastic Rubber Coverings on Leading Edges), NASA-TT-F-15454, Apr. 1974.
- Wright, M.C.M. and Nelson, P.A. (2000). Wind Tunnel Experiments on the Optimization of Suction for Laminar Flow Control, ISVR Contract Report No. 00/04, Institute of Sound and Vibration, University of Southampton, U.K., Jan. 2000.



- Wyser, K. and Yang, P. (1998). Average Ice Crystal Size and Bulk Short-wave Single-scattering Properties of Cirrus Clouds, *Journal of Atmospheric Research*, No. 49 (1998), pp. 315 - 335.
- Yajnik, K.S. and Subbaiah, M.V. (1976). Representation of the Drag Polar of a Fighter Aircraft, *Journal of Aircraft*, Vol. 13, No. 2, Feb. 1976, pp. 155 - 156.
- Yeo, C.Y., Tam, S.C., Jana, S. and Lau, M.W.S. (1994). A technical Review of Laser Drilling of Aerospace Materials, *Journal of Materials Processing Technology*, 42 (1994) pp.15 - 49.
- Young, T., Mahony, B., McClafferty, A., Corish, J., Humphreys, B. and Totland, E. (in press). Durability of Hybrid Laminar Flow Control (HLFC) Surfaces, *Journal of Aerospace and Technology*.
- Young, T. and O'Driscoll, D. (2002). Impact of Nd-YAG Laser Drilled Holes on the Strength and Stiffness of Laminar Flow Carbon Fibre Reinforced Composite Panels, *Journal of Composites, Part A: Applied Science and Manufacturing*, 33 (2002), pp. 1 - 9.
- Young, T., O'Driscoll, D. and Ryan, J. (1999). Assessment of Material Characteristics of Candidate Materials of the Nacelle Suction Surface, Confidential Report HYLDA TR-33, University of Limerick, Ireland, Mar. 1999. (Unpublished)
- Young, T.M. (2002). *Airplane Performance* in *The Standard Handbook for Aeronautical and Astronautical Engineers*, Davies, M. (Ed.), McGraw-Hill, New York.
- Young, T.M., Brown, P.R.A. and Fielding, J.P. (2002). The Impact of Cloud Encounter on Hybrid Laminar Flow Control Aircraft Operations, CEAS Aerospace Aerodynamics Research Conference, Paper 58, Cambridge, 10 - 12 June 2002.
- Young, T.M. and Fielding, J.P. (2000). Flight Operational Assessment of Hybrid Laminar Flow Control (HLFC) Aircraft, CEAS / DragNet European Drag Reduction Conference, Potsdam, 19 - 21 June 2000, Notes on Numerical Fluid Mechanics, Springer, Vol. 76, pp. 99 - 106.
- Young, T.M. and Fielding, J.P. (2001). Potential Fuel Savings due to Hybrid Laminar Flow Control under Operational Conditions, *Aeronautical Journal*, Paper No. 2670, Oct. 2001, pp. 581 - 588.
- Young, T.M., Humphreys B. and Fielding J.P. (2001). Investigation of Hybrid Laminar Flow Control (HLFC) Surfaces, *Journal of Aircraft Design*, 4 (2001), pp. 127 - 146.



# APPENDICES

- A ENVIRONMENTAL IMPACT**
- B HLFC TECHNOLOGY**
- C OVERVIEW OF MAJOR LFC AND HLFC STUDIES AND FLIGHT TEST CAMPAIGNS**
- D FUEL PLANNING AND PAYLOAD RANGE**
- E AIRCRAFT PERFORMANCE THEORY**
- F B757-200 CLASS AIRCRAFT DATA**
- G A330-200 CLASS AIRCRAFT DATA**
- H PERFORMANCE PROGRAMS**
- I HLFC SENSITIVITY STUDIES**
- J HLFC SYSTEM INSTALLATION**
- K CLOUD ENCOUNTERS**
- L INSECT CONTAMINATION**
- M MECHANICAL FAILURE, DAMAGE AND DURABILITY ASPECTS OF HLFC SYSTEMS  
AND SUCTION SURFACES**
- N NOMENCLATURE, DEFINITIONS AND GLOSSARY**



Blank page



**APPENDIX A**

**ENVIRONMENTAL IMPACT**

**TABLE OF CONTENTS**

A.1 Introduction..... 172

A.2 Types of Emissions ..... 172

    A.2.1 Carbon dioxide ..... 172

    A.2.2 Water vapour ..... 172

    A.2.3 Nitrogen oxides ..... 173

    A.2.4 Aerosol particles..... 173

A.3 Clouds and Contrails..... 174

    A.3.1 Clouds..... 174

    A.3.2 Contrail formation..... 174



## A.1 INTRODUCTION

Aircraft operations influence the atmosphere by introducing gases and particles into it and by forming contrails. The emissions include greenhouse gases, such as carbon dioxide and water, as well as chemically active gases that alter natural greenhouse gases, such as ozone and carbon monoxide. In this appendix, brief supplemental information is provided about dominant aircraft emissions and the formation of contrails. The following two important scientific works may be consulted for further information concerning the impact of aircraft on the atmosphere:

- (1) European Scientific Assessment of the Atmospheric Effects of Aircraft Emissions, Brasseur, G., Amanatidis, G.T. and Angeletti, G. (Editors), Special report for the European Commission DG XII, Science, Research, Development Environment and Climate Programme, published in *Atmospheric Environment*, Vol. 32, No. 13, July 1998, pp. 2327 - 2422.
- (2) Aviation and the Global Atmosphere, A Special Report of the Intergovernmental Panel on Climate Change (IPCC), Penner J. *et al.* (Editors), Cambridge University Press, 1999.

## A.2 TYPES OF EMISSIONS

### A.2.1 Carbon dioxide

Carbon dioxide (CO<sub>2</sub>) is by far the most important greenhouse gas and accounts for approximately 80% of the impact of these gases, when weighed according to their global warming potential (CEC, 1998). The effect of CO<sub>2</sub> on global warming is compounded by its exceptionally long lifetime in the atmosphere. Along with water, CO<sub>2</sub> is the most abundant of the products of jet fuel combustion. In 1992 the world aircraft fleet produced  $5.1 \times 10^{11}$  kg of CO<sub>2</sub> per year, which accounted for 2% of all anthropogenic CO<sub>2</sub> emissions (IPCC, 1999). The output is projected to rise threefold by 2050, even though the production per engine will be reduced due to new technologies.

### A.2.2 Water vapour

Water vapour is a greenhouse gas and its increase in the atmosphere due to aircraft operations tends to increase the rate of warming of the Earth's surface; although, by comparison to the effects of CO<sub>2</sub> and Nitrogen oxides (NO<sub>x</sub>), its impact is much smaller. The water vapour emissions of most subsonic aircraft are released into the troposphere and are then removed by precipitation within approximately nine days. A smaller fraction however, is released directly into the stratosphere, where it will remain for months or even years. As a result there is a build-up of aircraft-produced water vapour, which it is suspected could upset the natural hydrological balance in the upper atmosphere (Brasseur *et al.*, 1998; Moxon, 1999).



### A.2.3 Nitrogen oxides

NO<sub>x</sub> are influential in the chemistry of the atmosphere, particularly in the production and destruction of ozone. The processes by which NO<sub>x</sub> affect that chemistry are complex and differ according to factors such as season and location. At cruise altitudes, an increase in ozone (O<sub>3</sub>) leads to an increased greenhouse effect. The IPCC (1999) report indicates that in 1992 NO<sub>x</sub> emissions from subsonic aircraft were estimated to have increased ozone concentrations at cruise altitudes by up to 6%, and this was projected to grow to ~13% by 2050. NO<sub>x</sub> emissions also decrease the concentration of another greenhouse gas, methane (CH<sub>4</sub>). These reductions in CH<sub>4</sub> tend to cool the surface of the Earth. Although global average values for the two greenhouse influences, O<sub>3</sub> and CH<sub>4</sub> are of roughly similar magnitude, they do not cancel each other due to regional differences.

Atmospheric ozone, most of which is found in the stratosphere, provides a shield against solar ultraviolet (UV) radiation. The net effect of aircraft operations appears to be an increase in column ozone and hence a decrease in UV radiation, mostly as a result of the formation of nitrogen oxides (NO<sub>x</sub>). Much smaller changes in UV radiation are associated with contrails, aerosols and induced cirrus clouds. The erythemat dose rate<sup>1</sup> is expected to decrease due to aircraft operations. The impact of aircraft on the environment cannot however be seen in isolation. Ozone destruction by other causes such as chlorofluorocarbons (CFCs), has been considerable over the past twenty years and globally overshadows the impact of aircraft operations. However, on high density routes aircraft tend to create regional anomalies, which need to be considered in analysing the impact of ozone destruction.

NO<sub>x</sub> production by aircraft is related to combustion temperature and has increased in recent years as engine operating temperatures and pressures have gone up with more fuel-efficient designs. New dual annular staged combustors provide more control over a greater operating range, but are more expensive and suffer from extra weight and complexity (Moxon, 1999).

### A.2.4 Aerosol particles

Engines emit invisible aerosol particles, including soot, metals, sulphuric acid and unburned hydrocarbons (HC). Aerosol production by aircraft is very small compared to surface sources and is predicted to remain a very minor contributor to this form of atmospheric pollution. Aerosol particles stimulate chemical reactions in the atmosphere, absorb or scatter radiation and change cloud properties. They can seed contrails and cirrus clouds and may be a factor in increasing cloud cover; although the chemistry of aerosol production and its interaction with the atmosphere is little understood (IPCC, 1999; Moxon, 1999).

---

<sup>1</sup> Erythemat dose rate: UV irradiance weighted according to how effectively it causes sunburn.



## A.3 CLOUDS AND CONTRAILS

### A.3.1 Clouds

Clouds play a crucial role in the radiative heating and cooling of the earth-atmosphere system. The principle is described by London *et al.* (1991). Most clouds, depending on their physical properties and thickness, significantly reflect incoming short-wave solar radiation; but at the same time clouds (with the exception of thin cirrus) act as highly efficient infrared radiators of energy into space. Thus clouds act to heat and cool the system, and the net effect depends on the cloud properties. The emission of energy into space depends on the cloud-top temperature and this in turn depends on the height of the cloud-top.

Various cloud types thus affect the radiative forcing in different ways depending on their albedos<sup>2</sup> and the temperature of the emitting upper surface. High altitude clouds generally have low albedos and can be described as efficient "greenhouse" clouds. Low clouds have moderately high albedos and warm cloud-top temperatures, thus resulting in a significant cooling of the earth-atmosphere system. Clouds of large vertical extent have very high albedos, but also have a colder top temperature and thus tend to maintain "an approximate balance between net short-wave incoming and infrared outgoing radiation" (London *et al.*, 1991).

### A.3.2 Contrail formation

A major environmental concern is the formation of contrails and cirrus clouds. Contrails are triggered by emitted water vapour and particles in the engine exhaust plume. There is also strong evidence that the mere passage of an aircraft through a supercooled water cloud can alter cloud composition through the production of ice particles (Sasson, 1991). In 1992 contrails were estimated to cover about 0.1% of the Earth's surface on an averaged basis, with larger regional values associated with the popular air routes (Fig. A-1). Although contrail formation is extremely small compared to natural cloud formation, there is concern that contrails may have a disproportionate effect on global warming.

Contrails often occur in clusters in geographical regions that are cold and humid and have a substantial amount of air traffic, such as central Europe. Depending on the temperature and humidity conditions, contrails may dissipate rapidly or they may last for several hours, widening and becoming indistinguishable from cirrus clouds covering thousands of square kilometres. Furthermore, there is evidence that aircraft operations may perturb natural cirrus, through the addition of water vapour, solid emissions and turbulence (IPCC, 1999).

The increase in persistent contrail coverage on popular airline routes is evident by comparing the coverage for 1992 with the predicted coverage for 2050, as shown in

---

<sup>2</sup> Albedos: Fraction of the incoming solar energy reflected.



Fig. A-1 (from IPCC, 1999). The predicted distribution for 2050 is based on projected fuel usage and projected improvement in engine efficiency. The maximum contrail coverage is expected to occur over Europe (four times more than in 1992) and over the USA (2.6 times more). This increase in contrail coverage will have a direct impact on radiative forcing<sup>3</sup>, which will cause a global increase in temperature.

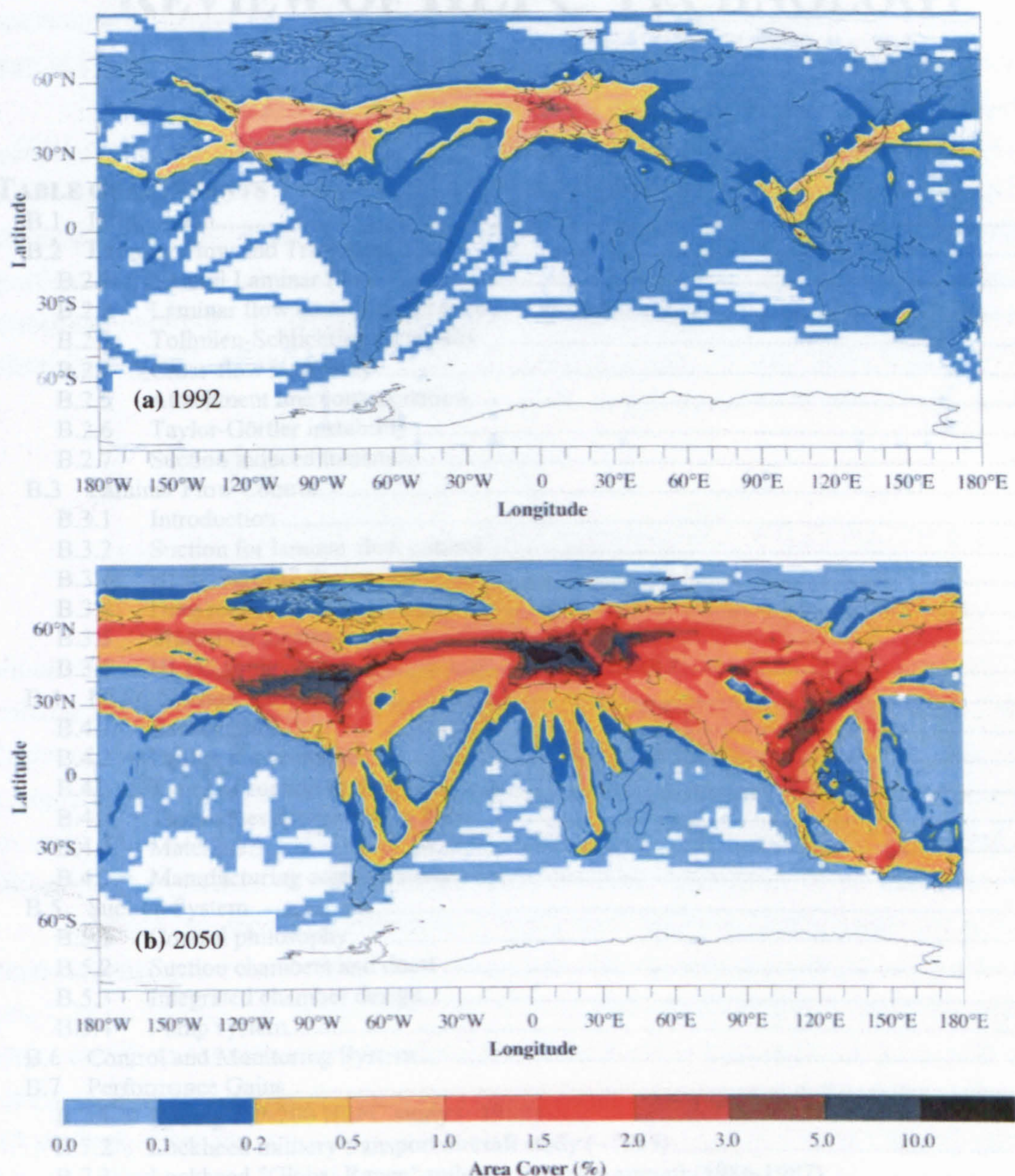


**Fig. A-1** Persistent contrail coverage (in % area cover) for: (a) 1992 and (b) 2050, based on projected fuel usage and improvements in engine efficiency (IPCC, 1999)

<sup>3</sup> Radiative forcing: A change in the balance between incoming solar radiation and outgoing infrared radiation. Used as a measure of the greenhouse effect.



Blank page



# APPENDIX B

## REVIEW OF HLFC TECHNOLOGY

### TABLE OF CONTENTS

B.1	Introduction.....	178
B.2	Laminar Flow and Transition.....	178
B.2.1	Natural Laminar Flow .....	178
B.2.2	Laminar flow control on jet transport aircraft .....	178
B.2.3	Tollmien-Schlichting instability .....	179
B.2.4	Cross-flow instability .....	179
B.2.5	Attachment line contamination.....	180
B.2.6	Taylor-Görtler instability.....	181
B.2.7	Suction induced transition .....	182
B.3	Laminar Flow Control.....	182
B.3.1	Introduction .....	182
B.3.2	Suction for laminar flow control .....	183
B.3.3	HLFC aerofoil design.....	183
B.3.4	Drag reduction.....	184
B.3.5	Transition location.....	186
B.3.6	HLFC application .....	187
B.4	HLFC Suction Surfaces .....	188
B.4.1	Introduction .....	188
B.4.2	Design requirements.....	188
B.4.3	Types of suction surfaces .....	191
B.4.4	Techniques for producing holes .....	191
B.4.6	Materials.....	194
B.4.7	Manufacturing considerations .....	196
B.5	Suction System.....	198
B.5.1	Control philosophy .....	198
B.5.2	Suction chambers and ducts .....	199
B.5.3	Integrated chamber design.....	199
B.5.4	Pump system.....	200
B.6	Control and Monitoring System.....	201
B.7	Performance Gains.....	201
B.7.1	Boeing 757-200 HLFC study (~1982).....	201
B.7.2	Lockheed military transport aircraft study (~1985).....	202
B.7.3	Lockheed "Global Range" military transport aircraft (1986-1987).....	202
B.7.4	Boeing 757 flight tests (1987 - 1991).....	203
B.7.5	GE / Rohr / AlliedSignal / NASA HLF nacelle (1991 - 1992).....	203
B.7.6	RR / DLR laminar flow nacelle (1990 - 1993).....	203
B.7.7	NASA 300 passenger long-range twin-engine HLFC study (1991).....	203
B.7.8	HLFC study on A320 and A340 classes of aircraft (1992) .....	204
B.7.9	Wilson (Cranfield University) HLFC study (~1997) .....	204
B.7.10	Airbus long-range aircraft estimate .....	205
B.7.11	Airbus HLFC fin .....	205



## B.1 INTRODUCTION

The purpose of this appendix is to provide an overview of Hybrid Laminar Flow Control technology, its theoretical basis, complexities and potential. A substantial literature exists on the subject, and reference is made to a number of publications relevant to the work herein reported. For a broader overview of the subject, the following sources may be consulted:

- (1) *Research in Natural Laminar Flow and Laminar-Flow Control* Symposium, Virginia, March 1987; proceedings published as NASA CP-2487, Hefner, J.N. and Sabo, F.E. (Ed.)
- (2) *The First European Forum on Laminar Flow Technology*, Hamburg, March 1992.
- (3) *The Second European Forum on Laminar Flow Technology*, Bordeaux, June 1996.
- (4) *Overview of Laminar Flow Control*, Joslin, R.D., NASA TP-1998-208705, October 1998.
- (5) *The CEAS / DragNet European Drag Reduction Conference*, Potsdam, Germany, 19-21 June 2000; proceedings published as *Notes on Numerical Fluid Mechanics*, Vol. 76, Thiede, P. (Ed.), Springer, 2001.

## B.2 LAMINAR FLOW AND TRANSITION

### B.2.1 Natural Laminar Flow

Natural Laminar Flow (NLF) results “naturally” from a correct aerodynamic profile. A favourable pressure gradient (i.e. reducing pressure) is created by the aerofoil shape, reducing boundary layer instabilities and delaying the point at which disturbances will cause transition. NLF aerofoils achieve laminar flow by having a sharp leading edge, followed by a gradual increase in thickness; thus the NLF pressure distribution has no leading edge suction peak found on most modern aerofoils, but rather a progressive reduction in pressure of up to approximately 50% of the chord.

Practical NLF wings have been designed for small to moderate size aircraft, without significant leading edge sweep. The 3D flow fields associated with highly swept wings of jet transport aircraft are vulnerable to Cross-flow Instabilities (see section B.2.4). A NLF aerofoil on a highly swept wing will thus become turbulent near to the leading edge.

A review of NLF theory and research programmes is presented by Holmes and Obara (1992), Wagner *et al.* (1992), Dziomba (1993) and Joslin (1998a).

### B.2.2 Laminar flow control on jet transport aircraft

Laminar flow control has been considered for the wing, horizontal tailplane, fin and engine nacelles of jet transport aircraft. The flow over three of these surfaces – the wing, horizontal tailplane and fin – is a complex 3D flowfield, which is significantly influenced by leading edge sweep. The engine nacelle is different, as there is essentially



no sweep on the nose section. The laminar to turbulent flow transition mechanisms which exist due to sweepback are thus not present on the nacelle.

For the 3D flow on the upper surface of a swept wing or empennage, there are three flow mechanisms which need to be controlled to prevent transition: Tollmien-Schlichting instability, Cross-flow instability and Attachment Line Contamination. A brief discussion of these laminar to turbulent transition mechanisms follows.

### B.2.3 Tollmien-Schlichting instability

Two-dimensional sinusoidal waves, called Tollmien-Schlichting (TS) waves, propagate within a laminar boundary layer (Fig. B-1). These waves may be gradually amplified or damped out as they travel downstream. The location of transition is dependent on the flow Reynolds number, pressure distribution and the presence of surface roughness elements. If a critical flow parameter like Reynolds number is exceeded, the waves will grow in strength, resulting in transition leading to turbulent flow (Joslin, 1998a).

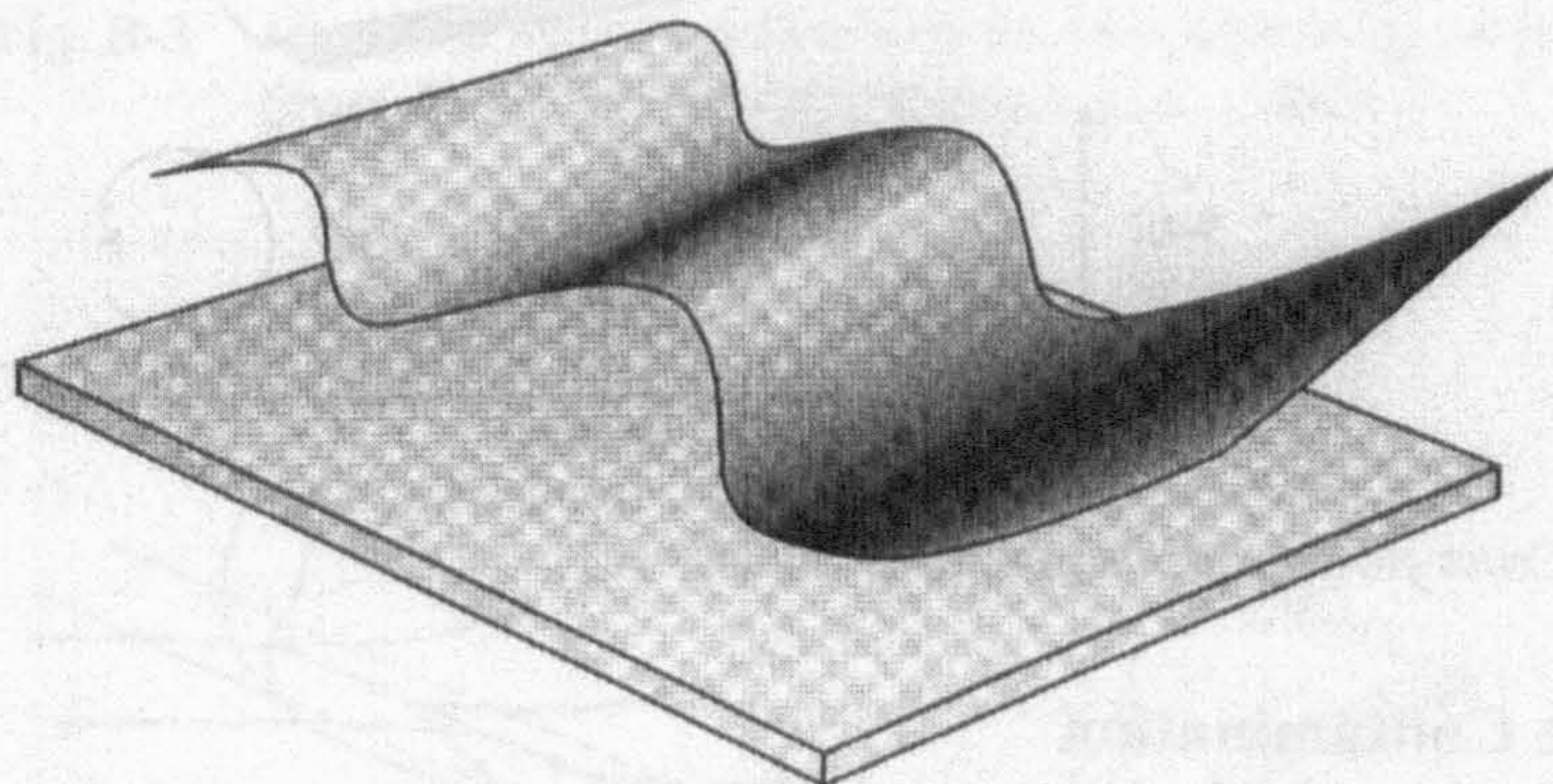


**Fig. B-1** Sketch of Tollmien-Schlichting waves (Joslin, 1998a)

### B.2.4 Cross-flow instability

In regions close to the leading edge of an infinite swept wing, the chordwise velocity component changes rapidly, while the spanwise component is essentially constant. Hence the streamlines are curved. The streamline curvature causes an imbalance between the pressure forces and centrifugal forces within the boundary layer, which in turn creates a boundary layer velocity distribution normal to the local external streamline. This has a point of inflection, which makes the profile intrinsically unstable (Joslin, 1998a). Cross-flow (CF) disturbances are characterised by co-rotating vortices, as shown in Fig. B-2.

The point of transition depends significantly on the airspeed, the sweep angle and the leading edge radius (Joslin, 1998a). For a given sweep angle, laminar flow is lost when the speed is increased to the critical value. The transition Reynolds number is dependent on the wing sweep, i.e. the transition point will move forward on the wing with an increase in wing sweep. This relationship is shown in Fig. B-3, which contains flight and wind tunnel data, collated by Wagner *et al.* (1992).



Cross-flow (CF) instability is a major concern for high Reynolds number flow over swept wing surfaces. Joslin (1998a) notes that "for a wing swept greater than  $30^\circ$ , CF disturbances dominate, amplify, and cause transition – often very near the leading edge of the wing". It is described as the predominant transition mechanism in the forward 5 - 10% of the chord, where the magnitude of spanwise flow is at its greatest (Poll and Danks, 1994).

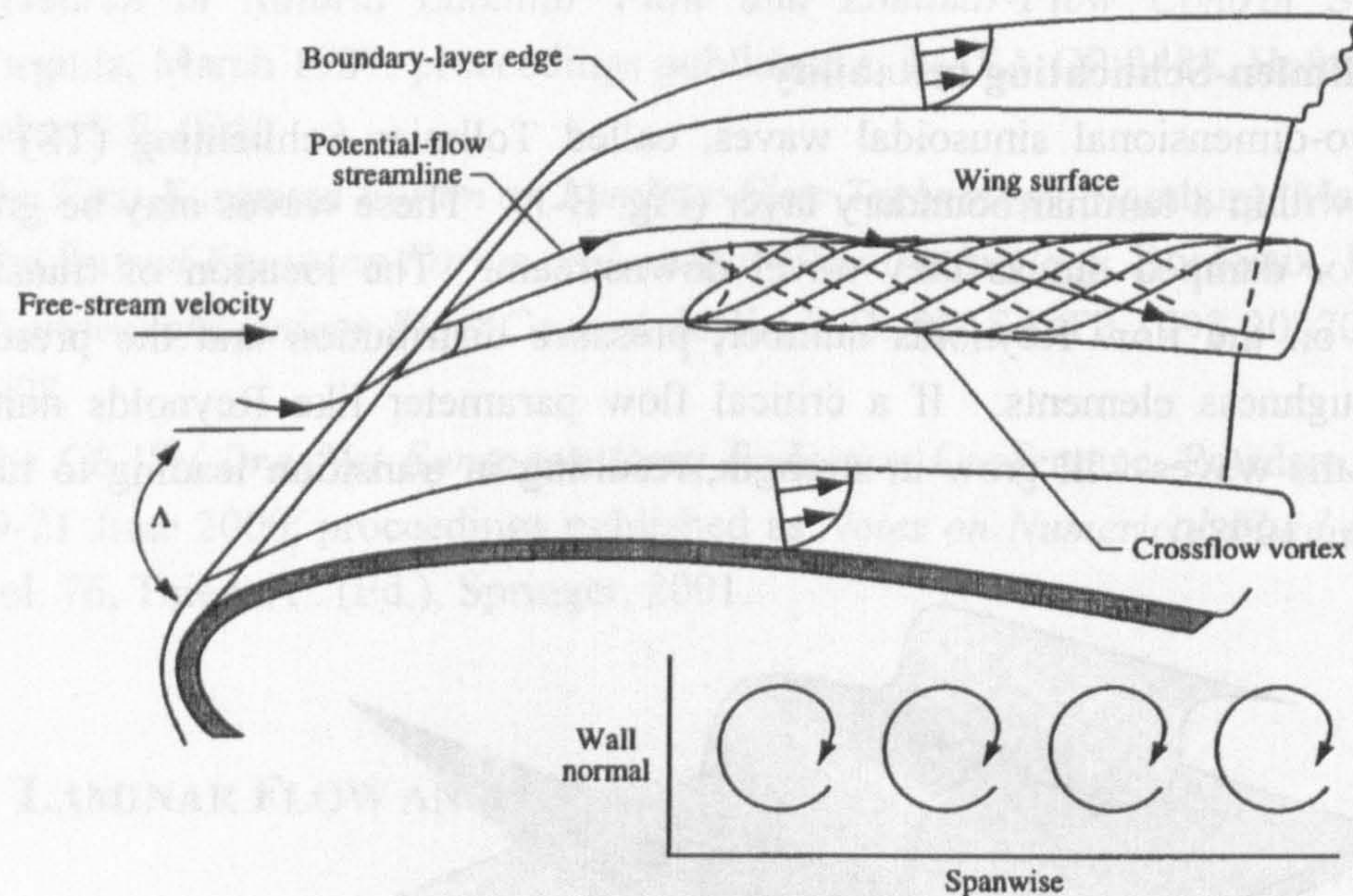


**Fig. B-2** Sketch of Cross-flow instability (Joslin, 1998a)

### B.2.5 Attachment Line Contamination

Laminar flow can only be obtained downstream of a laminar attachment line<sup>1</sup>. Thus, if transition were to occur at a point on the wing attachment line, the entire outboard portion of the wing would have turbulent flow. This can be instigated by the turbulent boundary layer on the fuselage, causing the local flow on the leading edge of the wing or empennage to become turbulent. Attachment Line Contamination is the phenomenon by which turbulent air at the wing root is propagated along the attachment line, causing flow over the whole of the wing to be turbulent (Fig. B-4).

The complete avoidance of Attachment Line Contamination is vital to achieve laminar flow on a swept wing. Maddalon and Braslow (1990) and Reneaux *et al.* (1996) report on alternative techniques that may be employed to delay the onset of Attachment Line Contamination. These include suction being applied at the leading edge, a sharp edge notch or a turbulence diverter on the attachment line. The latter concept – proposed by Gaster (1965) and commonly referred to as a Gaster bump – functions by stopping the propagation of the turbulence on the leading edge, which then allows a new laminar boundary layer to develop downstream (Fig. B-5). The

<sup>1</sup> Attachment line: The particular streamline which separates the flow over the upper and lower surfaces of the wing.



application of suction to prevent Attachment Line Contamination has been shown to work experimentally, as reported by Poll and Danks (1994), Juillen and Arnal (1994) and by Reneaux (1996).

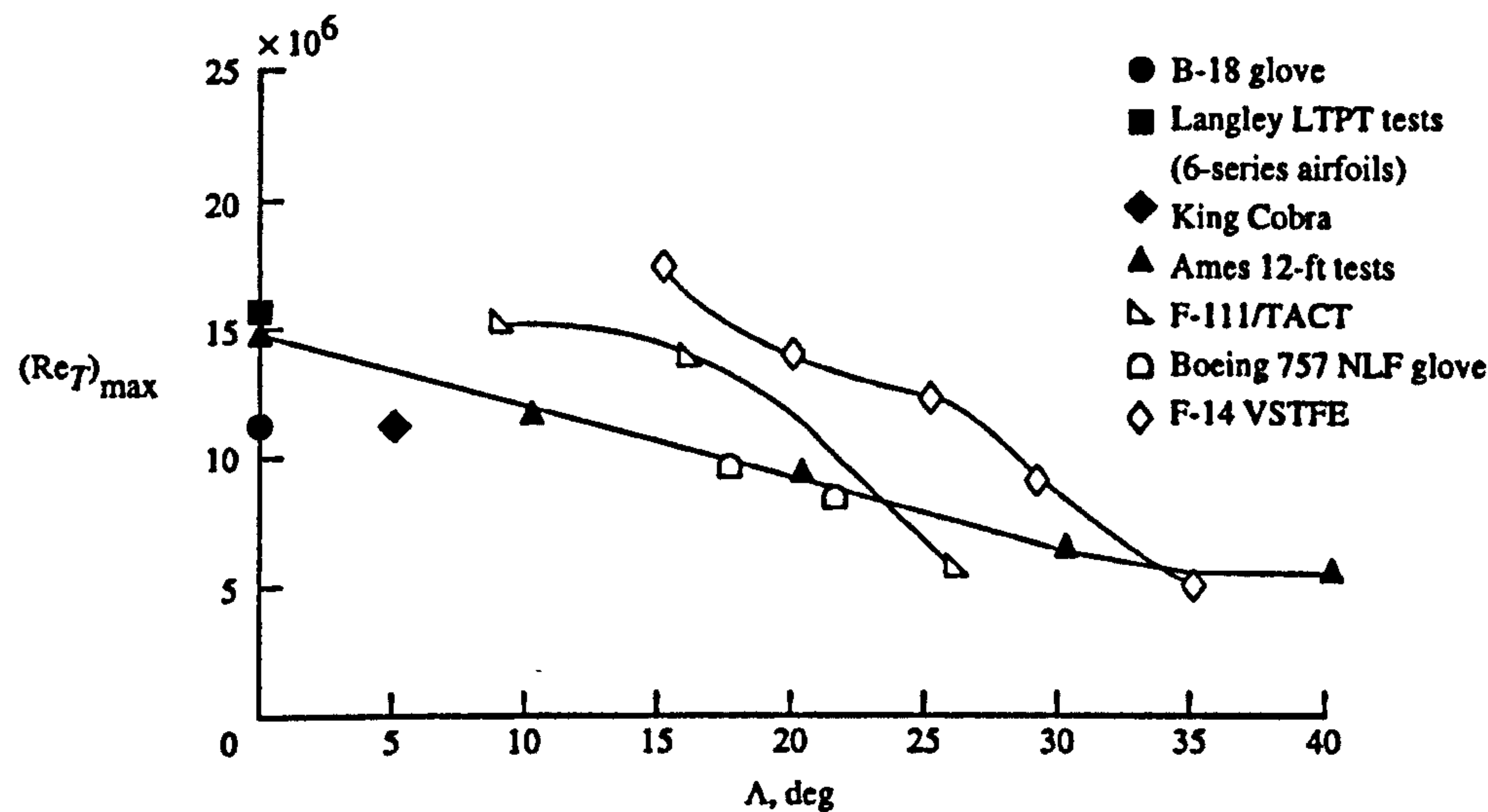


Fig. B-3 Maximum transition Reynolds number with wing sweep (from Joslin, 1998a; after Wagner et al., 1992)

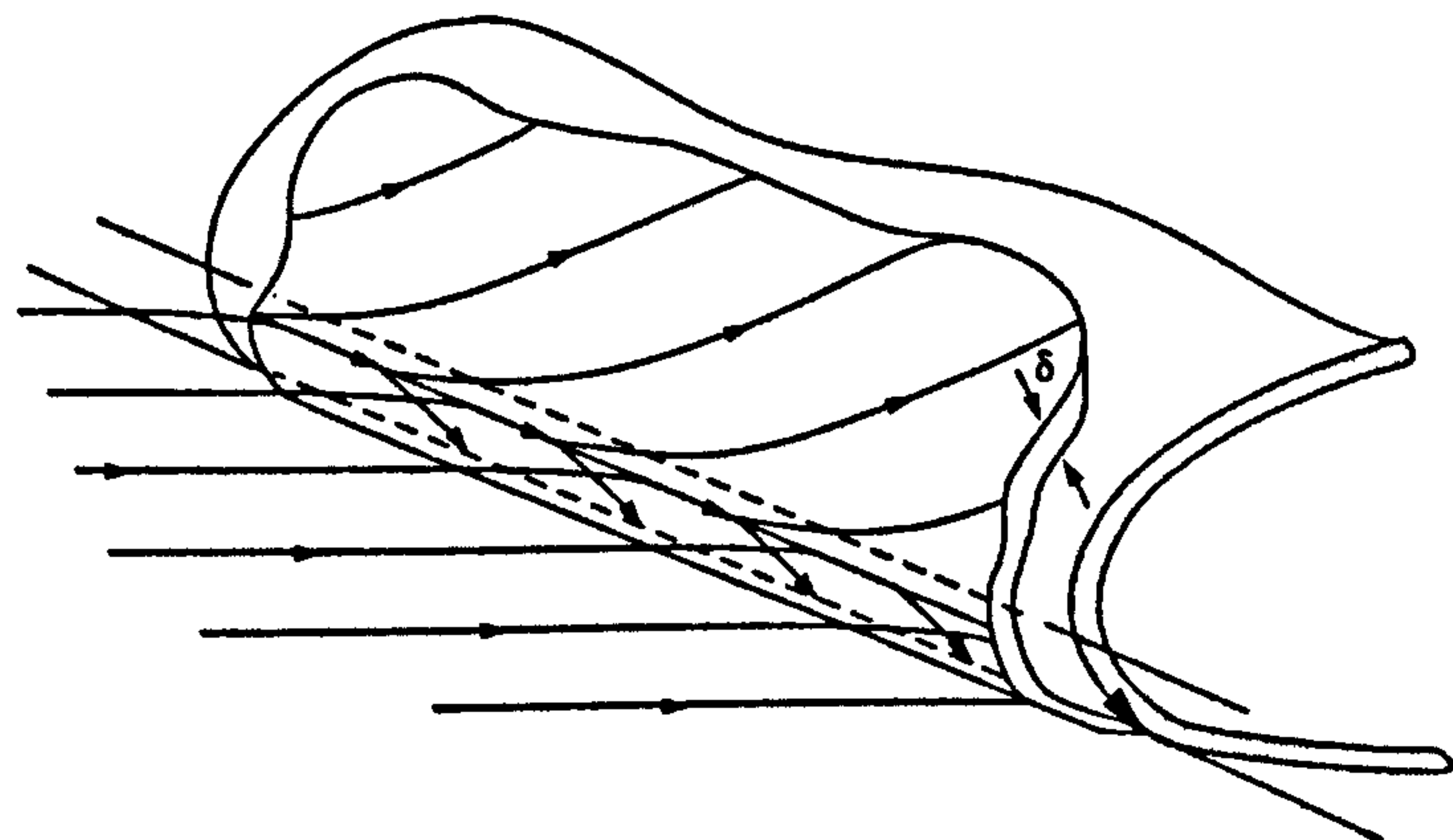


Fig. B-4 Sketch illustrating Attachment Line Contamination on a swept wing leading edge (from Joslin, 1998a; after Wentz et al., 1985)

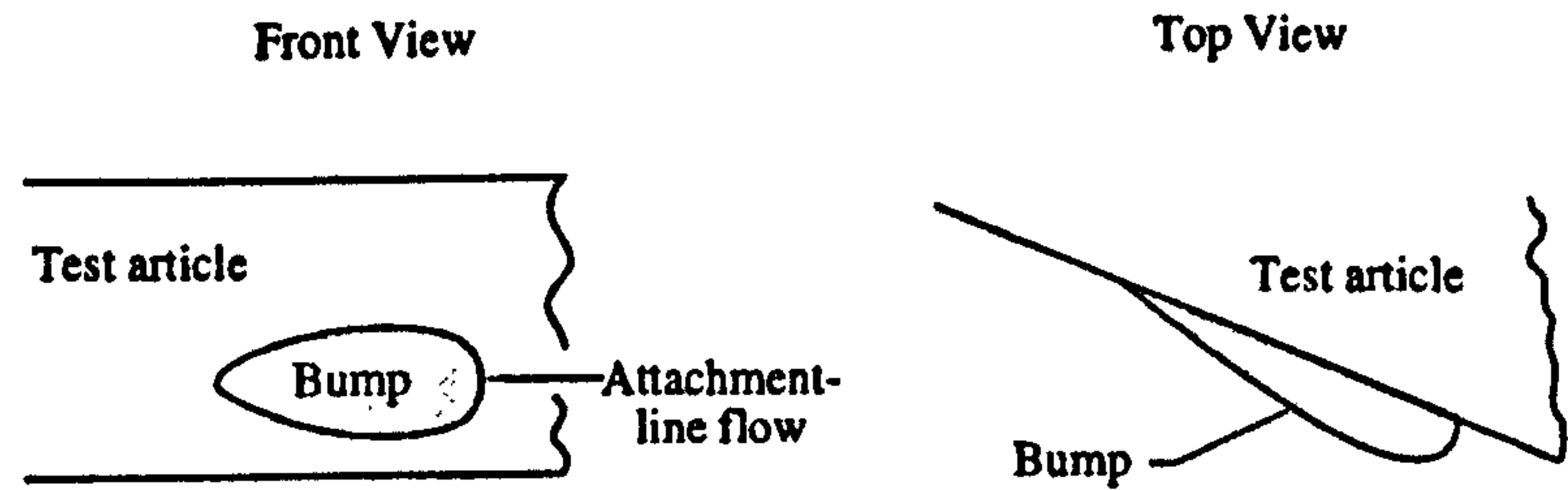


Fig. B-5 Sketch of Gaster bump (based on Maddalon and Braslow, 1990)

**B.2.6 Taylor-Görtler instability**

The Taylor-Görtler (TG) instability (Fig. B-6) is described as a centrifugal instability that occurs in viscous flows over concave surfaces (Boeing, 1982). If the



lower surface of the wing was considered for HLFC, then this instability would be of concern; however, for the upper wing section, nacelle and empennage, this flow instability mechanism does not arise, as the surfaces are not concave.

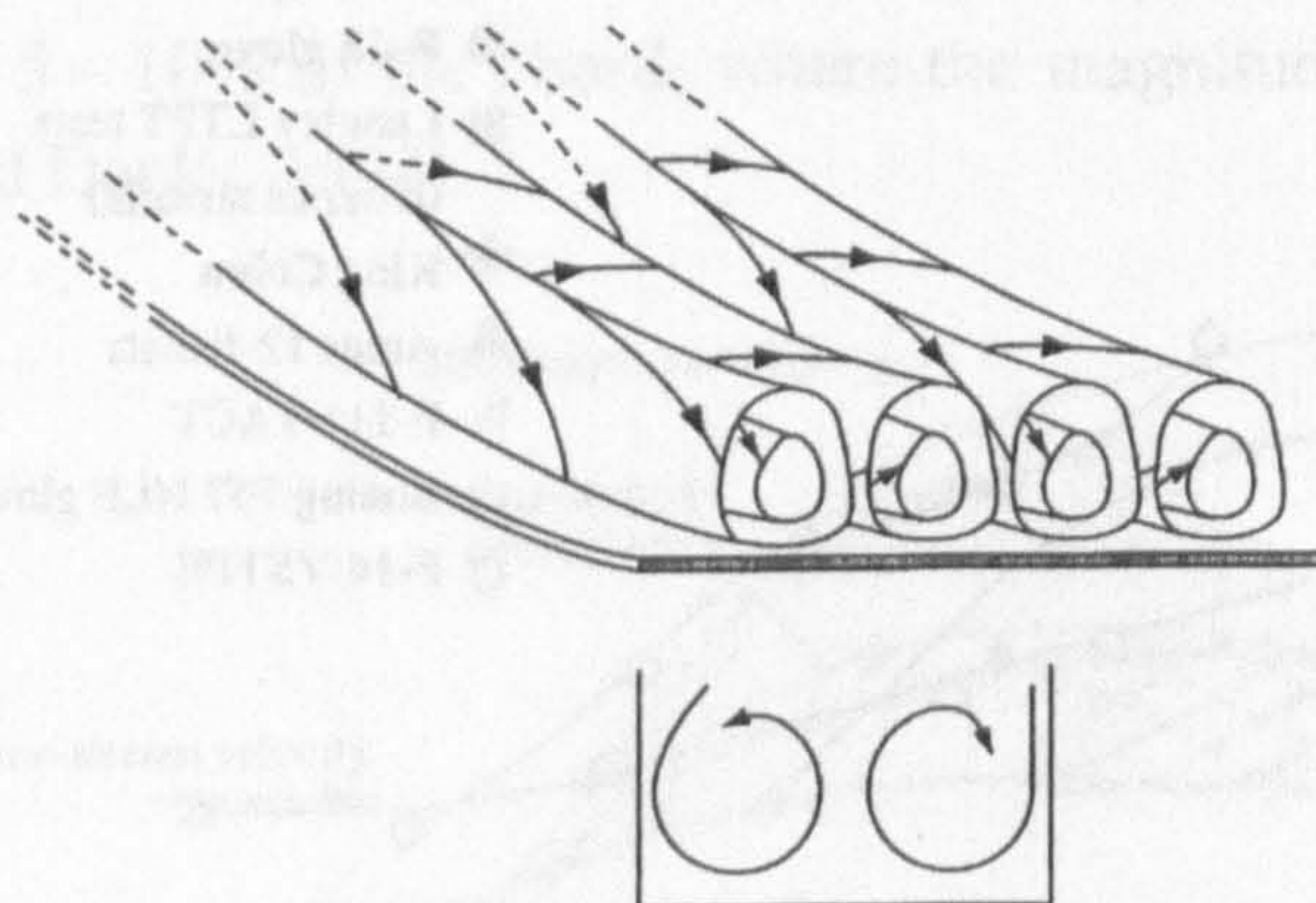


**Fig. B-6** Sketch of Taylor-Görtler instability (Joslin, 1998a)

### B.2.7 Suction induced transition

HLFC involves the sucking of a small amount of air from within the boundary layer through a porous or perforated skin surface, to suppress the boundary layer instabilities. A small increase in the suction beyond that which is required to stabilise the boundary layer, tends to have little impact on the flow; however, a substantial increase in the suction (i.e. over-suction) may result in a disturbance in the flow and cause transition. Recent experimental work into over-suction was reported by Reneaux and Blanchard (1992) and by Ellis and Poll (1996).

## B.3 LAMINAR FLOW CONTROL

### B.3.1 Introduction

Joslin (1998a; 1998b) described Laminar Flow Control (LFC) as “an active boundary layer control technique employed to maintain the laminar state at chord Reynolds numbers beyond that which is normally characterised as being transitional or turbulent in the absence of control”. Stabilisation of the boundary layer, to delay transition, can be achieved by a number of principles, including suction, blowing, thermal and the use of Micro Electro Mechanical Systems (MEMS). Of these LFC concepts, the one which has received greatest attention by researchers, is suction. The removal of a small amount of the air – from within the boundary layer, through the skin, via slots or through a porous / perforated surface – can suppress all instabilities and maintain a laminar flow for extended distances over a wing section (Fig. B-7). This may be achieved on highly swept wings and also in the presence of an unfavourable pressure gradient.



### B.3.2 Suction for laminar flow control

The required flow rate through the porous or perforated surface is a function of the predominant instability at that part on the wing. Generally, low suction rates are required to suppress TS instabilities, while higher rates are required to suppress CF instabilities and Attachment Line Contamination. Details of the impact of suction on delaying transition are provided by: Pfenninger and Reed (1966), Pfenninger (1977), Poll *et al.* (1992a), Arnal (1992), Ellis and Poll (1996), Hansen (1996), Bokser *et al.*, (1998), for example. Suction has also been shown to relaminarise the flow following a disturbance (Henke *et al.*, 1993; Poll and Danks, 1994). The degree to which this may be achieved depends on the state of the boundary layer at the point of transition and the size of the disturbance. Researchers would however, regard this as a different flow physics phenomena to LFC, which essentially maintains a laminar boundary layer (Joslin, 1998a).

The design implications of installing a suction system over the entire wing surface are considerable. It imposes significant design penalties in terms of structural and systems weight increases and results in reduced space in the wing for the housing of fuel.

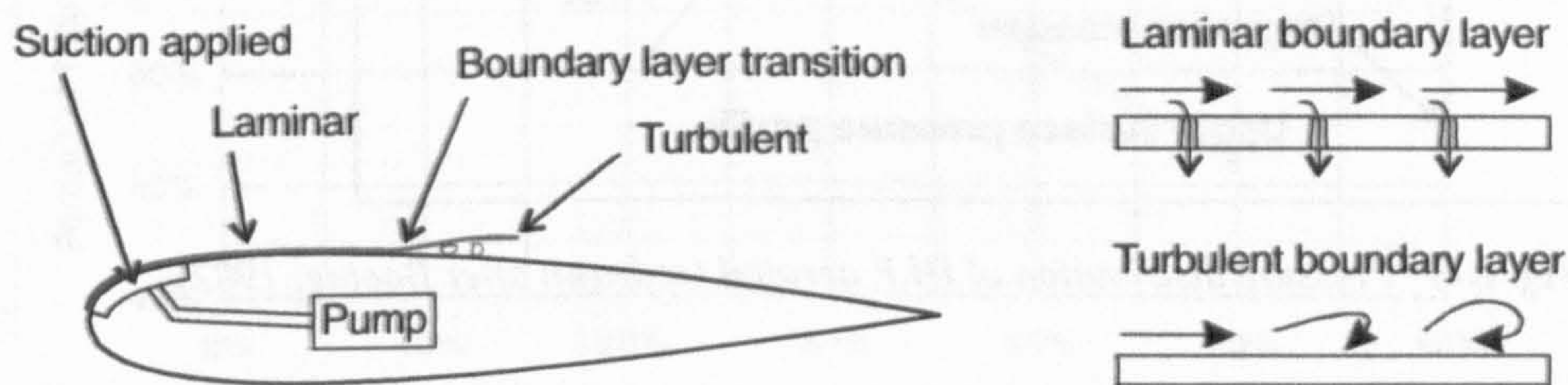


Fig. B-7 Principle of sucking the boundary layer to achieve laminar flow

### B.3.3 HLFC aerofoil design

A comparison of the pressure distributions of a NLF aerofoil, a LFC aerofoil and a HLFC aerofoil is given in Fig. 2-1. Hybrid Laminar Flow Control (HLFC) involves suction being applied to the leading 10 to 20% of the chord (i.e. ahead of the front spar) to suppress the boundary layer instabilities. The substantial pressure gradient in this region combines with the leading edge sweep to produce boundary layer cross-flow, which tend to amplify disturbances and promote transition. The fundamental strategy of HLFC is "to confine the unavoidable large negative gradients to the region ahead of the front spar and to use boundary layer suction to suppress disturbance amplification due to cross-flow here" (Boeing, 1982). Aft of the suction area, a correctly profiled aerofoil will produce a modest favourable pressure gradient (i.e. a falling pressure), which will tend to suppress the TS instabilities, ensuring extended laminar flow along the chord (Fig. B-8). The falling pressure is associated with an increase in local flow velocity, which can be expected to reach sonic speeds on the wing of a modern airliner. The compressibility effects on a HLFC wing must be modest, to ensure that the resulting weak shocks do not cause separation of the laminar boundary layer. Transition is



delayed and can be expected to occur early in the pressure recovery region, which would typically be located at 50 - 60% of the chord.

The pressure level on the lower surface is determined "by the desired lift coefficient and airfoil thickness ratio" (Boeing, 1982). The flow will normally be subsonic. Laminar flow can similarly be achieved on the lower surface up to the region of adverse pressure gradient. Practical design problems, which are discussed later, mean that it is unlikely that laminar flow on the lower wing surface will be realised.

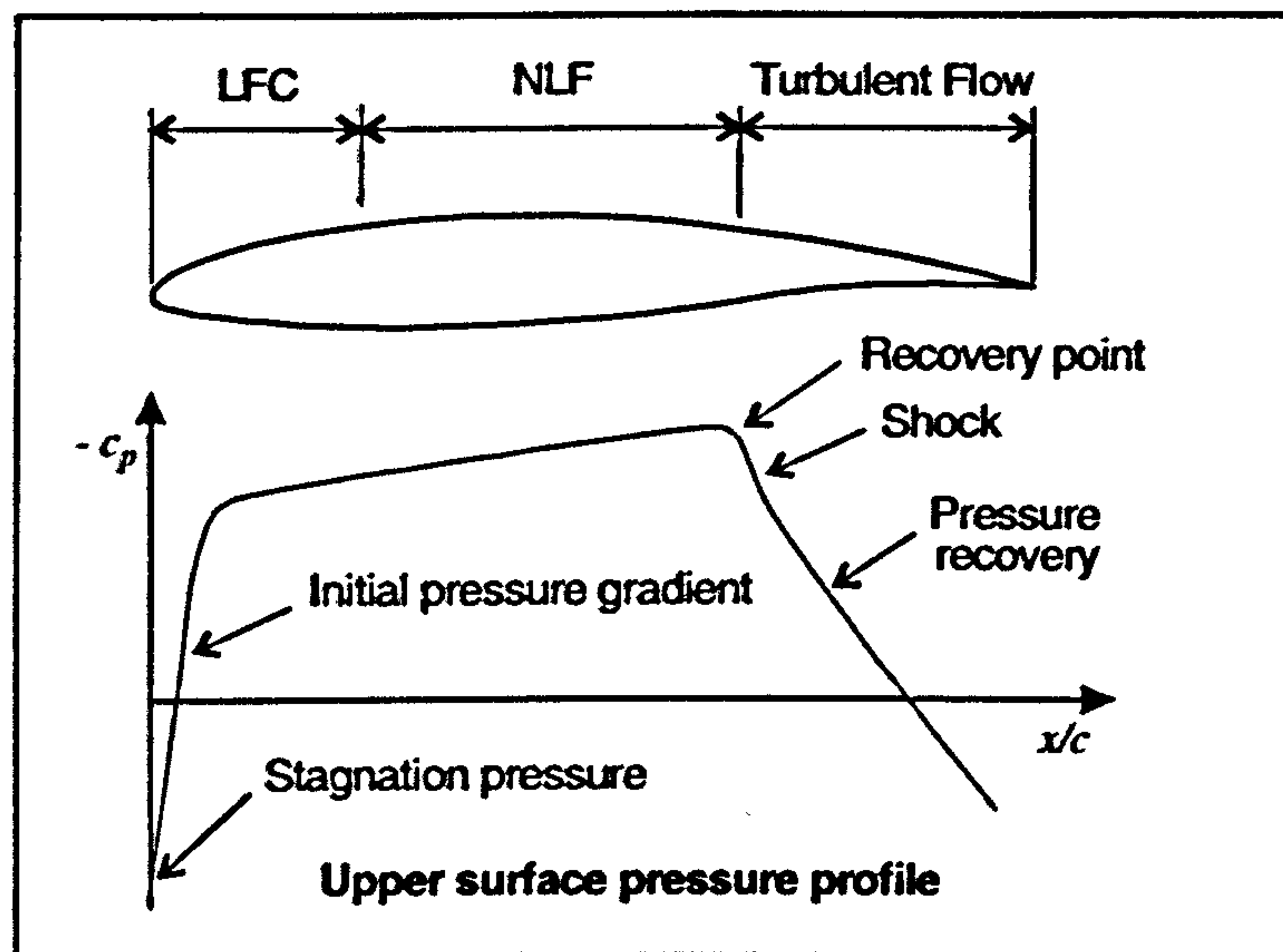


Fig. B-8 Pressure distribution of HLF aerofoil (redrawn after Boeing, 1982)

### B.3.4 Drag reduction

The introduction of suction stabilised laminar flow control "can be said to have only a secondary effect on the lift-dependent drag" (Sawyers and Wilson, 1996). However, current wing sections represent a highly-optimised design from the point of wave drag. Changes to the shape, to ensure long runs of laminar flow, can increase the wave drag. This penalty increases as the region of laminar flow extends further downstream. Research conducted by BAe Airbus (Sawyers and Wilson, 1996), indicated that HLFC aerofoils for new designs can be produced such that the wave drag penalty is avoided, but can still maintain the desired pressure gradients to achieve "an acceptable level of laminar flow". Atkins and Courteney (2002) considered wing modifications as part of a HLFC retrofit design for the A310 aeroplane. Their "baseline" design ensured laminar flow on the upper wing surface to 29 - 34% of the chord. Further studies considered a reduced nose thickness, reduced sweep, and a negative trailing edge flap. The modifications would all contribute to a greater extent of laminar flow, but would also induce a wave drag penalty, reducing the net drag benefit.

A standard method for estimating the  $C_{do}$  (zero lift drag coefficient) for a wing section is to scale the skin friction drag of a fully turbulent flat plate with a zero pressure gradient ( $C_F$ ) by a form factor; which depends on the section geometry of the



wing. A study conducted by Sawyers and Wilson (1996), utilising a BAe Airbus 2D Euler solver, coupled with a semi-inverse strip boundary layer method, investigated the variation of both  $C_F$  and lift-independent profile drag with transition location, for a series of infinite swept aerofoils. It was assumed that the attachment line was kept laminar across the wing span in order for the boundary layer in the chordwise direction to be laminar at the leading edge. Fig. B-9 is a result of this study. It indicates the variation of  $C_{do}$  as a percentage of the datum turbulent drag level for a given aerofoil section, calculated with form factors, that varied to account for the transition location. It is seen that for transition at 50% of the chord on both upper and lower surfaces, for example, the sectional drag coefficient of the HLFC wing section is ~52% of that of the fully turbulent wing.

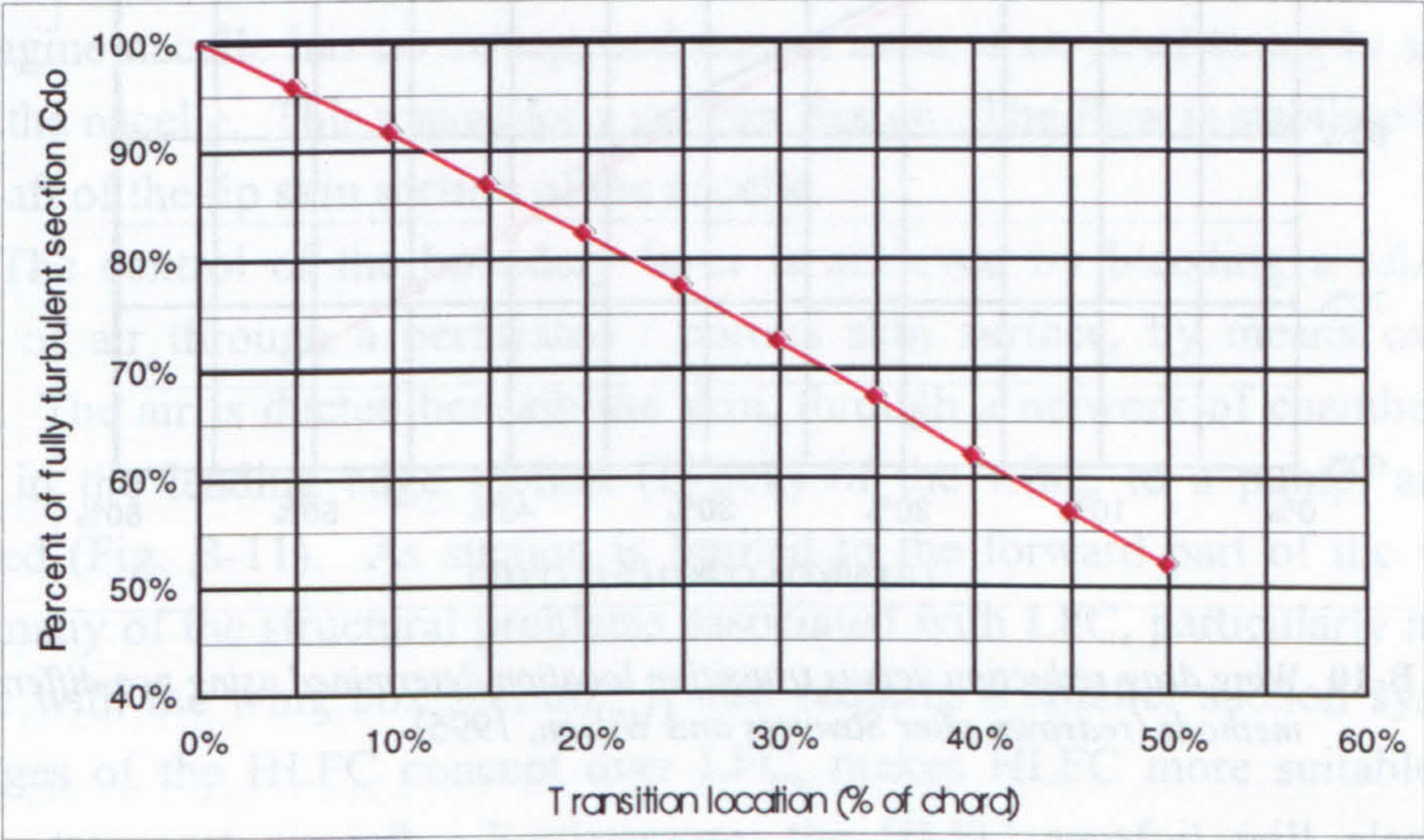


**Fig. B-9** Section drag reduction (upper and lower surface) with transition location (redrawn after Sawyers and Wilson, 1996)

Recent thinking is that it is highly unlikely that the lower surface on an actual wing, can be designed to be laminar, due largely to difficulties associated with the high lift devices and anti-contamination systems (Sawyers and Wilson, 1996; Robert, 1992). This is particularly true for a design that makes use of a Krüger flap. The relative proportions of  $C_{do}$  on the upper and lower surfaces, is thus of interest. Sawyers and Wilson (1996) determined this using the BAe 2D Euler solver code. It was found that at cruise  $C_L$  values, the upper surface profile drag is approximately twice that of the lower surface. This correlates very well with results determined by Boeing for the HLFC B757 study (Boeing, 1982) for the outer wing section. For the wing panel inboard of the wing "crank", the lower wing surface accounts for a larger portion of the section drag. At the body / wing interface, the ratio of the upper surface section drag to the total section drag was ~0.60. This increased to ~0.67 at the 40% semi-span position, which is the location of the wing "crank", and was seen to be approximately constant from this point outwards.



Sawyers and Wilson (1996) made the assumption that the one-third / two-thirds division in section  $C_{do}$  did not vary across the wingspan. Furthermore, they assumed that the spanwise transition location was constant. This enabled the variation in profile drag coefficient for a Large Subsonic Aircraft wing to be determined using two alternative methods. The results reported by Sawyers and Wilson (1996) indicate a good correlation between the methods (Fig. B-10). It was stated that with transition at the 50% chordwise position, there was a 32.7% reduction in wing  $C_{D_o}$ .

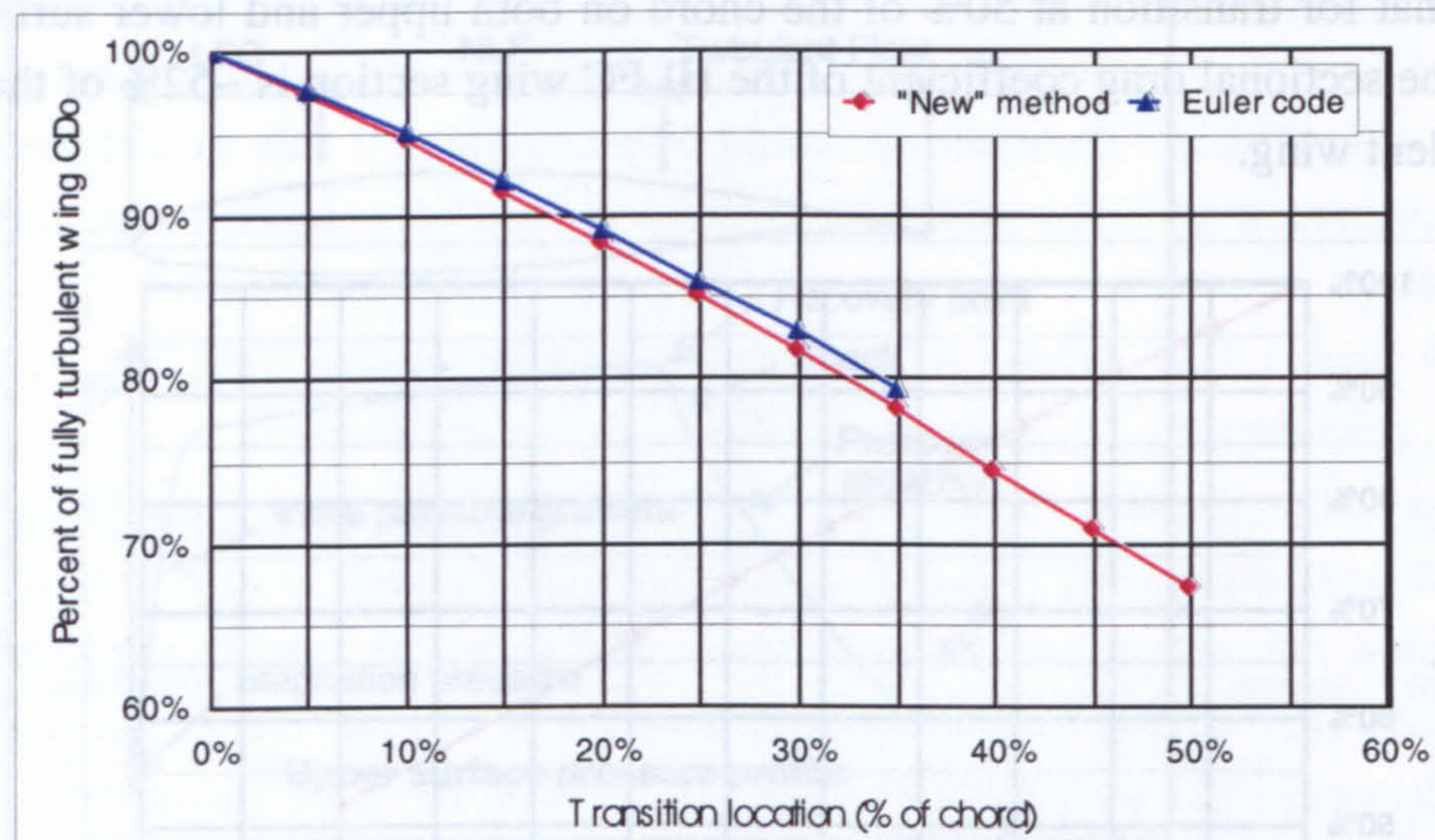


**Fig. B-10** Wing drag reduction versus transition location determined using two different methods (redrawn after Sawyers and Wilson, 1996)

### B.3.5 Transition location

The transition location is dependent on the flight Reynolds number and suction distribution. The further aft the transition, the greater will be the drag reduction. The standard tool for the analysis of the flow behaviour over Hybrid Laminar Flow surfaces, considered for transport aircraft, is the  $e^N$  method. The method is described by Schrauf and Horstmann (2000): "It is based on the computation of growth rates of wave-like disturbances in the boundary layer using linear stability theory. Transition is assumed to take place where the most unstable disturbances are amplified by a factor  $e^N$ , with  $N$  determined by correlations with experiments." In two-dimensional flow the amplification rate is characterised by the stability frequency. However, in three-dimensional compressible flow an additional parameter is required, details of which are given by Arnal (1994). The  $e^N$  method has been widely used for the prediction of CF and TS instabilities for HLFC designs (for example: Schrauf *et al.*, 1992; 1996; Atkin, 2000; Schrauf and Horstmann, 2000).

For conceptual design studies it must be possible to determine the transition location without having to perform complex stability analyses. The simplest way to define the point of transition is to assume that it occurs at the same chordwise location



across the wingspan. The point must be selected ahead of any shock location, which is the effective aft limit of transition location. The assumption of constant chord position is however unrealistic, as it ignores the effect of Reynolds number changes across the wingspan. Project studies performed at Cranfield University have used the concept of a transition Reynolds number to estimate the transition location (Wilson and Jones, 1995; Wilson, 1997). For a given suction distribution, this approach permitted the transition location to vary across the span.

### **B.3.6 HLFC application**

The principle of HLFC can be applied to the wing, empennage and engine nacelle. The prevention of Cross-flow instability and Attachment Line Contamination requires that suction be applied to the leading edge of the wing or tail. However, the lip of an engine nacelle has no sweep, and hence, there is no need to apply suction at the nose of the nacelle. This makes for a simpler design. The flow is stabilised by applying suction aft of the lip skin section of the nacelle.

The control of the boundary layer is achieved by bleeding a relatively small amount of air through a perforated / porous skin surface, by means of mechanical suction. The air is ducted beneath the skin, through a network of chambers and pipes located in the leading edge section (D-box) of the wing, to a pump, and is finally exhausted (Fig. B-11). As suction is limited to the forward part of the wing, HLFC avoids many of the structural problems associated with LFC, particularly as it does not interfere with the wing box section. It also requires a smaller suction system. These advantages of the HLFC concept over LFC, makes HLFC more suitable for use on subsonic transport aircraft. Furthermore, the HLFC aerofoil will also have good aerodynamic performance in the fully turbulent mode, which will not necessarily be the case for a NLF aerofoil.



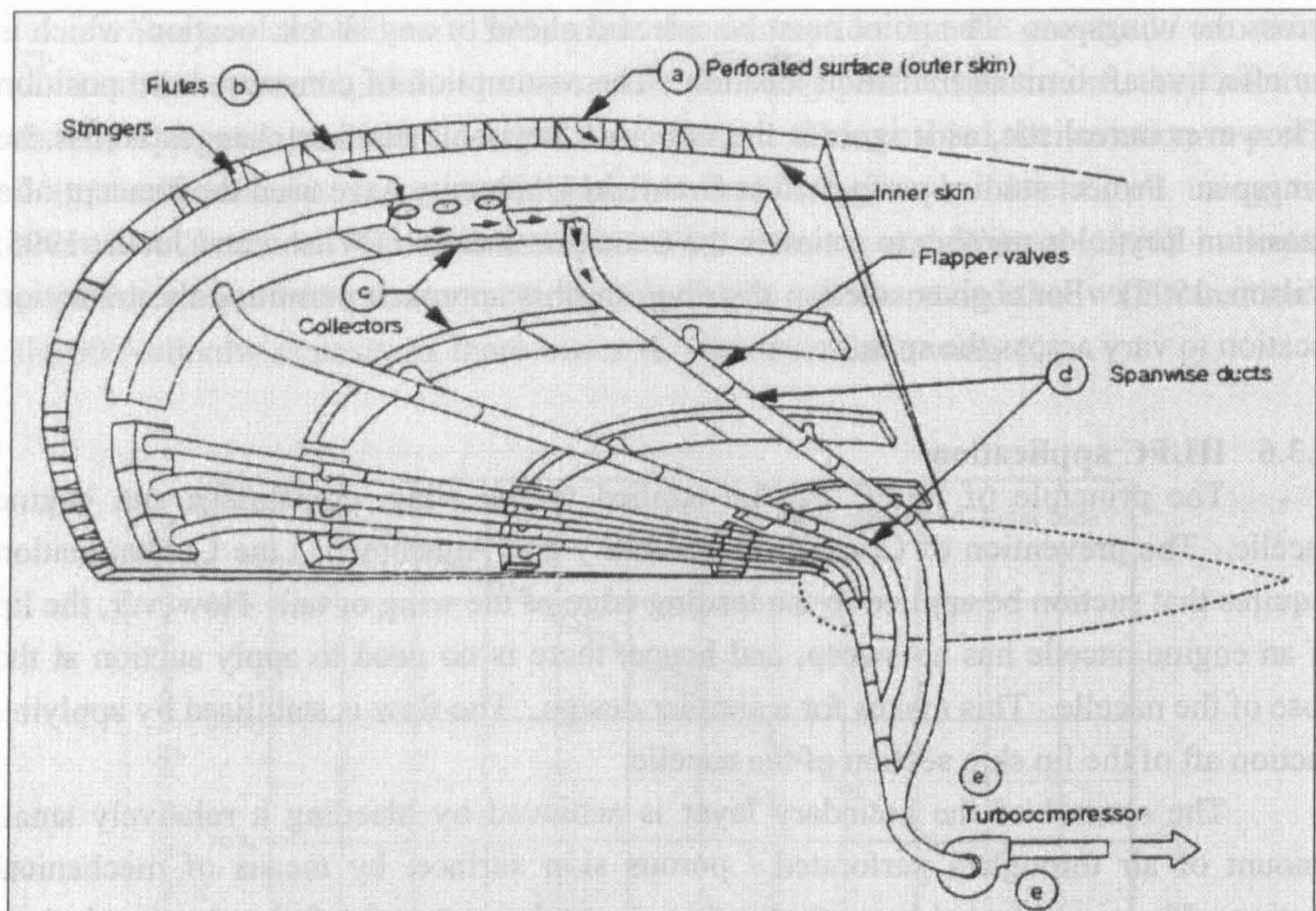


**Fig. B-11** Boeing 757 HLFC system concept (Boeing, 1999a)

## B.4 HLFC SUCTION SURFACES<sup>2</sup>

### B.4.1 Introduction

The design of the suction surface and the chambers underneath the perforated skin represents one of the most significant engineering challenges concerning HLFC. In addition to the manufacturing cost, which must be kept to a minimum, there are a number of specific design requirements that exist for the suction surface. These issues are discussed in this section.

### B.4.2 Design requirements

#### B.4.2.1 Aerodynamic contour

Stringent “mould line” requirements exist in terms of waviness and aerodynamic profile. The surface definition needs to be maintained when subjected to inertia, aerodynamic and suction loads.

<sup>2</sup> A review of suction surface design was presented in *Investigation of Hybrid Laminar Flow Control (HLFC) Surfaces* (Young *et al.*, 2001). Selected parts of this manuscript, relating to research conducted by the author, have been reproduced in this section (B.4). Contributions of the co-authors are cited where appropriate.



#### *B.4.2.2 Suction velocity*

Suction of the boundary layer through discrete holes can create local 3D disturbances in the boundary layer, and for this reason the mean suction flow velocity through the holes needs to be kept below a critical value. If the hole suction velocity exceeds this critical value (for a given hole size), then transition of the boundary layer will occur at the hole position or downstream of it (Priest and Paluch, 1996).

#### *B.4.2.3 Uniformity of hole size and shape*

It is known that inhomogeneities of suction velocity, resulting from non-uniformity of hole size and shape, can impact on the stability of the local boundary layer. Priest and Paluch (1996) report on the importance of uniformity of suction velocity across a HLFC panel; but state that the impact “remains difficult to assess due to lack of experimental data devoted to this subject and the complexity of the aerodynamics of a boundary layer with suction applied through discrete holes”.

#### *B.4.2.4 Mechanical properties*

The HLFC skin surface is a primary structural element. For certification purposes it must be treated as a Class 1 part, i.e. failure and separation of the panel from the wing structure must be prevented (Jagger and Davies, 1996). Satisfactory strength, stiffness and fatigue properties are required. Special considerations for composite materials include the effect of increased moisture absorption into the resin and UV damage (due to the fact that the surface cannot be painted). The skin panel thickness will be determined by considerations of deflection requirements under aerodynamic and suction loading, load transfer in the joints, panel buckling and impact resistance.

#### *B.4.2.5 Damage tolerance*

The most likely causes of in-flight damage are hailstone or bird impact. Ground handling impacts and FOD (Foreign Object Damage) during takeoff and landing, are also of concern. Current requirements in terms of impact damage on the leading edge are based on retaining structural integrity of the component, following an impact. In addition to these requirements, for HLFC surfaces, a surface dent is also of concern, as it could cause transition of the boundary layer, resulting in turbulent flow downstream of the impact site.

For carbon fibre reinforced composite materials, the presence of holes increases the electrical resistance in the panel and changes the nature of the damage caused by lightning strike. The author, with associates O'Driscoll, Hardwick and Ryan, evaluated this issue for a HLFC engine nacelle panel (which would not be protected by wire mesh). Contrary to expectation, the damage due to simulated lightening strike tests on Nd-YAG laser drilled carbon fibre epoxy panels, was less than that seen on the control panels, which represented a current nacelle design (O'Driscoll *et al.*, 2000).



#### *B.4.2.6 Durability, corrosion and erosion resistance*

The durability of the finished product relates to the long-term stability of the surface in terms of its dimensions, surface finish and porosity. Corrosion resistance of the base material is critical, as the final product cannot be painted, as this will block the holes. This is discussed further in section M.4 (Appendix M).

#### *B.4.2.7 Structural compatibility*

The HLFC surface must be compatible with the surrounding and supporting structure. The stiffness incompatibility between a titanium skin panel, for example, and an aluminium wing structure results in high strain-induced stresses, caused by wing flexure under load. For this reason, a relatively low modulus titanium skin would be better suited to this application than higher modulus titanium.

#### *B.4.2.8 Surface quality, steps and gaps*

Discontinuities, such as steps, gaps and surface irregularities may either “trip” the boundary layer or destabilise the flow, resulting in transition occurring at a finite distance downstream of the point of disruption. To prevent transition of the boundary layer, manufacturing tolerances at any manufacturing joint (or junction for an access panel, for example) in the suction surface or in the laminar flow region, will be substantially tighter than those used in current aircraft structures.

The critical height that will cause transition of the flow depends on the local boundary layer conditions. A small discontinuity could thus be tolerated at one location on the surface, but not at another location where the flow is less stable. The precise geometry of the discontinuity has been shown to be important. Forward facing steps, for example, are less of a problem than rear facing steps. Holmes *et al.* (1985) discussed the manufacturing requirements for laminar flow surfaces and reported on the stability of laminar flow over different shaped discontinuities.

#### *B.4.2.9 Repair*

In addition to the requirements for repair schemes to restore the structural integrity of the surface, it is necessary that the repair has a minimal aerodynamic impact. This implies that the repair is flush and perforated. Standard repairs for metal or composite material involve a patch that may not be flush with the original surface. A scarf repair on a composite surface, for example, will have a forward and backward facing step, equal to the thickness of a single ply (typically ~0.25mm). As stated earlier, the critical height that will cause transition of the flow depends on the local flow conditions; however, it is likely that this critical value will be exceeded in the case of such a repair. Furthermore, it will not be possible to “finish” the repair using a filler or paint, as this will block the holes.

The viability of re-drilling the repaired section depends on the detailed design of the structure. If it is possible to perform this operation in-situ, then the holes will be



larger on the outside than on the inside and this in itself may be a problem if the original design called for the smaller hole diameter to be on the outside. The presence of a non-perforated section with a step will result in a wedge-shaped area of turbulent flow downstream of the repair.

### **B.4.3 Types of suction surfaces**

The aerodynamic requirement is that air be sucked through the skin surface with minimal pressure loss, and in such a way that it does not instigate transition of the boundary layer. The suction surfaces that have been developed can essentially be divided into three categories:

#### *B.4.3.1 Porous materials*

Porous materials create little disruption to the flow and were used for much of the early LFC experimental work. Gregory (1961) provides a review of these suction surface designs. Porous materials like foams, fabrics, nylons and sintered meshes, tend however, to have little structural integrity and shear stiffness, rendering them unsuitable for use on their own as a skin material, unless supported by a load bearing sub-structure.

#### *B.4.3.2 Micro slotted surfaces*

The air can be sucked through narrow slots cut into the skin. Gregory (1961) describes the use of this technique in LFC experimental work. The Lockheed LFC wing design for the NASA Jetstar experiments (see section C.4, Appendix C), consisted of a titanium skin with 27 rows of 0.1mm wide slots (Joslin, 1998a). Slotted surfaces cannot however, be considered for highly swept wings, typical of a modern airliner, due to the flow disturbance caused by the slot.

#### *B.4.3.2 Discrete drilled holes*

Discrete holes can be produced by electron beam or laser drilling. The methods are reviewed in section B.4.4. Electron beam drilling was used for the Douglas designed right wing test section, for the LFC Jetstar tests. Drilling by Nd-YAG or Excimer laser has been the preferred technique since the mid-1980s. The Boeing 757 and F-16XL flight tests, as well the recent CEC supported HLFC research programmes (i.e. ELFIN, LARA, HYLDA, HYLTEC and ALTTA), have all used laser drilling for the production of the suction surfaces.

### **B.4.4 Techniques for producing holes**

#### *B.4.4.1 Electron beam*

Maddalon and Poppen (1986) report on the successful design and fabrication of a large suction wind-tunnel panel (~2.1m by 2.1m) that was produced using the Electron Beam (EB) technique. Schwab (1992) also investigated the drilling of holes for laminar flow control using an Electron Beam gun. He reported that this technique can produce



3000 holes per second, with hole diameters as small as  $60\mu\text{m}$  in 1.0 mm thick (and  $40\mu\text{m}$  in 0.5mm thick) stainless steel sheet. The cross-section of the holes was observed to be uniformly tapered with the hole diameter on the beam entry side approximately 2 to 2.5 times that of the beam exit side. Due to the "backing plate" technique adopted by Schwab (1992), the exit holes were reported to be burr-free and round.

#### B.4.4.2 Nd-YAG laser – single pulse

Holes can be drilled by a Nd-YAG laser, which produces pulses of radiation at a wavelength of  $1.06\mu\text{m}$  with a pulse duration of about 0.1 to 1ms (Williams and Marsden, 1996). The laser beam is focused by means of a lens to produce the holes individually by means of a single laser pulse. Fig. B-12 is a Nd-YAG laser drilled panel with typical HLFC hole sizes and spacing. The molten or vaporized material may not all be expelled and it would then re-solidify inside or around the hole. This is known as recast or resolidified material. Yeo *et al.* (1994) note that the "structure of the material lining the walls of the holes is considerably different from that of the parent material and shows evidence of substantial micro-cracking". The issue of cracking and its impact of the durability of the material were explored by the author. (See section M.4, Appendix M.)

Fig. B-13a is a SEM (Scanning Electron Microscope) image of a series of Nd-YAG laser drilled holes in a sheet of thermoplastic carbon fibre composite material. The heat from the drilling process results in a heat affected zone around the hole, which can affect the mechanical properties of the material.

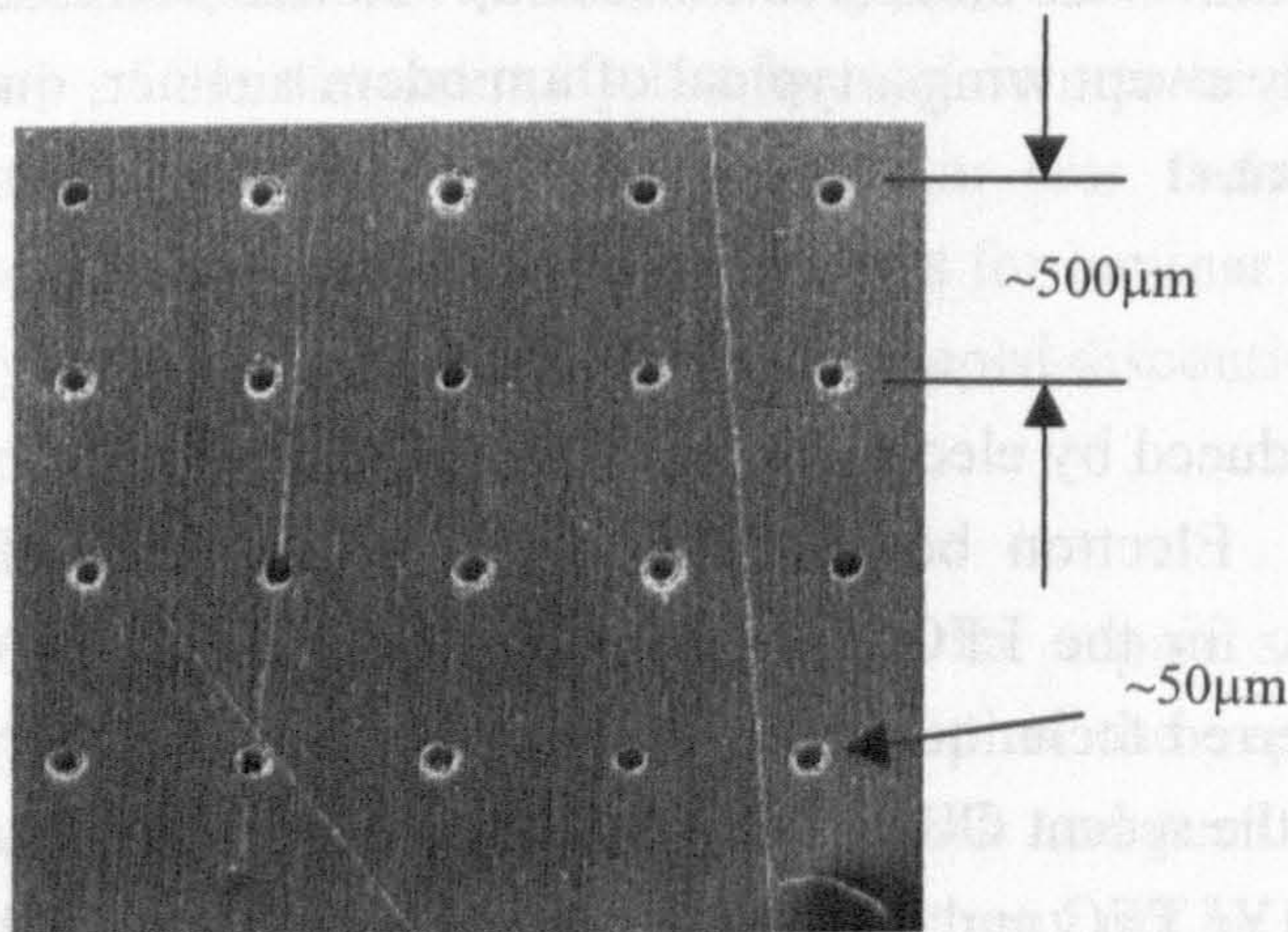


**Fig. B-12** Nd-YAG laser perforated aluminium sheet

#### B.4.4.3 Nd-YAG laser – multi-pulse

The multi-pulse method involves firing the laser several times in order to penetrate through the panel. The drilling technique can cause irregular shaped holes resulting from vibrations of the drilling process, which is not ideal for laminar flow.



The author (with Humphreys<sup>3</sup>) investigated the notion that this technique would reduce the size of the heat-affected zone, around the hole in carbon fibre composite epoxy panels; however, the extent of resin damage was observed to be very similar to that produced by the single pulse method.

#### B.4.4.4 Excimer laser

An Excimer laser produces pulses of radiation at a wavelength of 308nm with a pulse duration of 20 to 150ns (Williams and Marsden, 1996). The short pulse duration removes a small amount of material, necessitating several hundred pulses to penetrate a metal panel of 1mm thick. Practical techniques to produce large perforated panels use a diffractive lens array to drill an array of holes simultaneously. An advantage of this technique over the Nd-YAG laser is that smaller holes can be produced. Hole diameter of 10 to 50µm can be produced.

Williams and Marsden (1996) report that highly regular holes - in terms of shape and size - can be produced using this technique. However, any relative movement of the panel will result in holes that are not exactly round (Fig. B-13b).

#### B.4.4.5 Stitching

The concept of stitching a "fugitive" fibre in a lay-up of "prepreg" composite material, and then removing the fibre using solvents – after the laminate has been cured – to leave a hole in the panel, is described by Meade *et al.* (1977). Partial success with this method was reported. Recent studies conducted at the University of Limerick failed to replicate this process, as the acid baths did not completely remove the embedded fibres.

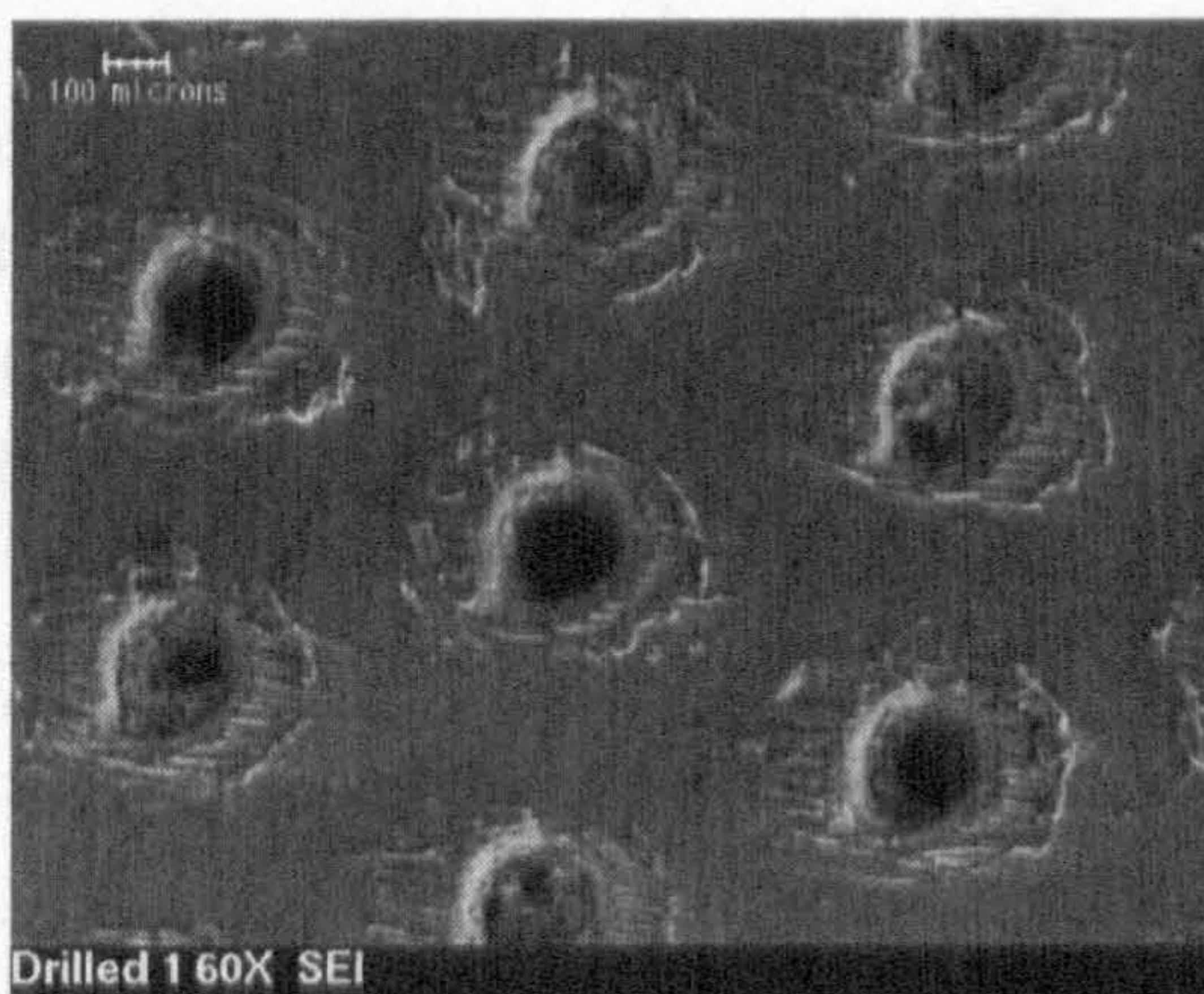


**Fig. B-13a** SEM image of Nd-YAG laser perforated APC-2 (Young *et al.*, 2001)

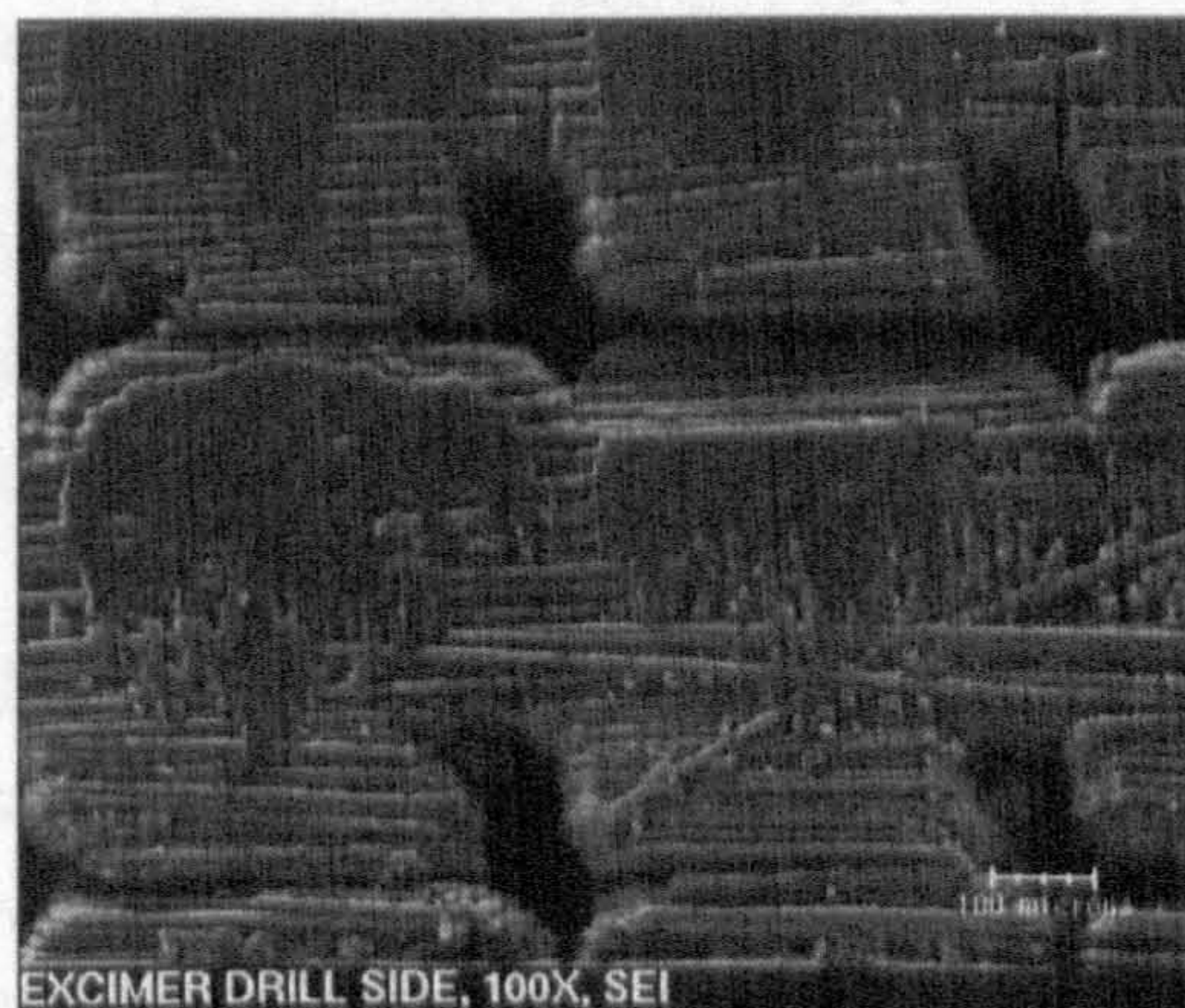


**Fig. B-13b** SEM image of Excimer laser perforated APC-2. Irregular hole shape caused by vibration. (Young *et al.*, 2001)

<sup>3</sup> B. Humphreys, Aerospace Systems and Technology, Consett, Durham, UK.



### B.4.5 Surface porosity, hole size and shape

The airflow through the suction surface is a function of the panel porosity. Referring to Fig. B-14, the porosity is calculated as follows:

$$\text{Porosity} = \frac{\pi \left( \frac{d_1^2}{AB} \right)}{4} = \frac{\pi \left( \frac{d_1}{A} \right)^2}{4} \text{ if } A = B \quad \text{--- [B-1]}$$

A typical hole diameter ( $d_1$ ) on the outer surface is 50 $\mu\text{m}$ , and the hole centre-to-centre distance, is 500 $\mu\text{m}$ . This gives a pitch to hole diameter ratio of 10 and a porosity of ~0.8%. (Details of hole measurements of laser drilled test panels are presented in section M.4, Appendix M.)

Ideally, the shape of the hole should be tapered with the larger diameter on the inside of the wing skin. The advantage of this is that should dust or any other particulate matter enter the hole, it will be sucked through and will not block the hole. This hole shape occurs naturally when holes are produced by electron beam or laser drilling, as the hole on the beam entry side is always bigger than on the exit side. For Nd-YAG drilled panels of about 1mm thick, the hole diameter on the beam entry side was established by the author to be about 2 to 2.6 times that of the beam exit side. Schwab (1992) indicates very similar ratios for electron beam drilled holes. However, there exists an aerodynamic advantage of having the larger hole diameter on the surface (i.e. having the taper in the opposite direction to that described above). For the same pressure drop and mass flow, the hole inlet velocity will be comparatively lower, because the hole area is larger, resulting in less disturbance to the external airflow.

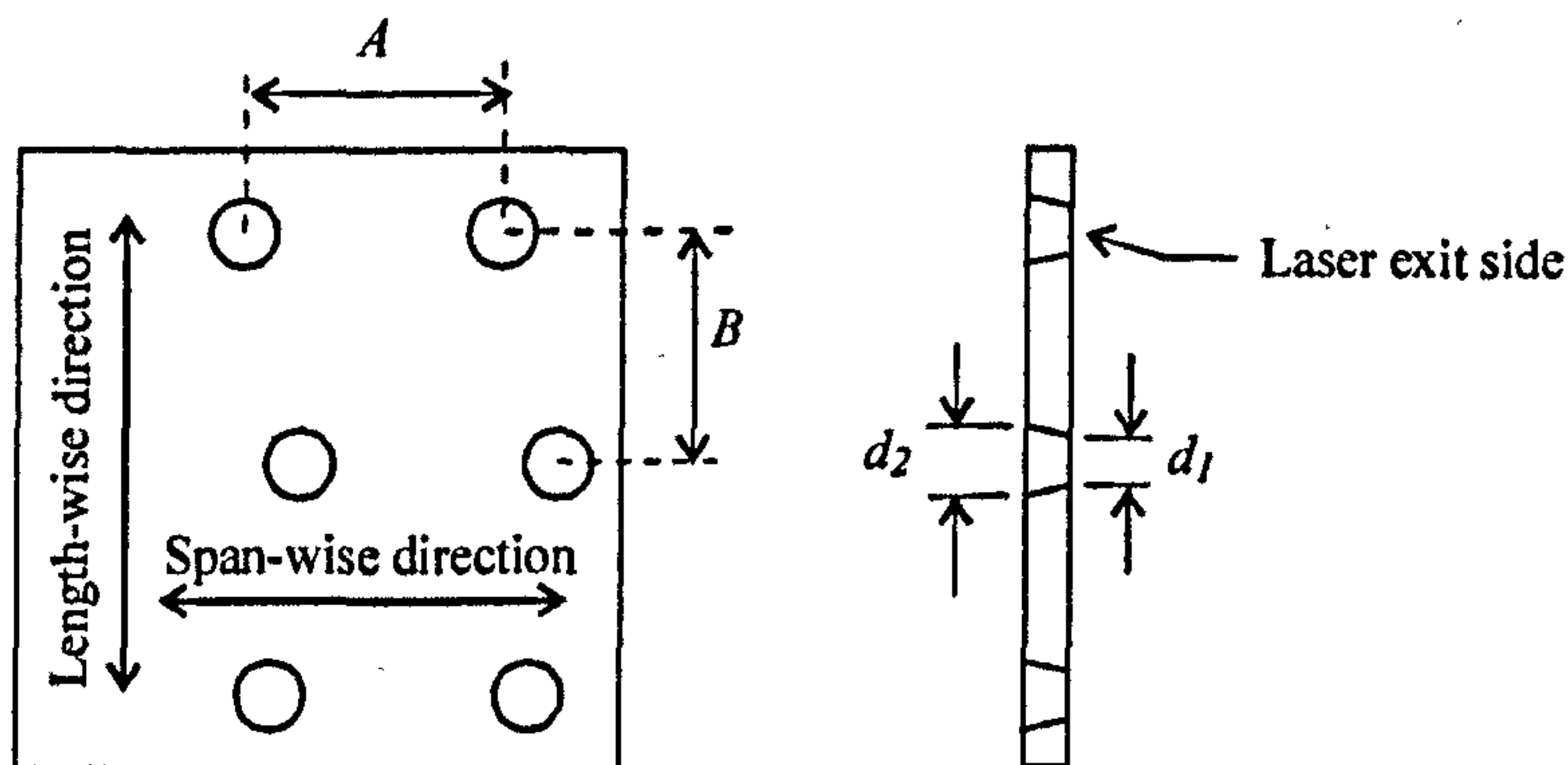


Fig. B-14 HLFC perforated panel

### B.4.6 Materials

#### B.4.6.1 Candidate materials

What is required is a light-weight material that can be drilled or manufactured in a way that produces an acceptable porosity for sucking the boundary layer and will still retain sufficient durability and structural integrity. Candidate materials are rated jointly by the author and Humphreys in Table B-1.



**Table B-1** *Candidate materials for HLFC suction surfaces*

Materials	Design strength	Corrosion resistance	Rain erosion resistance
Titanium	Fair	Good	Good
Stainless steel	Poor	Good	Good
Aluminium alloy	Good	Poor	Fair
Thermoset composites	Good	Good	Very poor
Thermoplastic composites	Good	Good	Fair

#### *B.4.6.2 Titanium*

Commercially pure (CP) titanium and titanium alloys have been the material of choice for many HLFC projects, as they may be slotted or drilled and will still retain adequate strength. Titanium has proven to be durable under harsh rain erosion tests and is regarded as the benchmark against which other materials are measured.

Candidate titanium materials are TA10 and Ti-15V-3Cr-3Sn-3Al. The advantage of the latter titanium alloy over the more widely used titanium alloy, Ti-6Al-4V, is that the former alloy has a lower modulus of elasticity (82GPa versus 110GPa) and this will reduce the strain-induced loads on the joint between the perforated skin and the primary wing structure (Timetal, 2002; Jagger and Davies, 1996).

#### *B.4.6.3 Stainless steel*

The material can be slotted or drilled by electron beam or laser. Like titanium, it does not suffer from corrosion problems, but results in a heavier structure, as the density of the material is about 1.8 times greater than that of titanium alloy.

#### *B.4.6.4 Aluminium alloy*

Aircraft grade aluminium alloys can be drilled without difficulty by electron beam or by laser. Unprotected aluminium alloy however, suffers from serious corrosion and erosion problems. The difficulty here is that the base material cannot be protected by cladding with pure aluminium or by painting the surface. Investigations conducted by the author in this regard are described in section M.4 (Appendix M).

#### *B.4.6.5 Carbon fibre reinforced epoxy materials*

Carbon fibre reinforced epoxy composite can be drilled by Excimer and Nd-YAG laser; however, the drilling process results in damage to the resin around the holes due to the heat from the laser being conducted along the fibres. The damaged area is equal approximately to one hole diameter on either side of the drilled hole (Fig. B-15a). This is a very serious concern for epoxy materials, as the 'resin burnout' around the holes leads to poor rain erosion characteristics (see section M.4, Appendix M). The laser drilled hole through the material is not uniform in diameter and features a bell-mouth opening on the laser entry side (Fig. B-15b).

Kevlar reinforced epoxy has also been successfully drilled using Excimer laser. Williams and Marsden (1996) report that uniform holes with a "lack of thermal effects"



were produced. Glass fibre composites do not lend themselves to laser drilling because the glass fibres tend to be transparent to the laser beam.

The author investigated the effect of single and multi-pulse Nd-YAG laser drilling on the mechanical properties of carbon fibre epoxy panels. It was noted that the ultimate tensile strength was reduced by between 2% and 48% depending on the drilling technique, material type and drilling pattern (Young and O'Driscoll, 2002).

#### B.4.6.6 Carbon fibre reinforced thermoplastic materials

Thermoplastic composite materials can also be drilled by Excimer and Nd-YAG laser. Because of the relatively good impact resistance of thermoplastic materials, they were investigated for use as the perforated suction surface. The two selected materials were APC-2, a carbon fibre composite of polyetheretherketone (PEEK) resin and carbon fibre reinforced PPS (polyphenylene sulphide). Quasi-isotropic APC-2 specimens of 1mm thickness were produced and drilled by Nd-YAG laser. Static testing conducted at the University of Limerick under the direction of the author, revealed an average reduction in ultimate tensile strength of ~30% compared to the undamaged material.

The Nd-YAG drilled APC-2 thermoplastic composite demonstrated superior rain erosion resistance to that of drilled carbon fibre epoxy composite, in spite of the presence of a heat affected zone around the hole.

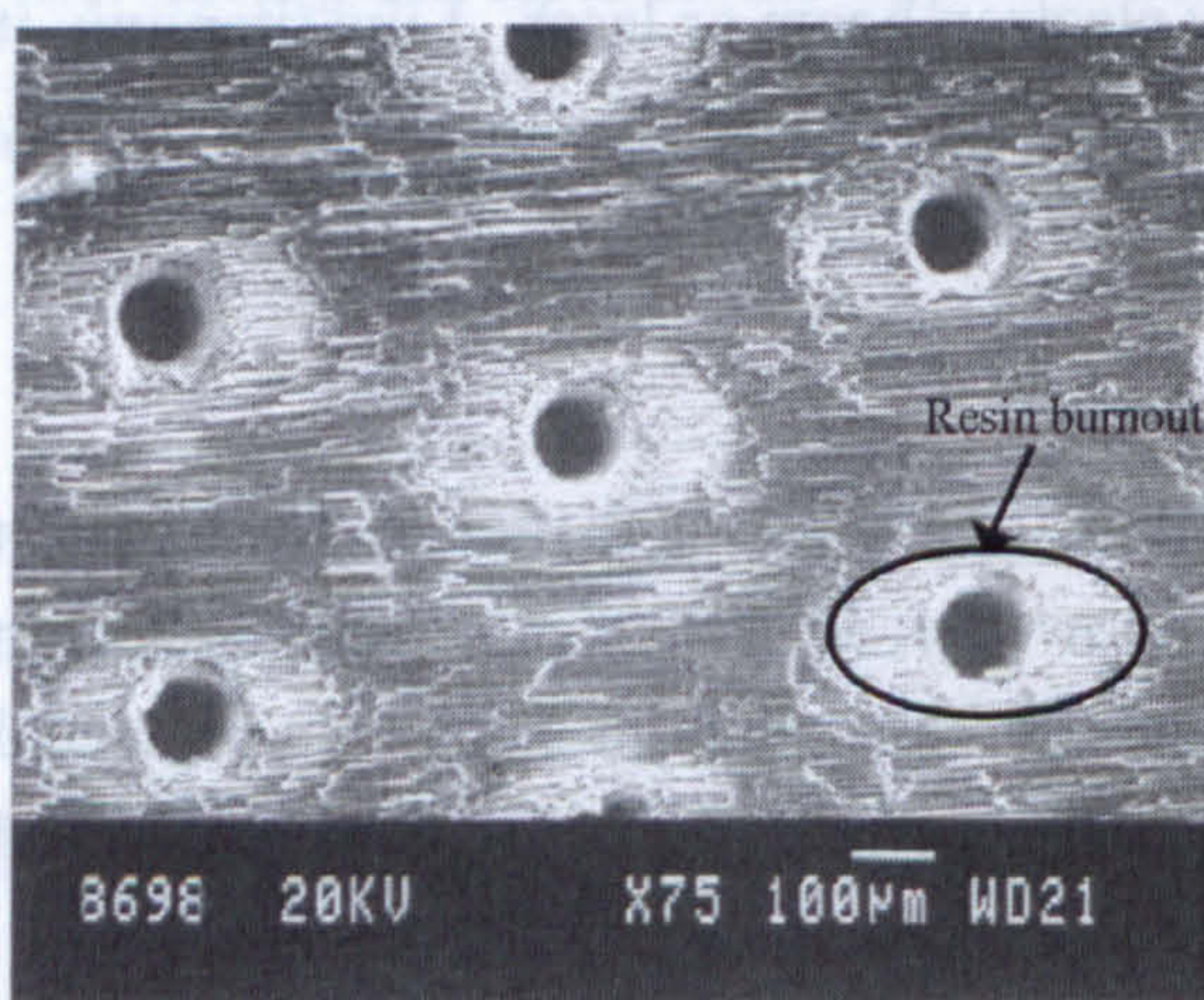


**Fig. B-15a** SEM image of laser entry of carbon fibre epoxy panel (Young and O'Driscoll, 2002)

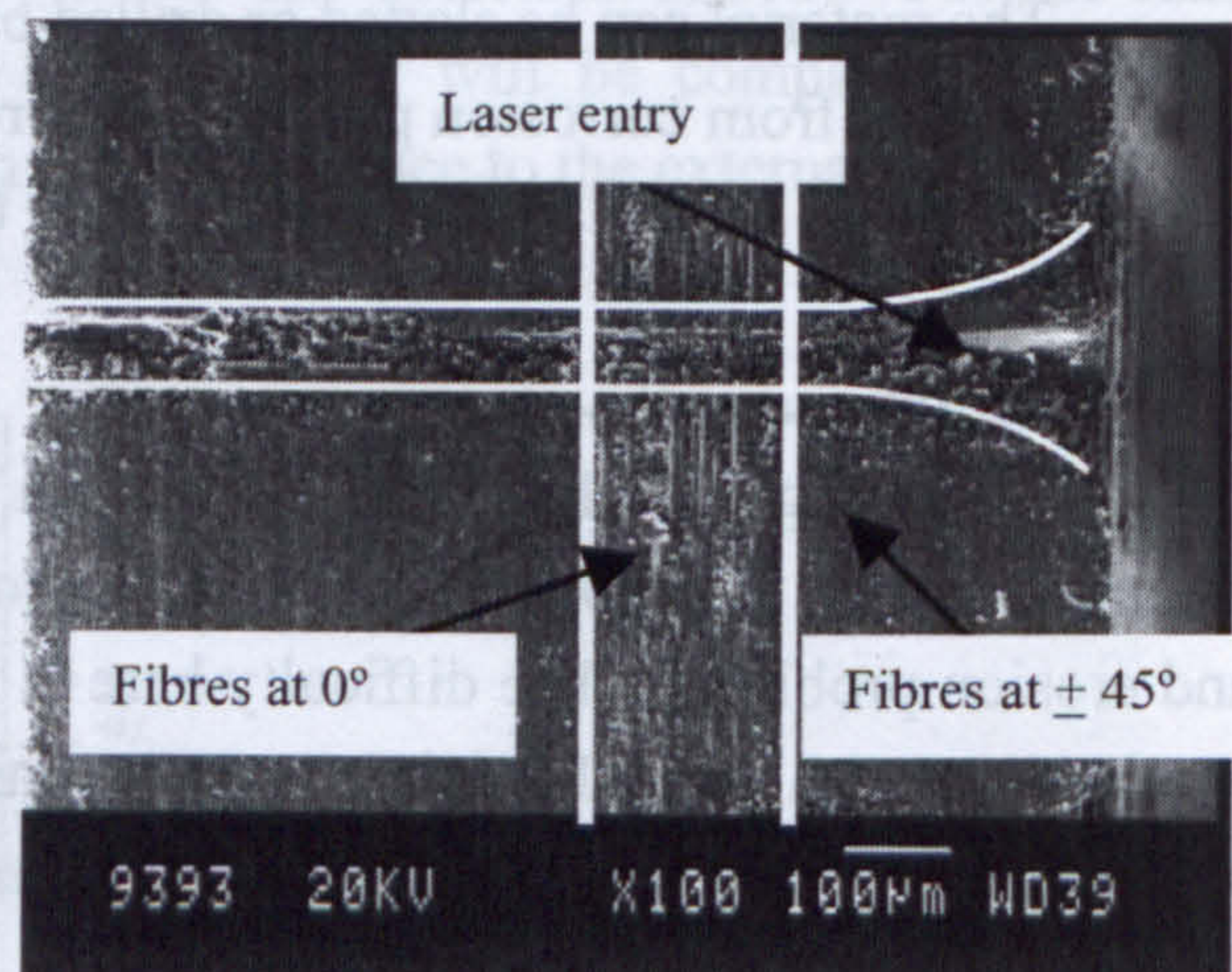


**Fig. B-15b** SEM image of laser drilled hole in carbon fibre epoxy panel (Young and O'Driscoll, 2002)

#### B.4.7 Manufacturing considerations

The material used for the suction chambers and the method of manufacture have to be considered in an integrated manner with the selection of the skin material. The requirement for an almost airtight seal between the suction chamber and skin surface complicates the manufacturing process. Brazing, welding, adhesive bonding and superplastic forming / diffusion bonding (SPDB) have all been considered for this



application. Providing a durable bond in a light-weight structure, without blocking too many holes, is the primary objective.

The relative merits of alternative manufacturing techniques are outlined by Humphreys (2001a; Young *et al.*, 2001). These options are illustrated in Fig. B-16. The superplastic forming / diffusion bonding technique initially proposed by Williams (1982) and Wilson (1982), offers the opportunity to manufacture a light-weight structure with little reduction in the porous area. The technique however, places a constraint on the allowable width of the suction chambers. One of the significant achievements of the HYLTEC projects was the successful development by Sonaca, of a practical HLFC test panel manufactured in titanium, using this technique (Fig. B-17).

To reduce the weight of the complete design, composite material has been considered for the suction chambers. The outer skin could be bonded or riveted to a light-weight substructure. This however results in an area along the bond line where no suction can be achieved. Molitor and Young (2002) report on alternative techniques for bonding carbon fibre composite to perforated titanium. Bonding does introduce concerns regarding delamination resulting from an impact (bird strike, for example).

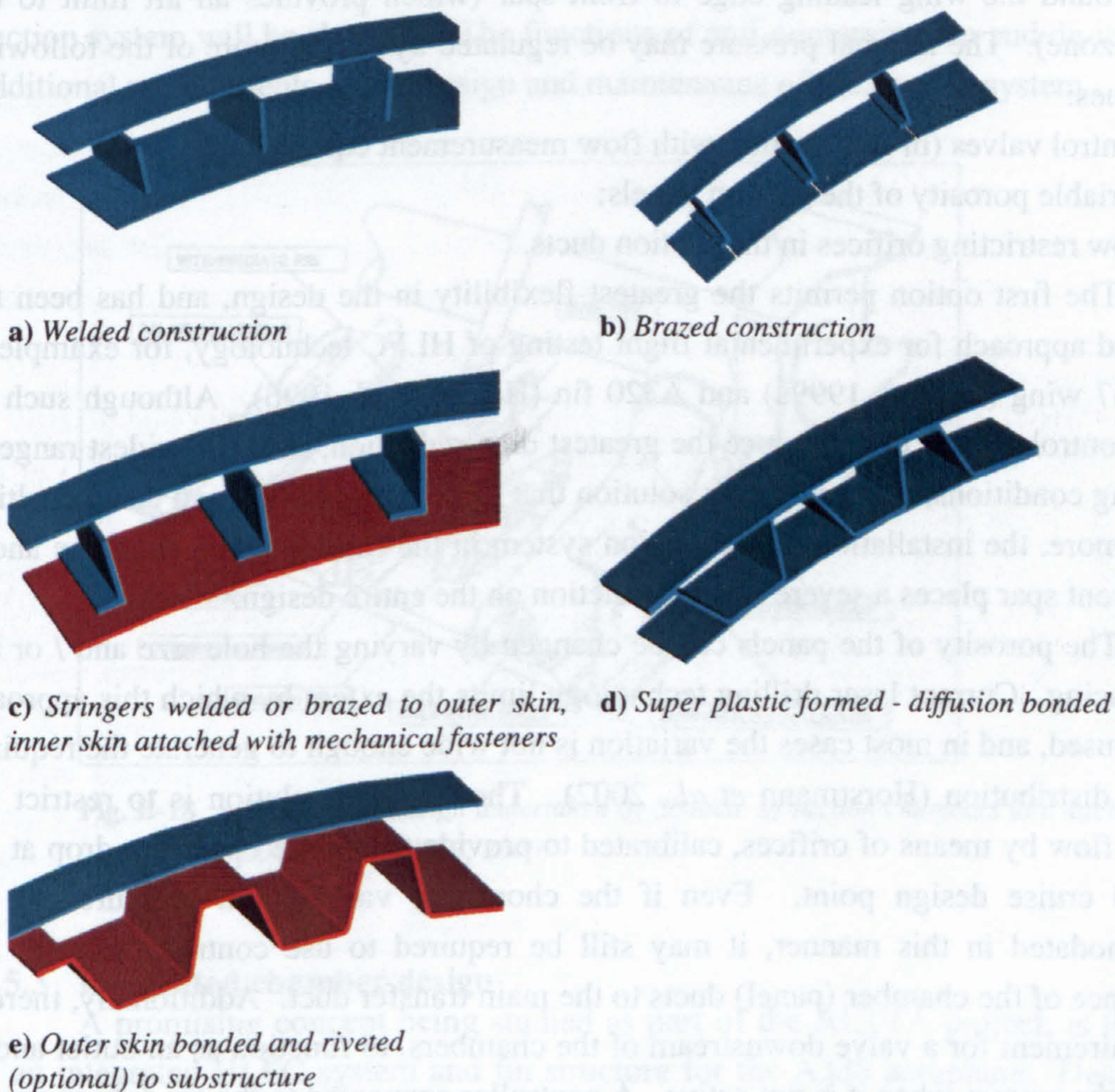


**Fig. B-16** Alternative manufacturing techniques for HLFC structures

(Humphreys, 2001a; Young *et al.*, 2001)



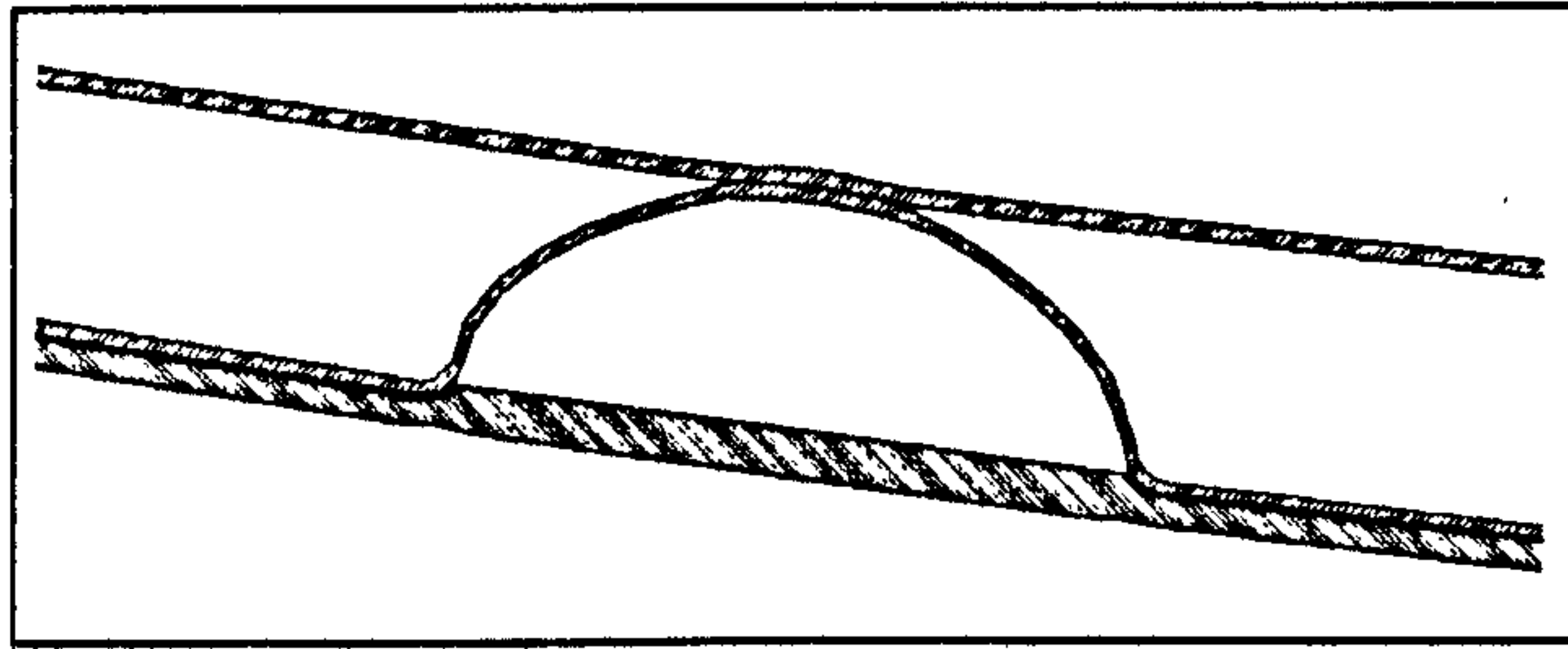


**Fig. B-17** Cross section of Super Plastic formed Diffusion Bonded (SPDB) test panel, manufactured by SONACA<sup>4</sup>

## B.5 SUCTION SYSTEM

### B.5.1 Control philosophy

To stabilise the laminar flow in the boundary layer, a certain pressure distribution has to be achieved within the suction chambers, which will ensure the desired flow velocities through the perforated panels. This is a difficult task as the pressure on the outer surface varies considerably, as the flow moves from the stagnation point around the wing leading edge to front spar (which provides an aft limit to the suction zone). The internal pressure may be regulated by one or more of the following techniques:

- (1) Control valves (in conjunction with flow measurement equipment);
- (2) Variable porosity of the suction panels;
- (3) Flow restricting orifices in the suction ducts.

The first option permits the greatest flexibility in the design, and has been the preferred approach for experimental flight testing of HLFC technology, for example in the B757 wing (Boeing, 1999a) and A320 fin (Henke *et al.* 1996). Although such an active control system may produce the greatest drag reduction, over the widest range of operating conditions, it is a complex solution that incurs both weight and cost penalties. Furthermore, the installation of the suction system in the limited space envelope ahead of the front spar places a severe space restriction on the entire design.

The porosity of the panels can be changed by varying the hole size and / or the hole spacing. Current laser drilling technology limits the extent by which this approach may be used, and in most cases the variation is not wide enough to generate the required suction distribution (Horstmann *et al.*, 2002). The simplest solution is to restrict the suction flow by means of orifices, calibrated to provide the desired pressure drop at the selected cruise design point. Even if the chordwise variation in pressure can be accommodated in this manner, it may still be required to use control valves at the confluence of the chamber (panel) ducts to the main transfer duct. Additionally, there is the requirement for a valve downstream of the chambers, to function as an outlet and to shutoff the system when it is not active. A controller connected to the air data computer

<sup>4</sup> Courtesy of Ch. Overbergh, Sonaca, Gosselies, Belgium



could automatically control this valve, switching on the system when the design point conditions (Mach number and altitude) are established. Depending on the design approach, valves may also be required for the anti-icing / anti-contamination system.

### B.5.2 Suction chambers and ducts

The function of the suction chambers (ducts or flutes as they may also be called) is to conduct the air bled from the external boundary layer to the pump. A series of narrow suction chambers will run under the skin, in the spanwise direction. The suction within the rows of chambers is not equal and is tailored to suit the external flow conditions (characterised by pressure, pressure gradient and Reynolds number). The suction chambers will convey the air to larger collection ducts or pipes, which will run to the pump (Fig. B-18). The design of the suction chambers must consider the skin material. For example, a titanium substructure was used on the A320 fin test (see section C.14, Appendix C) to eliminate problems with dissimilar materials.

For liquid anti-contamination systems, the ducts will also serve to conduct the liquid or foam from the reservoir to the skin. The alternative de-icing system is based on hot air, which may be ducted through the “suction chambers” (during which time the suction system will be shut off). The functions of anti-contamination and de-icing place additional requirements on the design and maintenance of the suction system.

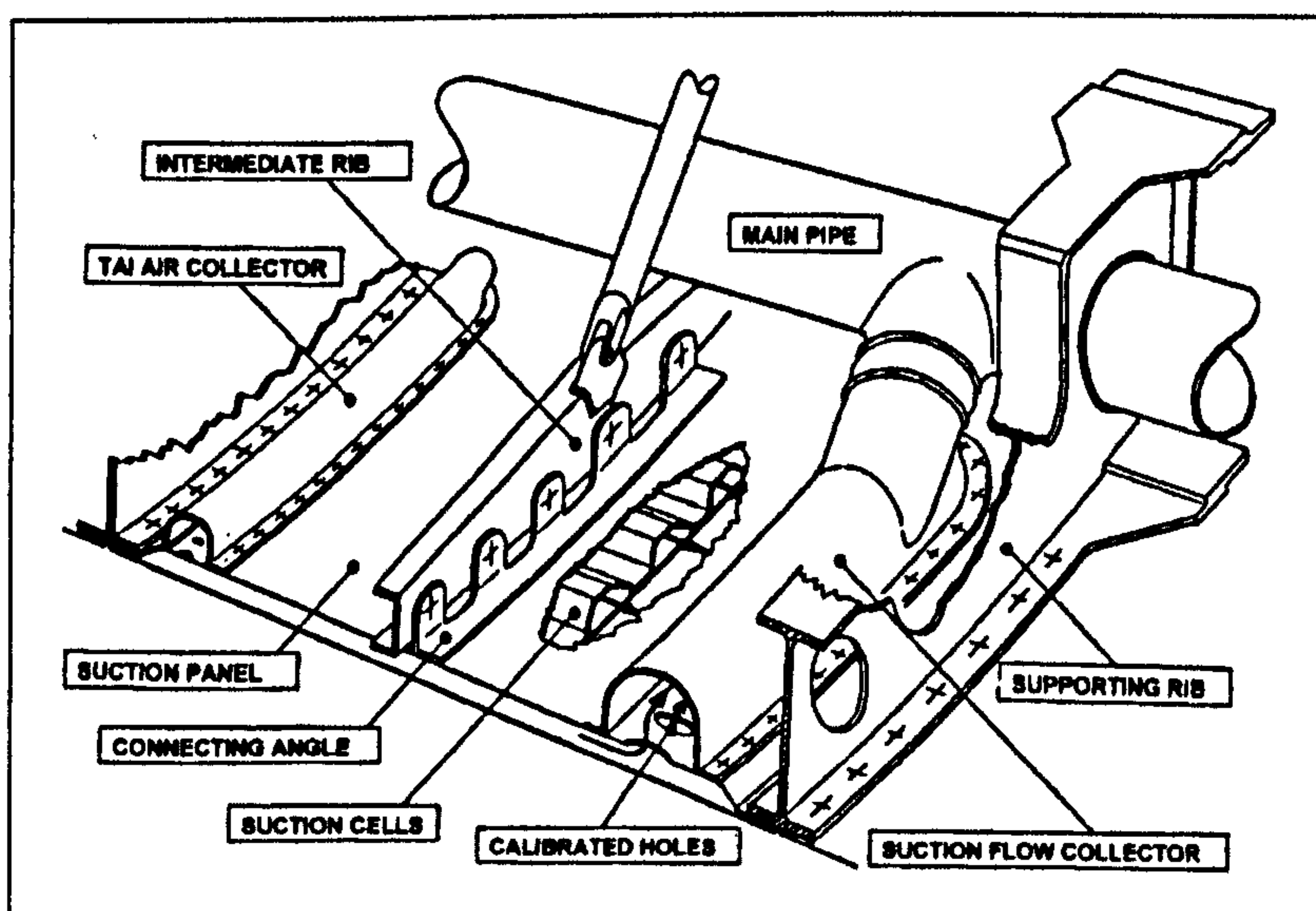


Fig. B-18 Conceptual design undertaken by Sonaca<sup>5</sup> of suction chambers and ducts installed in a slat (HYLTEC, 2000)

### B.5.3 Integrated chamber design

A promising concept being studied as part of the ALTTA project, is the design of an integrated HLFC system and fin structure for the A320 aeroplane. Described by Schrauf and Kühn (2001) and by Horstmann *et al.* (2002), the concept is based on the

<sup>5</sup> Sonaca SA, Gosselies, Belgium



use of the complete leading edge box as a large suction chamber, thus eliminating the ducts. A double-skin structure (first proposed within a German national RaWiD programme), is the key to the design (Fig. B-19). The perforated suction surface is supported by small chord-wise stringers, mounted on the inner metal sheet, in which metered holes are drilled. The suction ducts are eliminated in this concept and the whole inner space of the leading edge box is utilised as the suction chamber. Advantages of this design are a reduced weight penalty and a simpler control system. According to Horstmann *et al.* (2002), the design permits a "very efficient control of the suction distribution because the outer micro-perforated surface and the supporting stringers function as many small suction chambers, and the pressure in those small chambers can be adjusted by choosing suitable orifices in the inner sheet".

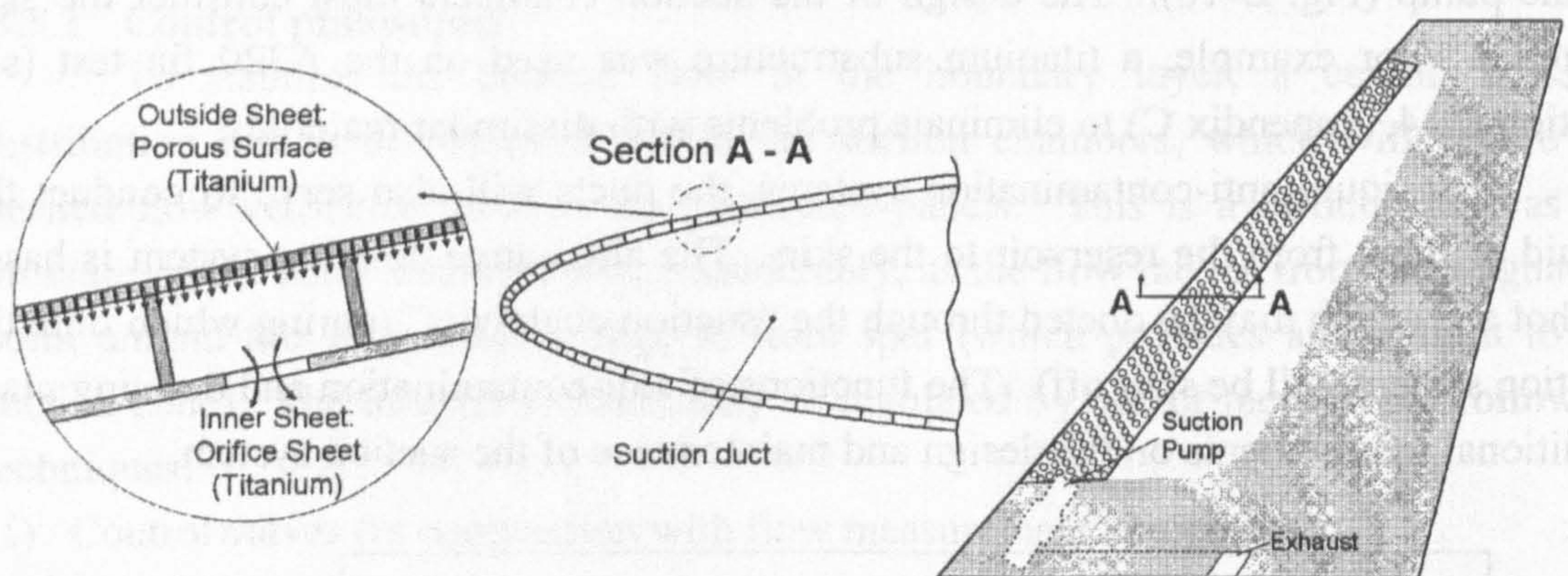


**Fig. B-19** ALTTA fin concept (from Horstmann *et al.*, 2002)

#### B.5.4 Pump system

In theory, two options exist to power the suction pump(s). The pumps may be driven by: (1) Bleed air taken from the Intermediate Pressure Compressor (IPC) or the HPC (High Pressure Compressor); or (2) Mechanical power off-take from the engine. For experimental work, pre-qualified aircraft components have been used. For example, suction for the F-16XL Ship 2 tests (see section C.7, Appendix C) was provided by a Boeing 707 turbo-compressor (Joslin, 1998a). Another option is a jet pump. Studies conducted during the HYLDA project (section C.16, Appendix C) came to the conclusion that an electric induction motor driving an axial turbo-compressor was the most efficient overall approach. On modern engines like the Rolls-Royce Trent, the HP shaft drives an accessory gearbox, which provides power to the Integrated Drive Generator (IDG). The IDG services the aircraft's complete electrical power requirement. For a new design it is possible, in theory, to increase the rating of the IDG to cater for the HLFC system.

An increase in fuel consumption results from the running of the pump(s), which reduces the gains due to the drag reduction. Wilson (1997) compared the electrical and bleed air drive options and concluded that an electrical drive was more efficient, with approximately half of the SFC penalty of that of the bleed drive option. However, he



had underestimated the SFC penalty for the electric system. A major advantage for the electrical system is the flexibility of locating the pump. The electric system has a large start-up power requirement and an attractive solution is to incorporate an air turbine, which will start the compressor.

## **B.6 CONTROL AND MONITORING SYSTEM**

The extent of the laminar flow on the skin can be measured in a number of ways. Hot film or hot wire sensors have been widely used in the wind tunnel and in-flight experimental work, described in Appendix C. Other techniques include infrared thermography, embedded microphones and liquid crystals. On the Boeing 757 and GEAE engine nacelle flight tests, wake-survey probes were used to infer local drag reduction values (Collier, 1993). In addition, static pressure ports have been used to measure the pressure on the external surface and also in the suction chambers.

For a production aircraft the requirements are different. A robust monitoring system is required, that will indicate to the pilot if the design target of HLF is being achieved. Blockage of the holes, for example, would change the pressure in the ducts and this could be used to indicate the state of the HLFC system. Wright and Nelson (2000) report on the successful use of miniature microphones to detect surface pressure fluctuations and thus distinguish between laminar and turbulent flow on a LFC wind tunnel model. Information on the static pressure and flow in the ducts, and the condition of the boundary layer, can be used in conjunction with the fuel flow monitoring system to ensure that the HLFC system is working correctly.

The control and monitoring system will receive information from the air data computer and initiate the start-up sequence, when the design flight conditions are reached. The controller will also be required to control the functioning of the anti-icing and anti-contamination system (if fitted). The intermittent loss of laminar flow, due to flight through cirrus clouds, would be detected by a loss of laminar flow as described above. If deemed necessary for operational requirements, the presence of cirrus cloud could be detected using a spectrometer (Knollenberg Probe) or a Charging Patch (as described by Davis *et al.*, 1989).

## **B.7 PERFORMANCE GAINS**

### **B.7.1 Boeing 757-200 HLFC study (~1982)**

Under contract to NASA (as part of the US Aircraft Energy Efficient (ACEE) Program), Boeing undertook a detailed study of the technical implications of HLFC using the B757-200 as the reference vehicle (Boeing, 1982). The mission specification was to transport 180 passengers at Mach 0.80 over a distance of 2100nm. Laminar flow was considered on the wing, with the assumption that it could be maintained to



approximately 60% of the upper wing chord and 40% of the lower wing chord. The mean drag reduction (for the aircraft) in the cruise condition at 35 000ft, was calculated for three design cases. The reduction in drag was: (1) 7.3% with laminar flow on the upper wing; (2) 10.9% with laminar flow on upper and lower wing surfaces; and (3) 15.1% with laminar flow on both upper and lower wing surfaces and on the empennage.

With HLFC on both upper and lower wing surfaces, a block fuel saving of ~8.1% was calculated over the baseline 757-200 aircraft for the reference mission, which included standard reserves based on US domestic rules. This would be increased to ~12% by applying HLFC to the empennage. The reduced thrust required in cruise implied that the HLFC aircraft was not optimised and that the SFC of the HLFC aircraft was a little higher than would be the case if the engine was re-sized to match the existing airframe. The incremental block fuel benefit for the resized engine was estimated to be about 1% (Boeing, 1982).

### **B.7.2 Lockheed military transport aircraft study (~1985)**

Lange (1987) reports on preliminary design studies conducted by Lockheed under a US Airforce "Technology Alternatives for Airlift Deployment" (TAFAD) contract. A preliminary design was completed for a Mach 0.80 cruise aircraft, with a payload of 96200kg, MTOW of 350400kg and a range of 5800nm. The design utilised LFC from the leading edge to 65% of the wing chord and to 75% of the chord of the empennage surfaces. As compared to a turbulent flow baseline design, the LFC design showed a 14% increase in range for the same payload, but with a 10% increase in empty weight. The LFC design had a 14% reduction in mission fuel, compared to the turbulent flow baseline aircraft.

### **B.7.3 Lockheed "Global Range" military transport aircraft (1986-1987)**

Lange (1987;1988) reports on a design study for a HLFC Mach 0.77 "Global Range" aircraft, designed to meet a mission requirement for a payload of 60100kg to be delivered over a range of 6500nm, and thereafter to return to the departing airport, without refueling. The work was co-sponsored by NASA and the USAF. The turbulent baseline design had a MTOW of 279500kg, whilst the HLFC baseline version had weight of 269700kg. The ground rules for the HLFC design study included:

- (1) HLFC only activated at initial cruise altitude;
- (2) Turbulent flow occurred for 6% of the cruise time (allowance for clouds);
- (3) 12% excess cruise thrust available to accommodate a loss of laminar flow.

Three versions of HLFC aircraft were derived, i.e. with HLFC on: (a) The upper and lower wing surfaces and on the empennage; (b) The upper and lower wing surfaces; and (c) The upper wing surface and the empennage. The wing design was optimised for the mission specification using a Lockheed computer program. The relative benefits of the three HLFC aircraft variants are given in Table B-2.



**Table B-2**    *Benefits of HLFC for "Global Range" military transport aircraft (Lange, 1987)*

	Change with respect to turbulent baseline aircraft (%)		
	a) HLFC baseline	b) No HLFC on empennage	c) No HLFC on lower wing surface
<b>OEW</b>	5.4	5.4	7.9
<b>MTOW</b>	-4.0	-4.2	-0.6
<b>Fuel consumption</b>	-13.4	-13.7	-7.9
<b>L/D ratio</b>	18.4	18.2	12.5

**B.7.4 Boeing 757 flight tests (1987 - 1991)**

Collier (1993) reported on the performance gains of the HLFC system tested on the wing of a Boeing 757. (See section C.6, Appendix C.) With laminar flow extending to 65% of the upper wing chord, a local drag reduction of 29% was deduced from the wake rake measurements, which if extended to the whole wing indicated a drag reduction of 6% for the aircraft. This value may be compared with the estimated 7.3% drag reduction, established in the earlier Boeing study (see section B.7.1).

**B.7.5 GE / Rohr / AlliedSignal / NASA HLF nacelle (1991 - 1992)**

A drag reduction on the nacelle of ~40% was deemed to be attainable for a HLF design (Tegarden, 1996). For a typical widebody aircraft, the nacelles represent between 4 - 5% of the total aircraft drag (Tegarden, 1996), implying that the potential benefit of HLFC on the nacelle would be a reduction in the aircraft drag of ~1.6 -2%. Following the HLF nacelle flight tests (see section C.10, Appendix C), it was reported that the "pre-flight predictions of 1% fuel burn savings for a hybrid laminar flow nacelle were validated" (Tegarden, 1996).

**B.7.6 RR / DLR laminar flow nacelle (1990 - 1993)**

Barry (1995) of Rolls-Royce, following the flight testing of the RR / DLR laminar flow engine nacelle on the DLR ATTAS test aircraft (see section C.11, Appendix C), stated that the "total aircraft drag could be reduced by up to 2% for a medium-sized twinjet airliner if laminar flow could be maintained over the nacelle". He reported that "this technology could provide an overall reduction of 1.5% or more in fuel consumption of engines powering an airliner during a five-hour flight". Mullender and Reidel (1996) concurred with this statement and indicated a net benefit of 1.5% in SFC for a laminar flow nacelle, based on Rolls-Royce studies.

**B.7.7 NASA 300 passenger long-range twin-engine HLFC study (1991)**

Arcara *et al.* (1991) reported on the results of a NASA study to evaluate the application of HLFC to a long-range, twin-engine subsonic transport aircraft. The study was performed using a conceptual design and analysis computer program, designed for the evaluation of advanced aircraft concepts. A 300 passenger twin-engine turbulent



baseline aircraft was defined for a 6500nm, Mach 0.83 mission, with FAR international fuel reserves (explained in section D.3, Appendix D).

The conceptual design was then resized for a HLFC system providing laminar flow to 50% of the chord on the upper wing surface and 50% of both upper and lower surfaces on the empennage. This resizing was done for three different sets of assumptions. The HLFC-1 concept was resized to meet the mission, but took no account of increased system mass and increased SFC. HLFC-2 represented a more realistic scenario and took account of the HLFC system. The assumed penalties for the HLFC system were a power requirement of 224kW, weighing 1361kg and resulting in an increased SFC of 0.3%. For both HLFC-1 and HLFC-2, it was assumed that if the system failed, then the aircraft would divert or complete the mission, using part of the reserve fuel. HLFC-3 was sized to complete the mission if the HLFC system failed at the start of the cruise, and still satisfied the reserve requirements. This aircraft was heavier than the baseline design, as it included (like HLFC-2) the penalties of system weight and SFC increase. Compared to the turbulent baseline, the block fuel was reduced by 16.8% for HLFC-1, 15.1% for HLFC-2 and 6.8% for HLFC-3 for the design range. The block fuel savings achieved by HLFC-2 for an “average operational stage length” of 3000nm, were calculated to be 14.0% less than that for the turbulent baseline.

#### **B.7.8 HLFC study on A320 and A340 classes of aircraft (1992)**

Robert (1992) reported on the results of a study to determine the potential benefits that HLFC could bring to the A320 and A340 classes of aircraft. He argued that because HLFC is a cruise technology, the A340 would benefit more than the A320. This statement was supported by the observation that for an A320 on a 500nm sector, the cruise represents only 35% of the fuel burn, whilst for the A340 on a 3000nm sector, the cruise represents 80% of the total fuel burn. A drag reduction of 14% was estimated for the A340 class aircraft, by using laminar flow on the wing, empennage and engine nacelles. Robert (1992) stated that 60% of the drag reduction came from the wing upper surface and 30% from the lower wing. The study concluded that there was no point in laminarising the lower wing surface due to the presence of Krüger flaps, doors and access panels.

#### **B.7.9 Wilson (Cranfield University) HLFC study (~1997)**

Wilson (1997) used a MVO (Multi-variate Optimisation) approach to investigate the potential fuel and DOC advantages of HLFC, for five classes of aircraft:

- (1) A Fokker 100 class Regional Jet (107 seats, 2963km stage length);
- (2) An A320-200 class Short-range Twin (150 seats, 5463km stage length);
- (3) An A330-300 class Medium-range Twin (336 seats, 8334km stage length);
- (4) An A340-200 class Long-range Quad (265 seats, 13700km stage length);
- (5) An A3XX class Super-Jumbo (615 seats, 13835km stage length).



A turbulent baseline aircraft was defined for each aircraft type to meet the design specification of payload and design range. Using the MVO tool, the designs were optimised for minimum DOC for “average missions”, which were between 17% and 40% of the design stage lengths. The impact of drag reduction due to HLFC applied to the wing, empennage and nacelles was considered, with a corresponding weight and SFC penalty. Using the MVO tool, HLFC designs were produced to meet the same requirements as those set for the baseline aircraft. Wilson concluded that the benefits generally increased with both design and average stage length. It was noted that the Super-Jumbo benefited less than the Long-range Quad, due to Reynolds number limits reducing the extent of laminar flow (expressed as a percentage of chord) on the wing of the larger aircraft (Wilson, 1997).

#### B.7.10 Airbus long-range aircraft estimate

The 3E/LaTec strategy of Airbus considered a phased approach for the implementation of HLFC, which in the mid-1990s centred on the A320 HLFC fin test (see section C.14, Appendix C). Schrauf of Airbus, who has been the Coordinator of a number of CEC funded HLFC projects, provided the following drag reduction estimate for a long-range aircraft in the class of the A340. He stated that a 16% reduction in total aircraft drag was possible (Schrauf and Kühn, 2001; Schrauf, 2001). This would come from laminar flow on the upper wing (~12%), empennage (~3%) and nacelle (~1%).

#### B.7.11 Airbus HLFC fin

It has been demonstrated during flight tests that laminar flow can extend to ~50% of the chord of an A330 fin (see Fig. B-20). Results from the ELFIN II wind tunnel tests, on a HLFC fin, indicated that a reduction of over 40% of the profile drag is possible (Schrauf, 2001). Tests repeated under the HYLTEC project, using an upgraded model, confirmed this result, with ~41% drag reduction measured at low angles of attack (Schrauf, 2001).

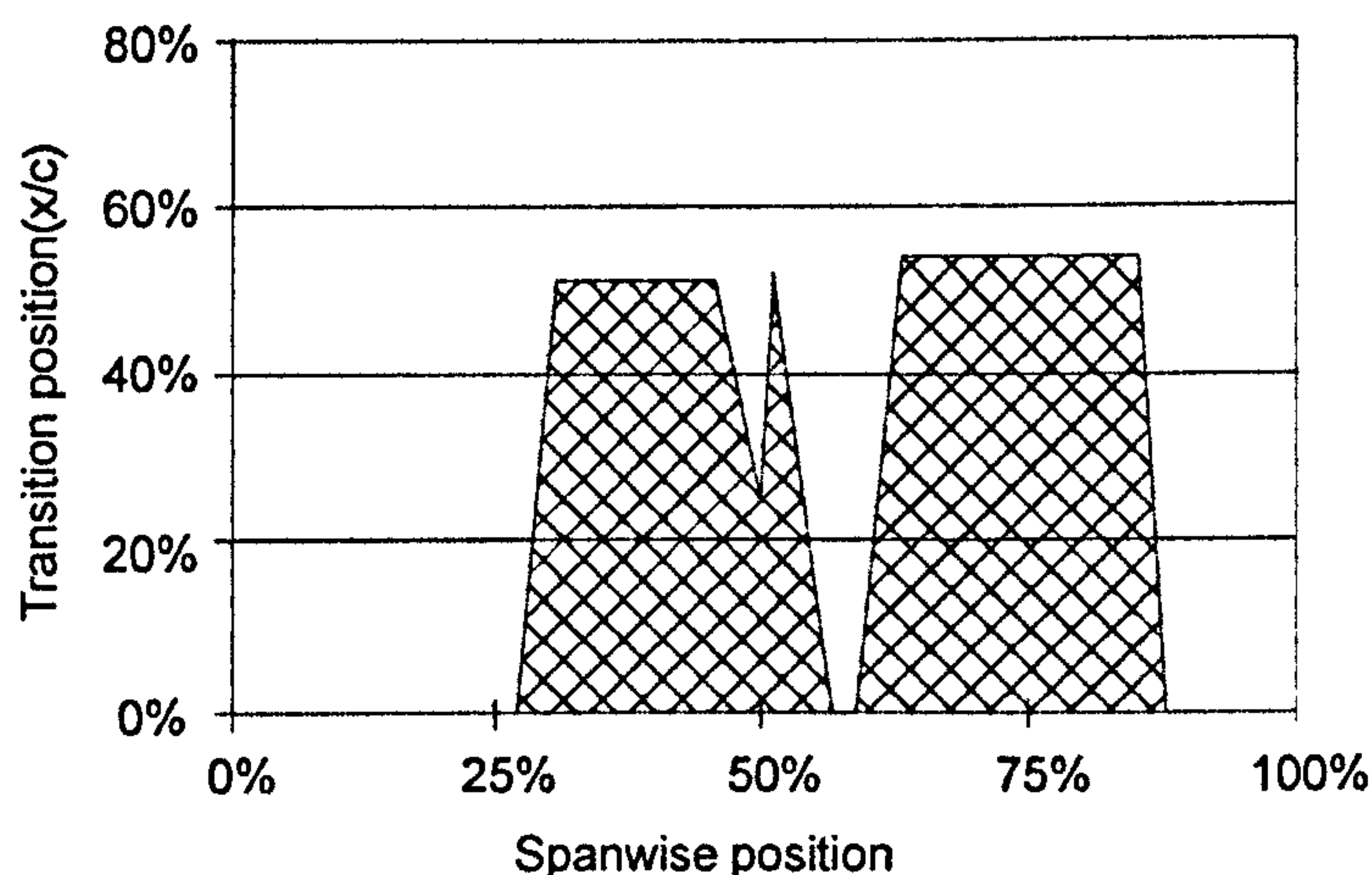


Fig. B-20 Measured laminar flow on A320 HLFC fin (redrawn after Henke, 2000)



Blank page



## APPENDIX C

# OVERVIEW OF MAJOR LFC AND HLFC STUDIES AND FLIGHT TEST CAMPAIGNS

### TABLE OF CONTENTS

C.1	Introduction .....	208
C.2	Early LFC Research (1939 - Late 1960s) .....	208
C.3	USAF / Northrop X-21A LFC Wing (Early 1960s) .....	210
C.4	NASA Jetstar LFC Wing (1983 – 1986) .....	211
C.5	Dassault Aviation NLF and HLFC Falcon 50 (1985 -1990).....	212
C.6	Boeing 757 HLFC Wing (1987 – 1991).....	212
C.7	F-16XL (1989 – 1996) .....	214
C.8	Project ELFIN (1989 – 1992) .....	215
C.9	Dassault Aviation Falcon 900 HLFC Wing (1990 - 1997) .....	216
C.10	GEAE / Rohr Industries HLF Nacelle (1991 - 1992).....	216
C.11	RR / DLR NLF and HLFC Nacelles (1990 - 1993) .....	217
C.12	Project LARA (1993 – 1994) .....	218
C.13	Project ELFIN II (1993 – 1996) .....	219
C.14	Airbus 320 HLF Fin (1993 –1998) .....	220
C.15	NASA / Boeing HLFC Wind Tunnel Tests (1993 –1995) .....	221
C.16	Project HYLDA (1996 – 1999) .....	221
C.17	Project HYLTEC (1998 – 2001).....	222
C.18	Project ALTTA (2000 – 2002) .....	224



## C.1 INTRODUCTION

The history of LFC research can essentially be divided into two time frames: from the late 1930s to the late 1960s, and then from the early 1970s to date. Two significant historical events separate the research efforts conducted before about 1970 and those conducted after that time period. At the end of the 1960s, the Vietnam War received the greatest priority for military and research resources in the USA. The result was a demise of interest in LFC research. Following the sharp rise in the cost of jet fuel in the mid-1970s (of the order of 300 - 400%), as a result of the OPEC oil embargo, there was much renewed interest in fuel saving technologies. The US Aircraft Energy Efficiency (ACEE) programme was the result (Povinelli *et al.*, 1976). Included as one element of this programme, was the objective to explore technologies that would significantly reduce viscous drag through LFC (Braslow and Muraca, 1978). This point also marked the start of a shift of emphasis away from military applications to civil transport aircraft applications. The strategy established in the late 1970s in the USA initiated a series of LFC and HLFC research programmes, which continued through the 1980s and early 1990s. From the early 1980s, there also emerged a renewed interest in Europe in LFC, partly as a response to the success achieved in the USA. The ELFIN (European Laminar Flow Investigation) project (1990 - 1992) was the first of a series of collaborative European laminar flow research projects that have made a large contribution to the current understanding of Laminar Flow Control.

In this appendix, the early research programmes are mentioned, and the major wind tunnel and flight test campaigns conducted since the late 1970s are reviewed.

## C.2 EARLY LFC RESEARCH (1939 - LATE 1960S)

The first LFC tests using suction are reported to have been conducted in the US by NACA in 1939 (Braslow and Muraca, 1978). Large scale wind tunnel models, with multiple suction slots, were used to demonstrate the viability of Laminar Flow Control. The successful tests were followed in 1941 by the first LFC flight experiments, performed with a B-18 aircraft. Over the next 30 years, steady and significant research progress was made by wind tunnel and flight experiments. Braslow (1999) traces the history of these early LFC research projects and Pfenninger (1977) provides a review of the significant technological achievements over the three decades. An important discovery was made in 1952, with the demonstration of Cross Flow Instability on the swept leading edge of an F86 by the RAE (Schrauf, 2001). In the US, the work culminated in the ambitious USAF / Northrop X-21A flight test campaign in the 1960s (see section C.3). Whilst in Britain, at about the same time, a swept slotted-suction wing was tested mounted vertically on the fuselage of a Lancaster bomber. A summary of the important early research milestones is presented in Table C-1.



Table C-1 Early LFC research (after Braslow and Muraca, 1978)

Where ?	What ?	How ?	When ?	Max. laminar R <sub>e</sub>	Major difficulty
USA (NACA)	Slots	Wind tunnel	1939	$7 \times 10^6$	Turbulence, noise
USA (NACA)	Slots	Flight – B – 18	1941	$4 \times 10^6$	Aircraft limit
Germany	Continuous	Analysis	Early 1940s	-	-
Germany	Continuous-perforations	Wind tunnel	Early 1940s	-	Hole disturbances
Switzerland	Slots	Wind tunnel	Early 1940s	$2.3 \times 10^6$	Turbulence, noise
USA (NACA)	Continuous-porous	Wind tunnel	1946 – 1952	$24 \times 10^6$	Surface roughness and buckling
USA (NACA)	Slots	Wind tunnel	Late 1940s	$10 \times 10^6$	Surface disturbances
USA (Northrop/NACA)	Slots	Wind tunnel	Late 1940s	$16\text{-}17 \times 10^6$	Surface disturbances
UK	Continuous	Analysis	1946 – 1950	-	-
UK (Cambridge Uni.)	Continuous-porous	Flight – Anson	1951	$3 \times 10^6$	Surface roughness
UK (RAE)	Continuous-porous	Flight – Vampire	1953	$29 \times 10^6$	Surface roughness
UK (RAE)	Continuous-perforations	Fight – Vampire	1954-1957	-	Hole disturbances
UK (Handley Page)	Strips-porous & perf.	Flt – Vampire Trainer	1951-1955	$15 \times 10^6$	Joint discontinuities, sweep
USA (Northrop/USAF)	Primarily slots- x-flow instability, slot design criteria, internal aero, acoustics, attach.-line contamination	Analysis & Experiments	1950s – early 1960s	-	-
USA (Northrop/USAF)	Slots	Flight – F-94	mid 1950s	$30 \times 10^6$	Local supercritical Mach, surface roughness
USA (Northrop/USAF)	Slots	Flight – X-21	Early 1960s	$40 \times 10^6$	Joint discontinuities, surface roughness, spanwise contamination, ice crystals
UK	Slots	Flight - Lanchester	Early 1960s		Spanwise contamination



### C.3 USAF / NORTHROP X-21A LFC WING (EARLY 1960S)

The USAF sponsored Northrop X-21A flight test programme – which evaluated a new laminar flow wing using two experimental aircraft, based on reconfigured WB-66D aircraft (Fig. C-1) – is described by Fowell and Antonatos (1965), Whites *et al.* (1966) and by Pfenninger and Reed (1966). The modifications included the installation of a new LFC wing, incorporating the suction system, new engines and the installation of LFC compressors in pods below each wing. The flight test programme, which started in April 1963, served to verify analytical studies and wind-tunnel tests of LFC swept wings; as well as to investigate manufacturing techniques and establish maintenance and operational data, applicable to LFC (Braslow, 1999).

According to Fowell and Antonatos (1965), the flight regime extended from about Mach 0.45 to Mach 0.80, and Reynolds numbers of 20 to 40 million (based on mean aerodynamic chord) were obtained. The suction was applied through slots, which covered ~95% of the wetted area of the upper wing surface and ~85% of the lower surface. The slots, flush with the surface, had widths ranging from ~80µm to ~250µm and the spacing between the slots varied between 10mm to 86mm. The air was channelled through internal ducts to the suction pumps. Laminarisation of 78% of the slotted area resulted in an aircraft drag change from  $C_D$  (turbulent) of 0.0220 to 0.0179, i.e. a reduction of ~18.6%.

Braslow and Muraca (1978) report that a number of fundamental difficulties of LFC were identified during these tests. The importance of surface smoothness and the avoidance of discontinuities (arising from spanwise wing splices) were vividly illustrated when premature transition of the boundary layer repeatedly occurred. Secondly, Attachment Line Contamination, which was not well understood at the time, was responsible for unexpected long runs of turbulent flow. It was also noted that partial or complete loss of laminar flow occurred temporarily when the aircraft flew through cirrus cloud and light haze.

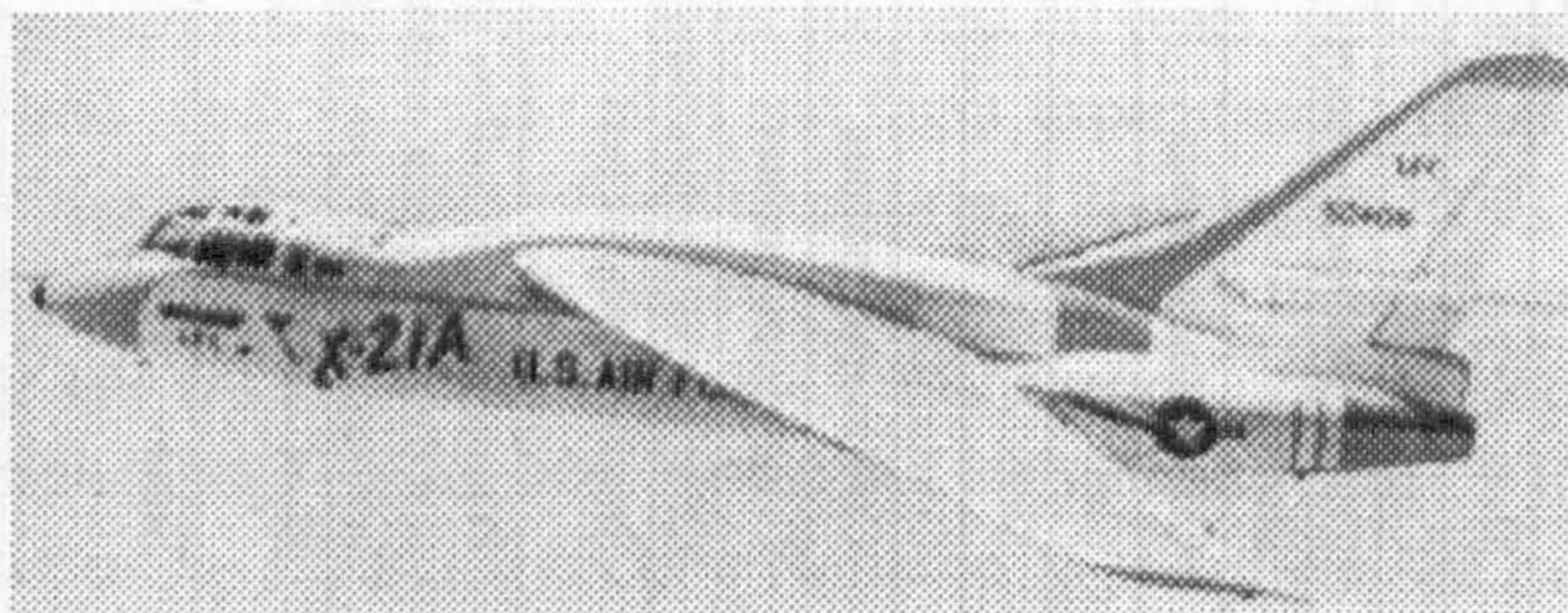


Fig. C-1 X-21A flight test aircraft (from Braslow, 1999)



#### C.4 NASA JETSTAR LFC WING (1983 – 1986)

A Jetstar (Lockheed C-140) aircraft was used as a test vehicle for LFC experiments by NASA, Douglas Aircraft and Lockheed-Georgia (Fig. C-2). Details of the aircraft modifications and the test flight tests are reported by Wagner and Fischer (1983), Davis *et al.* (1987; 1989) and Maddalon and Braslow (1990). The Lockheed designed concept (described by Etchberger, 1983; and by Lange, 1984; 1987) was tested on the port wing. It consisted of a titanium skin with 0.1mm wide slots, supported by a glass fibre-epoxy substructure. A fluid system for de-icing and for insect contamination protection utilised the forward slots near in the leading edge region, to expel a 60/40 mixture of propylene glycol methyl ether and water. After climb-out to 4000ft, the fluid was purged from the system and suction was initiated.

The Douglas designed article was tested on the starboard wing. It featured an electron beam drilled titanium skin, with holes of  $\sim 64\mu\text{m}$  diameter, in rows spaced  $\sim 890\mu\text{m}$  apart. The skin was bonded to a corrugated glass and carbon fibre substructure. The small channels formed by the corrugations (and the outer skin) formed the suction chambers (plenums), which ducted the air to the suction pump. A Krüger flap was used as an insect shield, which was retracted after reaching 6000ft. A TKS anti-icing system was installed on the nose of the flap, with aft-facing spray nozzles at the back of the flap for the protection of the wing upper surface (see Fig. 9-6, Chapter 9).

Both LFC test articles extended from the leading edge to the front spar and thereafter, a fairing extended the required profile back to  $\sim 65\%$  of the chord. A Gaster type bump was used to avoid Attachment Line Contamination, although other designs such as a leading edge notch were also tested. Laminar flow was observed to extend to between 83% and 97% of the glove (on the Douglas article) and between 74% and 97% (on the Lockheed article). In addition to demonstrating the viability of the LFC design, the aircraft was flown in a Simulated Airline Service (SAS) study to evaluate the LFC concept under operating conditions (Maddalon and Braslow, 1990).

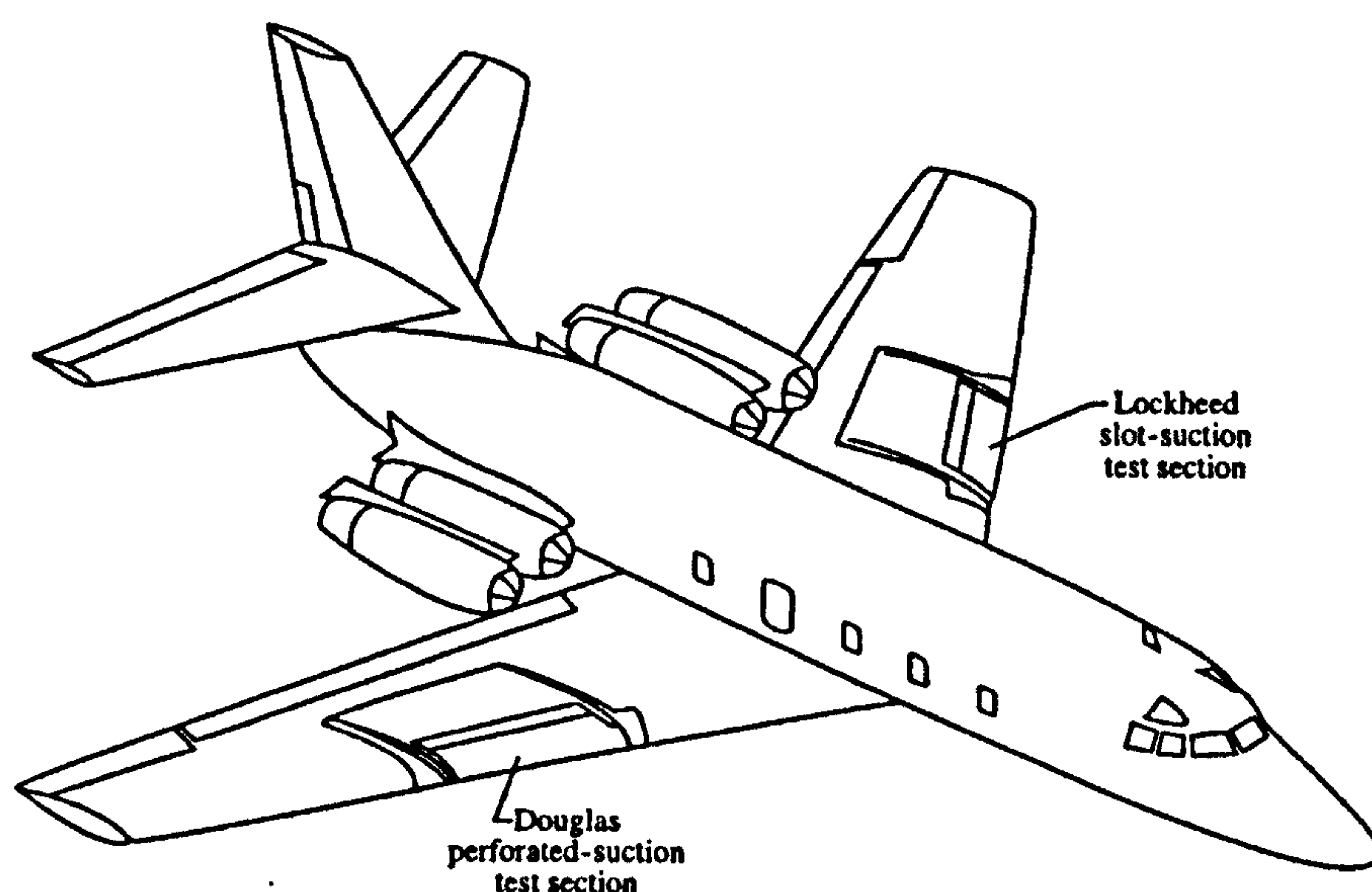
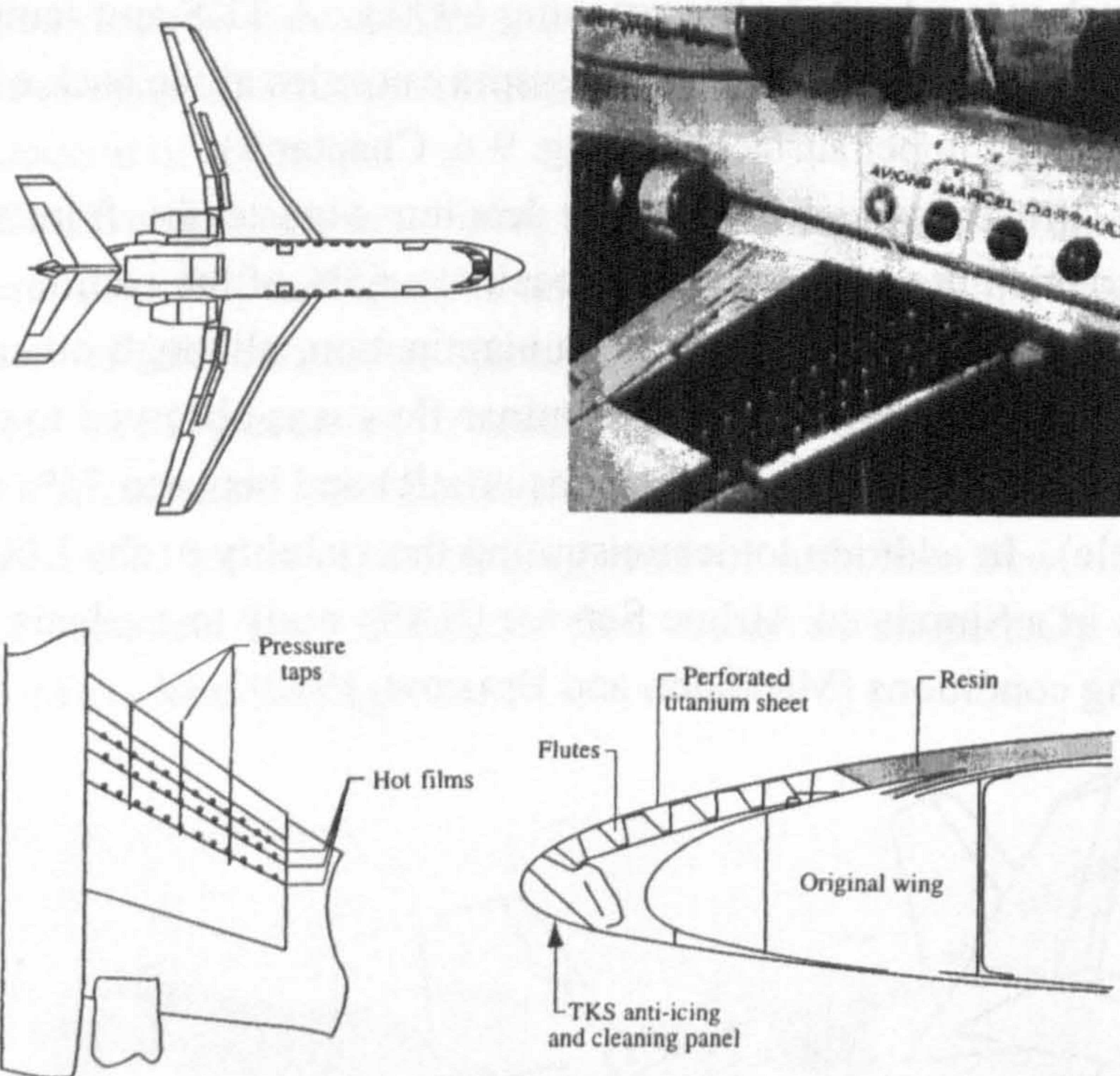


Fig. C-2 Jetstar LFC flight test aircraft (from Joslin, 1998a; after Fischer *et al.*, 1983)



### C.5 DASSAULT AVIATION NLF AND HLFC FALCON 50 (1985 -1990)

Between 1985 and 1987, Dassault Aviation performed a series of NLF tests on the fin of a modified Falcon 50 business jet (Bulgubure and Arnal, 1992). The test data was used to validate and extend the capabilities of transition prediction tools. These tests were extended to explore HLF by installing a test section on the right inboard wing, which has a leading edge sweep angle of  $35^\circ$  (Fig. C-3). Bulgubure and Arnal (1992) describe the design and manufacture of a new leading edge (which fitted over the original structure), incorporating the suction and anti-icing / cleaning system. Two TKS anti-icing panels, located on the attachment line, enabled monopropylene glycol to be applied to the leading edge surface. Suction through the laser perforated skin was achieved using six flutes (suction chambers) connected to a jet pump, via a plenum chamber. The ability of a leading edge "bump" to prevent Attachment Line Contamination, was verified. The tests, which continued to 1990, demonstrated that relatively low suction rates were required to develop controlled laminarity (Maestrati and Bulgubure, 1996).



**Fig. C-3** Dassault Falcon 50 HLFC demonstrator aircraft  
(from Joslin, 1998a; after Bulgubure and Arnal, 1992)

### C.6 BOEING 757 HLFC WING (1987 – 1991)

Boeing, NASA and the USAF Wright Laboratory initiated a cooperative flight programme in 1987, based on the use of a Boeing 757 (Fig. C-4). Test flights evaluated the performance of a 6.7m HLFC system installed on the outer left wing panel (Collier, 1993). The new leading edge section consisted of a perforated titanium outer skin,



suction flutes under the skin and collection ducts to allow suction control of boundary layer instabilities (see Fig. B-11, Appendix B). The re-designed leading edge contained a Krüger flap, which also functioned as an insect shield for takeoff and a hot air de-icing system. The main wing box portion of the test area consisted of the original Boeing 757 structure, and was only subjected to a "minor clean-up" that involved, for example, the shaving off of exposed rivet heads.

Flight testing took place in 1990 and 1991. The flight experiments were designed to: (1) Develop a database on the effectiveness of the HLFC concept, applied to a large, subsonic commercial transport; (2) Evaluate real-world performance and reliability at flight Reynolds numbers (including off-design conditions); and (3) Develop and validate integrated and practical high-lift, anti-ice, and HLFC systems (Collier, 1993).

Hot film sensors and limited infrared measurements were used for boundary layer transition detection. Wake-survey probes were used to infer local drag reduction estimates. The state of the boundary layer, internal and external pressure distribution and the suction system flow rates, were monitored "real time" during the flight test. The hot film sensors indicated laminar flow to beyond 65% of the chord, at suction levels substantially below those initially thought to be required (Maddalon, 1991; Collier 1993).

The wake-rate measurements indicated a local drag reduction of the order of 29% percent, with the HLFC system operational; which, if projected to the entire wing would result in a 6% drag reduction for the aircraft (Maddalon, 1991; Collier, 1993).

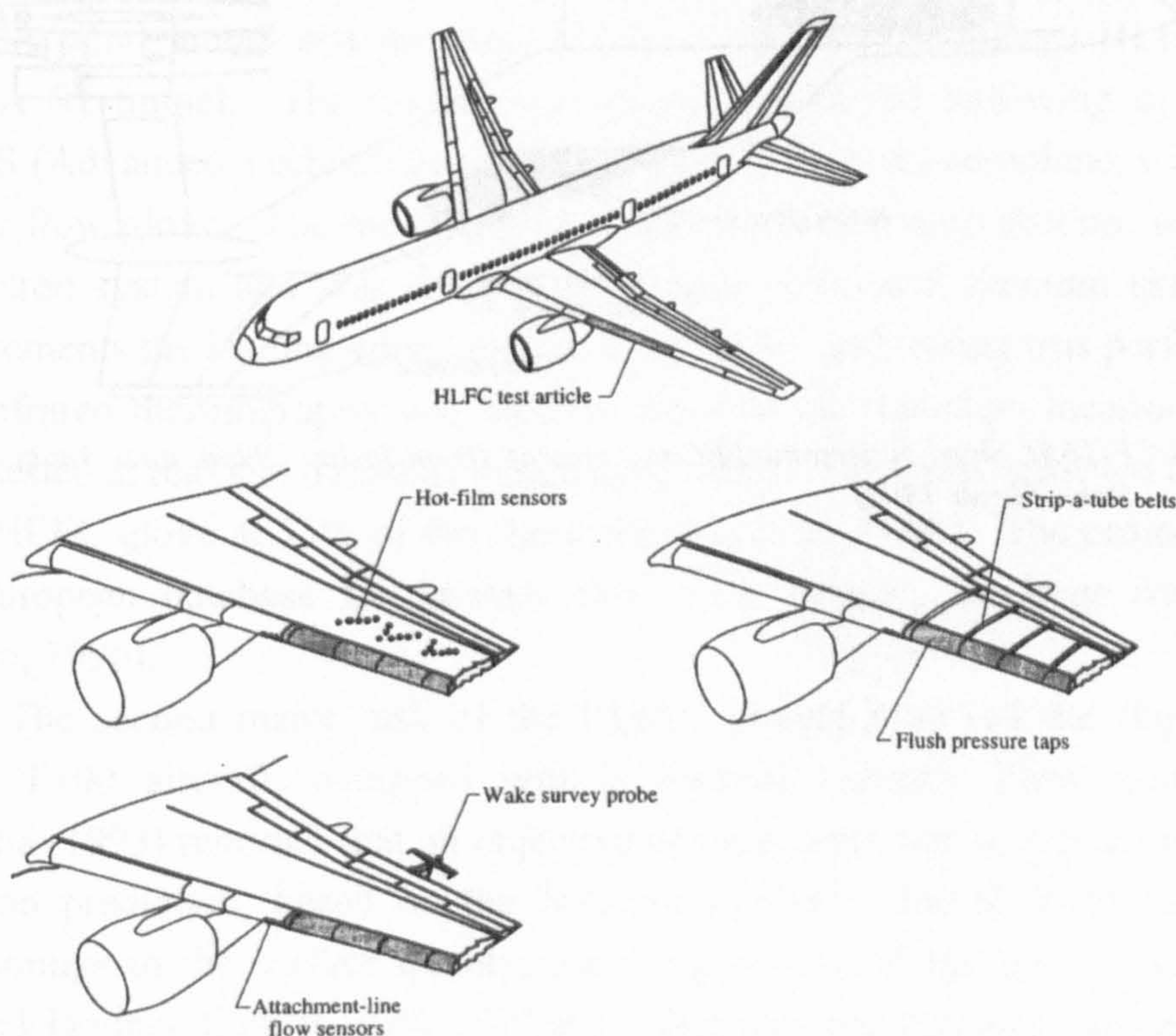


**Fig. C-4** Boeing 757 HLFC flight test aircraft with instrumentation  
(from Maddalon, 1991; Collier, 1993)



### C.7 F-16XL (1989 – 1996)

Supersonic LFC flight tests were conducted by NASA and a US industry team, on two delta wing F-16 XL testbed aircraft. NASA and Rockwell International carried out the flight tests with the F-16 XL Ship 1 (Fig. C-5), whilst a NASA, Rockwell, Boeing and McDonnell Douglas team, carried out the flight tests on Ship 2 (Fig. C-6).

A Rockwell designed suction glove was fabricated and installed on Ship 1. Flight testing took place in 1990. Because of the geometrical constraints of installing the glove, active suction was limited to the first 25% chord, and Attachment Line Instabilities were the primary focus of the tests (Joslin, 1998a).

The foam and fibreglass passive glove designed by McDonnell Douglas for Ship 2 had a 4.5m span and 10% chord section. The goals of the tests, conducted in 1991 and 1992, were to obtain surface pressure data to calibrate Euler design codes, and to study fuselage induced Attachment Line Contamination. Based on the results of these tests, a perforated suction glove, constructed of titanium skins and aluminium stringers, was installed on Ship 2. The supersonic flight tests conducted in 1996 had the objective of achieving laminar flow over 50 - 60% chord (Joslin, 1998a; 1998b).

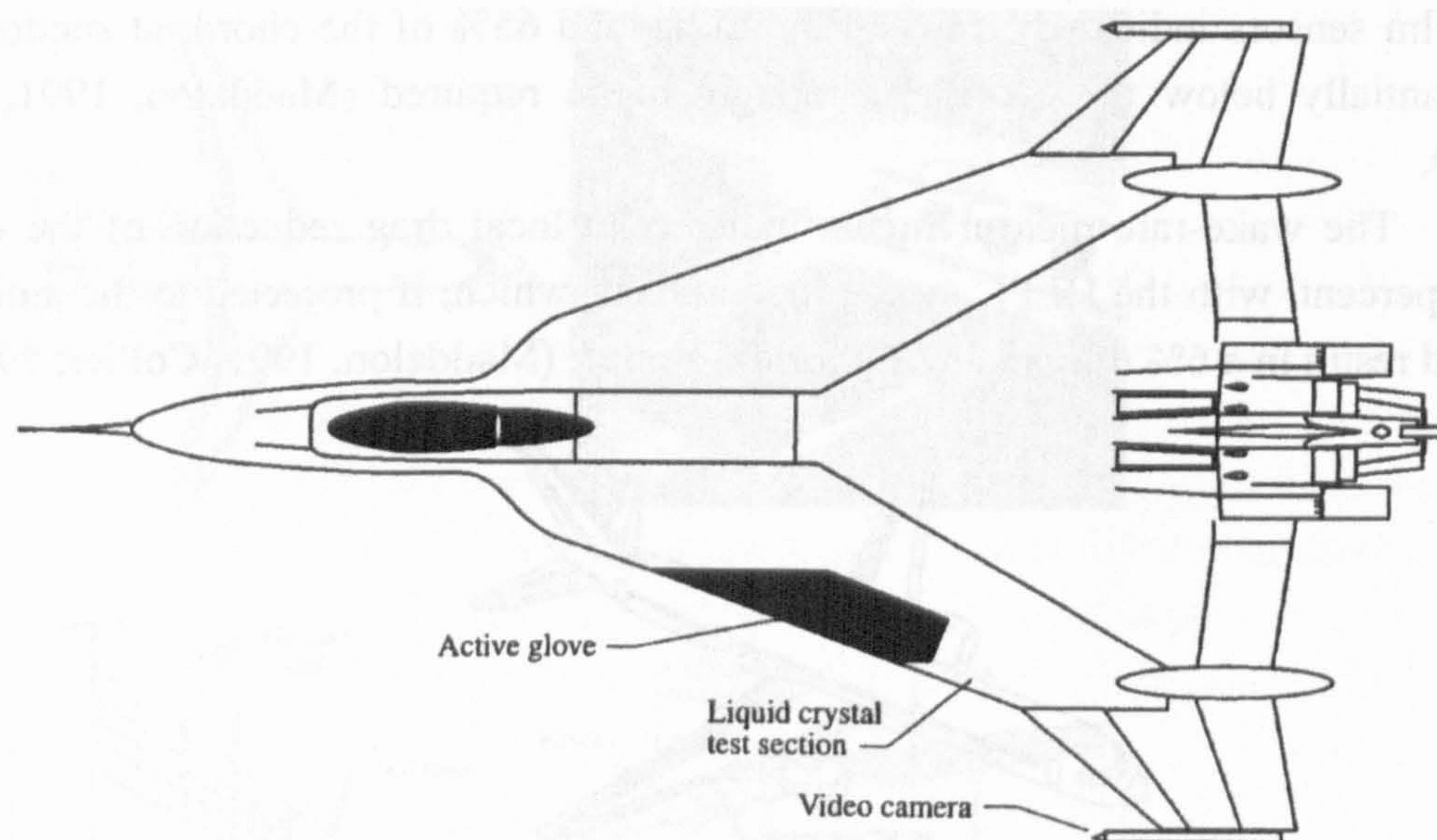


**Fig. C-5** *F-16XL Ship 1 supersonic LFC test aircraft (from Joslin, 1998a; after Anderson and Bohn-Meyer 1992)*



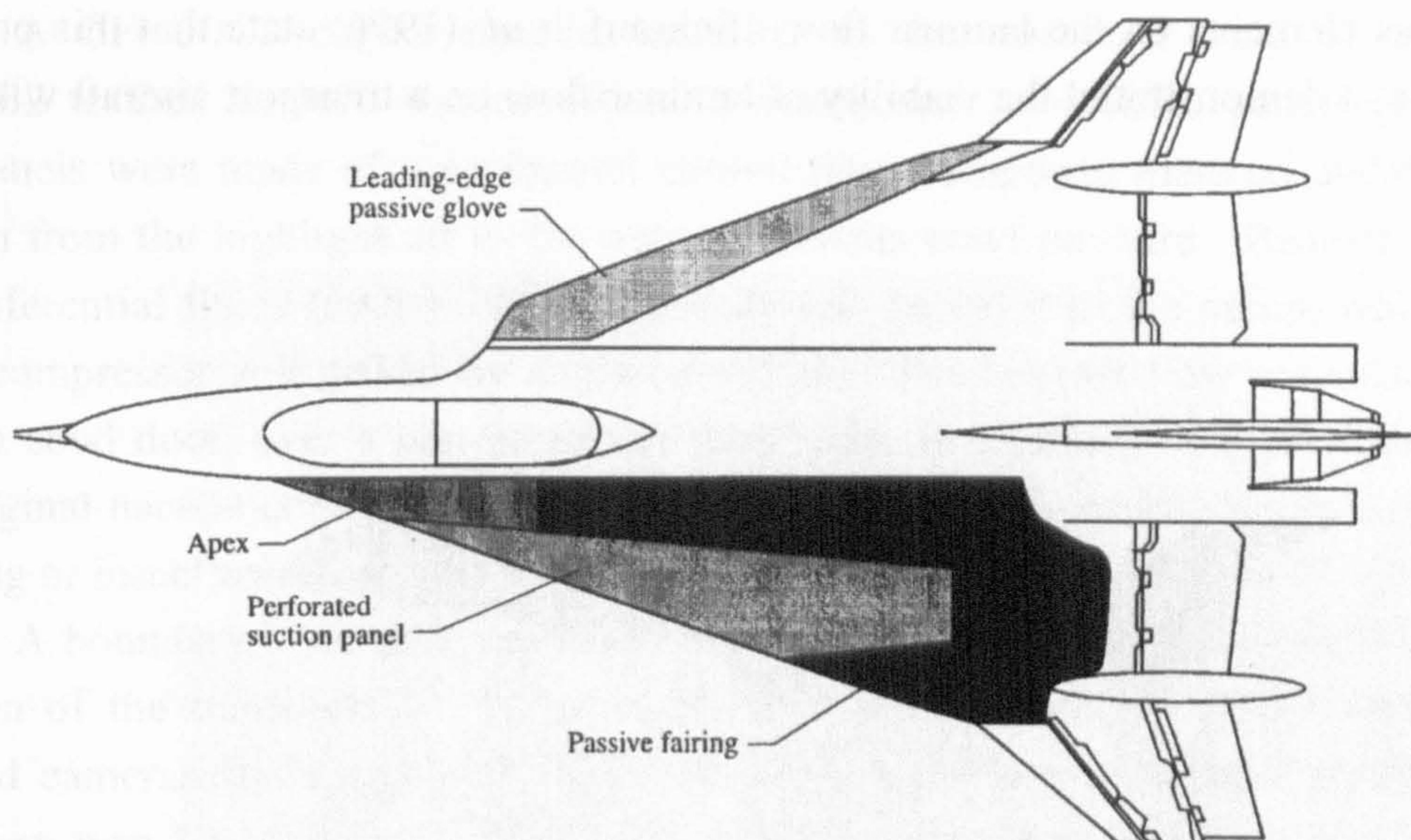


**Fig. C-6** *F-16XL Ship 2 supersonic LFC test aircraft (from Joslin, 1998a; after Smith, 1995)*

### C.8 PROJECT ELFIN (1989 – 1992)

The ELFIN (European Laminar Flow Investigation) project was conducted within the CEC Second Framework Programme by 24 partners, and was coordinated by Deutsche Airbus (Anon, 1992). The main objectives of the project were to prove the basic concepts of laminar flow technology, and "to prepare the tools, methods and systems required for its successful application to a wide range of practical airframes, from small subsonic commuters to large transonic transport aircraft" (CORDIS, 2001).

A wind tunnel test programme was completed on a large HLFC wing in the ONERA S1 tunnel. The model represented a modified half-wing of the VFW-614 ATTAS (Advanced Technologies Testing Aircraft System) aeroplane, with a 1.2m span laminar flow glove. The modification concerned a new nose section, which contained the suction system and was covered by a laser perforated titanium skin. For HLFC measurements the leading edge sweep was set at  $28^\circ$  and testing was performed at Mach 0.7. Infrared thermography was used to measure the transition location on the glove. When tested at realistic transonic conditions, laminar flow was achieved to the aft extent of the HLFC glove at 55% of the chord (Henke *et al.*, 1993). The project provided the first European database for laminar flow with suction, for large transport aircraft (Hansen, 1996).

The second major task of the ELFIN project involved the flight testing of a Fokker F100 aircraft, equipped with a Natural Laminar Flow glove (Fig. C-7). Dziomba (1993) reported that an objective of these tests was to refine the calibration of transition prediction, based on the N-factor method. Initial flight tests highlighted shortcomings in the surface quality, requiring rework of the glove. Subsequent tests achieved laminar flow to 40% of chord. The positive outcome resulted in industrial partners continuing the testing, primarily to evaluate the impact of artificial surface



roughness elements on the laminar flow. Schrauf *et al.* (1996) state that this proof-of-concept test demonstrated the viability of laminar flow on a transport aircraft with up to 130 seats.



**Fig. C-7** Fokker 100 with NLF glove on starboard wing (from Schrauf and Kühn, 2001)

### **C.9 DASSAULT AVIATION FALCON 900 HLFC WING (1990 - 1997)**

The positive results of the Falcon 50 tests, resulted in the FLAM (Falcon Laminar) programme, involving the installation of a HLF system in the inboard wing sections of a Falcon 900 business jet. According to Fiton (2000), the purpose of the demonstration was to “design, manufacture and certify an aircraft with Hybrid Laminar Flow with industrial methods with consideration of weight and cost constraints and then to put the aircraft into service to analyse the behaviour of the device and look for any operational problem there may be”.

After its certification in February 1995, the Falcon 900 went into service with Dassault Falcon Service for two years, in which it accumulated more than 1500 flight hours, including 1000 hours with HLF, reported Bulgubure (1999) of Dassault Aviation. The flight tests demonstrated the efficiency gains of the suction system and leading edge anti-contamination device, over a wide range of lift coefficients and Mach numbers. The in-service operations reported no failures of the suction / cleaning system. Contrary to expectations, no leading edge contamination and problems were observed; however, a mechanical design problem with a leading edge joint was reported (Bulgubure, 1999).

### **C.10 GEAE / ROHR INDUSTRIES HLF NACELLE (1991 - 1992)**

General Electric Aircraft Engines (GEAE) initiated a project, with Rohr Industries, AlliedSignal Aerospace and NASA, to explore the use of HLFC on nacelles. The main objective of the project was to demonstrate the feasibility of laminar flow nacelles for modern high-bypass engines, and to investigate the influence of aerodynamic characteristics and surface effects on the extent of laminar flow (Bhutiani *et al.*, 1993; Tegarden, 1996).



A CF6-50C2 engine nacelle, installed on the starboard wing of an Airbus A300/B2 testbed aircraft, was modified to incorporate two HLFC panels (Fig. C-8). The panels were made of a perforated carbon fibre composite material and permitted suction from the highlight aft to the outer barrel-fan cowl juncture. Beneath the skin, circumferential flutes (ducts) collected the air and ducted it to the pump, which was a turbo-compressor unit driven by engine bleed air. The laminar flow extended beyond the fan cowl door, over a non-perforated composite structure, which was blended into the original nacelle contour ahead of the thrust reverser. No provisions were made for de-icing or insect contamination avoidance on this experimental set-up.

A boundary layer rake was used to assess the state of the boundary layer. The position of the transition of the boundary layer was studied, using hot-film gauges, infrared cameras and surface embedded microphones. The duration of the flight test campaign was 50 hours. The HLFC concept was effective over the range of cruise altitude and Mach number, and resulted in laminar flow to 43% of the nacelle length (the design objective) independent of altitude (Bhutiani *et al.*, 1993; Collier, 1993). At this transition location, static-pressure sensors indicated the onset of the pressure recovery region, which caused the laminar boundary layer to become turbulent.

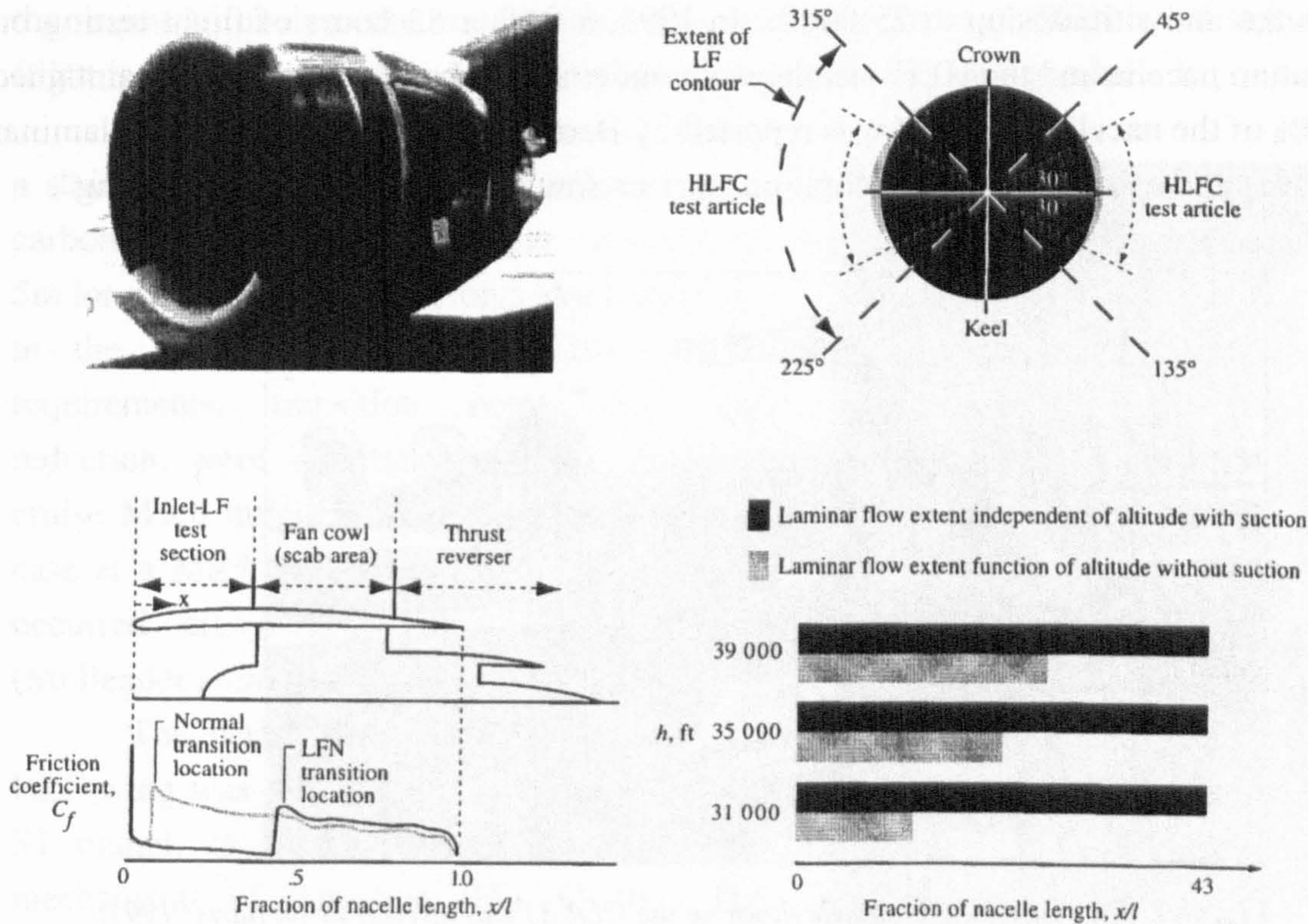


Fig. C-8 GEAE HLFC nacelle test article flown on an Airbus A300/B2 (from Joslin, 1998a, after Bhutiani *et al.*, 1993)

C.11 RR / DLR NLF AND HLFC NACELLES (1990 - 1993)

The joint Rolls-Royce / DLR laminar flow engine nacelle project is described by Barry (1995) and by Mullender and Reidel (1996). The project was launched in 1990,



with major subcontractors Hurel Dubois UK, MTU and Oxford University, supported financially by the UK Department of Trade and Industry. The DLR's ATTAS test vehicle (a VFW614 aircraft) was used. A laminar flow nacelle, which was later modified for HLF, was installed on one of the aircraft's Rolls-Royce Snecma M45H engines (Fig. C-9).

The suction surfaces were laser drilled carbon fibre composite. The holes had a nominal diameter of  $50\mu\text{m}$  and the pitch varied from 10 to 18 times the hole size. (The pitch governed the pressure drop through the surface.) The instrumentation included "axial rows of surface static pressure tapings, axial rows of flush mounted platinum-resistance thermometers, accelerometers, base pressure tapings on the trailing edge of the nacelle; Kulite pressure transducers and probe microphones mounted flush to the nacelle surface" (Mullender and Reidel, 1996). Infrared cameras and hot film gauges were used for transition detection. Insect contamination protection was provided by a cleaning fluid, exuded through a perforated region aft of the leading edge. The decontamination wash was switched on before takeoff and kept on until the aircraft climbed above the insect threat height, indicated by Barry (1995) as usually being 1000ft above the ground. It was also used during descent and landing.

Completed by 1992, 40 hours of flight testing were accomplished at speeds up to Mach 0.6 and altitudes up to 25 000ft. In 1993, a further 53 hours of flight testing on the datum nacelle and the HLF nacelle, were undertaken. Laminar flow was maintained to 60% of the nacelle chord. It was reported by Barry (1995) that "the extent of laminar flow was not affected by noise, vibration, surface finish, roughness or solar heating".

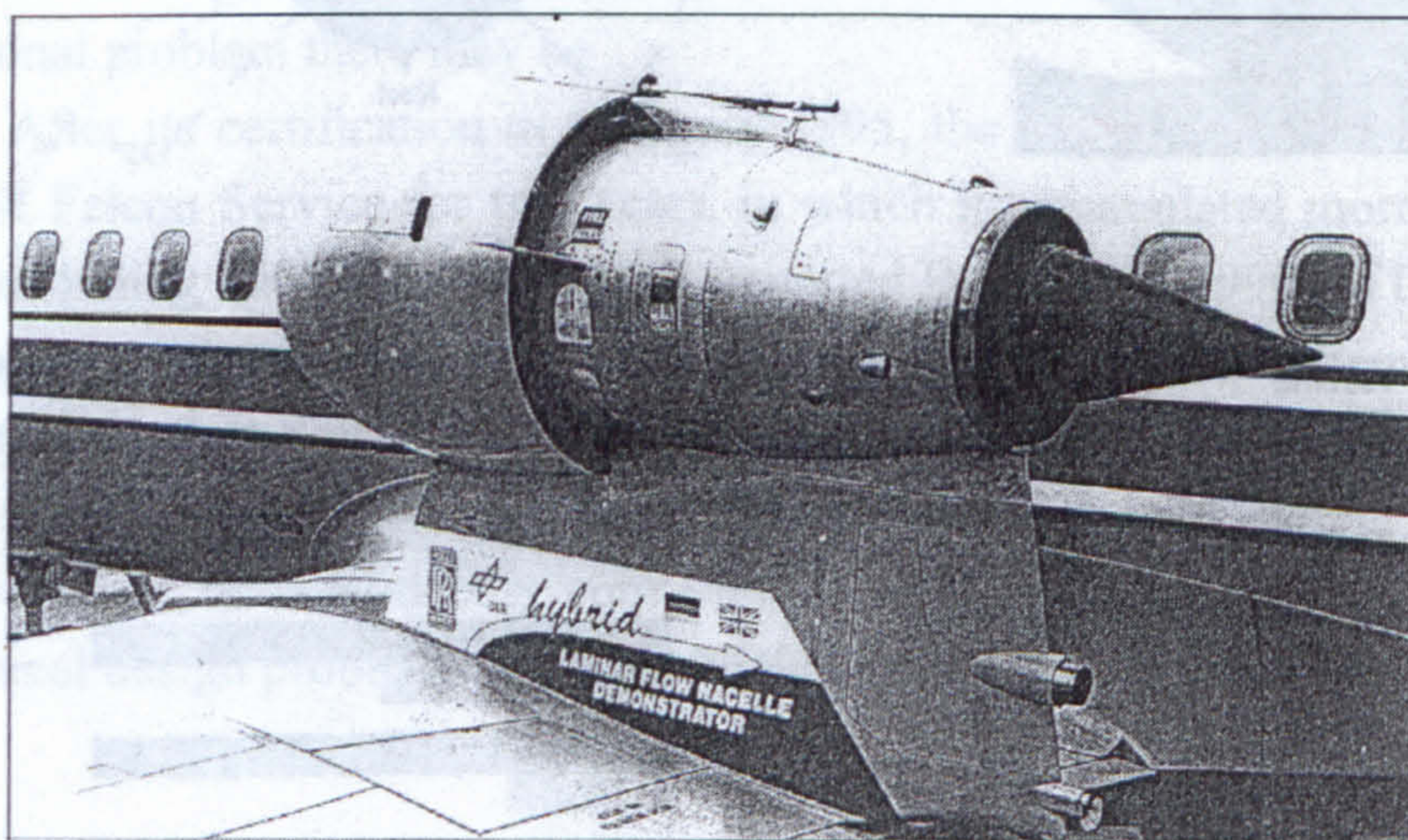


Fig. C-9 RR / DLR HLFC nacelle flown on the DLR ATTAS aircraft (from Barry, 1995)

## C.12 PROJECT LARA (1993 – 1994)

The LARA (Laminar Flow Research Action) project was a small offshoot programme of the ELFIN project, conducted under the CEC Third Framework Programme. A series of investigations were conducted, dealing with issues like off-



design behaviour of laminar flow nacelles, by means of large wind tunnel tests. Leading edge contamination was further explored in the project. The stability of the boundary layer after transition resulting from insect disturbance was studied (Barrett *et al.*, 1996). The effectiveness of insect contamination shielding by means of a Krüger flap, and the viability of protecting the leading edge using liquid systems, was also investigated (Dziomba, 1993).

A low speed laminar flow engine nacelle, designed and manufactured by Rolls-Royce, Snecma, DLR, ONERA and Hispano-Suiza was tested in the ONERA F1 wind tunnel in 1994 (Shipley, *et al.*, 1993; Mullender *et al.*, 1996). A companion high-speed model was manufactured and evaluated about the same time, but as part of the ELFIN II project.

Details on the experimental and theoretical work undertaken in projects ELFIN, ELFIN II and LARA, are described by Dziomba (1993).

### C.13 PROJECT ELFIN II (1993 – 1996)

The ELFIN II project, like the sister project LARA, followed on directly from the first ELFIN project, with many of the same research partners involved. It provided the means to analyse the considerable data generated in the ELFIN wind tunnel and flight test campaigns. A second wind tunnel test series was also conducted.

The HLF engine nacelle model featured a stainless steel suction region, followed by a carbon fibre composite aft section. It was over 5m long and was tested at cruise Mach numbers in the ONERA S1 tunnel. The suction requirements, transition point and drag reduction, were investigated over a range of cruise Mach numbers. For the zero incidence case at a Mach number of 0.78, the transition occurred aft of the 50% chord location (Mullender *et al.*, 1996).

The performance of a new large-scale HLF wing was also undertaken in the ONERA S1 tunnel, to investigate more precisely the mechanisms of transition (Fig. C-10). The performance of HLF aerofoils at off-design conditions was explored.



**Fig. C-10** ELFIN II HLF wing in ONERA S1 tunnel (from Schrauf and Kühn, 2001)



### C.14 AIRBUS 320 HLF FIN (1993 –1998)

The Airbus 320 HLF fin project, intended as the first step in a three part strategy under the name LaTec (Laminar Technology), was established by the (former) Airbus partners to develop HLF technology (Fig. C-11). The second step according to Thibert *et al.* (1992) was intended to be a laminar wing glove and the third step, a full laminar flow wing.

Flight tests of the HLF fin were conducted in autumn 1998, but the reduction of the flight test data continued for a number of years after the tests ended (Henke, 1999). The project also involved the testing of a half scale model of the fin, with leading edge suction in the ONERA S1 tunnel. The objectives of the A320 HLF fin programme were to calibrate transition prediction tools and establish LFC suction criteria. According to Henke (1999; 2000) the objectives of this programme were:

- To achieve laminar flow under cruise condition, for about half of the fin.
- To vary Mach number and altitude, so that that HLF can be studied for a wide range of Reynolds numbers.
- To use the test for rating HLF in general (i.e. to assess manufacturing tolerances, power supply, etc.).

The Laminar Flow Control section of the fin was constructed of a laser perforated titanium skin, with titanium suction chambers beneath the skin. The extent of laminar flow was measured using infrared photography, pressure measurements and piezoelectric sensors. These measurements were evaluated against wake rake data, temperature and pressure observations from the suction system, and against the power consumed by the suction system (Henke, 1999; 2000). The flight tests confirmed that HLFC can substantially reduce drag on a modern large transport aircraft. The suction system operated under a wide range of flight conditions, in order to explore the physical limits of applicability of HLF technology.



Fig. C-11 A320 test aircraft with HLF fin (from Schrauf and Kühn, 2001)



Henke (2000) makes a number of concluding statements based on the flight test campaign:

- Suction directly at the leading edge may not be necessary, if there is a functioning device against Attachment Line Transition, such as a Gaster bump.
- Surface imperfections in-flight are less critical than would be expected based on wind tunnel tests.
- There is a self-cleaning effect in-flight, especially when flying through clouds, but water ingress must be avoided.
- No degradation of surface or hole quality was experienced.
- The expected laminarity was reached, even with a test item that was partially outside of the specified limits (in terms of surface tolerances).
- By measuring the fuel flow at constant aircraft conditions, with and without suction, the expected drag reduction was demonstrated.

### **C.15 NASA / BOEING HLFC WIND TUNNEL TESTS (1993 –1995)**

A joint NASA / Boeing wind tunnel experiment was conducted in the Langley 8-foot Transonic Pressure tunnel, using a 2.1m span model. The objectives were to provide a better understanding of the flow over a swept wing geometry, to provide a calibration of the data base for LFC design tools, and to better understand the issues of suction system design (Joslin, 1998a).

### **C.16 PROJECT HYLDA (1996 – 1999)**

The CEC sponsored HYLDA (Hybrid Laminar Flow Demonstration on Aircraft) project was comprised of three main studies, involving the wing, the engine nacelle (Fig. C-12) and the A320 HLF fin. The project was coordinated by Airbus Germany (known as Daimler-Benz Aerospace Airbus at the time). It had 23 partners, including the University of Limerick, where the author was responsible for the University's contribution. The overall project objective was to investigate the factors that were needed to bring HLF technologies to the stage of readiness for flight demonstration.

The nacelle task group developed two conceptual designs for HLF nacelles, which were based on the CFM-56-5C engine, installed on the Airbus A340. According to Meyer

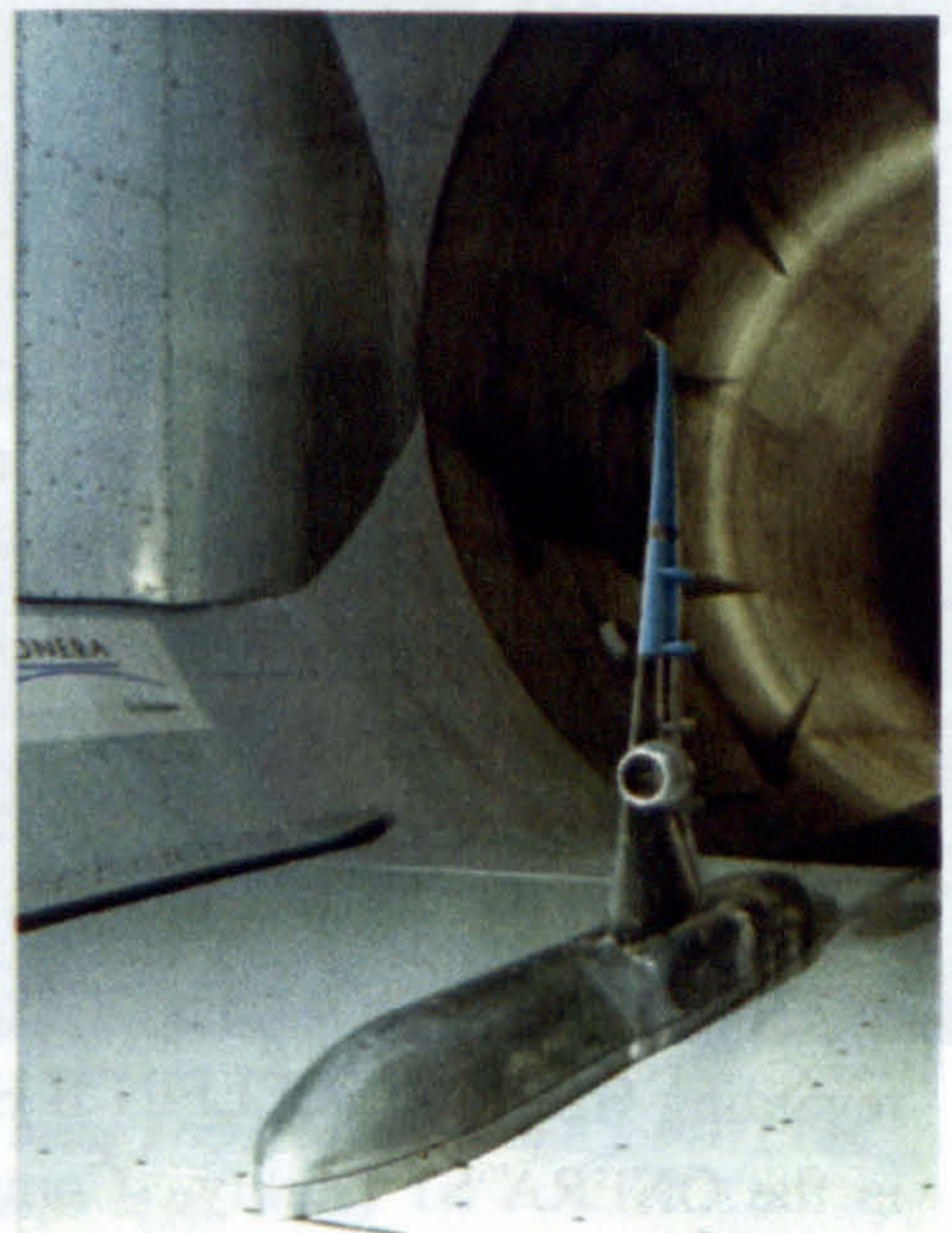


**Fig. C-12** HYLDA nacelle in the ONERA S1MA tunnel (from Meyer, 2000)



(2000) "both designs were based on the translating forebody concept: a demonstrator nacelle which replaces the existing intake and fan cowl doors, puts an overstructure on the thrust reverser unit and retains the production nozzle; and a notional production nacelle, where these constraints are removed" (Figures C-13). The goal of achieving laminar flow to 50% of the nacelle chord was "almost reached", with a resulting 35% reduction in nacelle friction drag predicted (Meyer, 2000).

The aim of the HLF wing task was to develop a wing glove, for a large transport aircraft, that would operate at Mach numbers in excess of 0.80 and at a Reynolds number greater than 30 million. The third element of the programme investigated the effects of surface roughness on laminar flow transition, by the application of artificial surface disturbances (Daimler-Benz Aerospace, 1995).

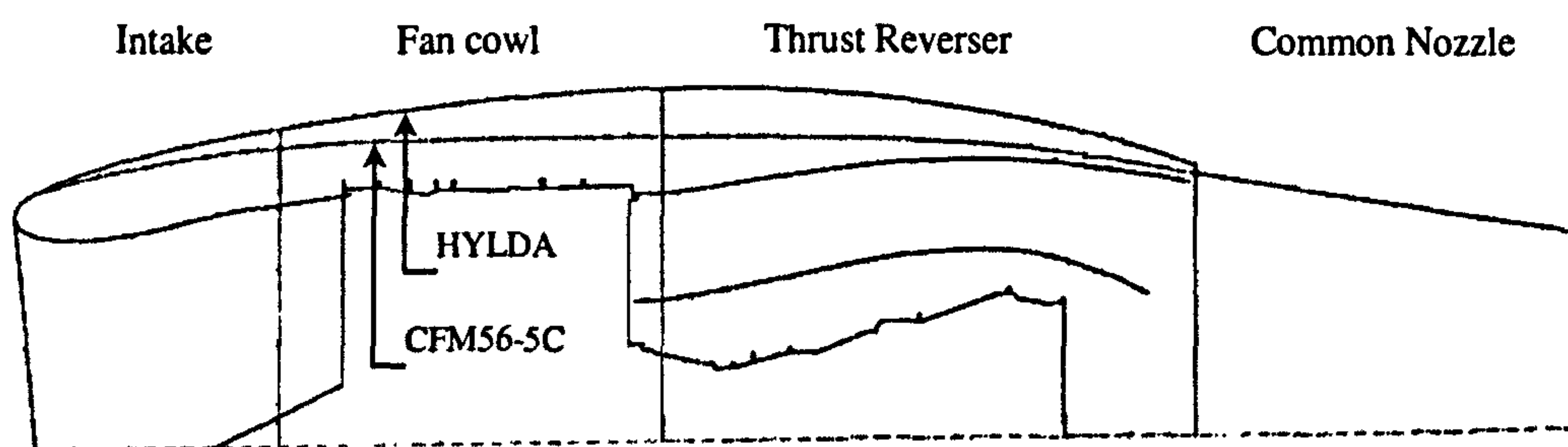


**Fig. C-13** Typical section showing the HYLDA loft lines over the original CFM56-5C lines (Courtesy Meyer<sup>1</sup>)

### C.17 PROJECT HYLTEC (1998 – 2001)

The HYLTEC (Hybrid Laminar Flow Technology) project focused on the technologies required for the full-scale development of a HLFC wing, with a particular emphasis on manufacturing and contamination related issues. The project was coordinated by Airbus Germany (formally DaimlerChrysler Aerospace Airbus). It had 15 partners, including the University of Limerick (where the author was responsible for the University's contribution).

The project had three major tasks, which are described by Bieler (1999a; 1998b) and Bieler *et al.* (2002). Task 1 considered manufacturing, systems and operational issues seen as critical, in terms of spoiling the performance of HLFC. Task 2 was devoted to HLFC retrofit studies for in service aircraft; whilst task 3 was concerned with the generation of new experimental data, needed for the validation of numerical predictions and the support of design strategies. Two wind tunnel test programmes and two flight test campaigns took place, to investigate specific elements of concern regarding HLFC. The ELFIN II HLFC wing model was tested at cruise Mach number in the ONERA S1 facility. Complementary data analysis of the A320 fin flight test results was also undertaken.

<sup>1</sup> P. Meyer, Rolls-Royce plc, Derby, UK



Humphreys and Totland (2000) describe the test program involving an in-service SAAB 2000 commuter aircraft (Fig. 9-5, Chapter 9). The tests commenced in August 1999 with the aircraft flying standard passenger service routes in Northern Europe. The objective was to investigate and gain experience in the aspects of contamination and durability of porous HLF surfaces. Two small panels were installed in the leading edge. Although no suction was applied, the natural pressure differential at the wing nose ensured that air passed through the panels. A Liquid Contamination Control System (LCCS) – incorporating a reservoir, mechanical pump and ducting to the perforated skin panel – was installed in the one wing; but the other wing panel was not cleaned. De-icing fluid was exuded onto the skin surface during the takeoff run and switched off at a height of 1500ft. The effectiveness of the LCCS in preventing insect and other contamination of the perforated surface was demonstrated. The durability of the laser perforated test segments, installed in the holder on the "passive" panel, was evaluated by the author in conjunction with HYLTEC research partners. (This is described in section M.4, Appendix M.)

The second flight test campaign was coordinated by the DLR and utilised a Do 228 aircraft (Fig. C-14). The objective of the tests was to investigate the performance of various combinations of suction, ice protection and insect contamination protection. The leading edge of the right wing was modified to incorporate three test sections. The innermost box contained a hot air de-icing system and a Krüger flap for contamination protection. The middle section was equipped with a liquid TKS de-icing system and a fluid anti-contamination system; whilst the outboard (reference) section had a liquid TKS de-icing system, but no insect protection.

An anti-contamination system was designed based on the transpiration of foam through the porous leading edge surfaces (see section 9.6, Chapter 9). Surfactants and enzymatic formulations, intended as additives to the fluidic anti-contamination system, were developed at the University of Limerick, under the direction of the author, for these trials (see section L.2, Appendix L).



**Fig. C-14** Do228 being prepared at the DLR for HYLTEC flight tests (from Bieler et al., 2002)



### **C.18 PROJECT ALTTA (2000 – 2002)**

The ALTTA (Application of Hybrid Laminar Flow Technology on Transport Aircraft) project, followed directly on from the HYLDA project and was funded under the CEC Fifth Framework Programme (CORDIS, 2001). The project was also coordinated by Airbus Germany (known as EADS-Germany at the time) and had not been completed at the time of writing. It had 23 partners, including the University of Limerick (where the author was responsible for the University's contribution).

The experimental HLC system installed in the Airbus A320 fin was used as a baseline in this project, with an objective of developing a simpler and more robust HLF system, designed for operational rather than experimental conditions (CORDIS, 2001). Schrauf and Kühn (2001) and later Horstmann *et al.* (2002) reported that a promising solution has emerged whereby a double skinned structure is created that allows for an integration of the load-carrying structure with the suction chambers and ducts. (This is described in section B.5.3, Appendix B.)

The second element of the project concerned a HLF nacelle, that would be designed to take into account the trade-off between aerodynamic drag reduction and penalties caused by the addition of the suction system. Meyer (2000) reported that a group of HYLDA partners, reinforced by an engine manufacturer, conducted a trade study to maximise SFC / DOC benefits and that they would focus on the "HYLDA identified risks that do not require a flight test sequence". Multi-variate Optimisation (MVO) forms a key element of this work.

The final element of this project dealt with the further development of analytical tools for modelling HLF, and the improvements in transition prediction techniques (i.e. database methods, linear and non-linear stability codes). A generic tool to optimise the trade-offs of HLF applications was to be developed and the system tools for laminar flow applications improved (CORDIS, 2001).



**APPENDIX D**

**FUEL PLANNING AND  
PAYLOAD RANGE**

**TABLE OF CONTENTS**

D.1 Introduction..... 226

D.2 JAR OPS 1 Requirements..... 226

    D.2.1 En route flight planning – fuel required ..... 226

    D.2.2 Extract from AMC OPS 1.255 "Standard" fuel policy..... 226

    D.2.3 Contingency fuel ..... 228

D.3 FAR 121 Requirements..... 229

    D.3.1 En route flight planning – fuel required ..... 229

D.4 Mission Profile..... 229

D.5 Payload - Range ..... 230



## **D.1 INTRODUCTION**

Specific requirements exist for the determination of the required fuel for the planned mission. These depend on the operator (flag or foreign), type of aircraft, route (domestic or international) and the availability of alternate airports (if, for any reason, the aircraft is unable to land at the destination airport). All aircraft engaged in public transport flights are required to meet a minimum standard of safety, deemed appropriate to the operation. The JAA and FAA regulations and requirements pertaining to the operation and planning of flights aeroplane are detailed in:

- JAR OPS 1 (Joint Airworthiness Requirement OPS Part 1) *Commercial Air Transportation (Aeroplanes)*.
- FAR 121 (Federal Aviation Regulation Part 121) *Operating requirements: Domestic, flag, and supplemental operations*.

The relevant requirements for the en route flight planning, specific to the fuel planning of missions for international routes, are outlined in this appendix.

Based on a defined set of mission requirements, or what the manufacturers call the "mission rules", the range of the aircraft is determined. On completion of this mission, the aircraft should have sufficient fuel onboard for the alternate leg and contingencies and allowances as set out in the mission rules. The payload range relationship is also briefly described in this appendix. The mission analysis required precise definitions of the weights, distances and times. These are given in section N.2.1 (Appendix N).

## **D.2 JAR OPS 1 REQUIREMENTS**

### **D.2.1 En route flight planning – fuel required**

The details regarding fuel planning policy are outlined in JAR OPS 1 Subpart D, section 1.255 and further elaborated in JAR OPS 1 Subpart D section AMC OPS 1.255. The fuel policy is described for four procedures:

- "Standard" procedure;
- Decision point procedure;
- Isolated aerodrome procedure;
- Pre-determined point procedure.

The details given in AMC OPS 1.255 are reproduced below for the "standard" policy.

### **D.2.2 Extract from AMC OPS 1.255 "Standard" fuel policy**

An operation should base the company fuel policy, including calculation of the amount of fuel to be carried, on the following planning criteria:

The amount of:



1. **Taxy fuel<sup>1</sup>**, which should not be less than the amount, expected to be used prior to takeoff. Local conditions at the departure aerodrome and APU consumption should be taken into account.
2. **Trip fuel**, which should include:
  - a. Fuel for takeoff and climb from aerodrome elevation to initial cruising level/altitude, taking into account the expected departure routing;
  - b. Fuel from top of climb to top of descent, including any step climb/descent;
  - c. Fuel from top of descent to the point where the approach is initiated, taking into account the expected arrival procedure; and
  - d. Fuel for approach and landing at the destination aerodrome.
3. **Contingency fuel**, which should be the higher of (a) or (b) below:
  - a. Either:
    - i. 5% of the planned trip fuel or, in the event of in-flight replanning, 5% of the trip fuel for the remainder of the flight; or
    - [ii. Not less than 3% of the planned trip fuel or, in the event of in-flight replanning, 3% of the trip fuel for the remainder of the flight provided that an en route alternate is available. The en route alternate should be located within a circle having a radius equal to 20% of the total flight plan distance, the centre of which lies on the planned route at a distance from the destination of 25% of the total flight plan distance, or at 20% of the total flight distance plus 50nm, whichever is greater; or]
    - iii. An amount of fuel sufficient for 20 minutes flying time based upon the planned trip fuel consumption provided that the operator has established a fuel consumption monitoring programme for individual aeroplanes and uses valid data determined by means of such a programme for fuel calculation; or
    - iv. An amount of fuel of not less than that which would be required to fly for 15 minutes at holding speed at 1500ft (450m) above the destination aerodrome in standard conditions, when an operator has established a programme, approved by the Authority, to monitor the fuel consumption on each individual route/aeroplane combination and uses this data for a statistical analysis to calculate contingency fuel for the route/aeroplane combination; or
  - b. An amount to fly for 5 minutes at holding speed at 1500ft (450m) above the destination aerodrome in standard conditions.
4. **Alternate fuel**, which should be sufficient for:
  - a. A missed approach from the applicable MDA/DH at the destination aerodrome to missed approach altitude, taking into account the complete missed approach procedure;

---

<sup>1</sup> The spelling of taxi as per JAR OPS 1 has been used in this section.



- b. A climb from missed approach altitude to cruising level/altitude;
- c. The cruise from top of climb to top of descent;
- d. Descent from top of descent to the point where the approach is initiated, taking into account the expected arrival procedure; and
- e. Executing an approach and landing at the destination alternate aerodrome selected in accordance with JAR OPS 1.295.
- f. If, in accordance with JAR OPS 1.295(d), two destination alternates are required, alternate fuel should be sufficient to proceed to the alternate which requires the greater amount of alternate fuel.

**5. Final reserve fuel, which should be:**

- a. For aeroplanes with reciprocating engines, fuel to fly for 45 minutes; or
- b. For aeroplanes with turbine power units, fuel to fly for 30 minutes at holding speed at 1500ft (450m) above aerodrome elevation in standard conditions, calculated with the estimated mass on arrival at the alternate or the destination, when no alternate is required.

**6. Additional fuel.** With the exception of Concorde operations, the minimum additional fuel which should permit:

- a. Holding for 15 minutes at 1500ft (450m) above aerodrome elevation in standard condition, when a flight is operated under IFR without a destination alternate, in accordance with JAR OPS 1.295; and
- b. Following the possible failure of a power unit or loss of pressurisation based on the assumption that such a failure occurs at the most critical point along the route, the aeroplane to:
  - i. Descend as necessary and proceed to an adequate aerodrome; and
  - ii. Hold there for 15 minutes at 1500ft (450m) above aerodrome elevation in standard condition; and
  - iii. Make an approach and landing,  
except that additional fuel is only required, if the minimum amount of fuel calculated in accordance with sub-paragraphs 2 to 5 above is not sufficient for such an event.

**7. Extra fuel, which should be at the discretion of the commander.**

**D.2.3 Contingency fuel**

The contingency fuel is described in JAR OPS 1.255 (c)(3)(i). The following is a direct extract from the requirements as described in IEM OPS 1.255(c)(3)(i). At the planning stage, not all factors which have an influence on the aircraft's fuel consumption (to the destination aerodrome), can be foreseen. Therefore, contingency fuel is carried to compensate for items such as:



- i. Deviations of an individual aeroplane from the expected fuel consumption data;
- ii. Deviations from forecast meteorological conditions; and
- iii. Deviations from planned routings and/or cruising levels/altitudes.

### **D.3 FAR 121 REQUIREMENTS**

#### **D.3.1 En route flight planning – fuel required**

US flag and supplemental operations on international routes where an alternate airport is specified, must comply with FAR 121.645. It is stated that no person may release for takeoff, a turbine-engine powered airplane (not including a turbo-prop airplane) unless, considering wind and other weather conditions expected, it has enough fuel: -

- (1) To fly to and land at the airport to which it is released;
- (2) After that, to fly for a period of 10 percent of the total time required to fly from the airport of departure to, and land at, the airport to which it was released;
- (3) After that, to fly to and land at the most distant alternate airport specified in the flight release; and
- (4) After that, to fly for 30 minutes at holding speed at 1 500 feet above the alternate airport under standard temperature conditions.

### **D.4 MISSION PROFILE**

The aircraft's flight profile may be divided into a number of segments for the purpose of flight planning, as discussed in section 3.2 (Chapter 3). Fig. D-1 illustrates the approach adopted herein, which conforms with the JAR OPS 1 fuel planning requirements. The climb and descent distances below 1500ft have been ignored in determining the trip distance. This assumption was introduced as JAR OPS 1 states that the trip fuel should take into account expected departure and arrival routing. Without actual route details, credit for these distances should not be taken. It is noted that this is not universally done and alternative definitions are in use that allow the climb or descent or both, to be included in determining the trip distance.

A difference between the JAR OPS 1 and FAR 121 requirements is the way in which the en route contingency fuel is specified. For the JAR requirements, it is stipulated in terms of a fixed percentage (3 - 5%) of the *trip fuel*, while for the FAR requirements, it is the fuel required to fly an additional 10% of the *trip time*.



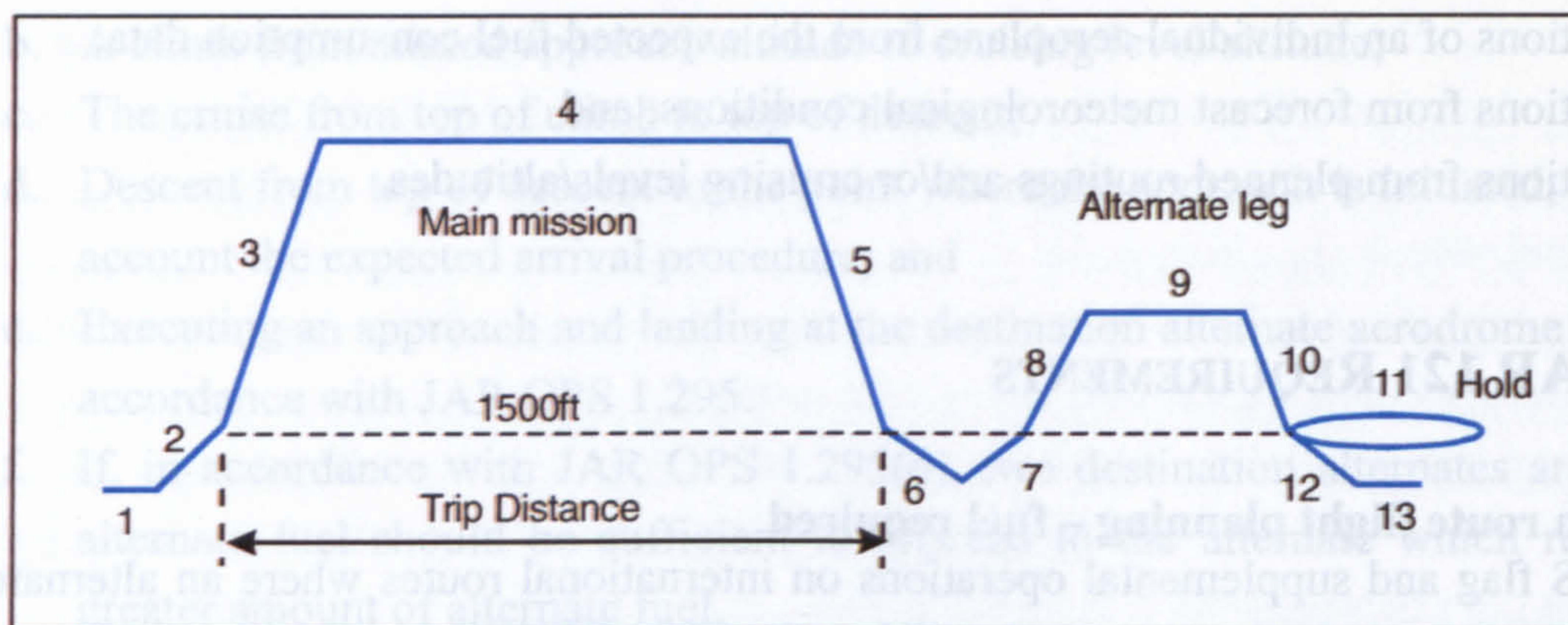


Fig. D-1 Flight profile for fuel planning

#### Index

- |                             |                                      |                        |
|-----------------------------|--------------------------------------|------------------------|
| 1 Engine start-up & taxi    | 6 Approach                           | 11 Hold for 30 minutes |
| 2 Takeoff & climb to 1500ft | 7 Missed approach & climb to 1500ft  | 12 Approach & land     |
| 3 Climb to cruise altitude  | 8 Climb to alternate cruise altitude | 13 Taxi & shutdown     |
| 4 Cruise                    | 9 Alternate cruise                   |                        |
| 5 Descent to 1500ft         | 10 Descent to 1500ft                 |                        |

## D.5 PAYLOAD - RANGE

A typical *payload* versus *range* graph for an airliner is illustrated in Fig. D-2. With the *maximum* allowable (or maximum structural) payload, the amount of fuel that can be taken onboard will usually be limited by the *allowable* maximum takeoff weight (MTOW) and not the tank capacity. The range that may be achieved under this condition is the *maximum payload range*. To increase the range it will be necessary to reduce the payload in order to take on more fuel, but without exceeding the MTOW. Progressively longer mission lengths may be achieved by trading payload for fuel. As indicated, a point is reached when the fuel tanks are full, and the only way the range can be increased is by further reducing the payload. The greatest possible range will correspond to zero payload.

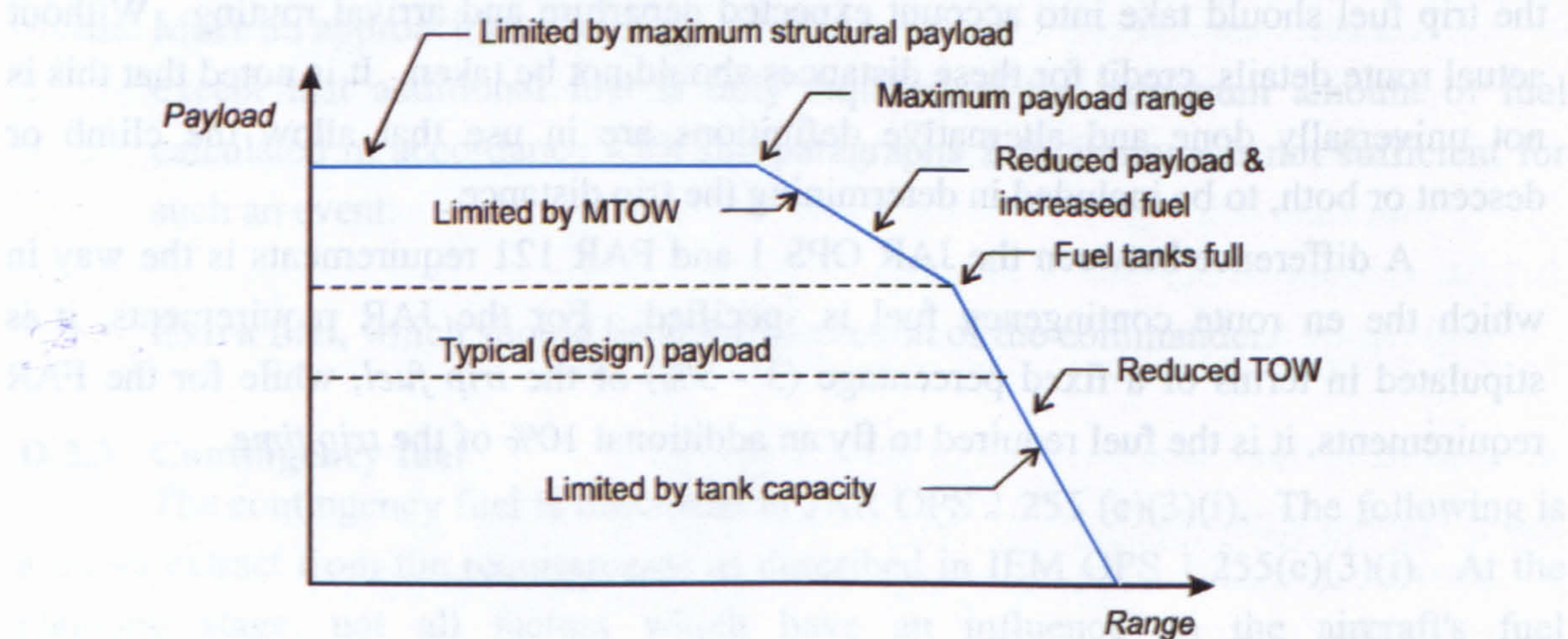


Fig. D-2 Typical payload range graph for an airliner



## APPENDIX E

# AIRCRAFT PERFORMANCE THEORY

### TABLE OF CONTENTS

E.1	Introduction.....	232
E.2	Jet Engine.....	232
E.2.1	Net installed thrust.....	232
E.2.2	Turbofan thrust variation.....	232
E.2.3	Specific fuel consumption.....	234
E.2.4	Corrected fuel flow.....	235
E.2.5	Fuel flow versus thrust.....	236
E.2.6	Pressure recovery losses.....	237
E.2.7	Off-take losses.....	237
E.3	Climb / Descent.....	238
E.3.1	Climb / descent angle.....	238
E.3.2	Rate of climb.....	239
E.3.3	Climb speed schedules.....	240
E.3.4	Time to climb.....	241
E.3.5	Distance covered in the climb.....	242
E.3.6	Descent.....	242
E.4	Cruise.....	242
E.4.1	Basic range equation.....	242
E.4.2	Solutions to the basic range equation.....	243
E.4.3	Further comments on the Breguet range equation.....	244
E.4.4	Integrated range method.....	246
E.4.5	Cruise speeds.....	246
E.4.6	Step climb.....	247
E.4.7	Trip fuel estimation.....	247
E.5	Hold.....	248
E.5.1	Equations for the hold.....	248
E.5.2	Integrated hold method.....	248
E.5.3	Holding pattern.....	249
E.6	Takeoff and Landing Performance.....	249
E.6.1	Takeoff and initial climb-out.....	249
E.6.2	Analytical evaluation of the takeoff run.....	250
E.6.3	Rotation distance and climb-out to screen height.....	251
E.6.4	Takeoff climb segment.....	251
E.6.5	Analytical evaluation of the landing distance.....	251
E.7	Conversion Factors / British Units.....	252
E.7.1	Introduction.....	252
E.7.2	Standard conversion factors.....	252
E.7.3	Airspeed.....	253
E.7.4	Fuel flow and specific fuel consumption.....	253
E.7.5	Range and endurance.....	253
E.8	International Standard Atmosphere (ISA).....	254
E.9	Drag.....	255
E.9.1	Drag components.....	255
E.9.2	Lift-dependent drag.....	256
E.9.3	Drag polar.....	257
E.9.4	Drag rise.....	259



## E.1 INTRODUCTION

The theory presented in this appendix concerns the en route aircraft performance and forms the basis for the computer performance models, developed for the B757-200 class and A330-200 classes aircraft (see Appendix H). The general expressions for the climb, descent, cruise and hold, are determined from fundamental equations of mechanics. Methods for the evaluation of fuel burn, distance covered and time elapsed during the mission, are presented. In particular, methods suitable for numerical analysis based on actual aircraft data are developed. Important engine performance characteristics are defined and explained, with the emphasis placed on the thrust and fuel flow, and the factors that influence these characteristics. The takeoff and landing performance is treated in a superficial manner, as these segments of the mission have a minor influence on the total fuel consumed. A description of the aircraft's drag breakdown is included and alternative representations of the drag polar are reviewed.

## E.2 JET ENGINE

### E.2.1 Net installed thrust

The baseline engine performance data supplied by an engine manufacturer is usually based on an assumed, rather than an actual inlet pressure recovery; furthermore, it may not include any corrections for bleed air or mechanical power extraction. Once installed in the airframe, it is necessary to take into account the actual inlet pressure recovery, the shaft power off-take, engine bleed and any secondary losses due to flow distortion, associated with the particular installation.

The thrust of the powerplant must thus be corrected for installation effects (pressure recovery, nozzle performance, power and bleed extraction, etc.) and for all drag contributions allocated to the propulsion system. In this work, the term *engine thrust* is taken to mean *net installed engine thrust*, and is given the symbol  $F_N$ .

### E.2.2 Turbofan thrust variation

The following functional relationship, given in ESDU 70020 (1970), describes the net thrust in terms of the dominant parameters:

$$\frac{F_N}{\delta} = f_1 \left( \frac{N}{\sqrt{\theta}}, M \right) \quad \text{--- [E-1]}$$

where  $\delta$  and  $\theta$  are the ambient pressure and temperature ratios respectively.  $N$  is the rotational speed of the engine, which is conventionally written as  $N_1$ . In the case of multiple shaft engines, the speed is usually defined as the speed of the fan or low speed compressor. Boeing (1989) provides a graphical illustration of this relationship (Fig. E-1), where  $\theta_{t_2}$  is the total temperature ratio for the engine at station 2 (described in section E.2.4).



For a particular engine setting (i.e.  $N$  is constant), the thrust is a function of the atmospheric conditions and the Mach number. It is useful to consider the effect of these variables for various flight conditions. For an airliner the cruise will generally be at a constant Mach number; if the height does not change very much, then from equation [E-1] it is seen that the thrust will be constant. In the Stratosphere where temperature is constant, the thrust for a given Mach number will decay linearly with pressure, as the height increases, i.e.

$$\frac{F_N}{\delta} \approx \text{constant} \quad \text{--- [E-2]}$$

In the Troposphere there will be a steadily decreasing thrust as the air pressure is reduced. Mattingly *et al.* (1987) indicate that for turbofan engines with high bypass ratios, the thrust will decay as an approximate power law function of the air density, for any constant Mach number up to 0.9, i.e.

$$\frac{F_N}{F_{N_{SL}}} \propto \sigma^n \quad \text{--- [E-3]}$$

where  $F_{N_{SL}}$  is the sea-level reference thrust. Mair and Birdsall (1992) demonstrate that this equation provides a good correlation to data provided by Rolls-Royce for the RB-211-535E4 engine for Mach 0.7, and suggest an exponent of  $n = 0.6$ . They report that a "further investigation has shown that this result is also true for other civil turbofans".

During the initial part of the climb, the Mach number cannot be constant as the TAS increases during the climb and the speed of sound drops. It is not possible to derive a simple thrust expression for the complex situation of changing height and increasing Mach number for this condition.

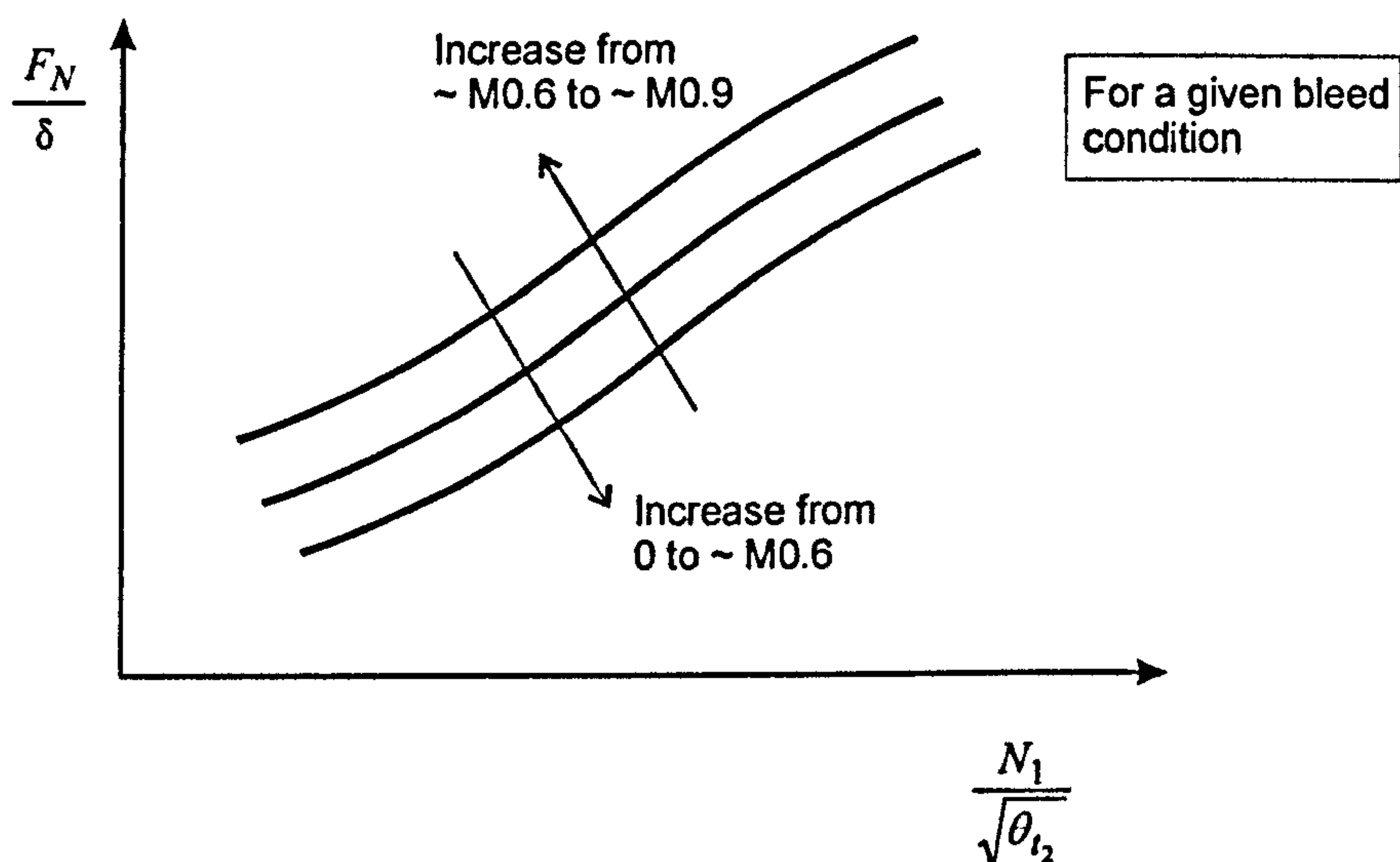


Fig. E-1 Engine thrust (redrawn after Boeing, 1989)



### E.2.3 Specific fuel consumption

The specific fuel consumption (SFC) is defined as the *mass* of fuel burned per unit time, divided by the thrust. The SFC of jet engines is usually given the symbol  $c$ . By definition:

$$\text{SFC} = c = \frac{\left( -\frac{dm_f}{dt} \right)}{F_N} = \frac{Q}{F_N} \quad \text{--- [E-4]}$$

where  $Q$  is the mass fuel flow. The reason for the minus sign is that the rate of change of aircraft fuel mass is negative, whereas SFC is positive. The following functional relationship (ESDU 70020, 1970) describes the fuel flow in terms of the dominant parameters:

$$\text{i.e.} \quad \frac{Q}{\delta\sqrt{\theta}} = f_2\left(\frac{N}{\sqrt{\theta}}, M\right) \quad \text{--- [E-5]}$$

Using equations [E-1], [E-4] and [E-5], the SFC may be expressed as:

$$c = \frac{Q}{F_N} = \sqrt{\theta} f_3\left(\frac{N}{\sqrt{\theta}}, M\right) \quad \text{--- [E-6]}$$

This equation is useful, as it indicates that SFC will depend on height and Mach number, for a given engine speed. For an aircraft cruising in the stratosphere the SFC will depend only on Mach number for a given engine speed.

ESDU 73019 (1982) states "that it is usually not practical to obtain general expressions for the functions  $f_1$ ,  $f_2$  and  $f_3$  and as an alternative, some simple algebraic expression is selected, which allows  $Q$  and  $c$  to be represented reasonably accurately over limited ranges of Mach number, engine speed and ambient conditions". Several such methods are described in the same source:

- (1) The simplest relationship is to assume that  $c$  is constant, i.e.  $c = c_1$ . The variation of  $c$  over segments of the cruise may be very small and the use of a mean value can yield "satisfactory" results.
- (2) "A more accurate method of representing the engine fuel consumption ... is to assume a law of the form:"

$$c = c_2 \sqrt{\theta} M^n \quad \text{--- [E-7]}$$

It is reported that this equation is derived from equation [E-6], but neglects the variation of  $c$ , with the engine speed parameter  $\left(\frac{N}{\sqrt{\theta}}\right)$ . The source (ESDU

73019, 1982) notes that: "This law may be applied over limited ranges of Mach number but is, strictly speaking, valid at only one value of  $\left(\frac{N}{\sqrt{\theta}}\right)$ ." With

suitably chosen values of the constants  $c_1$  and  $n$ , this expression is reported to provide an accurate approximation to measured SFC figures for turbofans, within the limited range of  $N$ ,  $\theta$  and  $M$  values associated with subsonic cruising flight



(ESDU 73019, 1982). Mair and Birdsall (1992) report that for the Rolls-Royce RB-211-535E engine, this equation gives a "reasonably good approximation to the variations of  $c$  due to changes of both Mach number and height". They concluded that the best results were achieved by setting the exponent  $n$  equal to 0.48 for a cruise altitude of 19700ft (6000m) and 0.45 for 29500ft (9000m).

(3) Another type of law that takes into account of the variation of  $c$  with  $M$ , is:

$$c = c_6 + c_7 M \quad \text{--- [E-8]}$$

It is reported that this usually provides a satisfactory approximation to the manufacturers' data (at constant height and engine speed) over a considerably greater range of values of  $M$  than is the case for equation [E-7] (ESDU 73019, 1982).

#### E.2.4 Corrected fuel flow

According to Boeing (1989), the fuel flow for the purposes of aircraft performance analysis, is usually specified as *corrected fuel flow*. By definition:

$$\text{Corrected fuel flow} = Q_{cor} = \frac{Q}{\delta_{t_2} \sqrt{\theta_{t_2}}} \quad \text{--- [E-9]}$$

where  $\delta_{t_2}$  and  $\theta_{t_2}$  are the total pressure and temperature ratio for the engine at station 2, as defined by equations [E-10] and [E-11] below.

$$\delta_{t_2} = \delta \left[ 1 + \frac{\gamma-1}{\gamma} M^2 \right]^{\left( \frac{\gamma}{\gamma-1} \right)} \quad \text{--- [E-10]}$$

$$\theta_{t_2} = \theta \left[ 1 + \frac{\gamma-1}{\gamma} M^2 \right] \quad \text{--- [E-11]}$$

As shown in Fig. E-2 the corrected fuel flow increases with an increase in  $\left( \frac{N_1}{\sqrt{\theta_{t_2}}} \right)$  for a fixed Mach number, and decreases with Mach number for the same value of  $\left( \frac{N_1}{\sqrt{\theta_{t_2}}} \right)$

By combining equations [E-9], [E-10] and [E-11], the actual fuel flow can be obtained from knowledge of  $Q_{cor}$ ,  $M$  and the atmospheric conditions, i.e.

$$Q = Q_{cor} \delta \sqrt{\theta} \left[ 1 + \frac{\gamma-1}{\gamma} M^2 \right]^{\left( \frac{1.5\gamma-0.5}{\gamma-1} \right)} \quad \text{--- [E-12]}$$

Boeing (1989) indicates that if the corrected fuel flow does not generalise completely, (i.e. one chart being valid for all altitudes), then a chart like that shown in Fig. E-2 must be generated for each altitude. It also states that if the fuel flow does not follow the mathematical analysis 100%, then equation [E-9] has to be modified "to cope with the



changes in design of the various types of engines". A correction factor ( $\lambda$ ), which is a function of the total temperature, is introduced:

$$Q_{cor} = \frac{Q}{\lambda \delta_{t_2} \sqrt{\theta_{t_2}}} \quad \text{--- [E-13]}$$

Since  $\lambda$  is a function of the total temperature, it can be combined with the temperature ratio, as follows:  $\lambda \sqrt{\theta_{t_2}} = \theta_{t_2}^x$ . The exponent  $x$  has to be determined experimentally for each engine. Typical values may vary from 0.5 (i.e. from the mathematical analysis) to 0.67 (Boeing, 1989). The general form of the corrected fuel flow is thus given as:

$$Q_{cor} = \frac{Q}{\delta_{t_2} \theta_{t_2}^x} \quad \text{--- [E-14]}$$

and taking  $\gamma=1.4$ , the actual fuel flow will be given as:

$$Q = Q_{cor} \delta \theta^x (1 + 0.2 M^2)^{3.5+x} \quad \text{--- [E-15]}$$

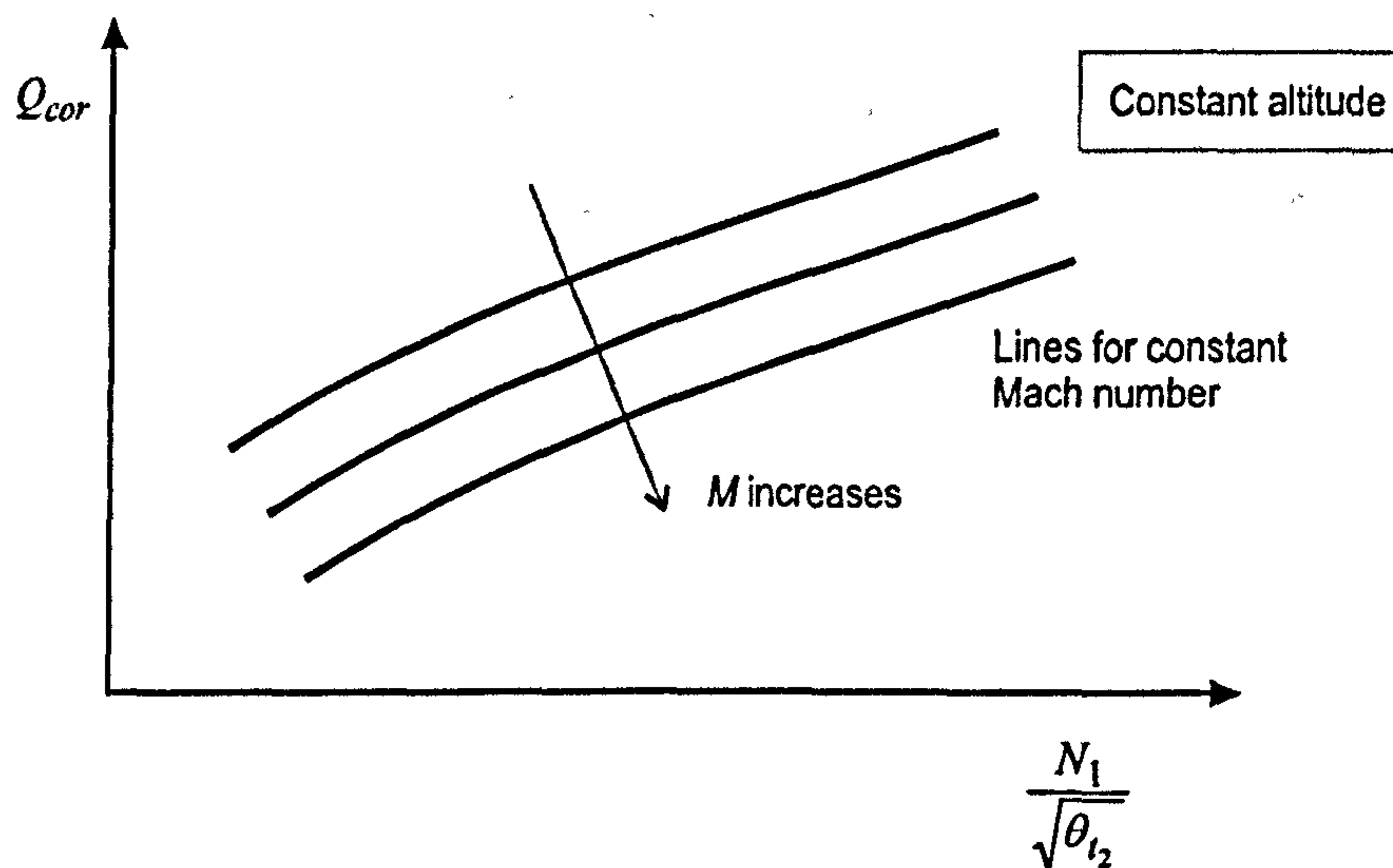


Fig. E-2 Corrected fuel flow (redrawn after Boeing, 1989)

### E.2.5 Fuel flow versus thrust

It is essential for the analysis of the en route aircraft performance to be able to obtain the fuel flow directly from the net thrust. During the cruise for example, the aircraft's drag can usually be determined from the drag polar, and this would equate to the net thrust. Using data of the form illustrated in Fig. E-1, the engine parameter

$\left( \frac{N_1}{\sqrt{\theta_{t_2}}} \right)$  can be established, which from Fig. E-2, would give the corrected fuel flow

for the desired Mach number. The final step is to use equation [E-15] to determine the



actual fuel flow. A cross plot of Figures E-1 and E-2 can be produced, eliminating the requirement to determine the engine speed parameter. Tables or graphs of  $Q_{cor}$  versus  $F_N/\delta$  for different Mach numbers for the specific aircraft / engine combination are thus the most convenient to use.

ESDU 73019 (1982) reports that for a range of turbo-jet and turbo-fan engines, the manufacturers' fuel flow data, at a given Mach number, may be satisfactorily expressed by the relationship:

$$\frac{Q}{\delta\sqrt{\theta}} = c_3 + c_4 \left( \frac{F_N}{\delta} \right) + c_5 \left( \frac{F_N}{\delta} \right)^2 \quad \text{--- [E-16]}$$

where  $c_3$ ,  $c_4$  and  $c_5$  are constants for a particular engine design and must be determined for each value of  $M$ .

### E.2.6 Pressure recovery losses

The inlet pressure recovery  $\left( \frac{p_1}{p_0} \right)$  is the total pressure at the engine front "face" divided by the total pressure in the freestream. According to Bewick (2001) for a modern engine nacelle, the maximum pressure recovery loss is ~0.5%; with a typical cruise condition having a pressure recovery loss of about half that value (i.e. ~0.25%). The same source indicated that the "exchange rate" of pressure recovery loss to SFC loss is about 1.5 to 2.0 for a modern engine. Combining these two estimates leads to the conclusion that in the cruise, the installed SFC will be about 0.38 - 0.50% lower than the uninstalled value.

The thrust loss due to an inlet pressure recovery loss, can be estimated using the equation:

$$\text{Percent thrust loss} = c_{ram} \left[ \left( \frac{p_1}{p_2} \right)_{ref} - \left( \frac{p_1}{p_2} \right)_{actual} \right] \quad \text{--- [E-17]}$$

where  $c_{ram}$  is approximately 1.35 for subsonic flight (Raymer, 1989). For a cruise pressure recovery of 0.25%, the thrust loss would be approximately 0.34%.

### E.2.7 Off-take losses

Aircraft systems driven by bleed air off-take from the HP compressor or direct shaft power off-take, reduce the available propulsive energy. For a given cruise speed and height, the TET (Turbine Entry Temperature) would have to increase to compensate for this loss. The effect of an off-take on the engine efficiency (as measured by the SFC) is a function of the engine thrust, the operating conditions (i.e. Mach number, height, atmospheric conditions) and the engine design parameters (e.g. bypass ratio, pressure ratio, etc.). This is discussed further in section J.5 (Appendix J).



## E.3 CLIMB / DESCENT

### E.3.1 Climb / descent angle

For this analysis the aircraft is considered to be performing a climb in *still air*, as shown in Fig. E-3. The angle between the flight path and the horizontal is  $\gamma$  (shown positive for a climb).

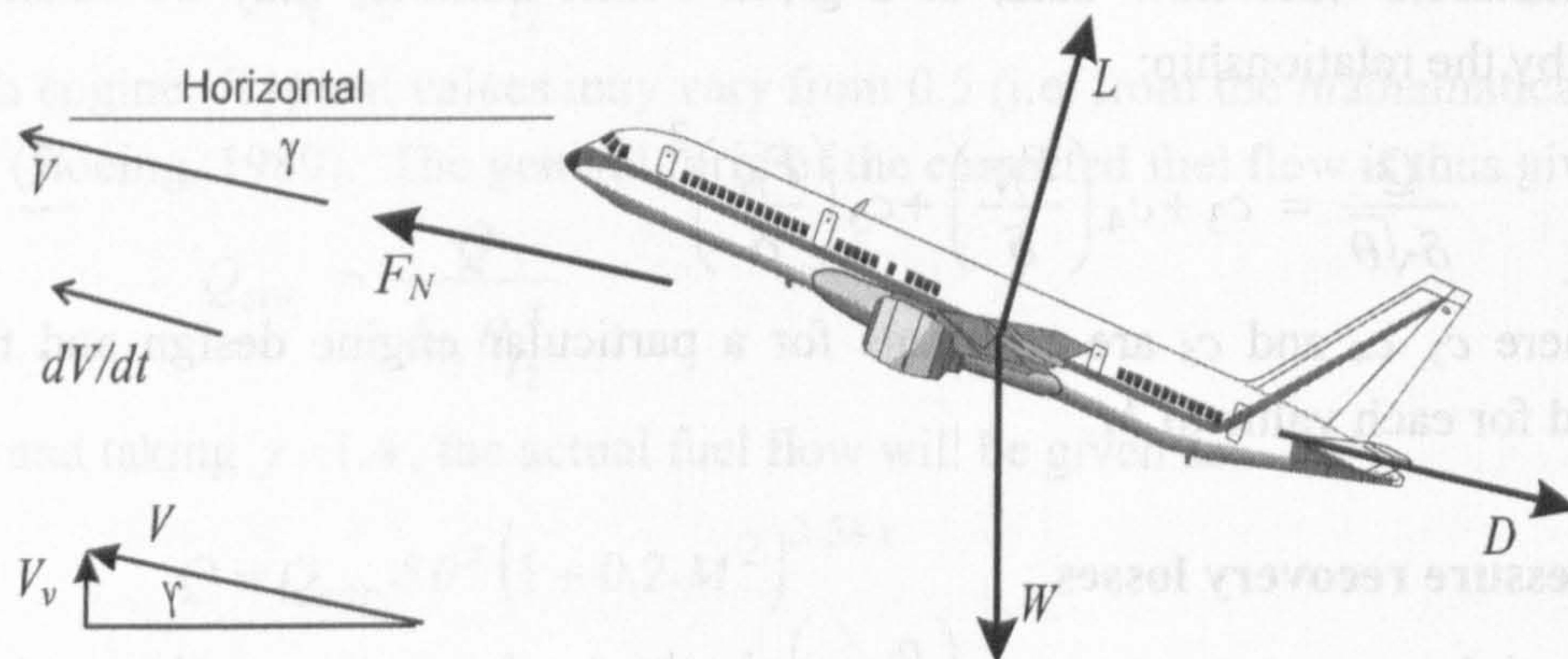


Fig. E-3 Climbing flight

The following assumptions are made:

- (1) The net thrust line is defined parallel to the line of flight, collinear with the drag line.
- (2) The acceleration normal to the flight path is considered to be negligible.

Considering the forces parallel to the flight path:

$$F_N - D - W \sin \gamma = \frac{W}{g} \frac{dV}{dt} \quad \text{--- [E-18]}$$

and normal to the flight path:

$$L - W \cos \gamma = 0 \quad \text{--- [E-19]}$$

From equation [E-18] the angle of climb may be expressed as:

$$\sin \gamma = \frac{F_N - D}{W} - \frac{1}{g} \frac{dV}{dh} \frac{dh}{dt} \quad \text{--- [E-20]}$$

The *vertical component* of the airspeed is given the symbol  $V_v$  and in the absence of updrafts (gusts), is equal to the change in height with respect to time, i.e.

$$V_v = V \sin \gamma = \frac{dh}{dt}$$

$$\sin \gamma = \frac{F_N - D}{W} - \frac{1}{g} \frac{dV}{dh} V \sin \gamma$$

$$\text{Thus:} \quad \sin \gamma = \frac{\frac{F_N}{W} - \frac{D}{W}}{\left(1 + \frac{V}{g} \frac{dV}{dh}\right)} \quad \text{--- [E-21]}$$



Equation [E-21] is the general expression for the climb angle, for an accelerated climb. For *steady* flight the rate of change of speed, with respect to height, is zero and the equation may be simplified.

$$\text{Then:} \quad \sin \gamma = \frac{F_N}{W} - \frac{D}{W} = \frac{F_N}{W} - \frac{D}{L} \cos \gamma \quad \text{--- [E-22]}$$

### E.3.2 Rate of climb

Using equation [E-21] the rate of climb (ROC) in the absence of updrafts is given by:

$$\text{ROC} = \frac{dh}{dt} = V \sin \gamma = \frac{\left( \frac{F_N}{W} - \frac{D}{W} \right) V}{\left( 1 + \frac{V}{g} \frac{dV}{dh} \right)} \quad \text{--- [E-23]}$$

The usual way of analysing this expression is by introducing an *acceleration factor*, defined as:

$$f_{acc} = \frac{V}{g} \frac{dV}{dh} \quad \text{--- [E-24]}$$

$$\text{Hence:} \quad \text{ROC} = \frac{dh}{dt} = \frac{\left( \frac{F_N}{W} - \frac{D}{W} \right) V}{(1 + f_{acc})} \quad \text{--- [E-25]}$$

For a constant CAS climb the *acceleration factor* will increase as the altitude increases. This is evident from the fact that the TAS increases and  $\frac{dV}{dh}$  (which is the reciprocal of the slope of the line shown in Fig. E-4) also increases during the climb. For the upper part of the climb, it is preferable to express the ROC in terms of Mach number, by making the following substitution:

$$V = Ma = Ma_o \sqrt{\theta} \quad \text{--- [E-26]}$$

Hence equation [E-25] may be rewritten as:

$$\text{ROC} = \frac{\left( \frac{F_N}{\delta} - \frac{D}{\delta} \right) Ma_o \sqrt{\theta}}{(1 + f_{acc}) \frac{W}{\delta}} \quad \text{--- [E-27]}$$

The reason for dividing both numerator and denominator by the pressure ratio ( $\delta$ ), is to write the thrust in a form consistent with the usual presentation of thrust data for a turbofan engine. The acceleration factor depends on the Mach number, the height and the climb speed condition. Boeing (1989) provides equations for the determination of the acceleration factor. These equations have been reproduced in a different format in Table E-1.



Table E-1 Acceleration factor (based on Boeing, 1989)

Acceleration factor: $f_{acc} = \frac{1.4 M^2}{2} \psi$		equation [E-28]
Where for:		and where:
Constant Mach No.	$\psi = -a$	$a = 0.190263$ (below the tropopause)
Constant EAS	$\psi = 1 - a$	$a = 0$ (above the tropopause)
Constant CAS	$\psi = \frac{\left\{ \left[ 1 + 0.2 M^2 \right]^{3.5} - 1 \right\}}{0.7 M^2 \left[ 1 + 0.2 M^2 \right]^{2.5}} - a$	

E.3.3 Climb speed schedules

The climb speed used by airliners is one that is usually calculated to reduce the total trip cost. The optimum speed that will reduce the total trip fuel is very close to the *maximum rate of climb* speed. The TAS for the best rate of climb varies with altitude, but corresponds closely to a constant CAS climb. In addition, there are operational constraints imposed by the aviation authorities. The FAA requires that a speed of 250 KIAS not be exceeded below FL 100 (Boeing, 1993). Depending on the aircraft type, climb speed schedules are established, either in terms of IAS (aircraft with pneumatic speed indicators), or CAS (aircraft with electronic speed indicators) (Boeing 1989).

A typical climb speed schedule may be written as 250/290/M0.8 (for example). This implies that the aircraft climbs until FL 100 is reached at a CAS of 250kt. Above this height the speed is held at 290kt, until Mach 0.8 is reached. This Mach number is held until the cruise height is reached. The speed variation is shown in Fig. E-4.

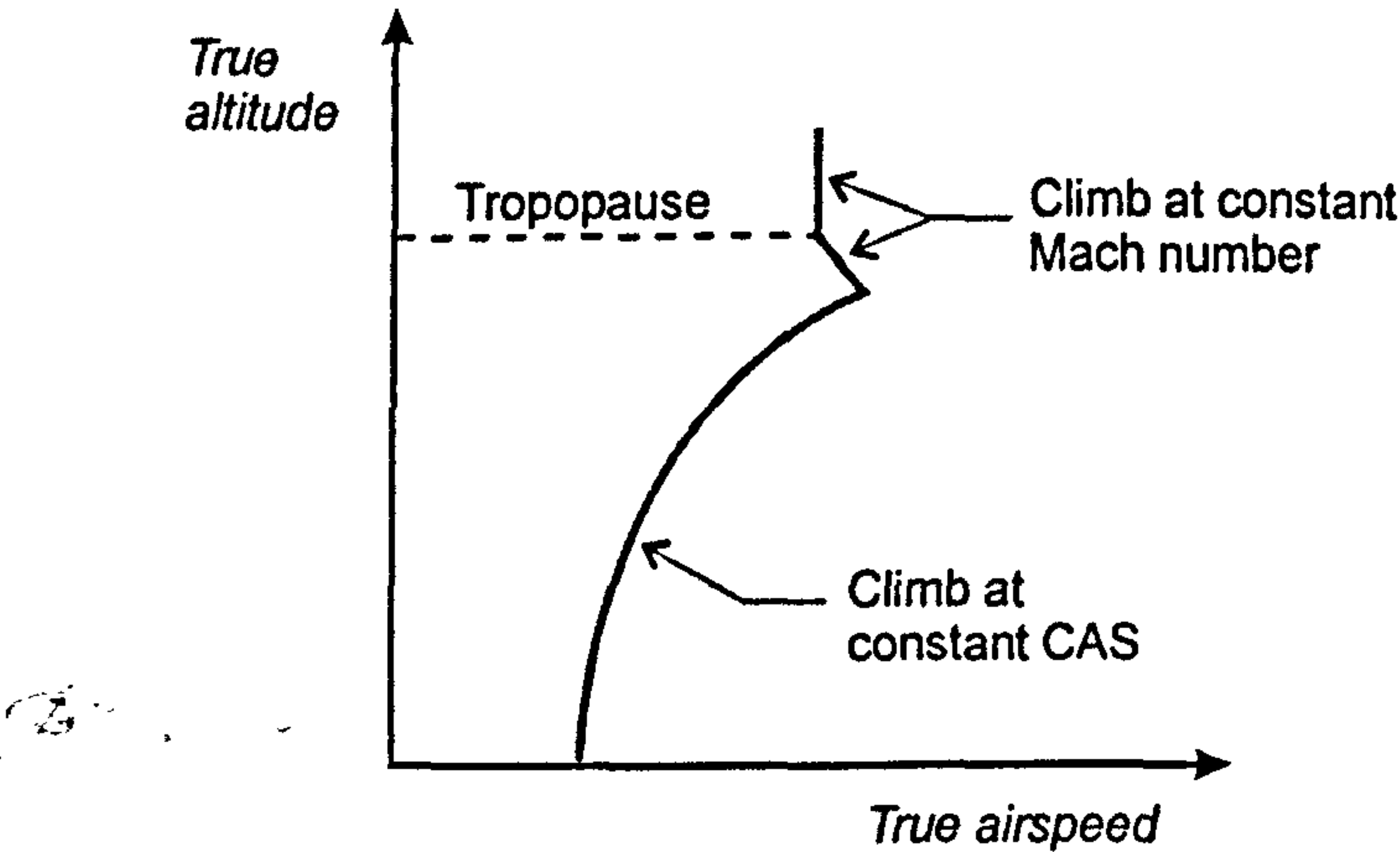


Fig. E-4 Typical airliner climb schedule: constant CAS, followed by constant Mach number



### E.3.4 Time to climb

The vertical component of the airspeed (or rate of climb) in the absence of wind, is equal to the change in height with respect to time, i.e.

$$\text{ROC} = V_v = \frac{dh}{dt} \quad \text{--- [E-29]}$$

The *time to climb* from height  $h_1$  to height  $h_2$  is given by:

$$t = \int_{h_1}^{h_2} \frac{1}{V_v} dh \quad \text{--- [E-30]}$$

where the ROC is given by equations [E-25] and [E-27].

The integration of equation [E-30] for a general problem is not easy, because of the interdependency of the many variables. As an illustration, consider the aircraft climbing from sea level to cruise altitude. As the aircraft climbs, fuel is consumed and the weight will be reduced. The fuel flow ( $Q$ ) is equal to the product of SFC and thrust. Although the SFC may be considered to be approximately constant, thrust will decrease with the reduction in air density, and will vary with changes in throttle setting. The drag depends on the air density, the aircraft weight, and the TAS.

As described earlier, it is typical for jet transport aircraft to initially climb at a constant CAS and to change later to climbing at constant Mach number. When the aircraft climbs at constant CAS, the TAS will increase as the air density reduces. Climbing at constant Mach number implies that there will be a slight decrease in TAS up to the tropopause, because the speed of sound will decrease. In the stratosphere, climbing at constant Mach number implies constant TAS.

A practical approach to determine the *time to climb* and *fuel burn* during the climb, is outlined below.

- Step 1* The climb is divided into  $n$  intervals, with each interval corresponding to a change of height  $\Delta h$ .
- Step 2* The ROC at the start of the  $i^{\text{th}}$  interval, designated as  $V_{vi}$  is determined using equation [E-25] or [E-27] based on the weight at the start of the interval  $W_i$  and the thrust and drag at the height  $h_i$ .
- Step 3* An estimate of  $t_i$  (*time to climb* through the interval) is then calculated from the ratio of  $\Delta h$  and  $V_{vi}$ . The fuel burnt in the interval is determined from the product of  $Q_i$  and  $t_i$ . By subtracting this from  $W_i$  an estimate of the weight at the end of the interval ( $W_{i+1}$ ) is obtained.
- Step 4* The ROC at the end of the interval ( $V_{vi+1}$ ) is now determined based on the weight, thrust and drag at the height  $h_{i+1}$ . A mean value of the ROC for the interval is then calculated from  $V_{vi}$  and  $V_{vi+1}$ .
- Step 5* In a repeat of step 3, revised estimates of  $t_i$  and  $W_{i+1}$  are determined using the mean value of the ROC.



*Step 6* The process (steps 2 to 5) is repeated sequentially for each interval. The total time to climb is given by:

$$\text{Total time} = T = \sum_{i=1}^n t_i \quad \text{--- [E-31]}$$

### E.3.5 Distance covered in the climb

The horizontal distance covered in the climb depends on the climb speed schedule and  $\gamma$ , the angle of the climb. As  $\gamma$  will change in the climb, this needs to be determined by dividing the climb into  $n$  intervals, as described earlier in section E.3.4. The horizontal distance (without wind) is given by:

$$\text{Still air distance} = \sum_{i=1}^n t_i V_i \cos \gamma_i \quad \text{--- [E-32]}$$

### E.3.6 Descent

The equations derived earlier, for the angle of climb (section E.3.1), rate of climb (section E.3.2), time to climb (section E.3.4) and climb distance (section E.3.5), are all applicable to the descent, where  $\gamma$  is negative. The standard engine rating for descent is "flight idle thrust" (Airbus, 2002a). Optimum glide conditions are achieved at the best  $L/D$  speed. However, for operational reasons, airliners descend at faster speeds and spoilers / speed brakes may be required to increase the rate of descent (ROD). The restriction of 250 KIAS applies to the descent below FL 100.

## E.4 CRUISE

### E.4.1 Basic range equation

The still air range ( $R$ ) that an aircraft travels, starting with an initial mass  $m_1$  and ending with a final mass  $m_2$ , is a function of aircraft design parameters (such as the lift-to-drag ratio), flight conditions, speed and SFC. The basic range equation may be derived starting from the definition of the *Specific Air Range* ( $r_a$ ), which is the distance travelled per unit fuel mass consumed, i.e.

$$r_a = \left( - \frac{dx}{dm_f} \right) \quad \text{--- [E-33]}$$

The minus sign is required because the change of fuel ( $dm_f$ ) is a negative quantity and Specific Air Range (SAR) is a positive quantity. The onboard fuel mass ( $m_f$ ) relates to



the fuel burned by the expression:  $Q = -\frac{dm_f}{dt}$ . This equation may be used to rewrite the definition of SAR in a more convenient form, i.e.

$$r_a = \left( -\frac{dx}{dm_f} \right) = \frac{\left( \frac{dx}{dt} \right)}{\left( -\frac{dm_f}{dt} \right)} = \frac{V}{Q} \quad \text{--- [E-34]}$$

where the true airspeed is given by:  $V = \frac{dx}{dt}$

For a turbofan powered aircraft in level flight, the fuel flow ( $Q$ ) may be written as:

$$Q = cF_N = cD = c \left( \frac{1}{L/D} \right) mg = \frac{cmg}{E} \quad \text{--- [E-35]}$$

The change in *aircraft* mass is equal to the change in total onboard *fuel* mass, i.e.

$$\left( -\frac{dx}{dm} \right) = \left( -\frac{dx}{dm_f} \right) = r_a \quad \text{and hence: } dx = -r_a dm.$$

This expression may be integrated from the starting condition (subscript 1) to the final condition (subscript 2).

$$R = \int_{start}^{end} dx = - \int_{m_1}^{m_2} r_a dm = - \int_{m_1}^{m_2} \frac{V}{Q} dm \quad \text{--- [E-36]}$$

$$\text{Hence: } R = - \int_{m_1}^{m_2} \frac{VE}{cgm} dm \quad \text{--- [E-37]}$$

This is the basic range equation.

#### E.4.2 Solutions to the basic range equation

To evaluate equation [E-37] it is necessary to describe the variables  $V$ ,  $E$  and  $c$  as functions of  $m$  during the cruise. Traditionally the approach adopted has been a two-step one. Firstly, assumptions regarding these variables are postulated that will allow the equation to be solved. This is followed by deductions into the implications of these assumptions for the pilot, in terms of actually flying the aircraft. Three alternative flight schedules (sets of assumptions) are possible, each of which will enable the integral to be solved:

- (1) Constant SFC, with cruise at constant *altitude* and constant *lift coefficient*;
- (2) Constant SFC, with cruise at constant *airspeed* and constant *lift coefficient*;
- (3) Constant SFC, with cruise at constant *altitude* and constant *airspeed*.

The second set of conditions are most commonly assumed. It is noted that the condition of constant  $C_L$  implies that the lift-to-drag ratio  $E$ , is constant. The second flight schedule is usually called the cruise-climb, as altitude is not constant. As  $c$ ,  $V$  and  $E$  are all constant, the integration is straight-forward, i.e.



$$R = - \frac{VE}{cg} \int_{m_1}^{m_2} \frac{1}{m} dm$$

hence:  $R = \frac{VE}{cg} \log_e \left( \frac{m_1}{m_2} \right)$  --- [E-38]

This equation is commonly known as the Breguet Range Equation, although the original postulation by Breguet was for piston engine aircraft and not for jets (Anderson, 1999). Mair and Birdsall (1992) and Eshelby (2000) (for example), describe alternative solutions to the basic range integral, corresponding to flight schedules 1 and 3. The cruise-climb is an elegant solution for obtaining the maximum range. The practical use of this equation is discussed further in section E.4.3.

The implications of these assumptions are deduced from the lift coefficient, which may be written as:

$$C_L = \frac{W}{qS} = \frac{W}{\frac{1}{2} \rho_o a_o^2 \delta M^2 S} = \frac{W / \delta}{\frac{1}{2} \rho_o a_o^2 M^2 S} \quad \text{--- [E-39]}$$

From this expression it is evident that the ratio of  $W / \delta$  must be kept constant, for  $V$  and  $C_L$  to be constant in the stratosphere (where constant Mach number implies constant TAS). This is possible if the aircraft is allowed to climb very slowly, so that the relative pressure decreases proportionally to the decrease in  $W$ . At the same time, as the thrust of a turbofan engine is approximately proportional to  $\sigma$  (in the stratosphere), it will automatically decrease as  $W$  decreases, without altering the throttle setting.

The initial conditions established for this analysis were for straight and level flight, where thrust equals drag and lift equals weight; but the above requirement for a climb clearly invalidates this statement. However, the climb angle required for a cruise climb is very small and the increase in thrust (of one or two percent required to maintain the climb angle), can be neglected for most range estimates.

#### E.4.3 Further comments on the Breguet range equation

The Breguet range equation [E-38] derived earlier is widely used because of its simplicity, and also because the error introduced by the assumptions are often not significant. The accuracy of the equation can be enhanced by selecting values for  $c$  and  $E$ , which are mean values evaluated for the cruise. The computer model for the B757-200 class aircraft (Appendix H) is based on representative aircraft performance data. This model was used to investigate the variation of the SFC and lift-to-drag ratio during a typical cruise. The results are shown in Fig. E-5. It is seen that the changes are non-linear with respect to the change in aircraft mass. The non-linear variation of  $L/D$  can be easily explained by recognising that the lift coefficient changes as the aircraft weight is reduced and  $L/D$  varies in a non-linear fashion with respect to  $C_L$ .

To investigate the accuracy of the Breguet equation, compared to the computer program described in Appendix H, the weight, drag,  $L/D$  and SFC were determined at



the start and at the end of the cruise, and at 19 intermediate points. Average values of  $L/D$  and SFC were determined as shown in Table E-2. The cruise range calculated using the computer model, was 2350nm, whilst that calculated using the Breguet equation was 2348nm. The difference between the two values is only 0.07%, which indicates that the equation can provide accurate solutions, providing that representative mean values of  $L/D$  and SFC are available.

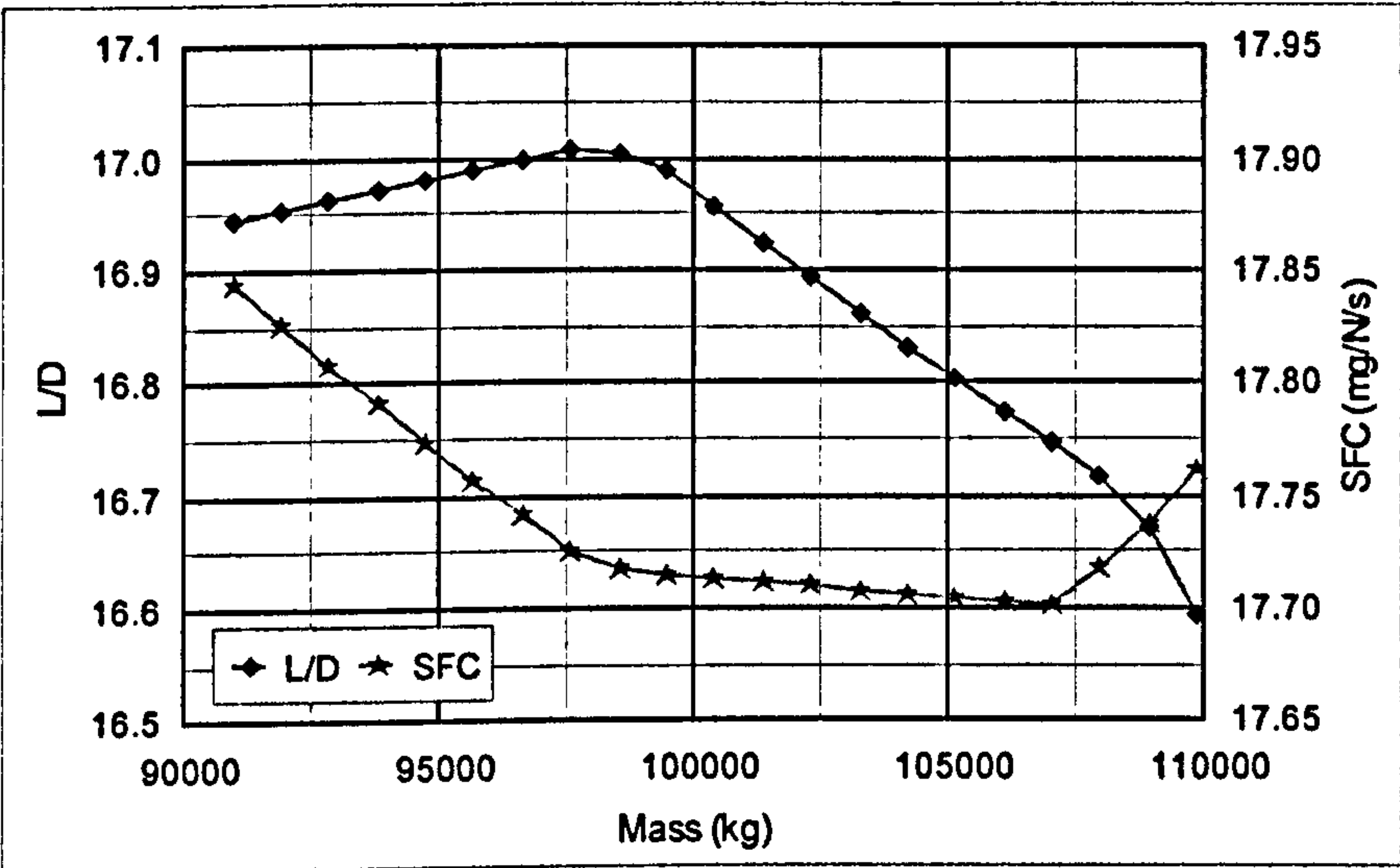


Fig. E-5 Typical variation of  $L/D$  and SFC during cruise

Table E-2 Typical cruise data for B757-200 class aircraft at FL 350 Mach 0.80 (TAS 461kt)

	Cruise Station	Mass (kg)	Drag (kN)	$L/D$	SFC (mg/N/s)
Start cruise ->	0	109914	65.0	16.59	17.76
	1	108968	64.1	16.67	17.74
	2	108022	63.4	16.72	17.72
	3	107076	62.7	16.75	17.70
	4	106130	62.0	16.77	17.70
	5	105185	61.4	16.80	17.70
	6	104239	60.7	16.83	17.71
	7	103293	60.1	16.86	17.71
	8	102347	59.4	16.89	17.71
	9	101401	58.8	16.93	17.71
	10	100455	58.1	16.96	17.71
	11	99509	57.4	16.99	17.72
	12	98563	56.8	17.01	17.72
	13	97617	56.3	17.01	17.73
	14	96671	55.8	17.00	17.74
	15	95726	55.2	16.99	17.76
	16	94780	54.7	16.98	17.77
	17	93834	54.2	16.97	17.79
	18	92888	53.7	16.96	17.81
	19	91942	53.2	16.96	17.83
End cruise ->	20	90996	52.7	16.95	17.84
Mean ->		100455	58.4	16.89	17.74



#### E.4.4 Integrated range method

A superior approach for range estimation, than the use of the Breguet formulation, is to perform a numerical integration of the basic range equation [E-36]. If a graph of SAR versus aircraft mass is produced for the required cruise conditions, then the range is the area under the graph between the points representing the end and the start of the cruise (Fig. E-6).

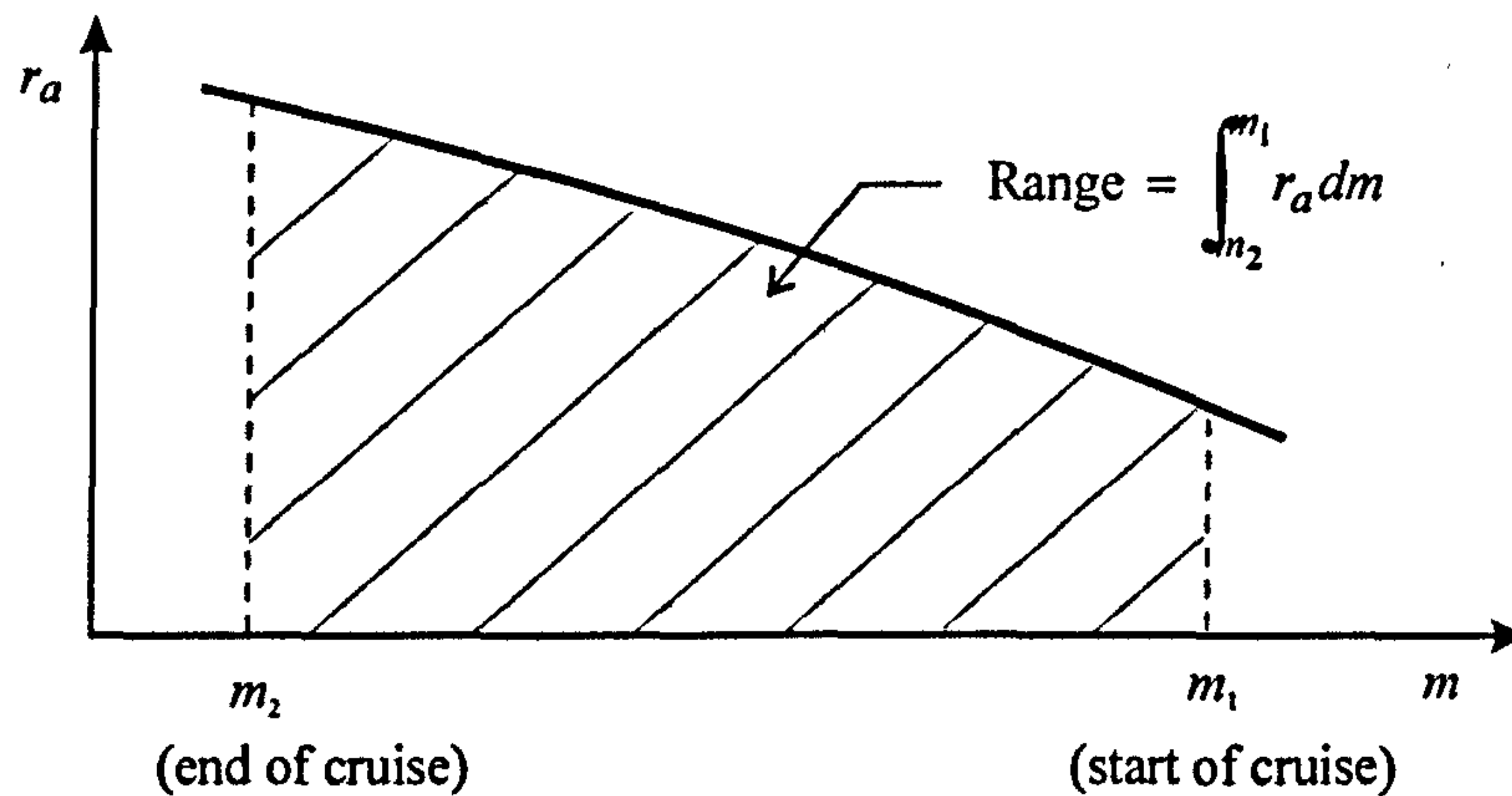


Fig. E-6 Integrated range method (Young, 2002)

The technique, usually called the Integrated Range Method, follows from equation [E-36] derived earlier. If the mass change is divided into  $n$  intervals, then the range is given by:

$$R = \sum_{i=1}^n \frac{V_i}{Q_i} (m_i - m_{i-1}) \quad \text{--- [E-40]}$$

#### E.4.5 Cruise speeds

The greatest possible range for a fixed fuel quantity, which an aircraft may achieve, is obtained by flying at all times at the condition for maximum SAR. This is called the Maximum Range Speed (MRS). The MRS decreases as fuel is burnt (at a fixed cruise altitude). In practice airliners usually fly faster than this, sacrificing a small increase in fuel to obtain a shorter cruise time (Boeing, 1996). As a portion of an airline's cost is proportional to the flight time, this is reduced by flying faster. The speed that will give the lowest total trip cost, for a particular set of operating costs, is called the Economy (Econ) Speed (Airbus, 2002). This can be difficult to calculate without complete cost data and a simpler approach is to fly at a fixed percentage faster than the MRS. The so-called Long Range Speed (LRS) is typically set about 2 to 4% faster than the MRS and has a 1% reduction in SAR, as shown in Fig. E-7. The alternate leg of a mission is usually planned to be flown at the MRS, or the LRS.



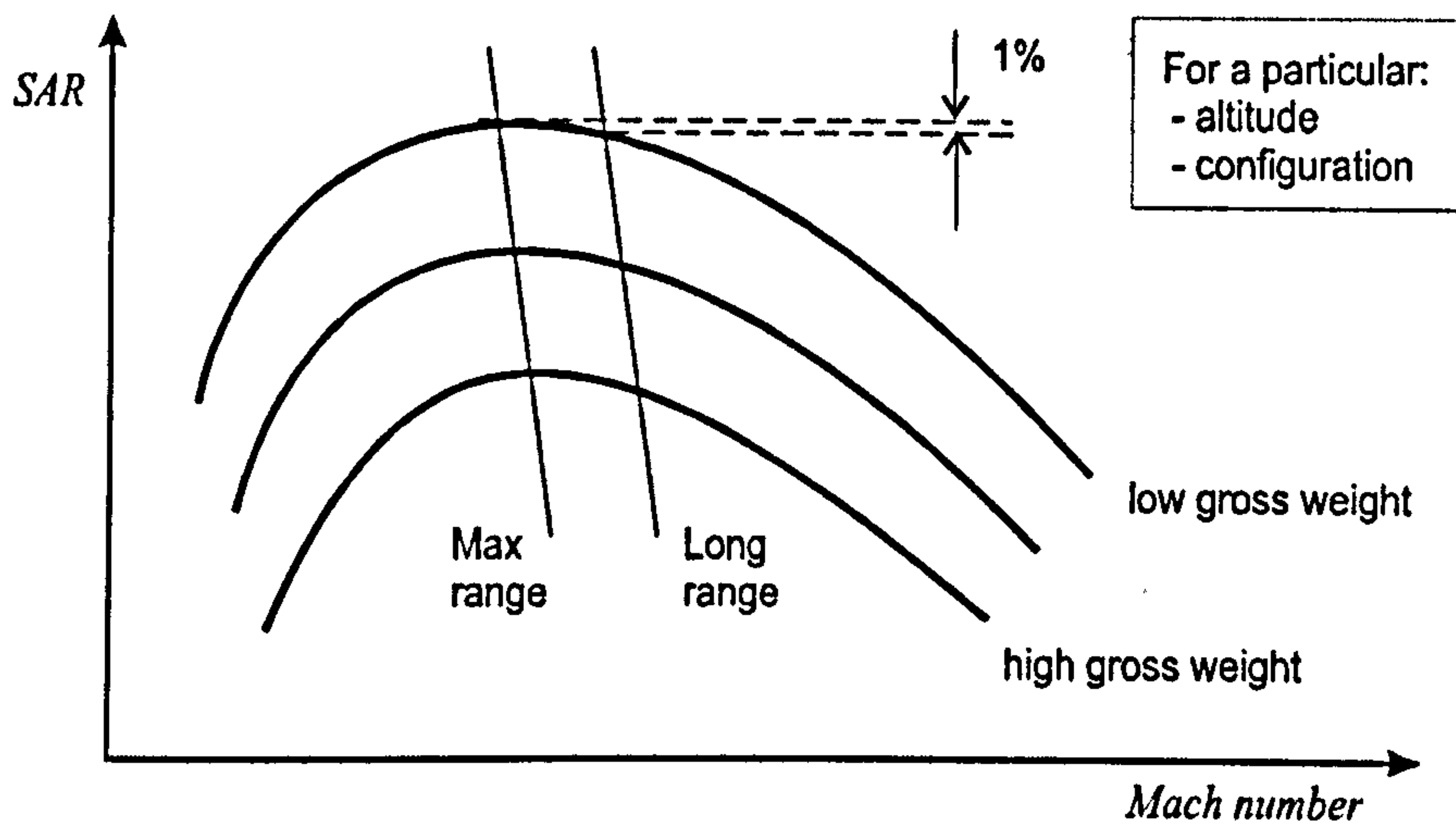


Fig. E-7 Max Range and Long Range Speeds (Young, 2002)

#### E.4.6 Step climb

The *cruise-climb* gives the greatest possible range. However, its practical use is limited by Air Traffic Control (ATC). As a result aircraft often fly a stepped approximation of the cruise-climb, climbing to a higher cruise altitude as fuel is burnt. The cruise is analysed as a number of fixed altitude segments and the additional fuel required for the step climb is added to the total.

#### E.4.7 Trip fuel estimation

A frequently used approach for estimating the trip fuel for a mission is to assume that the aircraft starts the cruise overhead the departure airfield and flies to a point overhead the destination airfield. The fuel is then estimated using the Breguet range, or similar equation, without the complexity of having to determine the climb and descent fuel quantities. From the brake-release to the Top of Climb (TOC), the approximation underestimates the required fuel, and from the Top of Descent (TOD) to the destination airfield, the approximation overestimates the required fuel (however this does not quite compensate for the error in the first part).

To explore the accuracy of the approximation, the results generated in section E.4.3 were used for a trip distance of 2350nm. In section I.2 (Appendix I) it is shown that the fuel consumed in the cruise ( $m_f$ ) can be expressed as a function of the end-of-cruise mass ( $m_2$ ). The data from section E.4.3, i.e.  $R = 4355\text{km}$  (2350nm),  $\bar{c} = 17.74\text{mg/N/s}$ ,  $V = 237.4\text{m/s}$  (461.1kt),  $\bar{E} = 16.89$  and  $m_2 = 90996\text{kg}$ ; was inserted into equation [I-4]. The resulting cruise fuel ( $m_f$ ) was evaluated to equal 18935kg. By comparison, the trip fuel calculated using the computer program (which would model the climb, cruise and descent), for the B757-200 class aircraft equalled 19841kg. The result of the approximate method differs from that produced by the more accurate computer model, by -4.6%. As stated earlier in section E.4.3, the problem with these



approximate methods is due to the difficulty that exists in obtaining accurate mean values, such as those given in Table E-2.

## E.5 HOLD

### E.5.1 Equations for the hold

An airliner may be required to *hold* at its destination, whilst awaiting ATC clearance to land. For standard fuel planning, a 30 minute hold at 1500ft overhead the alternate airfield is required at the end of the mission (see Appendix D). It is desirable that the aircraft fly, during this time, at the speed for lowest fuel consumption per unit time. The rate of fuel consumption for a turbofan engine is given by:

$$Q = cF_N = cD = c\left(\frac{D}{L}\right)W = \frac{c}{E}mg \quad \text{--- [E-41]}$$

Maximum endurance will be achieved at the condition that gives the least rate of fuel consumption. From equation [E-41] it is evident that this occurs when  $E$  is a maximum. The aircraft must therefore fly at its the maximum lift-to-drag ratio speed – the so-called *green dot* speed – to achieve the greatest endurance time (Airbus, 2002a).

The rate of change of aircraft mass is related to the fuel mass burned per unit time:

$$-\frac{dm}{dt} = -\frac{dm_f}{dt} = Q$$

If the initial mass is  $m_1$  and final mass  $m_2$ , the endurance time ( $t$ ) will be given by:

$$t = -\int_{m_1}^{m_2} \frac{1}{Q} dm = -\int_{m_1}^{m_2} \frac{E}{cgm} dm \quad \text{--- [E-42]}$$

In an almost identical manner to the range calculation it is possible to evaluate this integral for the three flight schedules, described in section E.4.2. With the assumption of constant lift coefficient (corresponding to flight schedules one and two) equation [E-42] can be evaluated. For constant  $E$  the endurance time  $t$  will be given by:

$$t = \frac{E}{cg} \log_e \left( \frac{m_1}{m_2} \right) \quad \text{--- [E-43]}$$

This equation is only valid if the aircraft is flown at a constant lift coefficient. Thus for flight at constant altitude, the pilot must reduce airspeed to compensate for the reduction in weight. If the aircraft is permitted to fly a *cruise-climb*, then it is possible to maintain a constant airspeed; however, this is not possible for an aircraft in a hold situation, where a fixed height must be maintained.

### E.5.2 Integrated hold method

In a very similar manner to that presented for the Integrated Range Method, the *holding time* can be estimated by a numerical integration, if fuel flow data is available.



$$t = \sum_{i=1}^n \frac{1}{Q_i} (m_i - m_{i-1}) \quad \text{--- [E-44]}$$

### E.5.3 Holding pattern

The conventional *racetrack* holding pattern consumes a little more fuel than a comparable straight and level flight at the same flight conditions. For example, the B757-200 will consume ~5% more fuel in a racetrack pattern (Boeing, 1993).

## E.6 TAKEOFF AND LANDING PERFORMANCE

### E.6.1 Takeoff and initial climb-out

For the purposes of analytical analysis, the takeoff distance ( $s$ ) may be divided into a ground segment ( $s_g$ ) and an air segment ( $s_a$ ). The ground segment is comprised of the distance from rest to the point where the aircraft rotates ( $s_R$ ) and the distance from the point of rotation to lift-off ( $s_{RL}$ ). At the rotation speed ( $V_R$ ), the angle of attack and lift is increased and lift-off occurs shortly afterwards. The aircraft climbs to clear the "screen" height of 35ft (10.7m). The flight path after takeoff may be divided into three segments (Fig. E-8). Specific requirements exist in terms of minimum climb gradients and speeds for each segment (as described in FAR 25 and JAR 25).

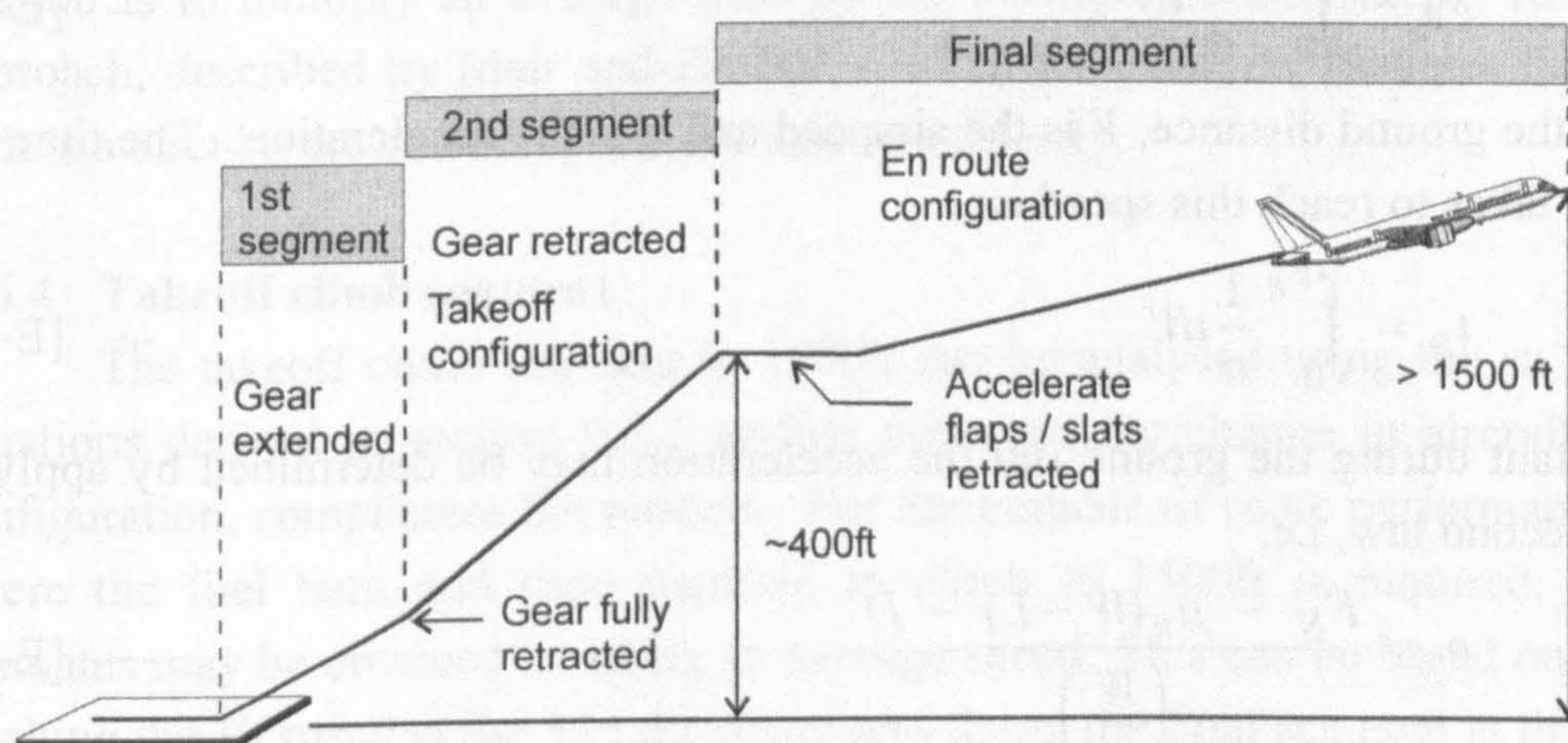


Fig. E-8 Takeoff path and initial climb segments

The first segment is from the 35ft height to the point of complete gear retraction. The aircraft will have the flaps and throttle set for takeoff. The second segment starts at the point of gear retraction and ends at a height ~400 ft (122 m) above the runway. In this segment the aircraft climbs at a speed of no less than the  $V_2$  speed, with the flaps set for takeoff. The final segment extends to a height of at least 1500ft (457m). During this segment the flaps are retracted and the aeroplane accelerates to the en route climb speed.



### E.6.2 Analytical evaluation of the takeoff run

The forces acting on an aircraft during takeoff are shown in Fig. E-9. During the takeoff the weight ( $W$ ) may be regarded as constant, but the other forces will change as the speed increases. The lift and drag coefficients will be essentially constant up to the point of rotation, hence the lift ( $L$ ) and drag forces ( $D$ ) will vary as functions of  $V^2$ . During the ground run the aircraft's lift-dependent drag is reduced by a *ground effect* correction factor ( $\lambda$ ), as a result of a reduction in the trailing vortex drag. In general the thrust ( $F_N$ ) will depend on the atmospheric conditions and the airspeed, and will vary during the takeoff run. For a hard dry surface, the "most usual value" for the rolling coefficient of friction ( $\mu_R$ ) that gets used is 0.02 (ESDU 85029, 1985).

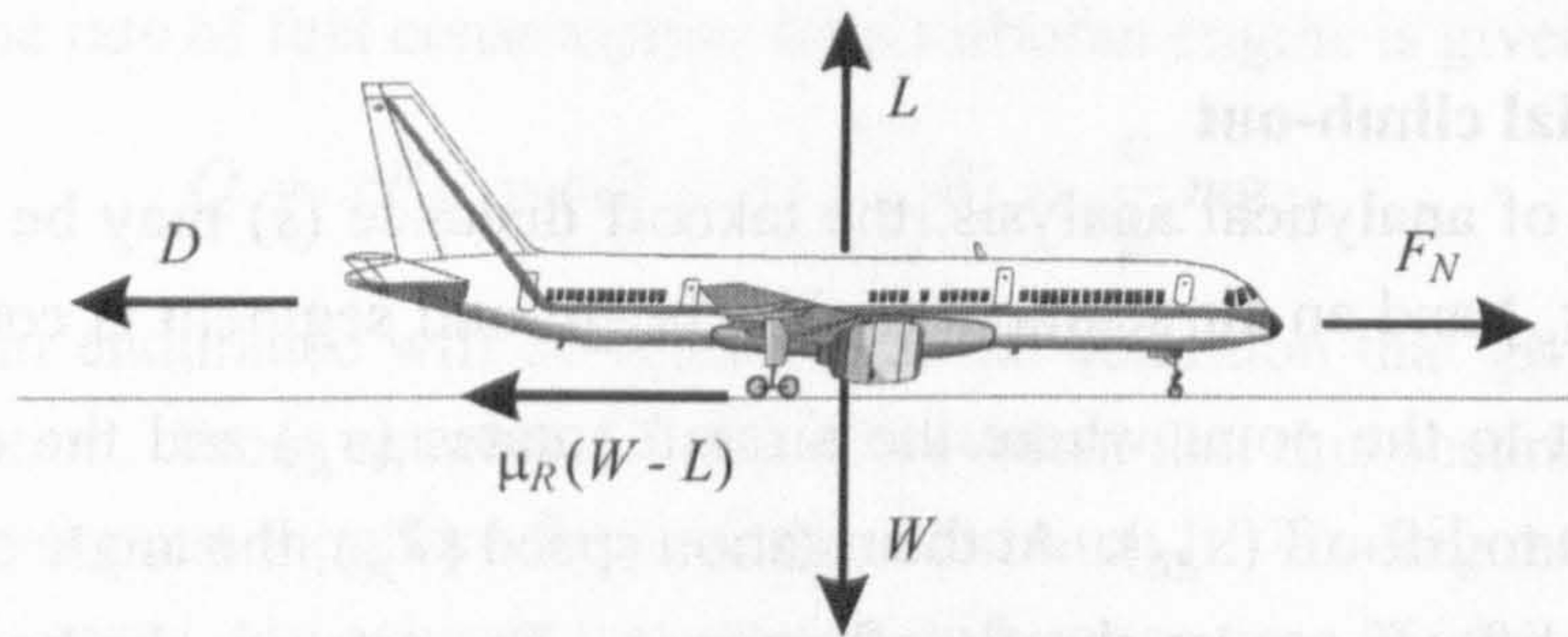


Fig. E-9 Forces acting on aircraft during takeoff

In the absence of wind the distance to the point of rotation ( $s_R$ ) is given by:

$$s_R = \int_0^{V_R} \frac{V}{a} dV \quad \text{--- [E-45]}$$

where  $s$  is the ground distance,  $V$  is the airspeed and  $a$  is the acceleration. The time ( $t_R$ ) the aircraft takes to reach this speed is:

$$t_R = \int_0^{V_R} \frac{1}{a} dV \quad \text{--- [E-46]}$$

At any instant during the ground run the acceleration may be determined by applying Newton's second law, i.e.

$$a = \frac{F_N - \mu_R(W - L) - D}{\left(\frac{W}{g}\right)} \quad \text{--- [E-47]}$$

By writing the lift as  $L = \frac{1}{2}\rho V^2 S C_L$  and the drag in terms of the parabolic drag polar, i.e.  $D = \frac{1}{2}\rho V^2 S (C_{D_0} + \lambda K C_L^2)$  the acceleration is given by:

$$a = \frac{g}{W} \left[ F_N - \mu_R \left( W - \frac{1}{2}\rho V^2 S C_L \right) - \frac{1}{2}\rho V^2 S (C_{D_0} + \lambda K C_L^2) \right] \quad \text{--- [E-48]}$$

The analysis may be simplified by assuming that the thrust is equal to  $\bar{F}_N$ , which is a value selected to give a good approximation of the takeoff distance. It has been shown



that for a jet aircraft, the acceleration varies approximately linearly with  $V^2$  from zero speed to the rotation speed (Boeing, 1989). The thrust and acceleration may thus be calculated at the speed  $V = \frac{1}{\sqrt{2}}V_R \approx 0.71V_R$ . With thrust taken as constant and all other variables written as functions of  $V^2$ , the integral expression [E-45] is evaluated to give:

$$s_R = \frac{1}{2gB_2} \ln \left( \frac{A_2 + B_2 V_R^2}{A_2} \right) \quad \text{--- [E-49]}$$

$$\text{where: } A_2 = \frac{\bar{F}_N}{W} - \mu_R \quad \text{and} \quad B_2 = \frac{\rho}{2(W/S)} \left( \mu_R C_L - C_{D_0} - \lambda C_L^2 \right)$$

### E.6.3 Rotation distance and climb-out to screen height

The rotation distance ( $s_{RL}$ ) is usually small in comparison to the distance  $s_R$ . The time that it takes for the aircraft to rotate depends on the rate that the pilot pulls the yoke back, and on the type of aircraft. An estimate of  $s_{RL}$  may be obtained by multiplying the rotation time, by the ground speed, which may be based on the assumption of zero acceleration, from rotation to lift-off.

The air segment ( $s_a$ ) is also difficult to calculate accurately, due to the variation of the governing parameters and the influence of varying pilot technique. The simplest method is to multiply an average time by the average ground speed. An alternative approach, described by Mair and Birdsall (1992), for example, assumes that the flight path is a circular arc and computes the distance directly.

### E.6.4 Takeoff climb segment

The takeoff climb segment to 1500ft can be analysed using the en route climb equations derived in section E.3.2 earlier; however, the change in aircraft speed and configuration, complicates the process. For the purpose of route performance analysis, where the fuel burn and time required to climb to 1500ft is required, satisfactory estimates may be obtained by using an average speed. This can be based on the aircraft reaching the  $V_2$  speed at the 35ft threshold and flying the final segment at the best climb gradient speed, which is equal to the  $\left( \frac{L}{D} \right)_{\max}$  speed.

### E.6.5 Analytical evaluation of the landing distance

The total landing distance is given by:

$$s = s_a + s_T + s_B \quad \text{--- [E-50]}$$

An estimate of the airborne distance ( $s_a$ ) can be obtained by multiplying the average time by the average ground speed. At the "screen" height of 50ft (15.2m), the approach speed is required to be not less than 1.3 times the stalling speed in the landing



configuration, according to the Airworthiness Regulations. The distance  $s_T$  is from touchdown to the point of brake application and can be determined from the delay time and the touchdown speed. (The speed at the touchdown will typically be about 5 - 15% higher than the stall speed.) The equations to be used to calculate the length of the ground run after the point where the brakes are applied, to standstill ( $s_B$ ), are essentially the same as those used for the takeoff. Equation [E-45] may be re-written to give the braking distance, i.e.

$$s_B = \int_{V_B}^0 \frac{V}{-a} dV \quad \text{--- [E-51]}$$

where  $a$  is negative and is given by equation [E-47]. The one significant difference is that a braking force replaces the rolling resistance. It is possible to estimate the maximum braking force, albeit with some difficulty. The braking coefficient of friction is not constant and will *increase* as the aircraft slows down. For initial estimations Raymer (1989) suggests typical braking coefficients ( $\mu_B$ ) of 0.3 – 0.5 for dry concrete or asphalt surfaces.

## E.7 CONVERSION FACTORS / BRITISH UNITS

### E.7.1 Introduction

Aircraft *operations* use a mix of units; altitude by convention is measured in feet, speed in knots or Mach number, and distance in nautical miles. These units are often used, even when other parameters, such as mass or density, are concurrently expressed in SI units. Converting between units poses no difficulty for most applications; however, in the case of aircraft performance analysis, the omission of the gravitational acceleration in the *definition* of parameters like fuel flow or SFC, can lead to errors. A description of the problem is presented in section E.7.4, together with range and endurance equations, which are conveniently defined for use with British units.

### E.7.2 Standard conversion factors

Conversion factors appropriate to the current study are given in Table E-3.

Table E-3 *Conversion factors*

	Aviation / British units	SI units	Conversion factor
Height, distance	ft	m	0.3048
Air distance	nm	m	1853
Speed	kt	m/s	0.5147
Area	ft <sup>2</sup>	m <sup>2</sup>	0.09290
Volume	USG	lt	3.785
Force	lb	N	4.448
Weight / mass equivalent under standard g	lb	kg	0.4536
SFC*	lb/lb/hr	mg/N/s	28.33

\* The conversion of SFC is not dimensionally consistent. See section E.7.4.



### E.7.3 Airspeed

The difference between CAS and EAS is the *compressibility correction*, and is designated as  $\Delta V_C$ . By definition:

$$V_C = V_e + \Delta V_C \quad \text{--- [E-52]}$$

and the magnitude of  $\Delta V_C$ , according to Boeing (1989), is given by:

$$\Delta V_C = a_o \left\{ \sqrt{5 \left\{ \left[ \delta \left\{ \left[ 1 + 0.2M^2 \right]^{3.5} - 1 \right\} + 1 \right]^{\frac{1}{3.5}} - 1 \right\}} - M\sqrt{\delta} \right\} \quad \text{--- [E-53]}$$

where  $a_o$  is the ISA sea-level speed of sound and  $M$  is the Mach number. A useful equation given in Boeing (1989) for converting CAS to Mach number, which accounts for compressibility correction, is:

$$M = \sqrt{5 \left\{ \left[ \frac{1}{\delta} \left\{ \left[ 1 + 0.2 \left( \frac{V_c}{a_o} \right)^2 \right]^{3.5} - 1 \right\} + 1 \right]^{\frac{1}{3.5}} - 1 \right\}} \quad \text{--- [E-54]}$$

### E.7.4 Fuel flow and specific fuel consumption

The *fuel flow* was defined in section E.2 as the *mass* of fuel burned per unit time. Equally correct it can be defined as the *weight* of fuel (under standard  $g$ ) burned per unit time (herein given the symbol  $Q'$ ). This is convenient for analysis performed using British units. Thus:

$$Q' = gQ \quad \text{--- [E-55]}$$

The SFC may be defined as, either the *mass* of fuel burned per unit time, divided by the thrust (as described earlier in section E.2.3), or the *weight force* of fuel burned per unit time, divided by the thrust, which is convenient when working in British units. Using the latter definition the SFC may be written as:

$$\text{SFC} = c' = \frac{\left( -\frac{dW_f}{dt} \right)}{F_N} = \frac{Q'}{F_N} \quad \text{--- [E-56]}$$

### E.7.5 Range and endurance

A summary of the range and endurance equations, expressed in terms of the mass flow and weight flow basis, are presented in Table E-4.



Table E-4 Summary of range and endurance expressions (Young, 2002)

	Mass flow basis	Weight flow basis
Fuel flow*	$Q = c g \left( \frac{D}{L} \right) m$	$Q' = c' \left( \frac{D}{L} \right) W$
Range	$R = \int_{m_2}^{m_1} \frac{V}{Q} dm$	$R = \int_{W_2}^{W_1} \frac{V}{Q'} dW$
	$R = \frac{V}{c g} \left( \frac{L}{D} \right) \ln \left( \frac{m_1}{m_2} \right)$ for constant $c, V$ and $C_L$	$R = \frac{V}{c'} \left( \frac{L}{D} \right) \ln \left( \frac{W_1}{W_2} \right)$ for constant $c', V$ and $C_L$
Endurance	$t = \int_{m_2}^{m_1} \frac{1}{Q} dm$	$t = \int_{W_2}^{W_1} \frac{1}{Q'} dW$
	$t = \frac{1}{c g} \left( \frac{L}{D} \right) \ln \left( \frac{m_1}{m_2} \right)$ for constant $c$ and $C_L$	$t = \frac{1}{c'} \left( \frac{L}{D} \right) \ln \left( \frac{W_1}{W_2} \right)$ for constant $c'$ and $C_L$

\* In level constant speed flight, where thrust equals drag and lift equals weight.

## E.8 INTERNATIONAL STANDARD ATMOSPHERE (ISA)

For aviation purposes, the ISA may be defined in two regions (ESDU 77022, 1986; ISO 2533, 1975):

- (1) The *Troposphere* extends from the ISA datum height (ISA sea-level) to the Tropopause, at a geopotential height of 11000m (36 089.24ft). The temperature is assumed to be exactly 15°C at the sea-level datum and to decrease linearly with altitude at a lapse rate of 6.5°C per 1000m.
- (2) The lower *Stratosphere* is the region above the Tropopause, to a geopotential height of 20000m (65616.80ft), in which it is assumed that the temperature is -56.5°C.

The standard values and equations for the ISA are given in Tables E-5 and E-6.

Table E-5 Equations for the ISA (Young, 2002)

	In the troposphere	Tropopause	In the stratosphere
Relative temperature	$\theta = \frac{L}{T_o} H$	$\theta^* = 0.751865$	$\theta = \theta^*$
Relative pressure	$\delta = \left[ 1 - \frac{LH}{T_o} \right]^{g_o / RL}$	$\delta^* = 0.223361$	$\frac{\delta}{\delta^*} = e^{(-g_o / RT^*)(H-H^*)}$
Relative Density	$\sigma = \left[ 1 - \frac{LH}{T_o} \right]^{(g_o / RL) - 1}$	$\sigma^* = 0.297076$	$\frac{\sigma}{\sigma^*} = e^{(-g_o / RT^*)(H-H^*)}$

Note: The conditions at the Tropopause are denoted by superscript asterisk (\*)



Table E-6 Standard values of the ISA (ESDU 77022, 1986; ISO 2533, 1975)

Standard values	Symbol	SI units	Equivalent
Temperature at sea-level	$T_o$	288.15 K	-
Lapse rate in Troposphere	$L$	6.5K per 1000 m	1.9812K per 1000 ft
Temperature of Tropopause	$T^*$	216.65 K	
Height of Tropopause	$H^*$	11000 m	36089.24 ft
Sea-level pressure	$p_o$	1013.25hPa	2116.217lb/ft <sup>2</sup>
Sea-level density	$\rho_o$	1.225 kg/m <sup>3</sup>	-
Gravitational acceleration	$g_o$	9.80665 m/s <sup>2</sup>	32.17405 ft/s <sup>2</sup>
Speed of sound at sea-level	$a_o$	340.294 m/s	661.4786kt
Gas constant	$R$	287.05287 m <sup>2</sup> /s <sup>2</sup> K	3089.811 ft <sup>2</sup> /s <sup>2</sup> K
Ratio of specific heats of air	$\gamma$	1.40	

E.9 DRAG

E.9.1 Drag components

There exist many different schemes for describing the drag on an aircraft. The subdivision shown in Fig. E-10 follows the approach and nomenclature described in ESDU 97016 (1997).

- *Friction drag (Skin friction drag)*

This is the viscous drag due to tangential forces on the surface of the body.

- *Pressure drag (Normal pressure drag)*

Pressure drag is the drag due to the normal pressures acting on the surface of a body. As tangential (Friction) and normal (Pressure) forces make up the resultant force on the body, the sum of *Friction* and *Pressure* drag is the total drag of the body.

- *Trailing vortex drag*

This is the drag produced on a finite wing due to the trailing vortex system formed when the wing is producing lift. In coefficient form, the *Trailing vortex drag* ( $C_{D_v}$ ) on planar wings with elliptic loading, is "well predicted" (ESDU 97016, 1997) by:

$$C_{D_v} = \frac{1}{\pi A} C_L^2 \tag{E-57}$$

where  $A$  is the wing aspect ratio. To allow for non-ideal conditions, the equation is often written as:

$$C_{D_v} = \frac{(1+\delta)}{\pi A} C_L^2 \tag{E-58}$$

where  $\delta$  is a planform correction factor.



- *Profile drag (Boundary layer drag)*

Profile drag is the drag arising due to the presence of a boundary layer on a body moving through the fluid.

- *Boundary layer normal pressure drag (Form drag)*

This is the Profile drag less the Friction drag. It depends on the shape of the body.

- *Interference drag*

Aerodynamic interference between adjacent airframe components arises due to the "coalescing of the pressure fields of the individual components and the confluence of their boundary layers in junction regions" (ESDU 97016, 1997).

- *Wave drag (Compressibility drag)*

Wave drag is the drag associated with the formation of shock waves in high speed flight. It has both lift and volume dependent components.

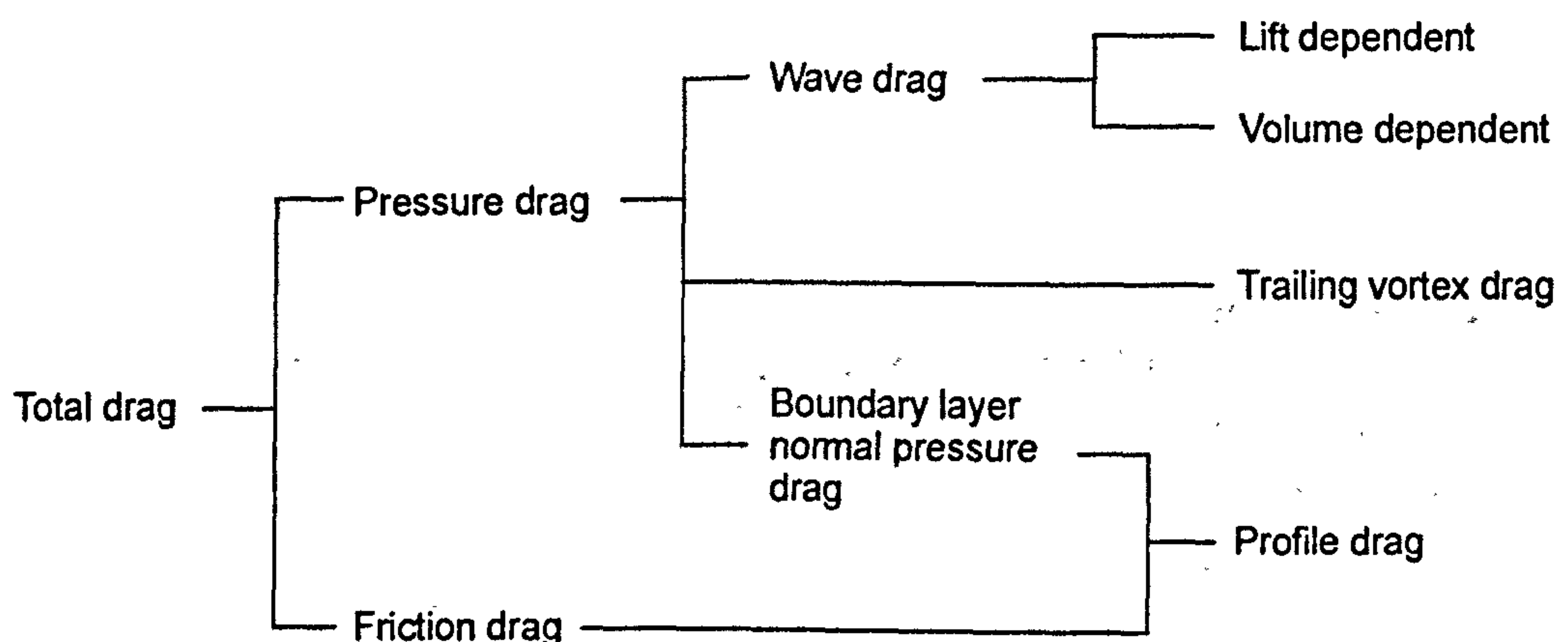


Fig. E-10 Drag components (ESDU 97016, 1997)

### E.9.2 Lift-dependent drag

The profile drag is largely *lift-independent*. In the drag breakdown shown in Fig. E-11 (after Bowes, 1974), the profile drag is the sum of the minimum profile drag  $C_{D_{pmin}}$  and a much smaller term  $\Delta C_{D_p}$  which is lift-dependent. The wing trailing vortex drag  $C_{D_v}$  is the major component of the *lift-dependent* (lift-induced) drag. Theoretical considerations suggest that the lift-dependent drag of a wing, is a quadratic form of the lift coefficient as  $Re \rightarrow \infty$  (Ardonceanu, 1994). Bowes (1974) states that a good airline wing design approaches an elliptic load distribution at the design condition and hence  $C_{D_v} \propto C_L^2$ . In the drag breakdown given in Fig. E-11, the non-elliptic vortex contribution, wing section camber influence, and the lift-dependent friction and pressure terms, are added to  $C_{D_v}$  to give the low speed lift dependent drag. The wave drag is the final component of drag in this breakdown.



As a matter of convenience the lift-dependent drag coefficient ( $C_{D_i}$ ) of the complete aircraft is frequently described by the expression:

$$C_{D_i} = K C_L^2 \quad \text{--- [E-59]}$$

where  $K$  is the *lift-dependent* drag factor. It is sometimes useful to express  $K$  in terms of a span efficiency factor; in which case the equation is written as:

$$C_{D_i} = \frac{1}{\pi A e} C_L^2 \quad \text{--- [E-60]}$$

where  $e$  is called the Oswald efficiency factor. ESDU 97016 (1997) indicates that "no genuine estimation method" exists for the value of this factor and traditional methods make use of data based on past experience.

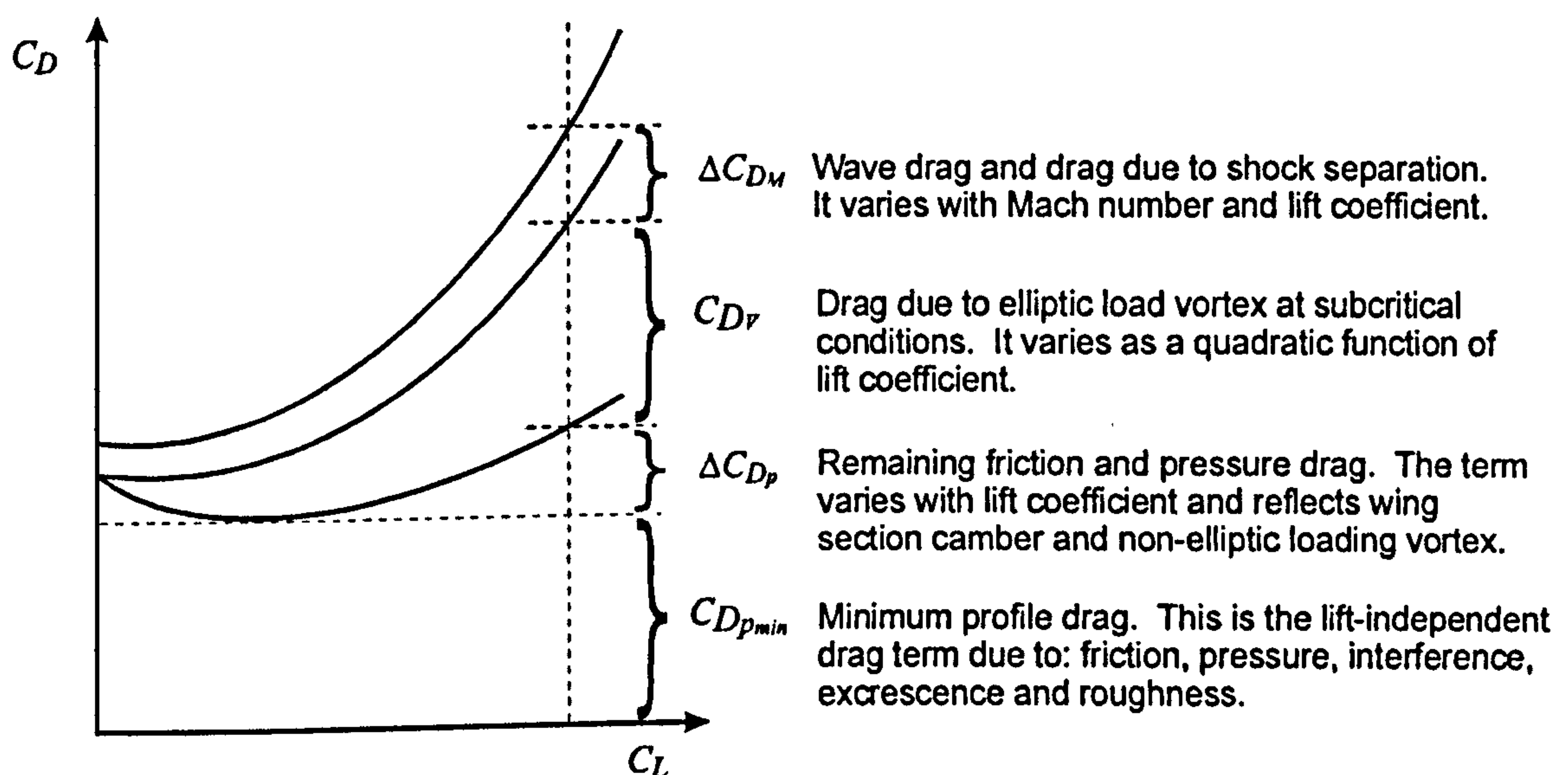


Fig. E-11 Drag breakdown (redrawn after Bowes, 1974)

### E.9.3 Drag polar

For the purpose of performance analysis, the aircraft's drag coefficient is usually divided into two components, i.e.

$$C_D = C_{D_o} + C_{D_i} \quad \text{--- [E-61]}$$

where  $C_{D_o}$  is the *zero-lift* drag coefficient. A number of formulations exist to mathematically describe the drag polar. A review of some of the drag representations is presented in this section.

- (1) Using the lift-dependent drag expression [E-59], the following well-known approximate drag representation is obtained:

$$C_D = C_{D_o} + K C_L^2 \quad \text{--- [E-62]}$$



Actual drag polars obtained from experimental results will usually differ from the idealised parabolic form, particularly at high or low AOA.

- (2) The effect of substantial camber on a wing will result in the minimum drag ( $C_{D_{min}}$ ) being slightly different to  $C_{D_0}$ . This is illustrated in Figures E-12a and E-12b. The drag polar shown in Fig. E-12b may be approximated by:

$$C_D = C_{D_{min}} + k \{C_L - C_L(C_{D_{min}})\}^2 \quad \text{--- [E-63]}$$

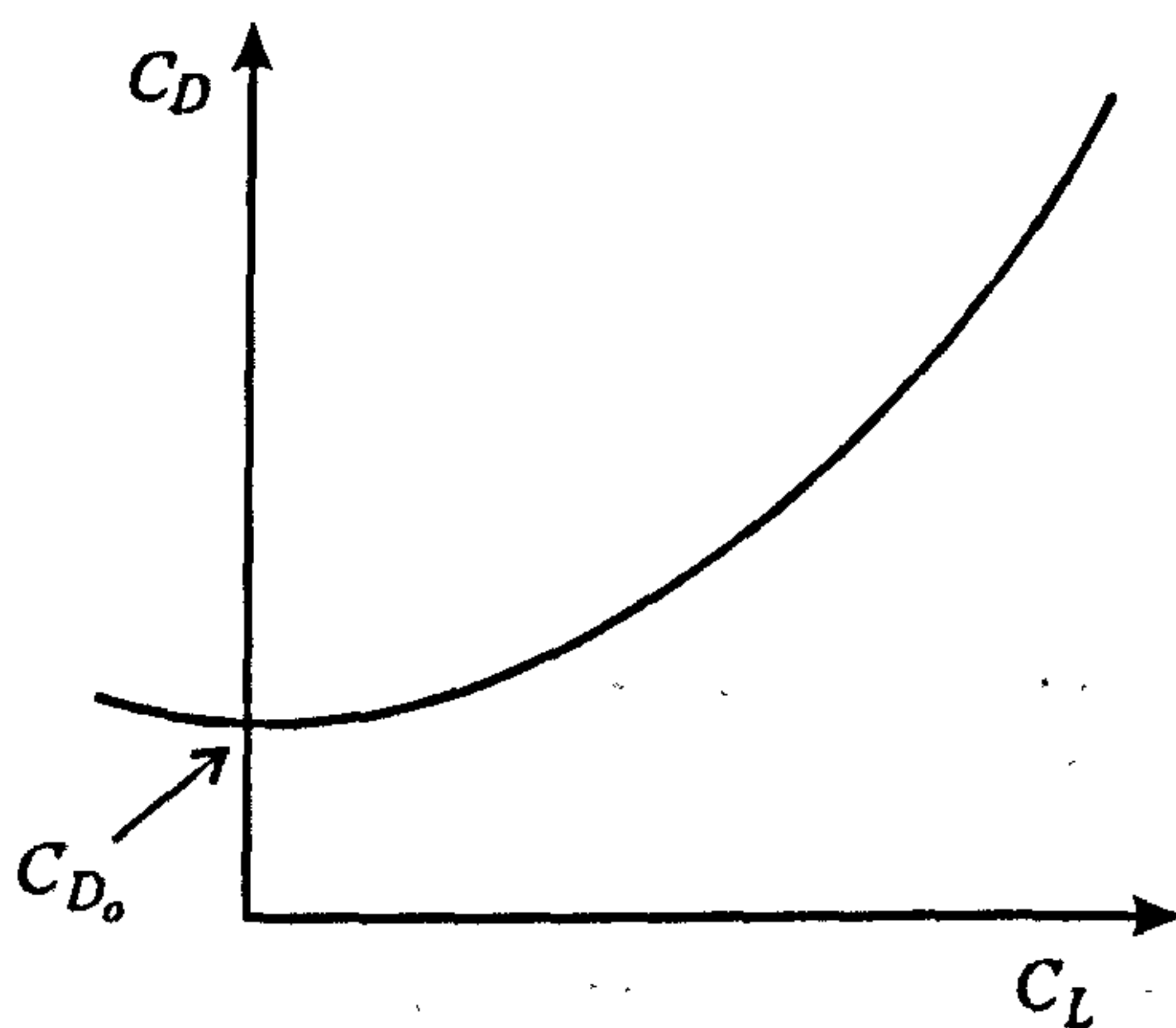


Fig. E-12a Idealised drag polar

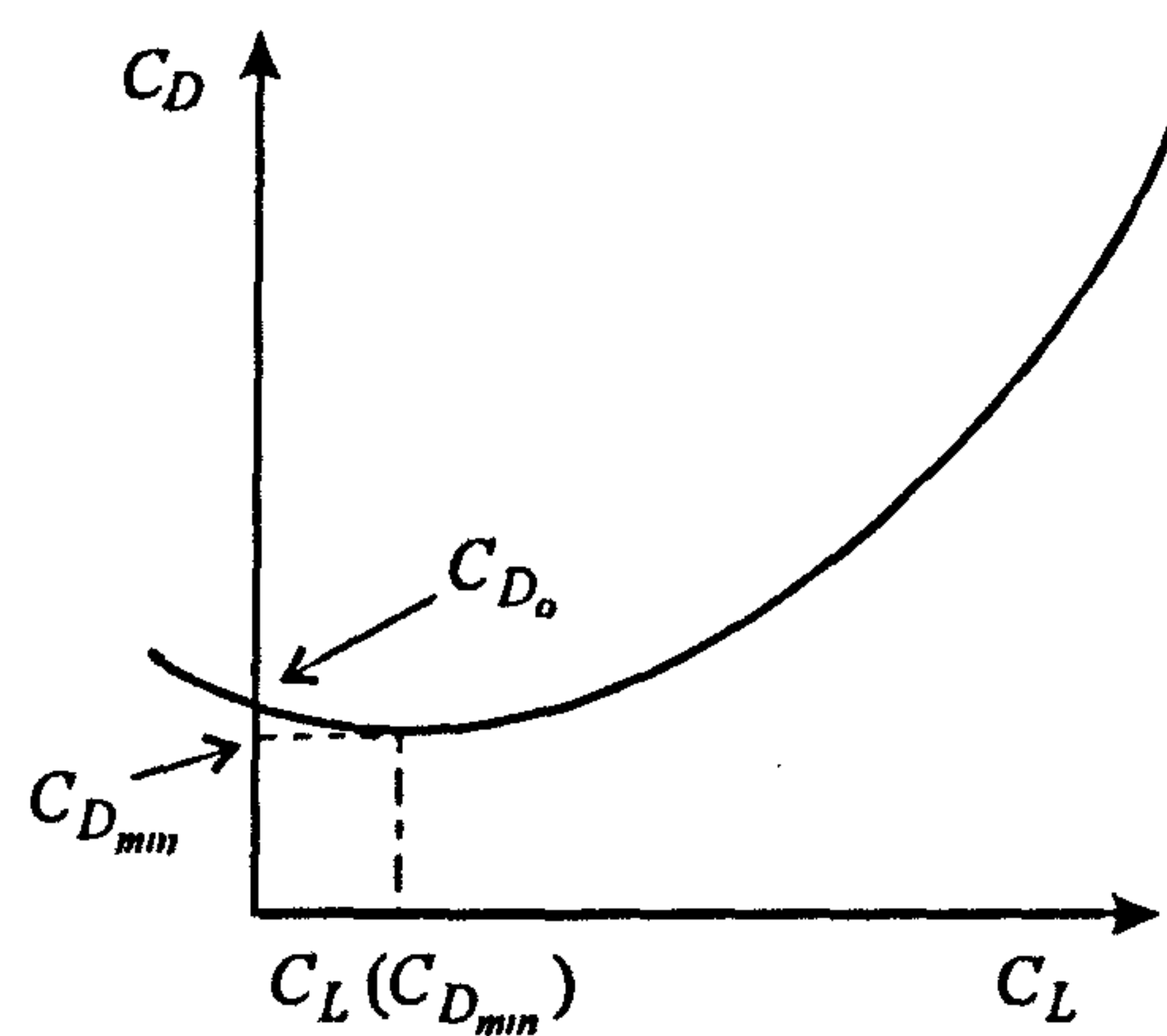


Fig. E-12b Drag polar for cambered wing

- (3) ESDU 66031 (1995) describes the drag relationship for a plane symmetrical section wing in terms of two parabolic segments. This can be seen on a plot of  $C_D$  versus  $C_L^2$  as shown in Fig. E-13. Up to a certain value of the lift coefficient ( $C_{L_K}$ ), the variation of  $C_D$  with  $C_L^2$  is linear and can be represented by the slope  $k_1$ . Above  $C_{L_K}$  the slope is given by  $k_2$ , where  $k_2 > k_1$ .

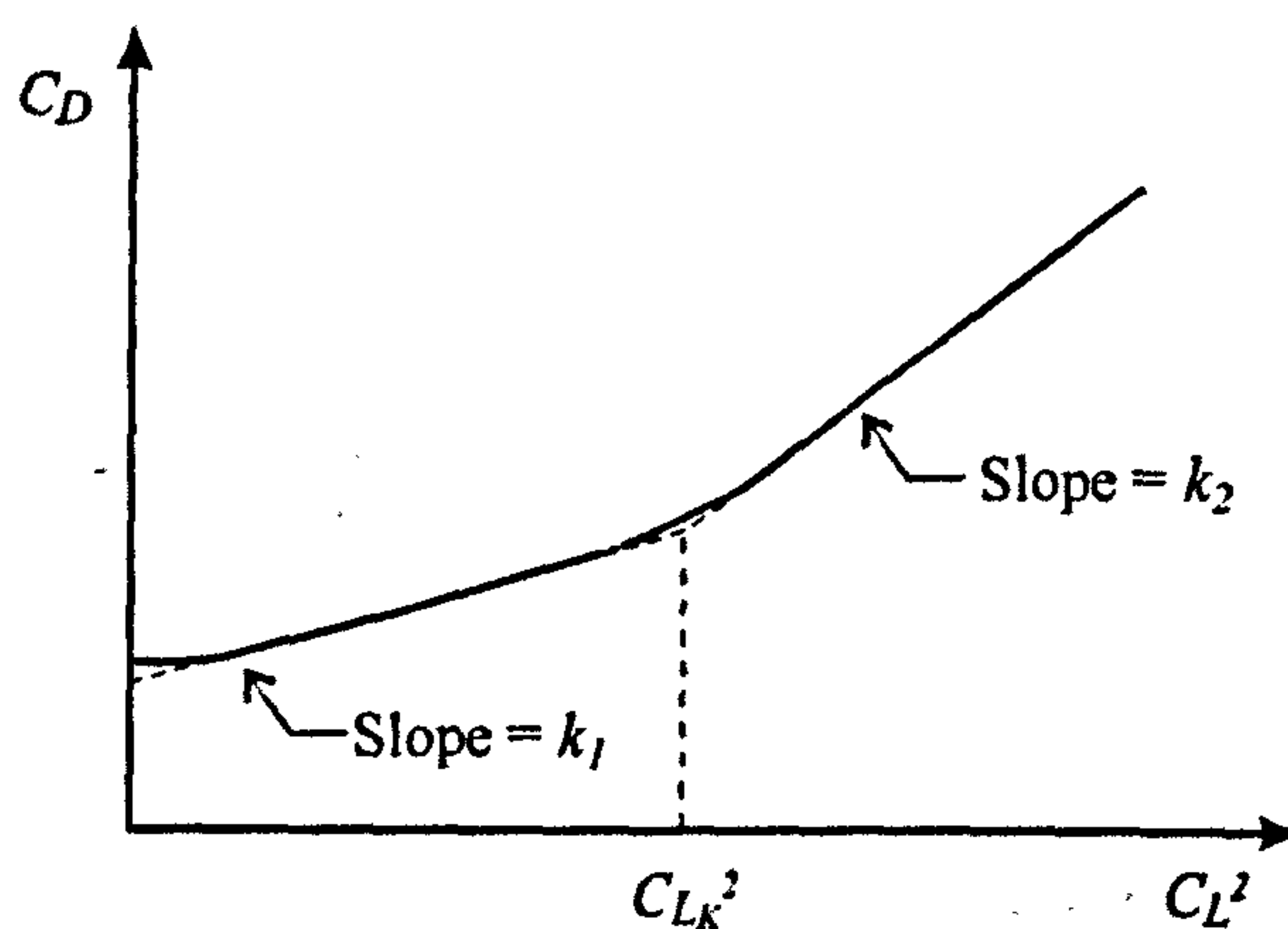


Fig. E-13 Drag approximation (based on ESDU 66031, 1995)



- (4) ESDU 66031 (1995) reports on unpublished Hawker Siddeley Aviation work, which indicated that "in some cases a term in  $C_L^4$  is not negligible" in drag representation. Inclusion of this term in the parabolic drag polar yields the expression:

$$C_D = C_{D_o} + K_2 C_L^2 + K_3 C_L^4 \quad \text{--- [E-64]}$$

Yajnik and Subbaiah (1976) showed that the drag polar of the YF-16 fighter aircraft, with manoeuvre flaps extended (i.e. with a cambered section), is well represented by the equation:

$$C_D = C_{D_o} + K_2 C_L^2 + K_3 C_L^n \quad \text{--- [E-65]}$$

They noted that the slope of the  $C_D$  versus  $C_L^2$  line did not change abruptly, as would be the case for the model described in (3) earlier, but instead a gradual change was evident. The exponent  $n$  was evaluated numerically and best fit values were shown to be in the range 3.4 to 4.2. They concluded that the exponent  $n = 4$  provided a simple, effective representation of the aircraft test data.

The experimental results of Ardonceau (1994), dealing with elliptic and crescent wing planforms, indicated that the "total induced drag... did not appear to be conveniently described by a parabolic relation with the lift coefficient". A better fit with the experimental data was obtained by raising the degree of the polynomial, and expressing the drag relationship in the form:

$$C_D = C_{D_o} + K_2 C_L + K_3 C_L^2 + K_4 C_L^3 + K_5 C_L^4 \quad \text{--- [E-66]}$$

#### E.9.4 Drag rise

The drag divergent Mach number ( $M_{DD}$ ) is a little greater than the critical Mach number (which is the speed when shocks begin to occur on the wing) and is associated with a significant increase in drag. Various interpretations exist of what constitutes a significant drag increase. The Boeing definition of  $M_{DD}$  is where the drag rise reaches 20 drag counts (Raymer, 1989). An estimate of  $M_{DD}$  (as per the definition of Boeing) may be obtained using the following equation (Raymer, 1998):

$$M_{DD} = M_{DD_{L=0}} LF_{DD} - 0.05 C_{L_{design}} \quad \text{--- [E-67]}$$

where:  $M_{DD_{L=0}}$  is the drag divergent Mach number for zero lift;  $LF_{DD}$  is a lift correction factor; and  $C_{L_{design}}$  is the design lift coefficient. Empirical data for  $M_{DD_{L=0}}$  and  $LF_{DD}$  (which are functions of the wing thickness to chord ratio) may be used to estimate  $M_{DD}$ .



Blank page



## APPENDIX F

# B757-200 CLASS AIRCRAFT DATA

### TABLE OF CONTENTS

F.1	Introduction.....	262
F.2	Leading Characteristics of the B757-200.....	262
F.3	Aerodynamic Data .....	263
F.4	Engine Data.....	264
F.4.1	Candidate engines.....	264
F.4.2	Available climb thrust .....	265
F.4.3	Fuel flow.....	267
F.4.4	Engine data at idle .....	269
F.5	Miscellaneous Performance Data.....	269
F.5.1	Initial climb data.....	269
F.5.2	Alternate leg cruise speed.....	270
F.5.3	Holding speed.....	270



## F.1 INTRODUCTION

The Boeing 757-200 is a short to medium range twin-turbofan airliner. It received FAA certification in December 1982, entered service in the same month and was granted 180 minutes ETOPS clearance in April 1992 (Boeing, 1999b).

## F.2 LEADING CHARACTERISTICS OF THE B757-200

Data for the B757-200 is given in Table F-1 and a "general arrangement" drawing of the aircraft is included as Fig. F-1.

**Table F-1** *Leading characteristics of the B757-200*

<i>Accommodation</i> <sup>(1,3)</sup>	Crew of two with five to seven cabin attendants. Design seating capacity for 201 (typical mixed-class) to 231 (economy) passengers.	
<i>Variants</i> <sup>(1)</sup>	757-200 passenger airliner, with extended range option 757-200PF a package freighter variant 575-200M a mixed cargo/ passenger Combi	
<i>Power plants</i> <sup>(2)</sup>	Rolls-Royce RB211-535C, RB211-535E4, RB211-535E4B Pratt and Whitney PW2037, PW2040	
<i>Fuel capacity</i> <sup>(1)</sup>	42597lt (11253 USG) or 34291kg (75594lb)*	
<i>Max. fuel capacity</i> <sup>(3)</sup>	43630lt (11526 USG) or 35123kg (77428lb)*	
<i>Dimensions</i> <sup>(4,1)</sup>	Wing span:	37.95m (124ft 6in)
	Wing aspect ratio:	7.95
	Length overall:	47.2m (155ft 3in)
	Height overall:	13.56m (44ft 6in)
	Wing sweep:	25° (25% chord)
<i>Areas</i> <sup>(1)</sup>	Wing gross area:	185.25m <sup>2</sup> (1994ft <sup>2</sup> )
<i>Areas</i> <sup>(4)</sup>	Wing reference area:	181.25m <sup>2</sup> (1951ft <sup>2</sup> )
<i>Aspect ratio</i>	7.95	Based on wing span and reference area
<i>Weights</i> <sup>(1)</sup>	With 186 passengers, Variants A RB211-535E4; B PW2037; C PW2040	
	OEW	A 57180kg (126060lb), B, C 57039kg (125750lb)
	MTOW (basic variant)	A, B, C 99 790kg (220 000lb)
	MTOW (long range)	A, B, C 113 395kg (250 000lb)
	MLW	A, B, C 89 810kg (198 000lb)
	MZFW	A, B, C 83 460kg (184 000lb)
<i>Weights</i> <sup>(3)</sup>	MTOW	115 660kg (255 000lb)
	Typical OEW	583 90kg (128 730lb)
<i>Weights</i> <sup>(5)</sup>	MZFW	85 280kg (188 000lb)
<i>Range</i> <sup>(1)</sup>	With 186 passengers:	
	at basic MTOW	A 2820nm (5226km), B, C 2980nm (5522km)
	at long range MTOW	A 3820nm (7079km), B, C 4000nm (7412)
<i>Range</i> <sup>(5)</sup>	With 201 passengers, "typical" mission rules, LRC, MTOW 115 660kg Range: ~ 3660nm (6782km)	

**Source:**

<sup>(1)</sup> Lambert (1992)

<sup>(2)</sup> Rolls-Royce (1998)

<sup>(3)</sup> Boeing (1999b)

<sup>(4)</sup> Boeing (1989)

<sup>(5)</sup> Boeing (2001)

\* Density of fuel: 0.805kg/lt (Ref. Boeing, 1996).



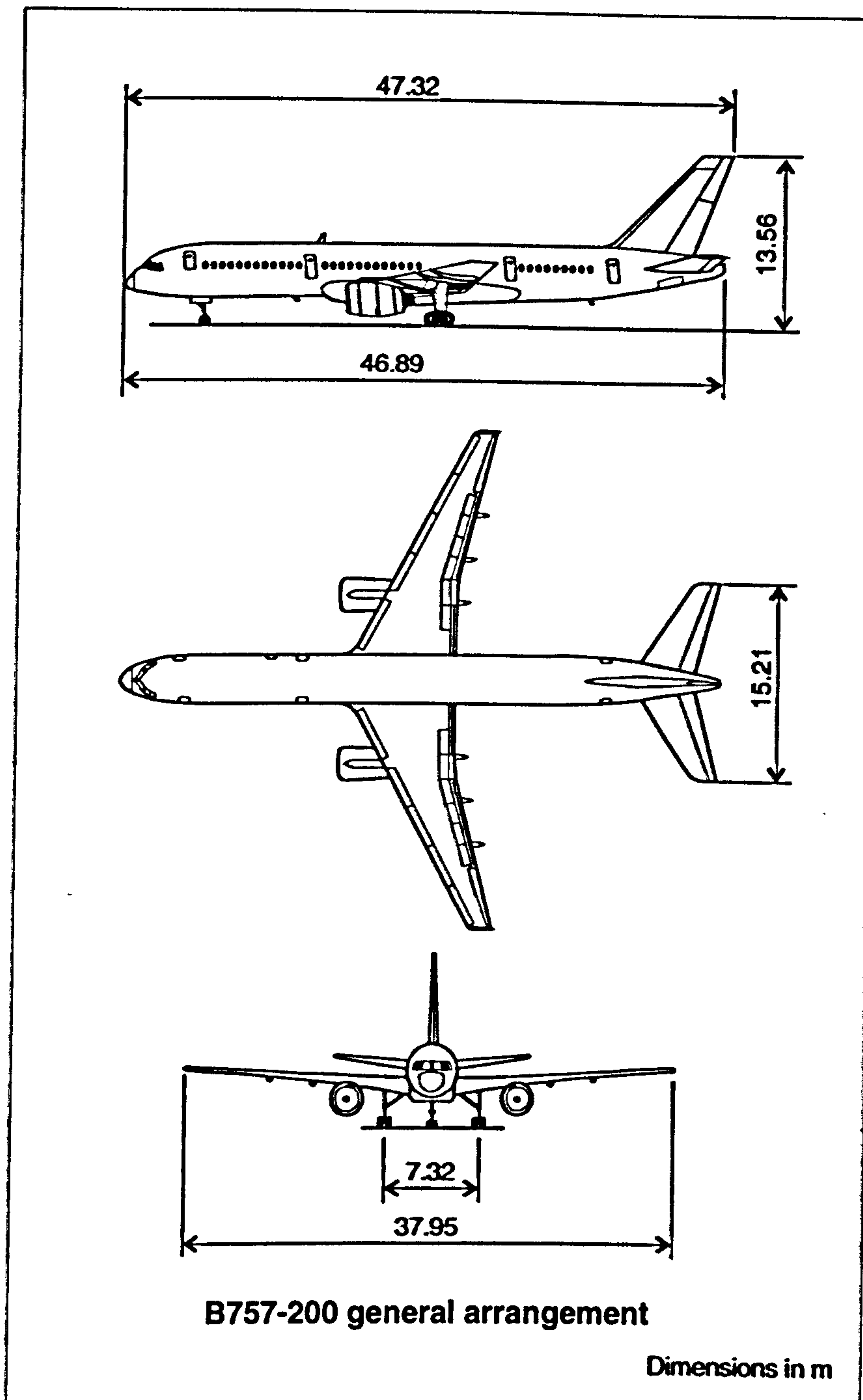


**Fig. F-1** General arrangement drawing of Boeing 757-200  
(Redrawn after Lambert, 1992; dimensions from Boeing, 1982)

### F.3 AERODYNAMIC DATA

The aerodynamic data for the performance model used in this study, was taken from a Boeing Performance Engineer's Manual (PEM) for a twin turbofan airliner in the class of the B757-200, which is referred to as the B7G7. In the PEM (Boeing, undated) the drag polar is presented as a table of  $C_D$  values against  $C_L$  values in steps of 0.05 for Mach numbers between 0.30 and 0.70 and then in steps of 0.1 for Mach 0.72 to 0.87.



To simplify the look-up process data for Mach 0.71 was obtained by linear interpolation and included in the database. The drag polars are shown in Figures F-2 and F-3.

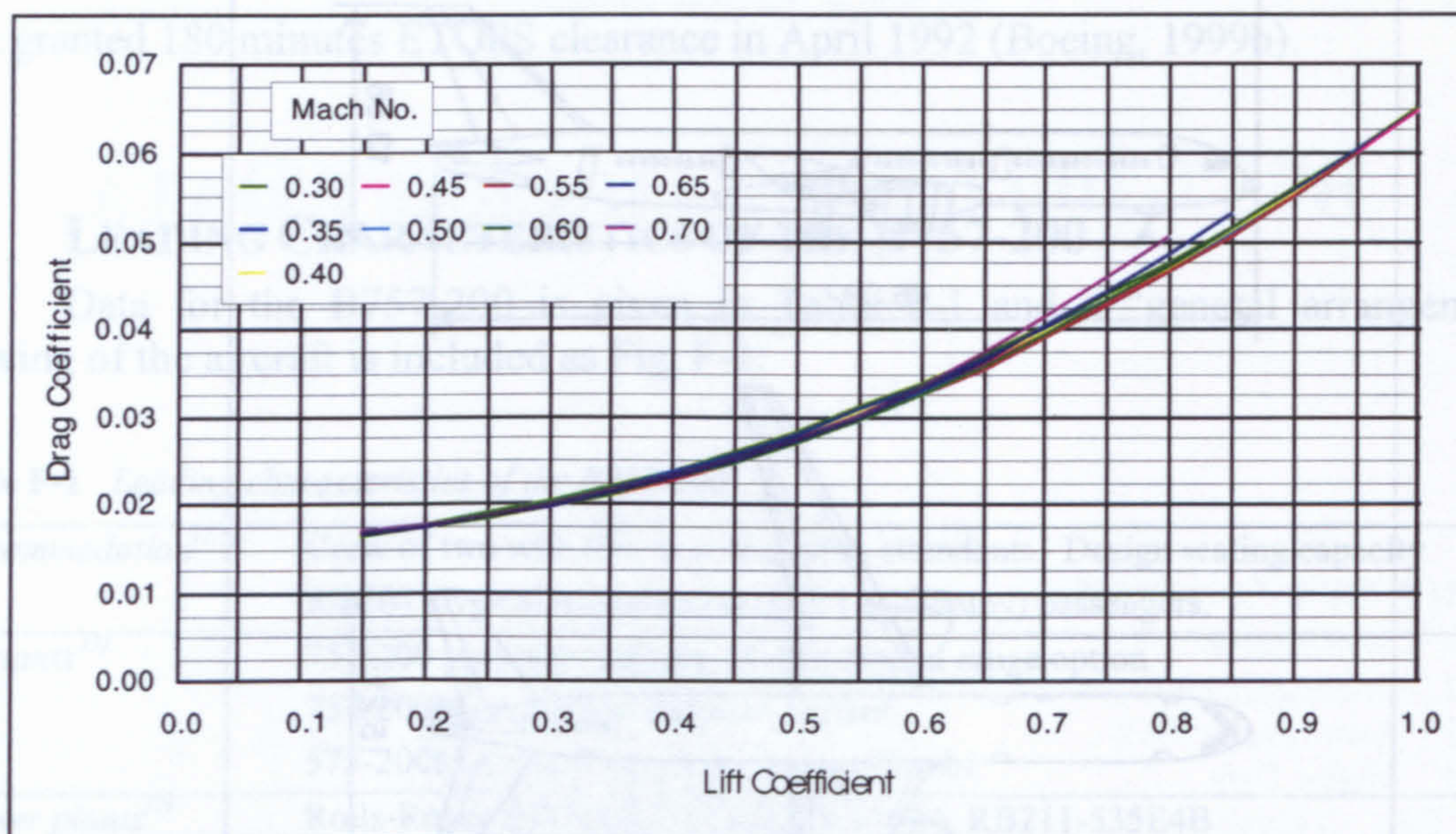


**Fig. F-2** Drag polar (Mach 0.30 to 0.70)

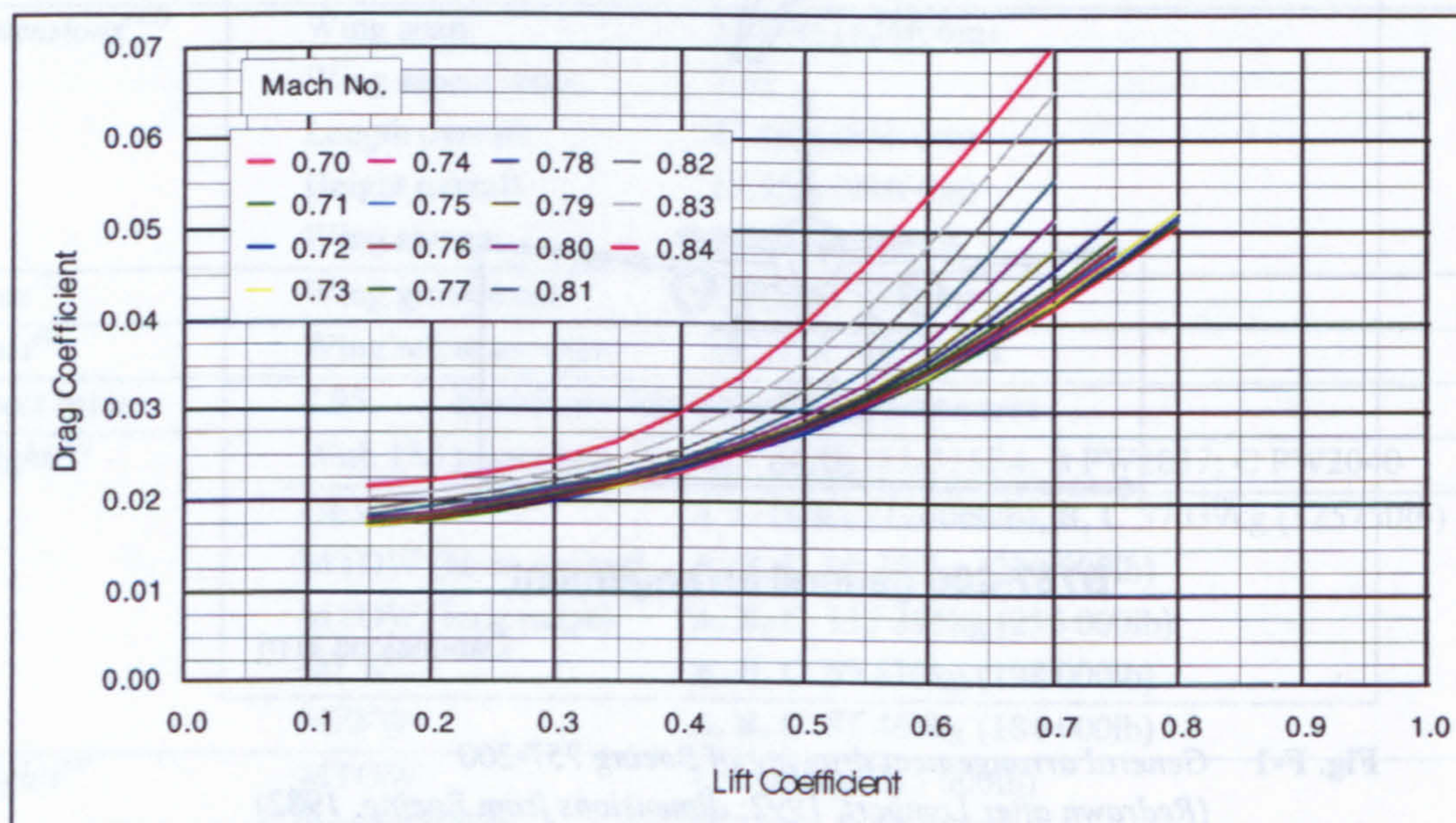


**Fig. F-3** High speed drag polar (Mach 0.70 to 0.84)

## F.4 ENGINE DATA

### F.4.1 Candidate engines

The B757-200 has been fitted with three versions of the Rolls-Royce RB211-535 engine and two Pratt and Whitney 2000 series engines. Leading parameters of



these engines are given below in Table F-2. The engine data for the B7G7 in the Performance Engineer’s Manual (Boeing, undated) closely matched that of the older RB211 engine, the RB211-535C. The data was then adjusted to get an engine database as close as possible to the more modern engine, the RB-211-535E4.

Table F-2 *Leading data of candidate engines (Rolls-Royce, 1998)*

Engine ->	RB211 -535C	RB211 -535E4	RB211 -535E4B	PW2037	PW2040
<b>Takeoff SLS</b>					
Thrust ISA	166kN (37400lb)	178kN (40100lb)	192kN (43100lb)	171kN (38400lb)	186kN (41700lb)
Bypass ratio	4.4	4.3	4.3	6.0	5.9
Pressure ratio	21.1	25.8	28.0	27.6	27.6
Mass flow	517kg/s (1140lb/s)	522kg/s (1151lb/s)	533kg/s (1177lb/s)	549kg/s (1210lb/s)	569kg/s (1255lb/s)
<b>Climb</b>					
Max thrust	40.5kN (9100lb)	40.5kN (9100lb)	40.5kN (9100lb)	37.8kN (8500lb)	41.1kN (9250lb)
<b>Cruise*</b>					
Thrust	37.6kN (8450lb)	37.8kN (8495lb)	N/A	28.9kN (6500lb)	28.9kN (6500lb)
SFC	18.3mg/N/s 0.646lb/lb/hr	16.9mg/N/s 0.598lb/lb/hr	N/A	16.5mg/N/s 0.582lb/lb/hr	16.5 mg/N/s 0.582lb/lb/hr

\* Note: Cruise at FL 350, M0.80 for RB211 engines; cruise at FL 350, M0.85 for PW2000 engines.

F.4.2 Available climb thrust

The maximum available climb thrust, tabulated in the Performance Engineer’s Manual (Boeing, undated) as  $F_N/\delta$ , was available for the speed range Mach 0.20 to Mach 0.90 for heights from sea-level to 42000ft. This was for the engine operating with two air-conditioning packs under normal conditions. It is evident from Fig. F-4 that the data is smooth; facilitating linear interpolation to be used to establish data points at Mach numbers and heights, which were not in the original database.

The climb thrust values were initially scaled by a factor of 1.072, which is the ratio of the quoted static thrust of the RB211-535E4 engine, to the RB211-535C engine (see Table F-2). The scaling factor was then adjusted within the computer program (Appendix H) and the climb results observed. The ROC (Rate of Climb) is dependent on the excess of thrust to drag for a given weight and speed. (See equation [E-25], Appendix E.) If the drag data is assumed to be correct, then the evaluated *time* and *distance* to the cruise height, provides a mechanism to check the climb thrust data. Following a number of trials a scaling factor of 1.080 was selected, as this gave the best set of overall results (given in Table 4-3). The results indicate a good correlation between the performance model and the Operations Manual data (Boeing, 1993).

The thrust that is available in the climb is shown in Fig. F-5. Also indicated in the figure is the Mach number for the B757 climb schedule, and the thrust at that Mach



number and height. The thrust parameter  $F_N/\delta$  during the climb is seen to be represented by three approximately linear segments, where the changes correspond to height changes in the climb speed schedule, i.e. at 1000, 31000ft and at the Tropopause.

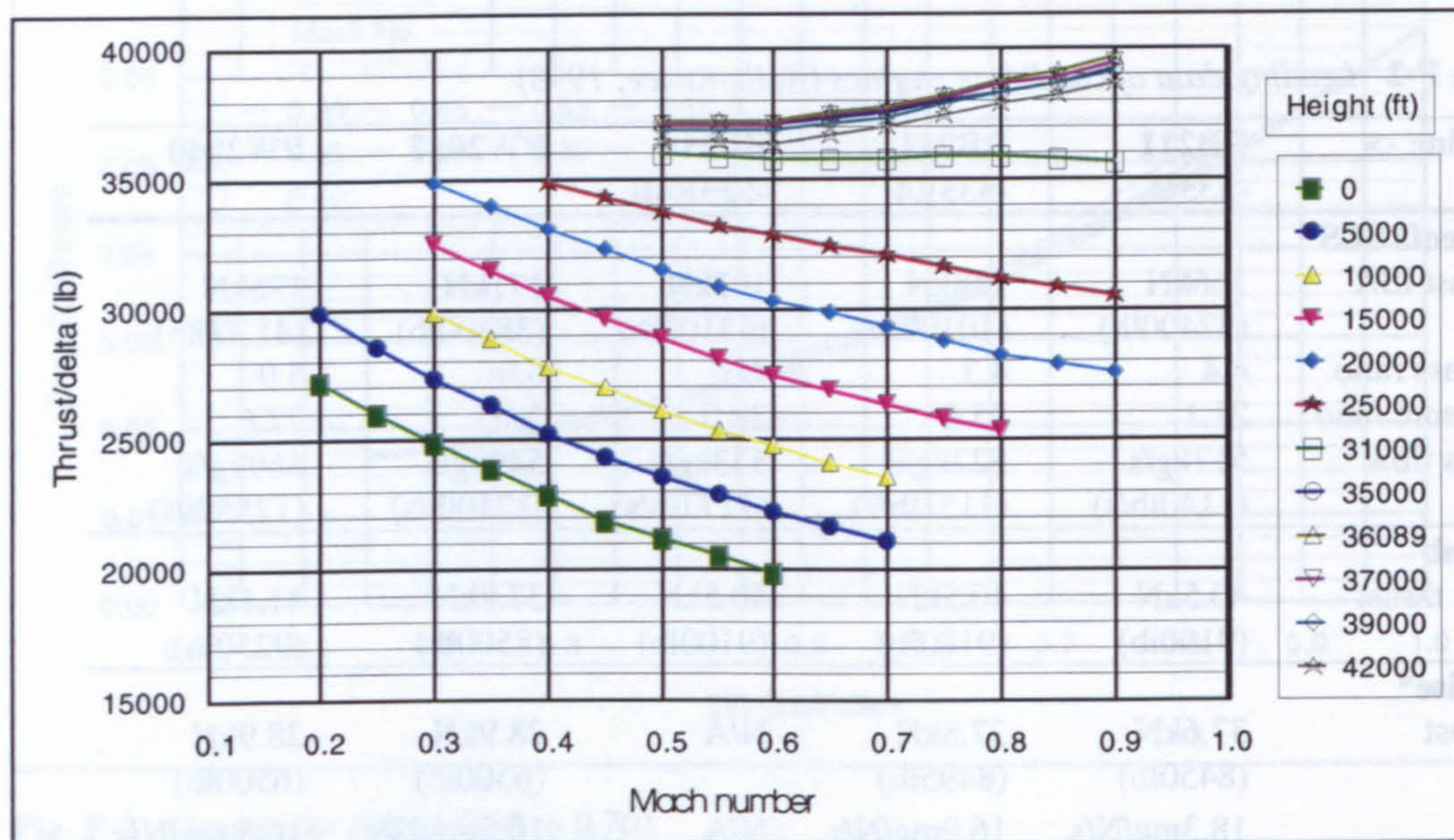


Fig. F-4 Maximum climb thrust  $F_N/\delta$  for various heights

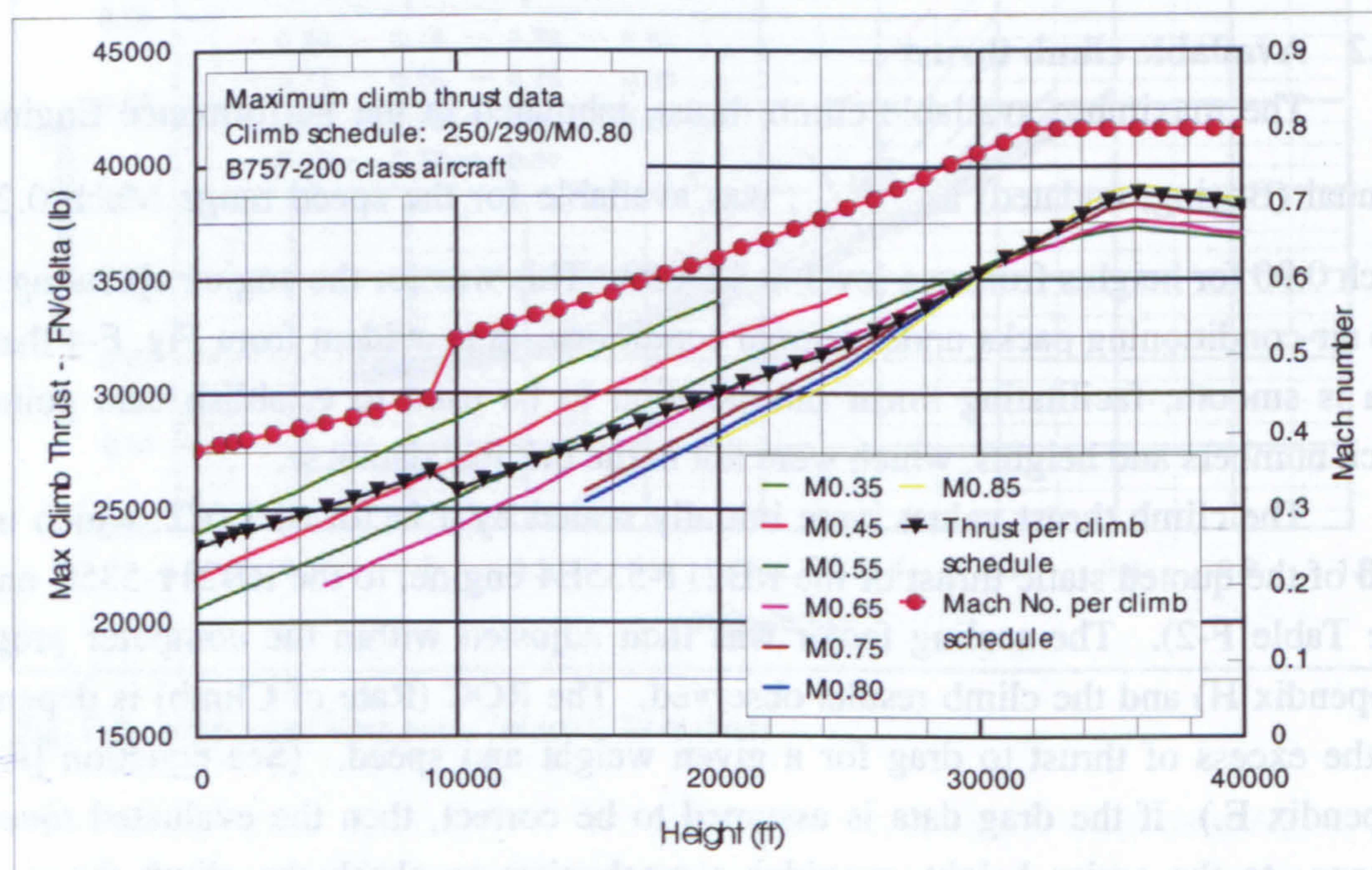


Fig. F-5 Maximum available climb thrust  $F_N/\delta$  for different Mach numbers versus height. Also indicated is the Mach number for the B757 climb schedule and the thrust at that Mach number and height.



F.4.3 Fuel flow

In the performance theory section E.2 (Appendix E) it was stated that the fuel flow is by convention "corrected" for atmospheric conditions, using the total pressure and temperature ratios. The form of the equation for the ideal engine installation is usually:

$$\text{Corrected fuel flow} = \frac{Q}{\delta_t \theta_t^{0.5}} \quad \text{--- [F-1]}$$

In the case of the B7G7 data the information is provided in the following form:

$$\text{Corrected fuel flow} = \frac{Q}{\delta_t \theta_t^{0.6363}} \quad \text{--- [F-2]}$$

where the exponent 0.6363 takes into account actual installation losses.

Seven tables of corrected fuel flow data were available, corresponding to heights of 0, 5000, 10000, 35000, 36089, 37000, 39000 and 42000ft. The values were tabulated as a function of  $F_N/\delta$  and Mach number (see Fig. F-6 for an example of the data). To facilitate the requirements of the mission calculations (see Appendix H), data was also required at other altitudes. For the hold calculation a table for 1500ft was derived by linear interpolation of the data given for 0 and 5000ft. Additional tables were created for heights of 32100 and 33000ft, by linear extrapolation of the 35000ft and 36089ft data, and by linear interpolation, a table was created for FL 410. For the climb analysis the heights selected, were 15000, 20000, 25000 and 29000ft. The data was obtained for these heights by linear interpolation of the 10000 and 32100ft data. The validity of this approach was assessed by plotting the interpolated / extrapolated values, as functions of height, for a fixed Mach number. The example given in Fig. F-7 is for Mach 0.6. It is evident that linear interpolation is acceptable in this situation.

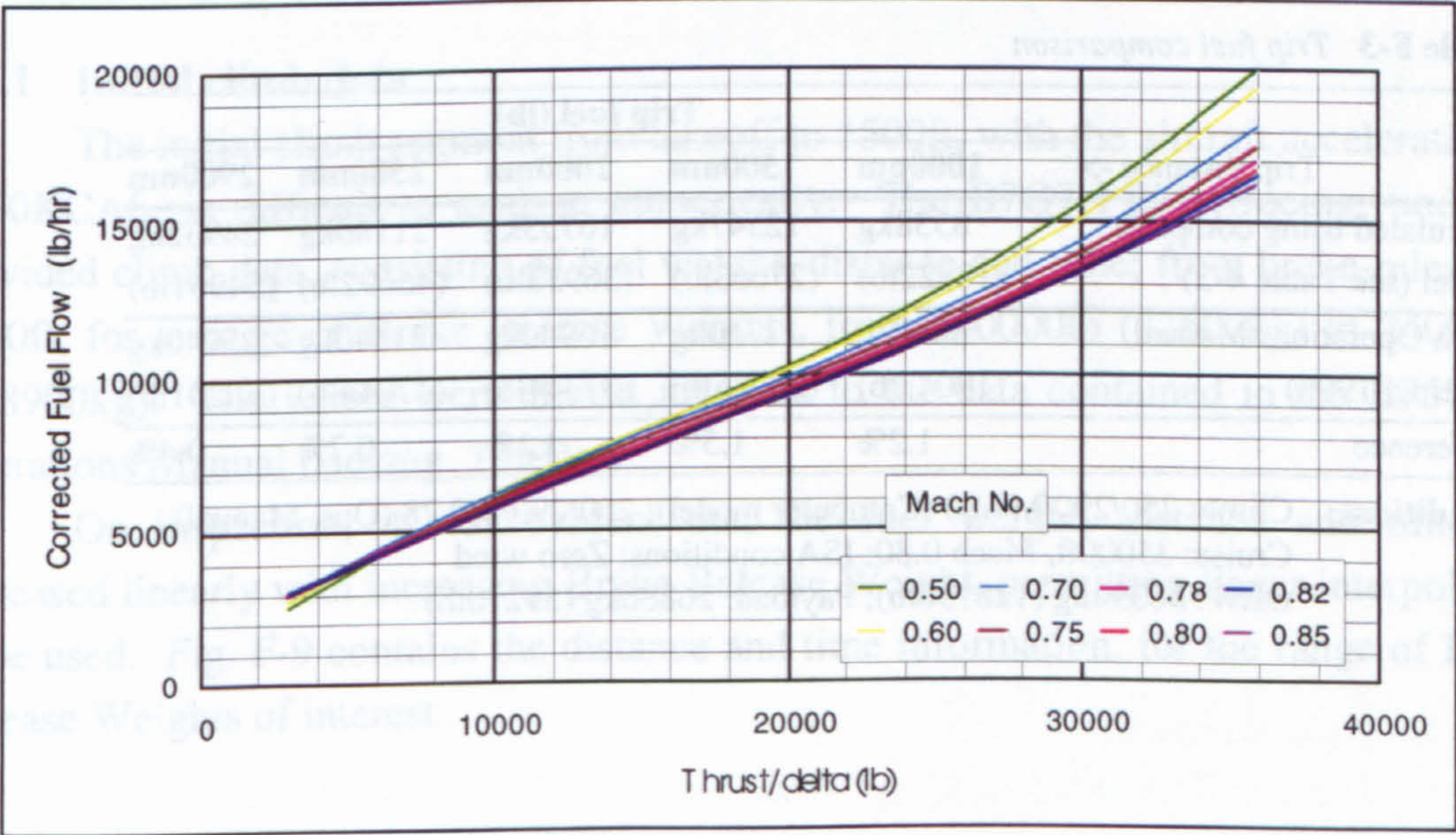
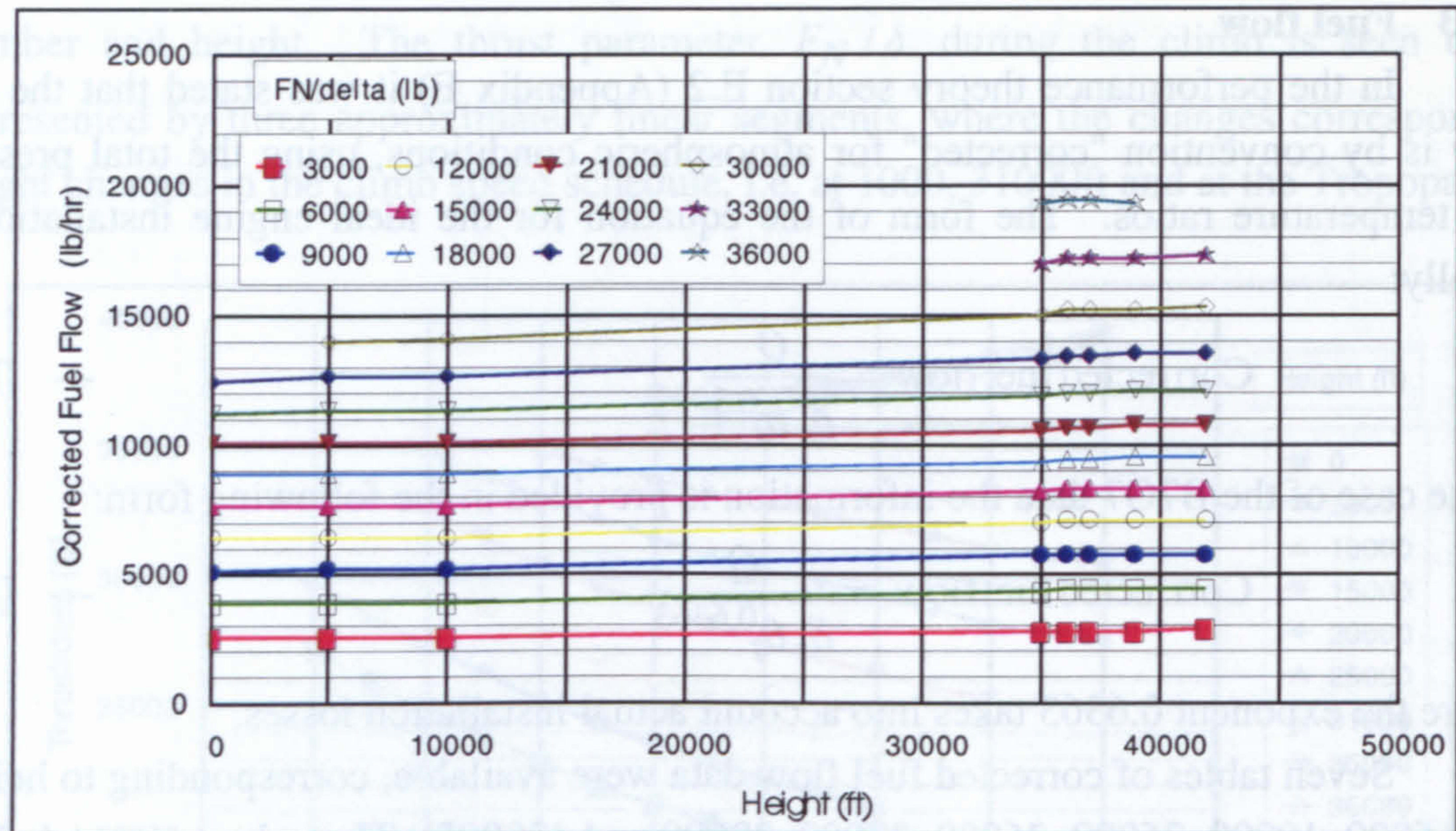


Fig. F-6 Corrected fuel flow at 35000ft for various Mach numbers





**Fig. F-7** Corrected fuel flow for Mach 0.6 at various thrust levels

As described earlier for the climb thrust data, the B7G7 fuel flow data was scaled to bring it as close as possible to the baseline engine, the RB211-535E4. An initial scaling factor of 0.926 was applied to all corrected fuel flow values in the tables. This factor was based on the ratio of the quoted SFC values of the RB211-535E4 and RB211-535C engines, as indicated in Table F-2 (Rolls-Royce, 1998). To validate the resulting data, checks were undertaken by evaluating the trip fuel predicted by the computer model (described in Appendix H) and comparing the results to data from the B757-200 Operations Manual (Boeing, 1993), for the identical mission conditions. The scaling factor was iterated until good agreement between the results was obtained. The selected factor of 0.937 yielded the results presented in Table F-3 below.

**Table F-3** Trip fuel comparison

Trip distance ->	Trip fuel (lb)				
	1000nm	1500nm	2000nm	2500nm	2900nm
Calculated using computer model (see Table 4-3)	8538kg (18822lb)	12547kg (27663lb)	16753kg (36933lb)	21180kg (46692lb)	24932kg (54961lb)
From Operations Manual (Boeing, 1993)	8640kg (19047lb)	12740kg (28085lb)	16940kg (37344lb)	21340kg (47044lb)	25040kg (55201lb)
Difference	1.2%	1.5%	1.1%	0.7%	0.4%

**Conditions:** Climb: 250/290/M0.80 (Computer model); 250/290/M0.78 (Ops. Manual)  
 Cruise: 35000ft, Mach 0.80; ISA conditions; Zero wind  
 OEW: 58394kg (128730lb); Payload: 26886kg (59270lb)



F.4.4 Engine data at idle

Minimum idle in-flight thrust, with two air-conditioning packs at normal flow, was provided in the B7G7 PEM (Boeing, undated) as  $F_N/\delta$  values for the speed range of Mach 0.20 to Mach 0.90 for heights from sea-level to 42000ft. Spillage drag around the nacelle at higher speeds was indicated as negative thrust. The corresponding fuel flow data was provided for the same conditions (Fig. F-8). These values were used without any changes.

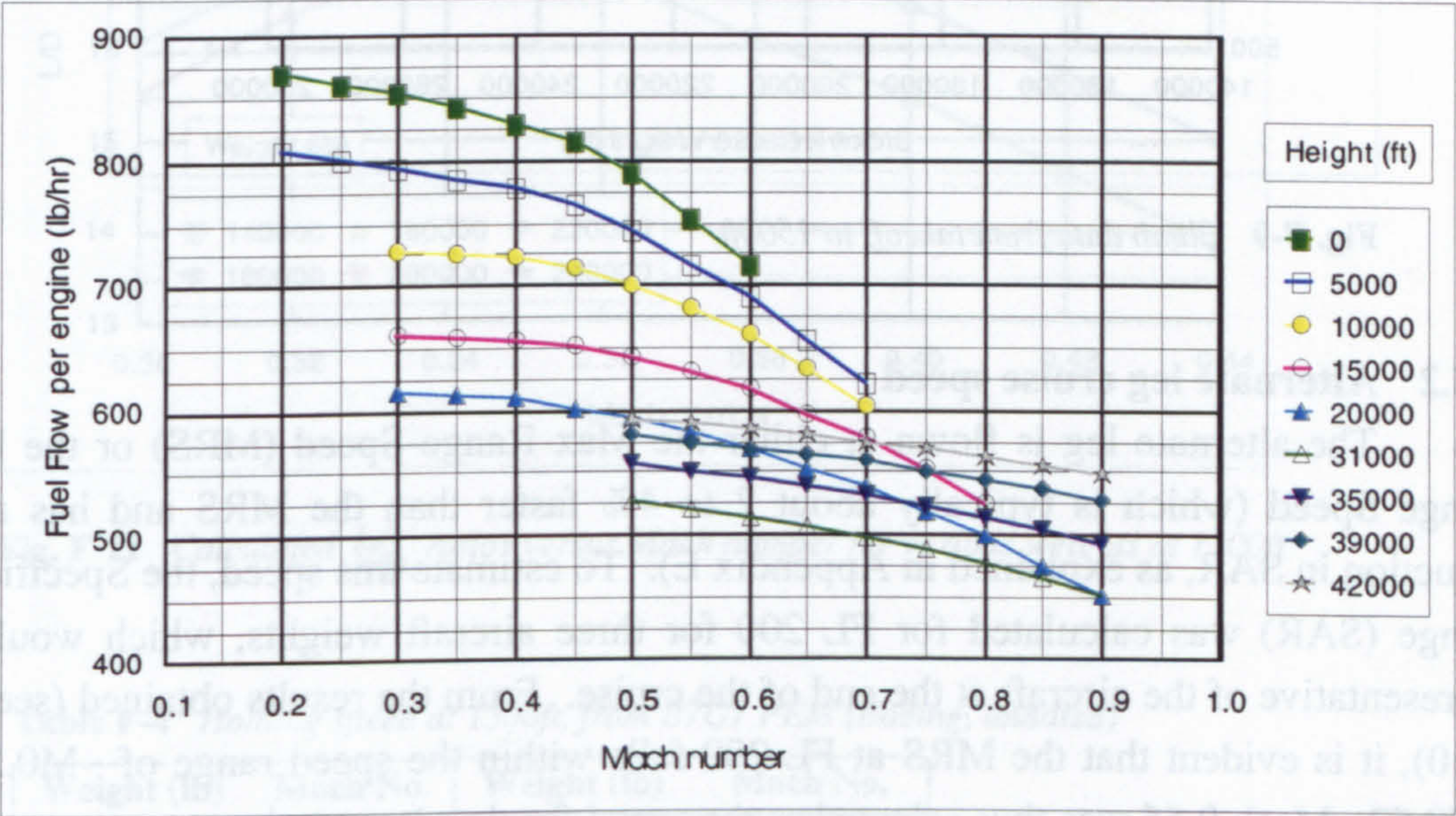


Fig. F-8 Idle fuel flow per engine for various heights

F.5 MISCELLANEOUS PERFORMANCE DATA

F.5.1 Initial climb data

The initial climb segment from takeoff to 1500ft, with the aircraft accelerating to ~250KCAS, is difficult to analyse numerically. The B7G7 PEM (Boeing, undated) provided climb data, consisting of fuel weight, distance and time; from brake-release to 1500ft; for a range of Brake Release Weights, from 160000lb (72600kg) to 240000lb (108900kg). The values were almost identical to the data contained in the B757-200 Operations Manual (Boeing, 1993).

On inspection, it was evident that the fuel weight, distance and time, all increased linearly with increasing Brake Release Weight, permitting linear interpolation to be used. Fig. F-9 contains the distance and time information, for the range of Brake Release Weights of interest.



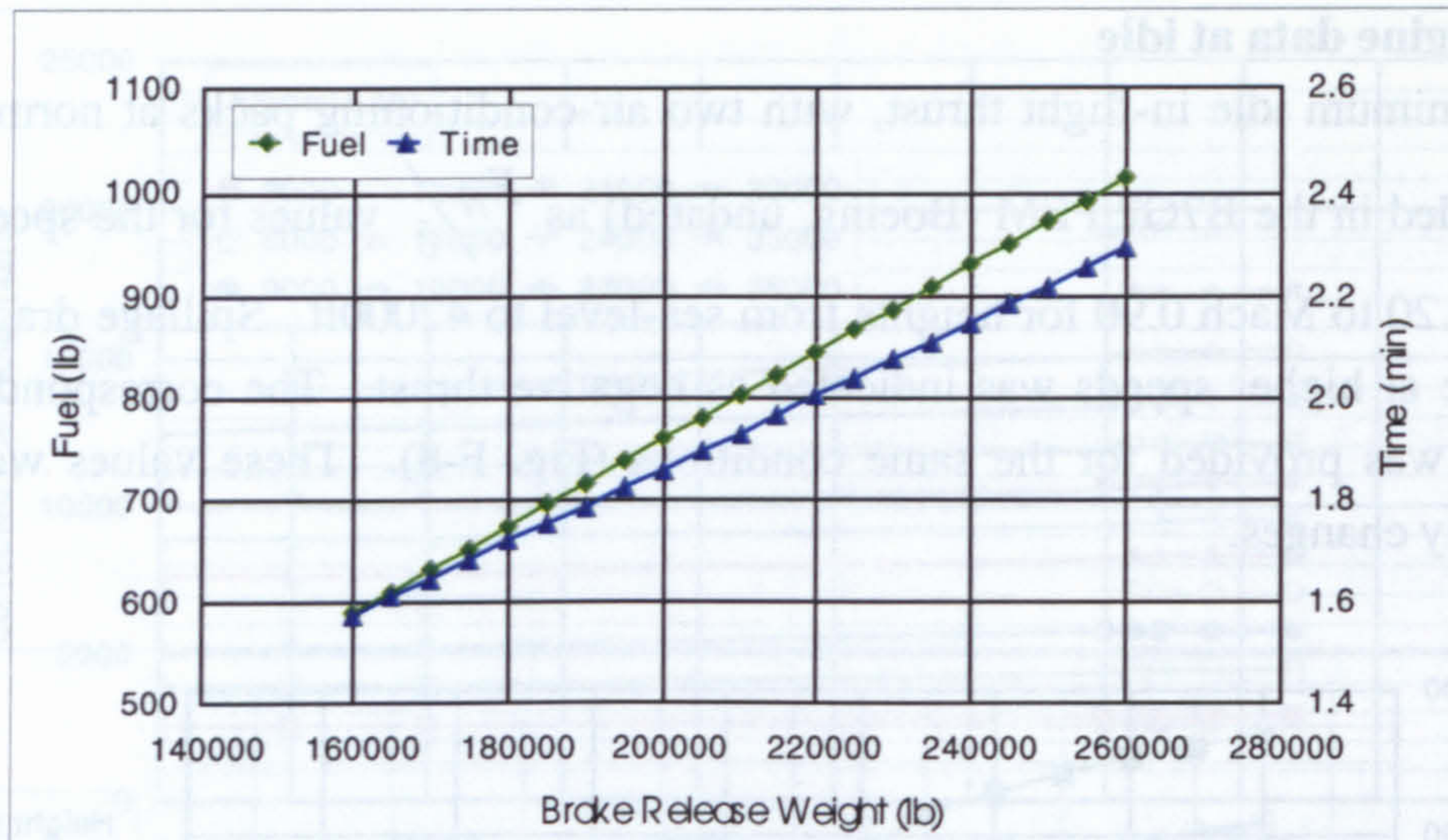


Fig. F-9 Climb data from takeoff to 1500ft

### F.5.2 Alternate leg cruise speed

The alternate leg is flown at either the Max Range Speed (MRS) or the Long Range Speed (which is typically about 2 to 4% faster than the MRS and has a 1% reduction in SAR, as explained in Appendix E). To estimate this speed, the Specific Air Range (SAR) was calculated for FL 200 for three aircraft weights, which would be representative of the aircraft at the end of the cruise. From the results obtained (see Fig. F-10), it is evident that the MRS at FL 200 falls within the speed range of ~M0.53 to ~M0.57. Mach 0.55 was thus selected as the speed for the alternate leg.

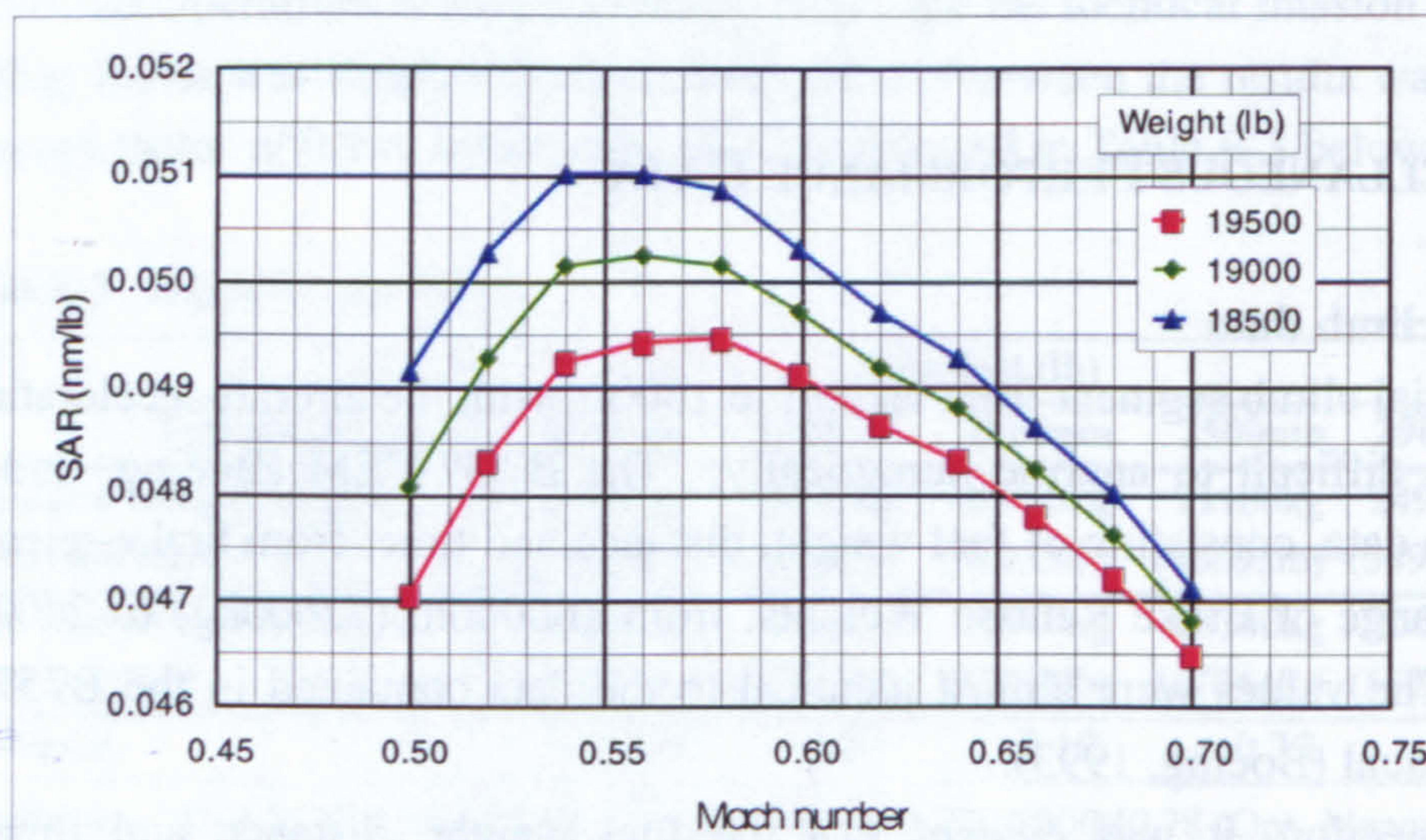


Fig. F-10 SAR at 20000ft for typical end of cruise weights

### F.5.3 Holding speed

The recommended holding Mach numbers at 1500ft for a range of aircraft weights were provided in the B7G7 PEM (Boeing, undated). As a cross check with the



aerodynamic data (section F.3), the green dot speed or  $(L/D)_{max}$  speed, was determined at these conditions. It is evident that the quoted holding speeds (Table F-4), correlate very well with the Mach numbers that gave the maximum  $L/D$  ratios in Fig. F-11.

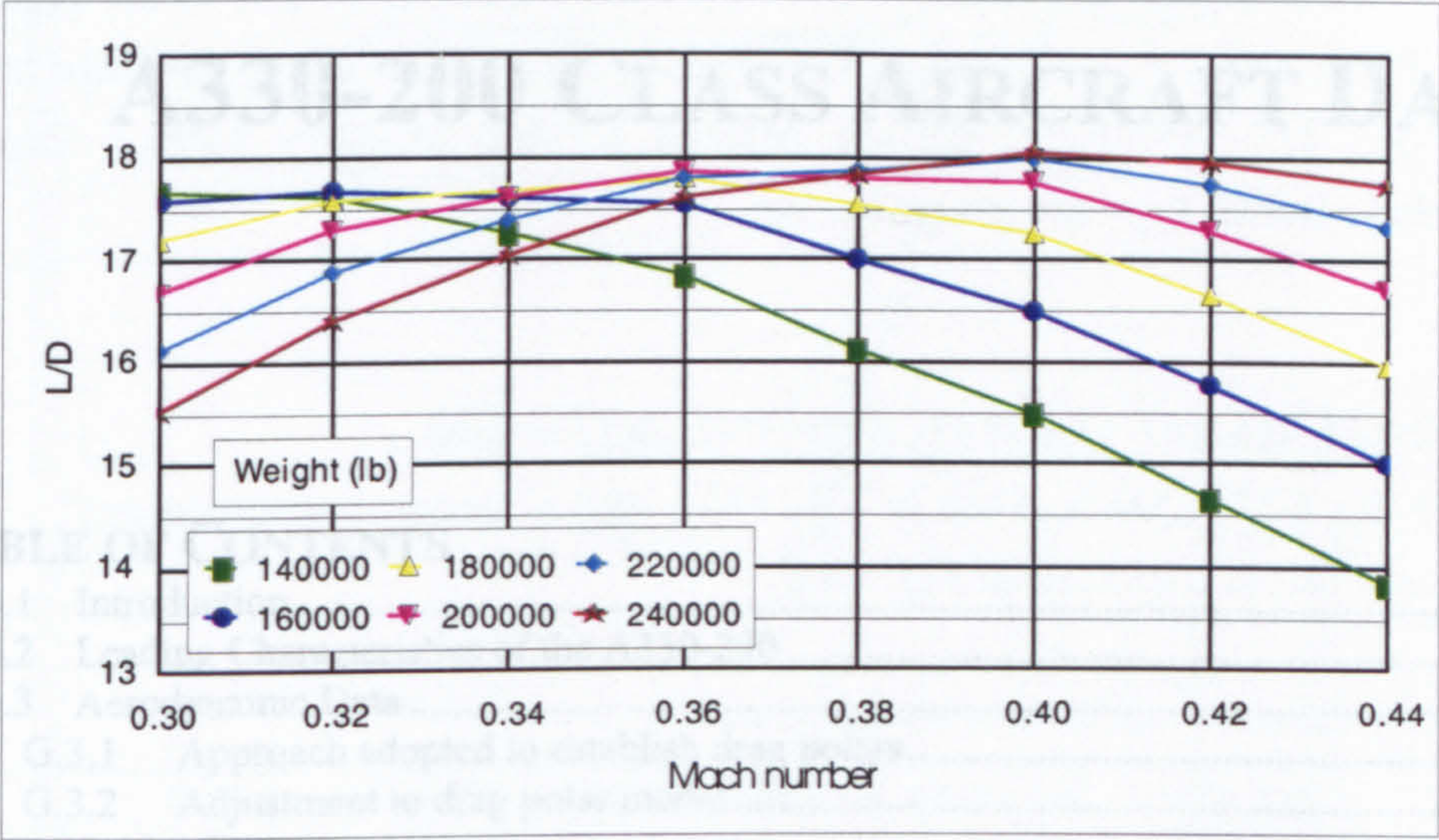


Fig. F-11 Calculated  $L/D$  ratios versus Mach number for various weights at 1500ft

Table F-4 Holding speed at 1500ft, from B7G7 PEM (Boeing, undated)

Weight (lb)	Mach No.	Weight (lb)	Mach No.
130000	0.305	190000	0.365
140000	0.315	200000	0.375
150000	0.325	210000	0.385
160000	0.335	220000	0.395
170000	0.345	230000	0.405
180000	0.355	240000	0.415



Blank page



## APPENDIX G

# A330-200 CLASS AIRCRAFT DATA

### TABLE OF CONTENTS

G.1	Introduction.....	274
G.2	Leading Characteristics of the A330-200 .....	274
G.3	Aerodynamic Data .....	275
G.3.1	Approach adopted to establish drag polars.....	275
G.3.2	Adjustment to drag polar model .....	276
G.4	Engine Data.....	278
G.4.1	Candidate engines.....	278
G.4.2	Available climb thrust .....	278
G.4.3	Fuel flow .....	279
G.5	Miscellaneous Performance Data.....	282
G.5.1	Initial climb data.....	282
G.5.2	Alternate leg cruise speed.....	283
G.5.3	Holding speed.....	284



## G.1 INTRODUCTION

The Airbus 330 is a widebody medium / long range twin-engine airliner. Simultaneous FAA and JAA certification for the A330-300 variant was received in October 1993, and the first delivery took place in December 1993 (Jackson, 1997). 180 minute ETOPS approval was granted in February 1995. The A330-200 is an extended range variant of the initial A330-300, with a ten frame reduction in the fuselage length (Airbus, 2000a). The A330-200 variant entered service in early 1998. Leading parameters of this aircraft type are given below.

## G.2 LEADING CHARACTERISTICS OF THE A330-200

Data for the A330-200 is given in Table G-1 and a "general arrangement" drawing of the aircraft is included as Fig. G-1.

**Table G-1** *Leading characteristics of the A330-200*

<i>Accommodation</i> <sup>(1)</sup>	Crew of two. Seating can accommodate between 253 (three classes) passengers and 293 (two class) passengers.
<i>Power plants</i> <sup>(3)</sup>	GE CF6-80E1A4, Rolls-Royce Trent 772, Pratt and Whitney PW4168
<i>Fuel capacity</i> <sup>(4)</sup>	139090lt (36744USG) 111967kg (246830lb)*
<i>Dimensions</i> <sup>(1)</sup>	Wing span: 60.30m (197ft) Length overall: 59.00m (193ft 7in) Height overall: 17.89 (58ft 8in) Wing sweep: 30° (25% chord)
<i>Areas</i> <sup>(2)</sup>	Wing gross area: 363.10m <sup>2</sup> (3908.4ft <sup>2</sup> )
<i>Areas</i> <sup>(4)</sup>	Wing ref. area: 361.6m <sup>2</sup> (3892ft <sup>2</sup> )
<i>Aspect ratio</i>	10.06 Based on wing span and reference area.
<i>Weights</i> <sup>(2)</sup>	(C with CF680E1A2, P with PW4168, T with Trent) OEW: C 120170kg (264920lb), P 120750kg (266200lb), T 120265kg (265150lb)
<i>Weights</i> <sup>(1)</sup>	MTOW: A 233000kg (513650lb), B 230000kg (507040lb) MLW: A 182000kg (401220lb), B 180 000 (396810lb) MZFW: A 170000kg (374760lb), B 168000kg (370360lb) Max. Struct. Payload: A 49500kg (109120lb), B 47500kg (104710lb)
<i>Weights</i> <sup>(4)</sup>	OEW: 120500kg (265640lb) typical
<i>Range</i> <sup>(1)</sup>	(With 253 passengers and baggage at typical OEW, with allowances for 200nm diversion and international reserves) A 6650nm B 6450nm

**Source:**

<sup>(1)</sup> Airbus (2000a) <sup>(2)</sup> Jackson (1997) <sup>(3)</sup> Rolls-Royce (1998) <sup>(4)</sup> Airbus (2001a)

\* Density of fuel: 0.805kg/lt (Ref. Boeing, 1996).



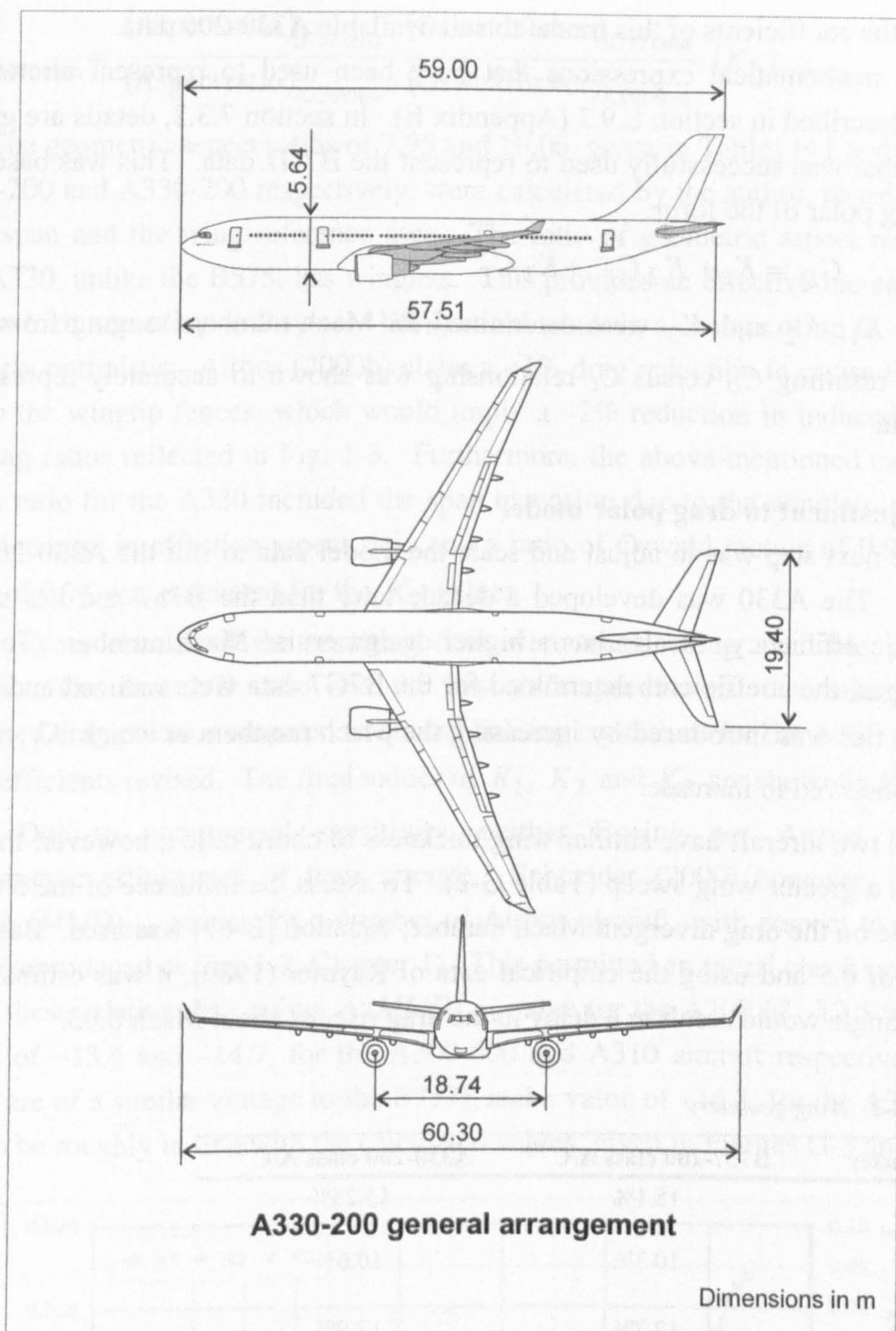


**Fig. G-1** General arrangement drawing of Airbus 330-200  
(redrawn after Airbus, 2002b; dimensions from Airbus, 2001b)

### G.3 AERODYNAMIC DATA

#### G.3.1 Approach adopted to establish drag polars

Unlike the situation that existed for the B757-200 class aircraft, there was no simple way of obtaining a representative set of drag polars for this class of aircraft, and so these had to be indirectly deduced from other information. The approach adopted to determine the drag polars for the A330-200 class aircraft was to:

- (1) Develop a mathematical model that approximated the B7G7 data; and



(2) Adjust the coefficients of this model to suit available A330-200 data.

Alternative mathematical expressions that have been used to represent aircraft drag polars are described in section E.9.3 (Appendix E). In section 7.3.2, details are given of the model that was successfully used to represent the B7G7 data. This was based on a generic drag polar of the form:

$$C_D = K_1 + K_2 C_L^2 + K_3 C_L^6 \quad \text{--- [G-1]}$$

Values for  $K_1$ ,  $K_2$  and  $K_3$  were determined for Mach numbers ranging from 0.3 to 0.84. The resulting  $C_D$  versus  $C_L$  relationship was shown to accurately represent the original data.

### G.3.2 Adjustment to drag polar model

The next step was to adjust and scale the model data to suit the A330-200 class of aircraft. The A330 was developed a decade later than the B757 and has superior aerodynamic efficiency. It also has a higher design cruise Mach number. To reflect these changes, the coefficients determined for the B7G7 data were reduced and a delay in the drag rise was introduced by increasing the Mach numbers at which  $K_1$ ,  $K_2$  and  $K_3$  were observed to increase.

The two aircraft have similar wing thickness to chord ratios; however, the A330 aircraft has a greater wing sweep (Table G-2). To assess the influence of the 5° greater sweep angle on the drag divergent Mach number, equation [E-67] was used. Based on a design  $C_L$  of 0.5 and using the empirical data of Raymer (1989), it was estimated that the sweep angle would result in a delay in the drag rise, of about Mach 0.03.

Table G-2 Wing geometry

Parameter	B757-200 class A/C <sup>(1)</sup>	A330-200 class A/C <sup>(2)</sup>
$(t/c)_{root}$	15.1%	15.25%
$(t/c)_{tip}$	10.3%	10.6%
$(t/c)_{mean}$	12.7%	12.9%
$\Lambda_{1/4}$	25°	30°

Source: <sup>(1)</sup> Lambert (1992); <sup>(2)</sup> Airbus (2000a)

At low Mach numbers the  $K_3$  term equals zero in the drag model described above. In which case, the drag representation reverts to the familiar parabolic function.

Writing the lift dependent drag term as:  $C_{D_i} = \frac{1}{\pi A e} C_L^2$ , enables an estimate of  $K_2$  to be established, i.e.



$$(K_2)_{A330\text{ class}} = \frac{(\text{Aspect ratio})_{B757\text{ class}}}{(\text{Aspect ratio})_{A330\text{ class}}} \frac{(\text{Oswald factor})_{B757\text{ class}}}{(\text{Oswald factor})_{A330\text{ class}}} (K_2)_{B757\text{ class}} \quad \text{--- [G-2]}$$

The geometric aspect ratios of 7.95 and 10.06, given in Tables F-1 and G-1, for the B757-200 and A330-200 respectively, were calculated by the author, based on the total wing span and the wing reference area. The ratio of geometric aspect ratios is 0.79. The A330, unlike the B575, has winglets. This provides an effective increase in aspect ratio, which according to Raymer (1989) could result in a change of up to ~20%. This is overly optimistic. Airbus (2000b) claim a ~1% drag reduction in cruise for the A310 due to the wingtip fences, which would imply a ~2% reduction in induced drag based the drag ratios reflected in Fig. 1-3. Furthermore, the above-mentioned calculation of aspect ratio for the A330 included the span extension due to the winglets. Based on a 1.5% increase in effective aspect ratio and a ratio of Oswald factors of 0.95, a scaling factor of 0.74 was estimated for the  $K_2$  values.

Cross checks of the resulting data were made using available performance figures. The best  $L/D$  ratio and the best  $L/D$  speeds were determined using the estimated drag polars, compared to quoted holding conditions for the A330 aircraft, and the coefficients revised. The final values of  $K_1$ ,  $K_2$  and  $K_3$  are shown in Fig. G-2.

Due to commercial sensitivity, neither Boeing nor Airbus publish the aerodynamic efficiencies of their aircraft. Schneider (2000) however, did indicate relative  $(ML/D)_{max}$  values for a number of Airbus aircraft, with respect to the original A300 (reproduced as Fig. 1-2, Chapter 1). This permitted an initial check on the results. Using these relative data points, a  $(ML/D)_{max}$  value for the A300 of ~12.5 would imply values of ~13.4 and ~14.7, for the A300-600 and A310 aircraft respectively (aircraft which are of a similar vintage to the B757), and a value of ~16.7, for the A330. This is seen to be roughly in line with the calculated values, given in Figures G-3 and G-4.

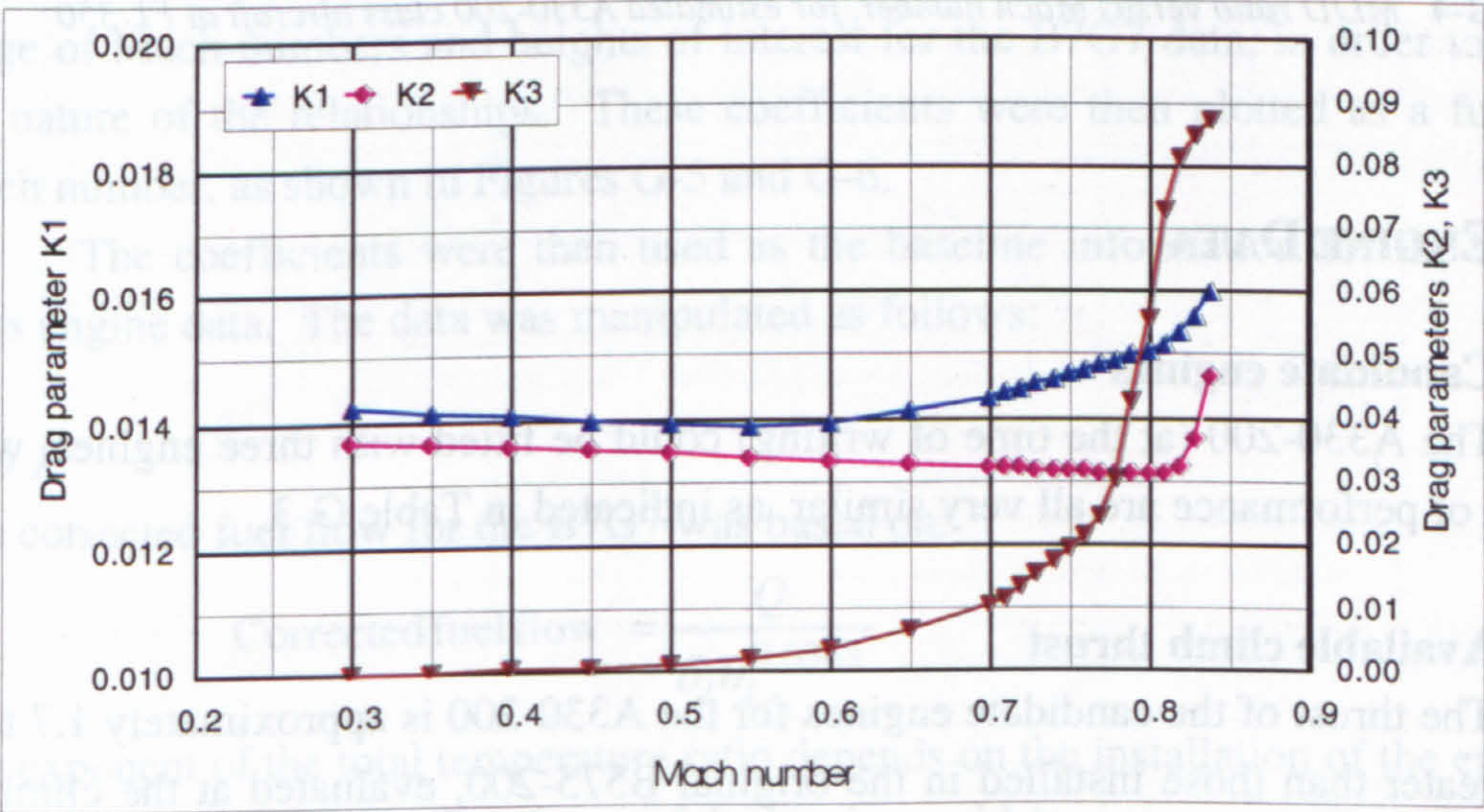


Fig. G-2 Estimated drag coefficients for A330-200 class aircraft



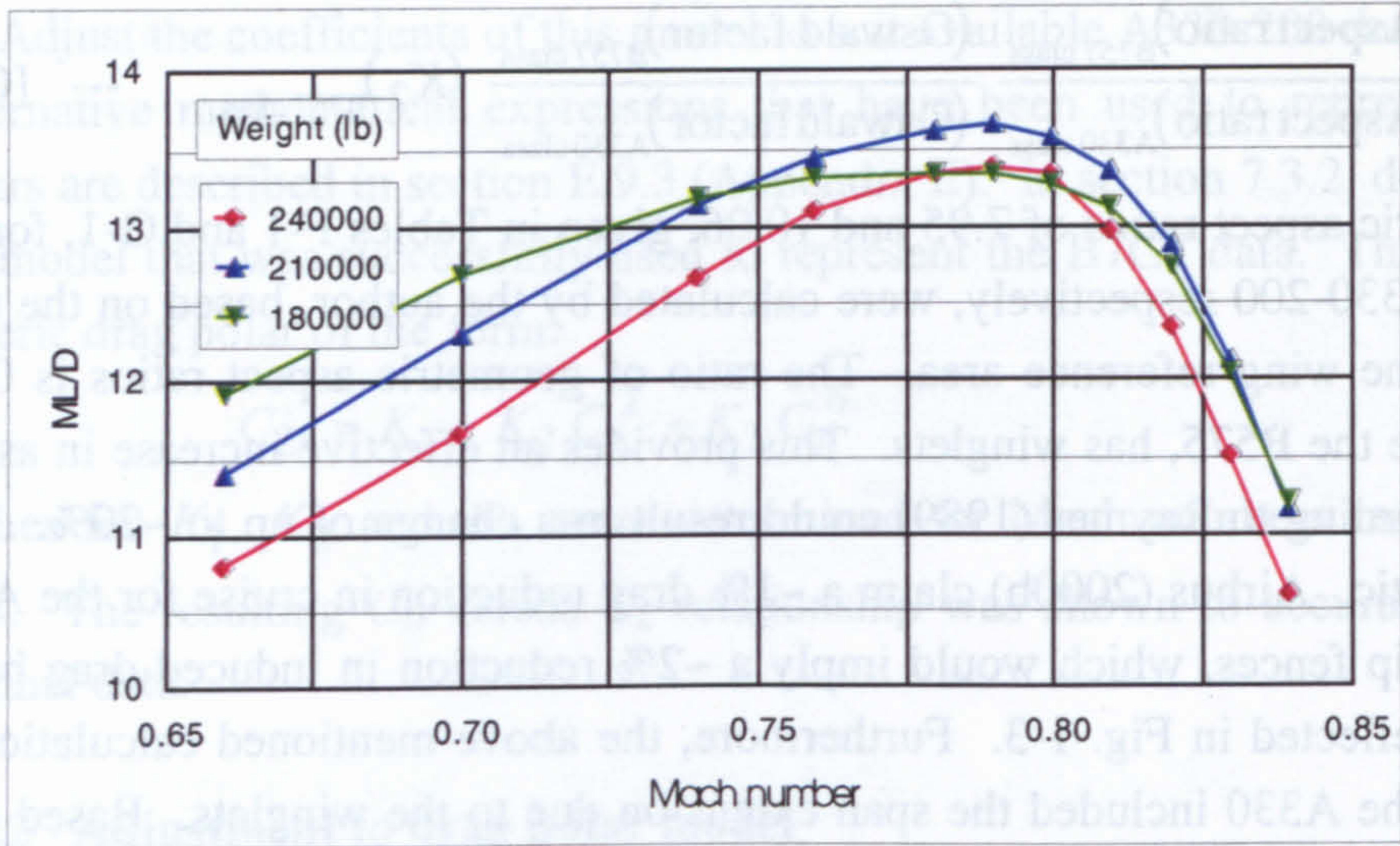


Fig. G-3 ML/D ratio versus Mach number, based on B7G7 data at FL 350

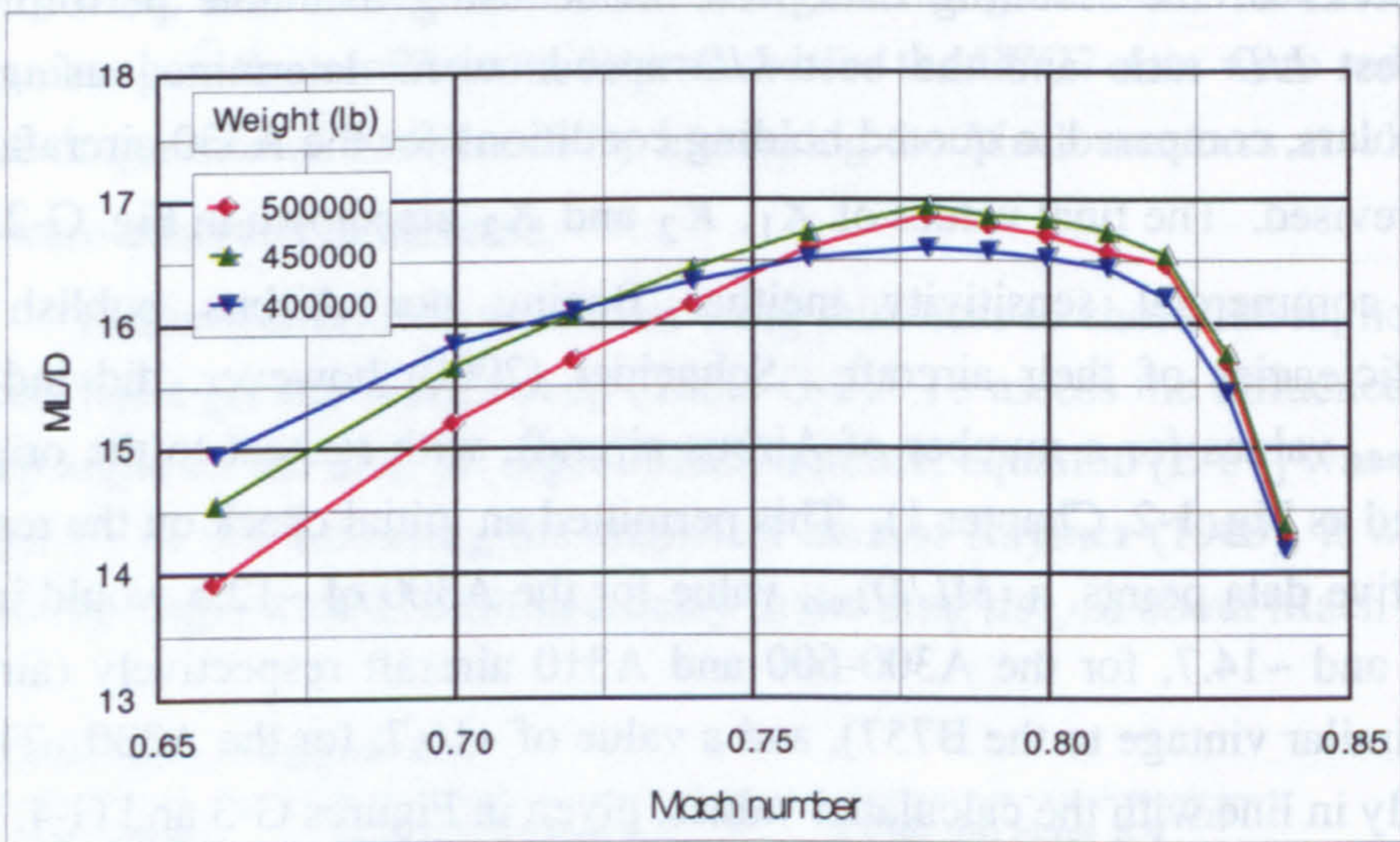


Fig. G-4 ML/D ratio versus Mach number, for estimated A330-200 class aircraft at FL 350

G.4 ENGINE DATA

G.4.1 Candidate engines

The A330-200 (at the time of writing) could be fitted with three engines, which in terms of performance are all very similar, as indicated in Table G-3.

G.4.2 Available climb thrust

The thrust of the candidate engines for the A330-200 is approximately 1.7 to 1.9 times greater than those installed in the original B575-200, evaluated at the climb and takeoff conditions, respectively. The B7G7 data was scaled to produce a trial data table for the A330-200 class aircraft and installed in the software model. As the rate of climb



is dependent on the excess of thrust over drag (for a given aircraft weight and speed), this provided a means to determine the scaling factor. By evaluating the time and distance to reach a specified cruising altitude, and comparing these values to quoted A330-200 Operating Manual values (Airbus, undated), the scaling factor was adjusted until the time matched to within 1%. A factor of 1.77 was selected.

**Table G-3** *Leading performance data of candidate engines (Rolls-Royce, 1998)*

	RR Trent 772	GE CF6-80E1A4	PW 4168
<b>Takeoff SLS</b>			
Thrust ISA	316kN (71100lb)	311kN (70000lb)	302kN (68000lb)
Bypass ratio	5.0	5.1	5.2
Pressure ratio	35.5	34.0	32.0
Mass flow	919kg/s (2027lb/s)	875kg/s (1930lb/s)	875kg/s (1930lb/s)
<b>Max climb</b>			
Thrust	68.4kN (15386lb)	67.2kN (15100lb)	67.1kN (15100lb)
<b>Cruise 35000ft, M0.82</b>			
Thrust	53.4kN (12000lb)	48.9kN (11000lb)	48.9kN(11000lb)
SFC	16.5mg/N/s (0.584lb/lb/hr)	16.5mg/N/s (0.584lb/lb/hr)	16.7mg/N/s (0.589lb/lb/hr)

**G.4.3 Fuel flow**

The establishment a fuel flow database for this class of aircraft was undertaken in an iterative manner. The corrected fuel flow relationship was modelled as two linear segments, where the change in slope occurred at the point of lowest SFC. For the lower part of the function, the equation:

$$\frac{Q}{\delta_t \sqrt{\theta_t}} = c_1 + c_2 \left( \frac{F_N}{\delta} \right)$$

--- [G-3]

was used. A “least squares” curve fit was used to determine  $c_1$  and  $c_2$  values for the range of Mach numbers and heights of interest for the B7G7 data, in order to establish the nature of the relationships. These coefficients were then plotted as a function of Mach number, as shown in Figures G-5 and G-6.

The coefficients were then used as the baseline information for the A330-200 class engine data. The data was manipulated as follows:

*Step 1*

The corrected fuel flow for the B7G7 was based on:

$$\text{Corrected fuel flow} = \frac{Q}{\delta_t \theta_t^{0.6363}}$$

--- [G-4]

The exponent of the total temperature ratio depends on the installation of the engine (see section E.2.4, Appendix E). It was felt that it would be incorrect to use the value of 0.6363 for any other engine, so the "theoretical" exponent of 0.5 was used.



i.e. 
$$\text{Corrected fuel flow} = \frac{Q}{\delta_t \theta_t^{0.5}} \quad \text{--- [G-5]}$$

This meant that the calculated coefficients had to be corrected, using factors that were dependent on the height and Mach number. The manipulation was undertaken for reasons of completeness rather than necessity, as the actual fuel (which is the parameter required in the software) is obtained by multiplying the corrected fuel flow by the appropriate denominator given in equation [E-4] or [E-5].

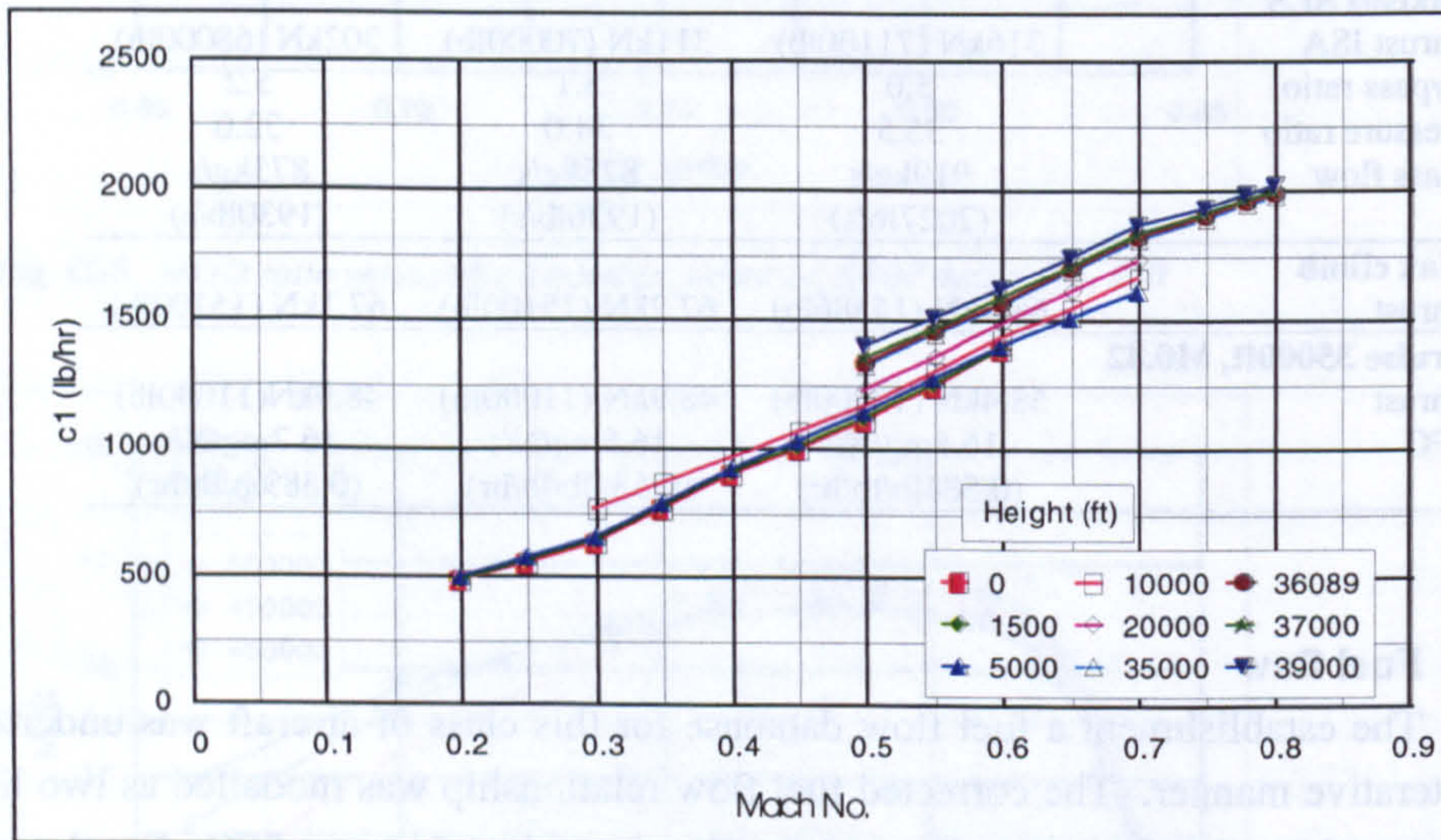


Fig. G-5 Corrected fuel flow factor  $c_1$  for B7G7

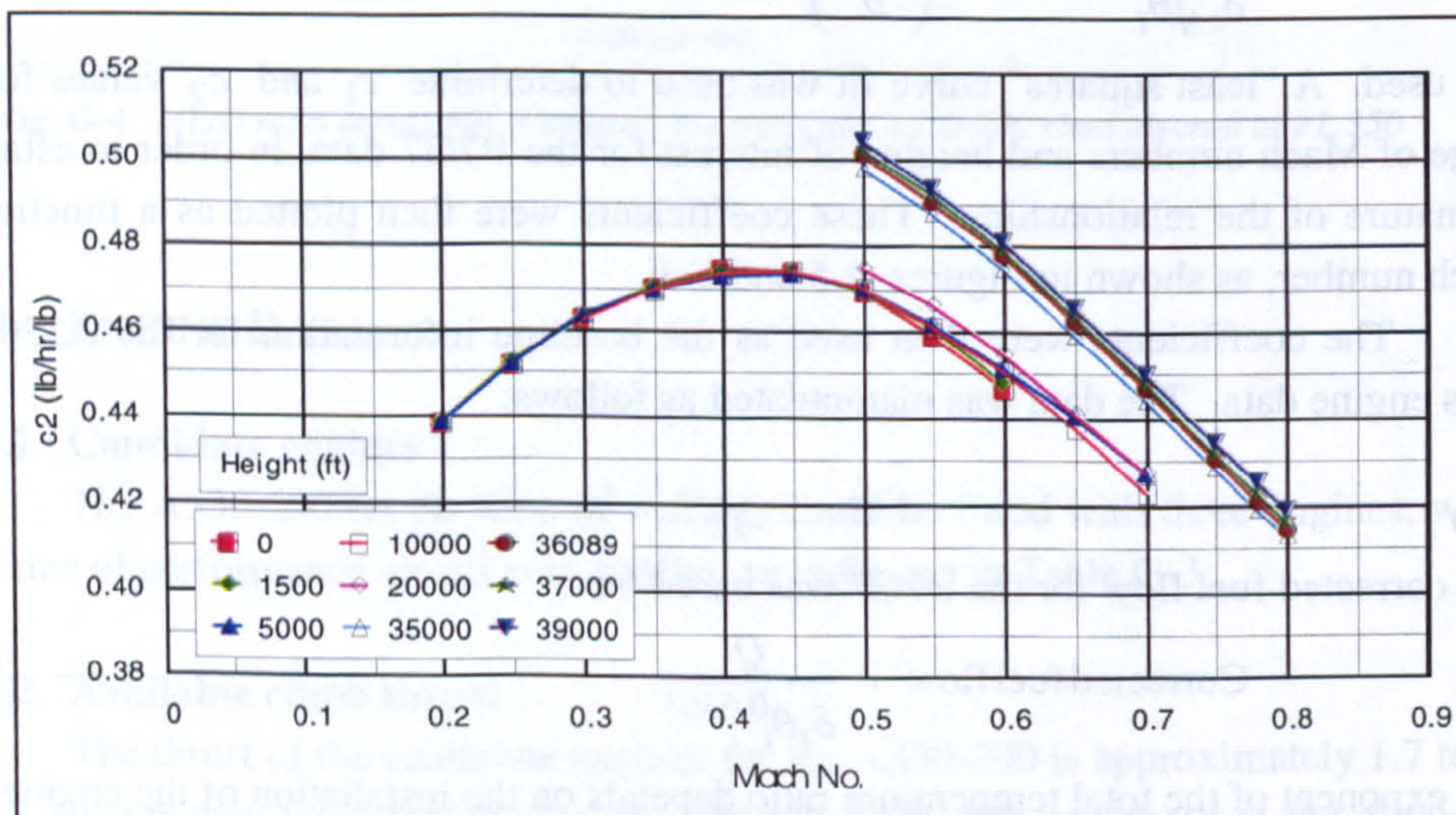


Fig. G-6 Corrected fuel flow factor  $c_2$  for B7G7



*Step 2.*

The  $c_1$  coefficients represent the intercept on the graph of corrected fuel flow versus thrust (i.e. where  $\frac{F_N}{\delta} = 0$ ). As seen in Fig. G-5, the  $c_1$  values increase approximately linearly with Mach number. The data was subsequently "linearised" by fitting straight lines through the data points for each height.

*Step 3.*

The coefficient  $c_2$  relates directly to the SFC and has the same units of SFC. Based on the fact that the more modern engine was about 7% more efficient than the older engine, trial values of  $c_2$  were obtained by scaling the B7G7 data by a factor of 0.93.

*Step 4.*

The models created in this way provide a good representation of the fuel flow data, up to point that corresponds to lowest SFC value. (This is shown in Fig. 4-5, Chapter 4.) Thereafter, the fuel flow versus thrust data shows a small but discernible increase. It was decided to model this change in slope, as the data would then give the characteristic SFC loop, with a minimum point. Without this adjustment, the linear representation of  $Q_{cor}$  would correspond to hyperbolic function for SFC. A correction was thus applied above  $\frac{F_N}{\delta} = 48000 \text{ lb}$ . This value was selected to represent the low point on the SFC loops. The correction was based on a linear increment to  $Q_{cor}$  above 48000, to a maximum of 8% applied at  $\frac{F_N}{\delta} = 72000 \text{ lb}$ . The 8% value was based on the increase observed in the B7G7 database.

*Step 5.*

The fuel burn was determined as a function of range at a fixed height, using the cruise subroutine of the performance model for the A330-200 class aircraft, based on the trail fuel flow database. The results were then compared to integrated range data, given in a Flight Crew Operating Manual for the A330-200 (Airbus, undated). Adjustments were made to the  $c_2$  coefficients, until a correlation of within 1% was achieved for all cruise segments.

*Step 6.*

Using the resulting corrected fuel flow data for Mach 0.82 at 35000ft (see Fig. 4-6, Chapter 4), a plot of SFC versus thrust (Fig. 4-7) was produced. This enabled a check to be undertaken against the information presented in Table G-3 (from Rolls-Royce, 1998). The SFC graph has a minimum of  $0.598 \text{ lbhr}^{-1}\text{lb}^{-1}$  at 11300lb (50.3kN). At the nominal cruise thrust of 12000lb (53.4kN) the SFC was  $0.602 \text{ lbhr}^{-1}\text{lb}^{-1}$ . These SFC



values, which represent an installed engine, with power and bleed air off-take, compared very well with the value of  $0.584 \text{ lb/hr}^{-1} \text{ lb}^{-1}$  for the Trent 772, which was for the uninstalled engine. Fuel and SFC data at 37000ft is presented in Figures G-7 and G-8.

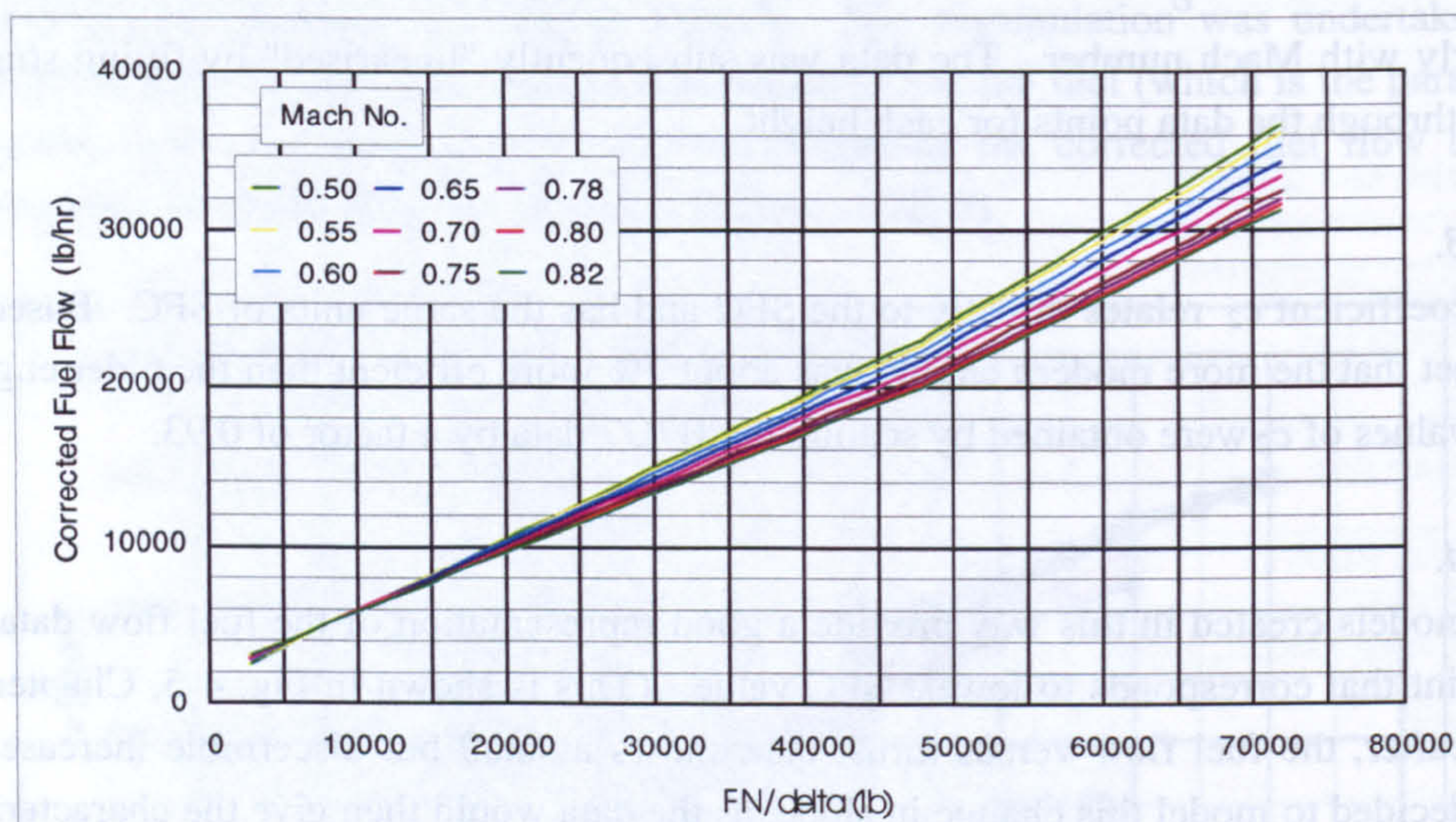


Fig. G-7 Corrected fuel flow at 37000ft for various Mach numbers

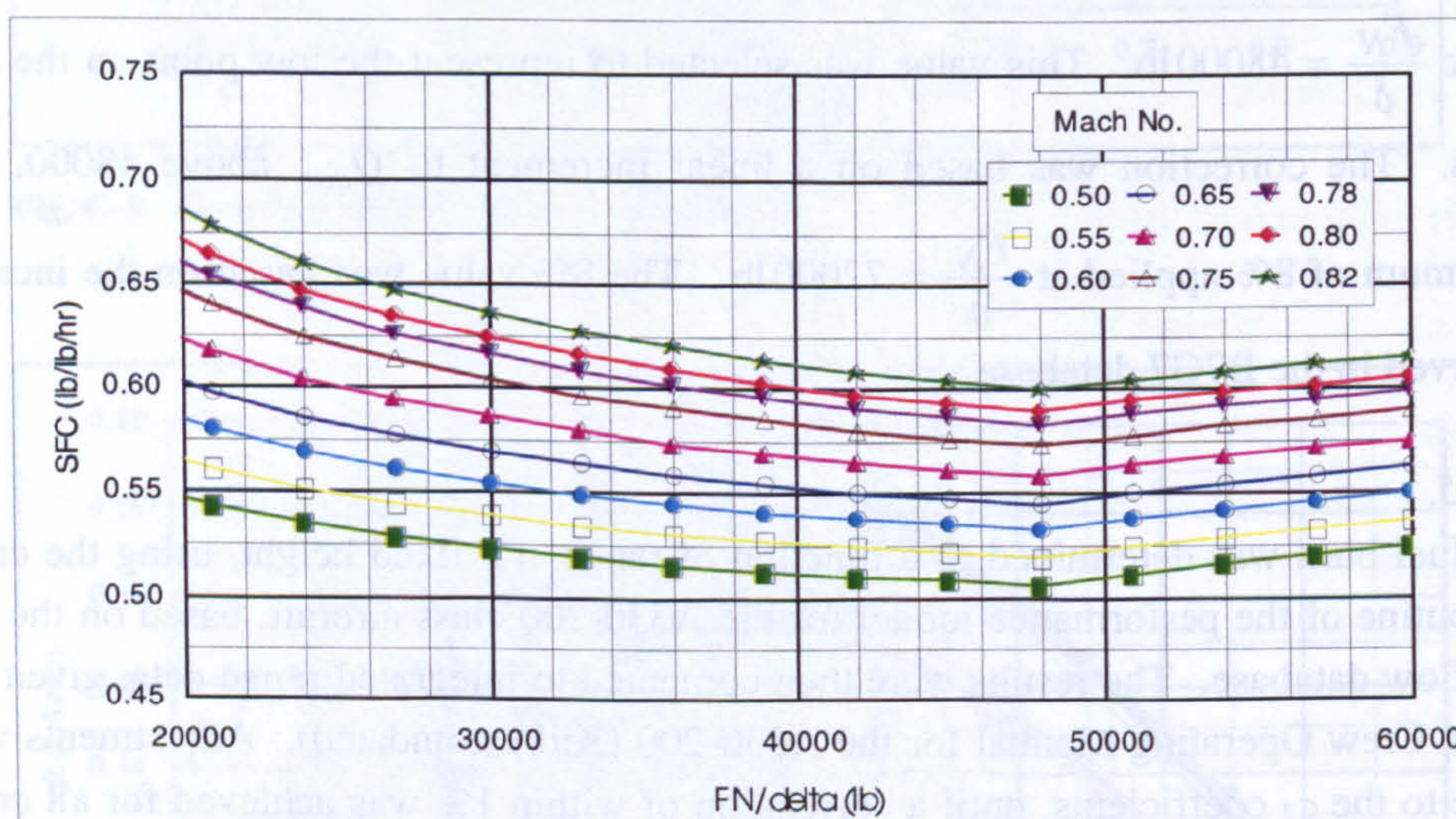


Fig. G-8 SFC versus thrust at 37000ft for various Mach numbers

## G.5 MISCELLANEOUS PERFORMANCE DATA

### G.5.1 Initial climb data

The time required during takeoff to accelerate from rest to the rotation speed ( $V_R$ ) depends on the aircraft's thrust-to-weight ratio, as is evident from the integral



expression [E-46] and from equation [E-47] in Appendix E. Similarly, the time to climb to 1500ft also depends on the thrust-to-weight ratio. From equation [E-25] it may be deduced that the ROC is given by:

$$\text{ROC} \approx \left( \frac{F_N}{W} - \frac{D}{L} \right) V \quad \text{--- [G-6]}$$

if the acceleration factor is ignored and the lift is taken as being approximately equal to the weight. For the purpose of estimating the time to climb to 1500ft, it may be assumed that  $\frac{F_N}{W}$ ,  $\frac{L}{D}$  and  $V$  will not differ greatly, within this class of medium size twin-engine airliner.

The time required for the A330-200 class aircraft to accelerate from standstill, rotate and climb to 1500ft was thus taken as being the same as that used for the B757-200 class aircraft. In Fig. F-9 (Appendix F) the times varied linearly from ~1.6 to ~2.3 minutes, with increasing aircraft weight. These times were used for the A330-200 class aircraft, but with corresponding Brake Release Weights appropriate to this aircraft type. The fuel required for this portion of the mission, was obtained by scaling the B757-200 class aircraft data, by a factor of 1.77 (i.e. the factor selected in section G.4.2, to scale the climb thrust data). The resulting fuel and the time values from brake-release to 1500ft are indicated in Fig. G-9, for a range of Brake Release Weights.

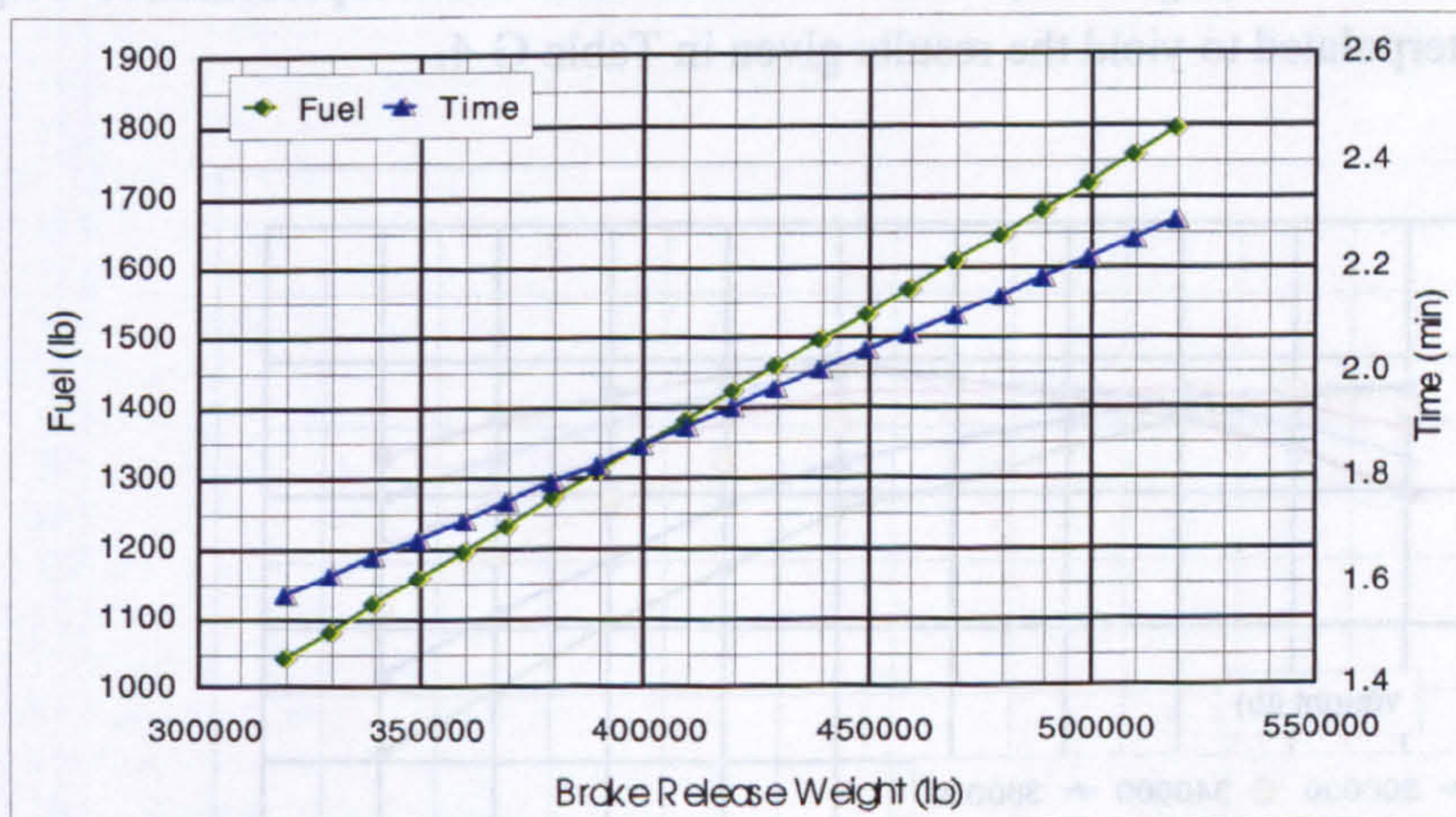


**Fig. G-9** Fuel and time required for initial climb to 1500ft

### G.5.2 Alternate leg cruise speed

The SAR was calculated for three aircraft weights in order to establish the best cruise speed for the alternate leg. From the results presented in Fig. G-10, it is seen that the MRS at 25000ft, falls within the range Mach 0.58 to Mach 0.62. Mach 0.60 was selected for the alternate leg for the performance analysis.



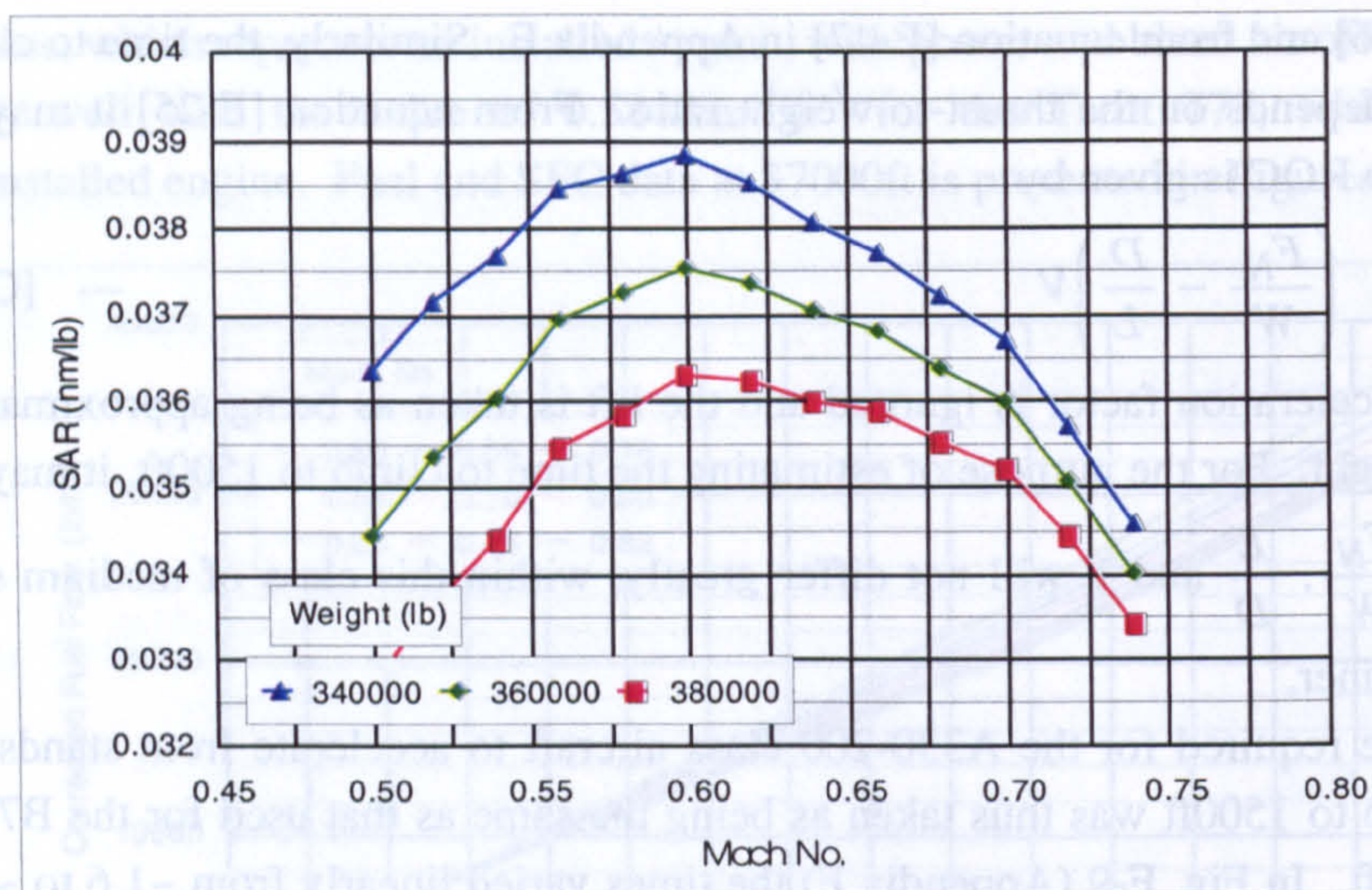


**Fig. G-10** Calculated Specific Air Range (SAR) versus Mach number at 25000ft

### G.5.3 Holding speed

The holding speed was set as the green dot speed, which was determined by plotting  $L/D$  ratios against Mach number, for the range of weights of interest at the holding height of 1500ft (Fig. G-11). This was undertaken at six representative weights and the data interpolated to yield the results given in Table G-4.

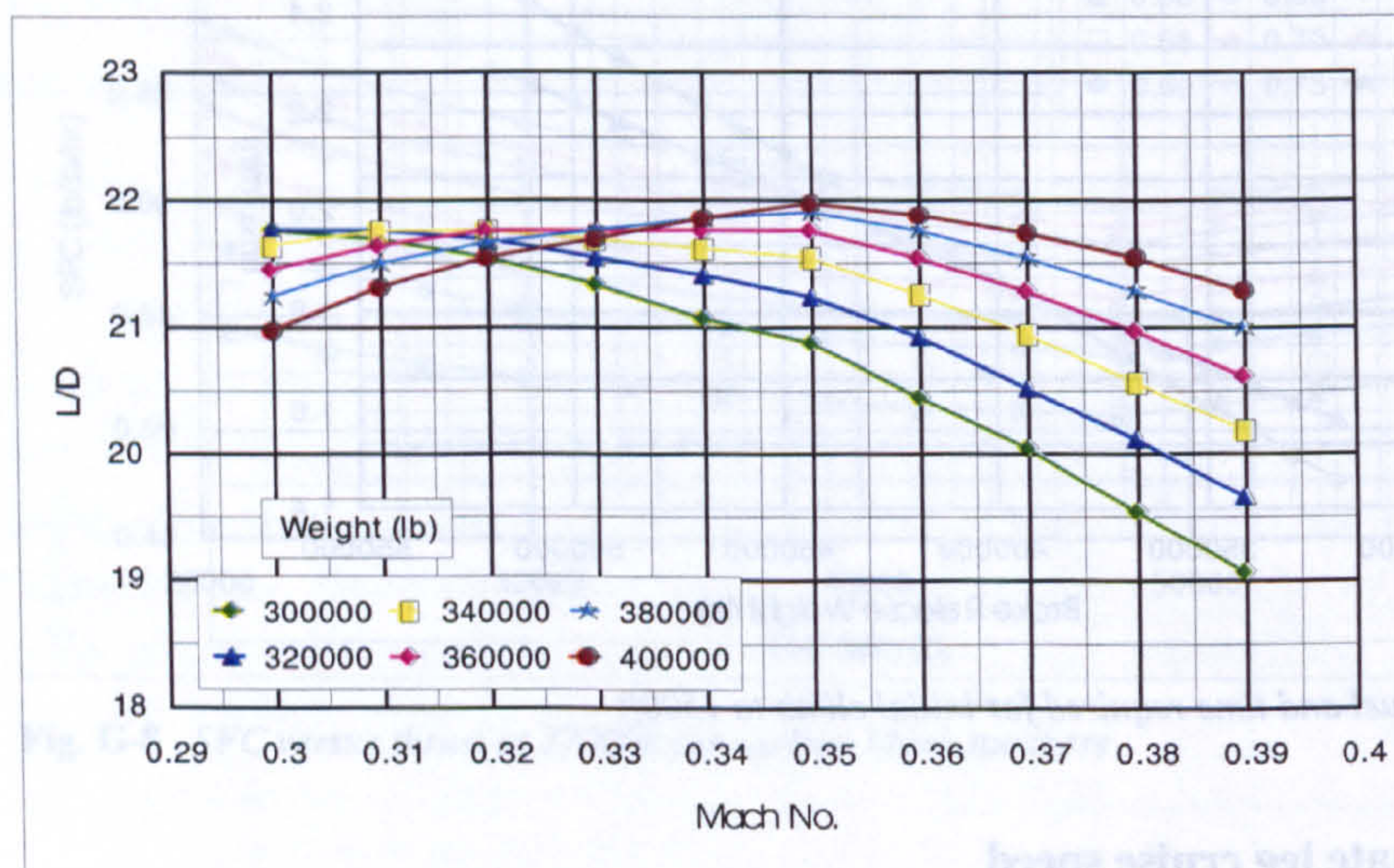


**Fig. G-11** Calculated  $L/D$  ratio versus Mach number for various weights at 1500ft



**Table G-4** *Calculated green dot speeds for holding at 1500ft*

Weight (lb)	Mach No.	Weight (lb)	Mach No.
240000	0.30	380000	0.34
260000	0.30	400000	0.35
280000	0.30	420000	0.36
300000	0.30	440000	0.37
320000	0.31	460000	0.38
340000	0.32	480000	0.39
360000	0.33		



Blank page



## APPENDIX H

### PERFORMANCE PROGRAMS

#### TABLE OF CONTENTS

H.1	Introduction.....	288
H.2	Program Outline.....	288
H.2.1	Program execution.....	288
H.2.2	Program structure .....	289
H.2.3	Units .....	289
H.3	Sheet A: Master Sheet.....	290
H.3.1	Sheet functions .....	290
H.3.2	Aircraft specific data .....	290
H.3.3	Mission specific input data .....	290
H.3.4	Software buttons.....	291
H.3.5	Master computing table .....	292
H.3.6	Results .....	293
H.3.7	Dialogue box and aircraft checks .....	293
H.3.8	Macro code.....	295
H.4	Sheet B: Cruise Calculation .....	298
H.4.1	Sheet functions .....	298
H.4.2	Cruise calculation .....	298
H.4.3	Step climb in cruise .....	299
H.5	Sheet C: Climb / Descent Calculation.....	301
H.5.1	Sheet functions .....	301
H.5.2	Climb speed schedule .....	301
H.5.3	Climb calculation .....	301
H.5.4	Descent calculation.....	302
H.6	Sheet D: Hold Calculation .....	305
H.7	Sheet E: Drag Polar.....	305
H.8	Sheet F: Corrected Fuel Flow Data.....	307
H.9	Sheet G: Climb and Idle Engine Data .....	307
H.10	Sheet H: Miscellaneous Tables .....	308
H.11	Sheet I: The International Standard Atmosphere (ISA) .....	308
H.12	Sheet J: Results .....	308



## H.1 INTRODUCTION

This appendix provides complete details on the two computer programs that were developed. The implementation of the performance theory (Appendix E) is described and the structure of the program outlined, together with sample runs and tables of applicable input data. A single computer file (program) has been developed for each of the two classes of aircraft, to compute the fuel and time required for a specified mission distance. Alternatively, the mission distance and time may be calculated for a specified fuel weight. The illustrative tables reproduced in this Appendix were taken from the program for the A330-200 class aircraft.

## H.2 PROGRAM OUTLINE

### H.2.1 Program execution

The spreadsheet software Lotus 123 (Release 9.6)<sup>1</sup> was used to develop two self-contained spreadsheet files:

- (1) *B757class.123* for the performance analysis of the Boeing 757-200 class aircraft; and
- (2) *A330class.123* for the performance analysis of the Airbus 330-200 class aircraft.

The files are run independently and almost identical in format and function. (The minor differences are explained in this Appendix.) To operate the program, the selected file is opened from within the software package Lotus 123. Each file is comprised of 10 sheets (or pages), designated as A through to J. These sheets contain the aircraft data, input parameters, program code and tables for the computed results. It may be run in one of three modes, depending on the nature of the problem and the input data (Table H-1). The user selects the required mode by clicking with the mouse on the appropriate software button, marked *Weight*, *Range* and *Fuel*, located prominently on the master sheet (A).

During the program execution, a "busy" message is displayed in a dialogue box, together with a counter that indicates the number of major iteration cycles performed. The Lotus 123 *trace* function is switched on during program execution, which is useful if the program terminates prematurely and also for stopping the program during operation. When the program stops, the message in the dialogue box indicates whether the program met the convergence criteria. The results are presented in a table indicating weight, time and distance, corresponding to each leg of the mission. After each run, the new set of results are appended to the results table, to facilitate subsequent analysis. A fourth software button marked *Clear*, deletes all entries in the results table and prepares the table for a new study.



Table H-1 Program modes of operation

No.	Mode	Function
1	<i>Weight</i>	The program computes the range for the user specific BRW and payload. (On landing at the alternate aerodrome, the fuel on board would match the specified reserve fuel.)
2	<i>Range</i>	The program computes the BRW, to satisfy the user specific range and payload. (On landing at the alternate aerodrome, the fuel on board would match the specified reserve fuel.)
3	<i>Fuel</i>	The program computes the fuel required to fly the user specified range, where the BRW and payload are also specified. (On landing at the alternate aerodrome, the fuel on board would not match the specified reserve fuel. The difference is reflected as <i>tankered fuel*</i> in the spreadsheet.)

\*Note: The *tankered fuel* is zero for modes 1 and 2; however, for mode 3, the *tankered fuel* is the output of the calculation where both range and BRW are specified.

### H.2.2 Program structure

The functions of the 10 sheets (pages) are outlined in Table H-2 below. Sheet A is the master sheet, used for running the program and for setting the input variables. Sheets B, C and D contain the computational spreadsheets. The data for the calculations are located in *look-up* tables, placed on sheets E, F, G, H and I. The final results are appended to a table on sheet J, for subsequent study.

Table H-2 Functions of the individual sheets

Sheet	Function	Contents of sheet	Described in:
A	Master sheet	Input tables; Master computing table; Macro code	Section H.3
B	Computational spreadsheets	Cruise calculations for mission and alternate legs	Section H.4
C	Computational spreadsheets	Climb / descent calculations for mission and alternate legs	Section H.5
D	Computational spreadsheets	Hold calculation	Section H.6
E	Look-up tables	Drag polar	Section H.7
F	Look-up tables	Corrected Fuel Flow	Section H.8
G	Look-up tables	Engine Climb and Idle Data	Section H.9
H	Look-up tables	Holding Mach No.; Initial climb data (to 1500ft); Mission allowances	Section H.10
I	Look-up tables	ISA tables	Section H.11
J	Output	Results	Section H.12

### H.2.3 Units

The units used in these programs are British / aviation units, i.e. weight and force in lb, area in ft<sup>2</sup>, speed in kt or Mach number, distance in nm, height in ft, fuel flow rate in lb/hr, SFC in lb/lb/hr and SAR in nm/lb. All input data, computations and results are in these units and are appropriately identified. Conversion factors are provided in Table E-3 (Appendix E).

<sup>1</sup> Lotus 123, a product of the Lotus Development Corporation, Staines, Middlesex, UK



## H.3 SHEET A: MASTER SHEET

### H.3.1 Sheet functions

Sheet A has seven main elements:

- (1) Table of aircraft specific data.
- (2) Tables of mission specific input data.
- (3) Software buttons to run the different calculation modes.
- (4) A master computing table.
- (5) A results table.
- (6) Dialogue and aircraft checks.
- (7) Macro (program) code.

### H.3.2 Aircraft specific data

The table of aircraft specific data is contained on sheet A. The required data is given in Table H-3. The aerodynamic and engine data for the aircraft are included in the look-up tables on sheets E, F, G and H.

Table H-3 *Aircraft specific data*

	B757-200 class A/C	A330-200 class A/C
Wing reference area	1951 ft <sup>2</sup>	3892 ft <sup>2</sup>
OEW	128730 lb	265640 lb
Max. BRW	255000 lb	513650 lb
Fuel capacity	77430 lb	246830 lb

### H.3.3 Mission specific input data

The required aircraft data for the basic program operation is shown in Table H-4, with typical values. All cells, with the exception of the *climb speed schedule* and *cruise height*, must have values entered. Two optional input cells are provided, which enable the user to study actual routes (as opposed to the idealised missions considered herein). The en route wind speed may be entered; however, the wind correction will only be applied to the cruise and not to the climb and descent. (This is limitation of the software.) Secondly, it is possible to increase the drag in the descent to emulate the effect of spoiler deployment. (This was not done for any of the studies reported herein.)

For the evaluation of the impact of HLFC, a separate input table is available. This enables the user to specify the change to the aircraft's drag, fuel flow and weight, due to the installation of the HLFC system. During the cruise the performance of the aircraft is evaluated at 21 points or stations. Correction factors for the drag and fuel flow can be individually applied at these stations, or they may be applied uniformly to the entire cruise.

An example of the HLFC input data is given in Table H-5, where station 0 designates the start of the cruise and station 20 designates the end of the cruise. The weight penalty due to the HLFC system is entered just once in the table (as it applies to



the entire mission). The drag change is given in terms of a drag coefficient and the fuel penalty, as a percentage increase in the fuel flow. (In the example given in Table H-5, the HLFC correction factors are not applied to all parts of the cruise.)

It is possible to introduce the effects of HLFC on the upper part of the climb, above 20000ft. This part of the mission is divided into four segments. As explained in Chapter 5, the pump power necessary to produce the desired panel flow velocity (and hence drag reduction), reduces with height. This was taken into account by multiplying the fuel flow penalty used for the cruise, by a factor that reduces with height (see section 5.2.3, Chapter 5). For the A330-200 class aircraft factors of: 1.7, 1.4, 1.2 and 1.1 were allocated to the climb segments of: 20000 - 25000ft, 25000 - 29000ft, 29000 - 31000ft, and 31000 - 35000ft, respectively. These values are shown in the right hand column, at the bottom of Table H-5. For the B757-200 class aircraft, the factors are identical, but the upper climb segment runs from 32100 to 35000ft (see Table H-9).

**Table H-4** *Mission input data (with typical values for A330-200 class aircraft)*

	Illustrative value	Instruction / Comment
<b>Main Input Data</b>		
Brake Release Weight	483425 lb	<i>Run either "Weight" or "Fuel" program modes, if Brake Release Weight is specified.</i>
Range (Trip distance)	5980 nm	<i>Run either "Range" or "Fuel" program modes, if Range is specified.</i>
Payload	52985 lb	<i>Must always set payload</i>
<b>Control Parameters</b>		
TOC to TOD for cruise	5691 nm	<i>Initial guess (provided by the user)</i>
TOC to TOD for alternate	77 nm	<i>Initial guess (provided by the user)</i>
<b>Other Data</b>		
Alternate cruise	200 nm	
Hold (Final reserve)	30.0 min	
Cruise height	37000/41000 ft	<i>Must also set height on sheets B and C</i>
Climb speed schedule	250/300kt/M 0.80	<i>Must also set schedule on sheets B and C</i>
Contingency fuel	5.00%	<i>Specified as percentage of the trip fuel</i>
Temperature: ISA plus	0 deg C	
Wind in cruise	0 knots	<i>Tail-wind considered +ve</i>
Spoiler drag (descent)	0	<i>Specify +ve value for drag increment</i>

### H.3.4 Software buttons

The software "buttons" that initiate the program to run the selected program mode are located adjacent to the input data tables on sheet A. (The mode functions are described in Table H-1.) The sequence of operations that follow the pressing of a software button is outlined in section H.3.8, which contains a description of the macro code.



**Table H-5** *Input table for HLFC correction factors (A330-200 class aircraft)*

	Drag decrease (Coefficient)	Q increase (%)	OEW increase (lb)	Suction power factor
Apply to all sectors ->	0.00362	2.00%	5313	
Or specify by cruise station:				
0	0.00000	0.00%		1.0
1	0.00000	0.00%		1.0
2	0.00362	2.00%		1.0
3	0.00362	2.00%		1.0
4	0.00362	2.00%		1.0
5	0.00362	2.00%		1.0
6	0.00362	2.00%		1.0
7	0.00362	2.00%		1.0
8	0.00362	2.00%		1.0
9	0.00362	2.00%		1.0
10	0.00000	0.00%		1.0
11	0.00000	0.00%		1.0
12	0.00362	2.00%		1.0
13	0.00362	2.00%		1.0
14	0.00362	2.00%		1.0
15	0.00362	2.00%		1.0
16	0.00362	2.00%		1.0
17	0.00362	2.00%		1.0
18	0.00362	2.00%		1.0
19	0.00000	0.00%		1.0
20	0.00000	0.00%		1.0
Climb (20000 - 25000ft)	0.00362	3.40%		1.7
Climb (25000 - 29000ft)	0.00362	2.80%		1.4
Climb (29000 - 31000ft)	0.00362	2.40%		1.2
Climb (31000 - 37000ft)	0.00362	2.20%		1.1
Descent (>20000ft)	0.00000	0.00%		0.0

### H.3.5 Master computing table

The master computing table (shown in Table H-6, with typical values) is the main computational framework for the program. The table provides a step-by-step calculation of the aircraft's weight, time elapsed and distance travelled, during the mission, starting with the aircraft at the ramp and sequentially updating the aircraft's status after each leg. Some of the values in the table are fixed, like the engine start and taxi fuel weight, but most are calculated on sheets B, C and D for the specific mission. During the computation, the subroutines continuously return values to the master table.

Lotus 123 has a powerful built-in *backsolver* feature. This is an iterative solver function, that may be used when the numerical answer to a defined function is known, but the variables needed to produce that answer, are not known. For example, the integrated range technique computes the still air distance travelled, for known weights at the TOC and at the TOD. However, when the distance (i.e. the answer) is known, the variable that must be determined, is one of the two weights – either the TOC or TOD weight, given that the other is specified. In Table H-6 three cell pairs are identified by a



gray background. These represent spreadsheet cells that are used by three separate *backsolver* routines. In the first pair the weight at the TOD (345071lb) was sought so that the computed distance equalled the required distance of 5690.7nm. Similarly for the hold, the weight at the end of the hold (331403lb) was iteratively sought so that the hold time equalled the user specified hold time of 30min.

At the bottom of Table H-6 the weight status of the aircraft when it lands at the alternative airport is given. Starting with the OEW, the payload is added to give the ZFW, then the contingency fuel and tankered fuel are added, to finally give the weight on landing at the alternate airport. In the example given in Table H-6, the program was run in the *range* mode with a specified distance. Hence, the program iterated until a result of zero tankered fuel, was determined. The fuel at the alternate airport is calculated and tabulated as a check against the contingency fuel. Note that in the *fuel* mode this value will generally not be zero.

### H.3.6 Results

The output of a single run is presented for easy reference in a table on sheet A. The results are also appended to a similar table on sheet J, which is able to store up to 20 sets of results (see Table H-13). This permits comparisons to be made between different runs, which are identified by a run number located at the top of each column.

### H.3.7 Dialogue box and aircraft checks

A dialogue (message) box indicates the status of the program during operation, by indicating one of three messages: "*Busy - please wait*", "*Converged*", or "*Did not converge*". A real time counter indicates the number of major (outer loop) iterations performed (see Table H-7). Associated with the dialogue box are the results of three checks that are performed. The format of these checks is shown in Table H-7 below the dialogue box.

- (1) The first check is central to the control of the "outer loop" iteration of the program. A mission OEW is determined by adding to the basic aircraft OEW, the weight penalty of the HLFC system. The specified payload and computed fuel from the last iteration, is added to the OEW to produce a "calculated" or trial BRW. This is compared to the value used during the last iteration to determine the trip fuel. The percentage difference is determined and indicated as a check adjacent to the "Calculated BRW" value in the table. Convergence is reached when the difference is less than 0.01%.
- (2) If the user enters a range that is beyond the capability of the aircraft for the specified payload, then the BRW that will be computed, will be higher than the allowable weight for the aircraft. This is checked. If the computed BRW is less than the MTOW, an "OK" message is returned when the program terminates.
- (3) A check is also made to determine if the fuel required to complete the mission is less than the maximum fuel capacity for the aircraft. This is based on the weight of



the fuel, rather than the volume. (The values used are reflected in Table H-3.) An "OK" message is returned if it is within the limit.

**Table H-6** Master computing table

MISSION	Weight (lb)	Time (min)	Distance (nm)
<b>MISSION</b>			
<b>Ramp weight</b>	484125	0.0	0.0
1 Start and Taxi	700	12.0	0.0
<b>At brake release</b>	483425	12.0	0.0
2 Takeoff & Climb to 1500 ft	1646	2.1	0.0
<b>At 1500ft</b>	481778	14.1	0.0
3 Climb to cruise altitude	9003	22.1	147.9
<b>At TOC</b>	472776	36.2	147.9
4 Cruise	127705	744.1	5690.7
<b>At TOD</b>	345071	780.4	5838.6
4.1 Step climb correction	350	0.0	0.0
<b>Corrected TOD</b>	344721	780.4	5838.6
5 Descent to 1500 ft	1153	23.1	141.4
<b>At 1500 ft</b>	343567	803.5	5980.0
6 Approach	450	4.0	0.0
<b>Landed at Destination</b>	343117	807.5	5980.0
13 Taxi & Shutdown	450	12.0	0.0
<b>Block weight/ time/ distance</b>	<b>342667</b>	<b>819.5</b>	<b>5980.0</b>
<b>ALTERNATE</b>			
<b>Depart for Alternate</b>	343117	0.0	0.0
7 Missed approach	1000	2.0	0.0
<b>At 1500ft</b>	342117	2.0	0.0
8 Climb	3670	7.7	41.8
<b>At TOC for Alternate</b>	338447	9.7	41.8
9 Alternate cruise	1983	12.8	76.8
<b>At TOD for Alternate</b>	336464	22.4	118.6
10 Descent to 1500 ft	844	15.5	81.4
<b>Overhead Alternate</b>	335619	37.9	200.0
11 Hold at 1500 ft	4216	30.00	0.0
<b>End Hold</b>	331403	67.9	200.0
12 Approach & Land	450	4.0	0.0
<b>Landed at Alternate</b>	<b>330953</b>	<b>71.9</b>	<b>200.0</b>
<b>LANDED</b>			
<b>Actual OEW</b>	<b>270953</b>		
Payload	52985		
<b>Zero Fuel Weight</b>	<b>323938</b>		
Contingency Fuel	7015		
Tankered fuel	0		
<b>Landed at Alternate</b>	<b>330953</b>		
<b>Fuel on board at Alternate</b>	<b>7015</b>		



Table H-7 *Dialogue box and checks*

Dialogue box and aircraft checks				
Iterations ->	26			
Message box ->	Converged			

Checks	Weight (lb)	Comment		
OEW (mission)	270953			
Payload	52985			
Zero Fuel Weight	323938			
Total fuel excl. start, taxi	159487			
Calculated BRW	483424	check ->	0.00%	
Max BRW	513650	check ->	OK	BRW must not exceed A/C limit
Fuel capacity	246830	check ->	OK	Total fuel must not exceed fuel capacity

### H.3.8 Macro code

Four software buttons start the operation of the subroutines (macros), as shown in Fig. H-1. The main subroutines: *submain1*, *submain2* and *submain3*, initialise the internal program counters, post a "busy" message to the user, activate the Lotus 123 trace function (useful for program debugging) and pass the command to the subroutines: *subweight*, *subrange* or *subfuel*, respectively. These subroutines are responsible for controlling the iterative computational cycles and checking for convergence within each iterative cycle. If convergence is not reached after 50 cycles, the subroutine posts a "Did not converge" message and terminates.

The central numerical part of the computation is performed by three "backsolve" functions in the subroutine *subsolve*. The backsolve functions are run sequentially to determine the fuel burn for the main mission, the alternative leg and for the hold. After each call to *subsolve*, the command returns to the appropriate subroutine (i.e. *subweight*, *subrange* or *subfuel*), which updates the master computational table (see section H.3.5) and checks if the convergence criterion have been met. If not, the program loops back to the start of the appropriate subroutine (i.e. *subweight*, *subrange* or *subfuel*). When convergence is reached, or the maximum permissible number of iterations reached, control is returned to the appropriate main subroutine, which then calls the subroutine *subprint*. This subroutine appends the final computed values to the results table on sheet J, before returning the command to the main subroutine; after which the operation is terminated.

The software button *clear* initiates the subroutine *subclear*, which resets the run counter and deletes all entries in the results table on sheet J.



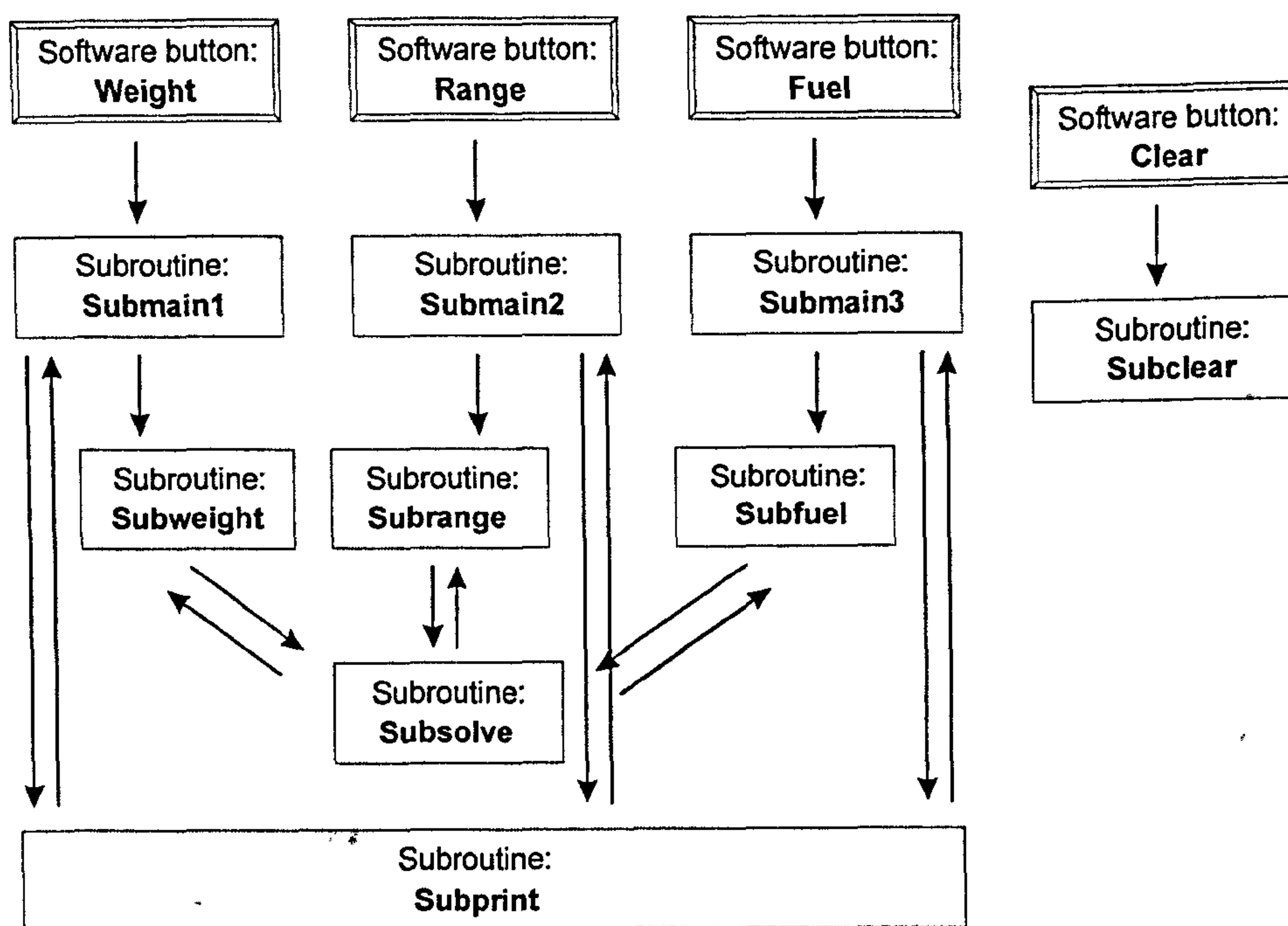


Fig. H-1 Subroutine hierarchy

### Macro code listing (for A330-200 class aircraft)

```

SUBROUTINE: SUBMAIN1
{SET "MACRO-TRACE";"ON"}
{LET RUN;RUN+1:V}
{LET COUNTER;0:V}
{LET MESSAGE;+"Busy - please wait":V}
{LET C123;0:V}
{SUBWEIGHT}
{SUBPRINT}
{SET "MACRO-TRACE";"OFF"}
{RETURN}

```

```

SUBROUTINE: SUBWEIGHT
{LET COUNTER;COUNTER+1:V}
{IF COUNTER>50}{LET MESSAGE;+"Did not converge":V}{QUIT}
{SUBSOLVE}
{LET C32;(C32*C27/H35):V}
{LET C28;C55:V}
{IF @ABS(ERROR1)>0.0001}{BRANCH SUBWEIGHT}
{LET C33;C33+C36-C60:V}
{IF @ABS((C36-C60)/C36)>0.002}{BRANCH SUBWEIGHT}
{LET MESSAGE;+"Converged":V}
{RETURN}

```

```

SUBROUTINE: SUBSOLVE
{BACKSOLVE A:E92;RANGE;A:C93}
{BACKSOLVE A:E109;ALTERNATE;A:C110}

```



```
{BACKSOLVE A:D113;HOLD;A:C114}
{RETURN}
```

```
SUBROUTINE: SUBMAIN2
{SET "MACRO-TRACE";"ON"}
{LET RUN;RUN+1:V}
{LET COUNTER;0:V}
{LET MESSAGE;+"Busy - please wait":V}
{LET C123;0:V}
{SUBRANGE}
{SUBPRINT}
{SET "MACRO-TRACE";"OFF"}
{RETURN}
```

```
SUBROUTINE: SUBRANGE
{LET COUNTER;COUNTER+1:V}
{IF COUNTER>50} {LET MESSAGE;+"Did not converge":V} {QUIT}
{SUBSOLVE}
{LET C32;C32+(C28-C55):V}
{IF @ABS((C28-C55)/C28)>0.002} {BRANCH SUBRANGE}
{LET C27;H35:V}
{LET COUNTER;COUNTER+1:V}
{SUBSOLVE}
{IF @ABS(ERROR1)>0.0001} {BRANCH SUBRANGE}
{LET C33;C33+C36-C60:V}
{IF @ABS((C36-C60)/C36)>0.002} {BRANCH SUBRANGE}
{LET MESSAGE;+"Converged":V}
{IF H35>H37} {LET MESSAGE;+"BRWeight exceeds maximum for A/C
type":V}
{RETURN}
```

```
SUBROUTINE: SUBMAIN3
{SET "MACRO-TRACE";"ON"}
{LET RUN;RUN+1:V}
{LET COUNTER;0:V}
{LET MESSAGE;+"Busy - please wait":V}
{LET C123;0:V}
{SUBFUEL}
{SUBPRINT}
{SET "MACRO-TRACE";"OFF"}
{RETURN}
```

```
SUBROUTINE: SUBFUEL
{LET COUNTER;COUNTER+1:V}
{IF COUNTER>50} {LET MESSAGE;+"Did not converge":V} {QUIT}
{SUBSOLVE}
{LET C32;C32+(C28-C55):V}
{IF @ABS((C28-C55)/C28)>0.002} {BRANCH SUBFUEL}
{LET C33;C33+C36-C60:V}
{IF @ABS((C36-C60)/C36)>0.002} {BRANCH SUBFUEL}
{LET C123;C124-(C121+C122+C123):V}
{CALC}
{LET MESSAGE;+"Converged":V}
{RETURN}
```

```
SUBROUTINE: SUBCLEAR
{LET RUN;0:V}
```



```
{SELECT J:D7..J:Y40;J:D7}
{EDIT-CLEAR}
{SELECT J:C7..J:C40;J:C7}
{RANGE-NAME-CREATE "RESULTS"}
{EDIT-GOTO A:E25}
{RETURN}
```

```
SUBROUTINE: SUBPRINT
{APPENDRIGHT RESULTS;OUTPUT}
{RETURN}
```

## H.4 SHEET B: CRUISE CALCULATION

### H.4.1 Sheet functions

Sheet B has two computational tables – one for the main mission cruise leg and one for the alternate leg. The first three rows of the main mission cruise spreadsheet table (corresponding to stations 0, 1 and 2) are shown in Table H-8. The calculations run from left to right across 39 columns in the spreadsheet (which because of space limitations on the page, have been split into four sections in Table H-8).

### H.4.2 Cruise calculation

If the distance from the TOC to the TOD is known, the required cruise fuel and cruise time can be computed; however, at the start of the calculation this is not known, due to the uncertainty of the climb and descent distances. It is thus required that the user enters an initial value of the TOC to TOD distance, and this is used to compute the fuel and time required for the entire mission. Any reasonable value will suffice, but poor estimates will imply a longer computational time. The calculated distance after each iteration is compared to the input data and the calculation repeated until convergence is reached.

As illustrated in Table H-8, the calculations run from left to right, beginning with the start and end weights for each segment. The start weight is obtained from the master table, corresponding to the TOC. As a trial value for the TOC to the TOD distance is available, the weight at the end of the cruise can be computed. This is done using the integrated range method (outlined in the theory section E.4.4, Appendix E), using 20 segments in the cruise. The end weight is found using the *backsolve* function (explained in section H.3.5). This function solves for a unique value of the end-of-cruise weight, which satisfies the requirement for the computed cruise distance, to equal the trial TOC to TOD distance.

The first few columns (after the weight) reproduce relevant data from sheet A, such as the altitude, atmospheric conditions and Mach number. For the given height, the temperature and pressure ratios and the speed of sound are obtained from the ISA look-up table (sheet J). The lift coefficient is then evaluated for the weight at that particular station. By linear interpolation, using the drag look-up table (sheet E), the



$C_D$  corresponding to the calculated  $C_L$  is determined for the appropriate Mach number. The next step is to apply the specified HLFC drag correction (which is stored on sheet A). Based on the revised  $C_D$  value, the parameter  $D/\delta$  is calculated and hence the thrust per engine is deduced. This provides the input data needed to determine the corrected fuel flow, which is obtained by linear interpolation using the fuel flow look-up tables (sheet F). The actual fuel flow is then computed using the total temperature ratio ( $\theta_t$ ) and total pressure ratio ( $\delta_t$ ), after which the HLFC correction to the fuel flow is applied. The SAR for this station, defined by the quotient  $SAR = V/Q$  is then determined.

All calculations to this point (i.e. across a single row in the spreadsheet) correspond to a particular station in the cruise (i.e. for specific weight, altitude and atmospheric conditions). This changes for the last five columns, where the calculation of *distance* and *time* is undertaken for the cruise sector *between* two stations. By numerical integration of the SAR, the air range increment for that sector is determined. The wind component is then added to give the ground range increment for that segment. A running summation of the range increments (from row to row) provides the cumulative ground range from the TOC. The time increment is obtained from the quotient of the range increment and the TAS, which is then summed to provide a running total of the cruise duration. The final cumulative values of the *range* and the *time* (for all sectors) are then passed back to the master table (on sheet A).

The cruise calculation described above, represents the "function" that is used by the *backsolve* routine to determine the TOD weight which will give a cumulative range that matches the trial TOC to TOD distance. The rest of the mission calculations (i.e. descent, alternative leg, etc.) are then undertaken, before the next calculation cycle begins.

The computational table for the alternate cruise is almost identical to that described above. The differences are that no HLFC correction is applied and that only two cruise segments are used in the analysis because of the short cruise distance.

#### H.4.3 Step climb in cruise

Maximum cruise efficiency for long range flights is achieved by permitting "step climbs" in the cruise. The cruise spreadsheet allows the user to specify different heights for each individual cruise sector. However, in this table no provision is made for the calculation of the small incremental fuel required for the step climb. To correct for this, an input cell is available in the mission look-up table on sheet H, where the fuel for the step climb may be inserted. For a constant height cruise, the correction in this cell is zero.



Table H-8 Cruise calculations (Note: Spreadsheet table in 4 parts)

Location	Weight (lb)	Altitude (ft)	Temp ISA +	Mach	Theta	Delta	a (kt)	W/delta (lb)	CL
0	472776	37000	0.0	0.80	0.7519	0.2138	573.6	2211368	0.59928
1	466390	37000	0.0	0.80	0.7519	0.2138	573.6	2181502	0.59119
2	460005	37000	0.0	0.80	0.7519	0.2138	573.6	2151635	0.58309

Interpolation for CD				CD Base	HLFC	CD	D/delta	FN/delta		
x1	y1	x2	y2		Drag		A/C	per eng	range	range
0.55	0.02610	0.60	0.02896	0.02892	0.00000	0.02892	106711	53356	MACH370	FUEL370
0.55	0.02610	0.60	0.02896	0.02846	0.00000	0.02846	105004	52502	MACH370	FUEL370
0.55	0.02610	0.60	0.02896	0.02799	0.00362	0.02437	89939	44970	MACH370	FUEL370

Interpolation for fuel flow				Cor. Q	theta T	delta T	Q	Q tot	HLFC	Q tot
x1	y1	x2	y2	per eng			per eng	A/C	Q	A/C
53000	21606	54000	23034	22114	0.8481	0.3259	6637	13274	Increase	(lb/hr)
52000	21606	53000	21606	21606	0.8481	0.3259	6484	12969	0.0%	13274
44000	17905	45000	19041	19006	0.8481	0.3259	5704	11409	0.0%	12969
									2.0%	11637

V	SAR	Sector	Still air dist	Ground	Ground	Time	Total
			Increment	Increment	Range	Increment	Time
(KTAS)			(nm)	(nm)	(nm)	(hr)	(hr)
458.9	0.03457		0.0	0.0	0	0.00	0.00
458.9	0.03538	0 - 1	223.3	223.3	223	0.49	0.49
458.9	0.03943	1 - 2	238.9	238.9	462	0.52	1.01



## H.5 SHEET C: CLIMB / DESCENT CALCULATION

### H.5.1 Sheet functions

This sheet has four computational tables:

- (1) Climb calculation for the main mission leg.
- (2) Climb calculation for the alternate leg.
- (3) Descent calculation for the main mission leg.
- (4) Descent calculation for the alternate leg.

### H.5.2 Climb speed schedule

The climb was broken into intervals of 5000ft or less, as shown in Table H-9 below. The climb speed schedule was 250/290/M0.80 for the B757-200 class aircraft and 250/300/M0.80 for the A330-200 class aircraft. The height at which the second climb speed equals Mach 0.80 (required for the remaining part of the climb) was determined to be ~32100ft for 290KCAS and ~31000ft for 300KCAS. Hence, these heights were required in the respective tables.

Table H-9 *Climb / Speed Schedule*

B757-200 class aircraft			A330-200 class aircraft		
Start height (ft)	End height (ft)	Speed	Start height (ft)	End height (ft)	Speed
1500	5000	250KCAS	1500	5000	250KCAS
5000	10000	250KCAS	5000	10000	250KCAS
10000	15000	290KCAS	10000	15000	300KCAS
15000	20000	290KCAS	15000	20000	300KCAS
20000	25000	290KCAS	20000	25000	300KCAS
25000	29000	290KCAS	25000	29000	300KCAS
29000	32100	290KCAS	29000	31000	300KCAS
32100	35000	Mach 0.80	31000	37000	Mach 0.80

### H.5.3 Climb calculation

The essential difficulty with the climb calculation is that the weight at the end of the interval depends on the rate of climb in the interval (which is not constant) and this in turn depends of the aircraft's weight during the interval. An iterative solution is thus required for each step of the climb. On inspection, it was found that two iterations permitted convergence within each interval. The approach adopted to analyse the climb is explained in the theory section E.3 (Appendix E). The sequence of calculations is shown in Table H-10, which is an extract from the computational table (located on sheet C).

The first part of this table is very similar to the cruise table up the point that  $C_D$  is determined. The spreadsheet permits HLFC correction to the drag coefficient and fuel flow, for heights above 20000ft. (The data is entered on sheet A). In the climb



(unlike the cruise) the thrust is independent of the drag and must be obtained from the appropriate look-up table (located on sheet G) by interpolation. The acceleration factor ( $f_{acc}$ ) is determined using the appropriate equation described in Table E-1 (appendix E). The appropriate equation depends on the speed schedule (i.e. constant CAS or constant Mach number) and thus, the equation in the cells of this column change when the climb speed schedule changes. The thrust, drag, start-of-interval weight and  $f_{acc}$  are then used to compute the ROC, according to equation [E-25]. The ROC (determined for conditions at the start of the interval) together with the change in height for the interval, yields an estimate of the climb time. Based on the climb thrust (also determined at the start of the interval) the corrected fuel flow is obtained using linear interpolation from the look-up tables, contained in sheet G. The fuel flow  $Q$  is then calculated. The first estimate of the fuel burnt in the interval is obtained from the product of  $Q$  and the interval time. This is subtracted from the aircraft's weight at the start of the climb interval, to give the first estimate of the aircraft's weight at the end of the interval.

The next part of the spreadsheet is almost an exact copy of the first part. The calculation is repeated, but the height is now taken for the end of the interval and the aircraft's weight is based on the estimated end-of-interval weight. The results of this second string of calculations are new values for ROC and for  $Q$ , corresponding to the estimated conditions at the end of the interval. Arithmetic means are then calculated for ROC and  $Q$ , using the start-of-interval and the end-of interval values.

Revised values for the climb time, fuel burnt and end-of-interval weight are finally calculated, using the mean ROC and  $Q$  values. The last part of the climb calculation uses equation [E-32] to calculate the horizontal distance travelled in the interval. This is summed in the last column of the table to give a cumulative climb distance. The final weight at the end of the interval is taken as the starting weight for the next interval and is passed to the appropriate cell in the next row of the spreadsheet, as shown in Table H-10.

#### H.5.4 Descent calculation

For the descent the idle thrust and fuel flow is obtained from the look-up tables on sheet G, but otherwise the calculations are identical to those for the climb. One minor change is incorporated that allows the user to specify a spoiler / speed brake drag increment (see Table H-4). This increases the drag below 20000ft.



Table H-10 Climb calculations (Note: Spreadsheet table in 8 parts)

Start	End	Temp	Constant	Constant	Start	At	Theta	Delta	Mach	a	W/Delta
Height	Height	ISA +	CAS	Mach	Weight	Altitude				(kt)	(lb)
(ft)	(ft)		(kt)		(lb)	(ft)					
1500	5000	0.0	250		481778	1500	0.9897	0.9470	0.388	658.1	508758
5000	10000	0.0	250		480973	5000	0.9656	0.8320	0.413	650.0	578059
10000	15000	0.0	300		479833	10000	0.9312	0.6877	0.541	638.3	697731

CL	interpolation for CD				Base	HLFC	L/D	Interpolation for thrust			
	Ref	CL	CD	CL	CD	Drag	CD	Mach	FN/delta	Mach	FN/delta
	Mach	x1	y1	x2	y2	Reduc		x1	y1	x2	y2
0.5861	0.400	0.55	0.02495	0.60	0.02703	0.02645	0.02645	0.35	40403	0.40	38756
0.5880	0.400	0.55	0.02495	0.60	0.02703	0.02653	0.02653	0.40	41453	0.45	40018
0.4134	0.550	0.40	0.01938	0.45	0.02084	0.01977	0.01977	0.50	42937	0.55	41698

FN/delta	Thrust	phi	f acc	V	sin	ROC	range	Ref	FN/delta	Cor. Q	FN/delta	Cor. Q
per eng	(lb)			(kt)	gamma	(fpm)		Mach	x1	y1	x2	y2
39151	74149	0.9640	0.08154	255.3	0.1006	2600.6	MACH15	0.40	39000	17242	40000	17242
41083	68365	0.9595	0.09180	268.4	0.0889	2415.3	MACH50	0.40	41000	17323	42000	18584
41919	57656	0.9328	0.15215	345.4	0.0628	2196.0	MACH100	0.55	41000	17643	42000	18901

Cor. Q	theta T	delta T	Q	HLFC	Q	Q tot	Estimate	Fuel	Estimate	At	Theta	Delta	Mach
per eng			per eng	Q	per eng	A/C	Climb time	Burned	Weight	Altitude			
(lb/hr)			(lb/hr)	Increase	(lb/hr)	(lb/hr)	(min)	(lb)	(lb)	(ft)			
17242	1.0195	1.0506	18338		18338	36676	1.346	822.7	480956	5000	0.9656	0.8320	0.413
17427	0.9985	0.9357	16291		16291	32582	2.070	1124.2	479849	10000	0.9312	0.6877	0.452
18799	0.9858	0.8392	15634		15634	31268	2.277	1186.5	478646	15000	0.8969	0.5643	0.593



Table H-10 continued

a	W/Delta	CL	Interpolation for CD					Base	HLFC	CD	L/D	Interpolation	
(kt)	(lb)		Ref	x1	y1	x2	y2	CD	Drag			Mach	FN/delta
			Mach						Reduc			x1	y1
650.0	578038	0.5880	0.40	0.55	0.02495	0.60	0.02703	0.02653		0.02653	22.16	0.40	41453
638.3	697754	0.5916	0.45	0.55	0.02475	0.60	0.02680	0.02646		0.02646	22.36	0.45	44252
626.4	848149	0.4184	0.60	0.40	0.01934	0.45	0.02078	0.01987		0.01987	21.06	0.55	46206

Mach x2	FN/delta y2	FN/delta per eng (lb)	Thrust (lb)	phi	f_acc	V (kt)	sin gamma	ROC (fpm)	range	range	Ref Mach
0.45	40018	41083	68365	0.95945	0.09180	268.4	0.0889	2415.4	MACH50	FUEL50	0.40
0.50	42937	44192	60781	0.95183	0.10905	288.7	0.0739	2160.2	MACH100	FUEL100	0.45
0.60	45101	45257	51080	0.92054	0.17974	371.5	0.0502	1888.5	MACH150	FUEL150	0.60

Interpolation for fuel flow										Cor. Q	theta_T	delta_T	Q	HLFC	Q	Q_tot	Ave	Ave
FN/delta	Cor. Q	FN/delta	Cor. Q	Cor. Q	per eng				per eng				per eng	Q	A/C	Q_tot	ROC	Q_tot
x1	y1	x2	y2		(lb/hr)				(lb/hr)				(lb/hr)	Increase	(lb/hr)	(lb/hr)	(fpm)	(lb/hr)
41000	17323	42000	18584	17427	0.9985	0.9357			16291				16291		32582		2508	34629
44000	19099	45000	20387	19346	0.9693	0.7913			15009				15009		30017		2288	31300
45000	20368	46000	20368	20368	0.9599	0.7159			14206				14206		28412		2042	29840

Revised Climb time (min)	Cumulative Climb time (min)	Fuel Burned (lb)	Cumulative Fuel burn (lb)	End Weight (lb)	Ave V (ktas)	Horizontal speed (ktas)	Distance (nm)	Cumulative Distance (nm)
1.40	1.40	805.4	805.4	480973	261.9	260.7	6.06	6.06
2.19	3.58	1140.1	1945.6	479833	278.6	277.6	10.11	16.18
2.45	6.03	1217.6	3163.2	478615	358.4	357.8	14.60	30.78



## H.6 SHEET D: HOLD CALCULATION

The hold calculation is very similar to that of the cruise and much of the computational table is identical (as shown in Table H-11). The hold Mach number is obtained from the look-up table on sheet H based on the aircraft's weight. No HLFC correction is applied, but the main difference comes about in the last few columns of the table. After the fuel flow  $Q$  is computed, the incremental time for each segment is determined. This is done by multiplying the reciprocal of  $Q$  (for the segment) by the weight change for that segment, as explained in the theory section E.5.2 (Appendix E).

The start weight comes from the master sheet. The end weight is determined by the *backsolve* routine, which solves for the appropriate weight to give the required hold time.

## H.7 SHEET E: DRAG POLAR

The drag polar look-up table is structured as follows. It has  $C_L$  values as headings for each column, from 0.15 to 1.0, increasing in steps of 0.05. The corresponding  $C_D$  values in each row are applicable to a single Mach number. The  $C_D$  data is provided for a range of Mach numbers, which increase in steps of 0.05 from Mach 0.30 to Mach 0.70, and thereafter in steps of 0.1 to Mach 0.84. Linear interpolation is used to determine the required  $C_D$  values, corresponding to the appropriate  $C_L$  values and Mach numbers. Due to the fact that the Mach number steps are relatively small, it is not required to perform a four-way interpolation of the data. The row containing the data for the Mach number closest to the aircraft's Mach number is used.

At each mission station in the cruise, climb, descent or hold computational tables (i.e. sheets B, C and D) the  $C_L$  is determined. To find the value of  $C_D$  corresponding to this value of  $C_L$ , the spreadsheet initially identifies two  $C_L$  values in the look-up table, which "bracket" the required  $C_L$  value and for which data is available. The two  $C_L$  values are designated as  $x_1$  and  $x_2$  in the computational tables (sheets B, C and D). The  $C_D$  values (designated as  $y_1$  and  $y_2$ ) corresponding to the two  $C_L$  values are then identified and returned to the appropriate computational table. For example, if the computed  $C_L$  equalled 0.6240 and the Mach number was 0.723, then  $C_D$  values would be returned for  $C_L$  values equal to 0.60 and 0.65, corresponding to Mach 0.72. Linear interpolation for the required  $C_D$  value is then performed in the computational table.



Table H-11 Hold calculation (Note: Spreadsheet table in 3 parts)

Weight (lb)	Altitude (ft)	Temp ISA +	Hold Mach	Theta	Delta	a (kt)	W/delta (lb)	CL	interpolation for CD			
									x1	y1	x2	y2
335619	1500	0.0	0.320	0.9897	0.9470	658.1	354414	0.60029	0.60	0.02757	0.65	0.02989
333509	1500	0.0	0.320	0.9897	0.9470	658.1	352185	0.59651	0.55	0.02544	0.60	0.02757
331403	1500	0.0	0.320	0.9897	0.9470	658.1	349962	0.59275	0.55	0.02544	0.60	0.02757

CD Base	D/delta A/C	FN/delta per eng (lb)	range	range	interpolation for fuel flow				Cor. Q per eng (lb/hr)	theta_T	delta_T	Q per eng (lb/hr)
					x1	y1	x2	y2				
0.02758	16285	8142	MACH15	FUEL15	6000	3597	9000	4355	4139	1.0100	1.0166	4228
0.02742	16189	8095	MACH15	FUEL15	6000	3597	9000	4355	4127	1.0100	1.0166	4216
0.02726	16094	8047	MACH15	FUEL15	6000	3597	9000	4355	4115	1.0100	1.0166	4204

Q_tot A/C	1/Q_T A/C	Time Increment	Time
(lb/hr)	(hr/lb)	(hr)	(hr)
8457	1.183E-004	0.00	0.00
8432	1.186E-004	0.25	0.25
8407	1.189E-004	0.25	0.50



## H.8 SHEET F: CORRECTED FUEL FLOW DATA

Sixteen look-up tables containing corrected fuel flow values as a function of  $F_N/\delta$  and Mach number (in steps of Mach 0.05), are included on sheet G. Each table is for a different height, from sea-level to 42000ft. For the hold calculation there is a table for 1500ft, and for the climb there are tables for flight levels 50, 100, 150, 200, 250 and 290. In order to analyze the cruise there are tables for flight levels 330, 350, 370, 390, 410 and 420. The climb / speed schedules stipulate a change from constant CAS to constant Mach number. To simplify the climb calculation, a fuel flow table was derived for 31000ft (for the A330-200 class aircraft) and for 32100ft (for the B757-200 class aircraft). Furthermore, the equation for calculating the acceleration factor (see Table E-1, Appendix E) changes at the tropopause and hence, data was required at 36089ft.

To ensure that the correct look-up table is used during the calculations, an index table is provided. This table, also located on sheet F, allocates two unique named ranges<sup>2</sup> to each of the 16 look-up tables. When the fuel flow at a particular height is sought, the program first "looks up" the corresponding range names in the index table and then uses the named ranges to identify the correct look-up table. In the computational tables (for the climb / descent, cruise and hold) these named ranges are written into the cells immediately prior the interpolation routine. This serves as a useful check to the user that the program is functioning correctly.

During the calculations two values of fuel flow are returned from the appropriate look-up table to the computational table, corresponding to values which "bracket" the actual value of  $F_N/\delta$ . A linear interpolation is performed in the computational table to calculate the desired value. This is done in an identical manner to that described earlier in section H.7 for the drag coefficient. As before, the data closest to the flight Mach number is used, to avoid the need for a second interpolation (for an arbitrary Mach number between table values).

## H.9 SHEET G: CLIMB AND IDLE ENGINE DATA

Sheet G contains three look-up tables:

- (1) The maximum climb thrust data, given as  $F_N/\delta$ , is presented as a table for the speed range of Mach 0.20 to Mach 0.90 (in steps of 0.05) and for heights from sea-level to 42000ft (in 1000ft steps).
- (2) The idle in-flight thrust, tabulated as  $F_N/\delta$ , is presented as a function of Mach number and height.

---

<sup>2</sup> Range: A name given to a spreadsheet cell (or range of cells) that may be used in place of the cell address(es).



- (3) Idle in-flight fuel flow is presented as a function of Mach number and height.

## H.10 SHEET H: MISCELLANEOUS TABLES

Sheet H contains three look-up tables:

- (1) Climb data, consisting of fuel, distance and time, from brake-release to 1500ft is presented for a range of Brake Release Weights.
- (2) The holding Mach number at 1500ft for a range of aircraft weights is tabulated.
- (3) Mission allowances of fuel, time and distance (as shown in Table H-12, below) are included in a table on this sheet. The table was based on data extracted from Airbus (undated), Boeing (1993), Boeing (undated) and Jenkinson *et al.* (1999). The values may be changed by the user, to suit a particular mission.

**Table H-12** *Mission allowances*

	B757-200 class aircraft			A330-200 class aircraft		
	Weight (lb)	Time (min)	Distance (nm)	Weight (lb)	Time (min)	Distance (nm)
<b>MISSION</b>						
1 Start and Taxi	500	12.0	0.0	700	12.0	0.0
4.1 Step climb correction	-	-	-	350	0.0	0.0
6 Approach	400	4.0	0.0	450	4.0	0.0
13 Taxi & Shutdown	400	12.0	0.0	450	12.0	0.0
<b>ALTERNATE LEG</b>						
7 Missed approach	700	2.0	0.0	1000	2.0	0.0
12 Approach & Land	400	4.0	0.0	450	4.0	0.0

## H.11 SHEET I: THE INTERNATIONAL STANDARD ATMOSPHERE (ISA)

Sheet I contains a look-up table for the International Standard Atmosphere. The required ISA values (i.e.  $\theta, \delta, \sigma, T, p, \rho$  and  $a$ ) were computed at 200ft intervals, from sea-level to 45000ft; and also at 36089ft, using the standard values and equations given in Tables E-5 and E-6 (Appendix E). The resulting values was checked for accuracy against data from ESDU 72018 (1972).

## H.12 SHEET J: RESULTS

Sheet J contains the table of results. After each run the final values are appended to the table. A maximum of twenty sets of results can be accommodated in the table. The software button marked *Clear* (see section H.2.1), is used to erase all values in the table (at the start of a new study, for example). Table H-13 illustrates the results table after 6 runs performed in *Range* mode for the A330-200 class aircraft. For runs 1 to 5, the range was progressively increased in steps of 1000nm, with all other input parameters remaining unchanged and the minimum trip fuel and BRW computed.



The payload was set equal to the design payload of 52985lb and the HLFC system was not "installed" (i.e. corresponding to the baseline aircraft, with no changes to OEW, SFC or drag). Run number 6 reflects the results obtained using the input parameters given in Tables H-4 and H-5. (Note the increased OEW and corrections to the fuel flow and drag.)

Table H-14 contains the output of a series of typical runs for the B757-200 class aircraft, conducted using the *Range* mode. The trip distance was 2603nm and a fixed payload of 59270lb was used (corresponding to the conditions stipulated for case 1A, as defined in Table 6-1 in Chapter 6). Run number 1 represented the baseline condition; run 2 had a 2% increase in fuel flow; run 3 had an increase in OEW of 2575lb; run 4 had a drag reduction of 42.2 drag counts, and run 5 had the aforementioned fuel flow, OEW and drag changes, simultaneously incorporated.

**Table H-13** Typical results for A330-200 class aircraft (program run in Range mode)

Run number		1	2	3	4	5	6
Ramp Weight	lb	358296	381918	406902	433516	462145	484124
Brake Release Weight	lb	357596	381218	406202	432816	461445	483424
Payload	lb	52985	52985	52985	52985	52985	52985
OEW	lb	265640	265640	265640	265640	265640	270953
HLFC drag reduction		0.00000	0.00000	0.00000	0.00000	0.00000	0.00362
HLFC fuel flow increase	%	0.00%	0.00%	0.00%	0.00%	0.00%	2.00%
Contingency	%	5.0%	5.0%	5.0%	5.0%	5.0%	5.0%
Wind in cruise	kt	0	0	0	0	0	0
Range (Trip distance)	nm	1000	2000	3000	4000	5000	5980
Trip fuel	lb	25757	48239	71995	97320	124547	140307
Trip time	hr : min	02:22	04:33	06:45	08:56	11:07	13:15
Block fuel	lb	26907	49389	73145	98470	125697	141457
Block time	hr : min	02:46	04:57	07:09	09:20	11:31	13:39
Alternate	nm	200	200	200	200	200	200
Hold time	hr : min	00:30	00:30	00:30	00:30	00:30	00:30

#### Fuel Breakdown

Start up and taxi	lb	700	700	700	700	700	700
Trip fuel	lb	25757	48239	71995	97320	124547	140307
Alternate and land	lb	7806	7826	7856	7878	7902	7948
Final reserve (Holding)	lb	4125	4133	4140	4148	4157	4216
Contingency fuel	lb	1288	2412	3600	4866	6227	7015
Tankered fuel	lb	0	0	0	0	0	0
<b>Total fuel on board</b>	<b>lb</b>	<b>39677</b>	<b>63309</b>	<b>88290</b>	<b>114913</b>	<b>143533</b>	<b>160187</b>

#### Trip Fuel Breakdown

Takeoff, climb to 1500 ft	lb	1195	1270	1383	1458	1571	1646
Climb to cruise altitude	lb	6220	6817	7510	8342	9394	9003
Cruise	lb	16757	38564	61512	85929	111988	128055
Descent to 1500 ft	lb	1135	1137	1139	1141	1144	1153
Approach	lb	450	450	450	450	450	450
<b>Total trip fuel</b>	<b>lb</b>	<b>25757</b>	<b>48239</b>	<b>71995</b>	<b>97320</b>	<b>124547</b>	<b>140307</b>



**Table H-14** Typical results for B757-200 class aircraft (program run in Range mode)

Run number		1	2	3	4	5
Ramp Weight	lb	249106	250182	252488	242363	246577
Brake Release Weight	lb	248606	249682	251988	241863	246077
Payload	lb	59270	59270	59270	59270	59270
OEW	lb	128730	128730	131305	128730	131305
HLFC drag reduction		0.00000	0.00000	0.00000	0.00422	0.00422
HLFC fuel flow increase	%	0.00%	2.00%	0.00%	0.00%	2.00%
Contingency	%	5.0%	5.0%	5.0%	5.0%	5.0%
Wind in cruise	kt	0	0	0	0	0
Range (Trip distance)	nm	2603	2603	2603	2603	2603
Trip fuel	lb	49041	50069	49736	42630	44117
Trip time	hr : min	05:52	05:52	05:52	05:52	05:52
Block fuel	lb	49941	50969	50636	43530	45017
Block time	hr : min	06:16	06:16	06:16	06:16	06:16
Alternate	nm	200	200	200	200	200
Hold time	hr : min	00:30	00:30	00:30	00:30	00:30

**Fuel Breakdown**

Start up and taxi	lb	500	500	500	500	500
Trip fuel	lb	49041	50069	49736	42630	44117
Alternate and land	lb	5662	5663	5702	5657	5697
Final reserve (Holding)	lb	3451	3452	3486	3447	3482
Contingency fuel	lb	2452	2503	2487	2131	2206
Tankered fuel	lb	0	0	0	0	0
<b>Total fuel on board</b>	<b>lb</b>	<b>61106</b>	<b>62186</b>	<b>61910</b>	<b>54365</b>	<b>56002</b>

**Trip Fuel Breakdown**

Takeoff, climb to 1500 ft	lb	973	973	973	930	951
Climb to cruise altitude	lb	5188	5295	5357	4353	4538
Cruise	lb	41846	42767	42370	36313	37591
Descent to 1500 ft	lb	634	634	637	634	636
Approach	lb	400	400	400	400	400
<b>Total trip fuel</b>	<b>lb</b>	<b>49041</b>	<b>50069</b>	<b>49736</b>	<b>42630</b>	<b>44117</b>



# **APPENDIX I**

## **HLFC SENSITIVITY STUDIES**

### **TABLE OF CONTENTS**

I.1	Introduction.....	312
I.2	Numerical Expression for Small Changes .....	312
I.2.1	Small increment equation .....	312
I.2.2	Fuel required for specified range.....	312
I.2.3	Impact of small changes on fuel required for a specified range .....	313
I.3	Impact of Change in Contingency Fuel on Trip Fuel.....	314



## I.1 INTRODUCTION

In this appendix a numerical expression for small changes is developed and the required partial derivatives established, using the Breguet range equation. The resulting linear expressions were evaluated using the computer model for the B757-200 class aircraft. Details of this study are discussed in Chapter 6. The objective was to investigate mathematically, the impact on fuel burn during cruise, due to an active drag reduction technology (which will simultaneously increase the SFC and  $L/D$  ratio, whilst adding weight to the aircraft).

## I.2 NUMERICAL EXPRESSION FOR SMALL CHANGES

### I.2.1 Small increment equation

If it is *assumed* that  $m_2$  (end-of-cruise mass),  $\bar{E}$  (mean lift-to-drag ratio) and  $\bar{c}$  (mean SFC) are mutually *independent* in the cruise, then a linear expression for small change may be written as follows:

$$\delta m_f = \left( \frac{\partial m_f}{\partial m_2} \right) \delta m_2 + \left( \frac{\partial m_f}{\partial \bar{c}} \right) \delta \bar{c} + \left( \frac{\partial m_f}{\partial \bar{E}} \right) \delta \bar{E} \quad \text{--- [I-1]}$$

where  $m_f$  is the cruise fuel and  $\delta m_f$  is the change in the fuel burn due to small changes to the variables  $m_2$ , SFC and  $L/D$ . It should be noted at the outset, that the variables are not mutually independent and the assumption of independence, introduces an inaccuracy. (This is discussed in section 6.4 of Chapter 6.) The next step was to determine mathematical expressions for the partial derivatives  $\left( \frac{\partial m_f}{\partial m_2} \right)$ ,  $\left( \frac{\partial m_f}{\partial \bar{c}} \right)$  and  $\left( \frac{\partial m_f}{\partial \bar{E}} \right)$ .

### I.2.2 Fuel required for specified range

The Breguet range equation (derived in Appendix E, as equation [E-38]) is repeated here as a starting point, with the difference that  $\bar{c}$  and  $\bar{E}$  represent *mean* SFC and lift-to-drag values in the cruise, i.e.

$$R = \frac{V \bar{E}}{\bar{c} g} \log_e \left( \frac{m_1}{m_2} \right) \quad \text{--- [I-2]}$$

This equation enables the range ( $R$ ) to be calculated for a given fuel mass and a specified start-of-cruise mass ( $m_1$ ) or end-of-cruise mass ( $m_2$ ). For the analysis of the impact of a HLFC system on the fuel burn, it is required that the fuel mass be expressed in terms of the cruise range. It is possible to derive this relationship, in terms of either range and  $m_1$ , or range and  $m_2$ . Both formulations are presented in this section.



Equation [I-2] is re-written as:

$$\frac{R\bar{c}g}{V\bar{E}} = \log_e \left( \frac{m_1}{m_2} \right)$$

hence: 
$$e^{\left( \frac{R\bar{c}g}{V\bar{E}} \right)} - 1 = \left( \frac{m_1 - m_2}{m_2} \right) = \left( \frac{m_f}{m_2} \right) \quad \text{--- [I-3]}$$

Expressing the fuel required in terms of the end-of-cruise mass, gives:

$$m_f = \left( e^{\left( \frac{R\bar{c}g}{V\bar{E}} \right)} - 1 \right) m_2 \quad \text{--- [I-4]}$$

Alternatively, the expression may be written for the start-of-cruise mass as follows:

$$e^{\left( \frac{R\bar{c}g}{V\bar{E}} \right)} - 1 = \left( \frac{m_1 - m_2}{m_2} \right) = \left( \frac{m_f}{m_1 - m_f} \right)$$

$$m_f = \left( e^{\left( \frac{R\bar{c}g}{V\bar{E}} \right)} - 1 \right) (m_1 - m_f)$$

$$m_f e^{\left( \frac{R\bar{c}g}{V\bar{E}} \right)} = \left( e^{\left( \frac{R\bar{c}g}{V\bar{E}} \right)} - 1 \right) m_1$$

Finally: 
$$m_f = \left( 1 - e^{-\left( \frac{R\bar{c}g}{V\bar{E}} \right)} \right) m_1 \quad \text{--- [I-5]}$$

### I.2.3 Impact of small changes on fuel required for a specified range

The linear expression for small changes, shown earlier as equation [I-1], assumes that  $m_2$ ,  $\bar{E}$  and  $\bar{c}$  are independent during the cruise. Using equation [I-4], the partial derivatives with respect to  $m_2$ ,  $\bar{E}$  and  $\bar{c}$  are determined:

$$\frac{\partial m_f}{\partial m_2} = e^{\left( \frac{R\bar{c}g}{V\bar{E}} \right)} - 1 \quad \text{--- [I-6]}$$

$$\frac{\partial m_f}{\partial \bar{c}} = e^{\left( \frac{R\bar{c}g}{V\bar{E}} \right)} \left( \frac{Rg}{V\bar{E}} \right) m_2 \quad \text{--- [I-7]}$$

$$\frac{\partial m_f}{\partial \bar{E}} = e^{\left( \frac{R\bar{c}g}{V\bar{E}} \right)} \left( \frac{-R\bar{c}g}{V\bar{E}^2} \right) m_2 \quad \text{--- [I-8]}$$



Repeating the linear expression for small changes:

$$\delta m_f = \left( \frac{\partial m_f}{\partial m_2} \right) \delta m_2 + \left( \frac{\partial m_f}{\partial \bar{c}} \right) \delta \bar{c} + \left( \frac{\partial m_f}{\partial \bar{E}} \right) \delta \bar{E} \quad \text{--- [I-1]}$$

and substituting from [I-6], [I-7] and [I-8], gives:

$$\delta m_f = \left( e^{\frac{R\bar{c}g}{V\bar{E}}} - 1 \right) \delta m_2 + \left( e^{\frac{R\bar{c}g}{V\bar{E}}} \frac{Rg}{V\bar{E}} m_2 \right) \delta \bar{c} - \left( e^{\frac{R\bar{c}g}{V\bar{E}}} \frac{R\bar{c}g}{V\bar{E}^2} m_2 \right) \delta \bar{E} \quad \text{--- [I-9]}$$

Finally, dividing through by  $m_2$  yields the required expression, which is given in the Chapter 6 as equation [6-4]:

$$\frac{\delta m_f}{m_2} = \left( e^{\frac{R\bar{c}g}{V\bar{E}}} - 1 \right) \frac{\delta m_2}{m_2} + \left( e^{\frac{R\bar{c}g}{V\bar{E}}} \frac{R\bar{c}g}{V\bar{E}} \right) \frac{\delta \bar{c}}{\bar{c}} - \left( e^{\frac{R\bar{c}g}{V\bar{E}}} \frac{R\bar{c}g}{V\bar{E}} \right) \frac{\delta \bar{E}}{\bar{E}} \quad \text{--- [I-10]}$$

Writing the final expression in this way is convenient, as the changes to  $m_2$ ,  $\bar{E}$  and  $\bar{c}$  are expressed as non-dimensional terms. The impact on fuel can thus be determined from relative (or percentage) changes to  $m_2$ ,  $\bar{E}$  and  $\bar{c}$ .

### I.3 IMPACT OF CHANGE IN CONTINGENCY FUEL ON TRIP FUEL

An expression for the change in trip fuel ( $m_f$ ), resulting from a change in the contingency fuel, is determined in this section. The viable  $x$  is introduced to define the contingency fuel, viz. contingency fuel =  $x m_f$ . Consider an aircraft being flown a fixed distance ( $R$ ), once with a standard contingency fuel (of say 5% of the trip fuel) and once with an increased contingency fuel (of say 8%). All aircraft parameters, such as payload, OEW, SFC  $L/D$  ratio, cruise speed, etc., are identical for the two flights. The difference in trip fuel between the two flights is of interest. Let the subscript *old*, designate the initial condition, where the contingency fuel is  $x_{old}$  and the subscript *new*, designate the revised condition, corresponding to an increased contingency fuel of  $x_{new}$ .

Hence:  $m_{2_{new}} = m_{2_{old}} + (x_{new} - x_{old}) m_{f_{new}}$

and:  $\delta m_2 = m_{2_{new}} - m_{2_{old}}$   
 $\delta m_2 = (x_{new} - x_{old}) m_{f_{new}}$

$$\delta m_2 = \delta x m_{f_{new}} \quad \text{--- [I-11]}$$

Recall equation [I-6] and let  $\beta = \frac{R\bar{c}g}{V\bar{E}}$

$$\frac{\partial m_f}{\partial m_2} = e^\beta - 1 \quad \text{--- [I-12]}$$

Substitute [I-11] into [I-12]



$$\text{i.e.} \quad \frac{\partial m_f}{m_{f_{new}}} = \{e^\beta - 1\} \delta x$$

$$\frac{\partial m_f}{m_{fold}} = \{e^\beta - 1\} \delta x \left( \frac{m_{f_{new}}}{m_{fold}} \right)$$

$$\frac{\partial m_f}{m_{fold}} = \{e^\beta - 1\} \delta x \left( \frac{m_{fold} + \delta m_f}{m_{fold}} \right)$$

$$\frac{\partial m_f}{m_{fold}} = \{e^\beta - 1\} \delta x \left( 1 + \frac{\delta m_f}{m_{fold}} \right)$$

$$\text{Finally:} \quad \frac{\partial m_f}{m_{fold}} = \frac{\{e^\beta - 1\} \delta x}{1 - \{e^\beta - 1\} \delta x} \quad \text{where: } \beta = \frac{R\bar{c}g}{VE} \quad \text{--- [I-13]}$$



Blank page



# APPENDIX J

## HLFC SYSTEM INSTALLATION

### TABLE OF CONTENTS

J.1	Introduction.....	318
J.2	Suction System.....	318
J.2.1	Generic suction system layout.....	318
J.2.2	Flow through suction (perforated) panel.....	318
J.2.3	Duct flow analysis.....	320
J.2.4	Orifices, valves and control / monitoring instrumentation.....	321
J.2.5	Pump power analysis.....	321
J.2.6	Suction system analysis for HTP of B757-200 class aircraft.....	322
J.2.7	Estimated power off-take for B757-200 and A330-200 class aircraft.....	323
J.3	Control and Monitoring System.....	327
J.3.1	Control requirement .....	327
J.3.2	Control system concept for HTP of B757-200 class aircraft.....	327
J.4	Anti-contamination System.....	328
J.4.1	System options .....	328
J.4.2	System concept for HTP of B757-200 class aircraft.....	328
J.4.3	Fluid consumption.....	328
J.5	SFC Penalty .....	329
J.5.1	Turbomatch software .....	329
J.5.2	SFC penalty per 100kW shaft power off-take.....	331
J.5.3	Concluding remarks - Turbomatch results .....	332
J.6	System Weight.....	333
J.6.1	Analysis approach.....	333
J.6.2	Mass estimation of HLFC system installed in B757-200 HTP .....	333



## J.1 INTRODUCTION

In this appendix an outline of a generic HLFC suction system is given. The process for analysing flow through the system is outlined and the relevant equations provided to calculate the pump shaft power, as a function of the flow through the suction surfaces. The SFC penalty resulting from the power off-take necessary to drive the pump is explored using the Cranfield University Turbomatch software program. The weight penalty of HLFC system is estimated.

## J.2 SUCTION SYSTEM

### J.2.1 Generic suction system layout

A sketch of a four-chamber, three-section layout is shown in Fig. J-1. The corresponding flow schematic is given in Fig. J-2. The number of chambers (which are aligned in the primary flow direction) depends on the design approach adopted to stabilise the external boundary layer. A typical wing upper surface layout, for example, may have six chambers – one on the leading edge to prevent attachment line contamination, followed by two in the CF and three in the TS regions. In the spanwise direction, the suction system is divided into a number of discrete sections. In Fig. J-2 three connector ducts are shown corresponding to a three spanwise sections. In the case of a wing or empennage, these sections have been called "noseboxes". For a nacelle, it would be typical – as was the case in the HYLDA project – to have four sections corresponding to the four quadrants of the nacelle.

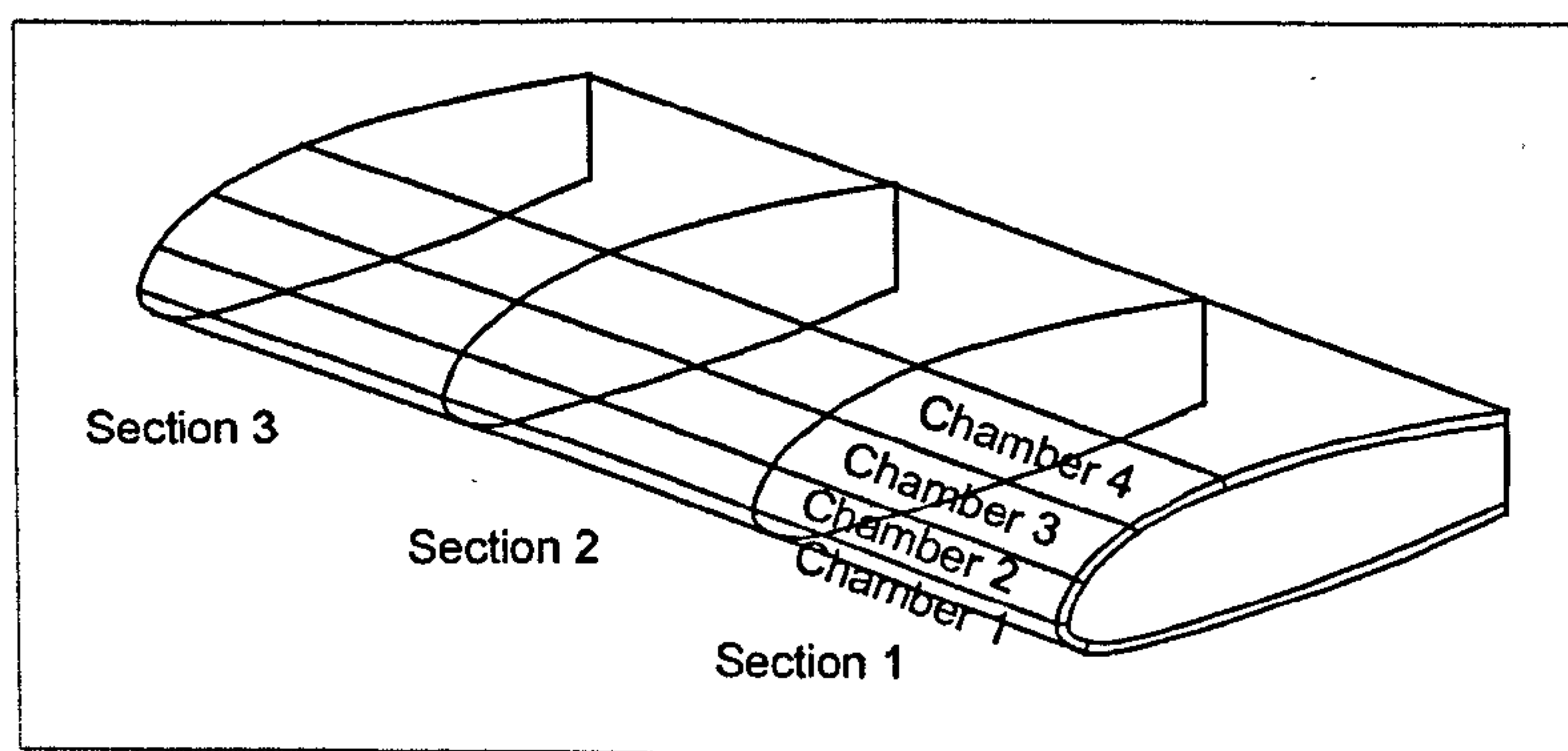


Fig. J-1 Sketch of suction chamber layout for a generic suction system

### J.2.2 Flow through suction (perforated) panel

The governing parameter for the analysis of the suction system is the panel velocity (or the mean velocity of air through the suction surface), which by convention is given the notation  $V_w$ . The panel velocity is the critical design parameter selected to stabilise the external boundary layer flow. Velocities of the order of 0.1 to 0.3 m/s have



been used in the HYLDA and ALTTA projects. The mass flow rate ( $\dot{m}$ ) is given by the equation:

$$\dot{m} = \rho V_w S_{panel} \quad \text{--- [J-1]}$$

where:  $\rho$  is the air density and  $S_{panel}$  is the panel area. The continuity equation – which stipulates that the mass flow into a closed system must equal the mass flow out of the system – may be used to establish flow velocities at flow stations of interest.

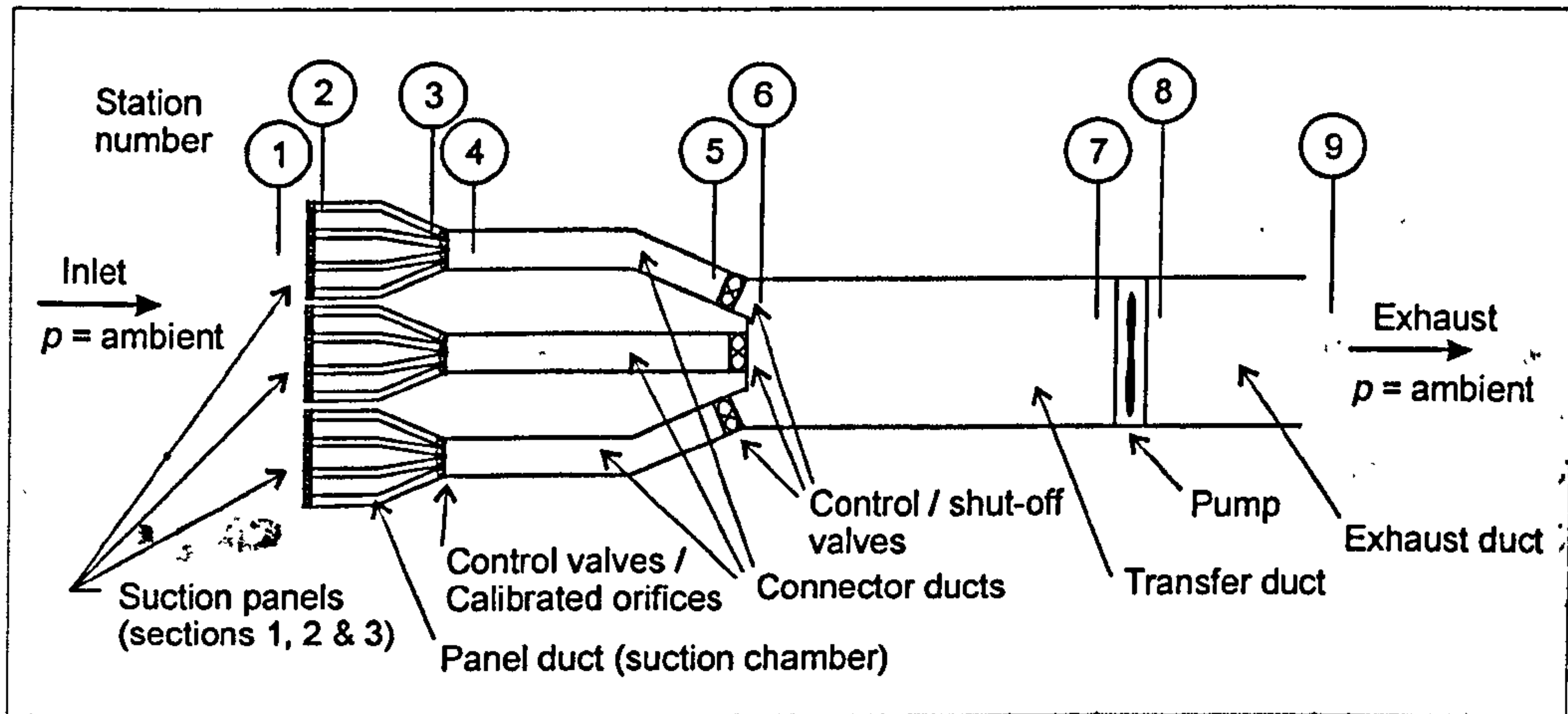


Fig. J-2 Flow schematic of generic suction system

The pressure drop characteristics of flow through HLFC perforated panels are described by Poll *et al.* (1992b) and by Preist and Paluch (1996). The following expression was devised by Preist and Paluch (1996) to represent their experimental data of pressure drop versus hole velocity:

$$\Delta p = K \frac{32\mu L_h}{d^2} V_h + \frac{C}{2} \rho V_h^2 \quad \text{--- [J-2]}$$

where  $L_h$  is the length of the hole (i.e. plate thickness) and  $d$  is the hole diameter (taken as the smaller diameter in the case of a tapering hole). The mean velocity of the flow in the hole ( $V_h$ ) may be approximated by:

$$V_h = \frac{V_w}{\text{Porosity}} \quad \text{--- [J-3]}$$

where the panel porosity is defined by equation [B-1] (Appendix B). The geometric constant  $K$  is given by:

$$K = \frac{1}{4} \left( \frac{d_1}{d_2} \right) \left( 1 + \frac{d_1}{d_2} \right) \left( 1 + \frac{d_1^2}{d_2^2} \right) \quad \text{--- [J-4]}$$

where the hole diameters ( $d_1$  and  $d_2$ ) are defined in Fig. B-14 (Appendix B). The constant  $C$  in equation [J-2] must be determined from experimental data (Preist and



Paluch, 1996). A value of  $C = 1.9$  was shown by McClafferty<sup>1</sup> (2002) to model the measured pressure drop across a "normal" taper (i.e. with the smaller hole diameter on the outside of the panel) titanium sheet; whilst a value of  $C = 1.6$  has previously been used, based on the work of Priest and Paluch at ONERA. The dynamic viscosity of the air ( $\mu$ ) can be computed using the Sutherland equation for a given air temperature ( $T$ ). According to ESDU 77022 (1986) this can be expressed as:

$$\mu = \frac{\beta_s T^{1.5}}{T + S} \quad \text{--- [J-5]}$$

where:  $\beta_s = 1.458 \times 10^{-6} \text{ N s/m}^2 \text{ K}^{0.5}$  and  $S = 110.4 \text{ K}$

The mathematical model given by equation [J-2] describes the pressure losses through the suction surface by a linear friction term and a quadratic dynamic term. It is noted that the friction term is the Hagen-Poiseuille law, multiplied by a hole "geometry" constant. The Hagen-Poiseuille law is strictly only applicable in piping with a constant cross section and fully developed flow (Massey, 1983). The constant  $K$  takes into account the effect of inlet distortion on the flow and the non-uniform cross section, typical of laser drilled holes.

### J.2.3 Duct flow analysis

The pressure ( $p$ ) at the start of the panel duct is the ambient pressure minus the pressure change across the suction panel. With knowledge of the pressure the air density may be determined from the equation of state:

$$\rho = \frac{p}{RT} \quad \text{--- [J-6]}$$

where  $R$  is the gas constant. For a design duct Mach number ( $M_{duct}$ ), the cross sectional area of the duct ( $S_{duct}$ ), can be calculated for the duct mass flow rate ( $\dot{m}$ ), i.e.

$$S_{duct} = \frac{\dot{m}}{\rho M_{duct} \sqrt{\gamma RT}} = \frac{\dot{m}}{\rho V_{duct}} \quad \text{--- [J-7]}$$

A maximum internal flow Mach number of 0.2 was recommended by Möller (2001) to limit frictional losses in the ducts. The frictional losses in the duct are a function of the duct geometry and the flow velocity ( $V_{duct}$ ). The pressure drop along a duct of length  $L_{duct}$  and diameter  $D_{duct}$ , may be determined from the following expression:

$$\Delta p = f \left( \frac{L_{duct}}{D_{duct}} \right) \rho \frac{V_{duct}^2}{2} \quad \text{--- [J-8]}$$

where, according to Miller (1990), the Colebrook-White friction coefficient ( $f$ ), may be approximated by:

---

<sup>1</sup> McClafferty worked with the author at the University of Limerick. See section M.4 (Appendix M).



$$f = \frac{0.25}{\left\{ \log \left( \frac{k}{3.7 D_{duct}} + \frac{5.74}{Re^{0.9}} \right) \right\}^2} \quad \text{--- [J-9]}$$

The parameter  $k$  is a roughness coefficient and the Reynolds number is based on the duct diameter, i.e.

$$Re = \frac{\rho V_{duct} D_{duct}}{\mu} \quad \text{--- [J-10]}$$

The pressure changes along the panel duct (stations 2 to 3, in Fig. J-1), the connector duct (stations 4 to 5), the transfer duct (stations 6 to 7) and the exhaust duct (stations 8 to 9) can be determined by the application of equation [J-8].

#### J.2.4 Orifices, valves and control / monitoring instrumentation

In the analysis of the suction system (which is performed in sequential order from station 1 to station 9) additional pressure drop terms are included to account for the flow through the control valves / orifices (i.e. from stations 3 to 4), control or shut-off valves (i.e. from stations 5 to 6), and through any additional flow monitoring instrumentation in the system. These elements have been seen to have a significant influence on the overall pressure drop.

#### J.2.5 Pump power analysis

Using the notation defined in Fig. J-2, the required pump power, according to Atkin and Courtenay (2002), can be determined using the following expression:

$$P_{pump} = \frac{\dot{m} c_p T_{o7}}{\eta_{pump}} \left\{ \left( \frac{P_{o8}}{P_{o7}} \right)^{\frac{\gamma-1}{\gamma}} \left( 1 + \frac{\gamma-1}{2} M_8^2 \right) - 1 \right\} \quad \text{--- [J-11]}$$

where:  $P_{pump}$  is the pump power,  $\dot{m}$  is the mass flow rate,  $c_p$  is the specific heat capacity at constant pressure,  $\eta_{pump}$  is the overall pump efficiency (representing both mechanical and isentropic efficiencies),  $\gamma$  is the ratio of specific heats and  $M$  is the Mach number. The subscript  $o$  designates a stagnation condition; subscript 7, the pump inlet condition and subscript 8, the pump exhaust condition (as shown in Fig. J-2).

The shaft power is seen to be critically dependent on the pump pressure ratio. The total pressure ahead of the pump ( $p_{o7}$ ) is determined from the sum of the static and dynamic pressures at station 7. This naturally depends on specific system design features, such as the length and diameter of the ducts and the control and monitoring valves / instrumentation installed. The total pressure after the pump ( $p_{o8}$ ) depends on the design of the exhaust. According to Atkin and Courtenay (2002), an exhaust Mach number of 0.2 was recommended during the HYLTEC project, as "providing a good balance between pump drag penalty and additional size and weight". This value was



also selected for the ALTTA fin design (Horstmann *et al.*, 2002). Based on the selected exhaust Mach number, the cross section area of the exhaust can be determined from equation [J-7]. The exhaust velocity can be calculated and hence the total pressure aft of the pump ascertained.

### J.2.6 Suction system analysis for HTP of B757-200 class aircraft

The HTP of the B757-200 class aircraft was selected as a reference design for the assessment of the suction system installation. The dimensions of the suction surfaces were defined in Fig. 7-4 (Chapter 7). Using this as a starting point, a conceptual layout of a suction system was developed, as shown in Fig. J-3. The lengths of the ducts were estimated (Fig. 7-9, Chapter 7). A flow analysis was performed on the concept system, using the equations described in sections J.2.1 to J.2.5, for a cruise altitude of 35000ft. A maximum flow Mach number of 0.20 was selected (as suggested by Möller, 2001) to reduce system pressure losses. This enabled the diameter of the connector and transfer ducts to be estimated. An initial check was performed to ensure that the duct diameter could be contained in the leading edge D-box (see Fig. 7-9 sections AA and BB). Constants and input data for the calculations are given in Table J-1 and the results of the calculations – given in sequential order in which the analysis was conducted – are recorded in Table J-2. The estimated pump power for the HTP (one side) was 17.2kW for a panel velocity of 0.13m/s.

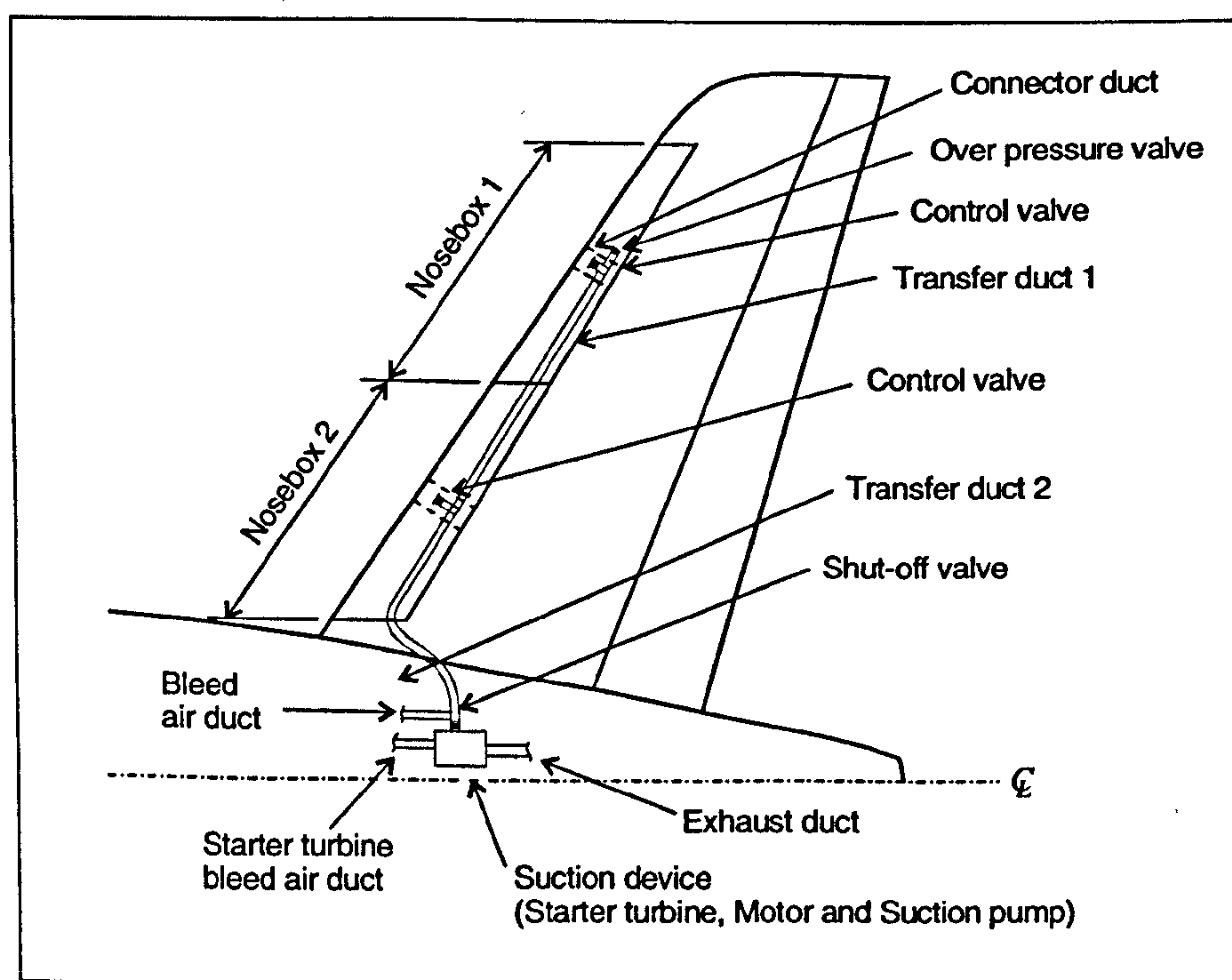


Fig. J-3 Schematic of suction system installation for HTP of B757-200 class aircraft



**Table J-1** Input data for HTP suction system analysis of B757-200 class aircraft

Atmospheric data		Notes / reference
$h$	35000 ft	Height
$T$	218.81 K	Ambient temperature
$\rho$	0.3796 kg/m <sup>3</sup>	Ambient density
$p$	23842 Pa	Ambient pressure
$\mu$	1.4334E-05 Pa s	Dynamic viscosity
Constants		
$g$	9.8067 m/s <sup>2</sup>	Gravitational acceleration
$R$	287.05 m <sup>2</sup> /s <sup>2</sup> K	Gas constant
$\gamma$	1.40	Ratio of specific heats of air
$c_p$	1004.7 m <sup>2</sup> /s <sup>2</sup> K	Specific heat at constant pressure
$\beta_s$	1.458E-06 N s/m <sup>2</sup> K <sup>0.5</sup>	Sutherland coefficient (ESDU 77022)
$S$	110.4 K	Sutherland coefficient (ESDU 77022)
Internal flow data		
Max. duct Mach No.	0.20	Möller (2001)
Mach No. of exhaust	0.20	Atkin and Courtenay (2002)
Compressor efficiency	0.80	Estimate
Electric motor efficiency	0.80	Estimate
Roughness	0.025 mm	Miller (1990)
Suction panel		
Small hole diameter	0.0716 mm	Young <i>et al.</i> (in press)
Large hole diameter	0.1351 mm	Young <i>et al.</i> (in press)
Hole pitch	0.7090 mm	Young <i>et al.</i> (in press)
$C$	1.9	Constant defined in equation [J-2]; data from McClafferty (2002)
Average panel velocity	<del>0.13</del> 1.20 m/s	Estimate

*Errata  
Jin Young*

### J.2.7 Estimated power off-take for B757-200 and A330-200 classes of aircraft

The complete analysis leading to the total power requirement for the HLFC aircraft can only be undertaken with a detailed knowledge of the suction system installation. Equation [J-11] can however, be used for the purpose of conceptual design studies, provided two critical parameters are known, viz. the mass flow and the pump pressure ratio. The other terms in the equation can be established with a satisfactory degree of accuracy. The mass flow can be determined using equation [J-1] based on a design panel velocity ( $V_w$ ) and an estimated panel area ( $S_{panel}$ ).

The pressure ratio across the pump can be estimated from previous studies. For the system designed for the HTP (described in section J.2.6 earlier), it can be seen from Table J-2 that the pump pressure ratio is 1.60. A one-stage radial compressor designed for the simplified ALTTA fin design (see section B.5, Appendix B), facilitated a pressure ratio range of 1.2 to 1.45 (Horstmann *et al.*, 2002). The pressure ratio was calculated to be in the range of 1.3 to 1.4, based on HYLDA nacelle design parameters provided by Möller (2001). However, this value would not be representative of a wing design, where higher upstream losses would be expected in the substantially more complex ducting system. It was assumed that the pressure ratio determined in Table J-



2, would represent an average value for all components (i.e. wing, empennage and nacelle), for both classes of aircraft. The results presented in Table J-3 are based on a panel flow velocity of 0.13 m/s and a pump pressure ratio of 1.60.

**Table J-2** *Summary of results for HTP suction system analysis of B757-200 class aircraft*

Suction panels	Total suction panel area	6.562 m <sup>2</sup>
	Small hole diameter ( $d_1$ )	0.0716 mm
	Large hole diameter ( $d_2$ )	0.1351 mm
	Hole ratio $d_1/d_2$	0.530
	Hole pitch	0.7090 mm
	Porosity	0.00801
	Thickness of panel	0.900 mm
	Panel velocity	0.130 m/s
	Volumetric flow	0.85 m <sup>3</sup> /s
	Mass flow suction panel	0.324 kg/s
	Hole velocity	16.2 m/s
	Constant $C$	1.9
	Constant $K$	0.260
	Panel pressure loss	190.3 Pa
Panel ducts (suction chambers) (12 off)	Mass flow - panel duct	0.027 kg/s
	Pressure - panel duct	23652 Pa
	Density - panel duct	0.377 kg/m <sup>3</sup>
	Volumetric flow rate - panel duct	0.072 m <sup>3</sup> /s
	Design flow velocity - panel duct	59.3 m/s
	Area - panel duct	0.00121 m <sup>2</sup>
	Diameter - panel duct	0.039 m
	Reynolds No. - panel duct	61110
	Roughness value ( $k$ )	2.5E-05 m
	Colebrook-White ( $f$ )	0.02238
	Length - panel duct	3.12 m
	Pressure loss - panel duct	1179 Pa
Connector ducts (2 off)	Mass flow - connector duct	0.162 kg/s
	Pressure - connector duct	22473 Pa
	Density - connector duct	0.358 kg/m <sup>3</sup>
	Volumetric flow - connector duct	0.453 m <sup>3</sup> /s
	Design flow velocity connector	59.3 m/s
	Area - connector duct	0.00763 m <sup>2</sup>
	Diameter - connector duct	0.099 m
	Dynamic pressure ( $q$ )	629.2 Pa
	Reynolds number - connector	145909
	Roughness value ( $k$ )	2.5E-05 m
	Colebrook-White ( $f$ )	0.0182
	Length of - connector duct	0.80 m
	Pressure loss - connector duct	93.1 Pa
Instrument	Pressure loss - sensor and valve	5034 Pa



Table J-2 Continued

Transfer duct number 1	Mass flow - transfer duct	0.162 kg/s
	Pressure - transfer duct	17346 Pa
	Density - transfer duct	0.276 kg/m <sup>3</sup>
	Volumetric flow - transfer duct	0.586 m <sup>3</sup> /s
	Design flow velocity - transfer duct	59.3 m/s
	Area - transfer duct	0.00989 m <sup>2</sup>
	Diameter - transfer duct	0.112 m
	Dynamic pressure - transfer duct	485.7 Pa
	Reynolds number - transfer duct	128189
	Roughness value ( <i>k</i> )	2.5E-05 m
	Colebrook-White ( <i>f</i> )	0.0184
	Length of - transfer duct	3.12 m
	Pressure loss - transfer duct	248.3 Pa
Transfer duct number 2	Mass flow - transfer duct	0.324 kg/s
	Pressure - transfer duct	17097 Pa
	Density - transfer duct	0.272 kg/m <sup>3</sup>
	Volumetric flow - transfer duct	1.190 m <sup>3</sup> /s
	Design flow velocity connector	59.3 m/s
	Area - transfer duct	0.02006 m <sup>2</sup>
	Diameter - transfer duct	0.160 m
	Dynamic pressure <i>q</i>	478.7 Pa
	Reynolds number connector	179984
	Roughness value ( <i>k</i> )	2.5E-05 m
	Colebrook-White ( <i>f</i> )	0.0171
	Length - transfer duct	2.90 m
	Pressure loss - transfer duct	148.4 Pa
Valves, etc.	Pressure loss - valve & junctions	2130 Pa
Pump system	Pressure pump inlet	14819 Pa
	Total pressure pump inlet	15304 Pa
	Mass flow pump	0.324 kg/s
	Pressure exhaust (ambient)	23842 Pa
	Density exhaust duct	0.380 kg/m <sup>3</sup>
	Volumetric flow rate exhaust duct	0.853 m <sup>3</sup> /s
	Design velocity exhaust	59.3 m/s
	Area exhaust duct	0.01438 m <sup>2</sup>
	Diameter exhaust duct	0.1353 m
	Dynamic pressure outlet	667.6 Pa
	Total pressure outlet	24510 Pa
	Differential pressure pump	9205 Pa
	Stagnation temperature	221 K
	Pressure ratio	1.60
	Suction power	10.99 kW
	Compressor efficiency	0.80
	Compressor shaft power	13.74 kW
	Motor efficiency	0.80
	Pump power	17.2 kW



**Table J-3** *Pump power estimation for B757-200 and A330-200 classes of aircraft*

[illegible]



### **J.3 CONTROL AND MONITORING SYSTEM**

#### **J.3.1 Control requirement**

The suction in each chamber must be maintained to within a relatively small margin about a nominal design value, which is not constant, but will vary depending on the atmospheric conditions, Mach number and angle of attack / sideslip. For most experimental work performed to date, this has been accomplished by means of an active control system – consisting of flow monitoring sensors, a computer and motorised control valves. The control system had the capability of adjusting the position of the valves during flight, thus tailoring the flow rates and pressures within the various parts of the system to pre-defined values. By reducing the range of operation of the system (e.g. by restricting the operating height envelope), a simpler design is possible. In this case it may be possible to produce the desired pressure distribution across the individual chambers by a combination of variable porosity and the use of calibrated orifices. In the ALTTA project (described in section B.5.3, Appendix B and in section C.18, Appendix C) this approach has been explored in the design of a HLFC fin for the A320 aircraft.

#### **J.3.2 Control system concept for HTP of B757-200 class aircraft**

The conceptual design of a control system for HTP of the B757-200 class aircraft was developed. This was primarily done for the purposes of estimating the weight of the installed system, and is based on the system layout reflected in Fig. J-3. The architecture of the basic system is shown in Fig. 10-1 (Chapter 10). The pressure within each suction chamber is controlled by an orifice cut in the inner wall of each chamber. The flow rate from the connector duct into the transfer duct will be governed by a control valve. This will receive instructions from a HLFC computer, based on data it receives from flow sensors in the ducts and from the aircraft's Flight Management Computer.

The HLFC computer will also control the start-up sequence. At a pre-defined height, instructions will be sent to open the bleed air duct, engage the starter turbine, and then, after the compressor has reached its normal operating condition, to close the bleed air duct. Purging of the system after water ingestion must also be managed without pilot intervention, again requiring the opening of valves in the bleed air duct and closing the Shut-off Valve (SOV) to the compressor. The status of the HLFC system will be determined and relevant data supplied to the cockpit via the Flight Management Computer.



## **J.4 ANTI-CONTAMINATION SYSTEM**

### **J.4.1 System options**

Details of alternative anti-contamination systems are reviewed in section 9.4, Chapter 9. For the wing the option of a Krüger flap may be preferential to a liquid system. A thermal anti-icing system will make use of the suction chambers to transfer hot air to the wing surface. For the empennage and nacelle, the option of a shield is not available and a liquid / foam system is the only viable solution.

For the purposes of estimating the weight and system reliability of the installed HLFC system, a conceptual design of an anti-contamination system was developed for the HTP of the B757-200 class aircraft. This was based on the foam concept, described in section 9.6, Chapter 9. There is generally no requirement for anti-icing on the HTP and therefore, the system will only have to be designed to cope with insect contamination.

### **J.4.2 System concept for HTP of B757-200 class aircraft**

The architecture of the system and its interface to the HLFC control system, is shown in Fig. 10-1, Chapter 10. The basic concept is to utilise the two leading edge suction chambers (i.e. numbers 3 and 4) on each nosebox to exude foam through the perforated skin. This will run back and protect both upper and lower surfaces. An electric motor and pump will be required to pump the anti-contamination fluid (i.e. a glycol based FPD / water mixture, with an appropriate surfactant added) from a reservoir through a SOV to the two noseboxes. Two foam generators installed in close proximity to the suction chambers will mix bleed air with the liquid. The foam will then pass into the suction chambers.

### **J.4.3 Fluid consumption**

Based on data from the HYLTEC SAAB 2000 flight trails, it was estimated that a flow rate of  $\sim 0.4$  lt/min per  $\text{m}^2$  of frontal area of the suction zone would be required. The SAAB 2000 wing has very little sweep; however the HTP of the B757-200 class aircraft has a leading edge sweep of  $\sim 34^\circ$ . This had to be taken into account in determining the HTP frontal area. The NACA 0009 aerofoil, which was used as a reference profile for the HTP, has a thickness to chord ratio of 8.48% at the 19% chord location (Abbott and von Doenhoff, 1959). The cross-sectional area of the HTP suction zone (i.e. from 22 - 90% of the semi-span, at 19% chord) was determined to be  $2.56\text{m}^2$ . The results of the calculations, which estimated the mass of the fluid, are given in Table J-4.



**Table J-4** *Estimated mass of anti-contamination fluid required for B757-200 HTP*

Parameter	Quantity	Notes
Flow rate	0.40 lt/min/m <sup>2</sup>	Estimate based on SAAB 2000 tests
Frontal area of suction surface*	2.56 m <sup>2</sup>	Based on Fig. 7-4 and NACA0009 aerofoil
Consumption	1.02 lt/min	
System operation per flight	6.0 min	Ref. Humphreys (2002)
Fluid used per flight	12.3 lt	
No. of flights between refills	4	Initial provision for sizing purposes
Density of fluid	1.06 kg/lt	Ref. Humphreys (2002)
Weight of fluid per refill	26.1 kg	For HTP one side

\* Normal to leading edge

## J.5 SFC PENALTY

### J.5.1 Turbomatch software<sup>2</sup>

The two reference engines, the Rolls-Royce RB211-535E4 and the Trent 772, were modelled using the Cranfield University Turbomatch software. The relationship between engine shaft power off-take and SFC increase was assessed, for a range of thrust values that would be typical of those used in the cruise of the B757-200 and A330-200 aircraft. Critical engine data, including takeoff SLS thrust and SFC, bypass ratio, pressure ratio and mass flow (see Tables F-2 and G-3), were used to establish the models. The model input parameters were then revised to get the SFC in cruise to within ~2% of the values established in Appendices F and G, for the two engines. The control (design point) data selected for this study are given in Table J-5.

Once the models had been established, two flight conditions were evaluated for the Trent 772 class engine and one for the RB211 class engine (details in Table J-6). The results for the RB211 class engine are shown in Fig. J-4 (at 35000ft) and for the Trent 772 class engine in Fig. J-5 (for 37000ft). The "bottom of the loop" SFC values correlated reasonably well, to within 1 - 2% of the values used in the performance models, described in Appendices F and G (at the same flight conditions).

The SFC penalty resulting from an increase in the power off-take, depends on the engine type (or specifically on the bypass ratio, overall pressure ratio and mass flow) and the operating conditions (atmospheric conditions, Mach number, thrust and baseline off-take). For a particular engine the effect is seen to depend significantly on the thrust, as shown in Figures J-4 and J-5, which are "cross plots" of thrust and SFC versus TET (Turbine Entry Temperature). Consider for example, the condition where the baseline off-take is 100kW and the net thrust is 27.5kN. For a 400kW increase in power off-take, the TET will have to increase from ~1205K to ~1230K to maintain the same thrust. This will increase the SFC from ~17.6 mg/N/s to ~18.2mg/N/s (a penalty of ~0.8% per 100kW). At higher thrust levels it is seen that the penalty is lower.

<sup>2</sup> It is acknowledged that P. Laskaridis, School of Engineering, Cranfield University, provided assistance in modelling the engines, using the Turbomatch program (Jan. 2002).

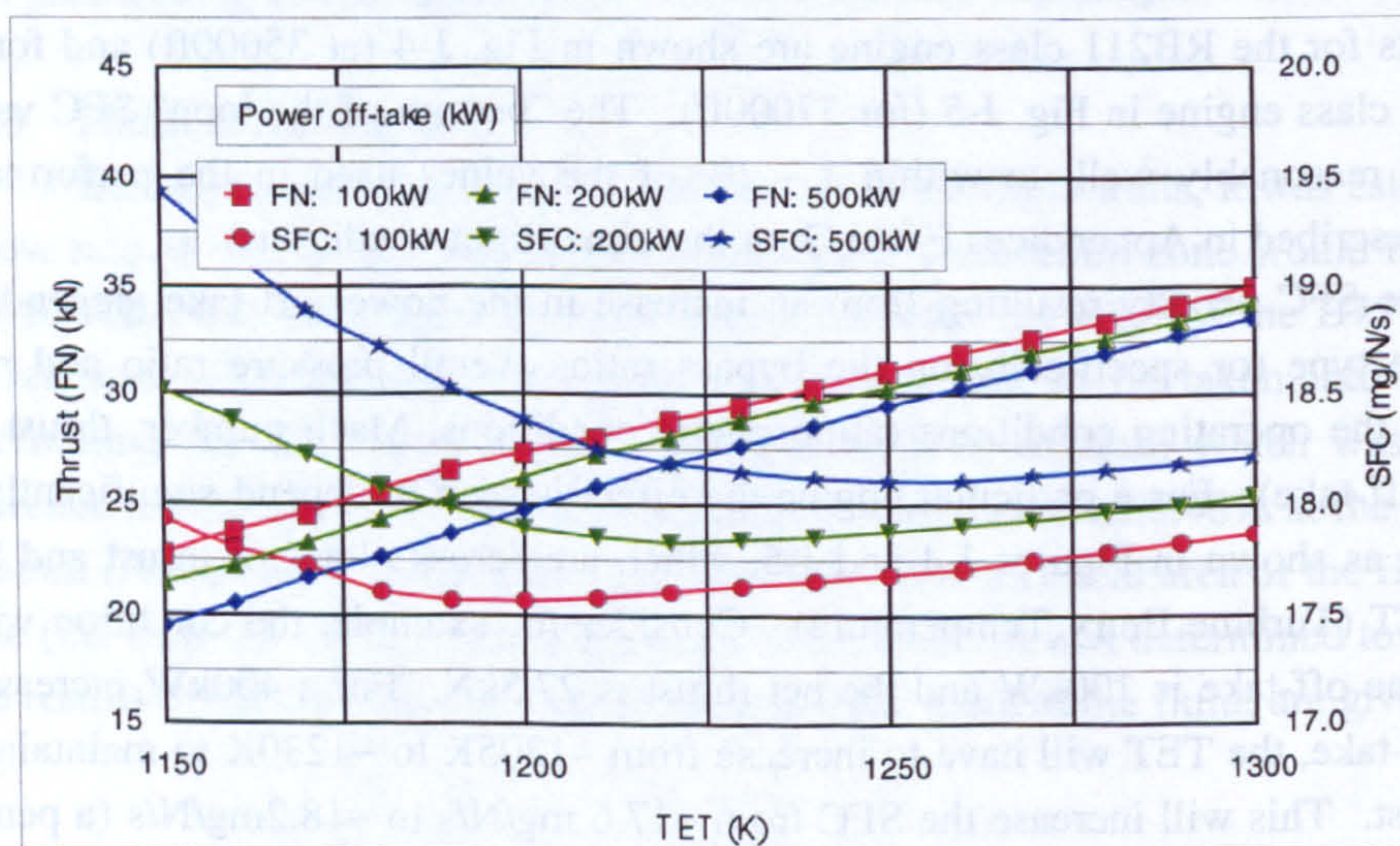


**Table J-5** Control (design) point data for Turbomatch program

	RB211-535E4 class engine	Trent 772 class engine
Fan pressure ratio	1.70	1.80
Inter. Compressor pressure ratio	3.90	4.44
High compressor pressure ratio	3.90	4.49
Overall pressure ratio	25.8	35.5
By-pass ratio	4.3	5.0
Turbine entry temp. (K)	1515	1600
Mass flow (kg/s)	522	919
ISA deviation (K)	14	0
Inlet recovery	0.99	1.0
Altitude (m)	0	0
Mach No.	0	0
Thrust (kN)	171	317
SFC (mg/N/s)	10.6	9.81
Bleed air (kg/s)	0	0
Shaft power off-take (kW)	0	0

**Table J-6** Input conditions / parameters used to assess the SFC penalty

	RB211-535E4 class engine	Trent 772 class engine	Trent 772 class engine
Mach	0.80	0.80	0.80
Height	35000ft	37000ft	41000ft
Thrust range	22 - 36kN	32 - 56kN	32 - 56kN
Bleed air off-take	0.25kg/s	1.13kg/s	1.13kg/s
Baseline power off-take	100kW	200kW	200kW

**Fig. J-4** Thrust and SFC variation against TET for RB-211 class engine with varying levels of power off-take (Conditions: 35000ft, M0.80, bleed air 0.25kg/s)



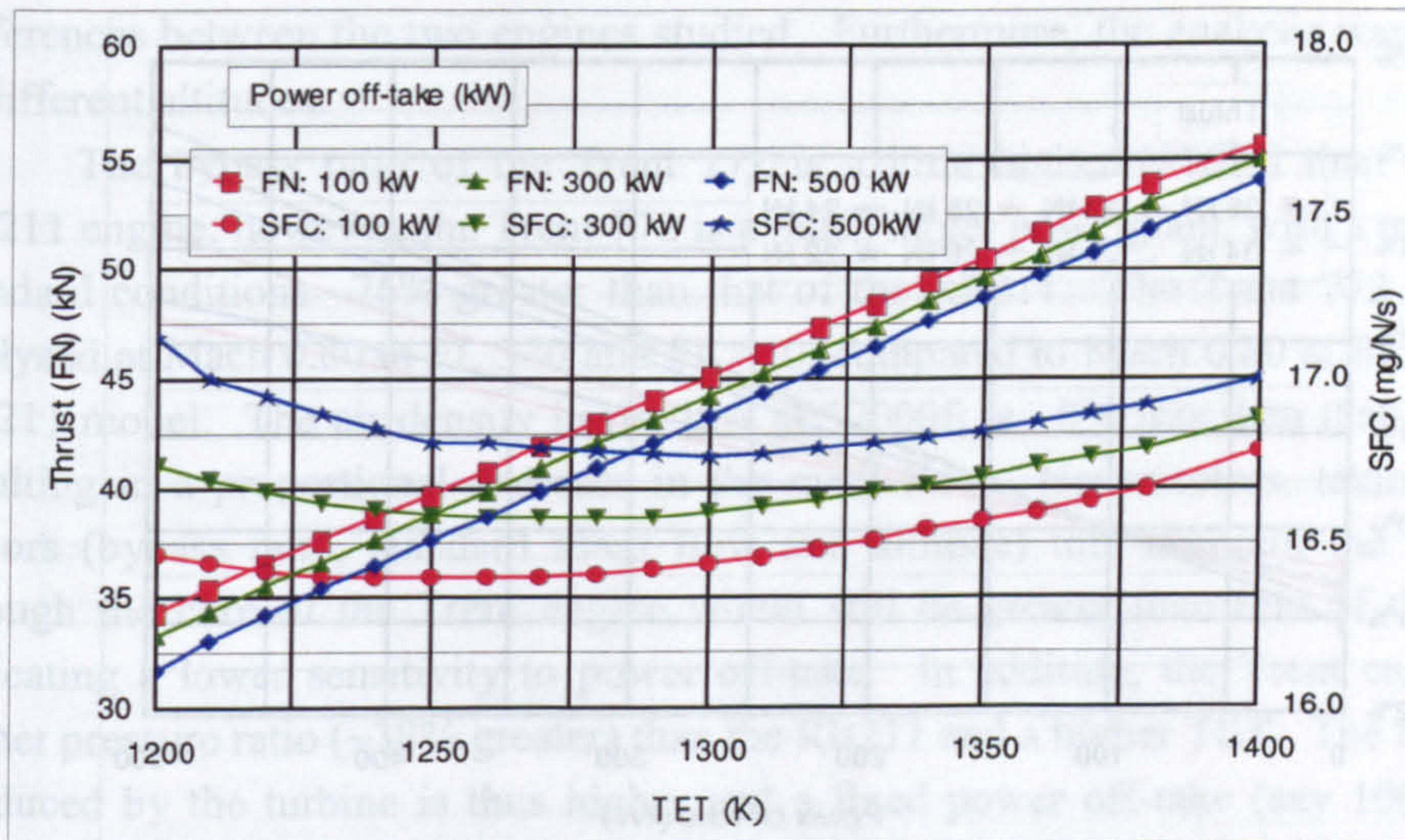


**Fig. J-5** Thrust and SFC variation against TET for Trent 772 class engine with varying levels of power off-take (Condition: 37000ft, M0.80, bleed air 1.13 kg/s)

### J.5.2 SFC penalty per 100kW shaft power off-take

For an assessment of the impact of HLFC, it was convenient to express the SFC increase relative to a unit increase in power off-take (taken as 100kW). The baseline condition was selected as 100kW off-take for the B757 and 200kW for the A330; and the impact of further increases, in steps of 100kW, was ascertained. The results are given in Figures J-6 and J-7. They indicate that the SFC change is linear beyond the baseline point (i.e. 200kW additional off-take results in twice the SFC change as 100kW; and 300kW, three times the 100kW change, etc.).

It is evident that the SFC penalty decreases with increasing engine thrust. To explore this further, the SFC penalty per 100kW was determined for the two engines. The results are included as Fig. 7-7 and Fig. 7-8 (Chapter 7) for the RB-211 class engine and Trent 772 class engines, respectively. It is seen that the SFC penalty decreases with increasing engine thrust and that the altitude change (37000 to 41000ft for the Trent 772 model) had only a minor influence on the SFC penalty. The mid-cruise thrust corresponded to a SFC penalty of ~0.72% per 100kW for the B757-200 class aircraft and a mean SFC penalty of 0.53% per 100kW was estimated for the A330-200 class aircraft.



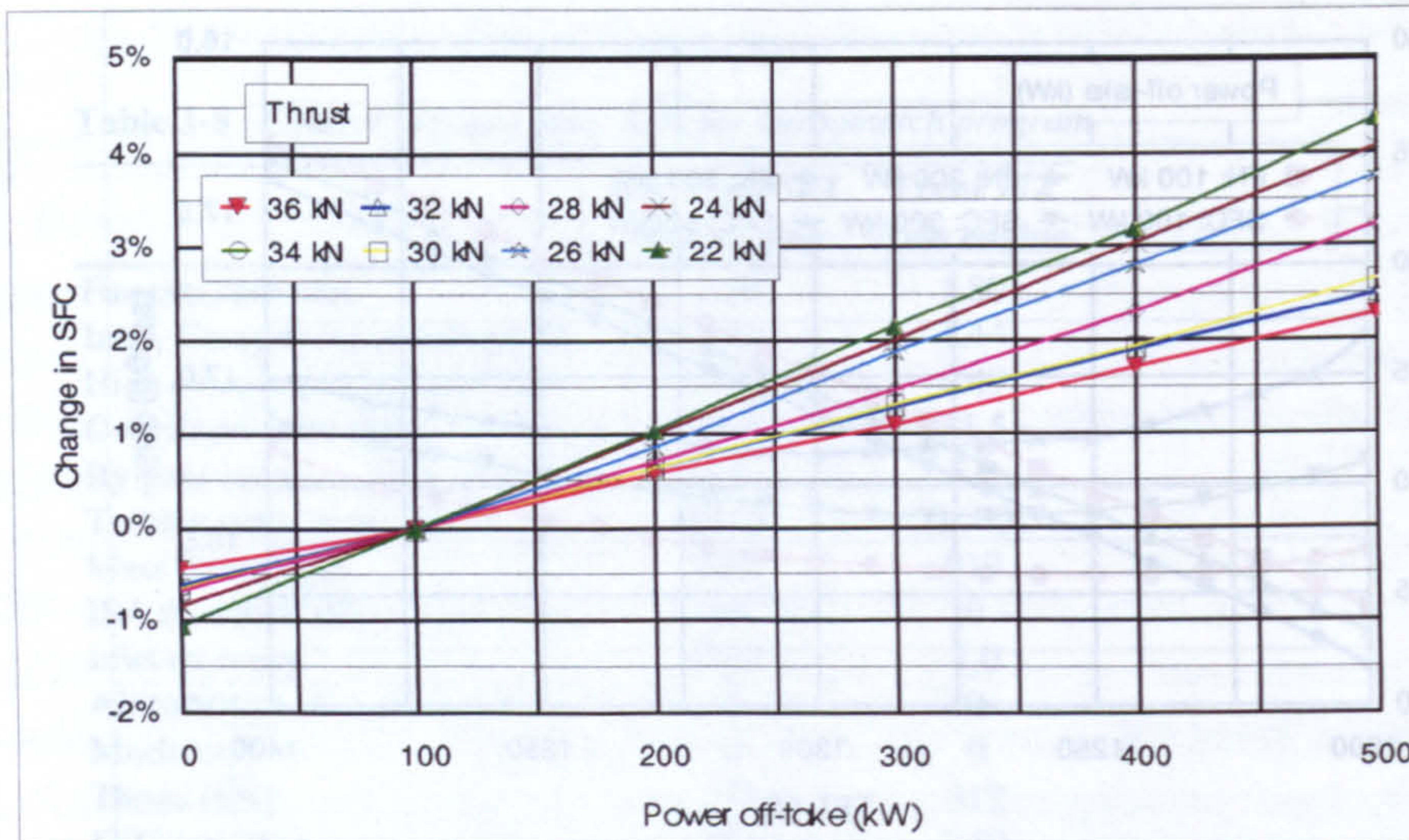


**Fig. J-6** SFC penalty versus power off-take for RB211-535E4 class engine (35000ft, M0.8, bleed air 0.25kg/s, baseline power off-take 100kW)

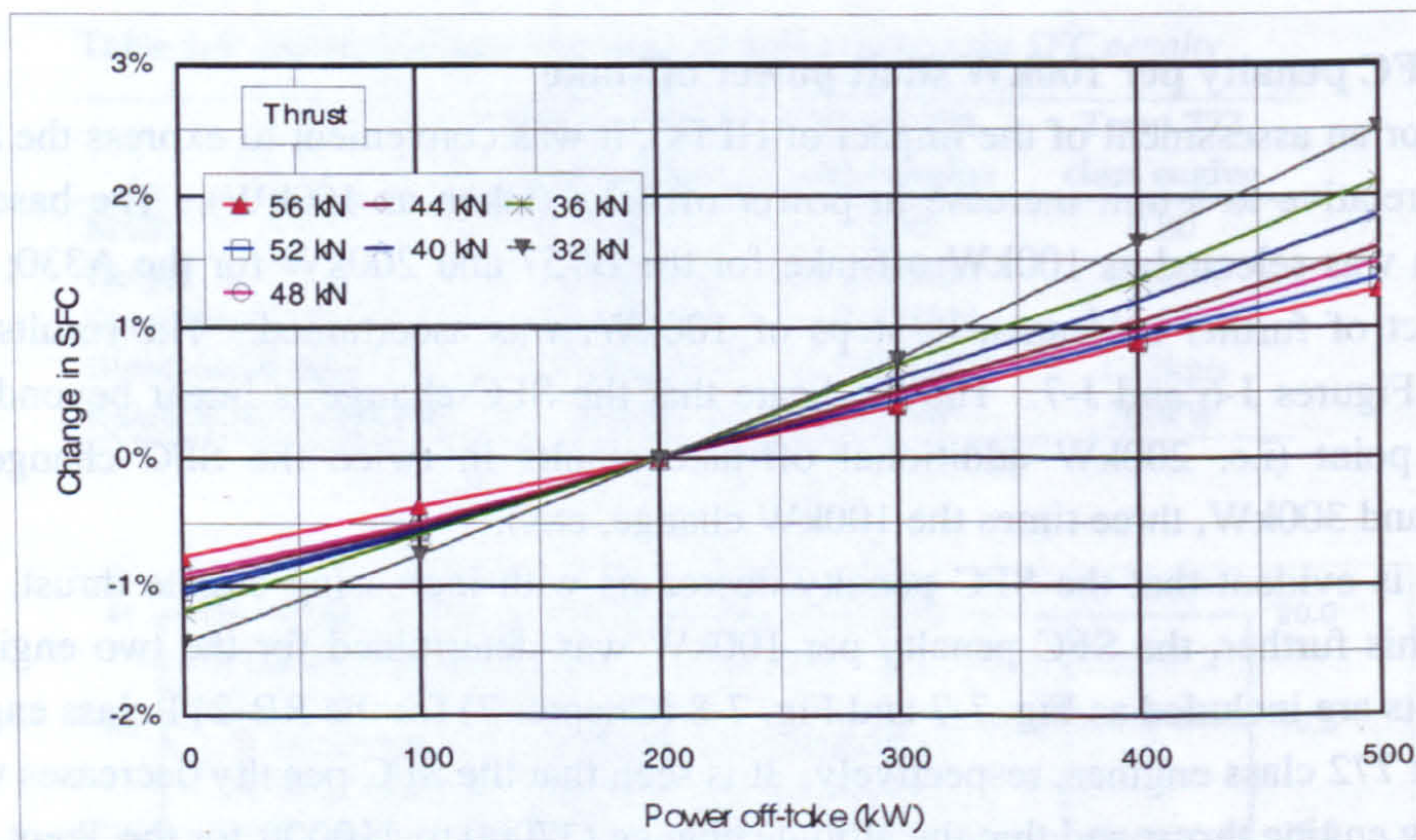


**Fig. J-7** SFC penalty versus power off-take for Trent 772 class engine (37000ft, M0.8, bleed off-take 1.13 kg/s, baseline power off-take 200kW)

### J.5.3 Concluding remarks - Turbomatch results

The Trent 772 class engine is less affected than the RB211 class engine, as measured by the percentage SFC change per 100kW power off-take. This observation cannot be attributed solely to the fact that the Trent is a larger engine. The effect of an off-take (shaft power in this case) on the engine efficiency (as measured by the SFC) is a function of the engine thrust, the operating conditions (Mach number, altitude) and the engine design parameters (bypass ratio, pressure ratio, etc.). In assessing the results presented above, it should be noted that there are a number of significant design



differences between the two engines studied. Furthermore, the analysis was performed at different altitudes.

The bypass ratio of the Trent 772 is a little higher (~16%) than that of the RB211 engine; however, the Trent 772 is a much larger powerplant, with a mass flow at standard conditions ~76% greater than that of the RB211. The Trent 772 model was analyzed at Mach 0.80 at FL 370 and FL 410, compared to Mach 0.80 at FL350 for the RB211 model. The air density in the ISA at 37000ft is ~8% less than that at 35000ft, resulting in a proportional decrease in the mass flow. Nevertheless, taking all three factors (bypass ratio, standard mass flow and altitude) into account, the mass flow through the core of the Trent engine would still be greater than that of the RB211, indicating a lower sensitivity to power off-take. In addition, the Trent engine has a higher pressure ratio (~38% greater) than the RB211 and a higher TET. The total power produced by the turbine is thus higher and a fixed power off-take (say 100kW), will constitute a lower percentage of the total power produced by the turbine, resulting in a lower SFC change.

## **J.6 SYSTEM WEIGHT**

### **J.6.1 Analysis approach**

The HTP of the B757-200 class aircraft has been used as a reference design for the system mass estimation. The mass of the installed HLFC system in the HTP was estimated based on the system definition outlined in section J.2.6 and illustrated in Fig. 7-9 (Chapter 7). The resulting mass value was then divided by the pump shaft power for the HTP and the ratio used to estimate the installed mass of the HLFC system for the wing, fin and nacelle. It is recognized that distinct differences will exist in the detail design of each of these components, especially with regard to the engine nacelle. Nevertheless it was felt that the approach would provide a reasonable estimate on an overall basis for the aircraft.

### **J.6.2 Mass estimation of HLFC system installed in B757-200 HTP**

Mass estimates for the individual components were established under four headings or mass groups, i.e. (1) Suction surface, ducts and valves; (2) Control and monitoring system; (3) Pump system and power generation; and (4) Anti-contamination system. It was necessary to make a number of assumptions regarding the system installation to complete the estimate. It was assumed that the suction surface, suction chambers, connector and transfer ducts, were manufactured from titanium and the wall thickness estimated. The density of titanium was taken as  $4.5\text{g/cm}^3$ , and for aluminium, it was  $2.78\text{ g/cm}^3$  (MatWeb, 2002). The diameters of the ducts had been determined as part of the flow analysis (Table J-2). This yielded an estimate of 24kg for the mass of these items, as shown in Table J-7. This value was carried forward to Table







**Table J-8** Mass estimation of HLFC system in HTP (one side) of B757-200 class aircraft

<b>(1) Suction surface, ducts, valves</b>		
Suction surface & ducting	23.7	kg
SOV (160 mm)	2.0	kg
OPV (112 mm)	1.5	kg
SOV for anti-contamination (4 off)	3.0	kg
Filter	0.5	kg
PRSOV (bleed air) (2 off)	4.0	kg
<b>Subtotal</b>	<b>34.7</b>	<b>kg</b>
Installation factor	1.10	
<b>Subtotal (installed)</b>	<b>38.1</b>	<b>kg</b>
Ratio of mass / power	2.23	kg / kW
<b>(2) Control &amp; monitoring system</b>		
Control valves & drives(2 off)	4.0	kg
Flow sensor (2 off)	2.0	kg
HLFC computer	5.0	kg
Wiring	5.0	kg
<b>Subtotal</b>	<b>16.0</b>	<b>kg</b>
Installation factor	1.15	
<b>Subtotal (installed)</b>	<b>18.4</b>	<b>kg</b>
Ratio of mass / power	1.07	kg / kW
<b>(3) Pump system &amp; Power supply</b>		
Compressor	10.0	kg
Electric motor	12.8	kg
Starter turbine	4.7	kg
Wiring harness	6.0	kg
Power generation (pro-rata provision)	9.0	kg
<b>Subtotal</b>	<b>42.6</b>	<b>kg</b>
Installation factor	1.15	
<b>Subtotal (installed)</b>	<b>49.0</b>	<b>kg</b>
Ratio of mass / power	2.86	kg / kW
<b>(4) Anti-contamination system</b>		
Reservoir	2.5	kg
Pump & motor	2.0	kg
Foam generator (2 off)	0.8	kg
SOV (2 off)	0.7	kg
PRSOV (bleed air)	1.5	kg
Ducting	3.0	kg
Anti-contamination fluid	26.1	kg
<b>Subtotal</b>	<b>36.6</b>	<b>kg</b>
Installation factor	1.15	
<b>Subtotal (installed)</b>	<b>42.0</b>	<b>kg</b>
Ratio of mass / power	2.45	kg / kW
<b>Total for HTP</b>		
Total installed mass	148	kg
Overall ratio of mass / power	8.61	kg / kW

Note: Suction power for one side = 17.1 kW



Blank page



# APPENDIX K

## CIRRUS CLOUDS

### TABLE OF CONTENTS

K.1	Introduction.....	338
K.2	Overview.....	338
K.2.1.	High level cloud types.....	338
K.2.2	Ice crystals.....	338
K.2.3	Current research thrust .....	339
K.2.4	Airborne observations .....	340
K.2.5	Instrumentation for airborne observations.....	341
K.2.6	Satellite and Space Shuttle observations .....	341
K.2.7	Average cloud amount.....	342
K.2.8	Subvisual cirrus .....	343
K.3	Jetstar Simulated Airline Service Flights.....	343
K.4	Global Atmospheric Sampling Program (GASP) .....	345
K.4.1	Data acquisition.....	345
K.4.2	Cloud climatology .....	345
K.4.3	Route data analysis.....	347
K.4.4	Frequency distribution based on GASP.....	348



## K.1 INTRODUCTION

In this appendix a review of cirrus cloud data is presented in support of the material given in Chapter 8. An overview of naturally occurring high-level cloud types that will impact laminar flow is presented, followed by a brief description of the research efforts concerning cirrus cloud physics. (Contrail formation is described in sections 8.3.7, Chapter 8 and in A.3.2, Appendix A.) Further details regarding the NASA Global Atmospheric Sampling Program (GASP) – that was used to establish the probability model of cloud encounters – is presented.

## K.2 OVERVIEW

### K.2.1. High level cloud types

Clouds are a visible aggregate of minute particles of water and / or ice in the atmosphere. *High level* clouds from an aviation perspective are clouds that have a base above 20000ft (Thom, 1997). This is also the height threshold above which it is likely that HLFC systems will be designed to operate. In this cold air clouds are largely composed of ice crystals, white in colour and from the ground tend to have a fine "texture". The appearance of cirrus, cirrocumulus and cirrostratus cloud types, found at these heights, is described by Thom (1997). Cirrus (Ci) are high altitude, detached clouds in the form of wispy filaments and narrow bands of fibrous appearance; cirrocumulus (Cc) are high altitude sheets of lumpy (cumulus) cloud, with grain or ripples more or less regularly arranged; cirrostratus (Cs) form a transparent veil that can partially or totally cover the sky, producing a halo around the sun or moon.

Although the base of cumulonimbus (Cb) clouds is typically only a few thousand feet, the tops can extend as high as the tropopause, reaching heights of 45000 to 55000ft in the tropics. The top of a mature cumulonimbus cloud tends to spread out in an anvil shape, in the direction of the upper winds. These cirrus outflows from cumulonimbus clouds can have extensive lateral and vertical developments, unlike the cirrus clouds that typify the mid-latitudes.

### K.2.2 Ice crystals

Cirrus clouds, unlike warm water clouds consisting of spherical liquid droplets, are composed almost entirely of non-spherical ice crystals of various sizes and shapes (as described by Hobbs, 1974; Mitchell, 1994; Wyser and Yang, 1998; and Lynch *et al.* 2002; for example). Cirrus clouds develop in the stable stratified air of the upper troposphere, with the crystals growing by vapour diffusion and aggregation. Fig. K-1 illustrates six principal crystal habits (characteristic forms) found in cirrus clouds. Based on the results of a large number of test observations (extensively reported by other researchers), Wyser and Yang (1998) noted that the predominant crystal habit in cirrus clouds are bullet rosettes, solid and hollow columns, plates and aggregates.



Numerous other forms and permutations of the basic shapes occur, as explained by Hobbs (1974). The relationship between the dimensions of the planar surfaces of a column crystal and the length of the column, vary considerably. Hollow structures of varying depth form at the ends of columns. Commonly found are aggregate ice crystals, which are formed by an arbitrary number of hexagonal elements of varying size and length. The bullet rosette can have a number of branches orientated three-dimensionally. It is evident that analysis performed by Hall (as described in section 8.2.2, Chapter 8), whereby he assumed that ice crystals were columnar in shape, is a simplification of the actual situation.

The size distributions of ice crystals have been observed in various field campaigns. The smallest crystals occur in the greatest numbers and the concentration tends to drop off with increasing crystal size. Wyser and Yang (1998) and Lynch *et al.* (2002), describe various mathematical attempts to model these distributions using alternative formulations (e.g. power-law, exponential, gamma and bi-modal). A common problem in modelling the crystal distribution is the difficulty in defining a simple size measure for the various and complex geometries. It is common practice to use the maximum dimension of the ice crystal as a characteristic measurement.

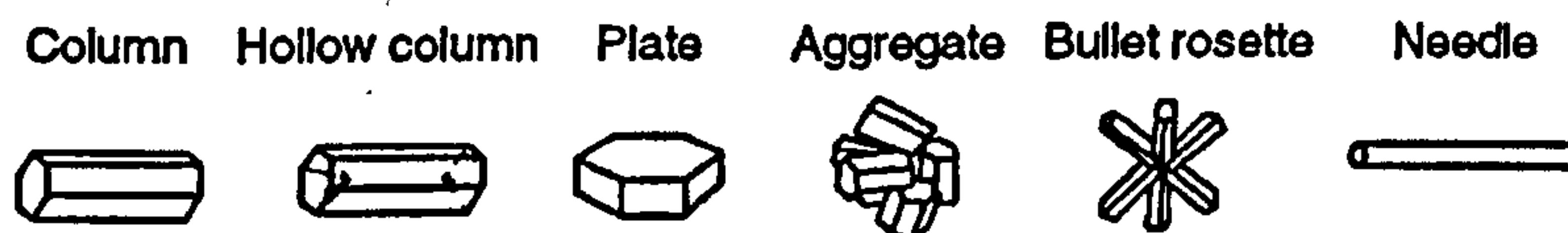


Fig. K-1 *Principal crystal habits (Wyser and Yang, 1998)*

### K.2.3 Current research thrust

Much of the current research into the nature of cirrus clouds is due to their role in the earth's radiation balance; research reported by Heymsfield and Platt (1984), London *et al.* (1991), Mitchell (1994), Khain *et al.* (2000) and Sprang *et al.* (2001), for example. The radiative property of cirrus clouds, which cover extensive regions of the earth at any one time, is recognised as having a significant climatological influence (see section A.3.1, Appendix A). Global numerical models of the earth's climate have indicated that the fraction of the incoming solar energy reflected (albedos) by cirrus is an important parameter; and for this reason the characterisation of the size, shape and concentration of ice crystals and their reflective properties, has generated considerable research interest. Notwithstanding this fact, Mitchell (1994) maintained that cirrus clouds are "probably the least understood cloud type in terms of their microphysics and life cycle". Wyser and Yang (1998) wrote: "The impact of these clouds on the climate and weather systems of various scales is far from being well-understood". In particular, tropical cirrus – generated by either deep convection (anvil clouds associated with thunderstorms) or by large-scale lifting – remain poorly understood, because of limited sampling data. These clouds, which may extend to 55000ft, are relatively inaccessible



by aircraft, because of the high altitude and geographical remoteness. Furthermore, because of the height at which they form, the particle sizes are often too small or irregular in size to be counted and sized accurately with optical instruments (Heymsfield and McFarquhar, 1996). Observations and experimental data are obtained from instrumentation mounted on: (1) Aircraft and balloons, (2) Spacecraft and (3) Ground based stations.

#### K.2.4 Airborne observations

Airborne observations of ice crystals taken *in situ* by aircraft flying through high altitude clouds date back more than 60 years. Flights using a Mosquito aeroplane were made in the UK, whilst in Germany a Henschel was used during World War II (Parungo, 1995). More recently, measurements have been made using a variety of aircraft, including the UK Meteorological Research Flight C-130 (Field, 1999), University of Washington B-23 (Hobbs and Rango, 1985), King Air (Sassen, 1991a), Learjet (Heymsfield and McFarquhar, 1996) and NASA's ER-2 and DC-8 aircraft (Heymsfield *et al.*, 1998).

For the purpose of studying the evolution of cloud particles, the aircraft needs to track a population of ice crystals. This can be achieved by the aircraft flying a spiral flight path in the cloud, drifting with the wind and descending at a rate close to the average ice crystal fall speed (Field, 1999). Although important in the study of cloud physics, such experimental work produces little information about the probability of aircraft flying through clouds on typical airline routes, which is required for the assessment of the impact of clouds on HLFC aircraft.

Commercial jet aircraft have been used since the 1960s to obtain data on the atmosphere whilst on routine service. These projects include: the Troposphärisches Ozon (TROZ) project conducted from 1970 - 1974 (Fabian and Pruchniewicz, 1977), Global Atmospheric Sampling Program (GASP), from 1973 - 1979 (described in section K.4) and MOZAIC (Measurement of Ozone on Airbus In-Service Aircraft) from 1993 - 1996, 1996 -1999 and 2000 -2003 (Marenco *et al.*, 1998; CORDIS, 2001). For these projects automatic units were installed for measuring atmospheric properties, such as  $O_3$ ,  $H_2O$ ,  $CO_2$ ,  $NO_x$  and  $C_2Cl_4$ . Since 1992, the CEC has supported a number of projects to assess the impact of aircraft emissions (CORDIS, 2001). These include: POLINAT (Pollution from Aircraft Emissions in the North Atlantic Corridor), from 1994 - 1996 and 1996 -1997; STREAM (from 1996 - 1997); AEROCONTRAIL (from 1996 - 1997) and AEROCHEM (from 1996 - 1997). From measurements of water vapour a substantial database has been established regarding the cloud climatology at flight levels associated with commercial aircraft traffic. Direct measurements of cirrus particles were not made, except in the case of the GASP. This database provides a unique insight into the distribution of cirrus particles in clouds along airline routes – precisely what is required to evaluate the impact of a loss of laminar flow of HLFC aircraft flying these routes.



### K.2.5 Instrumentation for airborne observations

Parungo (1995) reports on the earliest replication technique for ice crystals. Oil-coated slides were exposed to the air-stream during flight; these were allowed to dry, permitting images of the crystals to be seen by optical microscope after the flight. This technique is still used. Field (1999) provided a description of modern instrumentation as used on the UK Meteorological Research Flight C-130. The first was a PMS (Particle Measuring System) probe for particles in the size range 25 - 800  $\mu\text{m}$  and the second was a High Volume Precipitation Spectrometer (HVPS) for low concentrations of large particles. For both probes, the particles are "binned", according to an average particle diameter, calculated by taking a mean of the along-track and across-track maximum dimensions.

Of direct importance to the assessment of HLFC operations, are the X-21A and Jetstar flight experiments. Fowell and Antonatos (1965) described the continuous particle sampling apparatus used on the X-21A, which made replicas of the ice crystals on strips of resin coated plastic film. After heating, to drive off solvents, an optical system was used to size the particle imprints on the film. Davis *et al.* (1986; 1987) reported that two instruments were installed on the Jetstar for measuring the ambient free-stream particle environment. These were a cloud particle spectrometer (Knollenberg probe) and a charging patch, described as a "particle detector based on a triboelectric (frictional) charge-exchange principle". The spectrometer contained an optical system that imaged the particles passing through a laser beam enabling a measure of the particle size to be obtained to a resolution of 20 $\mu\text{m}$ , for particles greater than 60 $\mu\text{m}$ . The charging patch determined the number of individual impacts, by the level of charging current measured on the electrically isolated "patch". It was possible to identify smaller particles than was the case with the spectrometer.

### K.2.6 Satellite and Space Shuttle observations

Both shortwave (SW) and longwave (LW) measurements by satellite-borne instrumentation provide data on the radiance of cirrus, from which their optical thickness can be ascertained. The characterisation of clouds as part of the International Satellite Cloud Climatology Project (ISCCP) according to their optical thickness, is described by Heymsfield *et al.*, 1998. Optically thin clouds, which could potentially affect HLFC aircraft (see section K.2.8), cannot be accurately measured with these instruments. Research data on optically thin clouds has been acquired using the solar occultation technique<sup>1</sup> by the SAGE (Stratospheric Aerosol and Gas Experiment) II sensor on board the ERB (Earth's Radiation Budget) satellite (Wang *et al.*, 1996; 1998). Extensive cloud observations in the vicinity of the tropopause were obtained using CRISTA (Cryogenic Infrared Spectrometers and Telescopes for the Atmosphere) which

---

<sup>1</sup> Solar occultation: Technique used to monitor atmosphere as the instrument emerges from the dark side of the orbit (spacecraft sunrise) and then again when it re-enters the dark side (spacecraft sunset).



was flown on the NASA Space Shuttle in 1994 and 1997. This was a limb-scanning<sup>2</sup> instrument, which measured the thermal emission of trace gases, from which specific cloud features could be deduced (Sprang *et al.*, 2001).

### K.2.7 Average cloud amount

A substantial database exists on cloud coverage. Of interest to the work herein reported, are global trends in cloud amount (in particular high altitude clouds), as this affects the viability of HLFC. A study conducted by Angell *et al.*, (1984) concluded that there was a 3.7% increase in cloudiness over the contiguous United States, during the 33-year interval from 1950 to 1982, based on US Weather Service data.

Ship observations of cloud provide an excellent database for studying long term trends in global cloudiness. The Comprehensive Ocean Atmospheric Data set (COADS) has been used by researchers for this purpose. London *et al.* (1991) considered a subset of the data (for the tropical oceans) and concluded that cirrus (including cirrocumulus and cirrostratus) increased over the 30-year period from 1952 to 1981; but that cumulus (Cu) or stratus (St) cloud types decreased, or remained nearly constant.

From the same data set Parungo *et al.* (1993) determined annual mean oceanic cirrus cloud amounts for the period 1950 to 1981. An increase in cirrus was noted, and the rate of increase for the Northern Hemisphere was seen to be greater than for the Southern Hemisphere. This suggested possible anthropogenic causes. Parungo (1995) summarised the results from this study (Fig. K-2). Three general patterns were identified: (a) from 1951 - 1962, no discernible changes; (b) from 1962 - 1967, a negative trend; and (c) from 1967 - 1981, a positive trend. Parungo (1995) stated that the causes of these changes are uncertain, and discussed the results: "They may be natural variations, or anthropogenic effects or combinations of both. In searches of historical events, natural causes such as volcanic eruptions have not shown any systematic trends. However, human activities have augmented air pollution ever since the industrial revolution. In the past half century two specific activities that can deliver pollutants into the free troposphere and beyond, are nuclear bomb testing and high altitude jet travel. Both have the potential to alter cirrus cloud amount."

From Fig. K-2, it is seen that the greatest increase occurred in the Northern Hemisphere from 1967 - 1981. Parungo (1995) calculated this to be 2.0% for the Northern Hemisphere and 0.8% for the Southern Hemisphere, over the 14-year interval. A simple average of the two values indicates that the rate of increase of cirrus for the globe was of the order of 1% per decade.

---

<sup>2</sup> Limb-scanning: A view taken obliquely from a point in space through the atmosphere.



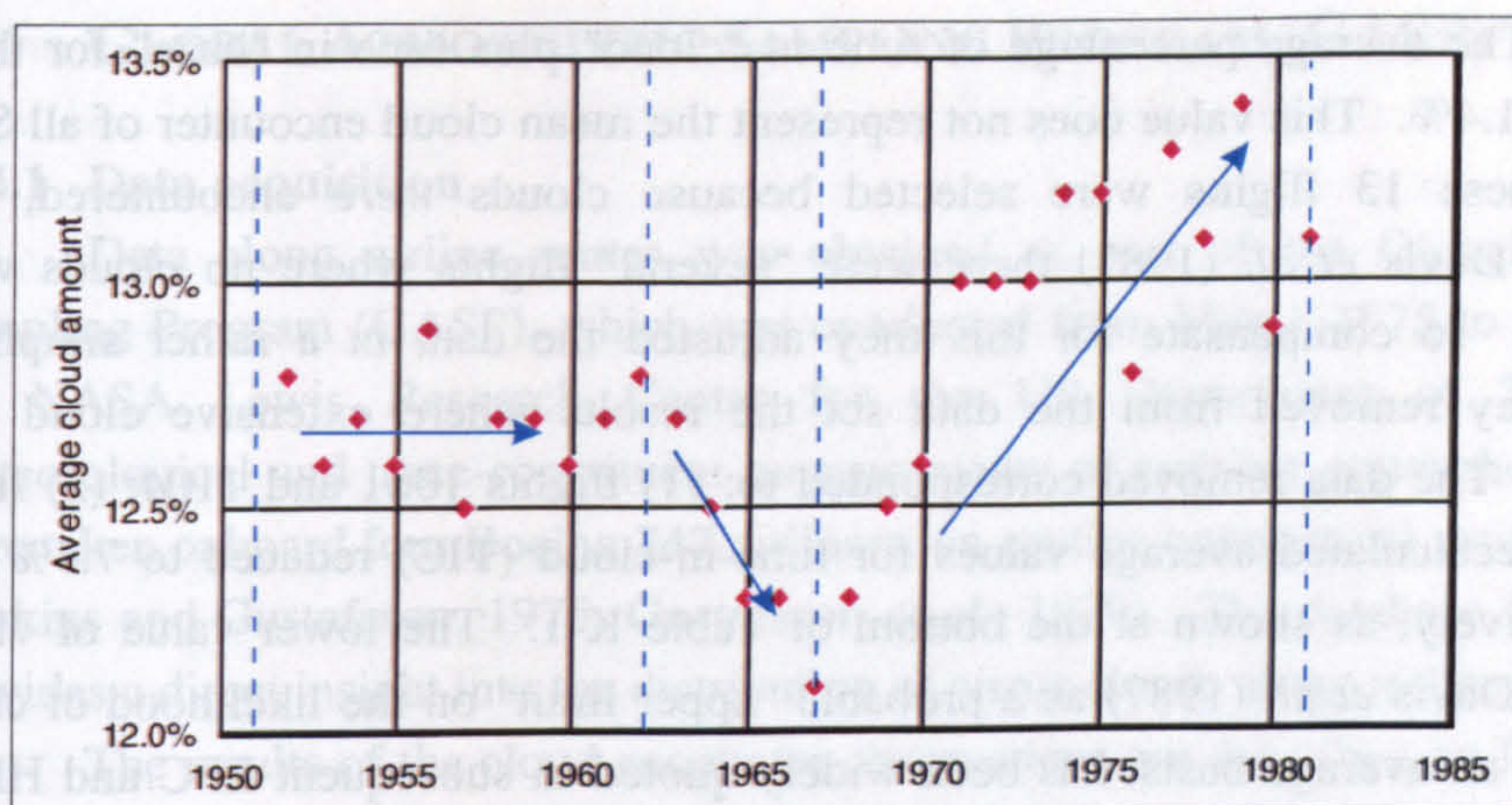


**Fig. K-2** Annual mean oceanic cirrus cloud trends between 1950 and 1981 for the globe (adapted from Parungo, 1995)

### K.2.8 Subvisual cirrus

Not all cirrus clouds are detectable to the naked eye. Pilot reports dating back to before World War II indicate the presence of clouds that could not be seen from the ground. Subvisual cirrus clouds (SVC) are described by Lynch *et al.* (2002), as being widespread, but virtually undetectable with existing passive sensors. The reason for this is that SVC have a low contrast at most solar-scattering angles. Orbiting solar limb occultation systems (such as that installed on SAGE) can detect these clouds, but only by looking at them horizontally, where the optical depths are significant.

SVC are usually found near the tropopause and are less than about 1000m thick vertically. They are reported to be not fundamentally different from ordinary, optically thicker cirrus; however, they do differ from average cirrus, by being colder and having smaller particles. Heymsfield (1986) investigated the composition of SVC based on high altitude aircraft studies. SVC particles were observed to be 1 - 50 $\mu$ m in diameter. Using passive remote sensing analysis of corona displays, particle diameters of 10 - 30 $\mu$ m were derived by Sassen (1991b). Based on the results of Hall (1964), it would appear that the particle sizes of SVC would be largely below that which would destroy laminar flow. However, partial degradation of laminar flow due to SVC (which, to the pilot would appear as a horizontal band of light haze), cannot be discounted.

## K.3 JETSTAR SIMULATED AIRLINE SERVICE FLIGHTS

During the NASA Jetstar LEFT programme (see section C.4, Appendix C), the Jetstar was flown under Simulated Airline Service (SAS) conditions (Maddalon *et al.*, 1987; Maddalon and Braslow, 1990). Unique in one respect, this test campaign simultaneously measured ambient cloud particles and the extent of laminar flow on the wing surfaces. The results are reported by Davis and Fischer (1983) and by Davis *et al.* (1986; 1987). Data for 13 flights studied by Davis *et al.* (1987) were reproduced in



Table K-1. The average percentage of time in "cloud" plus time in "haze" for these flights, was 11.4%. This value does not represent the mean cloud encounter of all SAS flights, as these 13 flights were selected because clouds *were* encountered, and according to Davis *et al.* (1987) there were "several" flights where no clouds were encountered. To compensate for this they adjusted the data in a rather simplistic fashion. They removed from the data set the results where extensive cloud was encountered. The data removed corresponded to: (1) flights 1061 and 1104; (2) flight 1061. The recalculated average values for time-in-cloud (TIC) reduced to 7.3% and 7.2% respectively, as shown at the bottom of Table K-1. The lower value of 7.2%, indicated by Davis *et al.* (1987) as a probable "upper limit" on the likelihood of cloud encounter on an average basis, has been widely quoted in subsequent LFC and HLFC studies and reviews.

Also indicated in Table K-1 are the results of the laminar flow measurements, taken on the Douglas Aircraft designed glove (installed on the Jetstar starboard wing). Fig. 8-2 (Chapter 8) was generated using this data. It illustrates the numerical correlation between the average level of laminar flow on the wing panel and the percentage clear air recorded for that particular flight (which is inversely related to the average particle concentration).

**Table K-1** *Meteorological conditions and laminar flow for SAS (Davis et al., 1987)*

Flight	Altitude (1000 ft)	Percent time in:			% laminar flow*	Particle Conc. (m <sup>-3</sup> )
		Clear	Haze	Cloud		
1059	32.7 - 36.9	90.23	5.57	4.21	93.51	1.07E2
1060	32.7 - 36.8	94.77	2.90	2.32	93.75	1.10E2
1061	28.7 - 32.0	37.16	4.24	58.60	56.47	2.29E5
1080	30.7 - 32.7	91.04	3.82	5.15	91.42	2.89E2
1081	32.7	94.91	11.29	3.95	89.07	8.15E3
1082	28.7 - 32.8	100.0	0.00	0.00	97.96	0
1085	30.8 - 32.8	97.55	0.76	1.69	96.74	1.97E2
1087	26.2 - 34.7	99.05	0.85	0.1	96.02	7.00E1
1094	32.5 - 32.8	84.37	5.89	9.75	86.28	3.16E2
1099	30.6 - 34.7	83.51	9.08	7.41	86.24	8.66E3
1100	22.5 - 35.7	81.56	8.79	9.64	84.90	3.98E2
1103	34.7 - 34.8	99.43	0.28	0.28	97.97	1.00E1
1104	27.4 - 34.7	93.78	1.47	4.77	**	2.57E2
Ave. (all 13 flights)		88.56	3.28	8.17		
Ave. (less 1061, 1104)		92.69	3.42	3.89		
Ave. (less 1061)		92.81	3.20	3.99		

Where: Clouds have a particle size > 60µm and a concentration > 1000 m<sup>-3</sup>; Haze has a particle size > 60µm and a concentration of 0 to 1000 m<sup>-3</sup>

Notes: \* For the Douglas Aircraft glove installed on the starboard wing.

\*\* No data due to icing.



## K.4 GLOBAL ATMOSPHERIC SAMPLING PROGRAM (GASP)

### K.4.1 Data acquisition

Data along airline routes was obtained as part of the Global Atmospheric Sampling Program (GASP), which was conducted from March 1975 to June 1979, by the NASA Lewis Research Center for the US Department of Transportation. Meteorological and trace-constituent measurements of ambient atmospheric conditions were taken onboard four Boeing 747 airliners, on routine commercial service worldwide (Perkins and Gustafsson, 1975; Gustafsson *et al.*, 1979). The database is unique, as it provides a direct insight into the distribution of cirrus clouds along airline routes.

The results of the cloud encounter observations are described by Nastrom *et al.*, (1981a; 1981b), (Davis and Fischer, 1983) and Jasperson *et al.* (1984a; 1984b; 1985). Some 88000 cloud encounter measurements were taken on more than 3000 flights (Davis and Fischer, 1983). In interpreting the results for a HLFC aircraft it is important to note that the data came from commercial flights on regular service, where no attempt was made to avoid the clouds. Observations of 256 seconds were recorded at nominal 5 or 10 minute intervals, at altitudes above 20000ft. For each observation the number of seconds that the aircraft was "in-cloud" was determined with a light-scattering particle counter. The cloud detection threshold was established on the basis of visual observation of light haze. This resulted in an "in-cloud" registration, whenever the local aggregate particle concentration (for all particles with diameters greater than  $3\mu\text{m}$ ) was greater than  $66\,000\text{ m}^{-3}$ . Meteorological information, such as the tropopause height, was subsequently estimated from data obtained from the US National Meteorological Center.

### K.4.2 Cloud climatology

Over the four-year period of the GASP, observations were made during all seasons, with a slight increase in the number of observations made in winter and spring. Most of the data came from the Northern Hemisphere, with about 3/4 of the data coming from flights in the latitudes 20 - 60 N. The calculated mean TIC values are thus weighted towards this region.

Nastrom *et al.* (1982) explained that many of the climatology observations were consistent with expectation and could be related to global-scale meteorological circulations. A number of conclusions in regard to the NASA study were noted.

- (1) The seasonal migration of the Inter-tropical Convergence Zone (ITCZ) was responsible for the observed north-south movement of the maxima and minima in cloudiness at low altitude.
- (2) A peak in mean cloudiness generally occurs near the subsolar latitude (sun overhead at noon), lagging by a few degrees. In winter in the Northern Hemisphere, it occurs near 15°S, while in spring at 5°S, summer at 15°N, and autumn at 5°N.



- (3) The associated minima also has a latitudinal displacement during the year. In winter (Northern Hemisphere), the feature is furthest south near 15°N and in the summer it reaches 35°N.
- (4) A secondary maxima occurs near 45°N, throughout the year. This is attributed to the increased cyclone encounter, along the Northern Hemisphere polar front.
- (5) The cloudiness is much greater in winter, as expected.
- Because of a shortage of flights in the Southern Hemisphere, no comparative conclusions were made for that region. The fraction of observations having clouds in vicinity (CIV) is the ratio of the number of observations where clouds were detected (irrespective of duration), divided by the total number of observations. It is thus a relative indication of the probability of cloud occurrence. Jasperson *et al.* (1984a; 1984b) make a number of observations concerning the data using the TIC and CIV parameters. The variations of TIC with respect to altitude, season and latitude, were reported to be significant at the 99% confidence level.
- (1) As shown in Fig. K-3, both the CIV and TIC cloudiness parameters tend to be approximately uniform in the troposphere, with a slight increase in the region of 5000 - 1000ft below the tropopause, followed by a rapid decrease just above the tropopause. It is evident that the tropopause acts as a lid on the weather system of the troposphere.
- (2) In Fig. K-4 the cloudiness parameters are plotted against pressure altitude, for the seasons in the Northern Hemisphere at 40° - 50°N latitude. Inspected individually, the lowest values of TIC correspond to the higher altitudes and to summer.
- (3) Due to the small sample size of data in the equatorial regions, statistical analysis was not performed. However, the data suggested that TIC is likely to increase with height in this region as a consequence of the high tropopause in the tropics (i.e. several thousand feet higher than typical aircraft flight levels).

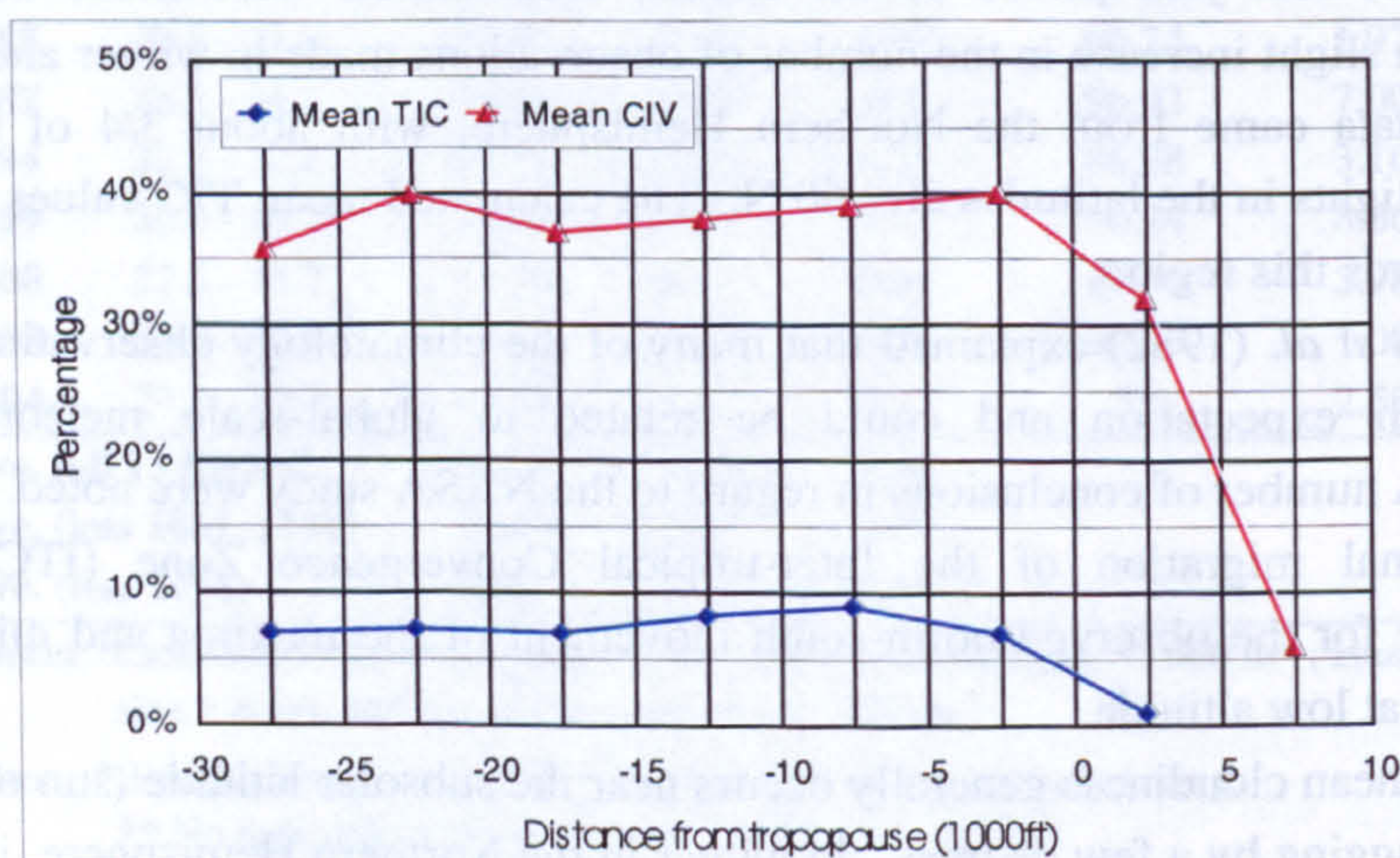


**Fig. K-3** Global annual mean values of cloudiness parameters with distance from the tropopause (redrawn after Jasperson *et al.*, 1984b)



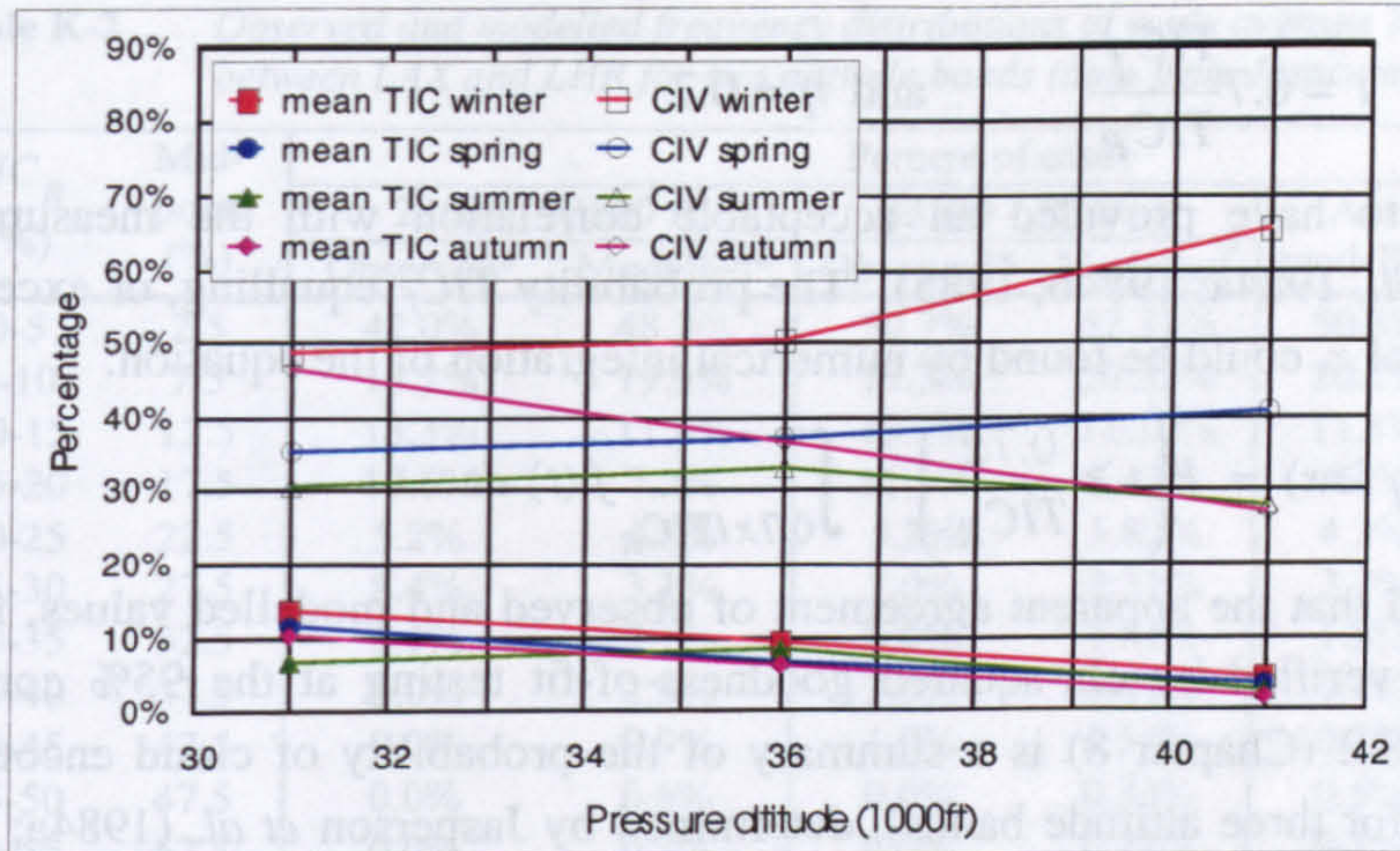


**Fig. K-4** Variation of cloudiness parameters with altitude and season for Northern Hemisphere at 40° - 50° N latitude (redrawn after Jasperson *et al.*, 1984b)

#### K.4.3 Route data analysis

Following the GASP data acquisition, a statistical analysis was undertaken by NASA to predict the probability of cloud encounter on airline routes, and its variations with altitude, season and location. Results based on a subset of the data, covering only 960 flights were reported by Nastrom *et al.* (1981a, 1981b). The probability of the aircraft encountering cloud for a fixed portion of the flight was estimated for three routes, i.e. New York (JFK airport) to London (LHR airport), New York (JFK) to Los Angeles (LAX) and Los Angeles (LAX) to Honolulu (HNL).

Davis and Fischer (1983) and later Jasperson *et al.* (1984a; 1984b; 1985), presented more detailed and updated analyses of the GASP cloud encounter statistics, based on the entire database of 88000 samples. The data were analysed to obtain summary statistics on the probability of cloud encounter at commercial airliner altitudes, for application in determining the feasibility of employing LFC on long-range aircraft. The following definitions were used in the analysis conducted by NASA (see also Fig. 8-3, Chapter 8):

$TIC_f$  = average fraction of time-in-cloud on one flight.

$TIC_R$  = average fraction of time-in-cloud for a sample of flights on one route.

$CIV$  = fraction of observations having clouds in vicinity.

All three quantities were expressed as percentages. It was reported that the observed behaviour could be modelled using a gamma probability density distribution. This function, given by:

$$f(t) = \frac{e^{(-t)(t)^{\eta-1}}}{\Gamma(\eta)} \quad \text{--- [K-1]}$$



$$\text{where: } t = 0.7 \frac{TIC_f}{TIC_R} \quad \text{and } \eta = 0.7$$

was reported to have provided an acceptable correlation with the measured data (Jasperson *et al.*, 1984a; 1984b; 1985). The probability  $TIC_f$  equalling, or exceeding a specific value of  $x$ , could be found by numerical integration of the equation:

$$P(TIC_f \geq x) = P\left(t \geq \frac{0.7x}{TIC_R}\right) = \int_{0.7x/TIC_R}^{\infty} f(t) dt \quad \text{--- [K-2]}$$

It was reported that the apparent agreement of observed and modelled values, for each data set, was verified by chi-squared goodness-of-fit testing at the 95% confidence level. Table 8-2 (Chapter 8) is a summary of the probability of cloud encounter on seven routes (for three altitude bands), determined by Jasperson *et al.* (1984a; 1984b), using this model.

#### K.4.4 Frequency distribution based on GASP

The frequency distribution of cloud on a particular route was illustrated for the US East Coast (LAX airport) - NW Europe (LHR airport) route by Jasperson *et al.* (1984a). In Table K-2, the GASP observed data is indicated as a frequency distribution for two flight level bands, i.e. from 28500 - 33500ft and from 33500 - 38500ft. There were 38 flights in the lower flight level bands and 99 flights in the sample for the upper flight level. The values were read off the graph of Jasperson *et al.*, 1984a. Also shown in the table, are the modelled values obtained using the gamma probability density distribution.

The equations used by Jasperson *et al.* (1984a) to calculate the model values, are:

$$\text{a) For 28500 - 33500ft: } f(TIC_f) = 3.147 \left(\frac{TIC_f}{100}\right)^{-0.3} e^{\left(\frac{-TIC_f}{21.72}\right)} \quad \text{--- [K-3]}$$

$$\text{b) For 33500 - 38500ft: } f(TIC_f) = 3.548 \left(\frac{TIC_f}{100}\right)^{-0.3} e^{\left(\frac{-TIC_f}{11.29}\right)} \quad \text{--- [K-4]}$$

A check on the modelled data was conducted by the author, using a statistical analysis computer package (MINITAB). Using a shape parameter of 0.7 and a coefficient of 11.29 (taken from equation [K-4]), the frequency distribution given in Table K-2 for the upper flight level band, was calculated. These values matched the data on the graph of Jasperson *et al.* (1984a).

Averages of the modelled values for the two flight level bands, were calculated by the author, and are also given in Table K-2. These average values were used to generate Fig. 8-4 (Chapter 8), and were used as the idealised model of probable cloud encounter for the HLFC fuel savings analysis, described in Chapter 11.



**Table K-2**      *Observed and modelled frequency distributions of route average TIC on GASP flights between LAX and LHR for two altitude bands (data from Jasperson et al., 1984a)*

<i>TIC<sub>R</sub></i> (%)	Mid-point (%)	Percent of cases					
		28500 - 33500 ft		33500 - 38500 ft		Ave. modelled <sup>†</sup>	Running total
		Observed*	Modelled*	Observed*	Modelled <sup>#</sup>		
0-5	2.5	42.0%	48.2%	50.7%	52.31%	50.3%	50.3%
5-10	7.5	18.2%	19.9%	13.3%	20.32%	20.1%	70.4%
10-15	12.5	13.3%	11.5%	15.0%	11.10%	11.3%	81.7%
15-20	17.5	10.6%	7.2%	11.1%	6.43%	6.8%	88.5%
20-25	22.5	5.2%	4.8%	5.2%	3.82%	4.3%	92.8%
25-30	27.5	8.4%	3.1%	1.0%	2.31%	2.7%	95.5%
30-35	32.5	3.1%	2.1%	0.0%	1.41%	1.8%	97.3%
35-40	37.5	0.0%	1.3%	2.0%	0.87%	1.1%	98.3%
40-45	42.5	0.0%	0.9%	1.0%	0.54%	0.7%	99.1%
45-50	47.5	0.0%	0.6%	0.0%	0.33%	0.5%	99.5%
50-55	52.5	0.0%	0.3%	0.0%	0.21%	0.3%	99.8%
55-60	57.5	0.0%	0.1%	1.0%	0.13%	0.1%	99.9%

Notes:    \* Observed data; values read off graph (*Jasperson et al., 1984a*)  
              <sup>#</sup> Values calculated by author using coefficients described by *Jasperson et al. (1984a)*  
              <sup>†</sup> Modelled data used to generate Fig. 8-4 (Chapter 8).



**Blank page**



# APPENDIX L

## INSECT CONTAMINATION

### TABLE OF CONTENTS

L.1	Introduction.....	352
L.2	Use of Surfactants and Enzymes.....	352
L.2.1	Foreword .....	352
L.2.2	Objective of the study.....	352
L.2.3	Surfactants for contamination alleviation.....	353
L.2.4	Foams .....	353
L.2.5	Enzymes for contamination alleviation .....	354
L.2.6	Contamination alleviation of favourable formulations.....	355
L.2.7	Discussion .....	357
L.2.8	Concluding remarks .....	358
L.3	HYLTEC SAAB 2000 Tests.....	358
L.3.1	Introduction .....	358
L.3.2	Objectives of contamination studies.....	358
L.3.3	Description of test equipment.....	359
L.3.4	Flight profile and test region .....	359
L.3.5	Data acquisition.....	360
L.3.6	Results .....	360
L.3.7	Discussion .....	361
L.3.8	Conclusions .....	361



## L.1 INTRODUCTION

This appendix provides supplementary information to Chapter 9, regarding insect contamination. It reports on work performed by the author, with colleagues and research partners, in project HYLTEC (see section C.17, Appendix C). Two areas of research are described: (1) The effectiveness of surfactants and enzymes, as additives to glycol based contamination alleviation fluids, and (2) The use of a liquid system in alleviating insect contamination during a flight test campaign, conducted using a SAAB 2000 aircraft.

## L.2 USE OF SURFACTANTS AND ENZYMES<sup>1</sup>

### L.2.1 Foreword

*An Investigation of Surfactant and Enzyme Formulations for the Alleviation of Insect Contamination on Hybrid Laminar Flow Control (HLFC) Surfaces*, by O'Donoghue, Young, Pembroke and O'Dwyer (2002), reports on novel research conducted at the University of Limerick, under the direction of the author from 1998 - 2001. The paper describes an experimental investigation into the potential use of surfactants and enzymes, as additives to contamination alleviation fluids. Section L.2 of this appendix is summary report based on the paper of O'Donoghue *et al.* (2002). It is acknowledged that O'Donoghue<sup>2</sup> was the principal researcher for this element of the work.

### L.2.2 Objective of the study

The objectives of the research were to advance the range of possible insect contamination alleviation fluids, for use on proposed HLFC surfaces.

- (1) The first aspect of the study was to identify and investigate the effect of surfactant additives, on the physical properties of fluids. The properties examined included:
  - Surface tension of fluid compositions;
  - Wing material wettability, by contact angle analysis of fluid compositions;
  - Effect on fluid viscosity, due to additives in fluid compositions;
  - Foaming and foam stability effects of additives, in fluid compositions.
- (2) A second aspect of the work involved the use of enzymes, as additives in proposed fluid compositions. The objectives were to:
  - Screen enzymes for activity in water/organic co-solvent mixtures, using aviation approved freezing point depressants (FPD) as organic co-solvents;
  - Select the favoured enzymes, for analysis in the presence and absence of other possible additives to insect contamination alleviation fluids.

---

<sup>1</sup> Reported by O'Donoghue *et al.* (2000; 2002). Selected parts have been reproduced in this section.

<sup>2</sup> D. O'Donoghue, M.Sc. student, CES Department, University of Limerick; 1998 - 2001.



(3) The final part of the research was to observe the tendency of insects to adhere to HLFC wing surface materials. Here, the objectives were to:

- Design and build an airgun for accelerating insects onto stationary perforated titanium plates and observe the rupture patterns, using Scanning Electron Microscopy (SEM) imaging;
- Use the airgun in conjunction with contamination alleviation fluids, determined to be potentially useful from bench tests, to mimic the effectiveness of these fluids at insect adhesion mitigation.

### **L.2.3 Surfactants for contamination alleviation**

Surfactants are chemical compounds, possessing both hydrophilic and hydrophobic fragments in their overall structure. In aqueous they reduce solution surface tensions by collecting at the liquid surface. A series of fluorinated and non-fluorinated surfactants, were examined for their ability to reduce the surface tension of solutions at room temperature. The fluorinated surfactants outperformed the non-fluorinated surfactants in water, the Type I de-icing agent TKS-80 and the Type II anti-icing agent Kilfrost ABC-3. The result was that five Zonal fluorosurfactants (FSA, FSD, FSJ, FSK and FS-300) were further assessed in water/TKS-80 solutions. In all cases where fluorosurfactants were added to solutions containing between 50 and up to 90% v/v TKS-80, significant surface tension reductions were observed.

Sessile Drop Contact Angle Analysis was conducted by photography on titanium alloy surfaces, using TKS-80 solutions containing 0.05, 0.2 and 0.6% v/v of the five fluorosurfactants considered for investigation. It was shown that all solutions could be readily spread over titanium alloy test plates. Zonyl FSA produced the least reduction in contact angles as a function of concentration. Zonyl FSD produced a large reduction in contact angles in the 50% v/v TKS-80 solution; though this was not the case in 80% v/v TKS-80 solution, whilst Zonyl FSK was most effective in each test solution at the 0.6% v/v fluorosurfactant concentration.

### **L.2.4 Foams**

The ability of the fluorosurfactants to produce stable foams at appropriate concentrations in 50% and 80% v/v TKS-80 solutions, was investigated using a foaming column based on gas sparging. Foams were produced by sparging air from the base of a column for 30 seconds; after which initial and final (5 minutes) foam heights were measured.

Fluorosurfactant foaming and foam stability was shown to be independent of the TKS-80 concentration, but dependent upon the fluorosurfactant concentration. Beyond appropriate surfactant concentrations, neither foam height produced, nor foam stability was significantly altered over the time course of experiments. Based on these test four fluorosurfactants were considered appropriate for use in insect contamination alleviation systems and were investigated in the airgun studies (described below).



## **L.2.5 Enzymes for contamination alleviation**

### ***L.2.5.1 Enzyme suitability***

Enzymes are proteins that are capable of catalysing reactions in an appropriate environment. Environmental conditions requiring control are the solvent medium used (normally aqueous), pH, temperature, and the presence or absence of stabilisers or denaturants. Protein degrading enzymes (proteases) are hydrolases, because the degradative reactions they use to catalyse the degradation of their substrates (proteins) require water.

Of particular interest in this context, are enzymes capable of degrading insect debris. The kinetic activity of enzyme catalysed reactions are monitored by observing the rate of product formation or disappearance of substrate. In the case outlined, the substrate would be insect debris protein or chitin, while the product would be a lower molecular weight material having greater solubility, less stickiness and be more easily removed by air currents flowing over the wing. The use of enzymes in this manner, is analogous to the incorporation of enzymes into detergent powders.

### ***L.2.5.2 Experimental screening of enzymes***

A series of non-specific proteases were selected for analysis in the presence of components with potential application in insect contamination alleviation systems. All screening experiments were conducted using the dye-labelled protein azoalbumin as substrate. The effect of ethylene and propylene glycol, and the influence of titanium filings were investigated.

### ***L.2.5.3 Results***

Results indicated that of all the enzyme preparations used, the most resilient enzyme was Subtilisin Carlsberg or commercial preparations of it (e.g. Alcalase) in up to 80% v/v glycol fluid. Whilst increasing concentrations of glycol fluids progressively reduced the aqueous-like activity of the enzymes, their stability in time was demonstrated for the preferred enzymes, Subtilisin Carlsberg and Proteinase K.

The heat stability of Subtilisin Carlsberg was examined to identify the optimum conditions for enzyme solution storage and the temperature range, wherein the enzyme solution retains 50% of its optimum temperature's activity. It was shown that the optimum temperature of activity was in the region of 40 to 50°C in the ethylene glycol range 0 to 80% v/v (Fig. L-1).

Enzymes were also tested in the presence of fluorosurfactants. From these experiments, only Zonyl FSK and, to a lesser extent, Zonyl FSA were found to be incompatible with the enzymes.



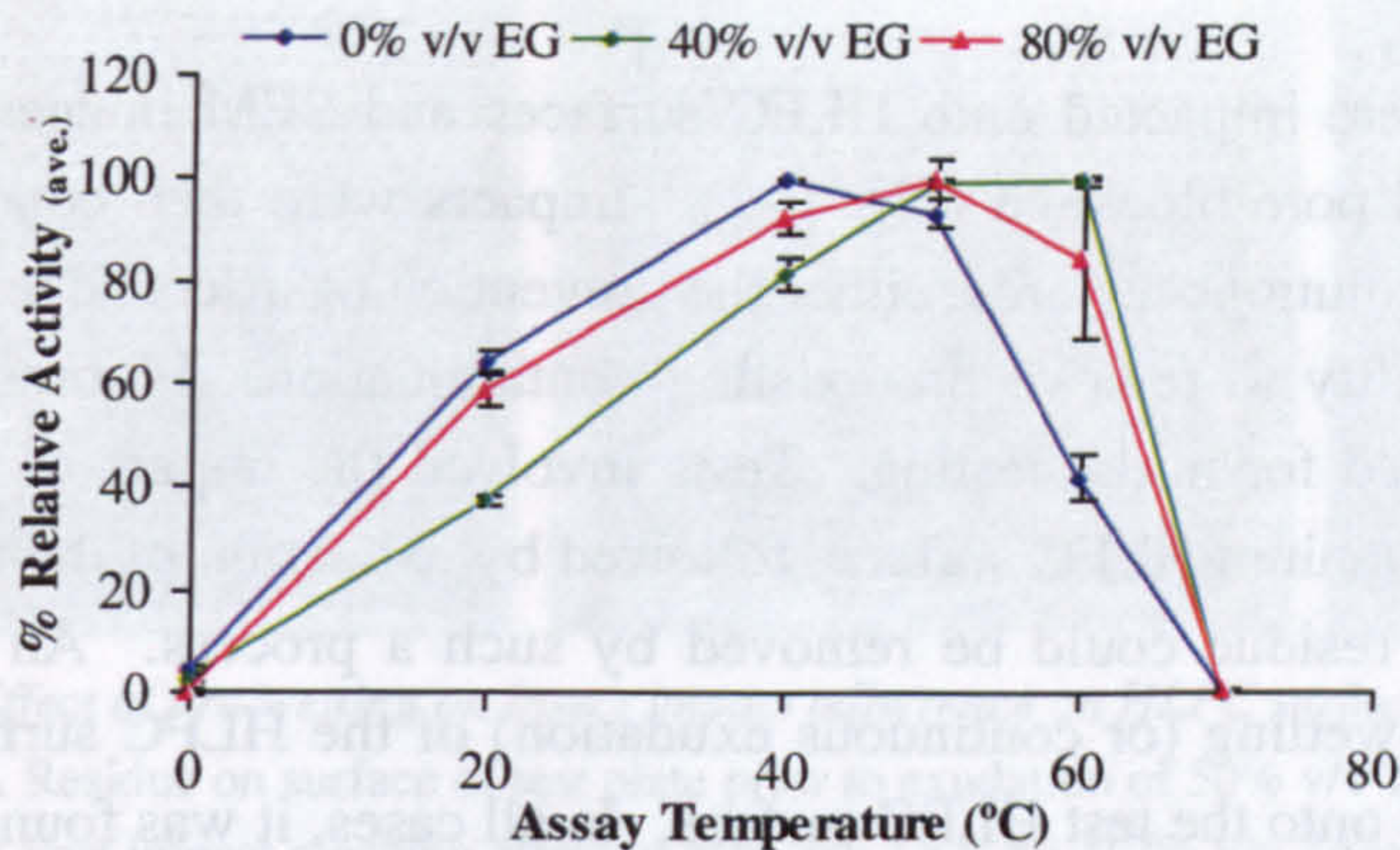


**Fig. L-1** Effect of ethylene glycol concentration (EG) and assay temperature on relative activity of Subtilisin Carlsberg (O'Donoghue et al., 2002)

**L.2.6 Contamination alleviation of favourable formulations**

**L.2.6.1 Methodology**

An airgun was constructed to test insect impacts on HLFC surfaces. This was constructed as a 25mm internal diameter copper gun barrel, in front of a gun stock containing a venturi flume, immediately below a hopper tube of stainless steel, placed at 45° to the gun barrel, and in front of a 4mm PVC tube supplying compressed air. Using this set-up (Fig. L-2), insect impacts onto test surfaces at speeds up to 150km/hr were possible (Fig. L-3). All insect impacts were conducted using insects either caught in the field or bred from the larval stage to maturity in the laboratory.

Given that Subtilisin Carlsberg gave the highest performance in ethylene glycol, and that the presence of other potential insect contamination alleviation additives had only a minimal affect on this enzyme's proteolytic activity, it was recommended for investigation in the airgun studies.

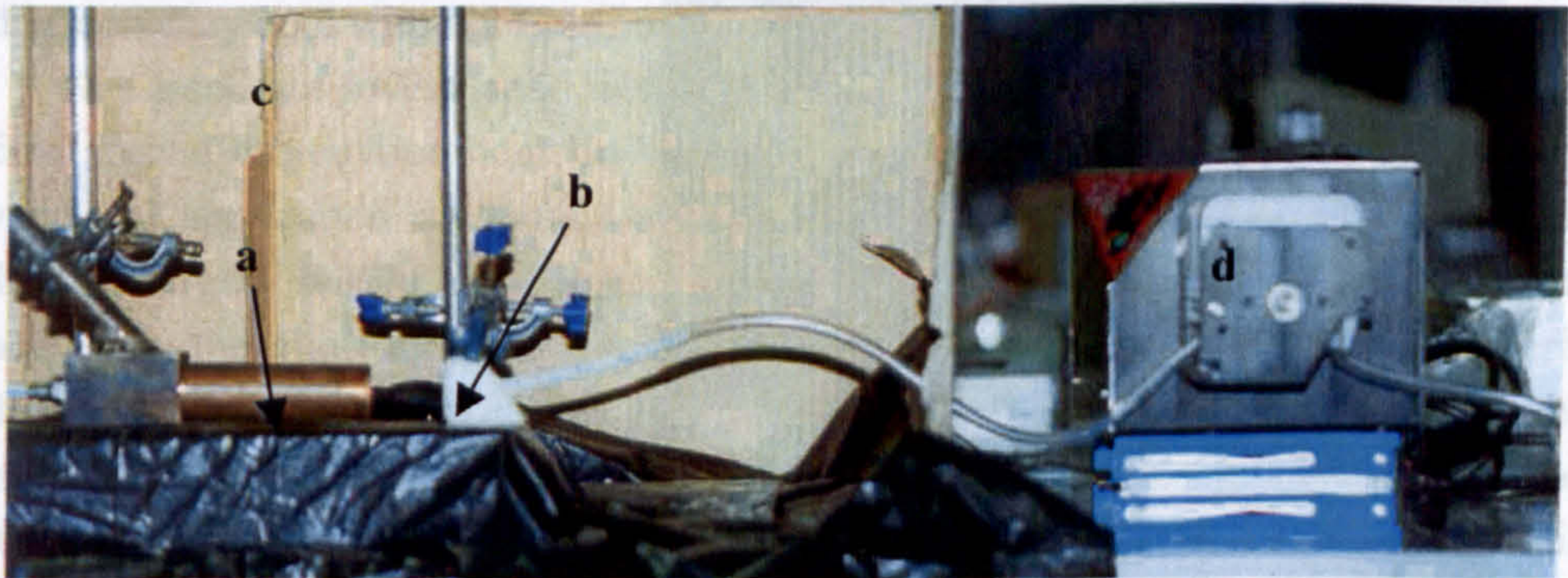


**Fig. L-2** Insect impact & fluid exudation experimental set-up a= Gun barrel, b= Plate holder, c= Shield, d= Pump (O'Donoghue et al., 2002)



### L.2.6.2 Results

Initially insects were impacted onto HLFC surfaces and SEM images showed evidence of adhesion and pore blockage (Fig. L-3). Impacts were then conducted to identify the effect of test solutions towards, either the prevention of insect adhesion onto wet surfaces, or their ability to remove pre-existing contamination. Fluorosurfactant compositions were selected for initial testing. Tests involved the impact of an insect onto a clean, perforated titanium HLFC surface, followed by exudation of the test fluid, to examine if the insect residue could be removed by such a process. An alternate experiment involved pre-wetting (or continuous exudation) of the HLFC surface, with concurrent insect impacts onto the test HLFC surface. In all cases, it was found that the emission of fluids onto an already contaminated wing, failed to remove insect residues, whilst pre-wetting experiments prevented the adhesion and build-up of insect residues onto wing surfaces (Fig. L-4).

Given that fluorosurfactant solutions appeared capable of preventing the build-up of residues on HLFC surfaces, enzyme-containing solutions were examined for passive dissolution of insect residues adhering to HLFC surfaces. This was to identify if such solutions could be used as films on wing surfaces prior to flight to degrade insect proteins enabling both fluid exudation and wind shear effects to wash away the insect residues during flight.

Results indicated that overall there would be no additional benefit from the use of enzyme-containing solutions, in insect contamination of HLFC surfaces. On the other hand, UV-visible spectroscopic measurement of solutions, used in dissolution test fluids, did show that irrespective of the duration of exposure of contaminated surfaces to test fluids, protein dissolution and the cleaning effect of wind was improved, as the water concentration of test fluids increased, coincident with reduced ethylene glycol concentrations in test fluids.

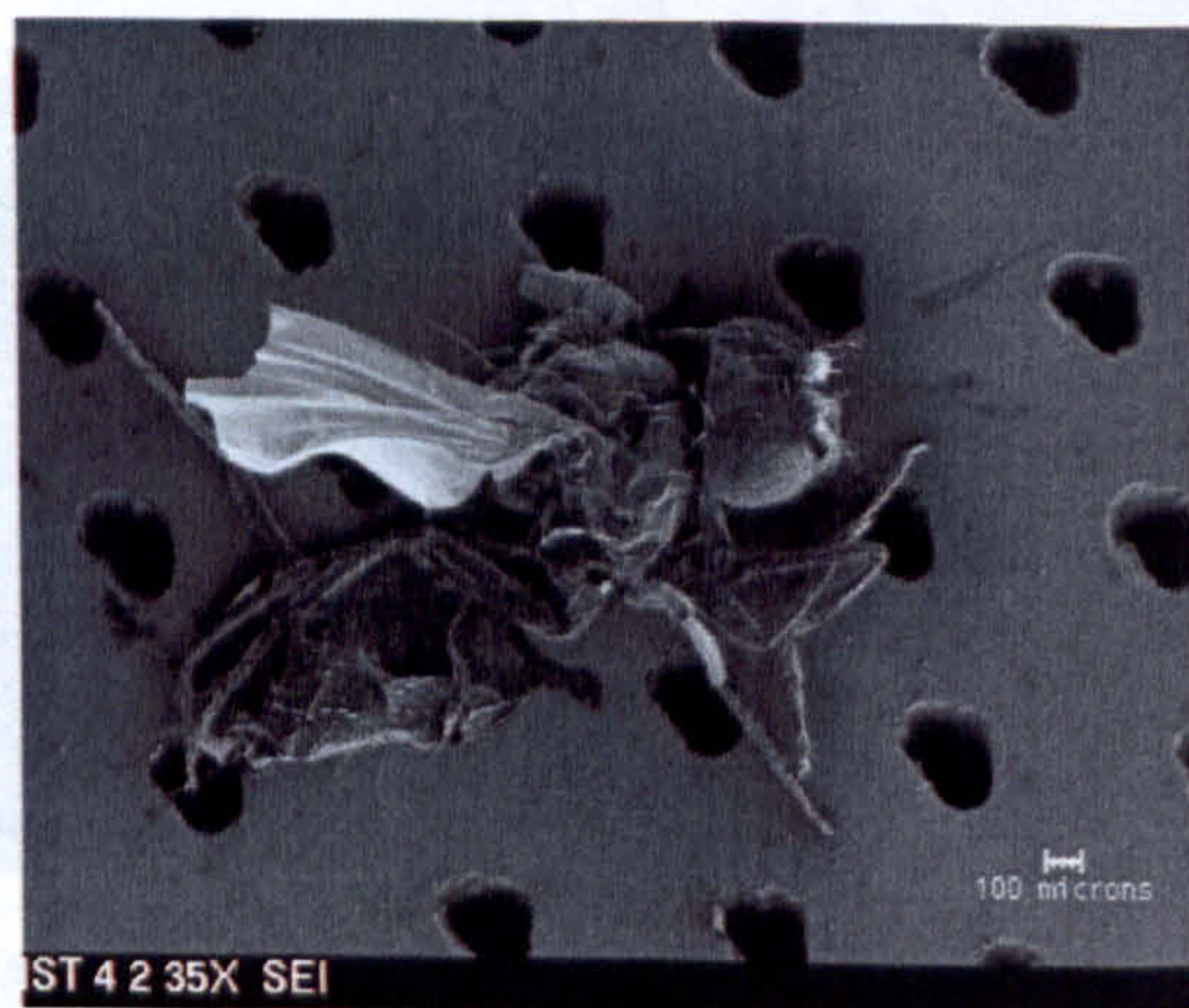
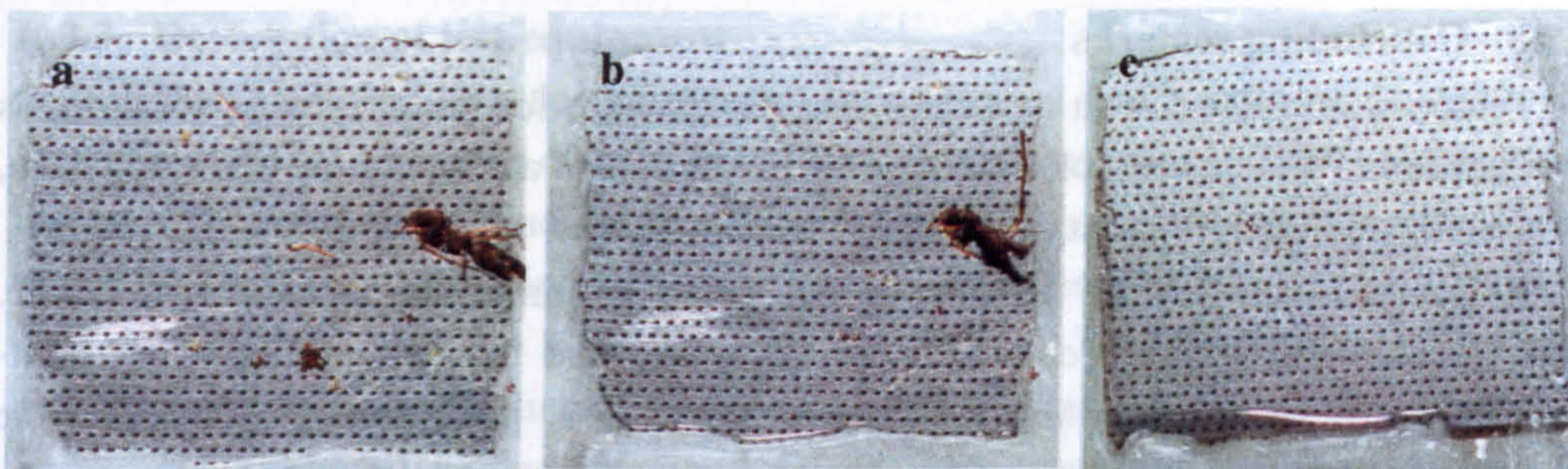


Fig. L-3 SEM image of insect on titanium test plates (O'Donoghue et al., 2002)





**Fig. L-4** Effect of pre-wetting on insect impact adherence on HLFC surfaces (O'Donoghue et al., 2002)

**A** Residue on surface of test plate prior to exudation of 50% v/v TKS-80 Zonyl FSD solution;

**B** Post impact cleaning effect of 50% v/v TKS-80, 0.2% v/v Zonyl FSD solution on titanium

plate; **C** Result of pre-wetting of test plates with Zonyl FSD solution

### L.2.7 Discussion

The study investigated two different potential mechanisms for insect contamination alleviation of HLFC surfaces; one having its basis in applied physical chemistry, the other in applied enzymology. On the basis of a direct comparison between each possible mechanism, it appears that the use of fluorosurfactant-containing solutions in the appropriate manner, is preferable to enzyme-borne solutions for insect contamination alleviation. From a practical and economic standpoint, this makes sense, as fluorosurfactant-containing solutions require few environmental controls to function effectively, whilst enzyme-borne solutions are operationally effective only within the correct ranges of pH, temperature, solvent composition and duration of exposure to their substrates; all of which add to fluid production, storage and application costs. Temperature represents a particular area for concern, as heating an enzyme solution requires the design of a temperature control system within the wing, thereby adding to the cost of HLFC. Furthermore, exudation onto HLFC surfaces places the fluid in an environment, which cannot be readily controlled. For example, the air temperature and wind effects may cool warmed fluids to sub-optimal temperatures.

One issue not investigated in this study, is the direct impact of fluid exudation systems around the environments in which they are applied. It is recognised that the conventional application of de-/anti-icing agents to aircraft is done under controlled conditions, largely within the boundaries of the airport, which limits environmental impact. For the fluid exudation system proposed for HLFC, even the short term exudation of a protective fluid from a wing surface, during the initial phases of flight, presents an uncontrolled introduction of fluids into the environment, with a pollution potential which may or may not be realised. It was therefore felt that this aspect of fluid exudation is worthy of investigation, prior to the application of such systems on a large scale.



### **L.2.8 Concluding remarks**

- Temperature represents a particular area for concern for the enzymatic solution, as the heating an enzyme solution requires the design of a temperature control system, thereby adding to the cost of the HLFC system.
- It was the view of the authors of the paper (summarised in section L.2), i.e. O'Donoghue, Young, Pembroke and O'Dwyer, that the use of fluorosurfactant-containing solutions in the appropriate manner, is preferable to enzyme-borne solutions for insect contamination alleviation.
- The introduction of glycol based decontamination fluids into the air during take off and landing, requires further study to investigate the potential of local environmental damage around the airport.

## **L.3 HYLTEC SAAB 2000 TESTS**

### **L.3.1 Introduction**

As part of the HYLTEC project (see section 9.3, Chapter 9, and section C.17, Appendix C), a SAAB 2000 aircraft was used to study insect contamination and material durability. A general description of these tests was given by Humphreys and Totland (2000); and by Humphreys (2001). Four organisations were involved: AS&T (Consett, UK) were responsible for the design and manufacture of the LCCS (Liquid Contamination Control System), the test panels and holders; SAAB Aerospace (Linköping, Sweden) jointly with AS&T, for certification and system installation; SAAB Aerospace for the management of the flight tests, inspections and data acquisition; SAS for aircraft operations; and the University of Limerick, for the analysis of the insect contamination data, and for the post flight-test inspection of the perforated panels. The work performed at the University of Limerick, was conducted under the direction of the author. It is acknowledged that the data reduction and analysis was performed by Whooley<sup>3</sup> and Corish<sup>4</sup>.

### **L.3.2 Objectives of contamination studies**

Two prime objectives were established. These were to:

- (1) Assess the effectiveness of a LCCS on preventing contaminants (particularly related to insects), from degrading simulated laminar flow surfaces, during routine in-service operation;
- (2) Investigate the insect threat environment in Northern Europe, in terms of weather and seasonal factors.

---

<sup>3</sup> A. Whooley, student, MAE Department, University of Limerick, Ireland; 1999 - 2000.

<sup>4</sup> J. Corish, student, MAE Department, University of Limerick, Ireland; 2000 - 2001.



### **L.3.3 Description of test equipment**

Two small holders, designed to house perforated test specimens (panels), were installed in the leading edge of a SAAB 2000 aircraft (illustrated in Fig. 9-5, Chapter 9), that was operating on routine airline service. The holders were approximately 300mm wide and extended to the wing forward spar. This location housed a flux gate when the aircraft was built, which later became redundant. The specimen holders were manufactured from aluminium alloy, and replaced the original leading edge section.

The starboard holder contained a laser perforated titanium sheet. This was protected from contamination during the takeoff and landing phases (below 1500ft) by the LCCS. The LCCS was based on proven ice protection system principles, and used standard aircraft components, where possible. The LCCS consisted of a reservoir for the de-contamination fluid and a pump, powered by an electric motor; all installed in the non-pressurised forward section of the starboard nacelle. An accumulator was placed in the leading edge, close to the test panel. The system was activated when the throttle lever was moved beyond the Ground Idle position or when the radar altimeter height indicated a height below 1500 ft.

The second panel holder, which was mounted on the port wing was passive (i.e. it was not protected by the LCCS). The objective here was to investigate the durability of candidate HLFC suction surface materials (see Fig. 10-5, Chapter 10) installed in the holder, and to provide a reference for the active panel in terms of contamination. No active suction system was installed; however, both test panels utilised the pressure differential that exists between the top and bottom of the wing, to ensure flow through the holes.

### **L.3.4 Flight profile and test region**

The SAAB 2000 is a much smaller and slower aircraft than the long-range airliners, for which the technology is being developed. Although cruise speed and sector lengths are very different, the speeds and times for climb and descent are not that dissimilar. As insect contamination and most atmospheric precipitation occurs below cruise levels, the SAAB 2000 turboprop aircraft was thus considered to be a useful test vehicle. The flights covered a large part of northern Europe, as illustrated in Fig. L-5.

The test programme started in July 1999 and continued for approximately 20 months, with the aircraft in typical airline operating conditions. Average utilisation was 200-250 flights per month.





**Fig. L-5** Primary routes flown by SAAB 2000 (after Humphreys, 2001)

### L.3.5 Data acquisition

Daily weather reports were obtained from the Swedish meteorological office, for the majority of the flight destinations. This information was in the form of METARs (meteorological aerodrome reports), which are routinely prepared for pilots and airline operators (described by Thom, 1997; for example). The METARs were decoded using a computer program<sup>5</sup>, and the required information extracted; this included: ambient temperature, dew point temperature, wind speed and the QNH pressure. As the aircraft flew to a number of destinations each week, and was only inspected at the end of the week, it was not possible to determine where the insects had been encountered. For this reason, average meteorological data for all destinations were determined on a daily basis, and weekly averages were then calculated.

At the weekly inspections, the level of contamination was recorded on pre-prepared cards using a rating scale. The fluid consumption was also noted. Records of flight times and destinations were obtained.

Each month a more detailed inspection took place. The panel porosity was measured using a flowmeter. Templates were placed over the leading edge, to ensure consistent positioning of the probe.

### L.3.6 Results

In almost 21 months of testing, the aircraft recorded over 4500 flights. The average flight time was 52 minutes, on legs ranging from 102 to 511nm. The average

<sup>5</sup> The computer program was written by A. Whooley, B.Eng. student, MAE Department, University of Limerick; 2000.



time of operation of the LCCS was approximately 6 minutes (3 min on takeoff and 3 on descent/landing) and the average fluid consumption was 13 ml/min of operation.

A graph indicating the observed level of insect contamination, based on a relative weighting scale, is shown in Fig. L-6. Also plotted on this graph is the weekly average ambient and dew point temperatures.

### **L.3.7 Discussion**

As expected, the insect data in Fig. L-6 has a distinct seasonal pattern. During the warmer months (i.e. April to September), when average temperatures range from approximately 10 - 20°C, relatively high levels of contamination were evident. The peak level was reported during the month of June. Conversely there was no contamination during the cold months, when the average temperatures fell below freezing (i.e. November to February). For the temperate periods of March / April, and October, a small amount of insect activity was evident.

An indication of the effectiveness of the LCCS system was obtained by comparing the contamination on the right hand (i.e. active) panels with that on the left hand (i.e. passive) panels. The LCCS malfunctioned on three occasions. One failure was during May - June 2000, which was unfortunate, as this would have provided the best information on the system performance due to the high level of insect activity. Little or no evidence of insect debris was observed on the active panel, when it was described as being "wet", i.e. resulting from the use of the LCCS during descent on the flight immediately prior to the weekly inspection.

It was observed that the average flow rate of 13 ml/min of operation was a little greater than the capacity of the pump, which was designed to deliver 10 ml/min. This apparent discrepancy can be explained by noting that the system had an accumulator, which was pressurised prior to the discharge of the fluid. This was required to give a rapid spreading of the fluid when operation of the LCCS commenced. The span of the active working section was 114mm, which gave an equivalent consumption of 114 ml/min per metre of span.

The insect debris on both the active and passive panels was usually described as "smears", having little or no perceptible height. This was in direct contrast to the adjoining rubber boots, where it was reported that numerous insect strikes of supercritical height were firmly attached.

### **L.3.8 Conclusions**

- (1) The overall conclusion was that the LCCS did effectively protect the wing leading edge. However, due to the uncertainty regarding the precise times when the system failed, no quantitative data regarding the effectiveness of the system over the test period, was obtained.
- (2) Insect contamination was only observed during the warmer months of April to October, with June representing the greatest activity.



### Correlation of Met data with Contamination Data

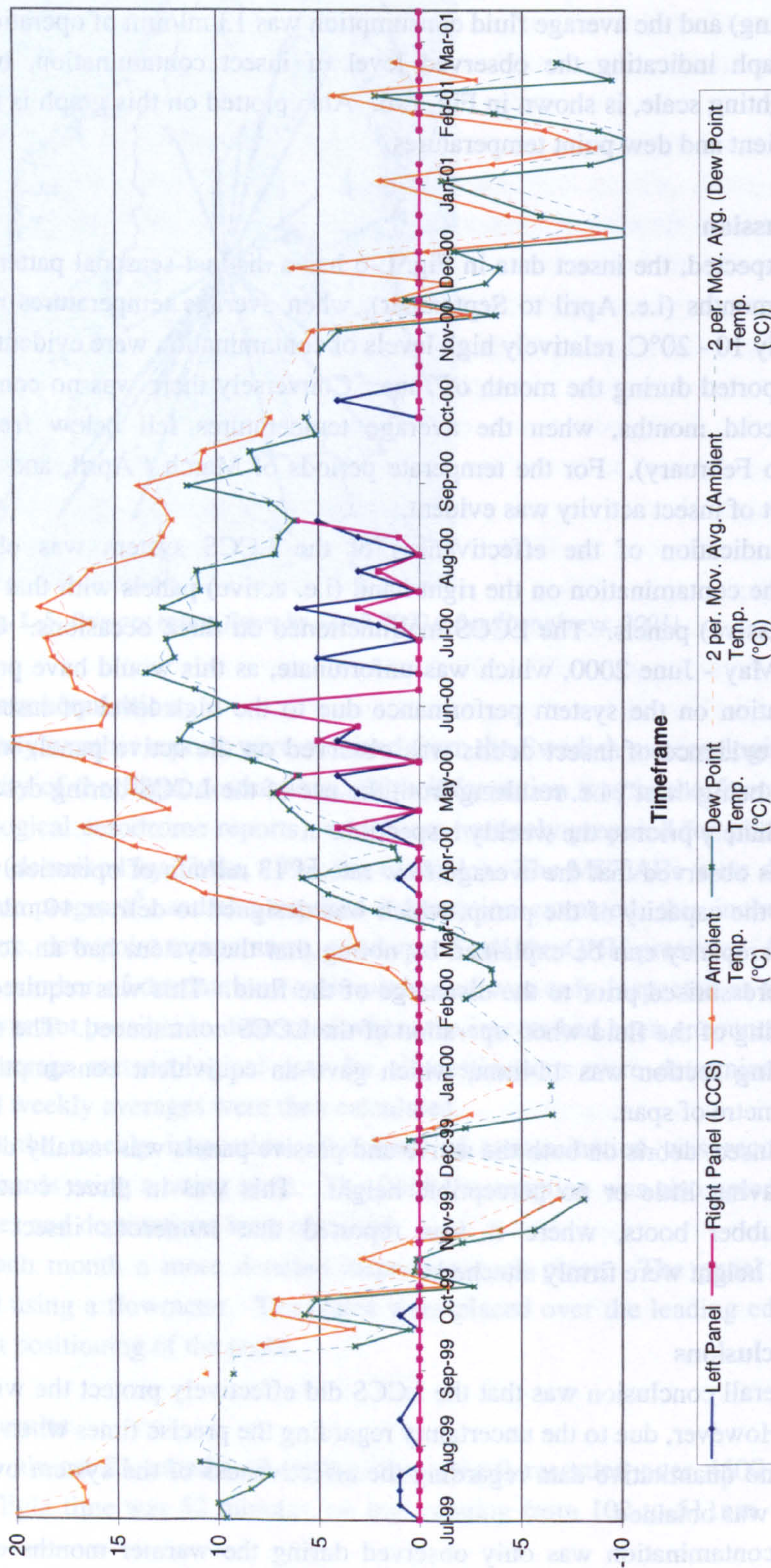


Fig. L-6 Comparison of meteorological data with insect contamination data<sup>6</sup> (figure by Corish<sup>7</sup>)

<sup>6</sup> The meteorological data for September 1999 and February 2000 was incomplete and trend values have been used.

<sup>7</sup> Graph produced by J. Corish, B.Eng. student, MAE Department, University of Limerick; 2001.



## APPENDIX M

# MECHANICAL FAILURE, DAMAGE AND DURABILITY ASPECTS OF HLFC SYSTEMS AND SUCTION SURFACES

### TABLE OF CONTENTS

M.1	Introduction.....	364
M.2	Mechanical Failure.....	364
M.2.1	Reference design .....	364
M.2.2	Component failure rate data .....	364
M.3	Bird Strike Data .....	366
M.3.1	Data collection.....	366
M.3.2	Data summary.....	366
M.4	HYLTEC Material Durability Trials .....	367
M.4.1	Introduction .....	367
M.4.2	Description of materials .....	368
M.4.3	Material inspection .....	368
M.4.4	Discussion - Corrosion, cracking and surface damage .....	370
M.4.5	Hole geometries.....	371
M.4.6	Discussion - Hole size .....	373
M.4.7	Flow measurements .....	374
M.4.8	Discussion - Flow measurement.....	376



## **M.1 INTRODUCTION**

Appendix M contains component failure rate data that was used in estimating the HLFC system reliability, as described in section 10.2 (Chapter 10). Information from the FAA National Wildlife Strike Database (FAA, 2001) on bird strikes has been reproduced in section M.3. This has enabled a preliminary estimate of the probability of a bird striking, and damaging, the laminar flow surfaces on the wing, empennage and nacelle of a HLFC commercial jet aircraft (see section 10.3, Chapter 10).

In section M.4 of this appendix, a detailed report is included on the durability of HLFC suction surfaces. A report is presented of work performed jointly by the author and other research partners as part of the HYLTEC project and associated research conducted by the author with students at the University of Limerick.

## **M.2 MECHANICAL FAILURE**

### **M.2.1 Reference design**

The HTP of the 757-200 class aircraft was selected as a reference design to estimate the suction power and installed weight of the system (described in Chapter 7). The conceptual design was extended to include the control and monitoring functions, so that a preliminary system reliability analysis could be performed. The system block diagram is shown in Fig. 10-1 (Chapter 10).

### **M.2.2 Component failure rate data**

Data for the selected reference components are given in Table M-1. The removal rate is the reciprocal of the MTBUR (Mean Time Between Unscheduled Removals). For items 1 to 7 the rate per 1000 hours has been calculated. A factor of 75% was used to estimate the failure rates from the quoted removal rates (i.e. assuming a “no fault found” rate of 25%). This was seen to be a representative value based on details given in Boeing (1976). A technology improvement factor of 5% per decade was assumed. The estimated failure rates for the reference components were obtained by dividing the unscheduled removal rate by these two factors. The resulting values were used in the reliability analysis described in section 10.2 (Chapter 10).



Table M-1 Aircraft component reliability data for selected reference items

Ref. No.	Item description	Raw data		Correction factors		Projected data		Source
		MTBUR (hr)	Unscheduled removal rate (per 1000hr)	Percent justified	Tech-nology factor	Estimated MTBF (hr)	Estimated failure rate (per 1000hr)	
1	Sensor pressure	25000	0.040	0.75	0.95	35088	0.029	For B767 air supply system. British Airways (1991)
2	Flow meter	17400	0.057	0.75	0.90	25778	0.039	For HS 125 fuel system British Aerospace (1979)
3	Control valve	32000	0.031	0.75	1.00	42667	0.023	For Airbus anti-ice system Airbus (2002c)
4	Shut-off valve (SOV)	10000	0.100	0.75	0.95	14035	0.071	For B767 cargo heating system British Airways (1991)
5	Shut-off valve (SOV)	100000	0.010	0.75	1.00	133333	0.008	For Airbus anti-ice system Airbus (2002c)
6	Shut-off valve (SOV)					70000	0.014	For aircraft ECS system Nord-Micro (2002)
7	Over pressure valve (OPV)	53000	0.019	0.75	1.00	70667	0.014	For Airbus bleed system Airbus (2002c)
8	Motor					20000	0.050	Electric motor Humphreys (2002)
9	Compressor	20000	0.050	0.75	1.00	26667	0.038	For Airbus air system Airbus (2002c)
10	Engine compressor	15000	0.067	0.75	1.00	20000	0.050	Engine compressor Hickey (2001)
11	Starter turbine	27000	0.037	0.75	1.00	36000	0.028	For Airbus air system Airbus (2002c)
12	PRSOV	5000	0.200	0.75	0.95	7018	0.143	For B767 pneumatics system British Airways (1991)
13	PRSOV	18000	0.056	0.75	1.00	24000	0.042	For Airbus pressurisation system Airbus (2002c)
14	Pressure regulator	17300	0.058	0.75	0.90	25630	0.039	For HS 125 ECS system British Aerospace (1979)
15	Valve	15000	0.067	0.75	0.90	22222	0.045	For HS 125 ECS system British Aerospace (1979)
16	Computer controller	20000	0.050	0.75	1.00	26667	0.038	For Airbus controller Airbus (2002c)
17	Pump de-icing system	8000	0.125	0.75	0.90	11852	0.084	For HS 125 TKS de-icing system British Aerospace (1979)
18	Pump					15000	0.067	De-icing system pump Humphreys (2002)



## M.3 BIRD STRIKE DATA

### M.3.1 Data collection

The United States Department of Agriculture's National Wildlife Research Center (NWRC), through an agreement with the FAA, began a project in 1995 to obtain more objective estimates of the wildlife strike problem in the USA for civil aviation (NWRC, 2001). Pilots, air traffic controllers, mechanics and others in the aviation field submit reports on a standard form, whenever there is an aircraft encounter with wildlife. From 1990 - 1998, the reported number of bird strikes to civil aircraft in the US, averaged over 2500 per year. Reporting is not mandatory and it was estimated by the NWRC that less than 20% of strikes were reported; however it is probable that the vast majority of strikes that caused damage to aircraft, were reported. A database has been established, and reports are published by the FAA (2001) and the NWRC (2001).

### M.3.2 Data summary

Tables M-2, M-3 and M-4 contain a summary of the data extracted from *Wildlife Strikes to Civil Aircraft in the United States, 1990 - 1999* (Cleary et al., 2000) as recorded on the FAA National Wildlife Strike Database (FAA, 2001). The analysis of the data is presented in section 10.3, Chapter 10.

**Table M-2** *Aircraft components reported struck and damaged by birds (Cleary et al., 2000)*

Aircraft component	Components struck	%	Components damaged	%
Radome / nose	5 906	25	678	14
Windshield	4 367	18	341	7
Engines	4 182	18	1 700	35
Wing / rotor	3 192	13	1 015	21
Fuselage	2 751	12	161	3
Landing gear	1 231	5	160	3
Propellers	856	4	100	2
Tail	362	2	170	4
Lights	212	1	173	4
Other	657	3	321	7
<b>Total</b>	<b>23 716</b>	<b>100</b>	<b>4 819</b>	<b>100</b>

**Table M-3** *Reported damage resulting from bird strike to civil aircraft (Cleary et al., 2000)*

Damage category	10-year total	% of total known
Minor	2 155	9
Uncertain	654	3
Substantial	1 331	6
Destroyed	7	<1
None	19 690	83
<b>Total known</b>	<b>23 837</b>	<b>100</b>
Unknown	3 5696	
<b>Total</b>	<b>27 433</b>	



**Damage codes:**

- Minor = The aircraft can be rendered airworthy by simple repairs or replacement and an extensive inspection is not necessary.
- Uncertain = The aircraft was damaged, but details as to the extent of the damage are lacking.
- Substantial = The aircraft incurs damage or structural failure which adversely affects the structural strength, performance or flight characteristics of the aircraft and which would normally require major repair or replacement of the effected component.
- Destroyed = The damage sustained makes it inadvisable to restore the aircraft to an airworthy condition.

**Table M-4** *Reported phase of flight of bird strike to civil aircraft (Cleary et al., 2000)*

Phase of flight	10-year total	% of total known
Parked	14	< 1
Taxi	104	< 1
Take off	4 564	20
Climb	4 370	19
En route	825	4
Descent / approach	9508	41
Landing roll	3 751	16
<b>Total known</b>	<b>23 136</b>	<b>100</b>
Unknown	4 297	
<b>Total</b>	<b>27 433</b>	

## M.4 HYLTEC MATERIAL DURABILITY TRIALS <sup>1</sup>

### M.4.1 Introduction

This section of the appendix contains an abridged version of the paper *Durability of Hybrid Laminar Flow Control (HLFC) Surfaces*, by Young, Mahony, McClafferty, Corish, Humphreys and Totland (in press). The work relates to material durability test conducted using a SAAB 2000 aircraft, as described in section 10.4 of Chapter 10. The post flight-test inspection and analysis of the panels was conducted under the direction of the author at the University of Limerick. Aspects of the work have been reported by Mahony (2002) and McClafferty (2002).

The objectives, outlined in section 10.4.3 (Chapter 10), are repeated here for completeness. The objectives were:

1. To examine the panels for cracking and corrosion, using optical and scanning electron microscopy<sup>2</sup>;
2. To measure the hole sizes using an optical technique and to statistically analyse the data to ascertain if the hole sizes changed due to exposure on the aircraft<sup>3</sup>;
3. To determine the pressure loss versus flow rate characteristics of the different panels and to relate, if possible, the results to the measured hole sizes<sup>4</sup>.

<sup>1</sup> Reported by Young *et al.* (in press). Selected parts have been reproduced in this section.

<sup>2</sup> Experimental work undertaken by J. Corish and B. Mahony (B.Eng. students, University of Limerick), under the supervision of the author.

<sup>3</sup> Experimental work undertaken by B. Mahony (B.Eng. student, University of Limerick), under the supervision of the author.



## M.4.2 Description of materials

The materials that were evaluated, were hard anodised non-clad aluminium, chromic acid anodised non-clad aluminium, titanium and APC-2, a thermoplastic carbon fibre composite of PEEK matrix (Table 10-3, Chapter 10). An aluminium panel which had not been was not installed on the aircraft, was used as a reference. All panels were drilled with a Nd-YAG laser using the single pulse method and Argon as the shielding gas. The panels were pressed, rolled to shape and installed in the holder (Fig. 10-5, Chapter 10), which was then attached to the leading edge of the port wing.

## M.4.3 Material inspection

### M.4.3.1 Apparatus and specimen preparation

An optical microscope (magnification 1660X) and Scanning Electron Microscope (SEM) were used to identify and record visual signs of cracking and surface corrosion. The surface analysis method EDAX (energy dispersive analysis x-ray) was used to identify the presence of selected elements on the surface.

Sectioning of the metal samples was done with a guillotine, and the composite material panel was cut using a diamond-edged saw. The aluminium and titanium specimens were mounted both in an epoxy and a phenolic resin, while the composite specimens were mounted in a softer thermoplastic resin, to aid with polishing. All specimens were ground and polished individually using isopropyl alcohol as a lubricant.

### M.4.3.2 Results - Hard anodised aluminium

The hard anodised aluminium panel had a very poor surface finish with a significant number of surface blemishes, which could be seen with the naked eye. (It was for this reason that the panel was removed prematurely from the test aircraft.) Under the optical microscope, large areas of pitting corrosion extending to ~1.5 mm in diameter, were clearly visible (Fig. M-1a). The EDAX surface analysis identified significant amount of sulphur, indicative of corrosion. Using the SEM, an oblique cut through one hole displayed extensive micro-cracking (Fig. M-1b). This feature was evident on other specimens cut from the same panel.

### M.4.3.3 Results - Anodised aluminium panel

To the naked eye, the surface of this panel was in better condition than the hard anodised panel. Sectioned specimens cut through the panel indicated many cracks on either side of the hole radiating outwards (Fig. M-2a) when viewed with the optical microscope, which were absent on the reference panel (Fig. M-3a).

Using the SEM, pitting corrosion on the test panel was clearly noticeable and a micro-crack was identified on the surface emanating from a hole (Fig. M-2b). Images of cross section specimens revealed crack lengths of up to 50  $\mu\text{m}$ . As with the hard

---

<sup>4</sup> Experimental work undertaken by A. McClafferty (B.Eng. student, University of Limerick), under the supervision of the author.



anodised panel, the EDAX inspection method confirmed significant amounts of sulphur on the surface of the panel.

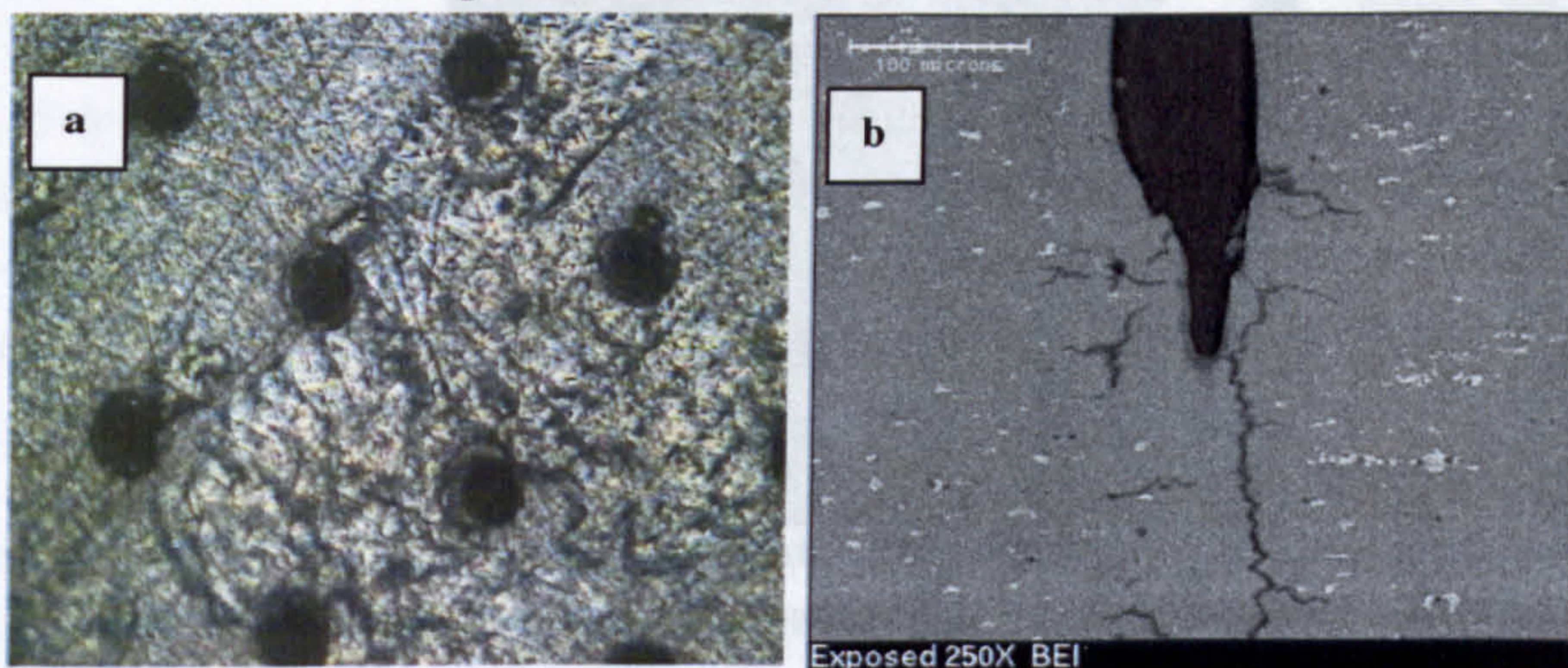


**Fig. M-1** Hard anodised aluminium panel: (a) Optical microscope image showing corrosion due to the hard anodising process; (b) SEM image of oblique cut through hole (after Young et al., in press)

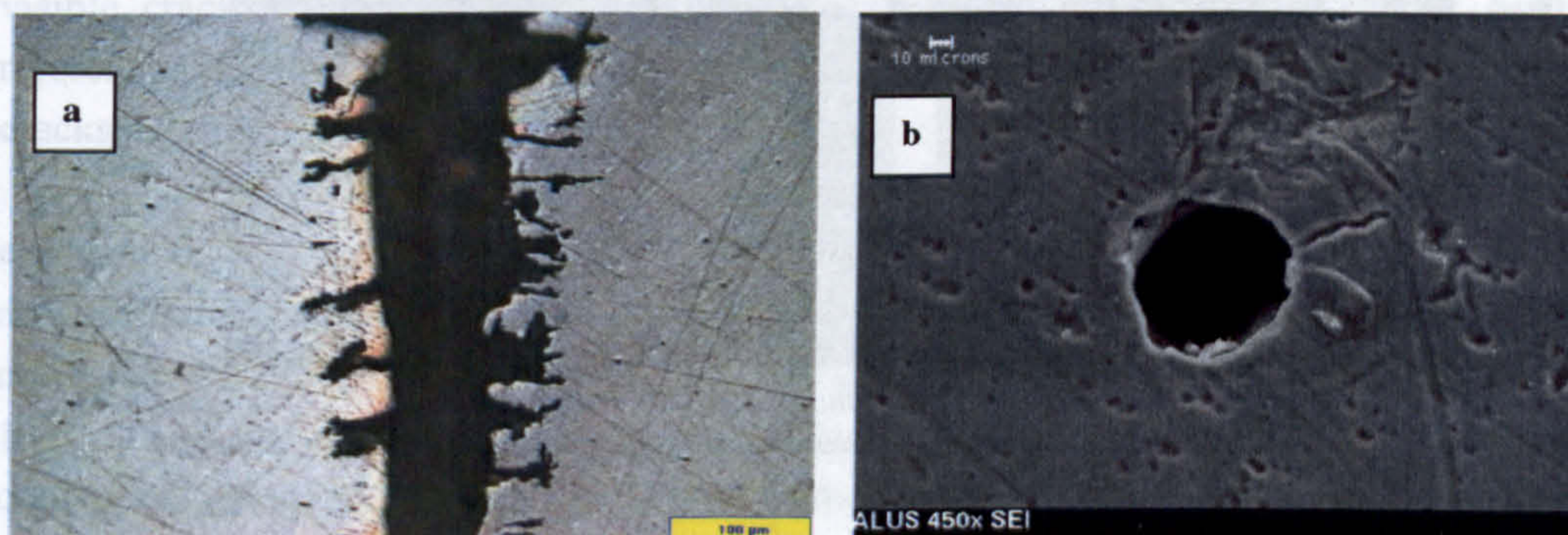


**Fig. M-2** Anodised aluminium panel: (a) Optical microscope image of cross section through holes in test panel; (b) SEM image of aluminium test panel showing micro-crack and pitting corrosion (after Young et al., in press)

#### M.4.3.4 Results - Titanium panel

The visual inspection of the surface of the titanium panel revealed no indication of pitting corrosion. Cross sections of the holes were examined using the optical microscope and the SEM; in contrast to the aluminium panel, there was no evidence of any micro-cracking (example seen in Fig. M-3b).

#### M.4.3.5 Results - APC-2 panel

The image quality from the optical microscope was substantially poorer for this material compared to the metals. The SEM was thus relied upon to evaluate the material. It is evident in Fig. M-4(a) that individual fibres had been stripped from the surface between the holes. Focusing on the hole itself (Fig. M-4b) it may be seen that matrix material had been removed in the vicinity of the hole, exposing the carbon fibres.



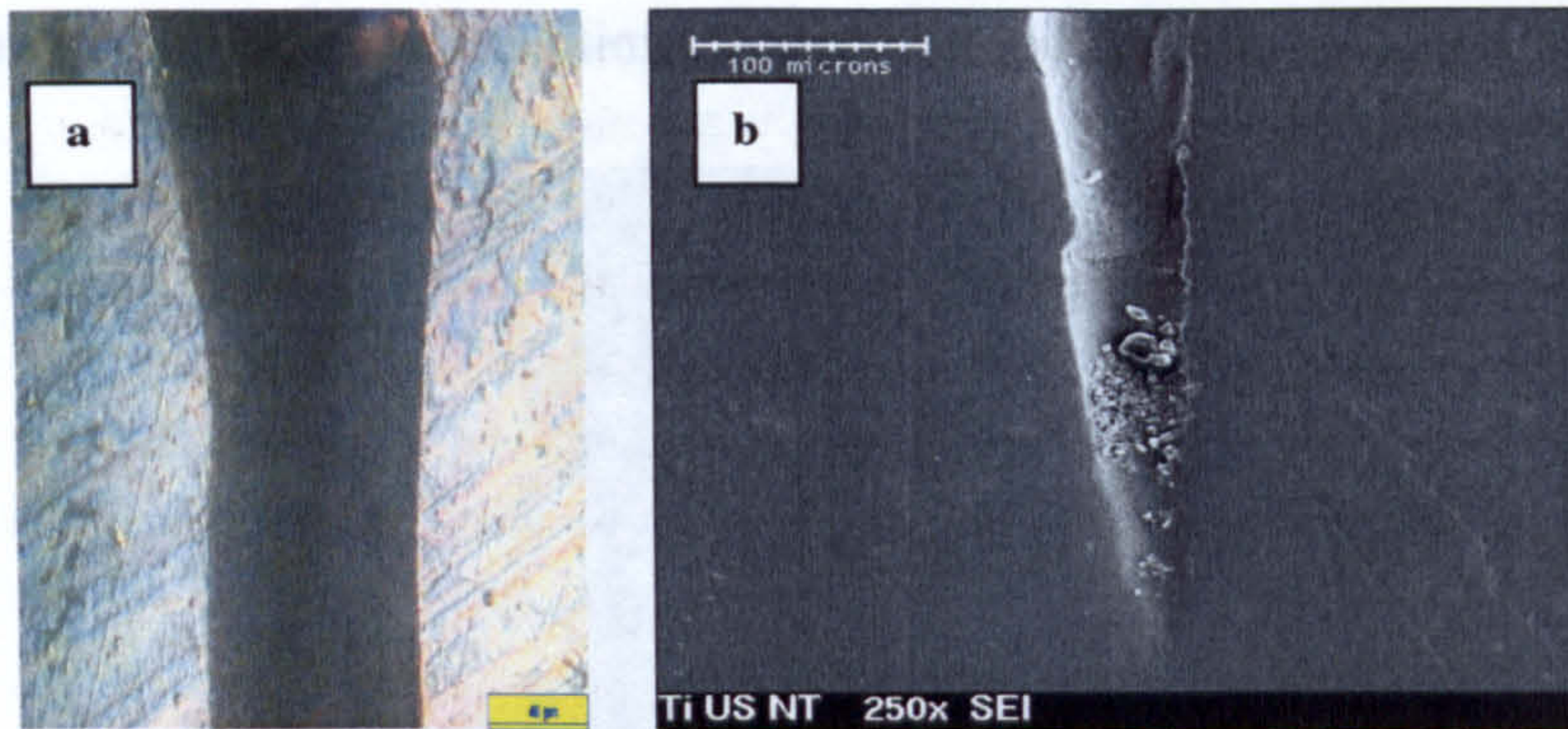


**Fig. M-3** (a) Optical microscope image of cross-section of hole in aluminium reference panel; (b) SEM image of oblique cut through hole in titanium panel, displaying no evidence of cracking (after Young et al., in press)

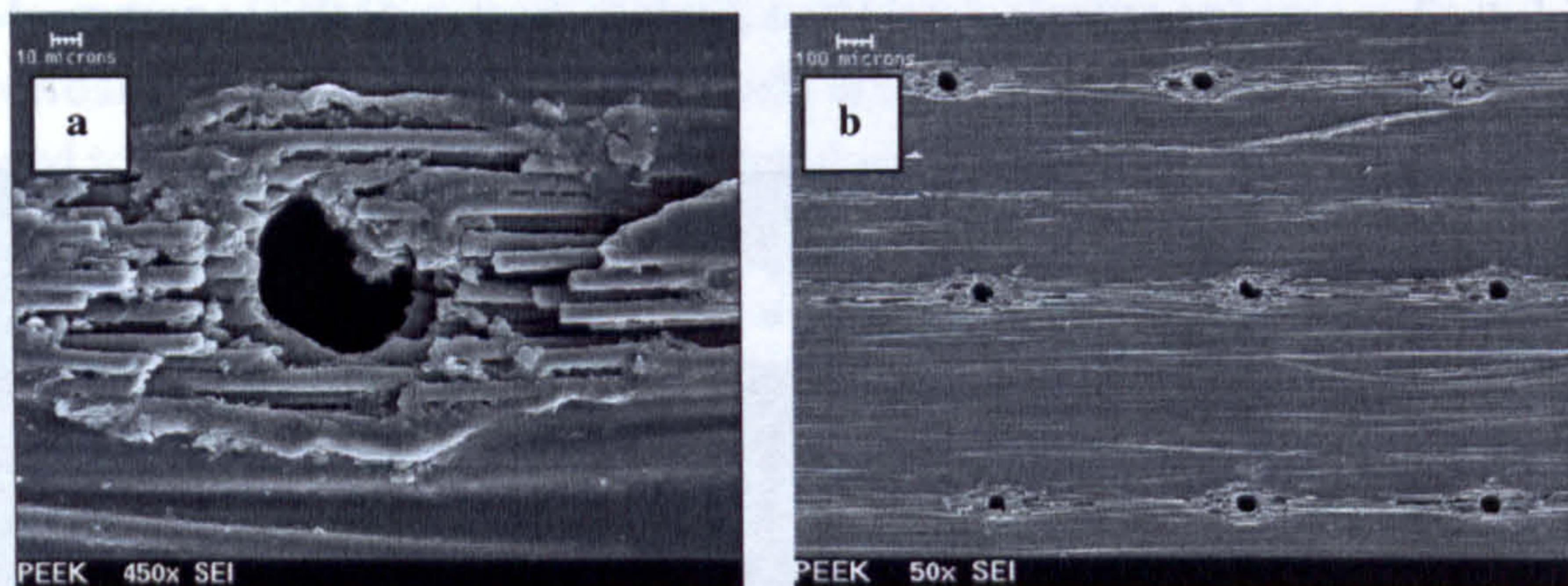


**Fig. M-4** Images of APC-2 panel: (a) SEM image showing "burnout" of matrix around the hole; (b) SEM image showing fibre removal between holes (after Young et al., in press)

#### M.4.4 Discussion - Corrosion, cracking and surface damage

Titanium is regarded as the benchmark material for HLFC applications; however, for an engine nacelle, the additional weight that results from the use of titanium (in place of the composite material used on most current designs), dramatically reduces the net performance gain from the HLFC system. Furthermore, the perforated suction area is not required on the leading edge of the nacelle, making the material durability less critical for this component, than would be the case for the wing or empennage. For these reasons, aluminium and carbon fibre reinforced PEEK have been considered.

The major difficulty in using aluminium – with its relatively poor corrosion resistance – for HLFC applications, is that the base material cannot be protected by cladding or painting. This led to the attempt to protect the material by anodisation. On inspection, it was observed that the surface of the hard anodised aluminium panel was characterised by large areas of pitting, known commonly as "burning". It was noted after the flight trials, that the major alloying element in this type of aluminium alloy is copper (typically 3.5 - 5%). When anodised in this way, the copper reacts with the sulphuric acid (hard anodise) process, in a way that prohibits the hard anodise from being uniform at the copper precipitates. For this reason, the chromic acid anodic



process is only recommended for use on alloys containing less than 3% Cu and less than 7% Si (ASM, 1980). The anodisation process was thus not suitable for the grade of aluminium selected.

Initial inspection of the chromic acid anodised panel indicated that it was in far better condition than the hard anodised panel; however, a serious concern regarding the durability of the material arose when a significant amount of cracking was observed emanating from the laser drilled holes. The mechanism by which these cracks formed could not be positively identified. As no cracks were seen on the reference panel, it may be deduced that they were the result of post drilling process(es), relating to the forming of the material and / or the environmental exposure it endured during the trials. This observation is however contrary to information presented by Yeo *et al.* (1994), who maintained that micro-cracking within the recast layer around the hole occurs due to the laser drilling process. Whether the cracks were initiated by the drilling process or not, the fact remains that after exposure on the aircraft, a substantial number of highly visible cracks were evident on the test specimens, which were not evident on the reference panel. It is suggested that corrosion has contributed to an opening-up of the cracks, as observed in Fig. M-2.

The titanium panel appeared to be entirely unaffected by the environmental exposure during the tests. Optical and scanning electron microscopy revealed no cracks at all in the material. The observation regarding the durability of the titanium panels is consistent with the results of the rain erosion tests, described in section 10.4.2 (Chapter 10). These findings would correlate with those of the NASA SAS programme, conducted using a Jetstar aircraft (see section C.4, Appendix C). Maddalon and Braslow (1990) reported that there was "no measurable degradation of the perforated titanium suction surface after four years of flight testing".

The surface damage mechanism of the thermoplastic composite material, whereby fibres were stripped from between the holes, is entirely consistent with the damage observed by the author on both the thermoplastic and epoxy rain erosion coupons, described in section 10.4.2 (Chapter 10).

## M.4.5 Hole geometries

### M.4.5.1 Hole measurement

The optical technique used to measure the hole areas followed a similar process to that outlined by Priest and Paluch (1996). Random sampling was used in selecting the holes to be measured. Image processing software was used to identify and measure the hole area. An equivalent hole diameter ( $d_e$ ) was determined for each hole measured

using the equation:  $d_e = \sqrt{\frac{4S}{\pi}}$  where  $S$  was the measured hole area. Referring to Fig.

B-14 (Appendix B), the hole pitch is defined as the distance  $A$  (in the span-wise direction) and  $B$  (in the length-wise direction). The panel geometric porosity was calculated using equation [B-1] (Appendix B), which was re-written as:



$$\text{Porosity} = \frac{\pi}{4} \left( \frac{\bar{d}_e^2}{\bar{A} \bar{B}} \right) \text{ where } \bar{d}_e \text{ is the mean panel equivalent hole diameter and}$$

$\bar{A}$ ,  $\bar{B}$  are the mean hole pitch values.

The analysis of variance (ANOVA) technique was used to examine the means of hole diameters of different data sets (from different samples) and to test the hypothesis that these means were statistically equal. This was done to determine if there was a change in effective hole diameter, due to the environmental exposure on the aircraft.

#### *M.4.5.2 Results - Hole pitch*

Table M-5 summaries the hole pitch and standard deviation ( $\sigma$ ) values determined in the span-wise and length-wise directions, for the three perforated panels tested. One hundred measurements were made for both the aluminium and titanium materials and 50 for the composite material.

#### *M.4.5.3 Results - Aluminium panel hole size*

A random sample of 100 holes on each side of the anodised aluminium test panel and the reference panel, was taken as the data set for the statistical analysis. The mean hole sizes, effective diameters and standard deviation results, are given in Table M-6. From the results of the ANOVA analysis, it was noted that there is a 99% probability that the laser entry holes on the reference panel were statistically equivalent in size to the laser entry holes on the test panel. Conducting a similar analysis on the samples of laser exit holes, it was concluded that statistically the two nominal hole sizes were significantly different.

#### *M.4.5.4 Results - Titanium panel hole size*

One hundred holes on each side of the titanium panels were examined (Table M-6). When evaluating this data, the laser exit holes on the reverse taper panel (i.e. where the smaller holes on the inner surface were not exposed on the aircraft) were used as a reference for assessing the normal taper panel laser exit holes (which were on the outside). Similarly, the laser entry holes on the normal taper panel acted as a standard for the laser entry holes on the reverse taper panel.

It was concluded from the ANOVA test that there is a 99% probability that the laser entry holes on the reverse and normal taper panels have the same nominal hole diameter. Furthermore, it was determined that there was also no significant difference in effective hole diameters between the laser exit holes on the two panels.

#### *M.4.5.5 Results - APC-2 panel hole size*

The carbon fibre composite was more difficult to inspect than the other panels, due to the fibres protruding through the surface of the material. This was particularly



evident when optical measurements of hole areas were attempted. Only five laser entry and exit holes were measured (Table M-6).

**Table M-5** Mean values and standard deviation for hole pitch (Young et al., in press)

	Anodised aluminium	Titanium	APC-2
$\bar{A}$ ( $\mu\text{m}$ )	700	722	708
$\sigma(\bar{A})$ ( $\mu\text{m}$ )	8.3	28.7	9.4
$\bar{B}$ ( $\mu\text{m}$ )	699	696	694
$\sigma(\bar{B})$ ( $\mu\text{m}$ )	49.3	29.7	24.9

**Table M-6** Geometric hole properties of aluminium, titanium and composite (Young et al., in press)

	Reference aluminium	Anodised aluminium	Titanium normal taper	Titanium reverse taper	APC-2
$\bar{d}_e$ laser entry ( $\mu\text{m}$ )	203.2	208.4	136.9	133.3	170.4
$\sigma(\bar{d}_e)$ laser entry ( $\mu\text{m}$ )	16.3	15.3	11.2	8.9	11.9
$\bar{d}_e$ laser exit ( $\mu\text{m}$ )	63.1	76.5	71.2	72.0	80.0
$\sigma(\bar{d}_e)$ laser exit ( $\mu\text{m}$ )	9.5	8.6	5.4	7.6	8.9
Porosity (based on $d_l$ )		0.94%	0.79%	0.81%	1.02%

#### M.4.6 Discussion - Hole size

An important result from this investigation concerned the mean hole sizes in the test panels. Concerns have been voiced regarding the effects on suction panel porosity, of long term environmental exposure on the leading edge of a wing (Humphreys and Totland, 2000). No comparative assessment of hole size was possible for the composite material; however, for both the anodised aluminium and titanium panels, this was possible. It was found that the laser exit holes (which were on the outside) on the anodised aluminium test panel, were significantly larger (~21%) than those on the reference panel (i.e. 76.5 $\mu\text{m}$  in comparison to 63.1 $\mu\text{m}$ ). The laser entry holes were also a little bigger for the test panel (208.4 $\mu\text{m}$  versus 203.2 $\mu\text{m}$ ); however, statistically (based on the ANOVA method) the mean hole diameters could be considered equivalent. It is suggested that the increase in hole diameter, is due to a depletion of the recast layer (formed during the laser drilling process) under the impact of airborne dust particles, rain and hail, assisted by the extensive cracking within the holes.

The ANOVA test revealed that statistically the laser entry holes on the reverse and normal taper panels, had the same nominal hole diameter. There was also no significant difference in effective hole diameters between the laser exit holes on the two panels; in spite of the fact that one surface was exposed to the external environment and the other was not. It was thus concluded, that any erosion affects on the external hole diameter, during the 20 months of in-flight exposure, were negligible.



The measured hole sizes and scatter of results for the titanium specimens were compared to the results of Priest and Paluch (1996). It should be noted that the drilling process was carried out with different drilling parameters in the two cases. It was thus not expected that the hole sizes would be identical; however, the results proved to be useful in comparing the pressure drop measurements (see section M.4.7 below). The mean hole diameter (laser exit) quoted by Preist and Paluch (1996) was about ~23% smaller than that given in Table M-6; but the standard deviation was observed to be similar.

## M.4.7 Flow measurements

### M.4.7.1 Experimental apparatus

A customised rig (Fig. M-5) was assembled to measure the flow characteristics of the laser drilled panels, enabling plots of pressure drop against net panel velocity ( $V_w$ ) to be produced. A compressor supplied air at one bar through a filter and a honeycomb flow "straightener" to the test section. The test section comprised of two stainless steel flanges, one male and one female, which clamped the test specimen between two nylon gaskets. The external diameter of the gasket was 35 mm and the internal diameter was 25 mm, matching the internal diameter of the test section. A Mass Flow Controller (MFC) was located down-stream of the test section and a digital hand-held manometer was used to measure the pressure drop across the test specimen. A thermocouple was used to measure the internal air temperature.

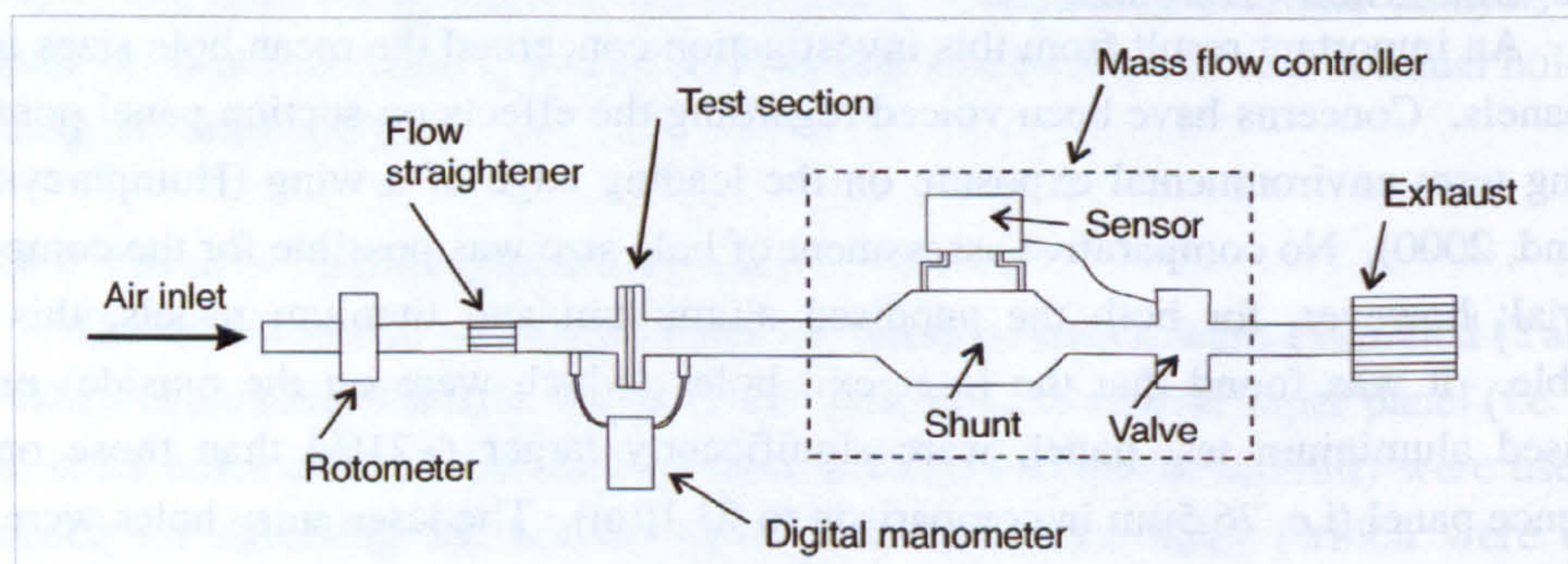


Fig. M-5 Schematic of flow rig (assembled at the University of Limerick)

### M.4.7.2 Test specimens and method

Three 35mm diameter specimens were cut from the test panels described in Table 10-3 (Chapter 10) – one anodised aluminium, one titanium and one APC-2 specimen. The hard anodised panel was not evaluated. A fourth specimen was cut from the aluminium reference panel. For initial tests, the specimens were left in the as-received condition and were later ultra-sonically cleaned to ascertain the effect on the airflow of debris in the holes. Pressure loss measurements were performed on the four specimens in both the normal and reversed flow directions (see Fig. 10-5, Chapter 10).



Mean pressure loss values were calculated from data recorded during ten experimental runs conducted on each specimen.

M.4.7.3 Results - Pressure drop

The pressure drop results are shown in Figures M-6a and M-6b. It was noted that prior to cleaning, the APC-2 specimen was almost completely blocked. This result was not included in these figures.

M.4.7.4 In situ pressure drop measurements

Humphreys and Totland (2000) describe the data collection of flow measurements taken *in situ* on the test panels installed on the SAAB 2000 aircraft at the monthly inspections during the flight tests. Fig. M-7 is a sample of the corrected data obtained during the programme, and included herein, to compare against the laboratory results given in Figures M-6a and M-6b. The ordinate variable indicates the panel porosity, which was measured at the same location on the panel each month, using a custom-built flow meter.

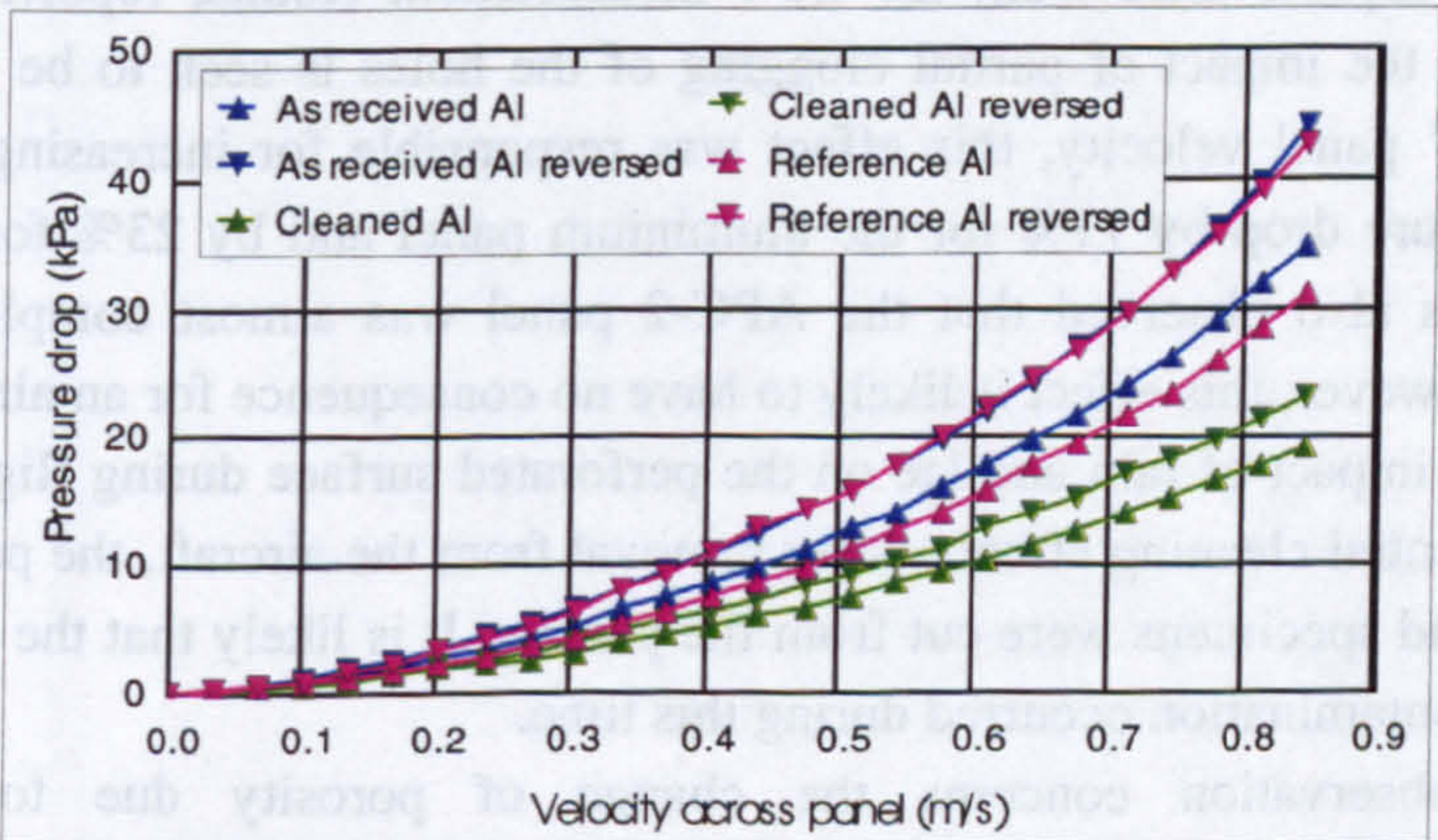


Fig. M-6a Pressure drop through perforated panels (based on McClafferty, 2002)

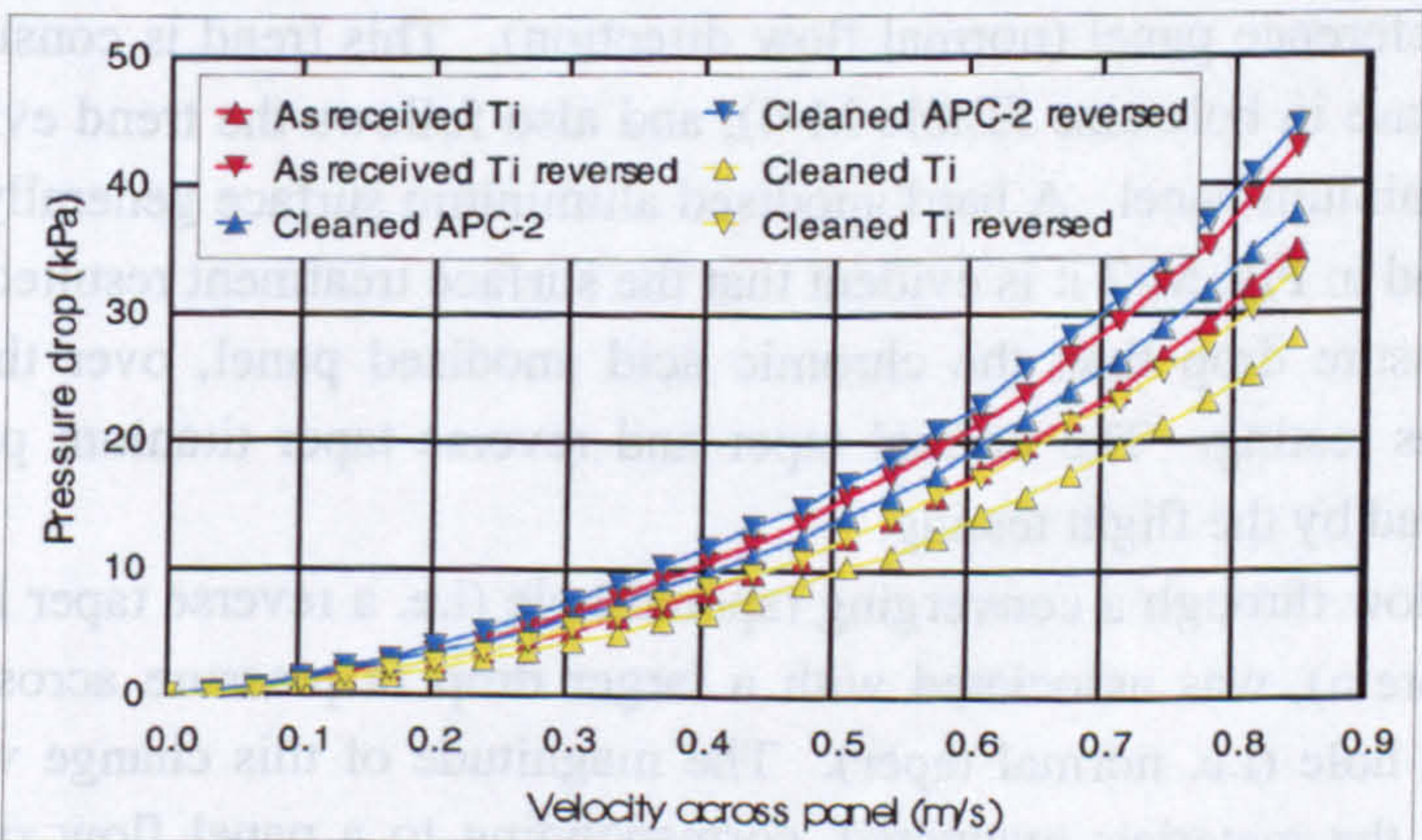
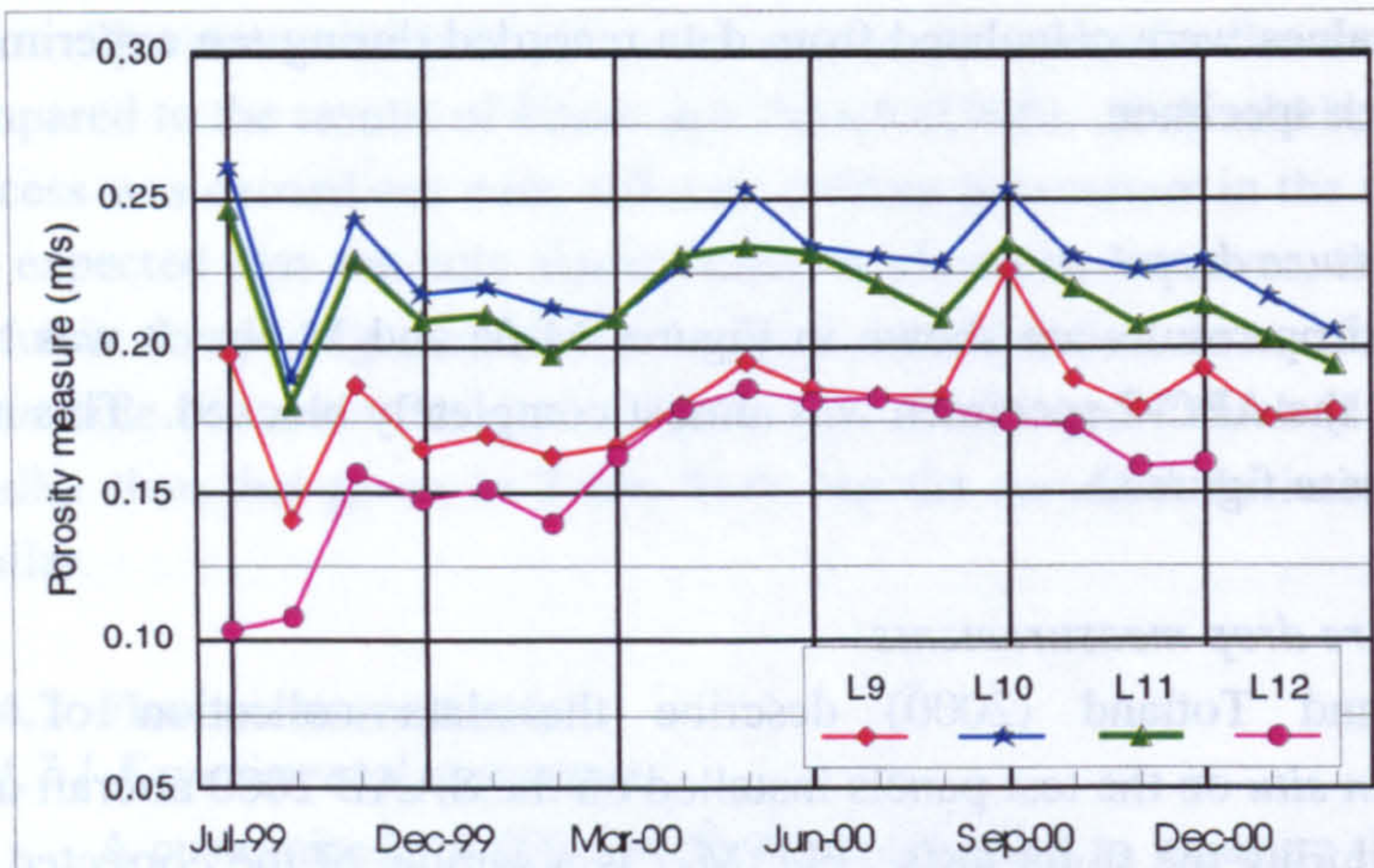


Fig. M-6b Pressure drop through perforated panels (based on McClafferty, 2002)





**Fig. M-7** Porosity results taken during the HYLTEC programme on the (passive) lower panel surface L9 - hard anodised aluminium; L10 - titanium normal taper; L11 - titanium reverse taper; L12 - anodised aluminium (after Young et al., in press)

#### M.4.8 Discussion - Flow measurement

Four important aspects arise from the flow measurement results, reported in section M.4.7. Firstly, the impact of partial clogging of the holes is seen to be very significant. At  $0.5\text{ms}^{-1}$  panel velocity, this effect was responsible for increasing the magnitude of the pressure drop by 71% for the aluminium panel and by 23% for the titanium panel. It was also observed that the APC-2 panel was almost completely blocked on receipt. However, this effect is likely to have no consequence for an aircraft flown regularly, as the impact of rain and ice on the perforated surface during flight is known to have a substantial cleaning effect. After removal from the aircraft, the panels were "handled" a lot and specimens were cut from the panels. It is likely that the most significant degree of contamination occurred during this time.

The second observation concerns the change of porosity due to the environmental exposure on the aircraft. For the anodised aluminium panel, the magnitude of the pressure drop across the test panel was  $\sim 32\%$  lower at  $0.5\text{ms}^{-1}$ , than that measured for the reference panel (normal flow direction). This trend is consistent with the observed increase in hole size (Table M-4), and also follows the trend evident in Fig. M-7 for the aluminium panel. A hard anodised aluminium surface generally has good wear resistance and in Fig. M-7 it is evident that the surface treatment resulted in a smaller change in pressure drop than the chromic acid anodised panel, over the 18 months of simultaneous testing. The normal taper and reverse taper titanium panels appeared to be unaffected by the flight testing.

In all cases airflow through a converging tapered hole (i.e. a reverse taper in the convention adopted herein), was associated with a larger drop in pressure across the panel than a diverging hole (i.e. normal taper). The magnitude of this change varied between 19 - 30% for the materials evaluated, corresponding to a panel flow rate of  $0.5\text{ms}^{-1}$ .



The pressure drop versus panel velocity characteristics were observed to follow the identical trend previously reported by Poll *et al.* (1992b) and Priest and Paluch (1996). The pressure drop of the normal taper titanium panels was observed to be a little lower than comparative values measured by Priest and Paluch (1996). Considering the fact that the holes in the HYLTEC panels were larger (see section M.6.4), this was consistent with expectation.



**Blank page**



# **APPENDIX N**

## **NOMENCLATURE, DEFINITIONS AND GLOSSARY**

### **TABLE OF CONTENTS**

<b>N.1</b>	<b>Nomenclature .....</b>	<b>380</b>
	<b>N.1.1</b> <b>Mathematical notation .....</b>	<b>380</b>
	<b>N.1.2</b> <b>Abbreviations .....</b>	<b>382</b>
<b>N.2</b>	<b>Definitions and Glossary .....</b>	<b>387</b>
	<b>N.2.1</b> <b>Definitions of mission weights, distance and time .....</b>	<b>387</b>
	<b>N.2.2</b> <b>Glossary of technical jargon .....</b>	<b>387</b>



## N.1 NOMENCLATURE

### N.1.1 Mathematical notation

$a$	Speed of sound; acceleration
$A$	Aspect ratio
$A, B$	Hole pitch in span-wise and length-wise directions, respectively
$b$	Wing span
$c$	Specific fuel consumption (mass flow basis); Chord length
$c'$	Specific fuel consumption (weight flow basis)
$c_p$	Specific heat capacity at constant pressure
$C_d$	Section (local) drag coefficient
$C_D$	Drag coefficient
$C_{D_i}$	Lift-dependent drag coefficient
$C_{D_{min}}$	Minimum drag coefficient
$C_{D_o}$	Zero-lift drag coefficient
$C_{D_P}$	Profile drag coefficient
$C_{D_S}$	Equivalent suction drag coefficient
$C_{D_V}$	Trailing vortex drag coefficient
$C_F$	Friction coefficient
$C_L$	Lift coefficient
$C_{L_K}$	Lift coefficient where drag polar changes (defined in Fig. E-13, Appendix E)
$C_p$	Pressure coefficient
$d_1, d_2$	Hole diameter on the laser exit and entry sides, respectively
$d$	Hole diameter
$d_e$	Equivalent hole diameter
$D$	Drag; Diameter of duct
$e$	Oswald efficiency factor
$E$	Lift-to-drag ratio
$f_{acc}$	Acceleration factor
$F_N$	Thrust (net)
$g$	Gravitational acceleration
$h$	Height
$H$	Geopotential height
$K$	Lift-dependent drag factor
$K_1, K_2, K_3$	Drag coefficient factors (defined in section E.9, Appendix E)
$L$	Lift; Lapse rate; Length
$L_h$	Length of hole
$m$	Aircraft mass
$\dot{m}$	Mass flow rate
$m_f$	Fuel mass



$M$	Mach number
$M_{DD}$	Drag divergent Mach number
$N$	Rotational speed of engine
$p$	Pressure
$P$	Power
$Q$	Fuel flow (mass flow basis)
$Q'$	Fuel flow (weight flow basis)
$Q_{cor}$	Corrected fuel flow
$Q_{tot}$	Total fuel flow
$r_a$	Specific air range (SAR)
$R$	Range; Gas constant
$Re$	Reynolds number
$s$	Ground distance (takeoff, landing)
$S$	Wing reference area; Panel area; Hole area; Sutherland coefficient
$S(t)$	Survivor function
$t$	Time; Chord thickness
$T$	Temperature (absolute); Time (total)
$TIC_f$	Average fraction of time-in-cloud on one flight
$TIC_R$	Average fraction of time-in-cloud for a sample of flights on one route
$V$	True airspeed (TAS)
$V_2$	Takeoff climb speed
$V_C$	Calibrated airspeed (CAS)
$V_e$	Equivalent airspeed (EAS)
$V_h$	Velocity through suction hole
$V_R$	Rotation speed
$V_v$	Vertical component of TAS
$V_w$	Mean panel flow velocity
$W$	Weight
$x$	Still air distance; Distance along chord
$x_1, x_2$	Abscissa variable used for data interpolation
$y_1, y_2$	Ordinate variable used for data interpolation

### Greek symbols

$\beta$	Range parameter, defined in equation [8-1] (chapter 8).
$\beta_s$	Sutherland coefficient
$\gamma$	Ratio of specific heats of air; Gradient angle
$\delta$	Relative pressure; Drag (planform) correction factor; Change
$\eta$	Efficiency; Non-dimensional semi-span coordinate
$\theta$	Relative temperature
$\Lambda$	Sweep angle
$\lambda$	Correction factor; Failure rate
$\mu$	Dynamic viscosity
$\mu_B$	Braking coefficient of friction



$\mu_R$	Rolling coefficient of friction
$\rho$	Density
$\sigma$	Relative density; Standard deviation
$\psi$	Parameter defined in Table E-1 (Appendix E) for acceleration factor

*Subscript*

$o$	Standard (sea level) value
$1$	Start of cruise / hold condition
$2$	End of cruise / hold condition
$a$	Air segment
$acc$	Accelerated
$B$	Brake
$f$	Fuel
$g$	Ground segment
$max$	Maximum
$min$	Minimum
$R$	Rotate
$RL$	Rotate to lift-off
$t$	Total
$T$	Touchdown
$TO$	Takeoff
$unacc$	Unaccelerated

*Superscript*

$*$	Conditions at Tropopause
-----	--------------------------

*Chemical symbols*

Al	Aluminium
CH <sub>4</sub>	Methane
CO	Carbon monoxide
CO <sub>2</sub>	Carbon dioxide
Cu	Copper
HC	Hydrocarbon
NaCl	Sodium chloride
NO <sub>x</sub>	Nitrogen oxides
O <sub>3</sub>	Ozone
Si	Silicon
SO <sub>2</sub>	Sulphur dioxide
Ti	Titanium

**N.1.2 Abbreviations and acronyms**

2D	Two Dimensional
3D	Three Dimensional
A/C	Aircraft



ACEE	Aircraft Energy Efficient
AFM	Atomic Force Microscopy
ALTTA	Application of Hybrid Laminar Flow Technology on Transport Aircraft
ANOVA	Analysis of variance
AOA	Angle of attack
APU	Auxiliary Power Unit
AS&T	Aerospace Systems and Technology
ASFR	Age Specific Failure Rate
ATC	Air Traffic Control
ATM	Air Traffic Management
ATTAS	Advanced Technologies Testing Aircraft System
Ave.	Average
BAe	British Aerospace
B.Eng.	Bachelor of Engineering
BR	Brake Release
BRW	Brake Release Weight
Cb	Cumulonimbus
Cc	Cirrocumulus
Ci	Cirrus
Cs	Cirrostratus
Cu	Cumulus
CAEP	Committee on Aviation Environmental Protection
CAS	Calibrated Airspeed
CASA	Construcciones Aeronáuticas SA
CD	Compact Disc
CEC	Commission of the European Communities
CERT	Centre d'Études et de Recherches de Toulouse
CES	Chemical and Environmental Science
CF	Cross Flow
CFC	Chlorofluorocarbon
CIV	Clouds in vicinity
CMC	Critical micelle concentration
COADS	Comprehensive Ocean Atmospheric Data set
Conc.	Concentration
CORDIS	Community Research & Development Information Service
CP	Commercial Pure
CPR	Component Performance Report
DASA	DaimlerChrysler Aerospace
DERA	Defence Evaluation and Research Agency
Dist.	Distance
DLR	Deutsche Forschungsanstalt für Luft- und Raumfahrt
DOC	Direct Operating Cost
DragNet	Drag Reduction Network
EAS	Equivalent Airspeed



EB	Electron Beam
EC	European Commission
ECMWF	European Centre for Medium Range Weather Forecasting
ECS	Environmental Control System
Ed.	Editor
EDAX	Energy dispersive analysis X-ray
EG	Ethylene Glycol
ELFIN	European Laminar Flow Investigation
EMD	Equivalent Melted Diameter
ETOPS	Extended Twin Engine Operations
FAA	Federal Aviation Administration
FAR	Federal Aviation Regulation
FFA	Aeronautical Research Institute of Sweden
FL	Flight Level
FLAM	Falcon Laminar
FOD	Foreign Object Damage
FPD	Freezing Point Depressant
GA	General Aviation
GASP	Global Atmospheric Sampling Program
GE	General Electric
GEAE	General Electric Aircraft Engines
HLF	Hybrid Laminar Flow
HLFC	Hybrid Laminar Flow Control
HNL	Honolulu International Airport
HP	High Pressure
HPC	High Pressure Compressor
HTP	Horizontal Tailplane
HVPS	High Volume Precipitation Spectrometer
HYLDA	Hybrid Laminar Flow Demonstration on Aircraft
HYLTEC	Hybrid Laminar Flow Technology
IAS	Indicated Airspeed
ICAO	International Civil Aviation Organisation
IDG	Integrated Drive Generator
IFR	Instrument Flight Rules
Int.	International
IOC	Indirect Operating Cost
IPC	Intermediate Pressure Compressor
IPCC	Intergovernmental Panel on Climate Change
ISA	International Standard Atmosphere
ISCPP	International Satellite Cloud Climatology Project
ISO	International Organization for Standardization
IWC	Ice Water Content
JAA	European Joint Aviation Authority
JAR	Joint Airworthiness Requirement
JFK	John F. Kennedy International Airport (New York)



KCAS	Knots Calibrated Airspeed
KIAS	Knots Indicated Airspeed
KTAS	Knots True Airspeed
LARA	Laminar Flow Research Action
LaTec	Laminar Technology
LAX	Los Angeles International Airport
LEFT	Leading Edge Flight Test
LCCS	Liquid Contamination Control System
LFC	Laminar Flow Control
LHR	London Heathrow International Airport
LRS	Long-range Speed
LTO	Landing / Takeoff (cycle)
LW	Long-wave
M	Mach number
MAE	Mechanical and Aeronautical Engineering
Max.	Maximum
MDA/DH	Minimum Descent Altitude/Decision Height
MEMS	Micro-Electro Mechanical Systems
Met.	Meteorological
METAR	Meteorological Aerodrome Report
MFC	Mass Flow Controller
Min.	Minimum
MLW	Maximum Landing Weight
MOZAIC	Measurement of Ozone on Airbus In-Service Aircraft
MRS	Maximum Range Speed
M.Sc.	Master of Science
MTBF	Mean Time Between Failures
MTBUR	Mean Time Between Unscheduled Removals
MTOW	Maximum Takeoff Weight
MVO	Multi-variate Optimisation
MZFW	Maximum Zero Fuel Weight
NACA	National Advisory Committee for Aeronautics
NASA	National Aeronautics and Space Administration
ND	Not determined
Nd-YAG	Neodymium doped - Yttrium Aluminium Garnet
No.	Number
NLF	Natural Laminar Flow
NWP	Numerical Weather Prediction
NWRC	National Wildlife Research Center
OEW	Operating Empty Weight
ONERA	Office Nationale d'Études et de Recherches Aérospatiale
OPEC	Organization of Petroleum Exporting Countries
Ops.	Operations
OPV	Over-Pressure Valve



Pax.	Passengers
PC	Personal Computer
PEEK	Polyetheretherketone
PEM	Performance Engineer's Manual
PMS	Particle Measuring System
POLINAT	Pollution from Aircraft Emissions in the North Atlantic Corridor
PRSOV	Pressure Regulating & Shut-off Valve
PVC	Polyvinyl Chloride
PW	Pratt and Whitney
RAE	Royal Aircraft Establishment
Ref.	Reference
Req'd.	Required
ROC	Rate of Climb
RR	Rolls-Royce
SAR	Specific Air Range
SAS	Scandinavian Airline System; Simulated Airline Service
SEM	Scanning Electron Microscopy
SFC	Specific Fuel Consumption
SI	Système International
SLM	Standard Litres per Minute
SLS	Sea Level Static
SOV	Shut-off Valve
SPDB	Super-Plastic forming / Diffusion Bonding
St	Stratus
SVC	Subvisual cirrus
SW	Shortwave
TAFAD	Technology Alternatives for Airlift Deployment
TAI	Thermal Anti-icing
TAS	True Airspeed
Temp.	Temperature
TET	Turbine Entry Temperature
TG	Taylor-Görtler
TIC	Time in Cloud
TOC	Top of Climb
TOD	Top of Descent
TOW	Takeoff Weight
TROZ	Troposphärisches Ozon
TS	Tollmien-Schlichting
TSFC	Thrust Specific Fuel Consumption
UNFCCC	United Nations Framework Convention on Climate Change
URL	Uniform Resource Locator
US	United States (of America)
USA	United States of America
USAF	United States Air Force
UV	Ultraviolet



VFW      Vereinigte Flugtechnische Werke  
ZFW      Zero Fuel Weight

## N.2 DEFINITIONS AND GLOSSARY

### N.2.1 Definitions of mission weights, distance and time

**Block fuel / time:** The block fuel / time equals the trip fuel / time plus the fuel / time required for the engine start-up and taxi and the taxi after landing. (The taxi-in fuel is taken from the reserve fuel.)

**Brake Release Weight:** The BRW is the aircraft weight when it commences the takeoff run. It is equal to the takeoff weight (TOW).

**Maximum Takeoff Weight:** The MTOW is the maximum structural limit weight.

**Maximum Zero Fuel Weight:** The MZFW is the Operating Empty Weight (OEW) plus the maximum structural payload weight.

**Ramp weight:** This is the aircraft weight at the ramp, before engine start-up.

**Range:** For the mission analyses the range is equal to the trip distance. In the case of a cruise only assessment the range is the horizontal distance covered in the cruise.

**Reserve fuel:** This is the fuel required for the overshoot at the destination, the alternate leg, the hold and the en route contingency fuel (as per JAR OPS 1, described in D.2, Appendix D).

**Tankered fuel:** For the purpose of this study, the tankered fuel has been defined as the "extra" fuel on-board after landing at the alternate aerodrome (i.e. that which is over-and-above the mission and reserve fuel).

**Trip distance:** The trip distance calculation ignores the climb and descent below 1500ft. In the absence of wind this is equal to the ground distance.

**Trip fuel / time:** This is the fuel / time calculated from "brake release" at the departure aerodrome to "touch down" at the destination aerodrome.

**Zero Fuel Weight:** The ZFW is the Operating Empty Weight (OEW) plus the payload.

### N.2.2 Glossary of technical jargon<sup>1</sup>

**Albedos:** Fraction of the incoming solar energy reflected.

**Anthropogenic:** Anything manmade or caused by humans.

**Assay:** Equivalent to the term experiment; most often used in the biological sciences.

**Attachment line:** The particular streamline, which separates the flow over the upper and lower surfaces of the wing.

**Block fuel:** The total fuel used from start-up to shut-down.

**Contact angle:** This is used to identify how well a liquid will wet a solid material. It is the angle made by a liquid on a solid at the three phase (solid/liquid/air) contact point in a two dimensional representation of a liquid drop on a solid surface.

---

<sup>1</sup> Definition of: Chemistry terms provided by D. O'Donoghue (CES Department, University of Limerick, Jan. 2001); Cloud physics terms explained by P. Brown (UK Met Office, Farnborough, Dec. 2001); Aeronautical terms by the author.



- Contrails:** Condensation trails are light, line-shaped clouds formed by high-flying aircraft in a cold, moist atmosphere.
- D-box:** This is the leading section of the wing, horizontal tailplane or fin ahead of the forward spar.
- Denaturant:** A compound or physical event (e.g. heating), which causes an enzyme structure to change from a native conformation to an inactive, unfolded protein structure. Denaturation may be an irreversible process.
- Drag count:** 1/10000 of a drag coefficient.
- Drag divergent Mach number:** The Mach number at which a significant increase in drag occurs due to shock formation. The Boeing definition is a 20 drag count increase.
- EDAX:** Energy dispersive analysis x-ray (EDAX) is a technique used to identify the presence of selected elements on the surface of a specimen.
- Empennage:** This is a collective term for the fin and horizontal tailplane on an aeroplane.
- Enzyme:** These are proteinaceous catalysts used by organisms for a multiplicity of purposes from the releases of energy to the synthesis of chemicals as building blocks for processes of cellular metabolism.
- Erythema dose rate:** UV irradiance weighted according to how effectively it causes sunburn.
- Fluorosurfactant:** Surfactants bearing fluorine on the hydrophobic chain(s).
- Flight level (FL):** This is pressure height expressed in hundreds of feet and is used for aircraft operations. FL 350 implies a pressure height of 35000ft.
- Freezing Point Depressant (FPD):** This is a solution, usually glycol based, with the ability to prevent the formation of ice, or to decompose pre-formed ice.
- Green dot speed:** Operational reference speed that gives the best lift-to-drag ratio for the aircraft.
- Greenhouse effect:** Greenhouse gases absorb infrared terrestrial radiation at specified wavelengths and in turn emit radiation from a level where the temperature is colder than at the surface.
- Habit:** The characteristic ice crystal geometry or shape, as formed in clouds.
- Haemolymph:** The "blood" of invertebrate species such as insects.
- Hydrolase:** A term used to describe an enzyme, which under normal circumstances catalyses the cleavage of chemical bonds in their substrates using water as part of the reaction.
- Hydrolysis:** This describes the decomposition of a substance by the addition of water. In aqueous solutions this is the typical reaction catalysed by proteases.
- Hydrophobic:** A term describing molecules, or fragments of molecules, which are *water hating*, meaning that they are not readily soluble in water.
- Hydrophilic:** A term describing molecules, or fragments of molecules, which are *water loving*, meaning that they are readily soluble in water.
- METAR:** This is a meteorological aerodrome report, prepared at regular times, for aviation activity. It provides coded details on actual temperature, dew point, wind, barometric pressure, clouds, etc.
- Nacelle:** This is the enclosure covering the engine on the aircraft.



- Native conformation:** A term describing the three dimensional structure of an enzyme in which it can display catalytic activity towards a substrate.
- Planform area:** This is the projected area of an aircraft component (or a part of the aircraft component) such as the wing or horizontal tailplane onto a datum plane, usually defined parallel with the fuselage horizontal datum.
- Polar:** Term describing a compound, which can ionise when dissolved. Generally, it is used to describe a compound, which will dissolve into water.
- Protease:** A class of enzyme for which proteins and peptides are the specific substrate catalytically decomposed by hydrolysis in aqueous media. They have been shown to be functional in non-aqueous media.
- QNH:** This is the standard code for a reference atmospheric pressure used routinely in aviation. On an aerodrome, the correct QNH setting on an altimeter, results in the instrument correctly reading the elevation of the aerodrome.
- Radiative forcing:** A change in the balance between incoming solar radiation and outgoing infrared radiation. Used as a measure of the greenhouse effect
- Relative activity:** This is the activity of an enzyme relative to some baseline value. It is usually expressed as a percentage of the maximum observed activity in a particular experimental reaction series.
- Revenue passenger-km:** This is a measure of the traffic carried by a commercial aviation operator and implies one revenue passenger carried 1km.
- Scanning Electron Microscopy (SEM):** A microscopy technique in which an image of a specimen is produced via detection of electrons emitted from a sample's surface.
- Sessile drop:** A static, immobile drop of liquid on a surface.
- Snowball effect:** This is used a term used to describe the cycle of weight increases that occur in the design of a new aircraft, for a given range specification. It implies that a less efficient aircraft will burn more fuel, which will result in more fuel being carried, which will imply a heavier aircraft, and yet more fuel being consumed.
- Sparging technique:** A technique in which a gas is introduced into a liquid via a glass column with a fritted element (e.g. a fritted disc) at some point along the glass column and beneath the surface of the liquid being sparged.
- Specific thrust:** The specific thrust (of a jet engine) is defined as the net thrust output divided by the mass flow through the engine.
- Substrate:** The general term used to describe the chemicals or materials on which an enzyme acts during enzyme catalysed reactions.
- Surface tension:** This is force acting at right angles to any line of unit length on the surface of a material.
- Surfactant (surface active agent):** These are chemicals, which alter the surface properties of solutions to which they have been added. They are composed of hydrophilic head groups and hydrophobic chains. The hydrophobic chain is normally a (branched) hydrocarbon chain.
- Turbomatch:** This is a Cranfield University computer program that is used to model jet turbine engine performance.
- Wetted area:** The surface area of an aircraft component (or a part of the aircraft component) such as the wing, empennage or fuselage.



**Wetting & Wettability:** Wetting is the displacement of one fluid by another and required three phases (e.g. solid, liquid, gas), two of which must be in contact. Wettability describes the ability of any solid to be wetted when in contact with a liquid and can be quantified by the contact angle.

**% v/v (percent volume/volume):** When a 10%v/v solution is prepared then the volume of substance used is 10mls and the final volume of the solution is 100mls.

**% w/v (percent weight/volume):** When a 10%w/v solution is prepared then the mass dissolved is 10g and the final volume of the solution is 100ml.

--- 0 ---